

RILEM State-of-the-Art Reports

Denys Breysse *Editor*

# Non-Destructive Assessment of Concrete Structures: Reliability and Limits of Single and Combined Techniques

State-of-the-Art Report of the RILEM



# Non-Destructive Assessment of Concrete Structures: Reliability and Limits of Single and Combined Techniques

# RILEM STATE-OF-THE-ART REPORTS

## Volume 1

---

RILEM, The International Union of Laboratories and Experts in Construction Materials, Systems and Structures, founded in 1947, is a non-governmental scientific association whose goal is to contribute to progress in the construction sciences, techniques and industries, essentially by means of the communication it fosters between research and practice. RILEM's focus is on construction materials and their use in building and civil engineering structures, covering all phases of the building process from manufacture to use and recycling of materials. More information on RILEM and its previous publications can be found on [www.RILEM.net](http://www.RILEM.net).

The RILEM State-of-the-Art Reports (STAR) are produced by the Technical Committees. They represent one of the most important outputs that RILEM generates – high level scientific and engineering reports that provide cutting edge knowledge in a given field. The work of the TCs is one of RILEM's key functions.

Members of a TC are experts in their field and give their time freely to share their expertise. As a result, the broader scientific community benefits greatly from RILEM's activities.

RILEM's stated objective is to disseminate this information as widely as possible to the scientific community. RILEM therefore considers the STAR reports of its TCs as of highest importance, and encourages their publication whenever possible.

The information in this and similar reports is mostly pre-normative in the sense that it provides the underlying scientific fundamentals on which standards and codes of practice are based. Without such a solid scientific basis, construction practice will be less than efficient or economical.

It is RILEM's hope that this information will be of wide use to the scientific community.



For further volumes:

<http://www.springer.com/series/8780>

Denys Breysse  
Editor

# Non-Destructive Assessment of Concrete Structures: Reliability and Limits of Single and Combined Techniques

State-of-the-Art Report  
of the RILEM Technical Committee 207-INR

 Springer



*Editor*

Denys Breysse  
I2M - Department of Civil and  
Environmental Engineering  
University Bordeaux 1  
Avenue des facultés  
33405 Talence  
France

ISBN 978-94-007-2735-9 e-ISBN 978-94-007-2736-6

DOI 10.1007/978-94-007-2736-6

Springer Dordrecht Heidelberg London New York

Library of Congress Control Number: 2012930139

© RILEM 2012

No part of this work may be reproduced, stored in a retrieval system, or transmitted in any form or by any means, electronic, mechanical, photocopying, microfilming, recording or otherwise, without written permission from the Publisher, with the exception of any material supplied specifically for the purpose of being entered and executed on a computer system, for exclusive use by the purchaser of the work.

Printed on acid-free paper

Springer is part of Springer Science+Business Media ([www.springer.com](http://www.springer.com))

# Foreword

The concrete infrastructure requires regular assessment in order to ensure public safety and cost-effective maintenance practice. Assessment efforts verify in place material condition, damage state, position and geometry of elements, and other important structural characteristics. But carrying out assessment using direct sampling and observation of the structure is not always possible, especially if the volume of interest is hidden from view (e.g. in the case of internal damage), or physical access to the structure of interest is restricted, or cost concerns limit the number of direct material samples that are collected.

Non-destructive assessment and evaluation (commonly referred to as NDE) methods offer the ability to infer material condition information where direct sampling and inspection cannot. And because of the inherent non-damaging nature of the tests, many data can be collected and analyzed without fear of adversely affecting the structure under inspection. In NDE, a specific test phenomenon is applied and the response observed. Many different types of phenomena are appropriate for application to concrete structures, including mechanical wave propagation, electromagnetic wave propagation, penetrating radiation, optics, magnetism, and heat transfer. Application of the phenomenon (test method) and observation of the observed phenomenological response (test data) is often made difficult by the nature of the concrete infrastructure: large size, difficult access and naturally inhomogeneous material makeup.

The nature of these different phenomena varies and the quality of the connection between the structural or material characteristic of interest also varies, depending on the particular phenomena employed and the characteristic of interest. After some processing, the observed test data, or in some cases judicious combination of distinct types of data, are normally related to the material property or structural condition of interest through some model. But in some cases, this connection is established by a normative rule set. For example, X-rays are less likely to be absorbed or scattered along paths within a solid that contain air-filled cracks and voids; thus we can infer that those paths that reveal higher X-ray intensity contain high amounts of such damage.

We see, though, that NDE relies on an indirect connection between the observed phenomena, and the quality of the NDE result depends as much on the appropriateness and rigor of this connecting model as on the quality of the observed phenomenological data themselves. Thus appropriate and effective use of NDE needs balance of requirements:

- (i) hold suitable understanding of the underlying phenomenon,
- (ii) deploy testing methods correctly, and
- (iii) apply appropriate and accurate connecting models in the analysis.

This book aims to give the reader a solid basis in these three areas, with a particular focus on complimentary combinations of techniques to improve the assessment.

Chapter 1 introduces the basic concepts of NDE, lays out the associated challenges for concrete structures and offers some solution to these challenges through the combination of distinct techniques. Chapter 2 provides fundamental information about the underlying phenomenological basis and principles of individual NDE test methods. Chapters 3 to 7 are devoted to specific NDE applications: strength assessment, defect characterization, geometry (thickness or depth) determination, etc. The last chapter revisits the concepts of test method combination, thoroughly addressing the challenges associated with NDE and proposing future directions of development.

This book is authored and edited under the auspices of RILEM Technical Committee 207-INR, which is made up of internationally recognized experts in the field. From this book, the reader will obtain a thorough background in non-destructive assessment methods that is essential for effective application to concrete structures, representing technical progress in an important field.



John S. Popovics, Ph.D.  
The University of Illinois at Urbana-Champaign

# Contents

<b>1 Non destructive assessment of concrete structures: usual combinations of techniques</b> .....	1
Denys Breysse	
1 Non-destructive assessment of concrete: objectives and key challenges.....	1
2 Added-value of combining techniques: traditional approaches.....	4
2.1 Purpose for combining techniques.....	4
2.2 Type [A] combination – confirmation of test results obtained with different techniques .....	5
2.3 Type [B] combination – improvement of test result interpretation obtained with different techniques .....	9
2.4 Type [C] combination – application of different techniques for “quick” localization of defected areas followed by detailed inspection with “slow” but more accurate measurements .....	12
3 Conclusions.....	14
References.....	15
<b>2 Presentation of common non destructive techniques</b> .....	17
1 Ultrasounds through transmission.....	17
1.1 Physical principles and theory .....	17
1.2 Correlation with the mechanical properties .....	18
1.3 Measuring Equipment and Handling .....	20
1.4 Guidelines, Recommendations .....	22
1.5 Common techniques and devices.....	22
1.6 Reliability and limitation of results.....	25
1.7 Developments.....	26
References.....	27
2 Ultrasonic Echo.....	27
2.1 Physical principles and theory .....	27
2.2 Measuring equipment and handling.....	28

- 2.3 Data processing: display and imaging techniques ..... 32
- 2.4 Guidelines, Recommendations ..... 34
- 2.5 Reliability and limitations..... 34
- 2.6 Developments..... 36
- References..... 38
- 3 Surface waves methods..... 39
  - 3.1 Physical principles and theory ..... 39
  - 3.2 Measurement equipment and procedure ..... 40
  - 3.3 Data analysis and interpretation..... 41
  - 3.4 Reliability and limitation of results..... 43
- References..... 43
- 4 Impact echo..... 44
  - 4.1 Physical principles and theory ..... 44
  - 4.2 Measurement equipment and handling ..... 46
  - 4.3 Guidelines, references and standards..... 47
  - 4.4 Calibration and interpretation of results ..... 48
  - 4.5 Reliability and limitation of results..... 50
- References..... 50
- 5 Impulse response..... 51
  - 5.1 Physical principles and theory ..... 51
  - 5.2 Measurement equipment and handling ..... 52
  - 5.3 Guidelines, references and standards..... 54
  - 5.4 Calibration and interpretation of results ..... 54
  - 5.5 Reliability and limitation of results..... 56
- References..... 57
- 6 Acoustic emission..... 58
  - 6.1 Physical principles and theory ..... 58
  - 6.2 Measurement equipment and handling ..... 59
  - 6.3 Guidelines, references and standards..... 60
  - 6.4 Calibration and interpretation of results ..... 61
  - 6.5 Reliability and limitation of results..... 62
- References..... 63
- 7 Ground Penetrating Radar..... 63
  - 7.1 Physical principles and theory ..... 63
  - 7.2 Equipment and handling ..... 66
  - 7.3 Guidelines and standards ..... 67
  - 7.4 Data processing, calibration and interpretation ..... 68
  - 7.5 Applications, reliability of results and limitations..... 69
- References..... 70
- 8 Capacitive technique..... 71
  - 8.1 Physical principles and theory ..... 71
  - 8.2 Measuring equipment and handling..... 73
  - 8.3 Data processing, calibration and interpretation ..... 74
  - 8.4 Limitations and reliability..... 76
- References..... 77

- 9 Electrical resistivity measurement ..... 77
  - 9.1 Physical principle and theory ..... 77
  - 9.2 Measurement techniques and handling ..... 78
  - 9.3 Calibration, data processing, interpretation of results ..... 82
  - 9.4 Reliability and limitation of results..... 82
  - 9.5 Guidelines for use, references, standards..... 83
  - 9.6 On-going developments: problems under research, new questions, specific developments ..... 83
- References..... 84
- 10 Infrared thermography ..... 85
  - 10.1 Physical principles and theory ..... 85
  - 10.2 Measuring equipment and handling: the infrared camera ..... 88
  - 10.3 Data processing, calibration and interpretation ..... 88
  - 10.4 Passive thermography applied to the investigation of discontinuities ..... 89
  - 10.5 Investigations with active thermography ..... 92
  - 10.6 Guidelines and Standards..... 97
- References..... 97
- 11 Radiography ..... 98
  - 11.1 Physical principles and theory ..... 98
  - 11.2 Measurement equipment and handling ..... 98
  - 11.3 Guidelines, references and standards..... 100
  - 11.4 Calibration and interpretation of results ..... 100
  - 11.5 Reliability and limitation of results..... 101
- References..... 101
- 12 Rebound hammer ..... 101
  - 12.1 Physical Principle and Theory ..... 102
  - 12.2 Measuring Equipment and Handling ..... 104
  - 12.3 Calibration and Interpretation of Results ..... 106
  - 12.4 Reliability and Limitation of Results ..... 107
  - 12.5 Guidelines for Use and Standards..... 109
- References..... 110
- 13 Pull-out testing ..... 110
  - 13.1 Physical principles and theory ..... 110
  - 13.2 Measurement equipment and handling ..... 113
  - 13.3 Guidelines, references and standards..... 114
  - 13.4 Calibration and interpretation of results ..... 115
  - 13.5 Reliability and limitation of results..... 116
- References..... 117

<b>3</b>	<b>Estimation of on-site compressive strength of concrete</b> .....	119
	Marios N. Soutsos, Denys Breysse, Vincent Garnier, Arlindo Goncalves, and Andre Valente Monteiro	
1	Introduction – definition of the problem.....	119
1.1	What is Looked For?.....	120
1.2	At What Scale? .....	122
1.3	For What Purpose?.....	123
2	Description of the Techniques .....	124
2.1	Penetration Resistance .....	124
2.2	Pull-out Test.....	125
2.3	Pull-off Test.....	128
3	Calibration Aspects and Assessment of Characteristic In-situ compressive strength .....	129
3.1	Calibration Aspects.....	129
3.2	Assessment of characteristic in-situ compressive strength by indirect methods .....	148
4	Multivariate analysis and modeling for strength assessment of concrete.....	156
4.1	Back into history: the SonReb method .....	156
4.2	Developing multivariate relationships as conversion curves .....	158
4.3	Understanding the possibilities and limits of multivariate correlations .....	161
4.4	Calibration process and combination of NDT on real data.....	166
4.5	The scope of investigation and its efficient planning .....	168
4.6	Conclusions about combination of techniques .....	170
5	Data fusion to better estimate strength.....	171
5.1	Why to use data fusion?.....	171
5.2	Data fusion in 1D.....	172
5.3	Data fusion in 2D.....	178
6	Conclusions.....	181
	References.....	182
<b>4</b>	<b>Control of thickness/dimensions of pavements, foundations, elements and piles</b> .....	187
	Johannes Huginschmidt, Martin Krause, Denys Breysse, Ernst Niederleithinger, and Alexander Taffe	
1	Problem description, testing tasks.....	187
1.1	Pavement.....	187
1.2	Thin elements.....	188
1.3	Shallow foundations.....	190
1.4	Deep foundations, piles and shafts.....	191
2	Common techniques.....	192
2.1	Pavement.....	192
2.2	Thin elements.....	196

- 2.3 Shallow foundations..... 201
- 2.4 Deep foundations, shafts and piles..... 206
- 3 Special techniques and enhanced methods ..... 213
  - 3.1 Possible enhancements..... 213
  - 3.2 Special techniques..... 214
- 4 Benchmarks and test sites ..... 216
  - 4.1 Pavements and sealings..... 217
  - 4.2 Thin elements..... 218
- References..... 225
- 5 Assessment of bonding, delamination and interfaces ..... 227**  
 Jean-François Lataste and Patrice Rivard
  - 1 Introduction to debonding and delamination ..... 227
  - 2 Description /definition of the problem treated ..... 228
    - 2.1 What is being looked for?
      - At what scale? For what purpose? ..... 228
    - 2.2 What level of interpretation? Required accuracy? ..... 229
    - 2.3 Why it is difficult? ..... 233
  - 3 Description of Techniques ..... 234
    - 3.1 Common techniques..... 234
    - 3.2 Special techniques..... 246
  - 4 Global strategy of approach towards diagnosis ..... 248
    - 4.1 Complementary techniques..... 248
    - 4.2 Use for better efficiency..... 250
    - 4.3 Use for more information..... 251
    - 4.4 Use for better reliability ..... 252
    - 4.5 Case study ..... 253
  - 5 Benchmark and test site ..... 255
  - 6 Conclusion ..... 259
  - References..... 260
- 6 Localization of grouting faults in post tensioned concrete structures ..... 263**  
 Martin Krause
  - 1 Introduction..... 263
    - 1.1 State of the art and existing guidelines and recommendations ..... 263
    - 1.2 Fields of application..... 264
  - 2 Overview of Methods..... 264
  - 3 Radiography with X- and  $\gamma$ -Radiation ..... 265
    - 3.1 X-rays..... 265
    - 3.2 Gamma-Radiation ..... 265
  - 4 Echo Methods with mechanical waves: Impact Echo..... 268
    - 4.1 Application of the impact-echo method for tendon ducts..... 268
    - 4.2 Point and Linear Measurement and evaluation..... 272
    - 4.3 Impact-Echo imaging..... 272
    - 4.4 Interpretation and research: the SIBIE procedure..... 278



5	Echo Methods with mechanical waves: Ultrasonic Echo .....	279
5.1	Introduction, principle.....	279
5.2	Ultrasonic Point Measurement and evaluation .....	280
5.3	Linear Measurement and 2D representation of the data .....	280
5.4	Linear and 2D Measurement followed by Imaging with Reconstruction calculation (magnitude evaluation).....	283
5.5	Reconstruction calculation using phase evaluation.....	287
5.6	Ultrasonic Echo with Linear Array.....	291
6	Ultrasonic Through Transmission.....	294
7	Other methods.....	295
7.1	Radar for plastic ducts .....	295
7.2	Active Thermography .....	297
8	Conclusions.....	298
	References.....	300
<b>7</b>	<b>Ruptures of prestressing cables .....</b>	<b>305</b>
	Jean-Paul Balayssac, Carmen Andrade, Javier Sanchez Monteiro, and Horst Scheel	
1	Definition of the problem.....	305
1.1	What is looked for?.....	305
1.2	At what scale?.....	307
1.3	For what purpose?.....	308
2	Description of the techniques.....	309
2.1	Radiography .....	310
2.2	Magnetic methods.....	312
2.3	Acoustic Emission .....	317
2.4	Special techniques.....	320
2.5	Calibration aspects.....	326
2.6	Evaluation and comparison of the techniques.....	326
3	What can be done for a better assessment? Combination possibilities .....	326
4	Benchmarking sites: examples.....	330
5	Conclusions.....	331
	References.....	332
<b>8</b>	<b>Non destructive assessment of concrete structures: combination of different techniques for addressing new challenges.....</b>	<b>335</b>
	Denys Breyse and Vincent Garnier	
1	Introduction: a new challenge for combination .....	335
2	The identification / inversion problem .....	338
2.1	Understanding the complexity of the problem.....	338
2.2	Formalizing the problem.....	339

- 3 Practical case of Type [D] combination for concrete properties assessment ..... 344
  - 3.1 Porosity and water content assessment by combining two NDT methods..... 345
  - 3.2 Young modulus assessment by combining two or more NDT measurements ..... 346
- 4 Data fusion ..... 350
- 5 Quality of techniques and quality of assessment ..... 353
  - 5.1 Effect of the noise ..... 354
  - 5.2 Quality of the models used for inversion/identification ..... 354
  - 5.3 Complementarity and efficiency of combination..... 355
- References ..... 357
  
- RILEM Publications** ..... 359
  - RILEM PROCEEDINGS ..... 359
  - RILEM REPORTS ..... 365
  
- RILEM Publications published by Springer** ..... 369
  - RILEM BOOKSERIES (Proceedings) ..... 369
  - RILEM STATE-OF-THE-ART REPORTS..... 369
  
- Index** ..... 371



# Authors and Contributors

This book is the result of a five year work of RILEM TC 207-INR. More than thirty core members and corresponding members were involved in twelve meetings and contributed to this report. They contributed either as “main authors” coordinating a chapter of the book, as contributors to these chapters or as reviewers. Their list is following. The name of authors and contributors is specified at the beginning of each chapter.

## Chairman

Denys Breysse                      Université Bordeaux 1, I2M, GCE (Civil and Environmental Engineering Department), France

## Secretary

Andrzej Moczko                      Wrocław University of Technology, Poland

## Core Members

Jean-Paul Balayssac                      Université de Toulouse, UPS, INSA, LMDC (Laboratoire Matériaux et Durabilité des Constructions), France

Xavier Dérobert                      IFSTTAR (formerly LCPC), Nantes, France

Roberto Felicetti                      Politecnico di Milano, Italy

Markus Fischli                      Proceq S.A., Switzerland

Vincent Garnier                      Université de la Méditerranée, IUT Aix-en-Provence, France

Arlindo Gonçalves                      Laboratório Nacional de Engenharia Civil, Lisbon, Portugal

Johannes Hugenschmidt                      EMPA, Zurich, Switzerland

Martin Krause                      BAM, Bundesanstalt für Materialforschung und –prüfung, Berlin, Germany

Jean-François Lataste                      Université Bordeaux 1, I2M, GCE (Civil and Environmental Engineering Department), France

Felicita Pires	Laboratório Nacional de Engenharia Civil, Lisbon, Portugal
Javier Sanchez Monteiro	Eduardo Torroja Institute for Construction Science, Madrid, Spain
Marios N. Soutsos	University of Liverpool, U.K.

### Corresponding members

Odile Abraham	IFSTTAR (formerly LCPC), Nantes, France
Carmen Andrade	Eduardo Torroja Institute for Construction Science, Madrid, Spain
Gérard Ballivy	Université de Sherbrooke, Québec, Canada
Muhammed P.A. Basheer	Queens University Belfast, U.K.
John H. Bungey	University of Liverpool, U.K.
Didier Defer	Université d'Artois, France
Michael C. Forde	University of Edinburgh, Scotland, U.K.
Pierre Gilles	Autoroutes et routes de Wallonie, Belgique
Apedovi Kodjo	Université de Sherbrooke, Québec, Canada
Christiane Maierhofer	BAM, Bundesanstalt für Materialforschung und –prüfung, Berlin, Germany
Ernst Niederleithinger	BAM, Bundesanstalt für Materialforschung und –prüfung, Berlin, Germany
Masayasu Ohtsu	Kumamoto University, Japan
Larry D. Olson	Olson Engineering Inc., USA
Claus Germann Petersen	Germann Instruments, Denmark
Marie-Aude Ploix	Université de la Méditerranée, IUT Aix-en-Provence, France
John S. Popovics	The University of Illinois at Urbana-Champaign, USA
Patrice Rivard	Université de Sherbrooke, Québec, Canada
Horst Scheel	Technische Universität Berlin, Institut für Bauingenieurwesen, Fachgebiet Baustoffe und Baustoffprüfung, Germany
Alexander Taffe	BAM, Bundesanstalt für Materialforschung und –prüfung, Berlin, Germany
Andre Valente Monteiro	Laboratório Nacional de Engenharia Civil, Lisbon, Portugal

Lastly, the authors of this book must also thank several experts for their participation and/or contribution: Ninel Alver (BAM, Germany), Alberto Gennaro-Santori (CND, Italy), Petr Konvalinka (Technical Univ. Prague, Czech Rep.), Adrian Long and Sreejith Nanukuttan (Queens Univ. Belfast, U.K.), Frank Mielentz (BAM), Carlo Pellegrino (Univ. of Padova, Italy) and Geoff Tickell (Univ. of Liverpool, U.K.).

# Chapter 1

## Non destructive assessment of concrete structures: usual combinations of techniques

Denys Breysse<sup>1</sup>

### 1 Non-destructive assessment of concrete: objectives and key challenges

Condition assessment of building materials is critical when reassessing existing structures, since material ageing can result in performance loss, degradation of safety, and maintenance costs. For these reasons, the use of non destructive testing (NDT) has become more common to assess the condition of existing reinforced concrete structures. The first part of this book shows the range of NDT methods that are available, which show some sensitivity to concrete properties or defects. Their use has become more common to assess the condition of existing reinforced concrete structures. When detecting or suspecting of a possible pathology, e.g. after visual inspection, the usual approach with application of NDE is the following:

- (a) to identify first the roots of the problem,
- (b) to know if there is a possible evolution of damage and, if any, at what rate, and
- (c) finally to know what is the severity level of the problem, its location and extent.

Much research has been aimed to developing techniques and data processing. Some standards have been developed for individual techniques and reference texts have been produced on individual problems, like strength assessment (EN 13791 2007). Some authors have also tried to synthesize the capabilities of techniques with

---

<sup>1</sup>Vincent Garnier, Martin Krause, Patrice Rivard, Felicita Pires and John Popovics have also contributed to this chapter.

D. Breysse (✉)

University Bordeaux 1, I2M, GCE (Civil and Environmental Engineering Department), France  
e-mail: denis.breysse@u-bordeaux1.fr

respect to a given problem (Bungey and Millar 1996, Uemoto 2000, IAEA 2002, Breyse and Abraham 2005) or to define the most promising paths for future developments (OECD 1998). The general agreement is that the quality of assessment is limited by various uncertainties caused by: the testing method, systematic interferences with the environment, random interference (due to intrinsic variability of materials), human factors, and data interpretation (Gehlen et al. 2006). The fact that concrete as a material is inherently variable also restricts the practical conclusions that can derive from NDT investigations. Thus, improved assessment can be achieved by reducing any of these sources of uncertainty/variability.

The lack of internationally acknowledged standards or guidelines is a significant limitation:

- the choice of the most appropriate technique for a specific problem is not simple,
- reference guidelines guaranteeing the relevance of the measurement protocol (preparation of the surface, number and mesh of measurement points...) are often lacking,
- the interpretation of measurement results to assess the structural properties can be difficult.

Until now, efforts undertaken to improve techniques (e.g. developing innovative equipment or post processing of data, numerical simulations, benchmarking techniques on pilot sites, etc.) have mainly been done at a national level with many work groups or national research projects in Germany, Britain, France, USA, and Japan. But these efforts have not lead to conclusions or proposals which could be used by the various participants in the field: building managers, contractors, regulators, NDT practitioners and consulting engineers. Due to these increasing needs (validated NDT protocols, quality control and structural assessment of ageing structures) we must now integrate – at an international scale – the huge amount of information and knowledge that has already been produced. For this reason, RILEM created a Technical Committee working on these questions, whose results are presented in this book. The text of this introductory chapter will mainly focus on material condition assessment, but the reader is invited to consider that the same principles will remain valid for other problems, like geometrical assessment or defect detection.

ICRI guidelines have synthesized the more common uses of NDT (ICRI 2009). These guidelines cover the assessment of all information which seems useful for condition assessment of structural concrete prior to repair design and execution: in-situ concrete strength, location and extent of delaminations, location and extent of concrete cracking, severity, location and extent of fire and frost damage, location and extent of void honeycombing, thickness of concrete members, and presence and rate of corrosion activity. Among all of these issues, which will be addressed in the following chapters, three of them illustrate the complexity of concrete assessment:

- Stiffness and strength assessment. The knowledge of the elastic modulus or of the compressive strength of concrete is necessary to perform a structural evaluation, as they are prerequisites for any safety or reliability analysis. These parameters can be determined from tests on core samples, but cores offer information of the

properties only at the point where the specimens have been taken. Thus it is difficult to obtain a representative view of the mechanical properties, since the material as well as the damage level can be spatially variable. NDT provides an interesting alternative since it enables wide coverage. The principal problem with NDE is correlating the values of the NDT measurements to the mechanical properties. Still, non-destructive techniques can be used to assess the structural condition, even if they only provide an indirect information (De Lorenzis et al. 2004). Rebound measurement and ultrasonic pulse velocity (UPV) are most suited NDT methods for this purpose (Malhotra 1981) and a recent European standard has given attention to this task (EN 13791 2007).

- Water content (or moisture content) assessment. Monitoring moisture content is important for two reasons: a high value of water content can be the sign of poor quality concrete, and moisture content enables damage mechanisms even if concrete is of good quality originally. Many NDT methods are sensitive to both material parameter (e.g. Young's modulus) and to moisture content. Due this double dependency, one cannot easily determine the cause for the measured variations in the NDT parameter. It has been shown that the question of damage detection and/or influence on deterioration process is similar in other building materials like timber or masonry (Breyse 2008). This problem has been named the "humidity paradox" (Shaw and Xu 1998).
- Corrosion assessment. This is an important problem since many reinforced concrete structures suffer severe damage due to corrosion of internal steel (due to chlorides in marine environment, deicing salts, or other causes). The cost of corrosion is estimated to be about 3 to 4 % of GNP in Western countries. The U.S. Federal Highway Administration (FHWA 2002) released a study in 2002 on the direct costs associated with metallic corrosion in nearly every U.S. industry sector. Results of the study show that the total annual estimated direct cost of corrosion in the U.S. is a staggering \$276 billion—approximately 3.1% of the nation's Gross Domestic Product (GDP). Corrosion attacks steel reinforcing bars and cables in pre-stressed structures, and material and structural assessment of such structures is critical when one wants to evaluate residual capacity, to design a reinforcing solution or to plan maintenance. The detection of defects like grout voids in tendon ducts, which favour corrosion, constitute another challenge. Some techniques have been standardized and make it possible to assess the material condition of corroding structures. However, many problems remain unresolved.

These three topics address the two domains of mechanical assessment and durability between which the boundary is not well defined: the mechanical properties of tomorrow are often dependent on the deterioration process of today. Different classes of concrete degradation can occur: either physico-mechanical (overloading, freeze and thaw, fire, restrained strains during shrinkage or temperature elevation, etc.) or physico-chemical (corrosion, alkali-aggregate reaction, sulfate attack, etc.). But regardless of the class of degradation, they result in distributed damage, which may take the form of a porosity increase or of a microcrack network, and local damage, which may take the form of delamination or macrocracks, which must be assessed (Breyse, 2010).



Three requirements should be satisfied for NDT assessment:

- (a) being able to detect defects or variation of properties, between two structures or within one structure,
- (b) being able to build a hierarchy (i.e. to rank on a scale) regarding a given property (e.g. mapping stiffness, plotting changes in dimensions...), between several areas in a given structure or between several structures,
- (c) being able to quantify these properties, e.g. comparing them to allowable thresholds or reference values (e.g. expected strength or planned dimension).

Of these three requirements, the last one is the most critical and also most difficult to satisfy. We propose that a well chosen combination of techniques can contribute to improved assessment of concrete structures.

In this chapter, we will first address the “traditional approaches” of NDT. In a second part, combinations of techniques will be analyzed from a formal point a view and illustrated by two practical examples. Finally, we will try to explain, relying on a single example, what can be the practical interest and the practical limits of such a combination. Throughout this book, many examples of combination of techniques will be presented. The reader is invited to keep in mind the opportunities and difficulties that will be discussed here when reading about combination of techniques for each specific application.

## **2 Added-value of combining techniques: traditional approaches**

### ***2.1 Purpose for combining techniques***

When addressing material condition, the expert can have different objectives. He can limit himself to a qualitative view, for instance by identifying spatial variations in the measured parameters, but he can be more ambitious and try to quantify these variations, for instance because he needs some input values for structural computations before repair or for reliability assessment. In this case, one needs a validated methodology such as to ensure the quality of estimates. Much research has been devoted to the development of techniques and data processing for improved assessment of building materials. Many case studies exist in which different techniques have been combined, but real added value can only be obtained if the issue of combination is correctly analyzed (Derobert et al. 2005). This added value can be defined in terms of (a) accuracy of estimation of properties, (b) relevance of physical explanations and diagnosis, (c) reduction in time to reach a given answer.

The combination of techniques can pursue various objectives, like confirming with a second technique what has been observed with a first one, zoning the area where a more sophisticated investigation will be performed in the following, decreasing the number of borings by identifying the areas where borings will be more informative.

**Table 1.1** Examples of Type A combination of non-destructive techniques

Reference	Techniques used	Structure	Objective
Scott et al., 2003	Impact echo, radar	Bridge deck	Comparisons between techniques
Alt et al., 1996	Infrared thermography, radar, electrical techniques	Bridge deck	Detection of delamination
Yong Hao & Kee Ee, 2003	Radar, impact-echo, dynamic response	Bridge deck	Detection of damage
Weise et al., 2008	Radar, udeckltrasonic	Hydraulic structures	Identification and zoning of damage (cores used for confirmation)
Maser et al., 2003	Radar, impact-echo	Pavement	Accuracy of results for depth evaluation
De Bold et al., 2010	Ultrasonic, impact echo, impulse response, radar, rebound hammer	Building (thick concrete)	Condition assessment
Parthasarathy et al., 2009	Radar, pulse echo	Slabs	Accuracy of results for defect detection (delamination, cracks, honeycombing)

We will refer now to to three possible types of combinations that will be illustrated by several examples (either in the laboratory or on site), all drawn from experiments performed in the frame a National Research Project (Balayssac 2008):

- Type [A]: comparison of results obtained via two or more techniques, so as to confirm measurements and recorded variations,
- Type [B]: comparison of results obtained via two or more techniques, so as to improve the interpretation of results. This improvement often needs some analysis (image analysis, statistical analysis), which enables one to go further than a simple visual confirmation,
- Type [C]: use of a “quick” technique to have a first rough mapping, followed by a second “slow” technique in the areas selected in the first step.

The following sections show only a few examples, from limited experience. Tables 1.1 to 1.3 provide additional references of similar combinations.

## 2.2 *Type [A] combination – confirmation of test results obtained with different techniques*

The combination of three techniques (infrared thermography, electrical resistivity and capacitance) to assess the moisture content / damage state of material along a profile is described in detail in (Naar et al. 2005) and (Sirieix et al. 2007). In this case study, a precast concrete duct in which some damage (crack patterns) had been

**Table 1.2** Examples of Type B combinations of non-destructive techniques

Reference	Techniques used	Structure	Objective
Romanescu et al., 2009	Ultrasonic, rebound	Bridge beams	Strength assessment
Scott et al., 2003	Impact echo, radar	Bridge deck	Assessment of damage and delaminations
Klysz et al., 2003	Radar, capacimetry, ultrasonic, infrared thermography	Bridge deck	Detection of damaged areas
Gardei et al., 2003	Radar, impact-echo, ultrasonic	Railway tracks	Quality control of the concrete
Lataste et al., 2003	Surface waves, electrical conductivity	Slab	Detection and sizing of cracks
Gucunski et al., 2010	Impact echo, radar, half cell potential, ultrasonic, electrical resistivity	Bridge deck	Detection and zoning of delamination, corrosion

**Table 1.3** Examples of Type C combinations of non-destructive techniques

Reference	Techniques used	Structure	Objective
Pina Santos et al., 2003	Thermography, US	Building wall	Detection of moisture and delamination
Maierhofer et al., 1998	Radar, US	Sluices	Decrease the number of borings
Arndt et al., 2010	Ultrasonic echo, radar, thermography, half cell potential	Laboratory slabs	Assess development of corrosion through periodic inspection

identified was inspected through several different techniques: capacimetry (measuring permittivity), infrared thermography and electrical resistivity. Radar and ultrasonic measurement were also tested but, for radar, the high density of rebars prevented any efficient processing of results, and reliable ultrasonic measurements were impossible with the device used due to the curvature of the surface. The longitudinal variations of the three measured properties along the duct profile show striking similarities (Figs. 1.1–1.3). In Fig. 1.1 the variation of a resonant frequency that is proportional to the material permittivity is shown. The variation of the electrical resistivity (Fig. 1.2) and the variation of the surface temperature, measured by infrared thermography (Fig. 1.3) show similar pattern. In all figures the black area indicates the part of the structure where the concrete had been repaired, because of extensive damage, which prevents any comparison. A dotted regression curve has also been added, which exhibits a parabolic shape for the three series of measurements.

The data scatter is indicated by error bars, which confirm that the magnitude of the longitudinal variation is much larger than the local variability/uncertainty. The similarities among the three NDT results illustrate their mutual confirmation. If a technique would have been used alone, a second technique (or a third one) would have reinforced the confidence in the assessment. This is a direct illustration of a Type [A] combination.

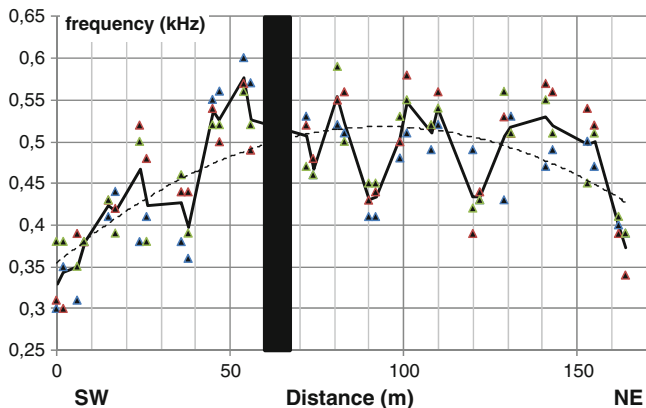


Fig. 1.1 Capacimetry: longitudinal profile of frequency (keystone)

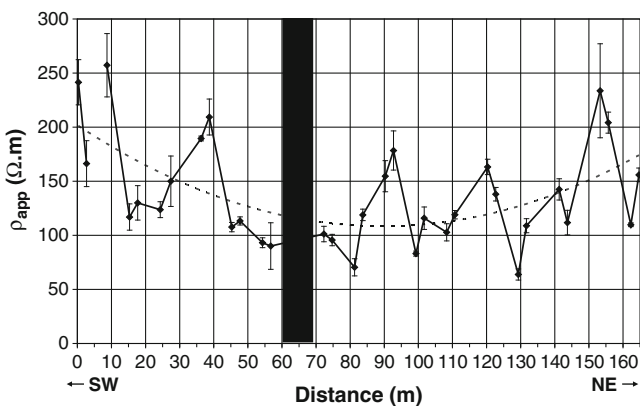


Fig. 1.2 Average electrical resistivity with error bars measured in three points, along the keystone of the duct

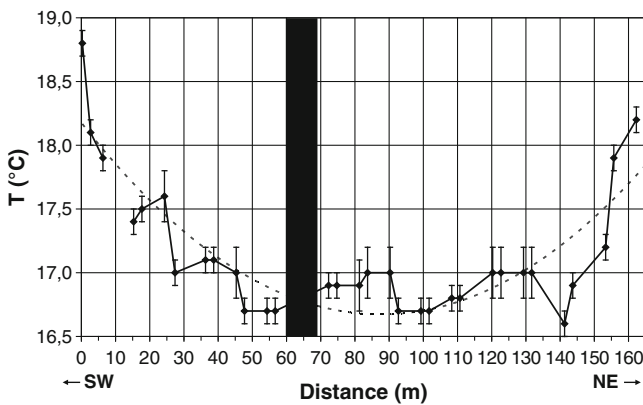
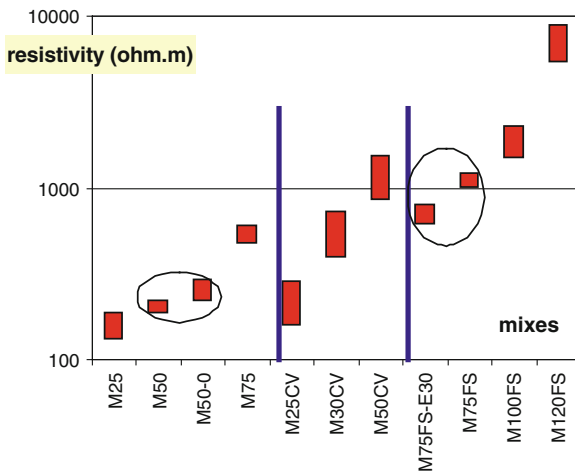


Fig. 1.3 Average temperature with error bars of the keystone measured with a thermal image ( $0.38 \times 0.46 \text{ m}^2$ )

**Fig. 1.4** Electrical resistivity of 10 concrete mixtures with various strengths (from left to right: normal concretes, CV = fly ash addition, FS = silica fume addition)



These similarities can be explained in terms of material moisture content and/or damage variation, since all three techniques are sensitive to these two causes. However, the measurements, even combined, do not provide any information about the reasons for these variations. Two opposite interpretations are suggested:

- It is possible that the material damage varies along the abscissa, which is interpreted as an increase in porosity; this leads to lower frequencies, lower resistivities and lower temperatures in the mid part of the duct, due to higher moisture content in the saturated concrete,
- It is also possible that the variations in the moisture content profile are caused by environmental conditions: the duct faces south-west on its left-end and north-east on its right-end, which favors a relative drying of the concrete cover near both ends. In this case, the longitudinal variations can be explained without any damage or cracking.

Going further in the interpretation would require a more detailed analysis of the parameters influencing each property measured; this will be discussed in § 3.1. This is the reason why recent efforts have been undertaken, in an extensive research project, to better understand (and quantify) how NDT parameters are sensitive to various possible influencing factors (Balayssac 2008). This issue is a central one, and will be addressed in detailed fashion in this book.

This type [A] of combination has also been carried out in another case study. The specimens, made of various types of concrete in the 25 MPa-120 MPa 28-day compressive strength range, had been subjected to marine attack (in the tidal domain in La Rochelle harbor) for several years. The specimens were investigated and ranked by various non-destructive techniques. Figure 1.4 illustrates how the electrical resistivity varied with the concrete mix. For each type of concrete, the corresponding rectangle marks the average value of resistivity plus/minus one standard deviation.

The very high sensitivity of resistivity to concrete strength is confirmed here. It enables to rank strengths for similar concretes (normal concrete, or concrete with fly ash addition or silica fume addition) kept in comparable environments. Figure 1.4 also confirms that various types of concrete cannot be directly compared.

The resistivity of M30CV (compressive strength 30 MPa with fly ash additions) is higher than that of M50 (normal concrete, compressive strength 50 MPa). Measurements performed by (Wolsiefer 1991) had yet shown the higher resistivity of concrete with silica fume addition, this increase being more important for low w/c ratios. The ranking of specimens based on electrical resistivity measurements (Lataste et al. 2005) was confirmed with radar measurements and capacimetry. However, as observed in the first case study, this confirmation (Type [A] combination) tells nothing about the physical explanation. The physics involved in each non-destructive technique is sensitive to many microstructural parameters (porosity and connectivity, properties of the particles...) as well as to parameters depending on environmental conditions (moisture content, chloride content...). Thus, the variation of a single physical property (radar attenuation, electrical resistivity, capacity...) can have various alternative explanations. For instance, the variation in electrical resistivity could be due to a variation in porosity (which changes greatly between different mixes), moisture content (which changes with time due to the tidal effects) or chloride content. The magnitude of influence of these possible causes must be assessed before interpretation.

Several influences control the NDT response: here the material strength cannot be deduced from the measurement of the resistivity alone, since the relation between strength and resistivity depends on the concrete mix. **This question will also be addressed in this book: since many NDT parameters are sensitive to individual influences, it is difficult to formulate “universal laws” which, after inversion, provide direct access to the property that is sought.** For this reason, the combination of NDT measurements can be fruitful. Table 1.1 gives some additional references where the authors have used a “Type A” approach when combining non-destructive techniques.

### ***2.3 Type [B] combination – improvement of test result interpretation obtained with different techniques***

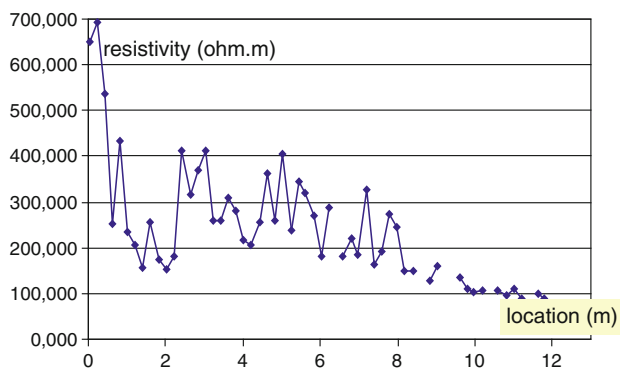
This type of combination is illustrated in the case of an abutment wall of a French bridge near Lilles, Nord (Fig. 1.5).

The inspected area, below the deck, is subject to alkali-aggregate reaction (AAR), and some cracking patterns can be seen on the concrete surface. The structure can only be investigated from one side. The same profile, approximately 12 m long, was inspected using radar and electrical resistivity measurements. The visible damaged area was localized between 9.8 m and 12.4 m.

Both techniques are potentially sensitive to AAR, since damaged areas have higher moisture content. A higher value of moisture content increases the attenuation



**Fig. 1.5** View of the bridge tested with combined techniques. White line below the deck gives location of the profile

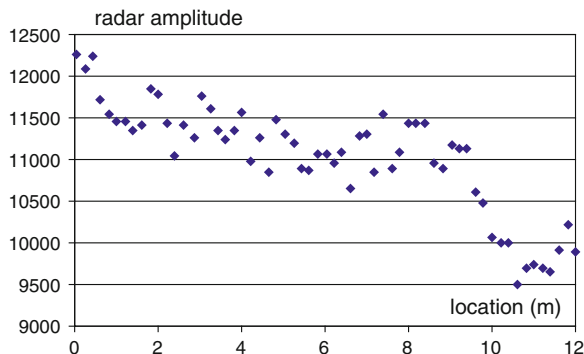


**Fig. 1.6** Electrical resistivity profile (ohm.m)

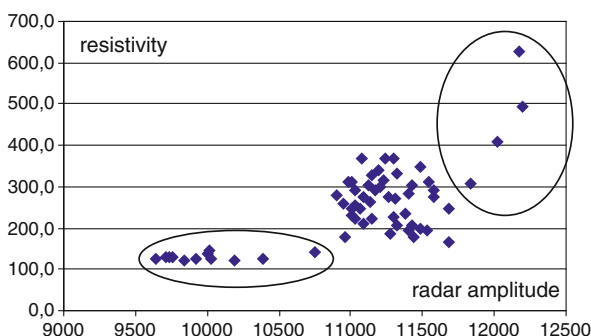
of the direct wave amplitude (radar) and decreases the resistivity. Thus the AAR assessment is only indirect, since the two techniques take advantage of moisture content sensitivity.

Figures 1.6 and 1.7 show the results obtained along the profile with a measurement step equal to 20 cm (each point is the average value of three neighboring measurements). The electrical resistivity is obtained using a 5-cm-square device. The repetition of measurements reduces the effects of noise measurements, as will be seen in §3.2. For both curves, the longitudinal profiles indicate a slow variation (decrease of radar amplitude, decrease of resistivity for electrical measurements) and a drop at the right end, more contrasted for radar. The two NDT also show a very different sensitivity: since resistivity is divided by a factor 6 between the left

**Fig. 1.7** Radar profile of the direct wave amplitude



**Fig. 1.8** Correlation between measurements obtained with two different techniques



end and the right end, the decrease of the amplitude of the radar wave is only about 20 %. **The question of sensitivity is a key issue, when performing NDT investigation, since one has to choose techniques that are the most sensitive as possible to the parameters that are sought.** This issue will be addressed into more details throughout this book.

Figure 1.8 illustrates the relations between the two measurements. Despite what appears as “noise” (the variations seen in the resistivity values between 2 and 8 m in the 200-400 ohm.m range are not correlated with any “structured” variation visible on radar measurements), two sets of points can be clearly distinguished:

- the first set corresponds to large values for both the radar amplitude (>11 800) and the resistivity (> 400 ohm.m),
- the second set corresponds to low values for both the radar amplitude (<10 800) and the resistivity (< 150 ohm.m).

It is important to note that these sets are not randomly spatially distributed. The first set is located at the left end of the profile (facing south) and the second at the right end of the profile.

The similarity of shapes between the two profiles is a good argument to justify the combination of techniques. It helps the interpretation since one can focus first on



the information that can be given by both techniques. (In a second step, it could be interesting to analyze whether some physical basis can explain the variations in the resistivity profile which were considered as “noise” in the first step.) The physical interpretation then stands on a more reliable basis:

- the variations at the left end can be interpreted as corresponding to drier material, probably due to environmental conditions (this end faces South),
- the variations at the right end can be interpreted as corresponding to the area where the alkali-aggregate reaction develops, as confirmed by visual inspection.

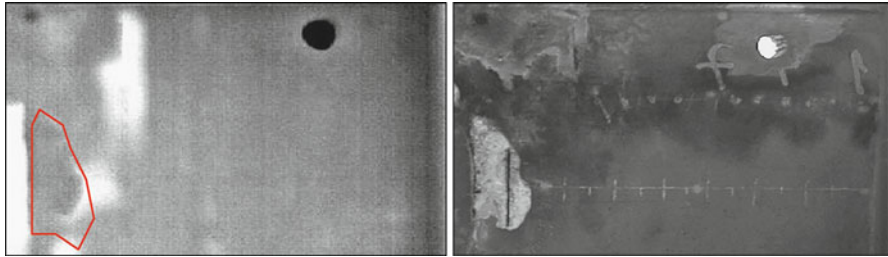
Another study (Rivard et al. 2005), performed on Bell’s Corner experimental site (Ottawa region, Canada) was devoted to the comparison provided by impact-echo, passive infrared thermography, electrical resistivity and radar measurements for assessing the alkali-aggregate reaction on concrete blocks of various mixes. It has shown that radar measurements (especially the magnitude of the direct wave) are the most promising method, when electrical resistivity is also sensitive to other factors, which makes data interpretation difficult.

In any case, the diagnosis of alkali-aggregate reaction is not direct, since it is only done through the variations in water content, which can be directly assessed by a simple visual inspection. In the case described here, NDT measurements provide, however, a more accurate estimation of the extent of the area affected by the chemical reaction. Another contribution is that they make it possible to quantify the material properties, opening the way towards the definition of critical values, which could be used for other structures, or for areas where the damage is not visible, but where NDT measurements would indicate values approaching critical values.

Table 1.2 provides some additional references in which the authors have used a Type [B] approach when combining non-destructive techniques. The combination used by (Romanescu et al. 2009) is usually referred to as the Sonreb method, which consists in combining ultrasonic velocity and rebound number for better assessing concrete strength. This question will be addressed into more detail in Chapter 3, devoted to strength assessment of concrete. Despite the high number of NDT used, the interpretation always remain a matter of expertise, since these techniques can show “clear similarities” on one instance and “significant differences” in another (Gucunski et al. 2010).

#### ***2.4 Type [C] combination – application of different techniques for “quick” localization of defected areas followed by detailed inspection with “slow” but more accurate measurements***

Some techniques have the particular advantage of enabling a quick overview of the structure, because they use a quickly moving set of sensors or because they are wide-field. This is the case, for instance, of infrared thermography, which can be used to monitor a large scene with an optical sensor that can be located at a certain distance from the surface under investigation (Sirieix and Defer, 2005).



**Fig. 1.9** Infrared thermography (left) and photograph (right). The image area is about 4 m x 1.5m; circle at upper right corner is a hole in the slab)

It is thus fruitful to use this technique in a first step and to investigate the areas where some interesting patterns are identified in greater detail (with a technique requiring more time or heavier equipment). The Empalot bridge case study, near Toulouse, provided us with such an opportunity. Figure 1.9 shows the infrared and visible pictures of one slab on the lower face of the deck. The two pictures were taken at the same time. The surface temperature range is [13.5 – 14.5] °C. The whitish areas indicate lower temperatures. Three of those areas can be seen on the infrared picture:

- the first one, on the left side of the red contour (which corresponds to an area where surface concrete has fallen) is the lower face of a transversal beam, which is not at the same distance from the camera as the deck surface,
- the two others, on the right side of the red contour do not correspond to any visible defect.

Since delamination was suspected on this 60-year-old bridge, these areas (and the full deck surface) were thoroughly investigated (with radar, electrical measurements, sonic waves and capacitometry), and delamination was confirmed. Thermography gave information on the existence and extent of the affected area from a distance, when all other techniques required heavy equipment (truck and platform) to reach the concrete surface with the measurement devices. The potential interest of such a combination is to provide information quickly, which helps the expert defining and planning detailed investigations. The interest of the second technique will be to provide quantitative information on material properties, since it is not straightforward to derive them from surface temperature measurements.

Naturally, the information gathered with the quick technique can also be processed to help the diagnosis. For instance, the variations in the temperature differences throughout the day between the delaminated area and the “good” surrounding concrete can be processed so as to give an estimation of the delamination depth. The potential interest of infrared thermography and the increasing capacity of numerical data processing algorithms explains the recent advances in this topic (Maierhofer et al. 2002, Valluzzi et al. 2009). If the surface is of easy access, it remains simpler to use sonic techniques that will provide the same type of information.

Another promising type [C] coupling possibility has been recently used (Dilek 2006), which combined stress wave measurements and dynamic elastic Young's modulus on thin disks from cores. Even if one of these two techniques cannot be considered as NDT, the interest is that the combination of NDT (stress-waves) and another technique provides very useful information for assessing near-surface gradients in fire or frost damaged concrete. In this case, NDT is used both for locating where coring is more relevant and for calibrating the results in terms of layering. Table 1.3 provides additional references in which the authors have used a Type [C] approach when combining non-destructive techniques. The recent work from (Arndt et al. 2010), even if limited to laboratory measurements, opens the way towards a more efficient long-term monitoring of corrosion, combining embedded sensors, quick techniques (like active infrared thermography) and slower techniques.

### 3 Conclusions

In the next Chapter, the common (and less common) non-destructive techniques will be presented. Each technique will be discussed in terms of the physics involved, which are the usual/possible use, which are the constraints and limits, etc. In this introductory chapter, we have shown how several different techniques can be combined to improve the assessment. We have defined three types of combination, according to their purpose. In most cases, this combination remains informal, which means that the understanding of the real added value of combining a second (or a third) NDT method simply does not exist. Thus, it is difficult to derive, from these individual experiences, any general conclusions that could be useful in other cases. It is only recently that this issue has been formally addressed by research (Balayssac 2008).

The chapters 3 to 7 will be devoted to five different practical questions engineers are faced with: strength assessment, voids detection in tendon ducts, damage and delamination detection, corrosion in cables, and geometry assessment. For each problem, we will explain which information NDT can provide, either used individually, or in combination. The text will be based on current engineering practice, but it will also present some innovative work. The issue of the combination of several NDT measurements will be specifically addressed. It is expected that the reader will find there new ideas and information about how better use NDT.

However we will see that, even in these situations, combination of NDT remains often informal. It is the reason why we will formalize this issue in Chapter 8. Our aim is that the reader becomes progressively more familiar with these central issues of variability (of the material), quality and sensitivity (of the NDT measurement) and complementary techniques. If so, he will be able to design and perform more efficient NDT investigation programmes, so as to get a more reliable view on the concrete structure.

## References

- Alt D., Meggers D. (1996) Determination of bridge deck subsurface anomalies using infrared thermography and ground penetrating radar, Kansas DOT, Report FHWA-KS-96-2, 18 p.
- Arndt R.W., Jalinoos F., Cui J., Huston D. (2010) Periodic NDE for bridge maintenance, Structural Faults and Repair, Edinburgh, June 2010.
- Balayssac J.P. (2008) SENSO: a French project for the evaluation of concrete structures by combining non-destructive methods, Sacomatis, RILEM conf., 1-2/9/2008, Varenna, It.
- Breyse D. (2008) Condition assessment of concrete, masonry and timber structures and the role of water: how far the problem is similar ?, SACoMaTiS Int. RILEM Conf., 1-2 sept. 2008, Varenna, Como lake, Italy.
- Breyse D. (2010) Overview of deterioration processes, in Non-Destructive Evaluation of Reinforced Concrete Structures, ed. C. Maierhofer, H.W. Reinhardt, Bertram publ.
- Breyse D., Abraham O. (2005) Guide méthodologique de l'évaluation non-destructive des ouvrages en béton armé. Presses ENPC, Paris, 550 pages.
- Bungey J.H., Millard S.G. (1996) Testing of concrete in structures, Blackie Acad. and Prof., 3rd edition, 286 p.
- De Bold R., Giannopoulos A., Forde M.C., Pareemamun K. (2010) Interpretation of NDT of thick concrete, Structural Faults and Repair, Edinburgh, June 2010.
- De Lorenzis L., Nanni A. (2004) Int. workshop on preservation of historical structures with FRP composites, Final Report, NSF.
- Dérobot X., Garnier V., François D., Latate J.F., Laurens S. (2005) Complémentarité des méthodes d'END, in Guide méthodologique de l'évaluation non destructive des ouvrages en béton armé, ed. Breyse D., Abraham O., Presses ENPC, Paris, 550 pages.
- Dilek U. (2006) Dynamic elastic Young's modulus of concrete disks in validation of stress wave based non-destructive testing technique results, 85th TRB Annual meeting, 22-26 Jan. 2006.
- EN 13791 (2007) Assessment of in-situ compressive strength in structures and precast concrete, CEN, Brussels, 28 p.
- FHWA (2002) Corrosion Costs and Preventive Strategies in the United States, Report from CC Technologies Laboratories, Inc. (Dublin, Ohio), for FHWA and NACE.
- Gardei A., Mittag K., Wiggenhauser H., Ripke B., Jovanovic M. (2003) Inspection of concrete-embedded tracks process development for the quality assurance of concrete-embedded tracks using non-destructive testing methods, NDT-CE, conf., Berlin.
- Gehlen C., Dauberschmidt C., Nürnberger U. (2006) Condition control of existing structures by performance testing, Otto-Graf-Journal, 17, 19-44.
- Gucunski N., Romero F., Kruschwitz S., Feldmann R. (2010) Comparative study of bridge deck deterioration detection and characterization by multiple NDE methods, Structural Faults and Repair, Edinburgh, June 2010.
- IAEA (2002) Guidebook on non-destructive testing of concrete structures, Training course series 17, International Atomic Energy Agency.
- ICRI (2009) Nondestructive evaluation (NDE) methods for condition assessment, repair, and performance monitoring of concrete structures, ICRI Guideline.
- Klysz G., Balayssac J.P., Derobot X., Aubagnac C. (2003) Evaluation of cover concrete by coupling some non-destructive techniques – Contribution of in-situ measurements, NDT-CE conf., Berlin.
- Latate J.F., Abraham O., Breyse D., Sirieix C. (2003) Sensitivity to crack parameters of two non-destructive techniques: electrical resistivity and acoustic methods, NDT-CE conf., Berlin.
- Latate J.F., Breyse D., Sirieix C., Naar S. (2005) Electrical resistivity measurements on various concretes submitted to marine atmosphere, ICCRC conf., Moscow, 5-9/09/2005.
- Maierhofer C., Bink A., Röllig M., Wiggenhauser H. (2002) Transient thermography for structural investigation of concrete and composites in the near surface region, Infrared Physics and Technology, 43, 271-278.

- Maierhofer C., Krause M., Wiggenhauser H. (1998) Non-destructive investigation of sluices using radar and ultrasonic impulse echo, *NDT&E Int.*, 31, 6, 421-427.
- Malhotra, V.M. (1981) Rebound, penetration resistance and pulse velocity tests for testing in place, The Aberdeen Group.
- Maser K.R., Holland T.J., Roberts R., Popovics J. (2003) Technology for quality insurance of new pavement thickness, *NDT-CE conf.* Berlin.
- Naar S., Sirieix C., Breyse D., Dérobert X. (2005) Assessment of water saturation rate in a reinforced concrete structures: non-destructive testing of Tarbes' precast duct, *ICCRC conf.*, Moscow, 5-9/09/2005.
- OECD Nuclear Energy Agency (1998) Development priorities for Non-Destructive examination of concrete structures in nuclear plant, *Nuclear Safety, NEA/CSNI/R(98)* 6, 25-39.
- Parthasarathy S., Murthy S.G.N., Sangoju B., Wiggenhauser H., Ravisankar K., Iyer. N.G., Lakshmanan N. (2009) Application of radar and ultrasonic pulse echo for testing concrete structures, *NDTCE'09*, Nantes, 30 june-3 july 2009.
- Pina Santos C., Matias L., Magalhaes A.C., Veiga M.R. (2003) Application of thermography and ultrasounds for wall anomalies diagnosis. A laboratory research study, *NDT-CE conf.*, Berlin.
- Rivard P., Naar S., Sbartai M.Z., Fournier B. (2005) Couplage de méthodes non destructives pour l'évaluation de l'endommagement du béton, *12th Conf. on Recherche Québécoise sur les Ouvrages d'Art*, 10-11/05/2005, Univ. Laval, Quebec.
- Romanescu C., Ionescu C., Scinteie R. (2009) The Romanian road administration experience in the field of NDT for bridges, *NDTCE'09*, Nantes, 30 june-3 july 2009.
- Scott M., Rezaizadeh A., Delahaza A., Santos C., Moore M., Graybeale B., Washer G. (2003) A comparison of nondestructive evaluation methods for bridge deck assessment, *NDT&E Int.*, 36, 4, 245-255.
- Shaw P., Xu A. (1998) Assessment of the deterioration of concrete in nuclear power plants – causes, effects and investigative methods, *NDTnet*, 3, 2.
- Sirieix C., Defer D. (2005) Méthodes thermiques, in : D. Breyse, O. Abraham (Eds), *Guide méthodologique de l'évaluation non destructive des ouvrages en béton armé*, Presses ENPC, Paris, 550 pages.
- Sirieix C., Lataste J.F., Breyse D., Naar S., Dérobert X. (2007) Comparison of nondestructive testing: Infrared thermography, electrical resistivity and capacity methods for assessing a reinforced concrete structure, *J. Building Appraisal*, 3, 1, 77-88.
- Uemoto T. (2000) Maintenance of concrete structure and applications of non-destructive inspection in Japan, in *Proc. of Non-Destructive testing in Civil Engineering*, Elsevier, 1-11.
- Valluzzi M.R., Grinzato E., Pellegrino C., Modena C. (2009) IR thermography for interface analysis of FRP laminates externally bonded to RC beams, *Mat. Str.* 42, 25-34.
- Weise F., Pirskawetz S., Meng B. (2008), Application of innovative testing methods for the quasi non-destructive assessment of the material condition in hydraulic engineering structures, *Sacomatis conf.*, Varenna, 1-2/9/2008.
- Wolsiefer J.T. (1991) Silica fume concrete: a solution to steel reinforcement corrosion in concrete, *Proc. 2<sup>nd</sup> Canmet/ACI Int. Conf. On durability of concrete*, pp. 527-553, ACI, Farmington Hills, MI.
- Yong Hao Z., Kee Ee Ng. (2003) Evaluation of concrete structures by advances nondestructive test methods – impact echo, impulse response test and radar survey, *NDT-CE conf.*, Berlin.

# Chapter 2

## Presentation of common non destructive techniques

Many experts contributed to Chapter 2. Their list is following

- |    |                                    |   |
|----|------------------------------------|---|
| 1  | Ultrasounds through transmission   | Vincent Garnier                               |
| 2  | Ultrasonic Echo                    | Martin Krause and Franck Mielentz             |
| 3  | Surface waves methods              | John Popovics and Odile Abraham               |
| 4  | Impact echo                        | Andrzej Moczko                                |
| 5  | Impulse response                   | Andrzej Moczko and Claus Germann Petersen     |
| 6  | Acoustic emission                  | Jean-Paul Balayssac and Masayasu Ohtsu        |
| 7  | Ground Penetrating Radar           | Johannes Hugenschmidt and Jean-Paul Balayssac |
| 8  | Capacitive technique               | Xavier Dérobert                               |
| 9  | Electrical resistivity measurement | Jean-François Lataste                         |
| 10 | Infrared thermography              | Didier Defer and Christiane Maierhofer        |
| 11 | Radiography                        | Jean-Paul Balayssac                           |
| 12 | Rebound hammer                     | Markus Fischli and Andrzej Moczko             |
| 13 | Pull-out testing                   | Andrzej Moczko                                |

### 1 Ultrasounds through transmission

**Vincent Garnier**

#### 1.1 *Physical principles and theory*

The ultrasonic method can be applied by the reflection or the transmission of elastic waves in the concrete or on its surface. The first method, called “ultrasonic echo” or “pulse echo” is explained in the next section (§2).

The second is the ultrasonic transmission method (also named “sonic pulse velocity” measurement). It is a common technique used by many companies to

evaluate the concrete in situ and to provide information on the quality of the concrete element. It allows measuring the velocity and attenuation of elastic waves. It consists to send the ultrasonic wave from a transducer “emitter” and to record the signal with a separate transducer “receiver”. Typical transducers generate the wave by exciting a piezoelectric disk.

The two transducers are generally identical in geometry and wave frequency range. The typical frequency range used for the concrete is from 20 kHz to 300 kHz. A usual device is proposed with 24 or 54 kHz transducers. The new devices propose higher frequency transducers but their attenuation is important. Pressure waves (P-waves, longitudinal waves) and surface waves (Rayleigh waves) are generally used. Shear waves (S-waves, transverse waves) are exploited only in specific cases.

The velocity  $C$  is the most currently and easily evaluated parameter by transmission technique.  $C$  is deduced from the measurement of the time of flight  $t$  and the distance  $L$  that the wave covers in the concrete.

$$C = \frac{L}{t}$$

The attenuation  $\alpha$  is deduced from the decrease of the amplitude  $A_1$  and  $A_2$  of the received signal for two paths with two different lengths  $L_1$  and  $L_2$ .

$$\alpha = \frac{20}{L_2 - L_1} * \log\left(\frac{A_1}{A_2}\right)$$

The current unit for attenuation is dB/m.

The attenuation measurement is not very easy because the contact conditions between the transducer and the concrete are not fully repeatable. Some new air coupling transducers (avoiding any contact) are in development today.

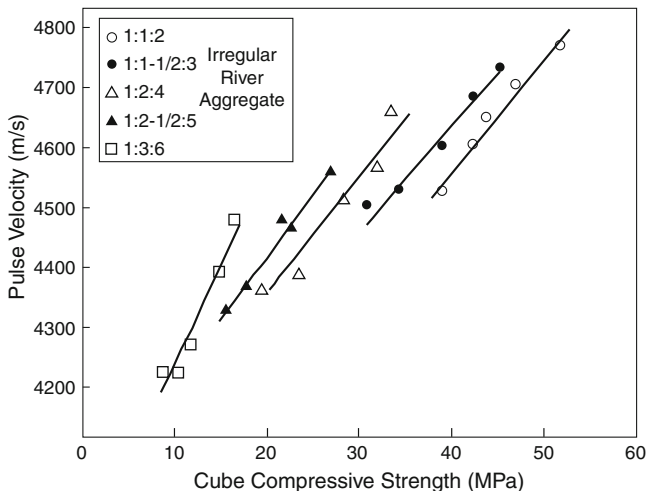
## 1.2 Correlation with the mechanical properties

Because the wave propagation is depending on the material mechanical properties, many tests are developed to link the compressive strength  $f_c$  or elasticity modulus  $E$  with the ultrasonic velocity. Since the propagation is modified by any defect in the material, the measurements can also inform about these defects.

The correlation with material properties can be calibrated with cores extracted from the structure or on a cubic specimen from the same concrete as the structure. For instance, ACI 228 1.R considers that  $V^4$  is proportional to  $E^2$  and to concrete strength. It is however not possible to define a general law. European standard EN13791 considers a polynomial relationship of order 2 between concrete strength and velocity. In a literature study [Evangelista et al., 2003] registered, without being exhaustive, 12 different laws (linear, exponential or power), from 1988 to 2000, establishing a relationship between the compressive strength  $f_c$  and the P-waves.

**Table 2.1** Usual values of velocity and attenuation of the P-wave in a concrete

Concrete condition	P-wave velocity (100 kHz)	P-wave attenuation (100 kHz)
Damaged	velocity < 3000 m/s	> 90 dB/m
Sound	velocity > 4500 m/s	< 30 dB/m



**Fig. 2.1** Effect of aggregate to cement ratio on the relationship between pulse velocity and compressive strength (after [Naik et al., 2004])

[Popovics, 2006] explains the problem and proposes to work with the surface waves to get an accuracy better than  $\pm 20$  percent.

It is suggested to estimate material properties after having fitted a specific correlation with velocity by using multiple regression techniques. One must keep in mind that a lot of parameters influence the ultrasonic velocities: the aggregate size, nature and rate, the ratio aggregate on cement or water on cement, the cement nature, the age of the concrete, the geometry of the tested structure or beam, the curing conditions, the porosity rate, the water contained in the pores and the cracks, the damage and also the rebar.

Typical values of velocity and attenuation are plotted on Table 2.1. These values depend on the wave frequency. So the transducers choice for a test can be very important.

An example of laws depending on the ratio aggregate to cement is given by Fig. 2.1. The figure shows that for a given value of pulse velocity, the higher the aggregate to cement ratio, the lower the compressive strength.

A solution exploited in situ is not to give the absolute value of the velocity but to compare the different zones (damaged or not). That allows defining the most suspect zones of the structure on which it is important to improve the tests or to develop some other complementary tests [Abraham and Dérobert, 2003]. It is possible either to work point by point and to move the two transducers each time, or to move only one of the two transducers. A third possibility is to work with a series



**Fig. 2.2** Ultrasonic Transmission device with plane coupling probes



**Fig. 2.3** Ultrasonic Transmission device with plane coupling probes (Pundit from CNSFarnell)



of transducers for the reception and / or for the emission. In each case, information got on each point is worked separately. It is also interesting to mix and to sum up all the information in order to get an image, for example to describe the structure. That is the ultrasonic tomography that is used to examine cracks, voids and other internal defects [Bond et al., 2000].

Today some new improvements are proposed in the modeling of the wave's propagation by the wave's homogenization, and in the signal analyses as well as in the surface wave applications (without contact and coupling).

### ***1.3 Measuring Equipment and Handling***

The typical industrial devices contain (Fig. 2.2 and 2.3):

- An electrical pulse generator (peak voltage from 150 V to 1000 V) and amplifier for the wave,
- an emitter transducer (mostly piezoelectric sometimes without contact). Sometimes the emitted wave is generated by an impact with a ball or a hammer,
- a receiver transducer (only one or several on a line to be precise on the distance value),

- sometimes, an automatic displacement device of ultrasonic displacement to obtain (A, B or C-scan),
- a calibration bar in metal or silica, to calibrate the measurement,
- an oscilloscope to see the signal and measure the time, or only a time calculator.

The transducers are generally plane with contact. To get a better transmission, the coupling is ensured by grease, paste or gel. Sometime the transducers can be bonded directly on the concrete surface. Some transducers include a cone for the tip to get a punctual contact that allows working, for the low frequencies, without coupling. Another specific air coupling transducers (piezo or capacitive) with specific amplifiers are developed to work without contact at a distance ranging from some millimeters to some centimeters between the transducer face and the concrete element. These transducers are new for NDT on concrete and they get rid of the sensitive problem of coupling. Then they allow working more easily on the attenuation properties. In some research works, the wave propagation can even be measured generated by laser interferometer without contact.

The equipment generally offers the direct digital read-out of transit time, the flaw detection, battery and A-C power, RS-232 output for computer uploading. The calibration can be done with the metallic bar to adjust the time measured or by an internal calibration.

The device can give the calculated P-wave or S-Wave velocity easily by direct reading. The elasticity dynamic modulus  $E_d$  or Poisson ratio  $\nu$  are calculated under some conditions.

To estimate the material properties, the relationships between elastic constants and the velocity of respectively ultrasonic pressure wave  $V_L$  and shear wave  $V_T$  are derived from equations in an isotropic elastic medium of infinite dimensions:

$$V_L = \sqrt{\frac{E_d(1-\nu)}{\rho(1+\nu)(1-2\nu)}} \quad V_T = \sqrt{\frac{E_d}{2\rho(1+\nu)}}$$

where:

$E_d$  = the dynamic elastic modulus (MPa)

$\nu$  = the dynamic Poisson's ratio.

$\rho$  = the density ( $\text{kg/m}^3$ ).

$V_L$  = the pressure (longitudinal) wave velocity (km/s).

$V_T$  = the shear wave (transversal) velocity (km/s).

The relation with  $V_T$  is difficult to exploit because the shear wave velocity is not easy to determine owing to the multiple scattering in the concrete. For the wave length  $\lambda$  generally used (from 10 to 150 mm), the concrete is a very heterogeneous material that generates a lot of scattering of the ultrasonic waves and that perturbs the shear waves exploitation. So the first relation is generally used to calculate the dynamic modulus  $E_d$ , with a prior assumption on the Poisson ratio and the measurement of the density.

## 1.4 *Guidelines, Recommendations*

AIEA, Guidebook on non-destructive testing of concrete structures, Vienna 2002  
 ASTM C 1383 Test method for measuring the P-wave speed and the thickness of concrete plates using the impact echo method Annual Book of ASTM Standards Vol. 04.02, ASTM, West Conshohoken, PA, USA, 2000  
 ASTM C 597 – 83 (91) Standard test method for pulse velocity through concrete  
 BS 86 (British Standards) Recommendation for the measurement of velocity of ultrasonic pulses in concrete, Testing concrete, BS 1881 : Part 203, 1986  
 D6760-02 Standard Test Method for Integrity Testing of Concrete Deep Foundations by Ultrasonic Crosshole Testing  
 EN 12504-4, Testing concrete in structures – Part 4: Determination of ultrasonic pulse velocity, Norme Européenne

## 1.5 *Common techniques and devices*

The common devices are used for concrete quality control and for the evaluation of the dimensions of structures. Under some conditions, they can also correlate concrete strength to standard velocity measurement, using correlation laws that are not universal.

If their sizes are important enough, it is possible to identify honeycombs, voids, frozen concrete, cracks, delamination and other non-homogenous areas like those resulting from thermal, mechanical or chemical damages in concrete. In a recent French research program [Balayssac et al., 2008], the influence on the velocity and attenuation waves of the water saturation rate, porosity, carbonization, chloride content and damage were tested.

An important way to assess the concrete condition is to determine the material variations in space or over time (this is mainly used for young age cementitious materials).

Ultrasonic testing can be applied to new and old structures, columns, walls, fire damaged areas, hydroelectric structures, bridge, piles, pipes, prefab and prestressed beams, cylinders and other concrete forms.

For transmission of P-waves, the emitter generates the signal and starts the time counting. The receiving transducer detects the arrival time of the leading vibration. For the low frequencies and if the length of the wave path is known, it is possible to measure the velocity in three directions depending on the accessibility of the structure faces [Farnell, 2008].

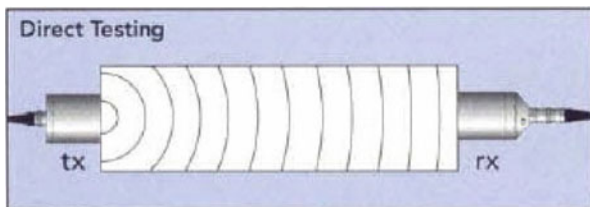
\* between opposite faces (direct transmission), see Fig. 2.4

\* between adjacent faces (semi direct transmission), see Fig. 2.5

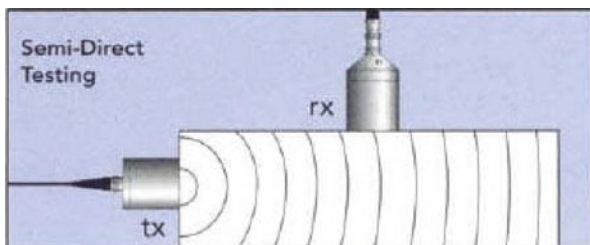
\* on a single face (indirect or surface transmission), see Fig. 2.6

The direct technique is the most accurate and must be chosen when possible. The difficulty is to access to the two sides. If the concrete is reinforced, the best solution is to locate first the rebar with an electromagnetic device and thus to test between them.

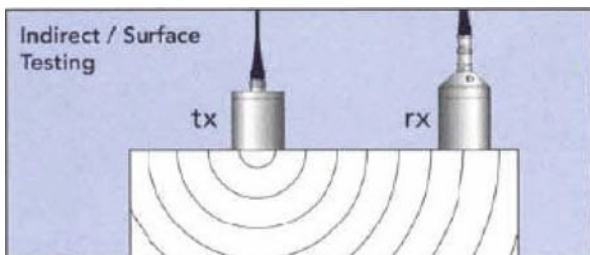
**Fig. 2.4** Direct transmission ultrasonic testing



**Fig. 2.5** Semi direct transmission ultrasonic testing



**Fig. 2.6** Indirect transmission ultrasonic testing



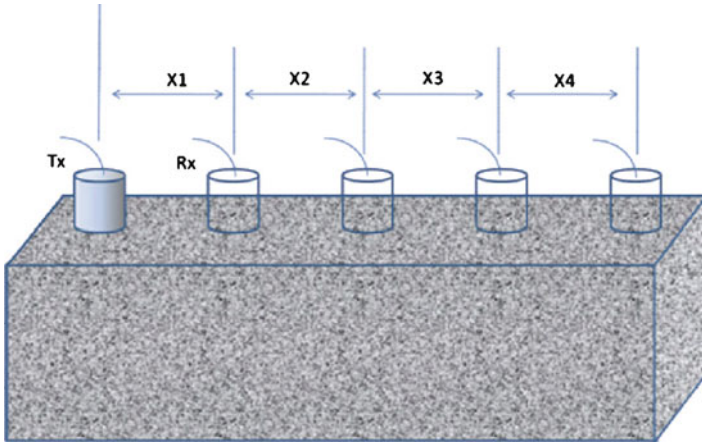
The semi direct technique is easy to use but the distance between the two transducers is less well defined than the previous case. Its accuracy is generally below the first.

The indirect or surface technique is easily exploitable in situ with different configurations. The access to only one face is simpler.

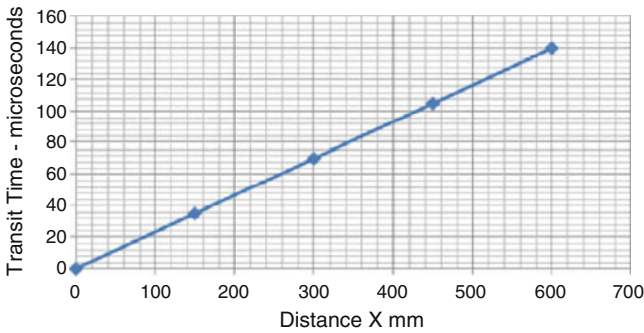
The three types of control are commonly used on site today.

To detail the indirect method, it must be said that the emitter is fixed and the receiver is placed at different positions ( $x_1$  to  $x_4$  on Fig. 2.7) on a line and the signal is recorded for each of them. The minimum length  $x_1$  inspected has to be more than 5 times the mean aggregates dimension. The general value is 100 mm or 150 mm. The time is plotted versus the distance (Fig. 2.8). This distance between the emitter and the receiver is measured from centre to centre of the transducers. The slope of the straight line gives the wave velocity. The indirect wave velocity is lower than the direct one by about 5 % to 20 %, the difference depending on the concrete type. To increase the measure quality, it is possible to work with a series of fixed transducers instead of moving a unique transducer.

By indirect transmission, the slope analysis allows detecting the presence of voids or cracks as presented in Fig. 2.9. The P-wave follows the shortest path, it is



**Fig. 2.7** Indirect method principle



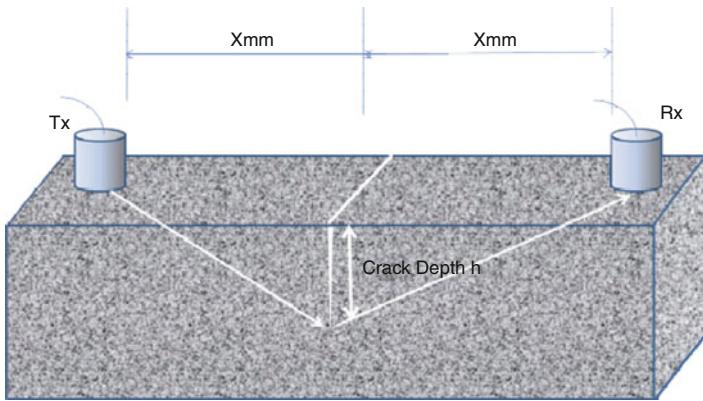
**Fig. 2.8** Time of flight versus distance

diffracted by the crack tip and transmitted to the receiver. A change of slope on the curve “time-distance” can give the position and the depth of the crack. However, in practice, the measurement is sometimes uneasy to work out because the partial closing or filling of the crack.

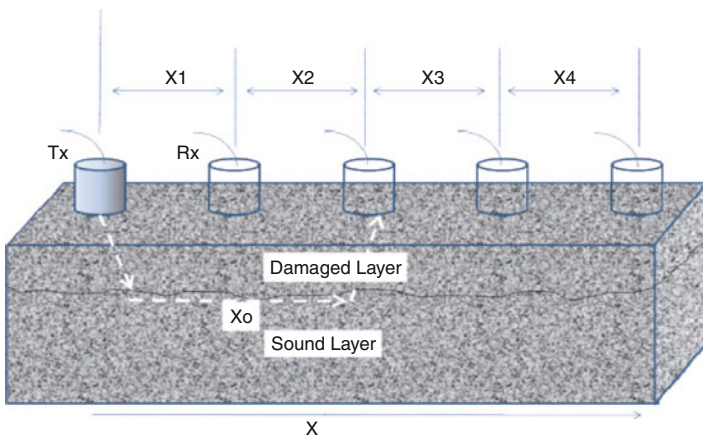
By indirect transmission, the slope analysis also allows to detect the presence of damaged layer as presented in Fig. 2.10. The variation of the slope can give the depth of the affected zone.

These evaluations can be perturbed by usual conditions on site:

- \* if the contact between the transducers and the concrete is irregular
- \* if the wave length is not adapted to problem: when the lengthwave is too high, small cracks cannot be detected; reversely, when the lengthwave is too small, an important attenuation increases the uncertainty
- \* if some water and /or some particles fill up the cracks, the diffraction doesn't occur on the crack tip.



**Fig. 2.9** Cracks detection principle



**Fig. 2.10** Damage detection principle

### 1.6 Reliability and limitation of results

Many parameters influence the wave velocity. The effect of some of them is known and can be corrected in the best case, but in industrial conditions, the best way is often to work by comparisons between the different points of measurement or with cores extracted from the structure.

The standards give information on how to adjust the velocity value as a function of the lateral dimension of the concrete elements, of the rebar presence, of the moisture and temperature.

Many bias factors exist:

- The coupling conditions highly change the amplitude of the wave, they can disturb the attenuation evaluation and sometimes the velocity estimation.
- The lateral boundaries of the tested structure can generate a new type of waves that modifies the velocity of the apparent P-wave analyzed (reflected or Lamb waves).
- The presence of reinforcing steel bars can accelerate the wave if they are in the same direction as the waves. They can also scatter the waves and decrease their velocity when they are perpendicular.
- The moisture, the porosity and the temperature of the concrete modify the velocity up to 20 %.
- The choice of the transducers (mainly frequency and size) can modify the velocity by 15 or 20 %.
- The concrete nature (aggregate size, cement nature, porosity rate and density) modify the velocity from 5 to 20 %

In any case, the technician must be qualified.

To conclude, the ultrasonic inspection by transmission is a technique accessible that can provide information on the concrete condition. In the simple case, it enables comparisons between different types or zones of concrete in a structure. If care is devoted to control some experimental parameters on site, it is possible to optimize the experimental device and the procedure to get more information attached to the material properties.

## ***1.7 Developments***

Today a lot of developments and researches are developed in order to help the operator to extract better and more reliable information from the transmitted ultrasonic waves.

- The tomography that is used in situ improves the quantity of information concerning the defect detected or the zone tested. It allows confirmation and increases the capability of detection.
- The Spectral Analysis of surface Waves analyzes the propagation mode of the dispersive waves (Rayleigh and Lamb) that propagate just below the surface or in plates. Derived from this method, the Multichannel Analysis Surface Waves method allows the assessment of delaminations.
- The cover concrete is the first protection of the structure regarding all the aggressions from the environment. It can be assessed by analysing the Rayleigh waves with automatic devices.
- Modeling of the waves' propagation is developed by some laboratories that are working on the concrete homogenization. The objectives are to understand the propagation in such a heterogeneous material and to predict the velocity and attenuation of the waves. Some Finite Element Methods are also developed in this way.



**Acknowledgments** The authors thank the Farnell company for having authorized the reproduction of several pictures.

## References

- Abraham O., Dérobert X. (2003) Non-destructive testing of fired tunnel walls: the Mont-Blanc tunnel case study, *NDT&E Int.*, 36, 411–418.
- Balayssac J.P., Arliguie G., Laurens S. (2008) Évaluation de l'état des ouvrages en béton par combinaison de techniques non destructives, *Proc. COFREND days*, Toulouse, May 2008.
- Bond L.J., Kepler W.F., Frangopol D.M. (2000) Improved assessment of mass concrete dams using acoustic travel time tomography (Part I-Theory, Part II-Application), *Constr. Build. Mat.*, 14, 133–156.
- Evangelista A.C., Shehata A.I., Shehata L. (2003) Parameters That Influence The Results of Non-Destructive Test Methods for Concrete Strength, *NDTCE Berlin*, 2003.
- Farnell (2008) Ultrasonic pulse velocity testing, Technical reference manual. CNS Farnell, August 2008.
- Naik T.R., Malhotra V.M., Popovics J.S. (2004) *CRC Handbook for NDT of Concrete*, Second edition, Carino N.J. and Malhotra V.M., eds Boca Raton, Florida, CRC press 2004.
- Popovics J.S. (2006) American Society for Nondestructive Testing, Analysis of the Concrete Strength versus Ultrasonic Pulse Velocity Relationship, 9 p.

## 2 Ultrasonic Echo

**Martin Krause and Franck Mielentz**

### 2.1 *Physical principles and theory*

Shortly described, the ultrasonic echo method (also named pulse echo method) measures the time of flight of elastic pulses, which are reflected at internal interfaces or are backscattered at internal objects, respectively. This method overcomes the drawback of ultrasounds through transmission that requires access to both surfaces. From the measured time of flight and the pulse velocity known from calibration measurements, the depth of the scatterers and interfaces can be deduced. Pressure waves (P-waves, longitudinal waves) as well as shear waves (S-waves, transverse waves) are used for NDT of concrete elements. For concrete, the typical frequency range is from 25 kHz to 300 kHz.

Generally the wave propagation velocity for a monochromatic wave (phase velocity) can be written as:

$$c = \lambda * f \quad (1)$$

where  $c$  is the wave velocity,  $\lambda$  is the wavelength and  $f$  is the frequency.

Pressure waves (P-waves) have a typical wave velocity of 4000 m/s in concrete, thus for a frequency of 100 kHz the wavelength is 40 mm.

The reflection  $R$  of P-waves at planar interfaces is defined by the difference of the acoustic impedance for two materials, whereas the acoustic impedance is



a material property defined as the density  $\rho$  multiplied by P-wave phase velocity:

$$R = \frac{z_2 - z_1}{z_2 + z_1} \quad (2)$$

where  $z$  is the acoustic impedance  $z$  in material 1 and 2, respectively, with:

$$z = \rho c \quad (3)$$

Since the acoustic impedance of air can be neglected compared to concrete, the reflectance at air interfaces is  $R = 1$ . When the impedance of material 2 is greater than for material 1, the sign of  $R$  is positive. When the acoustic impedance of the material 2 is smaller than for material 1, the sign of  $R$  is negative, that means that a phase jump of  $\phi = 180^\circ$  appears for the reflected wave pulse. This effect allows to distinguish between the reflection at the concrete/steel interface and reflection at the concrete/air interface.

Generally ultrasonic pulses are produced and measured with piezoelectric probes. Thus the measured AC voltage is proportional to the sound pressure  $P_s$  in the material, which is defined by:

$$P_s = \rho c \omega \zeta = z \omega \zeta \quad (4)$$

where  $z$  is the acoustic impedance (see (3)),  $\omega$  is the angular frequency (with  $\omega = 2\pi f$ ) and  $\zeta$  is the amplitude of particle oscillation.

The base for ultrasonic echo applications for concrete are low frequency transducers (probes, centre frequency around 100 kHz), which must transmit broadband pulses. After basic research in the 1990's, transducers and equipment were developed, which allow measuring the thickness of concrete elements even in single point measurement, if the site conditions are not too difficult. This means for instance not too dense reinforcing layers or not too bad surface conditions.

In order to measure the dimension of a reflecting area, several points can be combined for providing an imaging result. This can be done by measuring lines manually or by an automated scanning.

The ultrasonic echo method has the potential to locate and identify discrete defects or objects if sufficient focusing is achieved by the transducers. Because the concrete contains aggregates and air pores, structural noise always appears, reducing significantly the signal to noise ratio. In order to overcome this problem, special transducers and imaging methods based on array techniques and synthetic aperture have been developed (and are continuously ameliorated) in research and development activities.

## 2.2 *Measuring equipment and handling*

For single point measuring, there are generally two types of equipment: transducers with planar contact on the measuring surface and dry contact transducers

**Fig. 2.1** Array consisting of 10 broadband planar transducers for the frequency range of 80 kHz to 200 kHz



(point contacts). An instrument or development equipment contains four general features:

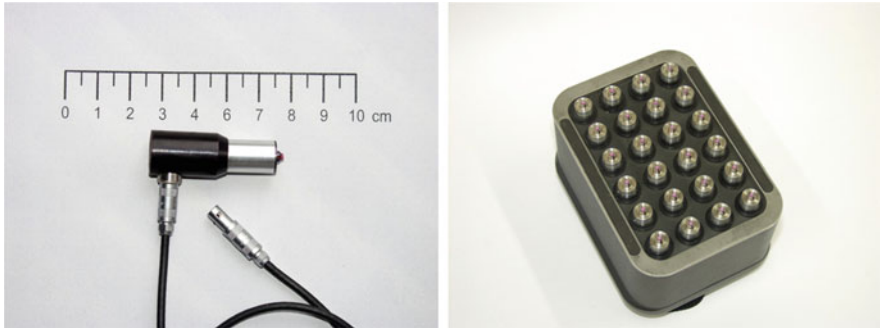
- A Electrical Pulse generation (AC Peak Voltage between 150 V and 1000 V)
- A piezoelectric Transducer
- A receiving unit and an amplifier
- Displacement device of ultrasonic measuring curve (amplitude vs. time; A-scan) and indication of time of flight or reflector depth.

Since the mid-1990s broadband transducers have been developed in the frequency range of 20 kHz to 300 kHz, for P-waves as well as for shear waves. Fig. 2.1 shows as an example ten pressure wave transducers arranged in a template to be applied as an array. They have a planar surface, which means that coupling agent is necessary (e.g. vaseline or glycerine) [Krause et al., 1997].

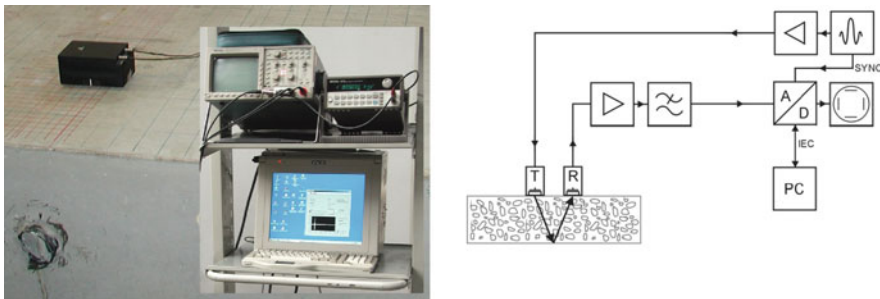
Low frequency shear wave transducers developed around 2000 have two main advantages: firstly the shear wave is directly generated by a ceramic tip pressed to the surface. There is no need for a delay wedge or coupling agent (dry contact). Thus, secondly, the polarisation axis of the shear waves can directly be aligned corresponding to the axes of symmetry [Kozlov et al., 2006].

Fig. 2.2 depicts some examples of dry contact transducers, which are available as single transducers and transducer arrays in different arrangements. The frequency ranges from 30 kHz to about 80 kHz (i.e. a wavelength range from about 100 mm to 33 mm for a typical wave velocity of  $C_s = 2700$  m/s in concrete). For manual measurements an electronic interface can be used. The probe has twelve transmitting and twelve receiving transducers, which are working simultaneously.

For developing and optimizing low frequency ultrasonic techniques, often arbitrary pulses are applied. A typical equipment is shown in Fig. 2.3.



**Fig. 2.2** left: Point contact transducer, right: T/R probe with 12 transmitting and 12 receiving point contact transducers



**Fig. 2.3** left: Excitation of transmitting/receiving (T/R) transducer with arbitrary function generator, power amplifier (not imaged) and oscilloscope, right: Principle sketch for working with arbitrary pulses and data processing

**Fig. 2.4** Ultrasonic Echo device with plane coupling probe (for thickness measurement of screed)



Two typical commercially available instruments are depicted in Figs. 2.4 and 2.5, left. Both permit point measurement with preferable separate transmitter and receiving transducers. For equipment 1, these are plane coupling transducers of the

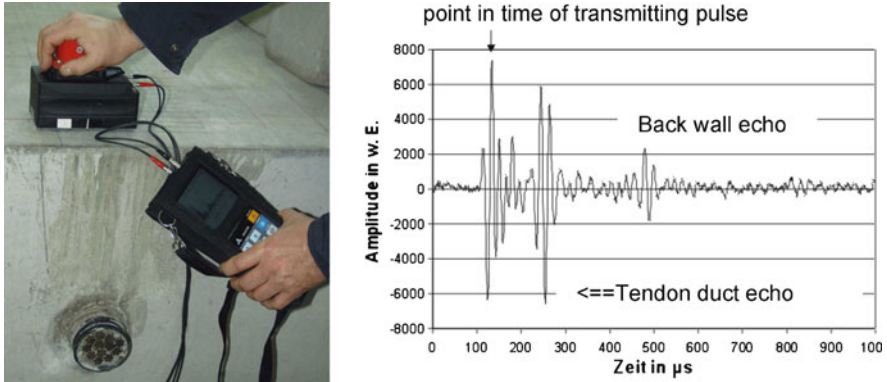


Fig. 2.5 left: Ultrasonic Echo Device with dry contact shear wave transducer and handheld electronic device, right: Ultrasonic time curve (Ultrasonic A-Scan)

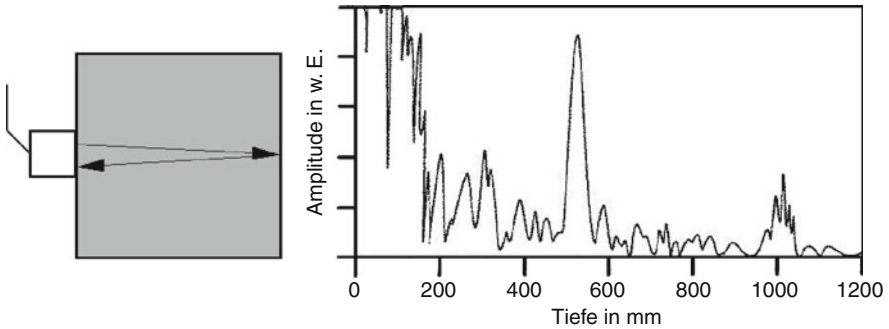
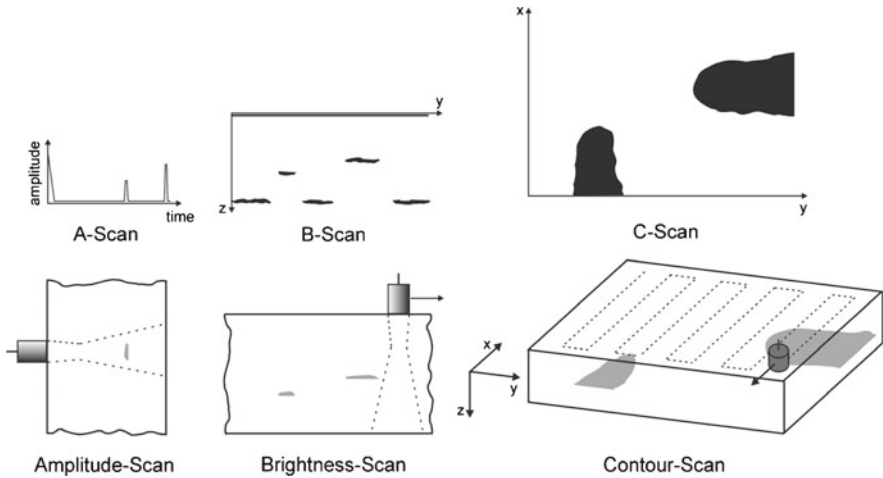


Fig. 2.6 Thickness measurement of concrete slab using a single probe in frequency range of 100 kHz

type explained above. Instrument 2 is constructed for point contact transducers, mainly for shear waves. Since the transducer tips are made of ceramic, they are simply pressed at the measuring surface without any need of coupling agent. The most frequent application for these transducers are shear waves (transverse waves) with a centre frequency of 55 kHz. The polarisation axis of these waves can be selected by the orientation of the device.

The handling of the electronic part of the device in Fig. 2.3 is similar to the frequently used commercial equipment, which is applied for ultrasonic testing steel in the frequency range between 1 MHz and 10 MHz. Fig. 2.5, right, shows as an example a typical ultrasonic time curve (*A-Scan*, see below) when the transducer is positioned above a tendon duct. The echo signals of the tendon duct and the back wall are visible. Around the origin of the time axis surface wave signals occur.

There are several systems working with the equipment explained in chapter 2. Typical testing tasks are e.g. measuring the thickness of concrete elements (Fig. 2.6)



**Fig. 2.7** Overview for general utilization of the terms A-scan, B-Scan, and C-Scan in ultrasonic echo measurement

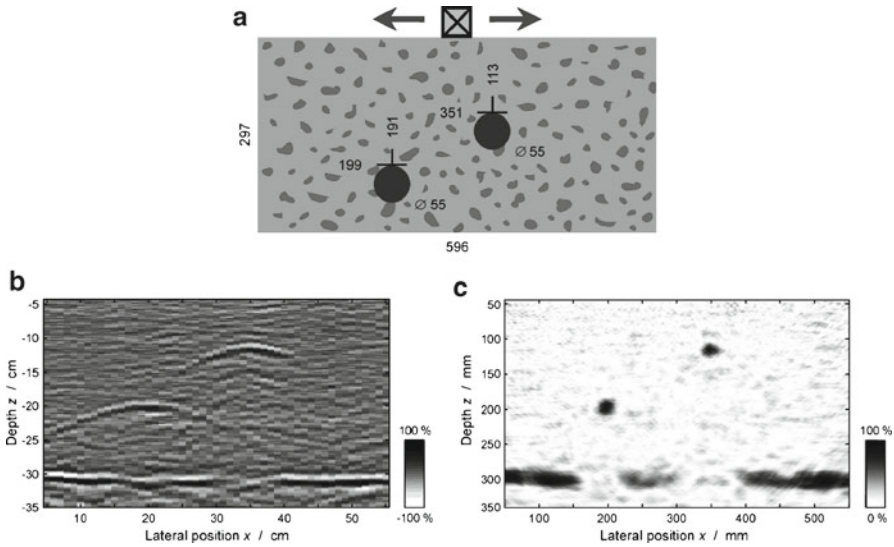
or localizing structural details. In some systems several measuring points can be stored in lines or/and 2D-Datasets for displaying them B-scans or C-scans, respectively ([Kozlov et al., 2006],[Krause et al., 1997]).

### 2.3 Data processing: display and imaging techniques

Generally the visualisations of ultrasonic measurement results are named A-scan, B-scan and C-scan. To say with usual words, these are respectively: the ultrasonic point measurement in the time domain (A-scan), an ultrasonic cross- or longitudinal section (B-scan) or a depth section, parallel to the surface (C-scan). These three types of visualisation are demonstrated in Fig. 2.7.

Especially in low frequency ultrasonic technique, a more general application of the terms is used.

- **A-scan:** Amplitude of the measured signal vs. time (output voltage proportional to the sonic pressure) vs. time. Three types of A-scans are used: HF-signal (not rectified), rectified and calculated envelope function. Fig. 2.5 (right) shows the HF Signal of an echo measurement of a tendon duct in a concrete slab.
- **B-scan:** Amplitude of the time signal along the measuring (or a selected) axis showing the depth information of the reflection (alternatively named: longitudinal or cross section of ultrasonic amplitude). It consists of a line (x-axis) of several A-scans and corresponds to the Radargram for Radar or sonogram of geophysical experiments. It is usually shown in a false colour (or grey scale) representation. The y-axis is either the time of the receiver after pulse excitation or the depth after calibrating the sound velocity (Fig. 2.8b)



**Fig. 2.8** B-scan of a measuring line above to bore holes in a concrete specimen. (a) plan specimen, (b) Ultrasonic B-scan of measuring line, axes in mm, (c) Reconstruction with SAFT (Linear Synthetic Aperture Focusing Technique, here 2-dimensional)

(after [Schickert et al., 2003]).

- **C-scan:** Amplitude of the measured signal parallel to the surface at a specific depth (alternatively named: depth section of ultrasonic amplitude). It corresponds to the “time slices” in case of Radar results.

For physical reasons, transducers having a diameter in the order of the wavelength or smaller produce a wave field with a large angle of aperture containing pressure and shear waves. For this reason ultrasonic measuring and evaluation methods known from material testing and medical diagnosis methods cannot simply be transferred to concrete testing. Therefore scanning and imaging methods have a special relevance in low frequency applications.

The measuring procedure depends on the testing task. For instance, for thickness measurement of concrete elements which are not densely reinforced, simple point measurements with handheld equipment can be applied. But in most cases the evaluation of data requires imaging methods, which means that the data are measured in lines or 2-dimensional grids.

In civil engineering the direct representation of measuring data is mostly applied for planar objects (e.g. layered structures) or wooden elements (timber). For more sophisticated testing problems, where spatial resolution is of importance, the results are calculated from linear or planar measured data sets. For this, several approaches of reconstruction calculation on the base of synthetic aperture exist (*SAFT: Synthetic Aperture Focusing Technique*).

Synthetic aperture techniques offer a flexible way of focusing. A synthetic aperture imitates a large transducer by sampling its area at many points. This can be done

either by an array of transducers measuring simultaneously, or by a single transducer approaching the aperture points in succession. Moved arrays, a combination of both, are also possible. Apertures considered here are linear or planar representing a large line or rectangular transducer, respectively [Schickert et al., 2003].

For focusing the pulse-echo measurements at the synthetic aperture, the received signals are processed using the SAFT-algorithm. The SAFT-algorithm focuses the received signals to any point of the reconstructed image by coherent superposition. In this way, a large virtual transducer with variable focus is synthesized. A high-resolution image results, which is two-dimensional (2D-SAFT) for the case of linear aperture, and three-dimensional (3D-SAFT) for the planar aperture. 2D-SAFT-images are B-scan cross sections, 3D-SAFT-images are often displayed as B-scan or C-scan sections through the three-dimensional data field.

In Fig. 2.8c) a simple example of 2D SAFT reconstruction is demonstrated for ultrasonic point measurements along a line of the specimen containing two drilled holes in concrete (already mentioned for the description of the B-scan (Fig. 2.8b)). Fig. 2.8c) depicts the result of a time domain reconstruction calculation resulting in imaging the top side of the holes at correct location and depth (example from [Schickert et al., 2003]). Another kind of reconstruction calculation is based on inverse scattering theory applying Fourier-Transform-SAFT (FT-SAFT) and is better suited for three-dimensional imaging [Mayer et al., 1990].

Ultrasonic elastic wave propagation in inhomogeneous materials can also be modelled by *EFIT* (*Elastodynamic Finite Integration Technique*). Here all elastic material properties as well as wave mode conversions are considered down to the mm scale [Mayer et al., 1990]. Comparing reconstruction results of synthetic data obtained from such elastic wave equations and real experimental data enables a much better understanding of the complex scattering processes in concrete. This may enhance the reliability of test results ([Mayer et al., 1990], [Krause et al., 2009]).

## 2.4 Guidelines, Recommendations

Merkblatt für Ultraschall-Impuls-Verfahren zur Zerstörungsfreien Prüfung mineralischer Baustoffe und Bauteile (B4), Deutsche Gesellschaft für Zerstörungsfreie Prüfung e.V., Berlin (1999)

*For pulse velocity (not echo)*

ASTM C 597 – 83 (91) Standard test method for pulse velocity through concrete

DIN EN 13296 Determination of ultrasonic pulse velocity (2004)

## 2.5 Reliability and limitations

There are additional points to be taken into account, when applying the equipment described in §2.2.



The performance of ultrasonic echo measurement for concrete elements has been growing very much since the beginning of the century. The equipment is rather easy to handle and procedures without coupling agent facilitate the measuring process. Nevertheless during training (basic instructions) the basic knowledge about ultrasonic methods in the low frequency range should be communicated.

The physical parameter to be measured is the time of flight (transit time) of the exited ultrasonic pulse in the concrete. This parameter allows calculating the depth of the reflector. There are mainly three possibilities for measuring it:

- 1) Calibration at a point of known thickness of the building element,
- 2) Taking a core of sufficient diameter and measuring the wave velocity through transmission mode (the radius has to be significantly larger than  $\lambda$ ),
- 3) Measuring the wave velocity of subsurface waves (longitudinal or shear waves corresponding to the applied wave mode). The homogeneity of ultrasonic wave velocity typically varies between about 2 % (for very homogeneous concrete) and 5 % (typical values, exceptions are possible).

Using the ultrasonic echo method one measures one or several reflectors/scatterers inside the concrete element. If it is an air-filled layer it leads to a total reflection of the ultrasonic waves. Because of the concrete heterogeneity, it may be difficult to distinguish actual defects. Large aggregate have a significant scattering effect, preventing the use of a too high frequency. Because of time frequency dependent attenuation and structural noise the pulse form depends on the length of the ray path in concrete. For concrete, the measurement from the maximum of the transmitting pulse to the maximum of the echo pulse seems to be the most appropriate way. Measuring from slope of transmitting to echo pulse is only recommended in case of weak structural noise.

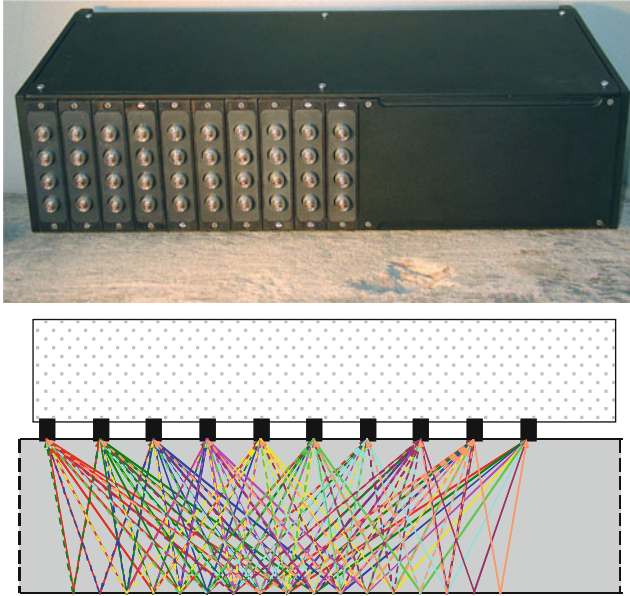
From all those influences on the depth value, the uncertainty of the result has to be estimated.

All low frequency transmitting transducers produce surface waves, which are captured by the receiver. These causes disturbing signals in the beginning of the measured time curve (compare Fig. 2.5, right, time range typically 50  $\mu\text{s}$  to 100  $\mu\text{s}$  after excitation). This is the reason, why the reliable measuring range of most equipment is limited. Another reason for that limitation is the wavelength in concrete, which is in the order of 30 mm to 60 mm for the most applications.

Especially when using dry contact transducers, users must be carefully with interpretations of single point results in case of bad surface conditions. At points with a rough surface, the transducers may oscillate in an undefined way, which will lead to misinterpretation in the time signal.

In the frequency range used for concrete the wavelength is mostly comparable to the transducer dimensions. The consequence is that not only the desired wave mode is transmitted in the concrete, but also shear waves and Rayleigh waves. The angle distribution of the applied transducers and the possible mode conversions in the concrete element should be taken into account for a proper interpretation of the results.





**Fig. 2.9** Linear array with dry contact transducers (top), principle of data acquisition (bottom)

## 2.6 Developments

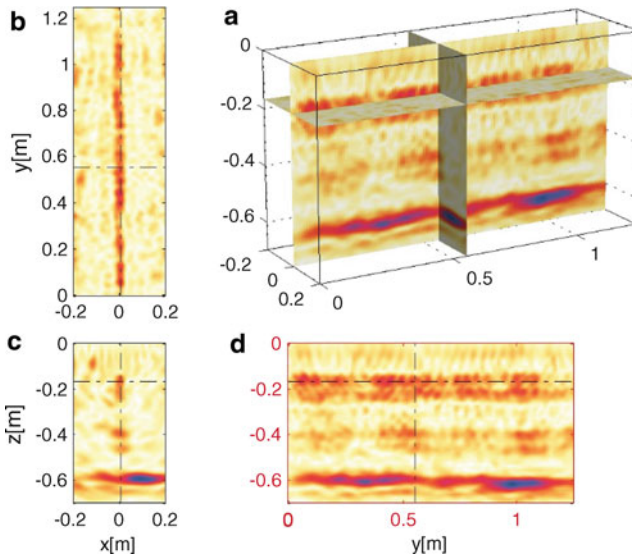
### 2.6.1 Linear Array

For automated measurement of larger surface areas linear arrays with multistatic triggering are available ([Kozlov et al., 2006], [Drinkwater and Wilcox, 2006]) (Fig. 2.9). Together with reconstruction calculation 3D imaging of section of building elements can be obtained very fast [Krause et al., 2008b].

Other approaches use differently controlled sensor systems [Schickert et Hillger, 2009].

An innovative device consists of 10 lines à 4 dry contact shear wave 50 kHz-transducers [Krause et al., 2008]. The distance of the lines is 35 mm in the current modification. The transducers and the electronics are mounted in a handheld box easily to be applied at concrete surfaces (Fig. 2.9 top). The ten lines are switched as a multistatic array, meaning that one line acts as transmitter, and all others as receiver, then the second as transmitter, and so forth as shown in Fig. 2.9 bottom. The data transfer is organized in the way that the whole data set is measured and stored in less than 1 second per location.

The data measured along a line can be combined to one data set and evaluated with fast FT-SAFT (Synthetic Aperture Focusing Technique) reconstruction calculation. Together with imaging technique, the scatterers and reflectors in the volume of interest can be analysed quickly on site with cross and longitudinal sections, as well



**Fig. 2.10** Example of measurement with linear array and 3D imaging with FTSAFT (case of a cross girder bridge [Taffe et al., 2005]) (a) Cuboid of the reconstructed volume, with different sections: (b) Depth section (C-scan), (c) Cross section (B-scan parallel x), (d) Longitudinal section (B-scan parallel y)

as depth sections and phase evaluation. There are different SAFT approaches for evaluation (2- and 3-dimensional).

In Fig. 2.10 one practical application is presented as an example. The aim was to localise tendon ducts in a cross girder, which is 60 cm thick. The data were measured along a line (length 1.16 m) with a 2-cm step width (orientation of the array is perpendicular to the measuring line).

The result was obtained with a research version of 3D-FT-SAFT reconstruction and is depicted in Fig. 2.10 [Krause et al., 2008]. The cuboid at the right (a) represents the reconstructed volume (surface: 0.40 m x 1.26 m, depth: 0.70 m). The other parts of the graph represent the different sections, which can be interactively adjusted by three planes.

## 2.6.2 Special Techniques based on the Ultrasonic echo principle

The ultrasonic echo methods for application in civil engineering are continuously ameliorated by several research and development activities. In the following only few examples can be briefly mentioned. For some of the subjects more examples are described in the corresponding chapters. The main points are:

- Automated scanning of large surface areas (see Fig. 2.11 [Krause et al., 2006])
- 2D and 3 D imaging with reconstruction calculation (SAFT) ([Krause et al., 2006], [Krause et al., 2008a])

**Fig. 2.11** 2D scanner working with linear drives and a pneumatic system to press the point contact transducers without coupling agent (BAM) [Beutel et al., 2006]



- Interpretation of the phase of the receiving signal in order to characterize the type of a reflector (steel or air) => investigating of tendon ducts ([Krause et al., 2008a], Krause et al., 2009], see also this book, Chapter 6)
- Application of contactless sensors as Laser Interferometer, imaging of ultrasonic wave propagation [Algernon et al., 2008]
- Application of air coupled ultrasonic transducers [Krause et al., 2008b].

Several testing problems are now solvable with common techniques, others with help of synthetic aperture methods (reconstruction calculation, SAFT). Numerous testing tasks are in the intermediate state between research and systematic application. The uncertainty of the results depends on details of the construction work and the site condition. Several parameters influence the wave propagation in the concrete. These are: the type and density of reinforcing bars, the concrete composition (aggregates and pores), the mechanical properties and the surface conditions. Each investigation corresponds to a specific structure or building element and it is mandatory to calibrate the measurements for reliable results. Here it is useful to describe the capability of the methods using examples of successful NDT results, mainly at test sites.

## References

- Algernon D., Gräfe B., Mielentz F., Köhler B., Schubert F. (2008) Imaging of the Elastic Wave Propagation in Concrete Using Scanning Techniques: Application for Impact-Echo and Ultrasonic Echo Methods, *J. Nondestructive Evaluation*, 2, 1–3, pp. 83–97.
- Beutel R., Reinhardt H.-W., Grosse Ch., Glaubitt A., Krause M., Maierhofer Ch., Algernon D., Wiggerhauser H., Schickert M. (2006) Performance Demonstration of Non-Destructive Testing Methods. In: *Proc. 9th European Conf. on NDT*, September 25–29, 2006, Berlin: DGZfP, BB 103-CD, Tu.3.2.2.
- Drinkwater B.W., Wilcox P.D. (2006) Ultrasonic arrays for non-destructive evaluation: a review, *NDT&E* 39, 525–546, Elsevier.

- Kozlov V.N., Samokrutov A.A., Shevaldykin V.G. (2006) Ultrasonic Equipment for Evaluation of Concrete Structures Based on Transducers with Dry Point Contact. In: Al-Quadi, I. and G. Washer (eds.); Proc. NDE Conf. on Civil Engineering, 14.-18. August 2006, St. Louis, MO, USA, pp. 496–498.
- Krause M., Bärmann R., Frielinghaus R., Kretzschmar F., Kroggel O., Langenberg K., Maierhofer Ch., Müller W., Neisecke J., Schickert M., Schmitz V., Wiggenhauser H. Wollbold F. (1997) Comparison of pulse-echo methods for testing concrete. In: NDT&E International Sonderheft Vol. 30, 4, pp. 195–204.
- Krause M., Gräfe B., Mielentz F., Milmann B., Friese M., Wiggenhauser H., Mayer K. (2008) Ultrasonic Imaging of Post-tensioned Concrete Elements: New Techniques for Reliable Localization of Grouting Defects, In: Alexander M. G., Beushausen H.-D., Dehn F. and Moyo P. (eds.); Proc. of the Concrete Repair, Rehabilitation and Retrofitting II, ICCRRR 2008, 24.-26.11.2008, Kapstadt, CD-ROM, pp. 521–527.
- Krause M., Mayer K., Friese M., Milmann B., Mielentz F., Ballier G. (2009) Progress in ultrasonic tendon ducts imaging. In: Derobert, X. and Abraham O. (eds.); 7th Int. Symp. NDT in Civil Engineering NDTCE 09, Nantes, F, 30.06.-03.07.2009, Proc. pp. 147–154 and CD ROM (77).
- Krause M., Milmann B., Mielentz F., Streicher D., Redmer B., Mayer K., Langenberg K.-J. Schickert M. (2008) Ultrasonic Imaging Methods for Investigation of Post-Tensioned Concrete Structures: A Study of Interfaces at Artificial Grouting Faults and its Verification. J. Nondestructive Evaluation, 27, pp. 67–82.
- Krause M., Milmann B., Schickert M., Mayer K. (2006) Investigation of Tendon Ducts by Means of Ultrasonic Echo Methods: A Comparative Study. In: Proc. 9<sup>th</sup> Eur. Conf. on NDT, September 25–29, 2006, Berlin: DGZfP, BB 103-CD, Tu.3.2.1.
- Mayer K., Marklein R., Langenberg K.J., Kreutter T. (1990) Three-dimensional imaging system based on Fourier transform synthetic aperture focusing technique. Ultrasonics 28, 241–255.
- Schickert M., Hillger W. (2009) Ein Ultraschall-Multikanal-Messsystem mit SAFT-Rekonstruktion für die Abbildung von Betonbauteilen, In: Berichtsband zur DGZfP-Jahrestagung 2009, 18.-20.05.2009, Münster, Beitrag auf BB 115-CD, Vortrag Mi.1.C.3, 10 Seiten.
- Schickert M., Krause M., Müller W. (2003) Ultrasonic Imaging of Concrete Elements Using Reconstruction by Synthetic Aperture Focusing Technique. Journal of Materials in Civil Engineering (JMCE), ASCE Vol. 15, 3, pp. 235–246.
- Taffe A., Krause M., Milmann B., Niederleithinger E. (2005) Assessment of foundation slabs with US-echo in the re-use process. In: Alexander M., Beushausen H.-D., Dehn F. and Moyo P. (eds); Proc. Int. Conf. Repair, Rehabilitation and Retrofitting (ICCRRR), 21.-23.11.05, Cape Town, South Africa, pp. 525–530, 2005.

### 3 Surface waves methods

**John Popovics and Odile Abraham**

#### 3.1 *Physical principles and theory*

The non-destructive testing (NDT) methods that use ultrasound, acoustics, seismic wave and vibration are based on mechanical wave (also known as “stress wave”) phenomena. Two types of mechanical waves can propagate within the body of a solid material: P-waves (also known as pressure waves or compressional waves) and S-waves (also known as shear waves). In addition, Rayleigh surface waves propagate along the free surface of a solid. P-waves travel with highest velocity and Rayleigh waves the lowest.

The characteristics of mechanical waves, such as propagating wave velocity or amount of wave energy reflected from an interface between two distinct media, are a function of the elastic properties and mass density of the solid materials. For example the velocity (speed) that these waves propagate through a material is controlled by the elastic moduli (Young's Modulus, Shear Modulus and Poisson's Ratio) and density of the material. Wave propagation characteristics are also influenced by the severity and location of internal defects such as cracking, honeycombing and delaminations. Thus mechanical wave measurements can be used to provide direct information about the condition of the material or structure under investigation.

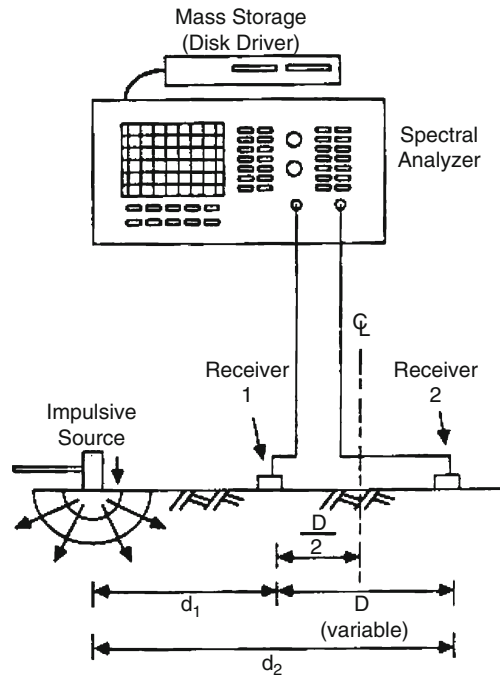
Surface-guided waves propagate along the free surface of solid materials. In the case of a single thick layer comprised of homogeneous material, surface-guided P-wave, S-waves and Rayleigh surface waves propagate along the surface. Rayleigh surface waves are used most often for non-destructive evaluation. These waves are most efficiently generated by a dynamic point load, such as an impact event, acting on a free surface of a solid. Unlike P-waves and S-waves, most of the energy of Rayleigh surface waves is relegated to the near surface region, to a depth of approximately one wavelength away from the surface (ACI, 2005). This near-surface behavior can be used to characterize the thickness and stiffness of the individual components of layered structures such as tunnel liners. Surface guided wave propagation is more complicated In the case of solids that are comprised of multiple distinct layers. The wave energy is distributed among distinct propagating wave "modes," which have particular characteristics that depend on the structure and frequency of the wave energy. At limit cases (e.g. thick top layer and high frequency), the modes converge to the more simple behavior of the single half space.

### ***3.2 Measurement equipment and procedure***

The following equipment is needed to perform these tests: a wave source, wave detection sensors, and a data acquisition and analysis system, see Fig. 2.1. The wave source is typically provided by a local impact event, for example the impact of a steel sphere or a hammer on the surface of concrete.

The size of the impactor controls the frequency content: smaller size provides higher frequency contents, normally up to 15 kHz. The wave detectors are surface-mounted sensors, usually geophones or accelerometers. These sensors measure the surface motion that is caused by the wave propagation events. The sensors provide an analog voltage output, which is collected over some time period to give a time domain signal. The data acquisition system digitizes the analog signal data, performs the analysis in either the time and frequency domain, and where needed performs the inversion (where the unknown structure of the test material is predicted based on collected wave data) and matching process. These processes can be carried out on PC-based computer systems, using commercially available software platforms.

**Fig. 2.1** Principle of Spectral Analysis of Surface Waves technique (after (Krstulovic-Opara et al., 1996))

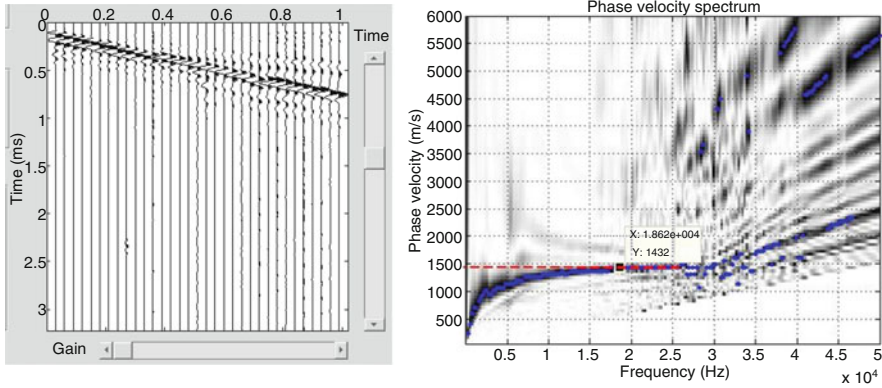


### 3.3 Data analysis and interpretation

Surface-guided waves can be analyzed and interpreted in the time domain or the frequency domain. Basic information about surface-guided wave arrival time and amplitude can be obtained from time domain signals, but this is only effective when the surface wave energy is principally relegated to the top surface, for example for high frequency waves or for a thick top layer. In these cases, the Rayleigh wave velocity of the top layer is obtained from determination for the group velocity arrival between two sensed locations on the surface. Group velocity is the measured wave velocity of an entire discrete packet or pulse of wave energy, as opposed to phase velocity, which is the measured velocity of a single phase value within the wave packet. For so-called “dispersive” materials both group and phase velocity vary with frequency.

Time domain analysis of surface-guided waves can also be carried out using multiple sensors to receive the wave data. This method, often called “seismic refraction”, allows the arrival of the first propagating wave front (surface guided P-wave) to be discerned as a function of distance from the wave source. A plot of wave front arrival time vs. distance should have linear form for a homogeneous material. Slope modifications in this plot indicate the presence of a distinct subsurface layer beneath the surface layer (Abraham and Derobert, 2003). When the wavelength of propagating





**Fig. 2.2** Illustration of multi-channel surface seismic data collected from a concrete slab: time domain signals (left) and constructed phase velocity spectrum using the MASW method (courtesy of Dr. Nils Ryden)

waves is of the order of the layer thicknesses, then frequency domain analysis methods are more appropriate. Two commonly applied frequency domain methods are the spectral analysis of surfaces method (SASW) and the multi-channel analysis of surface waves method (MASW) (Ryden, 2004). One main difference between these two analysis methods is the number of data points (collected wave signals) needed to carry out the analysis. SASW requires only two data points, whereas MASW requires more, on the order of tens of points, depending on the required depth of analysis and resolution. Another important difference is the number of wave modes that are assumed in the analysis. In the case of SASW, only one dominant wave mode is assumed to exist. In the SASW method, the surface wave dispersion curve is computed across a range of frequencies and, if needed, sensor spacing. The dispersion curve is a plot of surface wave phase velocity as a function of frequency. The dispersion curve is obtained from relative phase values, as a function of frequency, of the two measured signals. The obtained experimental dispersion curve is then matched to that computed for a specific layered structure of known thickness and mechanical properties. The computed curve is iteratively adjusted until a best match is obtained between experimental results and that of the model. In the MASW method, the surface/plate wave dispersion curves of all the excited wave modes are computed across a range of frequencies. The dispersion curves are computed by processing of the multi-channel signals that are collected from sensors placed along a line. The presence of multiple wave propagation modes is observed, providing plots of phase velocity dispersion curves for the excited modes. The obtained experimental dispersion phase velocity curves are then matched to those (called pseudo-Rayleigh wave curves) computed for a specific layered structure of known thickness and mechanical properties. The computed pseudo-Rayleigh wave curves are iteratively adjusted until a best match is obtained between experimental results and that of the model (Ryden, 2004). Figure 2.2 illustrates the MASW process in the case of a concrete plate above a subgrade for which a pseudo-Rayleigh wave mode dominates.

### 3.4 *Reliability and limitation of results*

Surface wave methods have been applied to obtain estimates of layer thickness and stiffness in a multi-layered system such as pavements and tunnel liners. For example the velocity of measured Rayleigh wave and refracted P-wave modes can be used to evaluate substrata conditions: low velocity values can indicate weak surface conditions due to scaling, spalling or minor cracking. The method can also be applied to detect the extent of a damaged zone near the surface of the tunnel liner, for example that caused by internal fire to a concrete (Abraham and Derobert, 2003).

These methods have the advantage that access to only one surface is needed. When applied properly, the methods provide an estimate of layer thicknesses and mechanical properties, although the accuracy of the thickness estimate is not as reliable as provided by other methods.

The analysis and inversion methods can be numerically intensive, and it may not always approach the correct solution; this is especially true for the SASW method. As a result, a considerable amount of user expertise may be needed to apply the SASW method. Because the sensors require physical contact with the surface of the tested specimen, the methods (using current, standard technology) are not readily applied for rapid scanning. Also, the surface conditions may adversely affect the results, and in some cases of extremely rough surface or limited access cannot be applied. However, recent developments in technology such as wheeled sensor systems and contactless air-coupled sensors may provide some solutions for the contact problem (Zhu and Popovics, 2005). Results collected from tunnels with cast iron liners may not accurately characterize the properties of the substrata.

## References

- Abraham O., Dérobert X. (2003) Non-destructive testing of fired tunnel walls: the Mont-Blanc tunnel case study, *NDT&E International*, Volume 36, pp. 411–418.
- ACI Committee 228 (2005) Non-destructive test methods for concrete, Committee Document 228.2R, American Concrete Institute, Farmington Hills, MI.
- Krstulovic-Opara N., Woods R.D., Al-Shayea N. (1996) Nondestructive Testing of Concrete Structures Using the Rayleigh Wave Dispersion Method, *ACI Materials Journal*, V. 93, No. 1, Jan-Feb 1996, pp. 75–85.
- Ryden N. (2004) Surface Wave Testing of Pavements, Ph.D. dissertation. Lund Institute of Technology.
- Zhu J., Popovics J.S. (2005) Non-contact imaging for surface-opening cracks in concrete with air-coupled sensors, *RILEM Concrete Science and Engineering/Materials and Structures*, Volume 38, pp. 801–806.



## 4 Impact echo

Andrzej Moczko

### 4.1 Physical principles and theory

Impact-Echo is based on the use of transient stress waves. The principle of measurement is described at Fig. 2.1. A short-duration stress pulse is introduced into the member by mechanical impact. This impact generated three types of stress waves that propagate away from the impact point. A surface wave (Rayleigh wave or R-wave) travels along the top surface, and a P-wave and an S-wave travel into the member.

In Impact-Echo testing, P-wave is of primary importance because the displacement caused by P-waves are much larger than those caused by S-waves at points located close to impact point. When the P-wave reaches the back side of the member, it is reflected and travels back to the surface where the impact was generated. A sensitive displacement transducer next to the impact point picks up the disturbance due to the arrival of the P-wave. The P-wave is then reflected back into the member and the cycle begins again. Thus the P-wave undergoes multiple reflections between the two surfaces. The recorded waveform of surface displacement has a periodicity related to the thickness ( $T$ ) of the member and the wave speed ( $C_p$ ).

The frequency of P-wave arrivals at the transducer ( $f$ ) is determined by transforming the recorded time-domain signal into the frequency domain using the fast Fourier transform technique (FFT). The frequencies associated with the peaks in the resulting amplitude spectrum represent the dominant frequencies in the waveform. These frequencies can be used to determine the distance to the reflecting interface. As a result the thickness of the member could be defined by simple equation:

$$T = \frac{C_p}{2f}$$

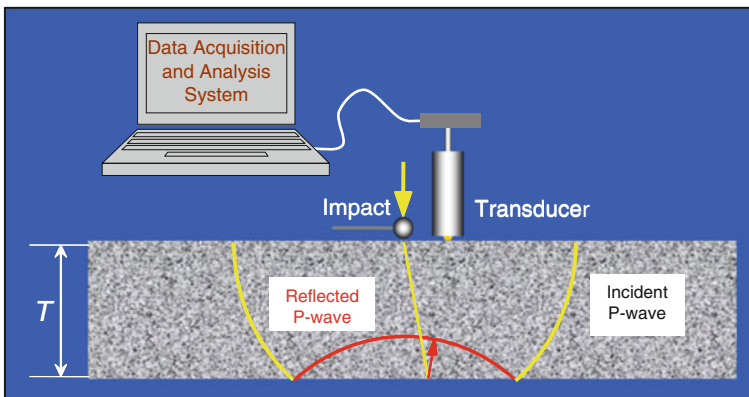


Fig. 2.1 Principle of impact echo measurement

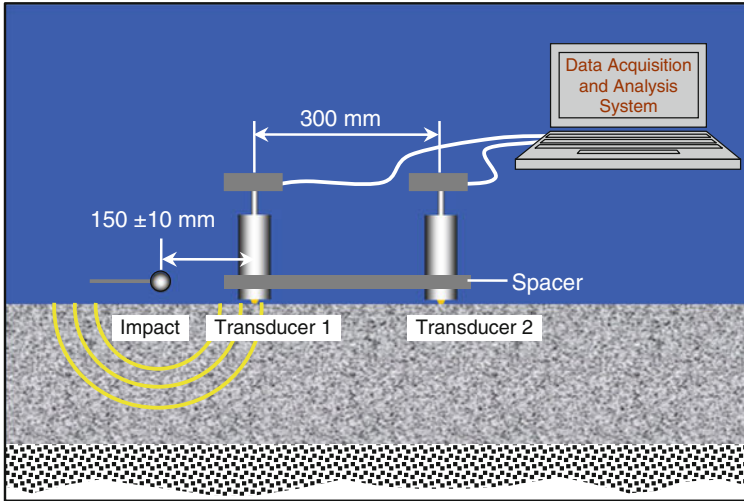


Fig. 2.2 Calibration principle for the P-wave speed determination

Naturally, to determine the thickness of concrete element the P-wave speed should be known. For determining the P-wave speed two methods are permitted. One method is by determining the thickness frequency and then measuring the actual plate thickness at that point.

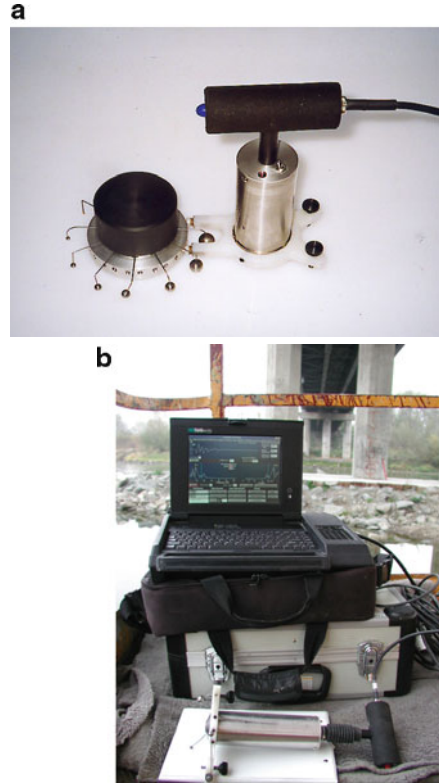
Alternatively,  $C_p$  may be determined by measuring the time for the P-wave to travel between two transducers with a known separation (Fig. 2.2). The transducers are placed 300 mm apart and the impactor is about 150 mm from one of the transducers on the line passing through the transducers. The distance  $L$  (300 mm) between the transducers, is divided by time difference  $\Delta t$  between arrival of the P-wave at the second and first transducers. When the wave speed is determined by the surface measurement method, the resulting value has to be multiplied by 0.96 prior to using it to calculate thickness. Thus the correct equation for thickness calculation in such case is:

$$T = \frac{0.96C_p}{2f}$$

The same principle applies to reflection from an internal defect (delamination or void). Thus, the impact-echo method is able to determine the location of internal defects as well as measure the thickness of a solid member.

The P-wave generated by impact will reflect at interfaces within the concrete where there is a change in acoustic impedance, which is defined by the density and wave speed of a material. At a concrete-air interface, there is complete reflection of the P-wave, and this permits the detection internal defects such as delaminations, cavities, and honeycombed concrete.

**Fig. 2.3** (a) Impactors and transducer (b) Acquisition system

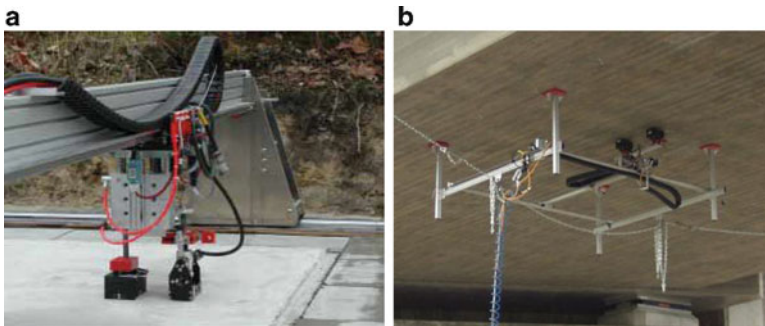


## 4.2 *Measurement equipment and handling*

Up to now the number of commercially available Impact-Echo devices is limited. The data acquisition and analysis capabilities of these systems are quite similar. In general Impact-Echo test system consists of three components (Fig. 2.3a and 2.3b): impactors, a receiving transducer and a portable computer with a data-acquisition card. The impactors are hardened steel spheres attached to spring steel rods to be operated by hand.

Typical diameters of impactors are 5, 8 and 12.5 mm. Testing are usually manual, performed from point to point. To do the measurement a spring is lifted with two fingers to a selected height and released for impact. There are also possibilities to perform impacts automatically for increasing the speed of testing what is especially suited when large areas need to be tested with close spacing between test points.

The receiving transducer is a broadband displacement transducer. A thin sheet (cap) of lead is used between the conical piezoelectric element and the concrete



**Fig. 2.4a-b** Examples of automatic scanning devices

surface. Always the test area has to be smooth to achieve good contact between the transducer element and concrete. A portable, computer-based, data acquisition system is used to capture the output of the transducer, store the digitized waveforms and perform signal processing and analysis.

It is particularly important that cap's intent has to rest against the surface when the handle is depressed. In general, it is recommended to start out testing with as big size of impactor as possible that can detect the solid frequency of interest.

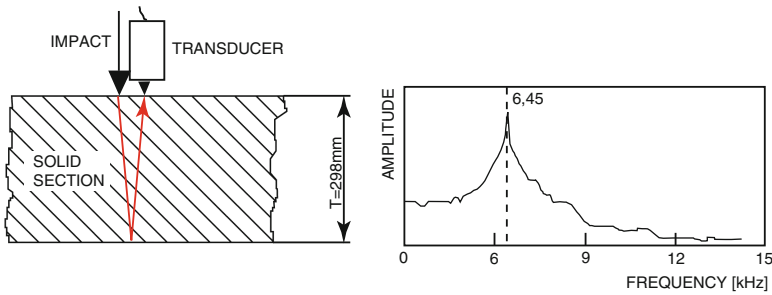
Should the measured frequency change compared to this frequency, a smaller impactor is chosen subsequently, in attempt to detect the depth of the defect causing the change of the solid frequency.

The surface at the transducer point has to be smooth. If not, it is necessary to grind a spot. It is imperative that there is electrical contact between the transducer tip/cap and concrete surface.

Point method of measurements has been improved by BAM (Federal Institute for Materials Research and Testing – Germany) into a scanning test method to visualize test results as an Impact-Echogram, similar to B-scan in ultrasonic pulse echo (see §2.3. in Ultrasonic echo) or a GPR radargram. A self driven scanner for horizontal surfaces was developed for both, Impact-Echo and ultrasonic sensors (Fig. 2.4a-b).

### 4.3 Guidelines, references and standards

- ASTM C1383-98 – Standard Test Method for Measuring the P-Wave Speed and the Thickness of Concrete Plates Using the Impact-Echo Method.
- Advice Notes NDT Highway Structures, UK, August 2006, Ed. Forde M., BA 86/06, Part 7, A.N. 3.1.
- Recommendation of Polish Highway and Road Directory concerning NDT “in-situ” quality control of concrete bridge structures during constructing process. Wrocław, 1998.



**Fig. 2.5** Principle of impact-echo for thickness measurement

- Recommendation of Polish Highway and Road Directory concerning NDT “in-situ” examination of existing concrete bridge structures. Wrocław, 1998.
- An Impact-Echo Guideline of DGZfD (German Society of Non Destructive Testing) – Working title: Application of Impact-Echo for NDT of construction elements (in preparation).

#### **4.4 Calibration and interpretation of results**

The Impact-Echo method is based on monitoring the arrival of reflected stress waves and is thus able to obtain information on the depth of the internal reflecting interface. The main application which was stimulating development of this technique was a need to identify the presence and depth of anomalies in concrete structures which are accessible only from one side. In particular, the possibility of thickness measurement of the solid plates, like pavements, asphalt overlays, slabs-on-ground and walls is worth of interest. In such case the spectrum of solid part of testing plate is dominated by a single large-amplitude peak – the plate thickness frequency (see Fig. 2.5).

However Impact-Echo can be also used for several other practical applications, as an example:

- detecting the presence and depth of voids and honeycombing,
- localization of delaminated surveys of bridge decks, piers, tunnel lining elements, cooling towers and chimneystacks,
- detecting voids below slabs-on-ground,
- detecting debonding areas between reinforcement and concrete, caused for example by corrosion,
- evaluation of the quality of grout injection in post-tensioning cable ducts,
- integrity testing of a membrane below an asphalt overlay protecting structural concrete.

In the case of a defect which is large enough to be detectable, the amplitude spectrum will show two peaks (Fig. 2.6): one corresponds to reflection from the

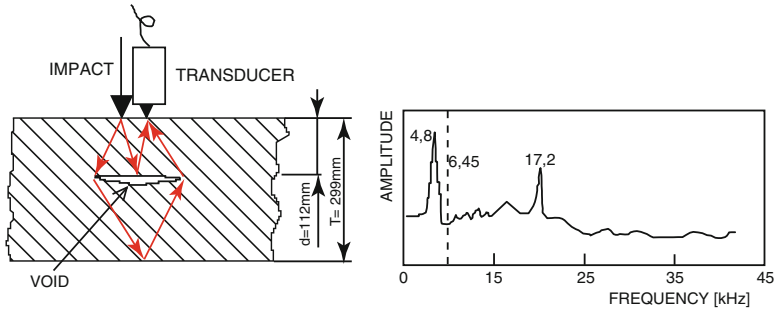


Fig. 2.6 Amplitude spectrum with two peaks, giving defect depth and total thickness

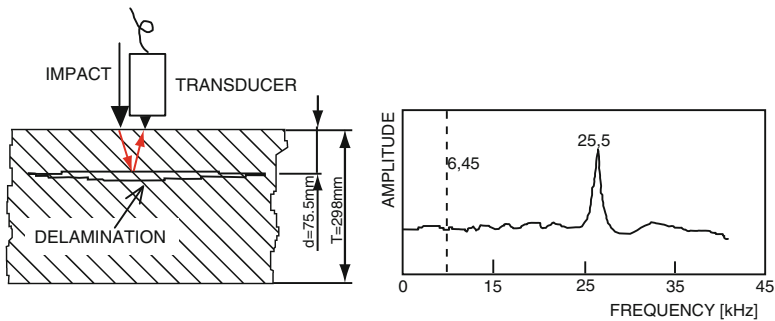


Fig. 2.7 Amplitude spectrum with screening effect of a large defect

interface and the other corresponds to the portion of the P-wave that travels around the defect and reflects from the opposite surface of the plate. The frequency associated with the portion of the P-wave that travels around the defect will be shifted to a lower value than the solid plate thickness frequency because the wave travels a longer distance than the thickness, and this provides further evidence that a defect is present.

If the plan area of the reflecting interface is larger (e.g. when the concrete section is delaminated), the generated stress wave does not propagate to the bottom of the testing plate. In such case all energy is reflected by the defect, which screens the bottom part of the concrete plate. The impact-echo response is shifted to a higher value and the plate thickness frequency is not observed at all (fig. 2.7).

As it has been shown above localization of different types of defects has been widely applied by identifying peak frequencies in the frequency spectrum. Nevertheless, the frequency spectrum can not be always interpreted successfully, because the peak frequencies in the frequency spectra can consists of reflections from the boundary surfaces of the structure and those of from the defects. To improve Impact-Echo measurements a rather new method for identification of the defects in concrete structures has been developed, applying a scanning procedure. Thus, stack imaging of spectral amplitudes based on impact-echo (SIBIE) was developed.

Among other things it has been proven that SIBIE procedure could be successfully applied for detection ungrouted tendon ducts of prestressed concrete elements, like an example bridge girders.

#### ***4.5 Reliability and limitation of results***

It is essential to ensure that the impact frequency, determined by the size of the ball bearing, is sufficiently high to identify existing defects. The interaction of stress waves with internal discontinuities depends critically upon the relationship between wavelength and the dimension and depth of the discontinuity. In general stress waves of wave length “ $\lambda$ ” will be reflected by defects having dimensions approximately equal to or greater than “ $\lambda$ ”, but will not see those that are smaller. The minimum depth at which discontinuity can be detected is assumed to be equal to half the minimum input wavelength.

Care should be also taken to ensure that the concrete surface does not crumble on ball bearing, otherwise the longer contact time will result in a lower frequency input signal with longer wavelength.

For P-wave speed determined by calibration with a known thickness, the error in thickness measured by the commercially available Impact-Echo systems is estimated to be within  $\pm 2\%$ . This assumes that the same P-wave speed is applicable at all test points. In the case of thickness measurement based on measuring the P-wave speed from surface measurements, the error in thickness dues to systematic errors associated with the digital nature of the measurements is about  $\pm 3\%$ . This assumes that the P-wave speed is uniform with depth.

## **References**

- Abraham O., Leonard C., Cote P., Piwakowski B. (2000) Time frequency analysis of impact-echo signals: numerical modelling and experimental validation., *ACI Mat. J.*, 97, 6, 645–657.
- Ata N., Mihara S., Ohtsu M. (2007) Imaging of ungrouted tendon ducts in prestressed concrete by improved SIBIE. *NDT&E Int.*, 40, No 3: 258–264.
- Carino N.J., Sansalone M.J. (1992) Void detection in grouted ducts using the Impact-Echo method. *ACI Materials Journal.*, 89, 3, 296–303.
- Colla C., Schneider G., Wostmann J., Wiggenhauser H. (1999) Automated Impact-Echo: 2 and 3-D imaging of concrete elements, *NDT*, 4, 2.
- Gipson A., Popovics J. (2005) Lamb wave basis for impact-echo method analysis, *J. Eng. Mech.*, ASCE, 5, 438–443.
- Jaeger B.J., Sansalone M.J. (1996) Detecting voids in grouted tendon ducts of post-tensioned concrete structures using the impact-echo method. *ACI Structural J.*, 93, 4, 462–472.
- Ohtsu M., Watanabe T. (2002) Stack imaging of spectral amplitude based on impact-echo for flaw detection. *NDT & E Int.*, 35, 189–96.
- Sansalone M.J., Impact-Echo (1997) The complete story. *ACI Structural Journal*, 94, 6, 778–786.
- Sansalone M.J., Streett W.B. (1997) Impact-Echo – Nondestructive Evaluation of Concrete and Mansory. Bullbrier Press.

## 5 Impulse response

Andrzej Moczko and Claus Germann Petersen

### 5.1 Physical principles and theory

The Impulse-Response technique was developed by Davis in the end of twentieth century. He adapted the Pile Integrity Testing procedure (cf Chapter 4, § 2.4.1.) for evaluating the integrity of concrete plate-like structures. A low-strain impact, produced by an instrumented rubber tipped hammer is used for sending stress waves through the tested element. The impact causes the element to vibrate and a velocity transducer (geophone), placed near the impact point, measures the amplitude of the response. The technique is based on the analysis of structural mode shapes. The hammer load cell and the velocity transducer are linked to a portable field computer with impulse-response software for data acquisition, signal processing and storage (Fig. 2.1). The time histories of the hammer force and the measured response velocity are transformed into the frequency domain using the fast Fourier transform (FFT) algorithm. The resultant velocity spectrum is divided by the force spectrum, to obtain the “mobility” as a function of frequency. The graph of the mobility plotted against frequency contains information on the condition and integrity of the structure.

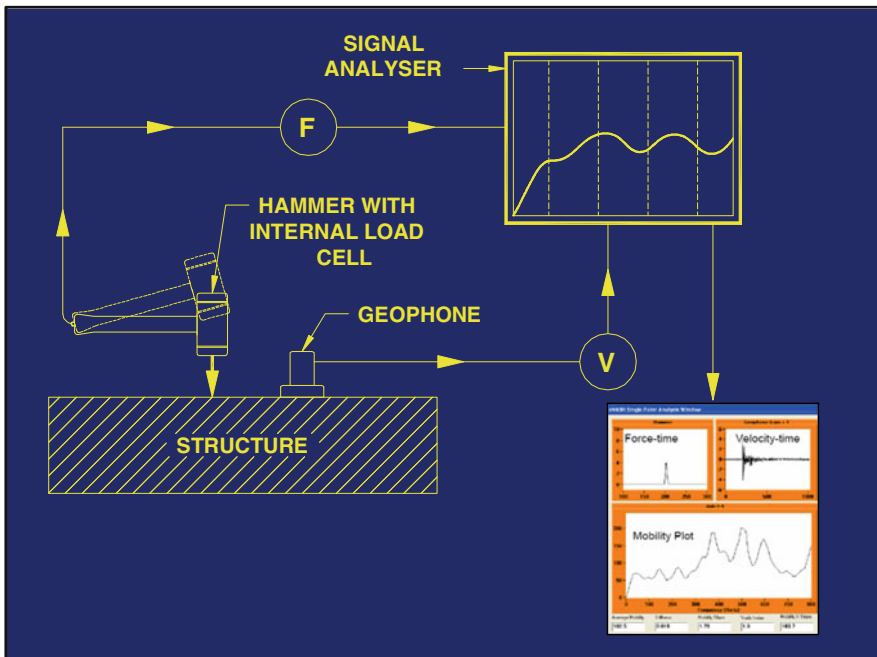
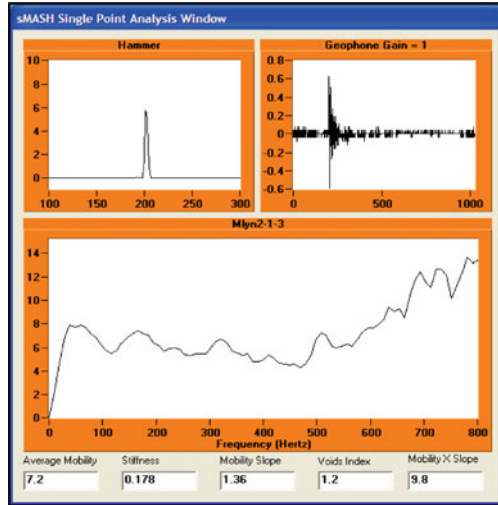


Fig. 2.1 Principle of the Impulse Response measurements



**Fig. 2.2** Building the mobility curve



An example of typical test results is given at Fig. 2.2. The top left window is the force-time curve obtained from the impact of the instrumented hammer. The top right window shows the velocity-time curve obtained from the geophone in contact with the concrete surface. The lower window shows the mobility plot obtained from the two previous wave forms. At the bottom part of the screen shot the various parameters calculated from the mobility plot are displayed. Mobility is expressed in units of velocity per unit force, such as (m/s)/N. In general, the integrity of the concrete element under test is evaluated using parameters obtained from the mobility plot-frequency plot over the 0-800 Hz range.

Impulse-Response testing method is mainly used for fast screening of large areas of concrete structures with the purpose to control their structural integrity and to determine local areas with possible flaws for subsequent detailed analysis, e.g. by the impact-echo test, ultrasound shear waves or by invasive inspection with drilled cores. In particular Impulse-Response inspection may be conducted for:

- locating delaminations and honeycombing in bridge decks, slabs, walls and large structures such as dams, chimney stacks and silos,
- detecting the curling of slabs,
- detecting voids beneath concrete slabs in highways, spillways and floors,
- detecting debonding of asphalt and concrete overlays and repair patches from concrete substrates,
- evaluating anchoring systems of wall panels.

## 5.2 Measurement equipment and handling

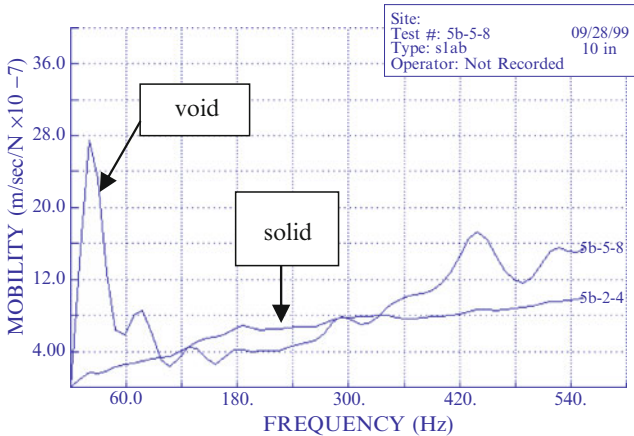
Up to now the number of commercially available Impulse-Response devices is limited. The data acquisition and analysis capabilities of these systems are quite

**Fig. 2.3** Typical equipment**Fig. 2.4** Measurement process

similar. In general Impulse-Response test system consists of three main components (see Fig. 2.3 and 2.4): instrumented rubber tipped hammer equipped with a load cell, broadband velocity transducer (geophone) which must have constant sensitivity over the range 15-1000 Hz and a portable field computer with proper software for data acquisition, signal processing and storage. Manual testing is usually performed across a grid of points marked on the surface of the structure. Grid node spacing normally ranges between 450 mm and 900 mm; however, grid spacing can be selected as a function of the size and shape of the element to be tested.

The velocity transducer has to be placed at a distance of between 75mm and 150mm from the point of impact. The test surface can be dry, moist or wet, but not inundated. It is necessary to remove any debris from the immediate vicinity of each test point. If the test surface is too rough, it can prevent to achieve good contact between the transducer and the concrete. In such a case, the surface should be ground so that good contact is achieved and loose material removed prior to placing the transducer on the surface.

The hammer-time graph must display a single positive voltage peak with a constant base voltage, not necessarily triangular like on Fig. 2.2. The velocity time curve must oscillate around zero, indicating that the transducer is stable during data acquisition.



**Fig. 2.5** Typical mobility curves in the case of a continuous material, and in the case of a void

### 5.3 Guidelines, references and standards

ASTM is preparing a proposal (not yet approved): ASTM C09.64 – Standard Practice for Measuring the Integrity of Concrete Plates Using the Impulse Response Method.

### 5.4 Calibration and interpretation of results

The main evaluation criterion for concrete structure integrity assessment is mobility plot obtained directly from the measurements. The test graph of mobility plotted against frequency from 0 to 800 Hz contains information on the relative quality of the concrete in the tested element (Fig. 2.5). In the case of the defect which is large enough to be detectable, a high mobility is measured at low frequencies (below 100 Hz). If there are not any significant delaminations or voids, mobility plot is rather stable over the frequency range.

For a more detailed **evaluation of Impulse-Response data, the following parameters are usually used:**

- Stiffness: the initial slope of the mobility frequency curve below 100 Hz defines the dynamic compliance or flexibility of the area around the test point for a normalized force input (Fig. 2.6). The inverse of this slope is the dynamic stiffness of the structural element at the test point. It is a function of concrete quality, element thickness and element support conditions.
- Average Mobility: the mean of the mobility measured at the point, calculated from the mobility curve between 100 and 800 Hz is related to the density and the thickness of a plate element (Fig. 2.6). A reduction in plate thickness corresponds

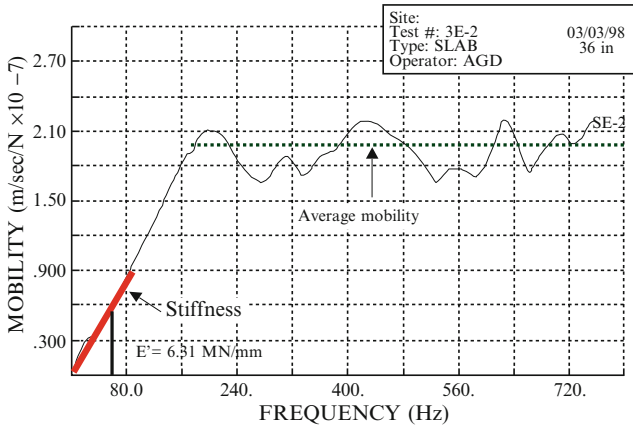


Fig. 2.6 Stiffness and average mobility determination on a mobility curve

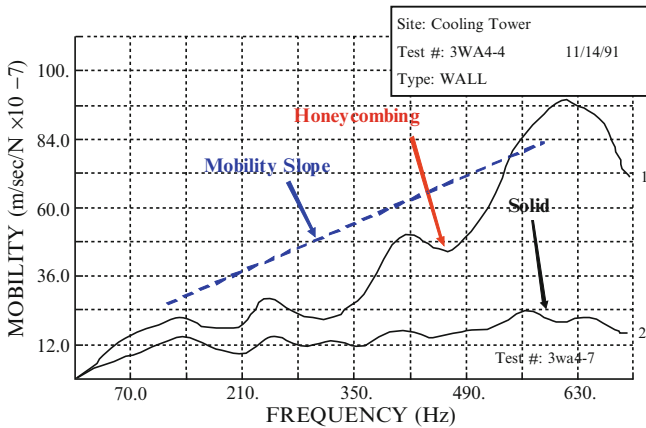


Fig. 2.7 Stiffness and average mobility determination on a mobility curve

to an increase in average mobility, even if these two parameters are not formally related to each other.

- **Mobility Slope:** this parameter is defined by calculating the linear best fit of the frequency spectrum between 100 and 800 Hz, then dividing the 800-Hz mobility by the 100-Hz mobility values on this linear best fit (Fig. 2.7). This parameter is considered as a function of concrete consolidation. When mobility slope values significantly increase, poor consolidation and honeycombing can be expected.
- **Void Index:** the ratio of the peak mobility value between 0 and 100 Hz and the average mobility between 100 and 800 Hz (Fig. 2.5). Void Index it is an indicator of the presence and degree of either severe debonding within the element or voiding. When debonding or delamination are present within a structural element, or when there is loss of support beneath a concrete slab on grade, the peak mobility below 100 Hz becomes appreciably higher than the average mobility between 100 and 800 Hz.

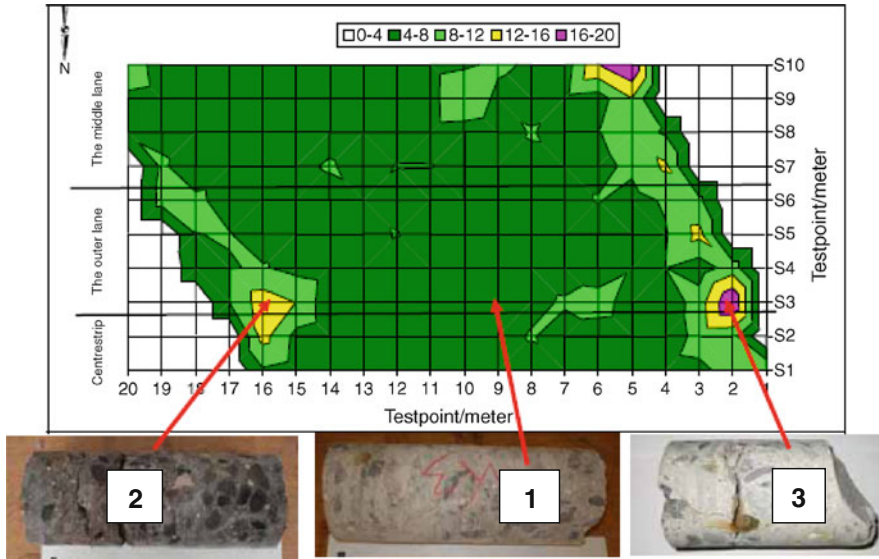


Fig. 2.8 Average mobility mapping on a bridge deck for detecting delamination

Results can be also presented as colour pictures showing the distribution of particular evaluation parameters on the surface of the tested element. As an example, a contour graph of the Average Mobility obtained by from measurements performed on the soffit of a bridge slab that was suspected of containing delaminations are shown at Fig. 2.8. Tests were performed on a 1 x 1 m grid. After testing, three locations were selected for drilling cores for experimental verification of the results obtained: (1) region of low value of average mobility, (2) region of intermediate mobility and (3) region of high mobility. Visual inspection of the cores confirmed that low mobility corresponds to a solid section of the concrete slab and higher values of average mobility correspond to the presence of delaminations.

### 5.5 Reliability and limitation of results

The main advantages of Impulse Response method are: access to only one face is needed, equipment is commercially available, the method does not require coupling materials and large areas can be tested in a relatively short amount of time. However, an experienced operator is required.

As any NDT method it is not recommended to use Impulse Response to evaluate concrete structures. The method is primarily considered as a relative method used for screening of large surfaces. The measurements should always be supplemented and verified with other more direct examinations. These verifications can be done

by means of drilling cores, breaking up concrete or the use a borescope. Screening with the impulse-response gives the possibility to identify potentially damaged areas. Because the physical properties of concrete can vary from point-to-point in the structure due to differences in concrete age or batch-to-batch variability, the measured mobility and dynamic stiffness can vary from point to point in a plate element of uniform thickness.

The impulse-response technique does not give any depth indications for the flaws. Only relative values of the various parameters can be evaluated for the structure in question, which give an indication of “good” and “bad” areas. Other tests or invasive verification are needed to confirm the interpretation from the measured mobility plots.

Any test results from within 300 mm of the edge of a plate-like structure should be disregarded, because of the edge effect of the plate on the test result. The effective radius of influence of the hammer blow limits the maximum concrete element depth or thickness that can be tested. This maximum depth can exceed 1000 mm; however, the apparatus shall not be used beyond these limits.

Impulse Response testing procedures are not influenced by traffic noise or low frequency structural vibrations set up by normal movement of traffic across a structure. They are also applicable in the presence of mechanical noise created by equipment (jack hammers, sounding with a hammer, mechanical sweepers, and the like) impacting on the structure. Nevertheless, Impulse Response technique is not applicable in the presence of high amplitude electrical noise, such as may be produced by a generator or some other sources, which can be transmitted to the data-acquisition system.

## References

- ASTM D 5882-00: Standard Test Method for Low Strain Integrity Testing of Piles. American Society for Testing and Materials, Philadelphia, PA. 19103, USA.
- Clausen J.S., Knudsen A. (2009) Nondestructive Testing of Bridges Decks and Tunnel Linings Using Impulse-Response, Proceedings of Tenth ACI Int. Conf. on Recent Advances in Concrete Technology and Sustainability Issues, Seville, Spain, October 2009, SP-261-19, pp. 263-275.
- Davis A.G. (2003) The Non-Destructive Impulse Response Test in North America: 1985-2001, NDT & E International, 36, pp. 185-193, Elsevier Science Ltd.
- Davis A.G., Hertlein B.H. (1987) Nondestructive Testing of Concrete Pavement Slabs and Floors with the Transient Dynamic Response Method, Proceedings International Conference on Structural Faults and Repair, London, July 1987, Vol. 2, pp. 429-433.
- Davis A.G., Hertlein B.H. (1995) Nondestructive Testing of Concrete Chimneys and Other Structures, Conference Nondestructive Evaluation of Aging Structures and Dams, Proc. SPIE 2457, pp. 129-136, Oakland CA, June 1995.
- Moczko A., Rybak J. (2010) Impulse Response – Modern NDT Technique for Concrete Structures Integrity Testing, Budownictwo Technologie Architektura, No 1, pp. 46-50.
- Otosen N.S., Ristinmaa M., Davis, A.G. (2004) Theoretical Interpretation of Impulse Response Test of Embedded Concrete Structures, ASCE Journal of Engineering Mechanics, Vol. 130, No. 9, Sept. 2004, pp. 1062-1071.

## 6 Acoustic emission

Jean-Paul Balayssac and Masayasu Ohtsu

### 6.1 Physical principles and theory

Acoustic emission (AE) is a stress wave emission technique used to monitor defect formation and failures in structural materials. What is the basic concept of AE? When an acoustic emission occurs at a source within a material due to inelastic deformation or to cracking it generates an elastic wave which can be detected by an adapted receiver (Fig. 2.1). The signal recorded by the receiver can be affected by the nature of the source, the geometry of the tested specimen and the characteristics of the receiver.

Acoustic emission testing is a “passive” monitoring method in which the detection system waits for the occurrence and capture of stress wave emissions associated with cracking, corrosion, or wire breaks. By contrast, classical flaw detection methods, such as those discussed in the previous sections (impact echo, surface waves...), are considered “active” because a stress wave is sent into the test object to identify the presence of defects. Moreover AE will be very sensitive to defect activity when a structure is loaded beyond its service activity in a proof test.

AE is used successfully in a wide range of applications including: detection and locating defects in pressure vessels or leakage in storage tanks and pipes, corrosion processes, removal of protective coatings... Concerning the application of acoustic emission for concrete assessment, three famous papers were historically

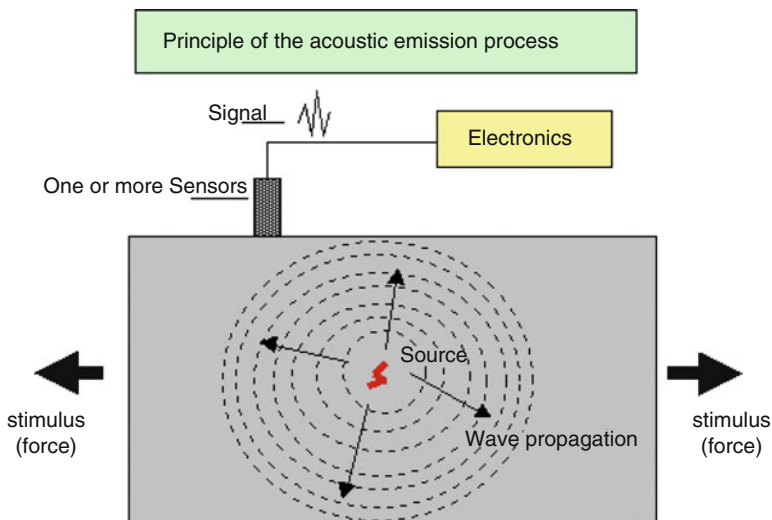


Fig. 2.1 Principle of acoustic emission



known, tracing back to 1960's. In 1959, H. Rusch studied the noise emitted during application of a compressive load in concrete. This is known as one of the first studies of the Kaiser effect in concrete. He found that AE events were recorded above 75% load level of failure load, and reported that generating behaviour of AE was closely related with the volumetric change and the absorption on ultrasonic waves. Applied researches are still in progress for instance for the detection of concrete reinforcement corrosion.

Even if AE is very reliable for the detection of the defects, it cannot provide quantitative information related to the extension of the damage. So other methods are still needed to provide such information. Moreover service environment is generally very noisy and the AE signals are usually very weak. Thus signal discrimination and noise reduction are not easy but extremely important for successful AE applications.

## ***6.2 Measurement equipment and handling***

The most widely used sensors are resonant piezo-electric accelerometers which convert the surface displacement into an electric signal. Resonant sensors are only very sensitive to a certain frequency but some wide band, high sensitivity sensors are now available. For civil engineering applications the sensor frequency is quite low (from 20 to 150 kHz). If several sensors are used and are located around the source, the mechanical wave will be successively received by each of these sensors, and so it will be possible to locate this source. The system consists on sensors, conditioners and a computer. The signal is amplified, conditioned and stored by a computer (Fig. 2.2). The conditioner can also provide solutions for the monitoring of additional parametric inputs.

Mainly due to practical reasons the implementation of the AE technique on site can be difficult. One of the difficulties is linked to the necessity of using a couplant between the sensor and the surface to ensure a good quality of the measurement and a good reproducibility. Like the test has to be performed during a long time the couplant qualities have to be preserved.

The number and the type of sensors (broad-band, resonant, bandwidth) must be defined in relation with the application. If the location is necessary, the definition of the sensor repartition grid is important. In this grid the distance between the sensors must be defined in relation with the attenuation of the waves.

The calibration of the acquisition system is very important. The quality of the sensor coupling and the accuracy of the source location must be assessed by mean of an artificial AE source (HSU Nielsen, also named pencil lead break).

AE waves are detected by AE sensor, which converts dynamic motions at the surface of a material into electric signals. Because AE signals are weak, they are normally amplified by two amplifiers (a pre-amplifier and a main amplifier). The signal-to-noise ratio of equipments used to be low, the amplifiers often provided more than 1000 times gain. Lately, it is normally 100 times or so.



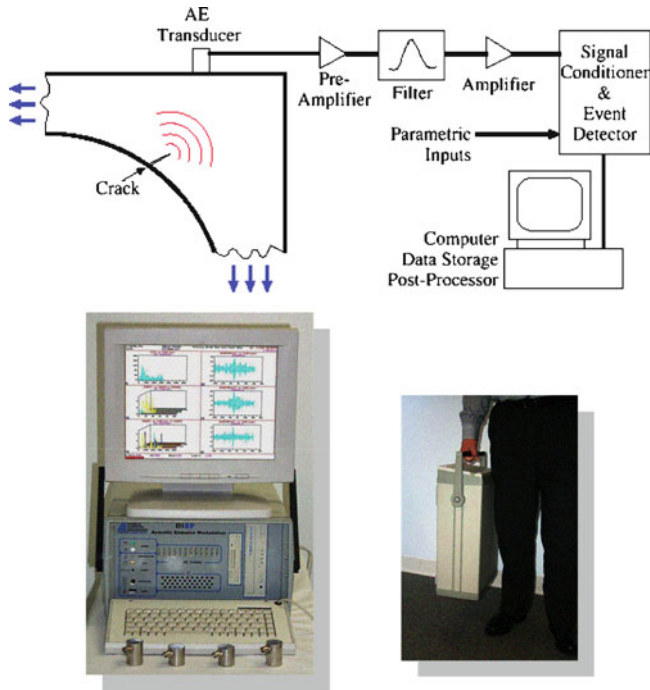


Fig. 2.2 Typical AE system

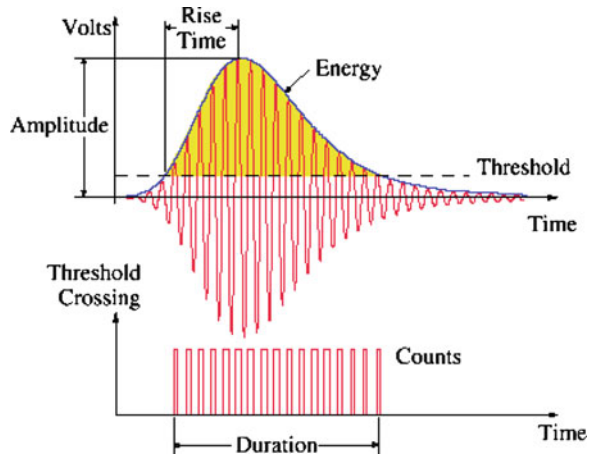
The band-pass filter is employed to eliminate the noises. In civil engineering materials, the band width from several kHz to several 100 kHz is recommended in the measurement.

Physically, AE waves are elastic waves due to dislocation motions (discontinuity of displacements as cracking) in a solid. As a result, they consist of P-wave (pressure wave, longitudinal wave or volumetric), S-wave (transverse wave or shear), and such other waves as surface waves (Rayleigh wave and Love wave), reflected waves, diffracted waves and interface wave (Lamb wave and other plate waves). The latter portion of AE waveform, in addition, is often associated with resonance vibration of AE sensor, which turns wave motions into electrical signals.

### 6.3 Guidelines, references and standards

The following standards concern terminology used for AE examinations, general principles and equipment characterisation. Regarding specific applications, standards are mainly focused on the examination of storage tanks or pressure vessels and from the point of view of materials, fiber-reinforced polymer-matrix composites, metals and ceramics. Regarding specific examinations of concrete structures

**Fig. 2.3** Typical burst and usual parameters



Japanese Standard and Recommendation are available. Some committees in RILEM (TC 212-ACD) have recently issued recommendations.

- ASTM E1316-07C – Standard Terminology for Non Destructive Examinations
- ASTM C1175-99A – Standard Guide to Test Methods and Standards for Non Destructive Testing of Advanced Ceramics
- EN 13554 – Non Destructive Testing – Acoustic Emission – General Principles
- EN 13477 – Non Destructive Testing – Acoustic Emission – Equipment Characterisation Part 1 & 2
- EN 1330-9 – Non-destructive testing – Terminology – Part 9: terms used in acoustic emission testing
- NDIS 2421, Recommended Practice for In-Situ Monitoring of Concrete Structures by AE, Japanese Society for Nondestructive Inspection, JNSDI, Tokyo, 2000
- JCMS-III B5706, Monitoring method for active cracks in concrete by acoustic emission, Federation of Construction Materials Industries, Japan, 2003.

#### **6.4 Calibration and interpretation of results**

The amount of charges measured by the sensor is translated in a transient signal in volts (V) or  $\text{dB}_{\text{AE}}$  versus time. The Fig. 2.3 shows an example of a received signal, the burst. A detected burst signal can also be named hit. After applying a threshold, the following AE parameters can be extracted from the burst:

- the maximum of amplitude: the amplitude of the maximum peak of the burst
- the number of counts: number of detected burst signals over the detection threshold
- the rise time: time interval between the first signal over the threshold and the maximum peak amplitude

- the duration: time interval between the first and the last time the detection threshold is exceeded by a burst
- the energy: relative energy of the acoustic emission burst. The measurement of the energy is depending on the acoustic emission equipment
- the number of counts up to the peak.

Up to now only the features previously listed were analyzed because of the limitations of the sensors as well as the data storage and the processing capabilities. In the recent years, wide band, high sensitivity sensors have been developed to capture the whole waveform. In the same time, the storage and the processing of these waveforms became possible with the advancement of computer technology. So it is now possible to characterize the nature of the AE sources from the waveform analysis.

When an array of sensors is used, by extracting the arrival times of the bursts received by each of them it is also possible to locate the source. Once a source is located it is usual to talk about acoustic events for the hits linked to this source. The location can be done in real-time (during the sounding) and the results can be displayed immediately. The location is achieved by means of specific algorithms and several approaches can be used. Linear location, i.e. one dimensional requiring two or more channels, planar location i.e. two dimensional requiring three or more channels and finally volume location i.e. three dimensional requiring five or more channels. Linear and planar locations are most widely used.

However, an important problem is how to differentiate the events of interest, for instance those due to crack growth or corrosion, from different noises in a large dataset. Often, the real AE events are measured in the presence of noise due to vibration, fretting and electromagnetic interference and so, an automatic procedure for noise rejection is required before correlating AE activities with crack initiations or progressive failures. In many cases, traditional signal processing techniques such as filtering, energy analysis and spectrum analysis are insufficient to achieve this separation. One possible approach is to use statistic tools like artificial neural networks (ANN) or wavelet analysis that are able to separate and cluster the different events. The classification and the clustering can be done with or without supervision. Generally a main components analysis is used before the implementation of the artificial neural network in order to reduce the number of events. Commercial softwares are available for this kind of application.

In the case of crack detection it is possible to distinguish different modes of cracking by the moment tensor analysis.

## ***6.5 Reliability and limitation of results***

If the attenuation is too high during the propagation towards the surrounding medium up to the sensor the event cannot be detected.

If the environment is very noisy the extraction of relevant information is difficult.

Like it is a passive technique it is necessary to make a monitoring and to wait for the occurring of damage.

The structure must be under loading to stimulate the evolution of the defect.

The choice of the sensors is a condition for obtaining reliable results.

The grid repartition of the sensors is important if the location of the events is required.

Up to now it is difficult to give accurate quantitative information on the defect range.

Up to now it remains difficult to cluster different events from a large dataset.

## References

- Breyse D., Abraham O. (2005) *Méthodologie d'évaluation non destructive de l'état d'altération des ouvrages en béton*, D. Presses de l'Ecole Nationale des Ponts et Chaussées, ISBN 2-85978-405-5.
- De Oliveira R., Marques A.T. (2008) Health monitoring of FRP using acoustic emission and artificial neural networks, *Computers & Structures*, 86, n. 3-5, p. 367–373.
- Grösse C.U., Ohtsu M. (2008) *Acoustic Emission Testing*, Springer Editions, 408 pp.
- Grösse C.U., Finck F., Kurz J.H., Reinhardt H.W. (2004) Improvements of AE technique using wavelet algorithms, coherence functions and automatic data analysis, *Construction and Building Materials*, Vol. 18, 203–213.
- Rusch H. (1959) Physical Problems in the Testing of Concrete. *Zement Kalk-Gips* 12, 1, 1–9.
- Shigeishi M., Ohtsu M. (2001) Acoustic emission moment tensor analysis: development for crack identification in concrete materials, *Construction and Building Materials*, Vol. 15, 311–319.

## 7 Ground Penetrating Radar

**Johannes Hugenschmidt and Jean-Paul Balaysac**

Ground-Penetrating-Radar (GPR) is an electromagnetic investigation method. It is also known as Surface Penetrating Radar, Electromagnetic Reflection Method or Radar. Main advantages of the method are that is non-destructive and fast (hundreds of measurements per second) and that it can be used in non-contact mode.

### 7.1 *Physical principles and theory*

Radar (**R**adio **D**etection and **R**anging) and Ground-Penetrating-Radar are electromagnetic methods. In principle GPR can be used in reflection or transmission mode. As reflection methods are by far the widely used, the following description will focus on this mode. The basic principle is presented in Fig. 2.1, where an electromagnetic pulse is emitted via a transmitter antenna, reflected at the surface and interior layer boundaries of an object and recorded via the receiver antenna.

Fig. 2.1 GPR principle

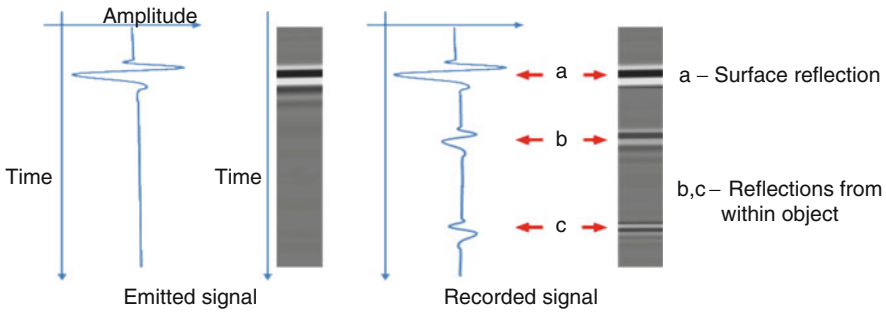
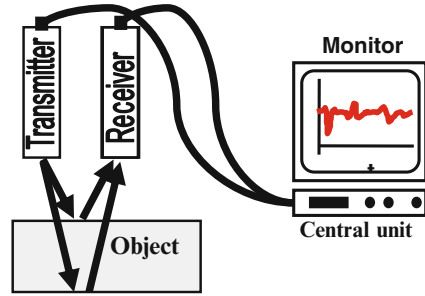


Fig. 2.2 Emitted and recorded signals

A sketch of the emitted and recorded signal is presented in Fig. 2.2 where the vertical axis is a time axis.

The following description will focus on Ground-Penetrating-Radar working in the time-domain. Systems working in the frequency-domain (stepped frequency systems) are also available but their dissemination is rather limited.

An electromagnetic impulse is emitted via an antenna. It propagates with the propagation velocity

$$v = \lambda * f \tag{Eq. 1.}$$

with  $v$  = propagation velocity,  $\lambda$  = wavelength,  $f$  = frequency.

In order to obtain an impulse of finite length, a range of frequencies is used. The larger the bandwidth of this range, the shorter is the emitted impulse. GPR antennas are therefore usually denoted by their centre-frequency. Typically antennas with a higher centre-frequency also have greater bandwidth and shorter pulse length.

The propagation of electromagnetic waves in materials is characterized by the dielectric permittivity  $\epsilon$  ( $\epsilon = \epsilon_r \epsilon_0$ ), conductivity  $\sigma$  and magnetic susceptibility  $\mu$  ( $\mu = \mu_r \mu_0$ ).  $\epsilon_0$  and  $\mu_0$  are constants with  $\epsilon_0 = 8.85 \cdot 10^{-12} \text{ A}^2 \text{ s}^2 / \text{Nm}^2$  and  $\mu_0 = 4 \pi \cdot 10^{-7} \text{ N} / \text{A}^2$ . From Maxwell's equations it can be derived that:

$$v = 1 / \sqrt{(\epsilon_r \epsilon_0 \mu_r \mu_0)} \tag{Eq. 2.}$$

In vacuum ( $\epsilon_r = \mu_r = 1$ ) this leads to

$$v = 1/\sqrt{(\epsilon_0 \mu_0)} = 2.998 \cdot 10^8 \text{ m/s} = \text{speed of light } c \quad \text{Eq. 3.}$$

For all non-ferromagnetic materials (ferromagnetic materials are not inspected with GPR due to their high conductivity)  $\mu_r$  can be approximated as 1 leading to  $\mu = \mu_0$ . Thus, the signal velocity for such materials can be described as

$$v = c/\sqrt{\epsilon_r} \quad \text{Eq. 4.}$$

which means that for practical purposes the signal velocity within a material depends on  $\epsilon_r$  only. If an electromagnetic wave hits an interface, part of the energy will be transmitted and part will be reflected. For a plain electromagnetic wave in a low loss material hitting at vertical incidence an interface between two materials with  $\epsilon_1$  and  $\epsilon_2$ , the reflected wave can be described as

$$\text{Reflected Wave} = R * \text{Incident Wave}$$

with

$$R = (\sqrt{\epsilon_1} - \sqrt{\epsilon_2})/(\sqrt{\epsilon_1} + \sqrt{\epsilon_2}) = \text{reflection coefficient} \quad \text{Eq. 5.}$$

This means that there is no reflection if  $\epsilon_1 = \epsilon_2$  (materials with identical properties) and the reflection amplitude becomes negative (phase shift by 180 degrees) if  $\epsilon_2 > \epsilon_1$ .

The time a GPR signal requires to travel through a material layer, get reflected and travel back through the layer is

$$\text{Two-way-traveltime} = \text{twt} = 2 D / v \quad \text{Eq. 6.}$$

with D being the thickness of the layer. If this thickness has to be computed from twt this equation can be rearranged to

$$D = \text{twt } v / 2 \quad \text{Eq. 7.}$$

This corresponds to the usual case where the thickness is computed with a known twt derived from the GPR data. The velocity v, necessary to compute depths or thicknesses from twt is a priori unknown. It can be estimated using experience or velocity tables, calibrated by comparison of twt with known thicknesses or by special setups during GPR data acquisition. Equation 0 is valid only if the distance between transmitter and receiver is zero or small enough to be neglected.

The ability of the method separating single objects (lateral resolution) is limited by the size of the Fresnel region which characterizes the area where reflected waves

add together constructively. Single points within this area cannot be distinguished by the GPR signal. The radius of the Fresnel region is described as

$$r = \sqrt{(D v / 2 f)} \quad \text{Eq. 8.}$$

Thus lateral resolution increases with frequency  $f$  and decreases with the depth (distance)  $D$  of the target.

## 7.2 *Equipment and handling*

Today a wide range of GPR-equipment from different manufacturers is available. A GPR system consists of one or several antennas, a central unit usually including a monitor for real time data display and accessories such as cables and energy supply.

### Antennas

The frequency content of the emitted and recorded GPR signal is mainly defined by the antenna. As a general rule of thumb it can be said that the higher the centre frequency of the antenna, the better the resolution but the lower the depth of penetration of the GPR signal and thus the possible depth of investigation. This means that the choice of the appropriate antenna(s) is crucial for the success of GPR investigations. Today antennas with centre frequencies between some MHz (low resolution, high depth of penetration, for geological applications) and some GHz (high resolution, low depth of penetration, used for non-destructive –testing) are available. Antennas can be monostatic (transmitter and receiver at fixed distance in the same box) or bistatic (transmitter and receiver as separate units. Depending on the antenna type and characteristics antennas are coupled to the object or used in non-contact mode (e.g. horn antennas).

### Central unit

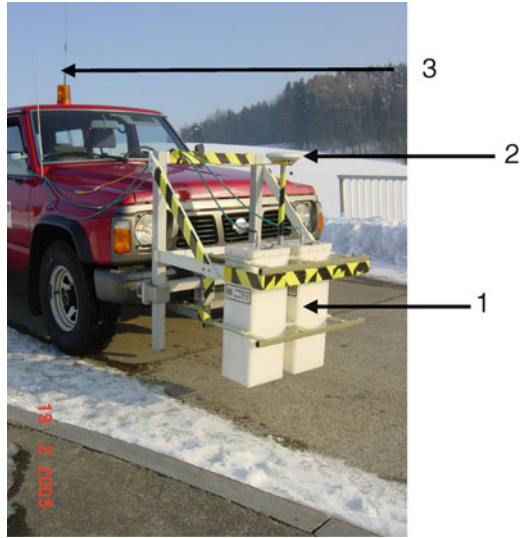
Central units have one or several channels for using one or several antennas at the same time. The possible data acquisition rate (number of measurements per second) depends mainly on the central unit and can reach up to several hundred of measurements per second. Data storage and real time display are other tasks performed by the central unit. Often data can be processed in real time for an enhanced display of the data.

### Accessories

As GPR is a fast and non-contact method, it can be used for the inspection of large structures such as roads or bridges. In this context the knowledge of the position of each measurement is essential. Modern surveying equipment such as GPS or automated theodolites can provide a means for an efficient position control.

Acquisition of GPR data is only one step of a GPR survey which is followed by data processing and interpretation. The availability of appropriate software is essential for performing those steps satisfactorily.

**Fig. 2.3** Mobile GPR-system  
(courtesy EMPA)



### Example

In Fig. 2.3 a mobile acquisition system is shown which is used for the inspection of roads and bridges. The two horn antennas (arrow 1, transmitter and receiver) are mounted in a height of about 0.25m above the ground. This facilitates data acquisition while the vehicle is moving. The GPS-antenna (arrow 2) is sitting on top of the GPR antennas for position control. A radio antenna (arrow 3) enables the communication of the on-board GPS-system with the GPS base-station thus ensuring an accuracy of the position control of some millimetres.

## **7.3 Guidelines and standards**

There is a range of standards and guidelines available describing the application of the GPR method to concrete and related problems. A selection is listed below.

- ASTM D4748-06 Standard Test Method for Determining the Thickness of Bound Pavement Layers Using Short-Pulse Radar
- ASTM D6087-07 Standard Test Method for Evaluating Asphalt-Covered Concrete Bridge Decks Using Ground Penetrating Radar
- ASTM D6429-99(2006) Standard Guide for Selecting Surface Geophysical Methods
- ASTM D6432-99 Standard Guide for using the Surface Ground Penetrating Radar Method for Subsurface Investigation
- DGZfP, Merkblatt über das Radarverfahren zur Zerstörungsfreien Prüfung im Bauwesen (B10), Deutsche Gesellschaft für Zerstörungsfreie Prüfung e.V., Berlin (2001) (Technical guideline, in German)
- The Concrete Society, Technical Report 48, Guidance on Radar Testing of Concrete Structures



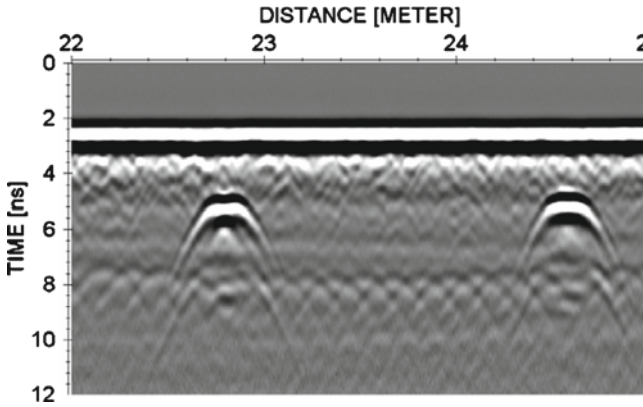


Fig. 2.4 Raw data

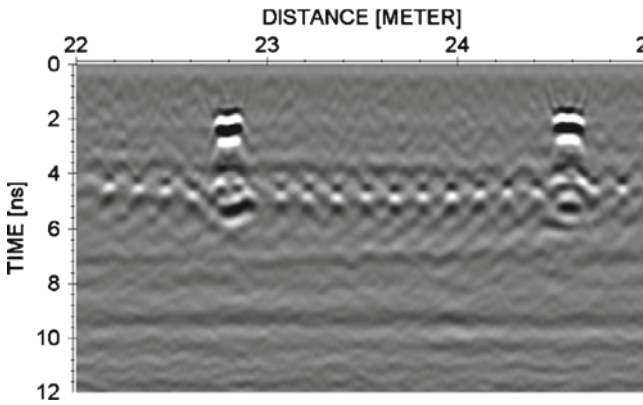


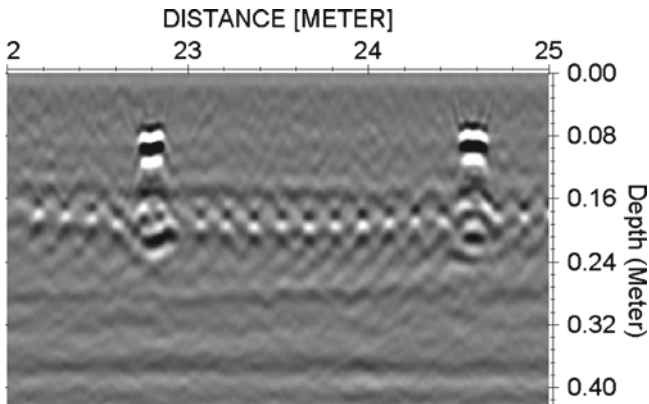
Fig. 2.5 Processed data

#### 7.4 *Data processing, calibration and interpretation*

Data processing is an essential step within a GPR survey. The optimal processing sequence depends on the GPR data, the object under inspection and the problem to be solved by the GPR survey. Some common aims of data processing are:

- Improvement of signal/noise ratio
- Correction of surface reflection to time/depth zero
- Migration (correction of the position of reflection energy that has been reflected sideways)
- Gain correction (amplification of signals depending on twt)

An example of a simple processing sequence applied to data acquired on an industrial railway track embedded in concrete is presented in Fig. 2.4 (raw data) and Fig. 2.5 (processed data). The length of the section shown is 3.0 metres, the vertical



**Fig. 2.6** Data with interpretation

time scale is 12 nanoseconds. The processing sequence included a bandpass filter (improvement of signal/noise ratio), the correction of the reflection at the concrete surface (black band in Fig. 2.4) to time 0, migration (focussing of energy that has not been reflected vertically but sideways) and gain correction (amplification with respect to twt).

In Fig. 2.6 the original time scale has been replaced by a depth scale. In order to do this the signal velocity within the material has to be calibrated with a core, obtained from the GPR data or estimated. In this example an estimated signal velocity within concrete of 0.08 m/ns was used for time-depth conversion.

Interpretation is the final step of a GPR inspection during which reflections are related to physical structures within the object. The many reflections distributed on the whole profile at 0.2 m in Fig. 2.6 have been interpreted as single bars of a layer of rebar, while the two reflections at 22.8 m and 24.6 m have been interpreted as sleepers embedded in concrete.

## 7.5 Applications, reliability of results and limitations

The GPR method can be applied to a wide range of problems, such as:

- Determination of layer thicknesses: concrete cover of rebar, asphalt pavement, concrete tunnel walls, subbase and geological layers
- Locating of structures: rebar, tendons or tendon ducts, anchors, dowels, cavities...
- Identification of material properties: humidity, chloride content, voids, air content. In general, it can be stated that the investigation of material properties is more demanding than the investigation of structural elements and in many cases still under development. In this case, other characteristics of the the GPR signal can be analyzed, like the direct wave propagation and its attenuation (Sbartai et al., 2007).

(Daniels, 2004) gives a detailed description of GPR and its applications.

Several studies have investigated the accuracy of GPR results [(Hugenschmidt and Mastrangelo, 2006), (Maser et al., 1994), (Maser (1996), (FDoT, 2000), (Willet and Rister, 2002), (Al Qadi et al., 2003)]. There are several limitations restricting the use of GPR and the accuracy of results. We have seen (equation 0) that a sufficient contrast in material properties is required if the interface between two materials has to be investigated. Without such contrast the boundary will not appear in the GPR data. If the thickness of a certain layer has to be investigated, the signal velocity within this layer has to be known (equation 0). If the velocity is calibrated with a single core and used for the time to depth conversion, this implies the assumption of constant velocity within the layer. This assumption is used successfully in many cases. However, it should be kept in mind that existing velocity variations will lead to errors in the result for the layer thickness.

The attenuation of the GPR signal within materials is caused by many factors, the electrical conductivity being an important factor for practical purposes. GPR waves in conducting materials lead to stray currents reducing the depth of penetration of GPR signals. Within certain limits this can be avoided using low frequency antennas (in most materials lower frequency waves experience less damping) but this will lead to a reduced resolution (equation 0) and may therefore not be feasible.

As described above interpretation links reflections in GPR data to physical structures within the object under inspection. In many cases an unambiguous relation between reflections and physical structures is not straightforward. In such cases it is a necessity to have additional information such as cores or plans available to support the interpretation, in all other cases the availability of such additional information is still desirable.

## References

- Al Qadi I., Lahouar S., Loulizi A. (2003) GPR, From State of the art to the State of the art of practice, Proc. NDT-CE 2003, Berlin, Germany.
- ASTM (2005) Standard Guide for using the Surface Ground Penetrating Radar Method for Subsurface Investigation, Book of Standards 04.09, D6432–99.
- ASTM (2006) Standard Guide for selecting Surface Geophysical Methods, Book of Standards 04.09, D6429–99.
- ASTM (2006) Standard Test Method for Determining the Thickness of Bound Pavement Layers using Short-Pulse Radar, Book of Standards 04.03, D4748–06.
- ASTM (2008) Standard Test Method for Evaluating Asphalt-Covered Concrete Bridge Decks using Ground Penetrating Radar, Book of Standards 04.03, D6087–08.
- Bungey J.H. (2004) Sub-surface radar testing of concrete: a review, *Constr. Build. Mat.*, 18, 1, pp. 1–8.
- Daniels D. (2004) *Ground Penetrating Radar*, 2nd edition, The Institution of Electrical Engineers.
- Deutsche Gesellschaft für zerstörungsfreie Prüfung (2008) Merkblatt über das Radarverfahren zur zertörungsfreien Prüfung im Bauwesen, Merkblatt B10.
- FDoT (2000) Florida Department of Transportation Research Center, Research Today, Fall 2000, Tallahassee, USA.

- Hugenschmidt and Mastrangelo (2006) GPR inspection of concrete bridges, *Cement & Concrete Composites*, 28, pp. 384–392.
- Maser K. (1996) Evaluation of pavements and bridge decks at highway speed using ground penetrating radar, ASCE Str. Congress XIV, Chicago, USA.
- Maser K., Scullion T., Roddis W.M., Fernando E. (1994) Radar for pavement thickness evaluation, Non-destructive testing of pavements and backcalculation of moduli, ASTM STP 1198, Philadelphia, USA.
- Sbartai Z.M., Laurens S., Rhazi J., Balayssac J.P., Arliguie G. (2007) Using radar direct wave for concrete condition assessment: correlation with electrical resistivity, *J. Appl. Geophysics*, Vol. 62, pp. 361–374.
- The Concrete Society (1997) Technical Report 48, Guidance on Radar Testing of Concrete Structures.
- Willet D.A., Rister B. (2002) Ground penetratin radar « pavement thickness evaluation », Res. Rep. KTC-02-29/FR101-00-1F, Kentucky Transp. Center, Univ. Kentucky, Lexington, USA.

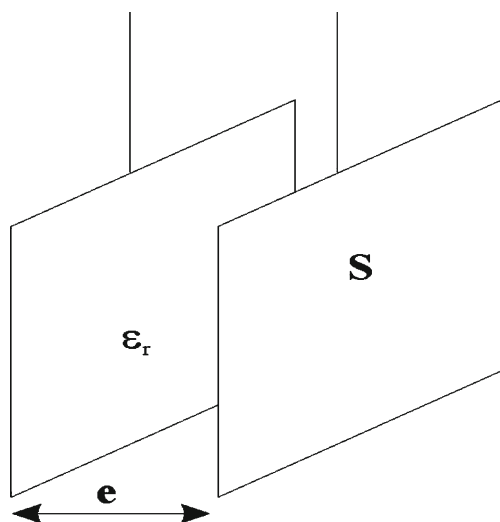
## 8 Capacitive technique

**Xavier Dérobert**

### 8.1 Physical principles and theory

The principle consists in placing two electrodes (or more) on the outer surface of a medium, and applying an electric current between them through a resonant circuit. The combination electrodes/medium forms a capacitor, and changes in capacitance are indicative of internal constituents of the medium (like the nature of its components or the moisture content).

Indeed, the configuration of a conventional parallel plate capacitor would require a contact with the material under study from two opposite sides (Fig. 2.1).



**Fig. 2.1** The simplest type of capacitive probe is based on the so-called parallel plate capacitor

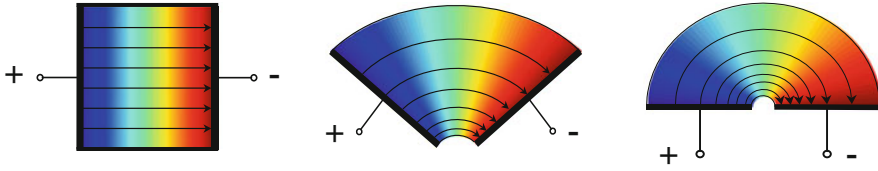


Fig. 2.2 Configuration of a capacitive sensor designed for cover concrete

As a first approximation (the result is only valid when the spacing between the plates is much smaller than their dimensions), the value of the capacitance  $C$  (in Farad) is obtained from the following formula:

$$C = \epsilon_0 \epsilon_r S / e \quad \text{Eq. 1.}$$

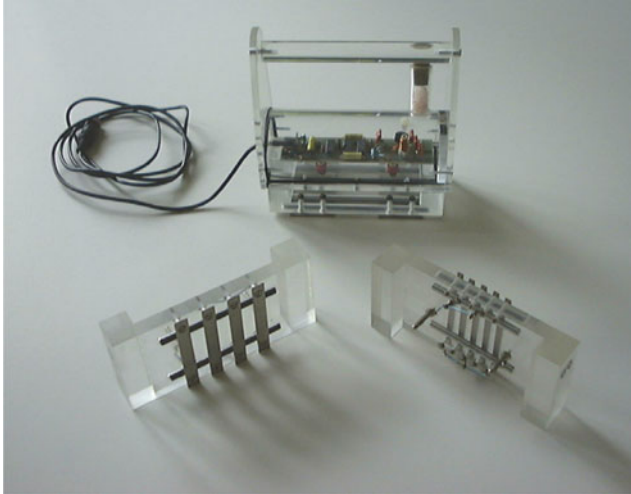
where  $S$  [ $\text{m}^2$ ] is area of the electrodes,  $e$  [m] the distance between them,  $\epsilon_0$  [ $\sim 8.854 \cdot 10^{-12} \text{ F}\cdot\text{m}^{-1}$ ] the permittivity of vacuum, and  $\epsilon_r$  the dielectric constant which determines some kind of ability to store electric charge.

For the application related to measurements of the moisture content of cover concrete, the difference is that the electrodes of the sensor are placed next to one another (Fig. 2.2), in order to provide a sufficient penetration depth of the electric field between sensing and driven devices on one side of the material under study. Then, this configuration can be seen as the result of gradually opening the angle between two electrodes of a parallel plate capacitor (Fig. 2.2, from left to right).

However, for measurements carried out from the surface, neither the volume of investigation, nor the penetration depth are precisely defined (which can vary from few millimeters to several centimeters depending to the geometry of the electrodes). Actually, the situation is complex, because the system appears as a heterogeneous mixing of dielectric materials and conductors. As a consequence, there is no analytical formulation (like for the parallel plate capacitor) giving the value of the capacitance as a function of the characteristics of the investigated media, and one has to calibrate the measurements on known homogeneous materials.

Spaces on both sides of the electrodes intervene, and the resulting layout doesn't constitute a single capacitor but a set of two capacitors in parallel. The first one ( $C_i$ ) incorporates the medium under survey and the second one ( $C_e$ ) the surrounding environment (principally air and Plexiglas making up the probe), so that the total capacitance is the sum.

The capacitance is determined by means of a (high frequency) resonant circuit delivering an alternative voltage. The resonant frequency shift is then obtained by a mere frequency analyzer. The relationship between the capacitance and the resonant frequency shift can be obtained, knowing the inductance of the circuit. For practical reasons, since we are interested in the changes (whereas  $C_e$  is a constant, provided that some precautions are taken to prevent "hands effect" and interference of external electrical field by adding a screen), we can deal with  $C_i$ , the capacitance of the inside volume.



**Fig. 2.3** Prototype of a capacitance probe for measuring the water content of flat concrete structures, with its sets of electrodes

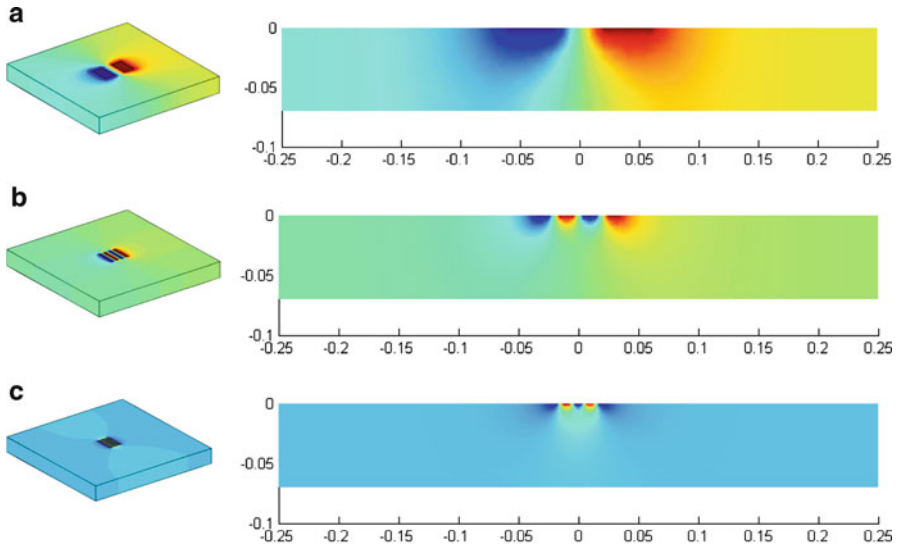
## 8.2 *Measuring equipment and handling*

Applications of capacitive techniques have been various in the civil engineering field, from the estimation of water content of soils (Eller and Denoth, 1996; Johnson et al. 2004), including the ice-water phase transition (Fen-Chong et al., 2006), and the snow (Louge et al., 1998) study, to the dielectric characterization of concrete mixing (Al-Qadi et al., 1995; Diefenderfer et al., 1998).

This technique has already been studied over few decades in the French network of Public Works Laboratories, initially for the measurement of water content in soils (Baron and Tran, 1977; Blaszczyk et al., 1993), and afterwards on reinforced concrete before being adapted to post-tensioned structures (Dupas et al., 2001; Iaquina, 2004). Lately, capacitive measurements were performed on concrete slabs, stored in homogeneous known water content (Derobert et al., 2008).

In order to minimize the influences of temperature and ionic conduction, the oscillator of the resonant circuit operates at 65 MHz. Practical reasons (related to the transmission of information over long distances) require the implementation of a frequency divisor to decrease the signal towards lower frequencies in the range of 5 000 Hz.

The current system can have the possibility of employing different configurations of electrodes in order to reach various depths of penetration, as illustrated on the Fig. 2.3: large plates (70\*40 mm, 40 mm spacing), average size plates (70\*10 mm, 10 mm spacing) and small plates (70\*5 mm, 5 mm spacing).



**Fig. 2.4** Comparison of electric potential calculations for a 70 mm-thick slab of 500x500 mm. On the left side, equipotential surfaces for: large, average size and small plates. On the right side are shown the corresponding vertical cross section plots in the center of the concrete slab

### 8.3 Data processing, calibration and interpretation

The main purpose, when employing electrodes of varied dimensions and spacing, is to reach different penetration depths in order to acquire an information about the gradient of moisture inside the cover concrete. Unfortunately, because of a strong dependency on the intrinsic material characteristics, it is rather difficult to delimit the investigation.

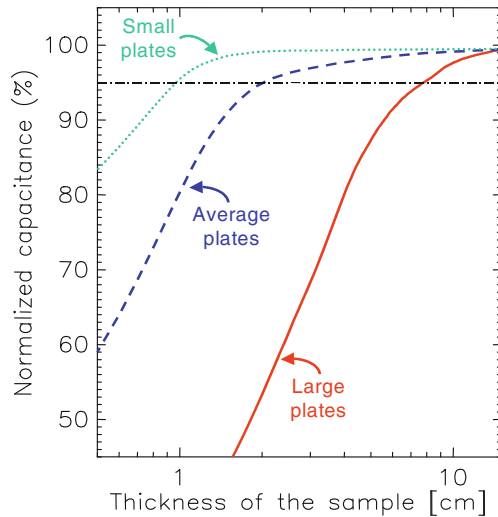
However, we can have an indication of the inspected volume by considering the three arrangements of electrodes placed in the center of the upper face of a concrete slab (homogeneous), as displayed on the Fig. 2.4a-c. These numerical simulations were conducted with the commercial finite elements software package FEMLAB 2.3 [FEM 03].

Basically, we handled a three-dimensional electrostatics model of the system with linear homogeneous isotropic materials. Modeling the electric field is carried out using the electric potential  $V$ , calculated from the Laplace equation (eq. 2). Regarding the boundary conditions, the electrodes are equipotential surfaces, and the remainder is considered as insulated electrically

$$\Delta V = 0 \quad \text{Eq. 2.}$$

From a qualitative point of view, the intensity of the electric field is extremely variable according to the configuration, in particular along the depth in the sample.

**Fig. 2.5** Normalized capacitance values as a function of the thickness of a concrete sample for the different probes geometry



Furthermore, the influence of the probe ranges from several centimeters (for that equipped with the larger set of electrodes), to a few millimeters (when the device is mounted with the smaller plates). Figure 2.5 presents the normalized capacitance values as a function of the concrete thickness coupled with the three sets of electrodes.

These values should be regarded as an order of magnitude (it may depend on the moisture content), but it can be taken as a good indicator of the penetration depth of the sensors (the effective penetration depth being identified at 5% reduction of from the maximum capacitance – arbitrary choice). Then we can estimate to 5-7 mm, 2-3 cm and 7-8 cm the depth penetration of the small, the average and the large size electrodes respectively.

Calibration can be done on homogeneous materials, which dielectric constants are known and non frequency dependent. For that, measurements were done with the panel of electrodes on PTFE, PVC, granite, marble and limestone respectively, thus corresponding to increasing dielectric constant. Results are presented in Fig. 2.6, and show linear relations between the measured frequency and the electromagnetic property of homogeneous media. The measurements are subtracted to a reference done in the air in order to remove the effect of the environment, including the sensor itself and the hand of the operator. The slopes of each calibration curve express the capacitance or the sensitivity of each electrode to the dielectric constant of the surveyed medium.

The various slopes showing the sensitivity of the electrodes are due to their dimension – and then their capacitance values – associated to the chosen frequency band in the resonant circuit of the sensor.

Then, capacitive measurements done on concretes, and transformed in dielectric constant values due to the calibration curves from Fig. 2.6, can provide information on the moisture of the mixing, the dielectric constant being related to the volumic



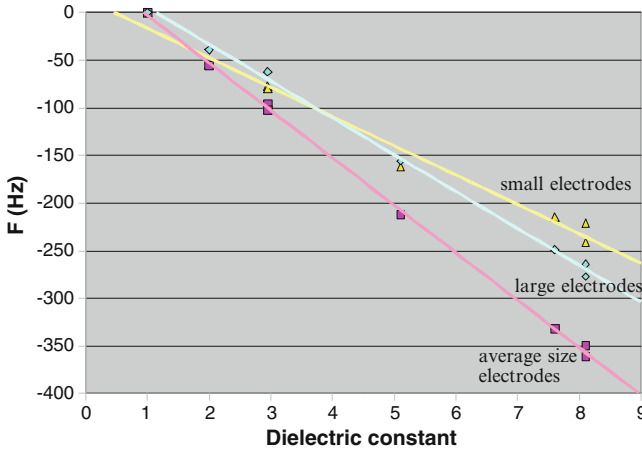


Fig. 2.6 Capacitive calibration of the set of electrodes on homogeneous media

water content of such material. Moreover, the variation of depth penetration of the set of electrodes can give an indication of the hydric gradient with depth.

### 8.4 Limitations and reliability

The most important limitations of the technique are related to the flatness of the concrete surface, the absence of knowledge of the location of the reinforcement and the need of calibration on the concrete material itself in order to obtain water content values.

Concerning the flatness of the surface, all the effects due to the building of the concrete structure, such as border of successive formworks presenting steps, or important spherical voids due to air bubbles, can lead to important errors.

For accurate measurements, we have to get the information of the location of the rebar in order to do punctual measurements in the center of the reinforcement mesh. Indeed, the presence of rebar in the coupling volume under the electrodes induces a slight decrease of the measurement values, which could be interpreted as a dryer material than the reality.

Then, the knowledge of an equivalence of dielectric constant remains insufficient to get water-content accurate values. Knowing the strength of concrete (C25, C40,...) can give a good indication of the relation between the capacitive measurements and the water content, but keeping in mind that the nature of the aggregates themselves biases the relation.

For the second aspect more related to the reliability, the relative measurements induce a strong limitation of the temperature influence and prevent any “hand effect”. Moreover, the average of elementary measurements (~5) a few centimeters around the

measurement location decreases the noise in the value and strongly diminishes the influence of the size of aggregates in the mixing considered as homogeneous material.

At last, this technique is limited to the water content estimation of homogeneous concrete which thickness should remain above 10 cm.

## References

- Al-Qadi I.L., Hazim O.A., Su W., Riad S.M. (1995) Dielectric properties of Portland cement concrete at low radio frequencies. *Journ. Mat. Civil Eng.*, 7, 192–198.
- Baron J.P., Tran N.L. (1977) Méthodes de mesure et de contrôle des teneurs en eau de matériaux dans les LPC. *Bull. Lab. Ponts Chauss.*, 87, 85–96.
- Blaszczuk F., Blaszczuk R., Trochet B., Bigorre M., Dupas A. (1993) Mesure de la teneur en eau en continu d'un matériau granulaire : TRITON II. Mesure à la jetée d'un transporteur. *Bull. Lab. Ponts Chauss.*, 186, 85–87.
- Dérobot X., Iaquina J., Klysz G., Balyssac J.P. (2008) Use of capacitive and GPR techniques for non-destructive evaluation of cover concrete. *NDT&E Int.*, 41, 44–52.
- Diefenderfer B.K., Al-Qadi I.L., Yoho J.J., Riad S.M., Loulizi A. (1998) Development of a capacitor probe to detect subsurface deterioration in concrete. *Mat. Res. Soc. Symp. Proc.*, 503, 231–236.
- Dupas A., Sudret J.P., Chabert A. (2001) Méthode de diagnostic de câbles de précontrainte externe contenus dans des gaines. French Patent n° 0107719, INPI, Paris.
- Eller H., Denoth A. (1996) A capacitive soil moisture sensor. *Journ. Hydro.*, 185, 137–146.
- FEMLAB (2003) Reference manual - Version 2.3. COMSOL, <http://www.comsol.com>
- Fen-Chong T., Fabbri A., Azouni A. (2006) Transient freezing-thawing phenomena in water-filled cohesive porous materials. *Cold Reg. Sci. Techn.*, 46, 12–26.
- Iaquina J. (2004) Contribution of capacitance probes for the inspection of external prestressing ducts. *World Conf. NDT Proc.*, Montréal.
- Johnson R.H., Poeter E.P. (2005) Iterative use of the Bruggeman-Hanai-Sen mixing model to determine water saturations in sand. *Geophys.*, 70, K33–K38.
- Louge M.Y., Foster R.L., Jensen N., Patterson R. (1998) A portable capacitance snow sounding instrument. *Cold Reg. Sci. Techn.*, 28, 73–81.

## 9 Electrical resistivity measurement

**Jean-François Lataste**

### 9.1 Physical principle and theory

Electrical resistivity measurements on reinforced concrete are used to assess probability of corrosion. They are sensible to factors influencing rebar corrosion (salt and moisture) and allow a more accurate interpretation of electrochemical measurement results (polarization resistance or half cell potential measurement).

Due to their sensitivity to on site concrete parameters, research is now oriented to the use of electrical resistivity to assess concrete conditions directly.

Electrical conduction in porous materials is described by the empirical Archie's law (Archie, 1942):

$$\rho_r = a \phi^{-m} s^{-n} \quad \text{Eq.1}$$

**Table 2.1** parameters of Archie's law, after (Naar, 2006)

Parameter	a	m	n
	Depend on lithology	Depend on cementation	
Value for rocks	0.6 to 2 (increases with porosity)	1.3 to 2.2 (increases with cementation)	About 2
Value for concretes	0.1 to 0.8	4.6	2.43

where  $\rho_r$  is the resistivity of rock,  $\phi$  the porosity,  $\rho_w$  the resistivity of the fluid in the rock,  $s$  the saturation degree,  $a$ ,  $m$  and  $n$  are three constants linked to the studied material.

This empirical relation has been established for rocks, but works show it is possible to use for concrete. Parameters have then to be determined (Table 2.1).

The measured resistivity is linked to nature and volume of fluids in concrete (parameters  $\rho_w$ , and  $s$  of Archie's law), but also to microstructural parameters of concrete (porosity, interconnectivity of pores, tortuosity (Andrade et al., 2000)). Thus, electrical resistivity is considered as an indicator of concrete transfer properties. Recent works suggest using it as an indicator of durability to characterize concretes (Baroghel Bouny et al., 2004).

Any significant change in porosity (between different types or because of an alteration) influence electrical resistivity properties of concrete. Any interface either electrically insulator or conductive can also have consequences for resistivity measurements.

## 9.2 Measurement techniques and handling

### 9.2.1 Laboratory

The laboratory measurement of the resistivity of concrete can be done using two probes or four probe equipment. In a two probe arrangement the sample (poured in mould, or from coring) is saturated by water and put between two metallic probes (equipped with moistened sponges to improve electrical contact – see Fig. 2.1). An electrical current ( $I$  in amperes) is injected between the probes and the potential difference ( $\Delta U$  in volts) is measured. The electrical resistance ( $R$  in Ohm) is calculated by Ohm's law:

$$R = \Delta U / I \quad \text{Eq. 2.}$$

The pressure on probes is constant and fixed by the constant mass. A calibration of sponge resistivity is done (a measure with the two sponges and without any sample), to extract the exact resistance of sample:

$$R_{\text{sample}} = R - R_{\text{sponges}} \quad \text{Eq. 3.}$$

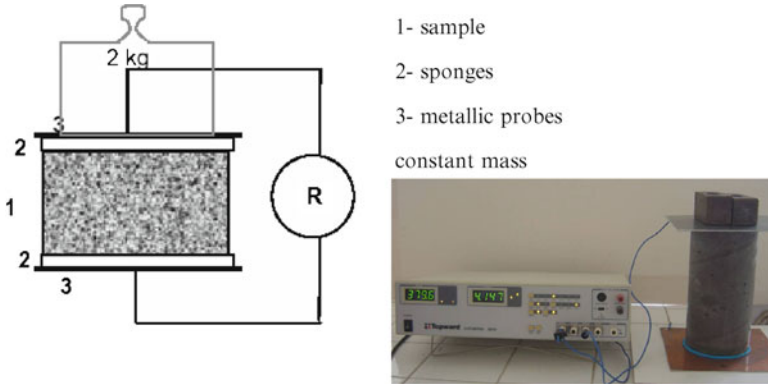
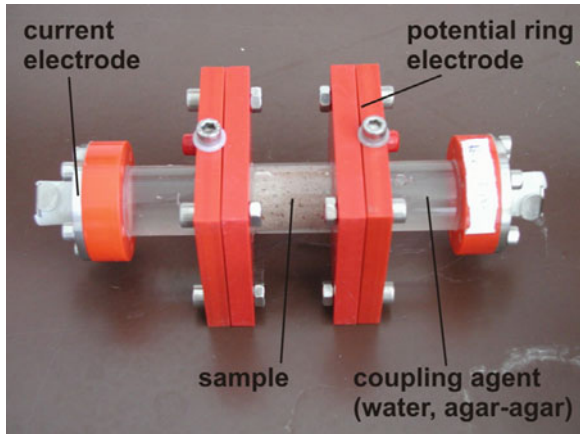


Fig. 2.1 Two probe laboratory electrical resistivity measurement device

Fig. 2.2 Four-probe laboratory electrical resistivity measurement device



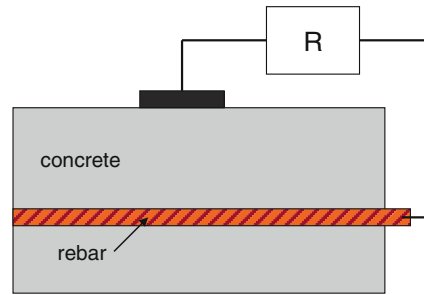
Measurement can also be done with a four probe arrangement. Only the device change, the principle is the same. The potential measurement is done at separate electrodes (Fig. 2.2.). Main advantage is the independence from any contact resistances ( $R_{\text{sponges}}$  in the formulation above). The measurement cell is somewhat more complicated, but accuracy is significantly higher. For impedance measurements (see §9.2.4) in the low frequency range the use of four electrode arrangements is a requirement.

Finally, the resistivity ( $\rho$  in Ohm.m) of material is deduced integrating geometrical factors (or cell factor): height ( $l$  in m), and section ( $S$  in  $\text{m}^2$ ):

$$\rho = R_{\text{sample}} S / l \tag{Eq. 4.}$$

Resistivity is independent of geometry and size of sample. The technique allows characterisation of concrete under controlled conditions. This resistivity is

**Fig. 2.3** Electrical resistivity measurement device for cover concrete characterization



representative of average properties of material at the scale of sample. A resistivity variation in the sample cannot be characterised.

This method is proposed to assess properties of initial concrete as a conformity test for new concrete, as for example today compressive strength test.

### 9.2.2 On site measurement of cover concrete resistivity

Electrochemical measurements to detect corrosion activity in reinforced concrete are strongly influenced by the concrete's resistivity. Simple two probe measurements are providing the required information. Resistance ( $R$  in Ohm) between a probe at the concrete surface (generally a little disc with  $D$  its diameter in m) and the reinforcement is measured (Fig. 2.3). The resistance ( $R$  in Ohm) is calculated from the potential drop measured by an electrical current impulse (Feliu et al., 1990). The resistivity ( $\rho$  in Ohm.m) is given as:

$$\rho = 2 R D \quad \text{Eq. 5.}$$

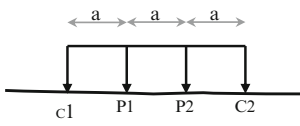

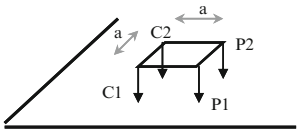
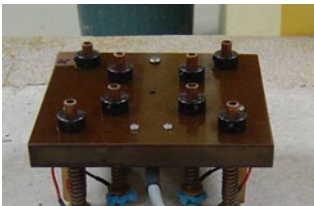
This approach is generally used simultaneously to electrochemical measurements because it needs to connect probe to reinforcement. The measure has to be done right to the rebar. It complete electrochemical measurement (corrosion rate).

### 9.2.3 On site measurement with four probe devices

General on site resistivity measurement have to be done with four probe devices. This approach is used to detect factors conditioning reinforcement corrosion (moisture, salts, etc.) and probability of corrosion (Polder et al., 2000). Some others applications have been developed independently of the rebar corrosion study (Sirieix et al., 2007), (Klysz et al. 2006).

An electrical current is between two probes ( $I$  in A). The potential difference ( $\Delta U$  in volts) is measured between two separate ones. By using Ohm's law  $R = \Delta U / I$ , the measured resistance ( $R$  in Ohm) is calculated. The size and geometry of the

**Table 2.2** devices for on-site measurements of electrical resistivity

Device	Geometrical factor
<p>Wenner configuration</p> 	 $k = 2 \cdot \pi \cdot a$
<p>Square configuration</p> 	 $k = \frac{2 \cdot \pi \cdot a}{2 - \sqrt{2}}$

electrode arrangement are taking into account to calculate the apparent resistivity ( $\rho_a$  in Ohm.m), by the geometrical factor  $k$  (in m):

$$\rho_a = k R \tag{Eq. 6.}$$

In homogeneous material the apparent resistivity equals true electrical resistivity. In structures with layers, inclusions or property variations, a mixed (“apparent”) resistivity is measured. True values can be approximately calculated from sets of measurements with different spatial sensitivity and mathematical inversion: this is called electrical resistivity tomography, still in development on concrete.

Two different electrode configurations are generally used (Table 2.2). The electrode distance  $a$  (m) influences the depth of investigation. Many devices are using  $a = 0,05$  m. By this way, concrete is characterised on the first few centimetres.

### 9.2.4 Frequency Domain Methods

Electrical resistivity measurements are normally done using direct current, in most cases alternating direction to avoid electrode polarisation. Using alternating currents at various frequencies additional parameters can be derived. Most of them are related to solid/liquid interfaces, thus providing information about the microstructure of concrete.

High frequency methods (several kHz – several MHz, Electrical Impedance Spectroscopy, EIS) can be used to assess the dielectric constant  $\epsilon$  (Ping Gu *et al.*, 1993). The technique consists in the measure of electrical responses (not only resistivity) of concrete for several signal frequencies. This technique is currently focused on the study of concrete hardening (Ping Xie *et al.*, 1993), or on the system

**Table 2.3** Corrosion speed probability from resistivity measurements

Electrical resistivity (Ohm.m)	Probability of corrosion speed
> 1000 – 2000	Negligible (concrete is too dry)
500 – 1000	Weak
100 – 500	Moderate to high (when steel is active)
< 100	Resistivity is not the driving factor of corrosion

rebar-concrete in the aim of rebar corrosion study (Koleva et al., 2008). The method is not well adapted to on site investigations, even some results are on monitoring of concrete structures (Ozyurt et al., 2006).

Low frequency applications (several mHz – several kHz, Spectral Induced Polarisation, SIP) are currently under research. Results from other material as masonry indicate, that SIP might be able to provide information about porosity and geometry related parameters as permeability or formation factors ( $F = a \varphi^{-m}$  in eq.1) as well as a method to distinguish between saturation and salt contamination effects (Kruschwitz, 2008).

### 9.3 Calibration, data processing, interpretation of results

As many factors are influencing the electrical resistivity the interpretation is mainly based relative variations. For characterisation of probability of corrosion by electrical resistivity, threshold values are proposed for on site assessment. The method measures only the presence of factors influencing rebar corrosion, which have both similar effects on resistivity: moisture and salts. Both decrease electrical resistivity (Table 2.3). But many cases prove the limitation of interpretation based on these thresholds. So today, engineers prefer to adapt the threshold values in each case by a visual inspection of rebars (opening a window in concrete).

### 9.4 Reliability and limitation of results

Resistivity of concrete is influenced by many parameters, linked with the material properties, with the structure or with the environment:

- Parameters depending on the concrete composition: cement type (Hammond and Robson, 1955), water/cement ratio (Hammond and Robson, 1955), (Whittington et al., 1981), aggregate (nature, quantity, etc.) (Millard, 1991),(Morris et al., 1996)
- Environmental factors: temperature (Spencer, 1937), moisture (Wolf and Lauer, 1980), salt ingress (Saleem et al., 1996)
- Geometrical effects: influence of rebar and edges (Millard, 1991), (Lataste et al., 2003b).

**Table 2.4** Some electrical resistivity ranges for concrete

Influence of concrete	Electrical resistivity (Ohm.m)	
Ordinary Portland Cement (35MPa)	500 – 1400	
Self compacting concrete (35MPa)	300 – 1000	
High Performance concrete (65MPa)*	850 – 1500	
Fibre Reinforced Concrete	80 – 400	

Influence of conditions	Electrical resistivity (Ohm.m)	
	Ordinary Portland Cement	Other concrete
Very wet, spayed atmosphere	50 – 200	300 – 1000
Natural atmosphere	100 – 400	500 – 2000
External atmosphere (she ltered concrete, 20°C/80%HR)	200 – 500	1000 – 4000
Carbonated concrete	1000 and more	2000 and more
Internal atmosphere ( 20°C, 50%RH)	3000 and more	4000 and more

\* Containing slag (>65%), or fly ashes (>25%), or silica fume (>5%)

The variation ranges for the resistivity depending on the value taken by some of these parameters are provided at Table 2.4. These multiple influences restrict the interpretation to the delineation of relative variations of resistivity. An isolated value of resistivity cannot be interpreted. However variations in time or geometry (lateral variations or in depth) make it possible to assess material or structure characteristics.

### 9.5 Guidelines for use, references, standards

Currently there are nor guidelines, references or standards available. Recommendations can be found. They give some elements allowing reliability of resistivity measurements (Polder *et al.*, 2000) (Chlortest, 2006)

### 9.6 On-going developments: problems under research, new questions, specific developments

Electrical resistivity is sensitive to many factors which are important for the assessment of concrete structures. Porosity, humidity and salt (e.g. chlorides) are three main parameters leading the electrical behaviour of material. So, resistivity has the potential to be used as an indicator for durability and to characterise the material. There for this this measure might be considered as laboratory conformity test in the future.

Main problem for interpretation of on site measurements in terms of the damage detection and assessment is to separate quantitatively the various factor influencing



the measurement. This point was studied in the frame of the French ANR-SENSO project, where two possibilities were identified:

- better definition of parameters  $a$ ,  $m$ , and  $n$  for concrete in the Archie law (for inverse analysis of measurements);
- using resistivity in combination with other techniques to assess values of porosity or saturation rate of concrete.

Others topics in progress are: on site crack investigation (Lataste et al., 2003a), characterisation of steel fibers in FRC (Lataste et al., 2008) (Ozyurt et al., 2006), electrical resistivity tomography (Chouteau et al., 2002), EIS for rebar corrosion assessment (Koleva et al., 2008), application of SIP techniques (Kruschwitz, 2008).

## References

- Andrade C., Alonso C., Arteaga A., Tanner P. (2000) Methodology based on the electrical resistivity for calculation of reinforcement service life. Fifth CANMET/ACI International Conference, 899–915.
- Archie G. (1942) The electrical resistivity log as an aid in determining some reservoir characteristics, Transaction of the American Institute of Mining and Metallurgical Engineers, vol. 146, pp. 54–62
- Baroghel-Bouny V. (2004) Conception des bétons pour une durée de vie donnée des ouvrages – maîtrise de la durabilité vis-à-vis de la corrosion des armatures et de l’alcali réaction, documents scientifiques et techniques de l’AFGC, 252p.
- CHLORTEST – Resistance of concrete to chloride ingress – From laboratory tests to in-field performance – Testing Resistance of Concrete to Chloride Ingress: – A proposal to CEN for consideration as EN standard (2006) 22 p.
- Chouteau M., Beaulieu S., Fréchette V., Toe E. (2002) Application de la tomographie de résistivité électrique aux infrastructures routières en béton, INFRA, Montréal, Québec.
- Feliu S., Andrade C., González J.A., Alonso C. (1996) A new method for in situ measurement of electrical resistivity of reinforced concrete, Material and Structures, vol. 29, pp. 362–365.
- Hammond E., Robson T. (1955) Comparison of electrical properties of various cement and concrete, The Engineer, vol. 199, pp. 78–80 and pp. 114–115.
- Klysz G., Lataste JF., Fnine A., Dérobert X., Piwakowski B., Buyle-Bodin F. (2006) Auscultation non destructive du chevêtre du pont de la Marque (59), Revue Européenne de Génie Civil, 10(1), pp., 1–24
- Koleva D.A., Van Breugel K., De Wit J.H.W., Van Westing E., Copuroglu O., Veleva L., Fraaij A.L.A. (2008) Correlation of microstructure, lectrical properties and electrochemical phenomena in reinforced mortar. Breakdown to multi-phase interface structures. Part I: Microstructural observations and electrical properties, Materials Characterization, vol. 59, pp. 290–300.
- Kruschwitz, S. (2008) Assessment of the complex resistivity behaviour of salt affected building materials. Ph.D. thesis, BAM/ TU Berlin.[http://www.bam.de/de/service/publikationen/publikationen\\_medien/dissertationen/diss\\_30\\_vt.pdf](http://www.bam.de/de/service/publikationen/publikationen_medien/dissertationen/diss_30_vt.pdf)
- Lataste JF., Behloul M., Breyse D. (2008) Characterisation of fibres distribution in a Steel Fibre Reinforced Concrete with electrical resistivity measurements, NDT&E international, 41(8), pp. 638–647.
- Lataste JF., Sirieix C., Breyse D., Frappa M. (2003a) Electrical resistivity measurement applied to cracking assessment on reinforced concrete structures in civil engineering, Non Destructive Testing and Evaluation International, vol. 36 n°6, pp. 383–394.
- Lataste JF., Sirieix C., Breyse D., Frappa M. (2003b) Improvement of electrical resistivity measurement for non destructive evaluation of concrete structures, 2nd International RILEM

- workshop on life and aging management on concrete structures, Paris (F), May 5-6 2003, pp. 93–102 (ISBN 2-912143-36-5).
- Millard S.G. (1991) Reinforced concrete resistivity measurements techniques, Proceedings of the Institution of Civil Engineers, Part 2, vol. 91, pp. 71–88.
- Morris W, Moreno E.I., Sagues A.A. (1996) Practical evaluation of resistivity of concrete in test cylinder using Wenner array probe, *Cement and Concrete Research*, Vol. 26, n 12, pp. 1779–1787.
- Naar S. (2006) Evaluation non destructive du béton par mesures de résistivité électrique et thermography infra rouge passive, Thèse de l'université Bordeaux 1, 248p.
- Ozyurt N., Mason T.O., Shah S.P. (2006) Non destructive monitoring of fiber orientation using AC-IS : An industrial-scale application, *Cement and Concrete Research*, Vol. 36, pp. 1653–1660.
- Ping Gu, Zhongzi Xu, Ping Xie, Beaudoin J.J. (1993) Application of A.C. Impedance techniques in studies of porous cementitious materials, (I) Influence of solid phase and pore solution on high frequency resistance, *Cement and Concrete Research*, vol. 23, pp. 531–540.
- Ping Xie, Ping Gu, Zhongzi Xu, Beaudoin J.J. (1993) A rationalized AC impedance model for microstructural characterization of hydrating cement systems, *Cement and Concrete Research*, vol. 23, n°2, pp.359–367.
- Polder R., Andrade C., Elsenser B., Vennesland O., Gulikers J., Weidert R., Raupach M. (2000) Rilem TC154-EMC: electrochemical techniques for measuring metallic corrosion, *Materials and structures*, vol. 33, pp. 603–611.
- Saleem M., Shameem M., Hussain S.E., Maslehuddin M. (1996) Effect of moisture, chloride and sulphate contamination on the electrical resistivity of Portland cement concrete, *Construction and Building Materials*, Vol. 10, n°3, pp. 209–214.
- Sirieix C., Lataste J.F., Breyse D., Naar S., Dérobert X. (2007) Comparison of non destructive testing : infrared thermography, electrical resistivity and capacity methods in a reinforced concrete structures Tarbes' precast duct, *Journal of Building Appraisal*, Vol. 3, n°1, pp.77–88
- Spencer R.W. (1937) Measurement of the moisture content of concrete, *Journal of the American Concrete Institute*, Vol. 9, n°1, pp. 45–61
- Whittington H.W., Mc Carter J., Forde M.C. (1981) The conduction of electricity through concrete, *Magazine of Concrete Research*, Vol. 33, n° 144, pp. 48–60.
- Woelfl G.A., Lauer K. (1980) The electrical resistivity of concrete with emphasis on the use of electrical resistance for measuring moisture content, *Cement Concrete and Aggregates*, Vol. 1, n°2, pp. 64–67.

## 10 Infrared thermography

**Didier Defer and Christiane Maierhofer**

### 10.1 Physical principles and theory

Infrared radiation covers the spectral range from 0.78 to 1,000  $\mu\text{m}$ . For standard application in infrared thermography, a range from 1.5 to 14  $\mu\text{m}$  is used. This type of radiation is mainly emitted by the object itself. Spectral range and intensity of the emitted radiation depend on the temperature, which describe the molecular movement, and the emissivity. For a black body, the spectrum of thermal radiation can be described by Planck's law (Eq. 1):

$$I_{\lambda}^{\text{black\_body}}(T) = \frac{C_1 \cdot \lambda^{-5}}{\pi \cdot \left[ \exp\left(\frac{C_2}{\lambda \cdot T}\right) - 1 \right]} \quad \text{Eq. 1.}$$

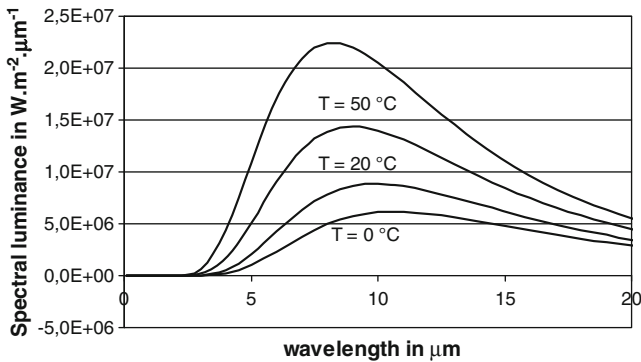


Fig. 2.1 Spectra of blackbody radiation vs wavelength for different temperatures

Table 2.1 Normal total emissivity at 20° C for classical building materials

Materials	Rough concrete	Asphalt	Red brick	Plaster	Dry soil
					Wet soil
$\epsilon$	0.92	0.93	0.93	0.91	0.9
					0.95

where  $L_{\lambda}^{black\_body}(T)$  is the spectral brightness ( $W.m^{-2}.\mu m^{-1}.sr^{-1}$ ) emitted by the black body,  $\lambda$  is the wavelength (m) and C1 and C2 are two constants of radiation.

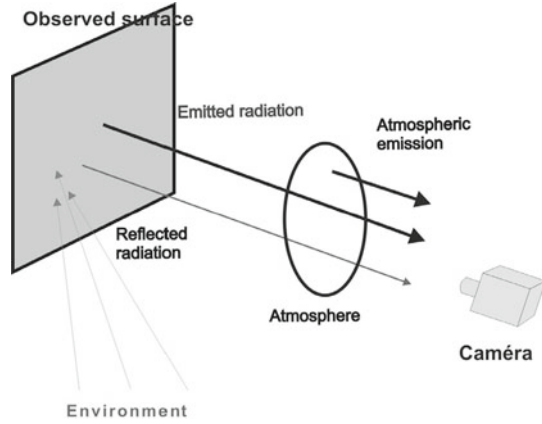
Fig. 2.1 shows the appearance of spectra of radiation of black bodies for various temperatures.

The emissivity  $\epsilon$  is the ratio between the radiated power emitted by a general structure in relation to the power emitted by an ideal radiator (black body). For a black body, the radiated power is independent of material properties and depends only on its temperature. Therefore, the emissivity of a blackbody is always 1. The emissivity of real structures varies between 0 and 1 ( $0 < \epsilon < 1$ ) and depends more or less on the temperature, the wavelength, the polarisation and the angle to the normal. This dependency is influenced by the surface properties like roughness and contamination. For each body, the directed spectral emissivity is equal to the directed spectral absorptivity (Kirchhoff’s law). Table 2.1 shows typical values of emissivity for some building materials.

At ambient temperatures, a large part of this radiation is situated in the spectral range between 1.5 and 20  $\mu m$  where the human eye is insensitive. To detect this radiation, infrared cameras are used which include one detector or a detector array (focal plane array, FPA) to convert this radiation into an electric signal. Two atmospheric transmission windows are used (3 to 5  $\mu m$  or 8 to 12  $\mu m$ ). For FPAs, each detector receives radiation from a small solid angle (instantaneous field of view, IFOV).

The radiometric equation (Eq. 2) describes the calculation of temperature from the measured radiation intensity. A camera which observes an object (Fig. 2.2) receives radiation that is made up of three parts: the radiation emitted by the object at a constant temperature  $T_0$ , the radiation of the environment at the temperature  $T_e$

**Fig. 2.2** Composition of the radiation received by the camera



reflected by the object (if the emissivity is  $< 1$ ) and the radiation emitted by the atmosphere between the object and the detector.

$$I' = \tau_{\text{atm}} [\varepsilon_0 I_0 + (1 - \varepsilon_0) I_e] + (1 - \tau_{\text{atm}}) I_{\text{atm}} \quad \text{Eq. 2.}$$

where the three parts  $\varepsilon_0 I_0$ ,  $(1 - \varepsilon_0) I_e$  and  $(1 - \tau_{\text{atm}}) I_{\text{atm}}$  respectively correspond to the surface emission, the reflected variation and the atmospheric emission, with:

$I'$  = radiation detected by the camera [ $\text{W} \cdot \text{m}^{-2} \cdot \text{sr}^{-1}$ ]

$I_0$  = radiation of the object itself [ $\text{W} \cdot \text{m}^{-2} \cdot \text{sr}^{-1}$ ]

$I_e$  = radiation of the environment [ $\text{W} \cdot \text{m}^{-2} \cdot \text{sr}^{-1}$ ]

$I_{\text{atm}}$  = radiation of the atmosphere [ $\text{W} \cdot \text{m}^{-2} \cdot \text{sr}^{-1}$ ]

$\varepsilon_0$  = emissivity of the object

$\tau_{\text{atm}}$  = coefficient of transmission of the atmosphere

The atmospheric transmission  $\tau_{\text{atm}}$  is a function of the distance between the surface under test and the camera and the atmospheric properties. For short distances, it can be approximated by 1. Beyond several metres the absorption and emission of the atmosphere itself can no longer be neglected. The humidity affects transmission in a great deal.

When the parameters of the radiometric equation are estimated, the average temperature of the surface may be deduced. The quality of the estimation of temperature values is directly linked to the validity of the hypotheses and the accuracy with which the various parameters are determined.

The methods of auscultation by infrared thermography may be classified in two categories:

- Passive methods, for which no additional source of heat is used specifically to carry out the auscultation.
- Active methods, for which the diffusion of heat is provoked by artificial means, set up to carry out the auscultation.

The characteristics of these two categories will be discussed in the following.

## ***10.2 Measuring equipment and handling: the infrared camera***

In the 1990s, focal plane arrays (FPA) were developed and the increase of array size, thermal resolution and image repetition frequency during the last ten years has accelerated the applications in several areas. Adjusted to the area of application and to the environmental conditions, different IR cameras can be used which are mainly distinguished by the detector types. Among others, these detectors are characterized by their spectral range, spatial resolution, noise equivalent temperature difference (NETD, thermal resolution), integration time and long term stability. With these detectors, commercial IR cameras with a full frame rate of up to 1 kHz for a FPA size of 256 x 256 were achieved. For lower frame rates, larger arrays (1024 x 1024) can be used. The maximum thermal resolution (NETD) is less than 15 mK.

For a thermographic study, the choice of camera's position results of a compromise between spatial resolution and size of observed area. Numbers of detectors (pixels) and optic system of the camera are parameters of the choice. The required objective has to be selected (wide angle, normal, tele). For example, with an objective of 24°x18° (horizontal field of view x vertical field of view) and a matrix of 320x240 detectors, the IFOV is 1.3 mrad. If the camera has a distance of one meter from the surface, the observed area is a 40 x 30 cm<sup>2</sup> rectangle. Each pixel corresponds to a 1.3 x 1.3 mm<sup>2</sup> rectangle.

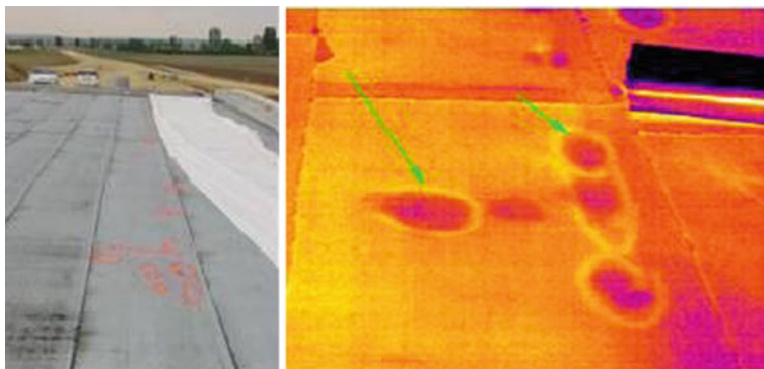
If possible, the camera should be positioned following the surface normal. Before starting data acquisition, the camera should be switched on for at least 30 min.

## ***10.3 Data processing, calibration and interpretation***

Infrared thermography allows observing a field of temperature on a surface. The information is extracted from gradients observed at the surface at one time. Information may also be deduced from evolutions of the temperature field with time. Temperature gradients or variations can only be observed if the system is submitted to heat transfer.

When considering the investigation of civil engineering structures by infrared thermography, we are faced with difficulties which make the exploitation of numerical values of temperature difficult. The temperature of the environment is an ideal that is hard to establish. The emissivity of the material is not known with great accuracy and it might vary along the surface and with the angle of observation. However surfaces of non-metallic elements in civil engineering have high emissivities and low reflection coefficients. Strong reflections due to direct sunlight for example must be avoided. Most of the applications developed up to now for testing of structural elements or buildings involve qualitative exploitation. They aim to interpret temperature differences. In a quantitative procedure, the analysis of absolute temperatures is envisaged.

In case of on-site applications, the influence of rain, fog and wind has to be considered.



**Fig. 2.3** Study of waterproof covering: visible image (left) and infrared image (right)

## ***10.4 Passive thermography applied to the investigation of discontinuities***

### **10.4.1 Principles**

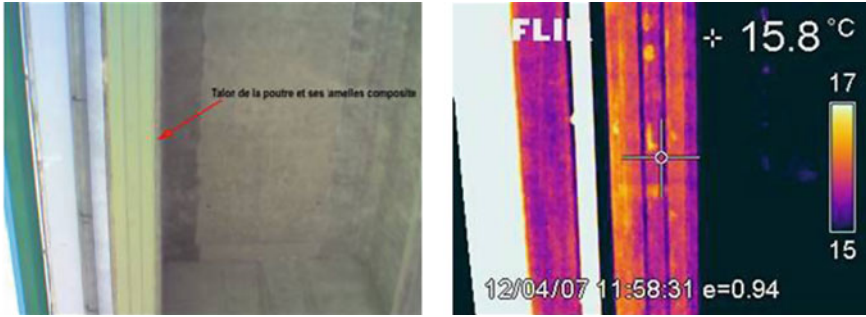
Temperature gradients at the surface may denote the presence of an anomaly under the surface of the material when the surface is exposed to the environment (sunshine, variation of the daily ambient temperature, etc.). If the surface is submitted to a thermal variation, the heat diffuses inside the material. The presence of a discontinuity such as a delamination, cavity or crack introduces a change of thermal properties which alters heat transfer. For instance, a hotter zone might appear at the surface depending on the thermal properties. Conversely, if there is heat loss (cooling), the signature will be a cold layer. Heat diffusion may also be modified by contrasting thermo-physical properties within the material.

The following example concerns the investigation of a waterproof covering on a bridge. The defects of adhesion of the covering are easily detected by using infrared thermography. The parts that have come unstuck appear warmer at the surface (see Fig. 2.3-right). Natural environmental effects are sufficient to generate a serious temperature contrast. Figure 2.4 shows the case of a concrete structure reinforced by composite plates. Preliminary thermography studies can be used to control the quality of reinforcement.

### **10.4.2 Limits and reliability**

For detecting inhomogeneities, the following conditions must be satisfied:

First, the thermo-physical properties of the defect and the material must be contrasted enough.



**Fig. 2.4** Study of the quality of interface between concrete and composite reinforcing plates: visible image (left) and infrared image (right)

For estimating the detectability of defects and inhomogeneities in structures, the heat transfer can be described by the thermal wave propagation (harmonic heating process with wavelike temperature field) (Maldague and Moore, 2001). In this model, the reflectivity of thermal waves at interfaces is determined by the differences between the effusivities of the contiguous materials. For the one-dimensional case, the reflection coefficient  $R$  of a plane thermal wave for transmission from medium 1 to medium 2 is equal to:

$$R_{12} = \frac{e_1 - e_2}{e_1 + e_2} = \frac{\sqrt{\rho_1 c_1 \lambda_1} - \sqrt{\rho_2 c_2 \lambda_2}}{\sqrt{\rho_1 c_1 \lambda_1} + \sqrt{\rho_2 c_2 \lambda_2}}$$

Thus, for a successful detection of inhomogeneities, there must be a sufficient difference between the thermal properties of medium 1 and 2. The larger the difference between the effusivities of the two media, the higher the thermal signature of the inhomogeneities is. For instance, the reflection coefficient at a concrete/air interface is about 100%, while the reflection coefficient of a concrete/steel interface is about -24%.

The second condition is on size: at a given depth, defects can be detected only when they are large enough. Typically, the size must be at least equal to the depth.

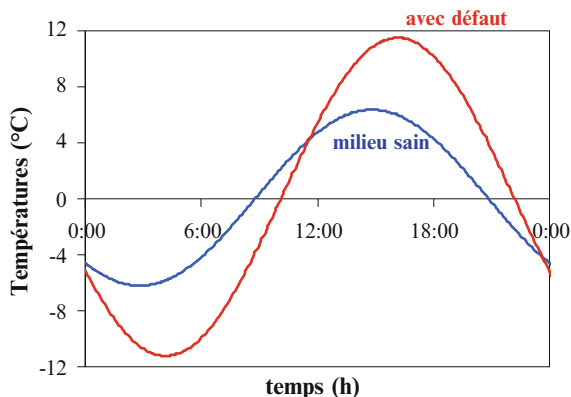
The third condition for detectability is linked to the heat wave penetration depth. The study of the heat wave propagation shows that a sinusoidal variation at the surface is propagated in the material with amplitude which decreases exponentially with the depth. The depth at which the amplitude is decreased to  $e^{-1}$  is the penetration depth  $p$ :

$$p = \sqrt{a / \pi f}$$

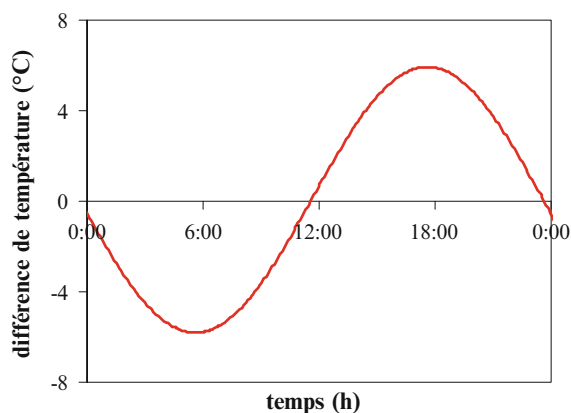
where  $p$  is the depth of penetration (m),  $a$  is the thermal diffusivity ( $m^2 \cdot s^{-1}$ ),  $f$  is the thermal excitation frequency (Hz).

At the surface, the response to thermal excitation is not sensitive to the presence of a discontinuity if its depth exceeds three times the penetration depth.

**Fig. 2.5** Temperature variations on the surface for a plain slab and a slab with delamination



**Fig. 2.6** Temperature difference between a point above the defect and a zone with defect

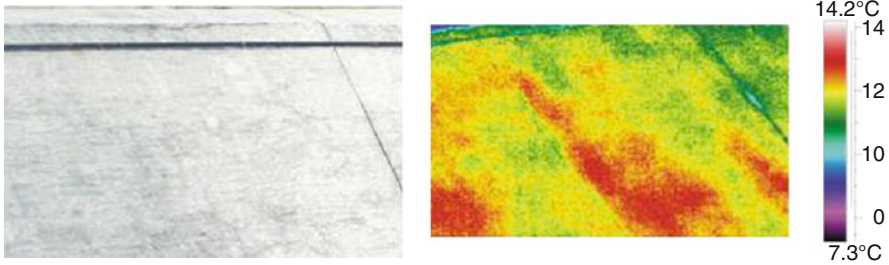


For example, a day-night cycle can be assimilated as a first approximation to a sinusoidal variation of  $1.16 \times 10^{-5}$  Hz. For concrete, the depth of penetration corresponding to this frequency is of the order of 10 cm. This means that defects deeper than 30 cm cannot be easily detected. Thus lower frequencies are required. For example, the response to the annual seasonal cycle can highlight anomalies situated at a few metres in depth. Day/night variations are often used for the detection of defects located near the surface.

Results of a simulation is presented there. A concrete slab in which a void is present at depth  $e$  is submitted to a 24h-harmonic thermal excitation. The imposed heat flux on the upper surface follows a sinusoidal variation. Fig. 2.5 show surface temperatures evolutions. In this case, a 1-cm thick air gap is situated 5 cm from the surface and above sound material.

The temperature time variations appear to be more contrasted above the delaminated zone, which are warmer during the day and colder during the night. The simulations show that the morning (6h) and the late afternoon (18h) are the most interesting times of the day, since they enable the highest temperature differences between the zones with and without a defect to be observed (see Fig. 2.6).





**Fig. 2.7** Study of a concrete siding: visible image (left) and infrared image (right)

The fourth condition is to have a thermal excitation whose amplitude is sufficient. The thermal contrast may be reduced if the convection at the surface that is too strong (e.g. due to wind).

Figure 2.7 illustrates the investigation of a concrete facing installed on the edge of a lock. Delaminations are detected by a thermogram recorded at the end of the day.

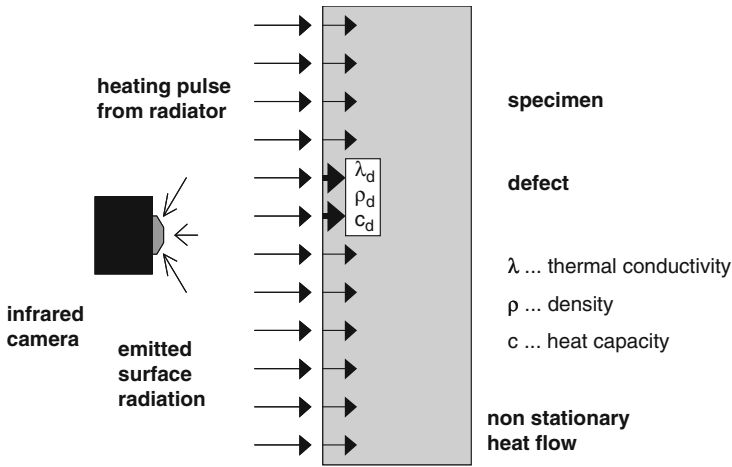
## 10.5 Investigations with active thermography

### 10.5.1 Principles

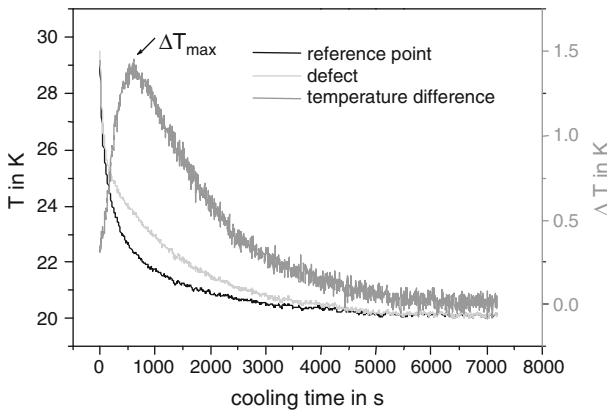
Active infrared thermography methods are based on the active heating or cooling of the structures under test to provide an unsteady temperature gradient (Maldague and Moore, 2001). In civil engineering, two of these active methods, impulse-thermography (IT) and pulse phase thermography (PPT), have been proven to be very useful for the investigation of structures close to the surface.

Experimental set-up and data acquisition are identical for IT and PPT: the surface of the structure to be investigated is heated by using a radiation source (also other energy sources are applicable depending on the testing problem) as visualised in Fig. 2.8. After switching off the heating source, the cooling down behaviour is recorded in real time with an infrared camera. The propagation of the heat depends on the material properties like thermal conductivity, heat capacity and density. If there is an inhomogeneity in the near surface region of the object with different thermal properties, the heat flow will slow down or accelerate in these local areas. While observing the temporal changes of the surface temperature distribution with the infrared camera, near surface inhomogeneities will be detected if they cause measurable temperature differences on the surface.

The main approach of IT in analysing the thermal data was to interpret the function of surface temperature versus cooling time (see Fig. 2.9) for selected areas with and without inhomogeneities. These selected transient curves were compared and difference curves (difference between transient above a void and transient above a



**Fig. 2.8** Principle of impulse-thermography and pulse-phase-thermography. The surface is heated up with a heating impulse and the cooling down behaviour is observed with an infrared camera



**Fig. 2.9** Transient curves above a reference point and above a defect and the respective difference curve with a maximum temperature  $\Delta T_{max}$  at a distinct time  $t_{max}$

sound area) were calculated as shown in Fig. 2.9. The difference curves usually have a maximum of the temperature difference  $\Delta T_{max}$  at a distinct time  $t_{max}$ , which depends mainly on the difference of the thermal properties, the depth of the void and the heating time. For solving the Inverse Problem, i. e. to get information about the thermal and geometrical properties of the detected defect from the difference curves, numerical simulations are performed (Maldague and Moore, 2001).

PPT is based on the application of the Fast Fourier Transformation (FFT) to all transient curves of each pixel. Thus, one obtains amplitude and phase images for all

frequencies. Amplitude images show the internal structure of a specimen up to a maximum available depth depending on the frequency (low pass filter behaviour). Phase images show the internal structure within a certain depth range depending on the frequency (band pass filter behaviour) [(Maldague and Moore, 2001), (Maldague, 2001), (Wedler et al., 2003), (Maldague, 1993)].

### 10.5.2 Measurement equipment and handling (general)

The experimental set-up consists of a thermal heating unit, an infrared camera and a computer system, which enables digital data recording in real time.

For the civil engineering applications, the heating pulse is realised as a square pulse, which can be described as a superposition of different frequencies with varying amplitudes.

In most cases, infrared radiators have been proven to be the most suitable sources, being fast and efficient and generating a homogeneous temperature increase. For this, the heating procedure is usually done dynamically by moving the radiators (computer-controlled) at an appropriate distance from the surface and by using an automatic scanner system to obtain the best possible homogeneous heating. The heating time varies from several seconds up to 60 min. It must be considered that the surface temperature should not rise higher than 50°C to avoid any damage. This temperature has to be even less for sensitive surfaces. The cooling down process of the surface is observed with an infrared camera. This camera and the related software for data acquisition and analysis should at least fulfil the following conditions:

- availability of recording of sequences of thermal images with a minimum frame rate of 1 to 10 Hz to record fast cooling down processes;
- known file format of thermal sequences for further data analysis;
- extraction of transient curves (temperature as a function of time for one pixel) must be possible;
- for on-site measurements, the heating source has to be placed close to the surface under investigation (distance 10 to 20 cm) and should be moveable to obtain a homogeneous heating. A respective power supply must be available.

An operational test should be performed measuring the surface temperature of a known object (reference object). A first thermogram of the surface to be investigated should be recorded to have a reference image in more or less thermal equilibrium. During the whole time range of data recording, it should be ensured that nothing and nobody is crossing in the area between camera and observed surface.

### 10.5.3 Data Processing related to impulse-thermography (IT)

Data processing related to IT is performed if qualitative and quantitative information is needed about inhomogeneities and defects near below the surface.

As raw data, temporal sequences of thermograms are available containing information about environmental and measurement parameters in the header. The single steps of IT data processing are the following:

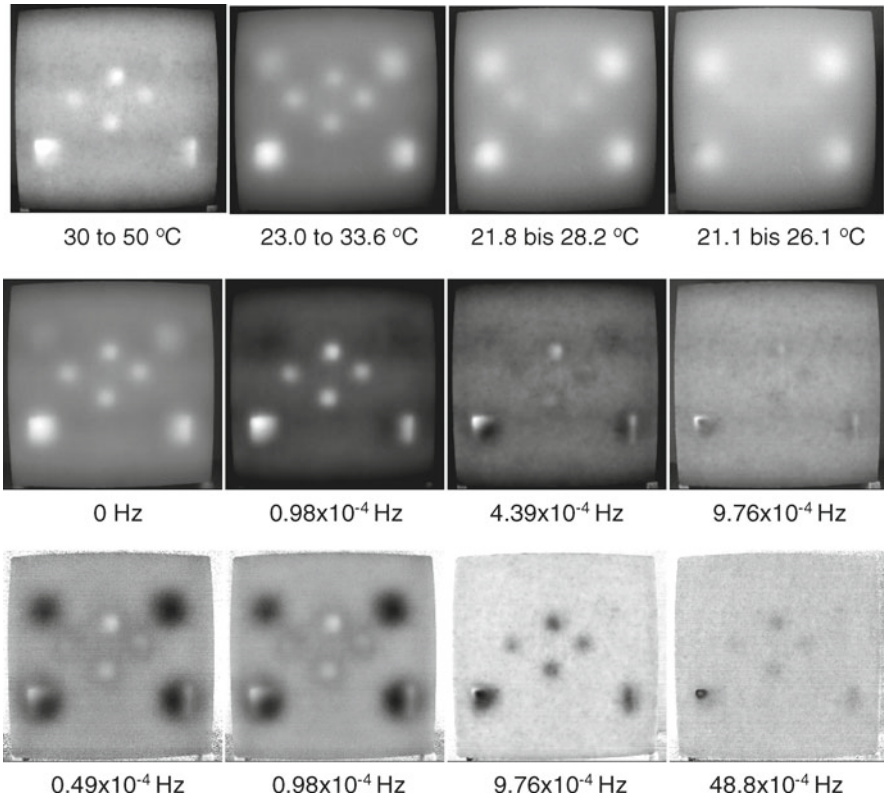
- Correction of temperature data related to surface emissivity and environmental parameters, if this has not been already performed on-site;
- enhancement of the signal to noise ratio, e. g. by averaging of thermograms or spatial or temporal filtering;
- location of defect areas by visual examination of the thermograms. Contrast areas can be accentuated by edge filtering or through further steps of image processing;
- transformation of geometrical parameters (size and position of measurement area, planar size and position of inhomogeneities or defects);
- selection of transient curves (temperature of a pixel as a function of time during cooling down) of pixels above sound and defect area, calculation of the difference curve;
- calculation of maximum thermal contrast  $\Delta T_{\max}$  and the respective time  $t_{\max}$  after the switching off of the heating source by analyzing the temporal variation of contrast, as on Fig. 2.9;
- from calibration curves and/or numerical simulations, the Inverse Problem can be solved, e. g. quantitative information can be obtained about the depth (concrete cover). But this is only possible if a lot of prior knowledge is available, e. g. the thermal properties of sound and defect material must be known.

#### 10.5.4 Data processing related to Pulse-phase thermography

Data processing related to PPT is also performed if qualitative and quantitative information are needed about inhomogeneities and defects near the surface. In PPT, non unique emissivity at the surface and indirect reflection have a reduced influence on the results. The sensitivity to deeper defects is thus enhanced.

As raw data, temporal sequences of thermograms are available containing information about environmental and measurement parameters in the header similar to IT. The single steps of PPT data processing are the following:

- Correction of temperature data related to surface emissivity and environmental parameters, if this has not been already performed on-site;
- enhancement of the signal to noise ratio, e. g. by averaging of thermograms or spatial or temporal filtering;
- calculation of Fast Fourier Transformation (FFT) of each transient curve resulting in amplitude and phase spectra. For enhancing the frequency resolution, zero padding of the transient curves can be performed (enhancing the transient curves in total time range with room or offset temperature). Since most of the information in the spectra is included in the very low frequencies, zero padding is essential;



**Fig. 2.10** Images built at respective times ( 0, 34.5, 68.5 and 102.8 min after 30 min heating time): thermograms (top), amplitude images (middle) and phase images (bottom). The concrete specimen contains voids at varying depth from 2 to 8 cm

- for each frequency, amplitude and phase can be presented for each pixel resulting in amplitude and phase images. Thus also in amplitude and phase images can be presented in sequences (as a function of frequency).

As an example, selected thermograms, amplitude and phase images of the concrete test specimen with voids at different depths are shown in Fig. 2.10. In the phase image at the lowest frequency in Fig. 2.10, all defects can be clearly seen with better contrast as in the time sequences. With increasing frequency, the deeper defects disappear in the amplitude as well as in the phase images, but earlier in the amplitude images.

The data processing described above might lead to identify inhomogeneities inducing after thermal activation a lower or a higher surface temperature than in the sound area. As mentioned above, the thermal properties and the depth of these inhomogeneities can only be determined if comprehensive prior-knowledge is available.

In most cases, further quantitative results will be available only on the depth of inhomogeneities or defects, which will have more or less large relative errors.

## 10.6 Guidelines and Standards

For the applications of active thermography for concrete testing, at time there are no standards. Guidelines for the investigation of historic masonry structures have been developed during the EC funded project ONSITEFORMASONRY and will be enhanced by the RILEM TC SAM.

In the following, related standards concerning passive and active thermography are listed:

- ASTM C 1046, Standard practice for in-situ measurement of heat flux and temperature on building envelop components, 1995
- ASTM C 1060, Standard practice for thermographic inspection of insulation installations in envelope cavities of frame buildings, 1990
- ASTM C 1153, Standard practice for location of wet insulation in roofing systems using infrared imaging, 2003.
- ASTM D 4788, Standard test method for detecting delaminations in bridge decks using infrared thermography, 2003
- DGZfP-B, Guideline for thermographic investigations at building elements and building structures, Edition 1993-10 (in german)
- DGZfP-TH 1, Characterization of thermography systems, Edition 1999-03 (in german)
- DIN 54162, Non-destructive testing – Qualification and certification of personnel for thermographic testing – General and special principles for level 1, 2 and 3, Edition 2006-09
- DIN 54190-1, Non-destructive testing – Thermographic testing – Part 1: General principles, Edition 2004-08
- DIN 54190-2, Non-destructive testing – Thermographic testing – Part 2: Equipment, Edition 2005-08
- DIN 54190-3, Non-destructive testing – Thermographic testing – Part 3: Terms and definitions, Edition 2006-02
- DIN EN 13187 Thermal performance of buildings – Qualitative detection of thermal irregularities in building envelopes – Infrared method, Edition 1999-05

## References

- Busse G., Wu D., Karpen W. (1992) Thermal wave imaging with phase sensitive modulated thermography, *J. Appl. Phys.*, 71, 3962.
- Maldague X. P. (1993) *Nondestructive Evaluation of Materials by Infrared Thermography*, Springer-Verlag.
- Maldague X.P., Couturier J.P. (1997) Review of pulsed phase thermography, *Atti della Fondazione G. Ronchi, Carloma G.M. and Corsi C. (eds), pp. 271–286.*
- Maldague, X. P. (2001a) *Theory and Practice of Infrared Technology for Nondestructive Testing*, Wiley.
- Maldague, X. P., Moore P. (2001) *Nondestructive testing handbook, Infrared and thermal testing*, ASNT.
- Vavilov V., Marinetti S. (1999) Thermal Methods Pulsed Phase Thermography and Fourier-Analysis Thermal Tomography, *Russian Journal of Nondestructive Testing*, 35, 134-145.
- Wedler G., Brink A., Röllig M., Weritz F., Maierhofer C. (2003) *Active Infrared Thermography in Civil Engineering - Quantitative Analysis by Numerical Simulation*, Int. Symposium NDT-CE, Berlin.

## 11 Radiography

Jean-Paul Balayssac

### 11.1 *Physical principles and theory*

Radiography in civil engineering can concern a lot of structures. Theoretically the limitations are only related to the penetration depth of the rays and to the exposure rate of the emitter. It can be used on concrete, reinforced or prestressed concrete, stone, mortar and steel.

Like it is a transmission technique, it needs to access to the two opposite faces of the structure. One face is highlighted by the source and the sensitive film is placed on the other one. In radiography, the radiation is either X-ray or gamma-ray. Gamma rays are emitted by an artificial source (Cobalt 60 or Iridium 192). In the case of X-rays, accelerators are used to obtain higher energy. For usual applications, the radiation attenuation through the material is measured with a sensitive film located on the opposite face (Fig. 2.1).

Field applications of radiography include the detection of reinforcement location, voids, cracks, the quality of grouted post-tensioned tendons and the failure of cables. As well, radioscopy is a different form of radiography in which the transmitted radiation is converted into a visible light and recorded by a video camera. Radioscopy has been used in France for the detection of grouting defects.

Classically, industrial radiography is able to observe:

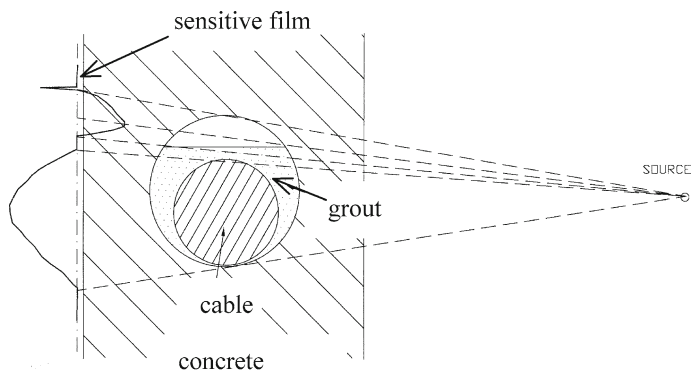
- the presence of cavities inside the concrete
- the presence of grout inside the prestressing ducts and also its defects
- the localization of tendons
- the localization of the reinforcement and the diameter of the rebars
- the discontinuities of the ducts
- the broken wires or cables in some cases.

### 11.2 *Measurement equipment and handling*

The source is chosen in relation with the scope of the investigation (size of the target, thickness of the concrete element, implementation conditions and radioprotection). The weight of the source is linked to its power of penetration through the material. Table 2.1 gives examples of source characteristics. The picture of Fig. 2.2 illustrates an example of a source of Iridium 192.

The choice of the source depends on the exposure time, the thickness of the element and the required resolution.

For the receptors, the use of photographic films (emulsion) is very usual and the different categories of films are defined by standards. The film is always associated to a filter and a reinforcing screen. The choice of the film is done regarding the thickness



**Fig. 2.1** Principle of radiography

**Table 2.1** Source characteristics

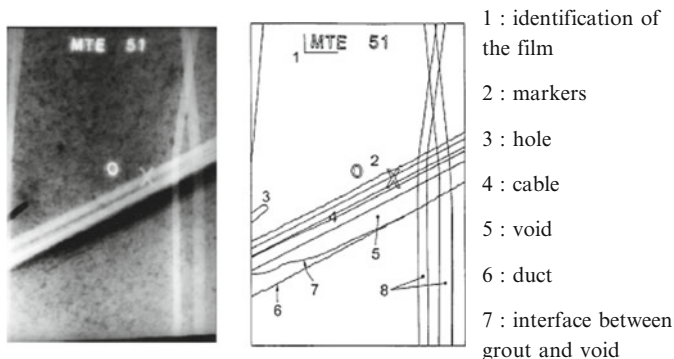
Source	Radioactive half-life	Weight of the source (kg)	Maximal thickness (cm)
Iridium 192	74 days	25	30
Cobalt 60	5.3 years	120	40
Cobalt 60	5.3 years	350	65
X-rays		45 to 120	130

**Fig. 2.2** Source of Iridium 192



of the element, the required sensitivity and also the exposure time. The image quality depends on the emitter, the distance between the source and the film, the incidence of the rays, the choice of the film, the reinforcing screen and the filter. The distance between the source and the film depends on the thickness of the element.





**Fig. 2.3** An example of radiogram and interpretation – sounding of an internal tendon [NF A 09-202]

The use of radioactive sources being very hazardous, specifically trained and accredited persons for implementing the technique and for protection aspects are required. A protection area must be defined around the sounded structure and it is necessary to move away all the persons from it, during the entire test. It can be disturbing for the users, particularly if the structure is a flat building.

### ***11.3 Guidelines, references and standards***

NF A 09-202 : principes généraux de l'examen radiographique, à l'aide de rayons X et gamma, des matériaux béton, béton armé et béton précontraint

NF EN 1330-3 : Essais non destructifs – Terminologie – Partie 3 : Termes pour le contrôle radiographique industrielle (indice de classement : A09-020-3)

BS 1881: Part 205, Recommendations for radiography of concrete, British Standards Institute, London, 1986.

### ***11.4 Calibration and interpretation of results***

The optical density related to the grey levels of the sensitive film is analysed. The quality of the images is generally good because the attenuating characteristics of steel, concrete, and air differ greatly (Fig.2.3).

The radiographic techniques can provide very useful information because of their ability to observe cross-sectional images of the object. They are applicable for every kind of concrete structures. However, these methods currently pose the problem of safety and other limitations. With further advancements in portable radiography equipment for field applications, such devices could have widespread use. In particular, safety increasing, and imaging speed advances to permit practical scanning rates should greatly improve the technique.

### ***11.5 Reliability and limitation of results***

Despite its high interest of providing an image of the internal structure of concrete, radiography has several limitations:

- Being a technique by transmission, two faces of the structure must be accessible
- Depth limitation: 60 cm for penetration of gamma rays is a limit, but 120 cm can be reached with X-rays
- Only small surfaces can be sounded due to the limited size of sensitive film
- The time of exposure is rather long (especially for gamma-rays)
- Steel bars (cables or reinforcement bars) can mask the target
- Important weight of the usual radiation sources can prevent the investigation of some parts of a structure
- The use of radioactive source being hazardous, a safety area is required around the structure. It is sometimes impossible to restrain the access of the surroundings
- The implementation of the technique is expensive if very large areas need to be sounded (especially with X-rays). For this reason, radiography is sometimes relegated for use in specific conditions only
- The image does not provide any information about the depth of the defect.

## **References**

- Mitchell T.M. (1991) Radioactive/Nuclear Methods, in *CRC Handbook on Non Destructive Testing of Concrete*, Malhotra and Carino Editors, CRC Press, 1991, p 235.
- Roenelle P. (2005) Méthodes radiographiques d'évaluation non destructive, Chapter B7, in *Méthodologie d'évaluation non destructive de l'état d'altération des ouvrages en béton armé*, Ed. D. Breysse et O. Abraham, Presses de l'Ecole Nationale des Ponts et Chaussées, pp. 305–328.

## **12 Rebound hammer**

### **Markus Fischli and Andrzej Moczko**

The Rebound Hammer was developed in 1948 and patented in 1950 by Ernst Schmidt, a Swiss engineer. The device is based on the rebound principle, which is an indicator of the hardness of concrete. In the rebound hammer test, a spring loaded mass has a fixed amount of energy imparted to it by extending the impact spring to a fixed position, this is achieved by pressing the plunger against the surface of the concrete under test. Upon release, the mass impacts on the plunger, rebounds and the distance traveled by the mass expressed as a percentage of the initial extension of the spring, is called the rebound number. The rebound distance is measured on an arbitrary scale marked from 10 to 100 (Kolek, 1958, Carino, 1974). Schmidt

standardized the hammer blow by developing a spring-loaded hammer and devised a method to measure the rebound. Several models of the device were built (Greene, 1954) and patented, with further developments.

## 12.1 Physical Principle and Theory

The Rebound Hammer (Proceq, 2007a) is principally a surface hardness tester. With this instrument the user presses a plunger against the surface under test and a spring then releases a mass to impact on the plunger. Inside the instrument a spring provides a defined impact energy for each measurement. After the impact the mass rebounds a certain distance and this is shown on the scale by a pointer. Before removing the instrument from the concrete element the impact mechanism can be locked by the locking button and the rebound value R be read. The position of the pointer indicates the rebound as a percentage of forward hammer travel. Equation 1 explains how the rebound value R is calculated:

$$R = 100 \cdot \sqrt{\frac{E_{\text{reflected}}}{E_{\text{forward}}}} = 100 \cdot \sqrt{\frac{1/2Dx_R^2}{1/2Dx_0^2}} = 100 \cdot \frac{x_R}{x_0} \quad (1)$$

where D is a spring constant,  $E_{\text{forwar}}$  is the energy before the impact,  $E_{\text{reflected}}$  is the energy following the impact,  $x_0$  is the displacement at triggering of impact and  $x_R$  is the displacement following the impact (rebound distance).

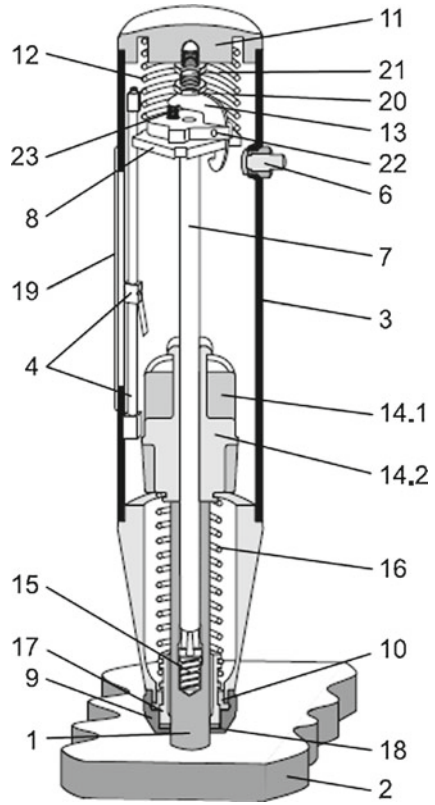
Figure 2.1 shows the moment of the impact of the hammer mass 14 on the plunger 1. Other main parts are impact spring 16, the pawl 13 which releases the hammer mass, and pointer 4.

The most suitable surfaces for testing by this method are vertical faces of the concrete structure, which means the impact is produced in horizontal direction. Impact directions up and down on horizontal surfaces plus at angles of 45° up and down are also possible. For these measurements a correction of the measured values due to gravity has to be considered.

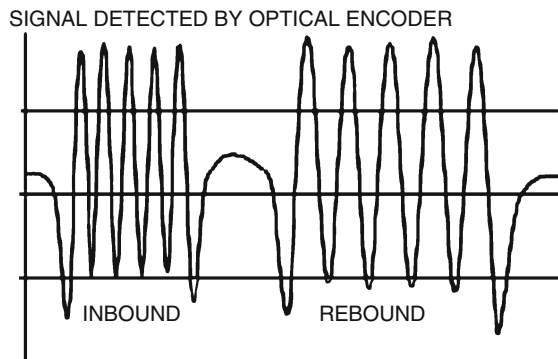
The classic “R”-value is the mechanical travel of the hammer mass on rebound. It is affected by its friction on the guide rod, the friction of the drag pointer on the scale, the influence of gravity during its travel, the relative velocity between unit and mechanical parts. The R value is measured as characteristic of the energy that is not absorbed by the material under test.

Some years ago a development led to a new instrument that combines innovative ideas with the advantages of the classical rebound hammer. The new instrument (Proceq, 2007b) measures the velocity of the hammer mass immediately before and after the impact and calculates the quotient Q (Fig. 2.2, Eq. 2). Based on the same physics the measurement is not affected by friction between hammer mass and guide rod and the one of the pointer and there is no need to

**Fig. 2.1** Sectional view of Concrete Test Hammer Model



**Fig. 2.2** Signal detection



compensate for the impact direction. Equation 2 explains how the rebound value R is calculated:

$$Q = 100 \cdot \sqrt{\frac{E_{\text{reflected}}}{E_{\text{forward}}}} = 100 \cdot \sqrt{\frac{1/2mv_R^2}{1/2mv_0^2}} = 100 \cdot \frac{v_R}{v_0} \quad (2)$$

where the rebound value Q is expressed as a function of the respective kinetic energies before ( $E_{\text{forward}}$ ) and after ( $E_{\text{reflected}}$ ) the impact. These two quantities depend on the mass m of the hammer and on the respective velocities immediately before ( $v_0$ ) and after ( $v_R$ ) the impact.

An ergonomic housing accommodates the impact mechanism and the optical absolute velocity encoder that measures the velocity of the hammer mass. There are integrated electronics as well as the LCD that process the data and display the concrete strength plus all other information of the measurement series. The impact spring initiates an impact of the hammer mass on the plunger. According to the surface hardness of the concrete element the rebound velocity of the hammer mass is lower or higher.

## 12.2 *Measuring Equipment and Handling*

The Rebound Hammer is a portable instrument that can easily be operated by one person. Inside the cylindrical housing there is the impact mechanism that activates the plunger which protrudes from the housing on the front end. The plunger has to be pressed perpendicularly against the surface of the test specimen and the pressure has to be increased until the hammer impacts. Inside the instrument the impact spring provides a constant impact energy for each measurement, which is 2.207 N.m for the normal (Type N) hammer. After the impact the mass rebounds a certain distance and this is shown on the scale by a pointer. Before removing the instrument from the concrete element the impact mechanism can be locked by the locking button and the rebound value be read. The position of the pointer indicates rebound as a percentage of forward hammer travel.

The instrument is immediately ready for the next measurement. The plunger can be placed on the desired measuring spot which according to the standards should be at least 25mm away from the previous one. The instrument is pressed towards the concrete surface. This unlocks the impact mechanism and the instrument housing is moved away from the structure under the force of the loading spring. At the end position the concrete test hammer is automatically loaded and ready for the next impact. Because of the influence of surface condition on test results, if the surface is too rough it should be smoothed with a grinding stone.

For structures with low strength and wall thickness below 100mm the Model L with smaller impact energy was developed. The normal energy would damage the structure or the reading could be affected. The instrument is basically the same but



Fig. 2.3 Typical digital Rebound Hammer

Fig. 2.4 Measurement with the new device developed (Q measurement)



the impact energy is only 0.635 N.m, i.e. one third of the one of the standard Model N. For both types there are also the versions NR and LR that register the readings as a graph on a paper roll.

In modern versions of rebound hammer an electronic measuring unit has been added to help ensure proper test results which can be recorded for later review or uploaded to a personal computer. The scale is replaced by a displacement sensor which measures the rebound value. Impact direction, carbonation depth can be entered in addition to other options and the unit is capable of direct statistical analysis as shown in Fig. 2.3.

With the new device (Q measurement, Fig. 2.4), the measuring procedure is the same as with the classic rebound hammer. The user can perform test series of a specified number of impacts. Manual cancellation of obvious outliers is possible. Operation with the “one button” user interface is simple. To obtain a reading in units of compressive strength the user can select the desired unit, the length of the series and the averaging mode, carbonation depth (if applicable), conversion curve for

concrete mixture and form factor. At the end of the series the instrument will display the average Q value converted to the desired concrete compressive strength unit. The instrument is suitable for testing a wide variety of concrete, mortar, rock on site as well as in the laboratory. It is handy for difficult to access or confined test areas (i.e. working overhead) and especially convenient for testing on tunnel linings as measurements are independent of impact direction.

### ***12.3 Calibration and Interpretation of Results***

An initial test series at the Swiss Federal Materials Testing and Experimental Institute (EMPA) was successful and application was made to patent the instrument world-wide. A correlation was developed between the compressive strength of standard cubes and rebound number. The first successful reports appeared in 1951. The new method of non-destructive concrete testing was acclaimed throughout the world. DIN 4240 was published in 1962 dealing with the SCHMIDT Hammer and its use.

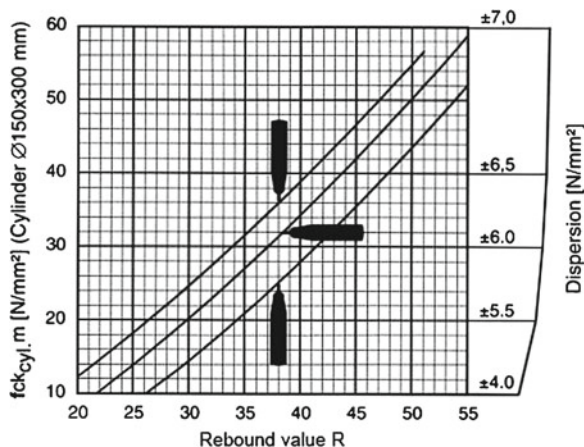
However, as other investigators began to develop correlations between strength and rebound number, it became evident that there was not a unique relationship between strength and rebound number (Kolek, 1959). This led to the often-stated recommendation that a correlation should be developed using the same concrete and forming materials as used in construction. Without such a correlation, the rebound hammer is useful only for detecting gross changes in concrete quality throughout a structure (Carino, 1994). The issues of reliability of the rebound measurement and of calibration are key issues.

The rebound number is first very sensitive to the very local properties of concrete, i.e. to the fact that the impact occurs just above an aggregate or a volume of cement paste. Thus, a series of measurements must be performed in a limited area around the same point, whose values are averaged such as to obtain a representative value for R. For instance, ASTM C 805 requires that 10 rebound numbers be taken for a test.

The first correction corresponds to the direction of impact (horizontal, vertical up and down), for which the calibration curve (which expresses the estimated compressive strength as a function of rebound number) must be shifted, as shown on Fig. 2.5. The test hammer symbols in the diagram indicate the impact direction and the respective conversion curve. In many countries cubes of 150x150x150mm are used as test specimens for which conversion curves are available as well.

A common factor that influences the reading is the carbonation of the concrete which starts from the surface and penetrates into the structure. Rebound numbers on a carbonated surface can be as much as 50% higher than non-carbonated surfaces. Correction factors have been proposed by (Tanigawa et al., 1988) and in Japanese and Chinese guidelines (AIJ, 1983, JGJ/T 23-2001), but their values are very different and the more efficient way to compensate for this effect remains the calibration of the rebound values against the strength of core specimens taken from the structure.

**Fig. 2.5** Conversion curve for the average compressive strength measured on cylinders ( $\phi 150$ , H300mm)



Many other factors have been recognized as influencing the rebound number, the most influent being (Evangelista et al., 2003):

- the moisture condition, a dry surface giving higher values,
- the surface texture, a smoother surface giving higher values than a rough one,
- the type of aggregate.

The influences of these factors are so great that it is very unlikely that a general calibration curve relating rebound hammer to strength, as provided by the equipment manufacturers, will be of any practical values, even by using a series of corrective coefficients. It is the reason why the EN 13791 has chosen a different approach for calibration: it gives a “basic curve” linking the rebound number and the estimated strength and the calibration process consists in shifting this basic curve accordingly to the results given by comparing the values of rebound number and true core strength measured at a given number of points. This calibration method does not explain why one has to shift the curve but is able to account for the effect of any influential factor.

On the innovative device which measures energy and gives a Q factor instead of R, the correlation between the Q value and the compressive strength of a concrete element is represented by another conversion curve which covers a large range of concrete strengths (from 10 MPa up to 100 MPa). The use of the device is easier because the effect of the direction of the test and that of the carbonation depth can be automatically corrected. The issue of calibration is however the same. A more precise derived compressive strength can be achieved by creating site specific (custom) conversion curves.

## 12.4 Reliability and Limitation of Results

Owing to its simplicity, speed and low cost the rebound hammer is, by far, the most widely used non destructive test device for concrete. Another main advantage of rebound measurement for strength estimation is that this technique has a more direct



**Fig. 2.6** Test anvil with hammer under test



link with mechanical properties of concrete than most others. But this simplicity can be misleading and results sometimes in careless handling. For instance, manual corrections for impact direction can occasionally be “forgotten”. Such omissions are less likely with the improved electronic concrete test, since such corrections are made automatically, providing these have been switched on.

A periodic function test is indispensable, since concrete dust penetrates the instrument and can change the characteristics of the impact. A function test must be carried out on a calibrated test anvil Fig. 2.6 before and after important assignments. Every 1000 – 2000 test impacts, the instrument should be thoroughly cleaned and then checked on the test anvil. If the readings get smaller than the lower limit the mechanism of the hammer usually has to be cleaned which can be done by the user. If the readings persist to be too low the hammer needs re-calibration. This should be done by a certified service centre in order to perform the calibration in the right way.

The test anvil is standardized. EN 12504-2 specifies the steel block with a hardness of minimum 52 HRC, a mass of  $16 \pm 1$  kg and a diameter of approximately 150 mm. Typical R-values are 81 for N-type and 75 for L-type hammers, tolerance is  $\pm 2R$ . Each anvil is calibrated with selected Master Equipment and the calibration of Rebound hammers and anvils is traceable back to the Master Anvil.

According to the European standard a minimum of 9 dm<sup>2</sup> of concrete surface with 10 cm thickness is needed. The rebound hammer Model N can be used on surfaces of concrete elements of any direction that have a minimal thickness of 100mm and are fixed with the structure, or if the thickness is less the specimen must be rigidly supported or Model L must be used. Moreover, the temperature during the tests must be between 10 and 35°C.

Statistical evaluations of test results should also be performed according to national specifications and requirements.

The evaluation of concrete compressive strength using the rebound hammer gives in any case valuable information about the quality of concrete. Another application of this technique consists in the localization of the coring zone for optimizing the number of cores to be tested in a laboratory

However, there is a large variance in opinions as to the accuracy of estimating the compressive strength. In any case, the accuracy can be increased by performing a proper calibration, such as to reduce the main causes of bias. The FHWA guide (FHWA, 1997) states that for a properly calibrated device, the accuracy is  $\pm 15$  to 20 percent for test specimens cast, cured and tested under laboratory conditions and that it is approximately  $\pm 30$  to 40 percent for in place compressive strength. Malhotra considers that the uncertainty is more probably  $\pm 25\%$  in a structure (Malhotra and Carino, 2004).

This variety of opinions is explained because experimental correlations and correlation curves have not been established in a standard context. The type of concrete, shape and size of reference specimens (cores taken from the structure or cubes or cylinders from the laboratory) have widely varied. More often carbonation and moisture have not been controlled. It results a wide variety of calibration curves, which are not strictly valid for extrapolation in a different context. It is the reason why another calibration approach is proposed by EN 13791, in which the exact correlation curve is not *a priori* known, but built on the basis of few additional destructive tests.

One also must note that since the rebound number is indicative of the near-surface properties of concrete (about 3 centimeters), it may be not indicative of the bulk concrete in a structure. It is influenced by local properties (air voids, higher content in cement, carbonation, effect of formwork and curing conditions...).

## 12.5 Guidelines for Use and Standards

The method is covered by several standard specifications including:

- ASTM C 805, Standard test method for rebound number of hardened concrete, in: Annual book of ASTM standard, ASTM C805-85, Detroit, 1994.
- BS 1881 - Part 202 - Recommendations for surface hardness tests by the rebound hammer, BSI, UK 1986.
- DIN 4240, Kugelschlagprüfung von Beton mit dichtem Gefüge, Richtlinien für die Anwendung, 4-1962.
- EN 12504-2, Testing concrete in structures – Part 2. Non destructive testing – determination of rebound number, 2001.
- EN 13791, Assessment of in-situ compressive strength in structures and precast concrete, CEN, Brussels, 28p., 2007.
- JGJ/T 23-2001, J 155-2001, Technical specification for inspection of concrete compressive strength by rebound method, 2001 (in Chinese).

Some guidelines are also available:

- AIJ, Architectural Institute of Japan, Manual of nondestructive test methods for the evaluation of concrete strength, p. 26, 1983 (in Japanese)
- FHWA, Guide to non destructive testing of concrete, FHWA-SA-97-105, USDOT, Washington DC, 1997.
- Malhotra V.M., Carino N.J., Handbook on non destructive testing of concrete, CRC Press, 2004.

## References

- Carino N.J. (1994) Nondestructive testing of concrete: history and challenges, in ACI SP-144, Concrete Technology – Past, Present and Future, P.K. Mehta Ed., ACI, Detroit, MI, pp. 632–678.
- Evangelista A.C., Shehata I., Shehata L. (2003) Parameters that influence the results of non destructive test methods for concrete strength, NDT-CE 2003, Berlin.
- Greene G.W. (1954) Test hammer provides new method of evaluating hardened concrete, ACI J., vol 26, n. 3, pp. 249–256.
- Kolek J. (1958) An appreciation of the Schmidt rebound hammer, Mag. Concr. Res., 10, 28, pp. 27–36.
- Proceq S.A. (2007a) Product brochure Original Schmidt hammer.
- Proceq S.A. (2007b) Product brochure SilverSchmidt hammer.
- Tanigawa Y., Baba K., Mori H. (1988) Estimation of concrete strength by combined non destructive testing method, ACI SP 82, pp. 57–76.

## 13 Pull-out testing

**Andrzej Moczko**

This technique is the only not fully non destructive technique described in this section. It was however considered useful to describe it briefly, since (a) it is of common practice in structural assessment and (b) it provides an output directly correlated with mechanical properties of concrete. Thus, this test can bring valuable information on the material condition, either used alone or in combination with other (non destructive) techniques.

### *13.1 Physical principles and theory*

The fundamental principle behind pull-out testing is that accurate estimation of the strength on-site can be obtained, as the peak-force (the pull-out force) correlates accurately to the concrete compressive strength measured by standard cylinders or cubes in the laboratory.

A metal insert is either cast into fresh concrete or installed into hardened concrete. When an estimate of the in-place strength is desired, the insert is pulled by means of a jack reacting against a bearing ring. The pullout strength is determined

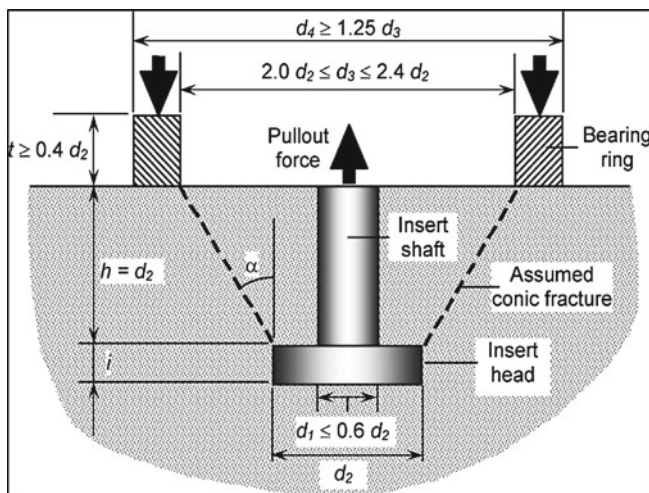


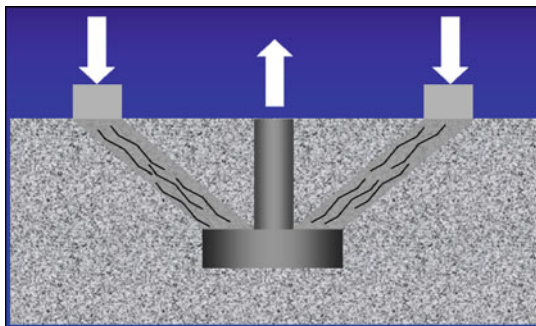
Fig. 2.1 General principles of the pull-out test

by measuring the maximum force required to pull the insert from the concrete mass. Alternatively, the insert is loaded to a specified load to verify whether a minimum level of in-place strength has been attained. It is essential to ensure that the dimensions of the pull-out test shall be determined according to Fig.2.1.

The diameter of the insert head ( $d_2$ ) is the basis for defining the test geometry. The insert head diameter shall be greater than or equal to  $2/3$  of the nominal maximum size of aggregate. A typical value is 25 mm. The thickness of the insert head and the yield strength of the metal shall be sufficient to prevent yielding of the insert during test. The sides of the insert head shall be smooth. The length of the pullout insert shaft shall be such that the distance from the insert head to the concrete surface ( $h$ ) equals the diameter of the insert head ( $d_2$ ). The diameter of the insert shaft at the head ( $d_1$ ) shall not exceed  $0.60 d_2$ . The counter pressure ring shall have an inside diameter ( $d_3$ ) of 2.0 to 2.4 times the insert head diameter ( $d_2$ ), and shall have an outside diameter ( $d_4$ ) of at least 1.25 times the inside diameter. Usually diameter of such ring is assumed to be about 55 mm. The thickness of the ring ( $t$ ) shall be at least 0.4 times the pullout insert head diameter. Finally, inserts are pulled out using a hydraulic pull machine reacting against a counter pressure ring and the force required to pull-out the insert is measured (Petersen, 1997, Petersen and Poulsen, 1993).

Internal rupture during pull-out test is a multistage process where three different stages, each with different fracture mechanisms, can be observed. In the first stage, at a level of about 30-40% of ultimate load, tensile cracking begins, starting from the notch formed by the upper edge of the insert's head. These cracks run out in the concrete at pronounced open angle (Fig. 2.2). The total length of these first cracks is typically 15-20 mm from the edge of the insert's head. In the second stage of internal rupture a multitude of stable microcracks are formed in the above mentioned truncated zone. These cracks run from the top of the insert's head to the

**Fig. 2.2** Schematic damage and cracking pattern during the pull-out test



bottom of the counter pressure ring. The formation of this second cracking pattern is similar to that of vertical microcracks inside a concrete cylinder or cubes during ordinary uniaxial compression tests.

Finally, when the load reaches ultimate value, third stage of rupture occurs. This forms a tensile/shear crack running all the way around from the outside edge of the insert head to the inside edge of the counter pressure ring. Since the second microcracking stage of rupture is responsible for and directly correlated with the ultimate load in this testing procedure, it can be accepted that pull-out force is directly proportional to the compressive strength of concrete (Krenchel, 1982, Krenchel and Shah, 1985). Moreover, it can be observed that the failure obtained in such test is caused by crushing of the concrete. This fracture mechanism has been also confirmed by nonlinear finite element analysis (Ottosen, 1981).

There are two basic categories of pull-out tests: one which involves an insert having to be cast into the concrete and the other where the expanding ring insert is fixed into a drilled hole and undercut groove in the hardened concrete.

The first procedure is mainly used to obtain a reliable estimation of the in-place strength of concrete in newly cast structures, with following main applications:

- determining whether in-place concrete strength is sufficient for early application of loads, such as due to formwork removal or application of prestressing.
- determining whether the in-place strength is sufficient for terminating curing and thermal protection.

The second pull-out procedure, based on the post-installed inserts, has been developed for determining on site compressive strength of existing concrete structures. In this case following practical application can be considered:

- evaluation of the actual compressive strength in existing concrete structures during technical surveys,
- verification of in-place strength when strength of standard-cured specimens fails to meet acceptance criteria,
- testing of the residual strength of concrete elements prior to further loading,
- quality control of the structure after completion.

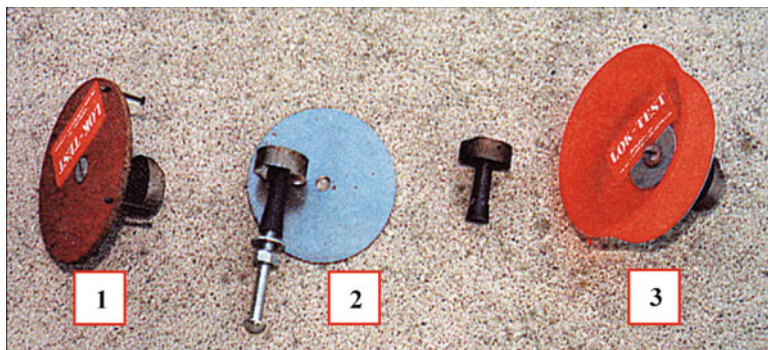


Fig. 2.3 Insert hardware

### 13.2 Measurement equipment and handling

In the case of testing focused on the estimation of the in-place strength of concrete in newly cast structures special inserts (Fig.2.2) have to be casted into the fresh concrete. Cast-in-place inserts shall be made of metal that does not react with cement. The insert shall consist of a cylindrical head and a shaft to fix embedment depth. The shaft shall be attached firmly to the center of the head. The insert shaft shall be threaded to the insert head so that it can be removed and replaced by a special bold relevant to pullout the insert. Such inserts can be installed as inserts nailed to formwork (Fig. 2.3 – type 1), as inserts attached to formwork cutouts (Fig.2.3 – type 2) or as floating inserts (Fig. 2.3 – type3). The inserts shall be embedded into the fresh concrete by means that ensure a uniform embedment depth and a plane surface perpendicular to the axis of the insert shaft.

Load is applied through a manually operated hydraulic pull-machine. The loading rate must be uniform, so that the nominal normal stress on the assumed conical fracture surface increases at a rate of  $70 \pm 30$  kPa/s. For a pullout test system in which  $d_2 = 25$  mm and  $d_3 = 55$  mm, the specified stress rate corresponds to a loading rate of approximately  $0.5 \pm 0.2$  kN/s. If the insert is to be tested to rupture of the concrete, the test is carried on until rupture occurs. If the insert is to be tested only to a specified load to verify a minimum in-place strength, the specified uniform rate is kept until the specified pullout load is reached. The specified load is maintained for at least 10 seconds. The pull-out force is recorded and correlated to compressive strength by means of a general calibration curve.

Application of pull-out technique for testing existing concrete structures needs different procedures of insert preparation. In the first stage, using special staff of equipment, a 18.4 mm diameter hole is drilled perpendicular to the surface, outside reinforcement disturbance. Next a recess (slot) is routed in the hole to a diameter of 25 mm and at a depth of 25 mm. A special split ring is inserted through the hole in the recess until it fits in the inside diameter of the recess and expanded by means of a special expansion tool (Fig. 2.4). Finally, the insert is pulled out using a pull



**Fig. 2.4** Ring expansion hardware



**Fig. 2.5** Applying the loading on the insert



machine reacting against a counter pressure ring (Fig. 2.5). As a result of the measurements pull-out force is defined and similar procedure, as in the case of in place casted inserts, is applied for determining concrete in-situ compressive strength.

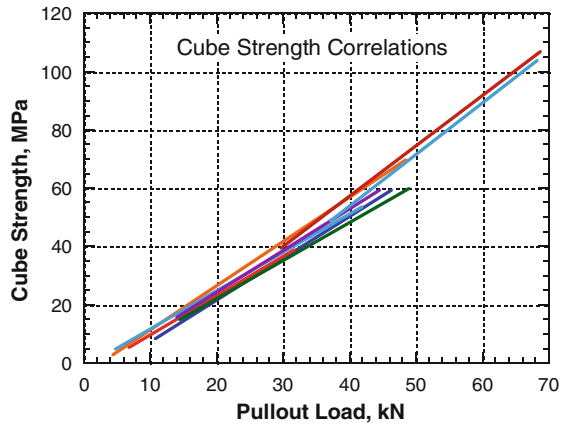
### ***13.3 Guidelines, references and standards***

ASTM C900-06, Standard Test Method for Pullout Strength of Hardened Concrete. ACI Committee 228, In-place Methods for Determination of Strength of Concrete, Technical Committee Document 228.1R-03, American Concrete Institute, PO Box 19150, Detroit, MI 48219, 2003, p. 44.

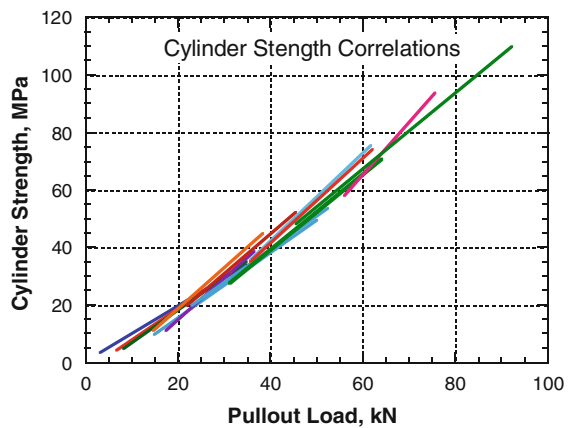
Canadian Standard CSA A23.2, Methods of Test and Standard Practices for Concrete, Test Procedure A23.2-15C – Evaluation of concrete strength in-place using the pullout test.

EN 12504-3: 2005, Testing Concrete in Structures, Part 3: Determination of „Pull-out” Force.

**Fig. 2.6** Some examples of calibration curves for cubes



**Fig. 2.7** Some examples of calibration curves for cylinders



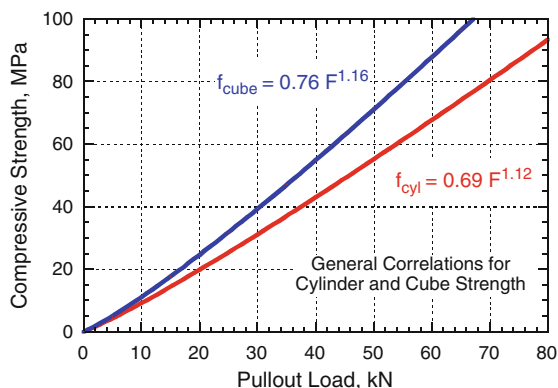
### 13.4 Calibration and interpretation of results

Several investigations have shown that the pull-out measurements provides an accurate estimate of in-place strength because the peak pullout force has a well-defined correlation to compressive strength measured using standard cylinders (Fig. 2.6) or cubes (Fig. 2.7).

More than 20 years of correlation experience from all over the world indicates close agreement, suggesting that one general correlation is applicable for all normal density concrete mixtures [(Bickley, 1982), (Carino, 1990), (Petersen and Poulsen, 1993), (Petersen, 1997)]. It is only for lightweight aggregate concrete and for mixes with maximum aggregate size larger than 40 mm that such relationships are not valid.



**Fig. 2.8** General correlation curves proposed by ACI



As an example, two following calibration equations can be assumed as a relevant approximation of the curves shown with relation to cube strength:

$$f_{c,cub} = 1.41 P - 2.82 \quad \text{for strength under 50 MPa}$$

$$f_{c,cub} = 1.59 P - 9.52 \quad \text{for strength over 50 MPa}$$

The general correlations shown in Fig. 2.8 is a more recent proposal of calibration suggested by (Carino, 1990) and recommended by equipment producer, providing sufficient accuracy for all normal density concrete mixtures. It is however necessary to mention that project specifications may require development of mixture specific correlations.

### 13.5 Reliability and limitation of results

Inserts shall be located in those portions of the structure that are critical in terms of exposure conditions and structural requirements. When pull-out tests are used for other purposes, the number of tests shall be determined by specification but at least 3 measurements for one testing area. Pull-out test locations shall be separated so that the clear spacing between inserts is at least seven times the pullout insert head diameter. Clear spacing between the inserts and the edges of the concrete shall be at least 3.5 times the head diameter. Inserts shall be placed so that reinforcement is outside the expected conical failure surface by more than one bar diameter, or the maximum size of aggregate, whichever is greater. It is not allowed to perform pull-out tests for frozen concrete.

Experience indicates that pull-out strengths are of lower value and more variable for manually-placed surface inserts than for inserts attached to formwork. In the case of post-installed inserts it is crucial to remove free-standing water from the hole at the completion of the drilling and undercutting operations. Protect the hole from ingress of additional water until completion of the test. Penetration of water into the failure zone could affect the measured pullout strength; therefore,

water must be removed from the hole immediately after drilling, grinding, and undercutting operations.

For concretes with a maximum aggregate size of 38 mm, tested by means of pull-out method, with assumption that the confidence level is equal to 95 % and for an average of at least 4 tests, the estimated compressive strength based on the general correlations indicated is within  $\pm 6$  % of the strength measured from standard specimen tests (cylinders or cubes). The average coefficient of variation for individual result is about 8% for normal density concrete.

If the range of tests results exceeds the acceptable range, further investigation should be carried out. Abnormal test results could be due to improper procedures or equipment malfunction. The user should investigate potential causes of outliers and disregard those test results for which reasons for the outlying results can be identified positively. If there are no obvious causes of the extreme values, it is probable that there are real differences in concrete strength at different test locations. These differences could be due to variations in mixture proportions, degree of consolidation, or curing conditions.

## References

- Bickley J.A. (1982) The Variability of Pullout Tests and In-Place Concrete Strength, *Concrete International*, ACI, Vol. 4, No. 4, April 1982, pp. 44–51.
- Bickley J.A. (2009) A brief history of pull-out testing with particular reference to Canada – A personal journey, *Proc. 10<sup>th</sup> ACI Int. Conf. on Recent Advances in Concrete Technology and Sustainability Issues*, Seville, Spain, oct-2009, SP-261-20, pp. 277–286.
- Carino N.J. (1990) Statistical methods to evaluate in-place test results, *RILEM, Testing during concrete construction*, Chapman & Hall.
- Krenchel H. (1982) Lok-strength and Capo-strength of concrete, ABK publication, Serie I, 71, Structural Research Laboratory, Techn. Univ. of Denmark, Lyngby.
- Krenchel H., Bickley J.A. (1987) Pull-out testing of concrete—Historical background and scientific level today, *The Nordic Concrete Federation*, No.6.
- Krenchel H., Shah S.P. (1985) Fracture analysis of the pullout test, *Materials and Structures*, *RILEM*, Vol. 18, No 108.
- Malhotra V.M., Carrette G. (1980) Comparison of Pullout Strength of Concrete with Compressive Strength of Cylinders and Cores, Pulse Velocity and Rebound Number, *ACI J.*, Vol. 77, No. 3, May–June 1980, pp. 161–170.
- Ottosen N.S. (1981) Nonlinear Finite Element Analysis of a Pull-Out Test, *Journal of the Structural Division*, *Proc. ASCE*, Vol. 107, No ST4, USA.
- Petersen C.G., Poulsen, E. (1993) Pull-out Testing by LOK-test and CAPO-test with particular reference to the in-place concrete of the Great Belt Link, Revised Edition, November 1993.
- Petersen C.G. (1997) LOK-TEST and CAPO-TEST Pullout Testing – Twenty Years Experience, *Proc. Int. Conf. NDT-CE*, British Institute of Nondestructive Testing, U.K., J.H. Ed. by J.Bungey, Liverpool, 8–11 April 1997, pp. 77–96.
- Soutsos M.N., Bungey J.H., Long, A.E. (2005) Pullout Test Correlations and In-Place Strength Assessment The European Concrete Frame Building Project, *ACI Materials Journal*, Vol. 12, No. 6, Nov-Dec 2005, pp. 422–428.
- Stone W.C., Carino N.J., Reeve C.P. (1986) Statistical Methods for In-Place Strength Prediction by the Pullout Test”, *ACI Journal*, Vol. 83, No. 5, Sept-Oct. 1986, pp. 745–755.
- Yun C.H., Choi K.R., Kim S.Y., Song Y.C. (1988) Comparative evaluation of non-destructive test methods for in-place strength determination, *ACI Special Publ.*, SP 122-6, 1988, Detroit, USA.

# Chapter 3

## Estimation of on-site compressive strength of concrete

Marios N. Soutsos, Denys Breysse, Vincent Garnier, Arlindo Goncalves, and Andre Valente Monteiro<sup>1</sup>

### 1 Introduction – definition of the problem

The finding that concrete strength in a structure was not correctly described by the strength of specimens moulded and stored under controlled standard conditions, led to the study of the relation between actual and potential strength of concrete. To avoid damaging the structure it became later necessary to develop non-destructive techniques to assess the in-situ concrete compressive strength.

According to (Petersons, 1964), the first studies were performed in 1915 by Berndt and Preuss (Germany), who compared the concrete strengths of moulded cubes and of cubes sawn from large concrete blocks. In the 1930s several authors, especially in the USA, reported experimental results obtained during the execution of concrete pavements, where cores were drilled to determine the compressive strength and thickness of concrete and the results compared with those of moulded specimens.

The first attempts made to assess concrete strength using non-destructive techniques were, most likely, performed in Germany in 1934 (Jones, 1962). The

---

<sup>1</sup>Other contributors to this chapter are: J. Bungey, M. Fischli, A. Gennaro-Santori, J.F. Lataste, A. Moczko, F. Pires and M.A. Ploix. The authors also thank corresponding members: G. Tickell, P.A.M. Basheer, A.E. Long, S. Nanukuttan, C.G. Petersen and P. Gilles.

M.N. Soutsos (✉)  
University of Liverpool, U.K.  
e-mail: M.N.Soutsos@liverpool.ac.uk

D. Breysse  
Université Bordeaux 1, I2M, GCE (Civil and Environmental Engineering Department), France

V. Garnier  
Université de la Méditerranée, IUT Aix-en-Provence, France

A. Goncalves • A.V. Monteiro  
Laboratório Nacional de Engenharia Civil, Lisbon, Portugal

strength determination relied upon indentation methods, in which the diameter of the impression made by a metallic sphere having a given initial amount of kinetic energy was measured. The diameter and/or depth of the indentation were considered as being a measure of the concrete hardness, which, in turn, was an indicator of the compressive strength of concrete. Several indentation type methods were developed shortly after, namely the Testing Pistol by Williams, the Spring Hammer by Frank, and the Pendulum Hammer by Einbeck (Malhotra and Carino, 2004), with the first results being presented in 1936 by Williams.

Nevertheless, the main increment in the use of these techniques was verified only after 1948, when Ernst Schmidt, a Swiss engineer, developed the so called “Rebound Hammer” method, which was inspired in the Shore method used to determine the metals surface hardness.

As the above methods assessed only the condition of the concrete surface, new test methods were developed to evaluate the concrete below the surface, based on the determination of the depth of penetration of probes (steel rods or pins) into concrete. This provides a measure of the penetration resistance of the material, which is an indirect measure of its strength. The first results were published in 1954 (Voellmy, 1954), however it was only after the development, in 1965, of a device known as the Windsor probe, that this technique has registered a significant widespread, especially in the USA.

Meanwhile, since the 1930s, several resonant frequency methods were being used in the laboratory to assess the concrete elasticity modulus, and later on the pulse velocity method was also adopted to assess the degradation and cracking of concrete.

From the 1960s onwards, this method started to be used in-situ to estimate the concrete strength, and still on the same decade, combined methods have emerged. For instance, (Skramtaev and Leshchinsky, 1966) in Russia, and (Facaoaru, 1970) combined ultrasonic pulse velocity and hardness measurement techniques (rebound hammer) to improve the reliability and precision of the concrete strength estimation.

Another way to improve the concrete strength estimations was achieved from 1970 onwards, through the development of methods like pull-out test, pull-off test, internal fracture test and break-off test. All these techniques measure some type of strength, but they cause some damage to the concrete surface. By far, the most popular method has been the pull-out test, while the pull-off test has been used mainly to assess the adhesion between layers, mostly in repair works.

Combining more than two non destructive techniques and analysing the results by multivariate analysis or data fusion methodology, significant improvements on concrete strength estimation may still be obtained.

## ***1.1 What is Looked For?***

The development of in-situ tests is linked to the perceived needs for assessing in-situ concrete quality. Determination of in-situ concrete strength has traditionally been performed for two reasons:

- (a) Evaluation of an existing structure: There is a great deal of interest in in-situ testing of hardened concrete, largely as a result of an increase in the number of

concrete structures showing signs of deterioration. To investigate the nature and extent of the problem, and to ensure that new structures are built to appropriate standards, a range of in-situ test methods has continued to be developed and assessed in relation to materials developments, e.g. high strength concrete (Price and Hines, 1996).

- (b) Monitoring strength development during new construction: In-situ tests are needed to determine the concrete strength at critical locations in a structure and at times when crucial construction operations are scheduled (ACI, 1995). Traditionally, some measure of the strength of the concrete in the structure has been obtained by using field-cured cubes or cylinders. These are supposedly cured on or in the structure under the same conditions as the concrete in the structure. However, measured strengths of field-cured specimens are often significantly different from in-situ strengths because it is difficult, and often impossible, to have identical bleeding, compaction, and curing conditions for concrete in specimens and concrete in structures. Differences in internal temperature at early ages due to differences in volume may be especially important. Field cured specimens can also give rise to errors due to improper handling or inappropriate storage, which may result in misleading data for critical operations. To meet rapid construction schedules, form removal, application of post-tensioning, termination of curing, and the removal of props must be carried out as early and safely as is possible. The determination of in-place strength to enable these operations to proceed safely at the earliest possible time requires the use of in-situ tests which have been established as reliable. The need for such strength information is emphasized by several construction failures [(Carino et al., 1983), (Lew, 1980)] which could have been prevented had in-place testing been used. The use of in-situ tests not only increases safety but can result in substantial savings in construction costs by permitting accelerated construction schedules. Guidance on formwork stripping on the basis of insitu tests has been given by (Harrison, 1987).

In-situ testing has been shown, by recent construction projects, to offer the opportunity to lessen the reliance on the testing of standard-cured cubes or cylinders as the only method to judge acceptability of the concrete delivered to site. The added benefit of in-situ testing is that it provides assurance that the finished construction has the properties intended by the designer. This has been demonstrated by projects in Denmark and Canada, described below:

- The Great Baelt Link – Denmark (Petersen and Poulsen, 1993)  
It is becoming recognised that the durability of exposed structures is dependent strongly on the curing history. Therefore, it is desirable to have assurance that the finished structure has the necessary properties to attain the desired level of performance. The Great Baelt Link project in Denmark is one of the first large-scale construction projects in which the owners relied on in-situ testing (pullout tests) to assess the acceptability of the concrete layer protecting the reinforcement.
- The Trinity Square Head Office and The College Park Phase II Building – Canada (Bickley, 1984)

Bickley has reported on two demonstration projects where in-situ testing was used not only for early-age strength determination of horizontal elements but also for confirmation of the 28-day design strength. Permission to waive standard cylinder testing was obtained from the Building Official. Innovative clauses were included in the project specifications that defined the frequency of in-place tests and the procedures to follow in performing the tests and reporting the results. Acceptance of the concrete was based on the results of pullout tests performed on the structure at 28 days. Individual pullout tests were converted to compressive strengths based on predetermined strength relationships. The standard deviations of these estimated strengths were computed and subsequently the expected percentages of strength below the characteristic strength were shown to be less than 10 percent. The in-situ test results demonstrated that the concrete had acceptable strength.

Another factor that has promoted interest in in-situ testing is the introduction of performance related specifications [(Sanja and Verikari, 1996), (Concrete, 1995), (Kropp and Hilsdorf, 1995), (Harrison, 1996) (RILEM TC-230, 2008) (Fib TG8.10, 2011)], particularly in highway construction. The argument is that the change will result in innovation by contractors and in better quality products with reduced life-cycle costs (Carino, 1994).

## 1.2 At What Scale?

The principal application of in-place tests is to *estimate* the compressive strength of the concrete. Most design codes, e.g. ACI 318 (ACI, 2005) and Eurocode 2 (BS EN, 2004) are based on the compressive strength of standard cylinders or standard cubes. Although in-place tests can be used: (a) during construction, so that operations that require a specific strength can be performed safely or curing procedures can be terminated, and (b) during the evaluation of existing structures, the significant characteristic of most of these tests is that they *do not directly* measure the compressive strength of the concrete in the structure. Instead, they measure some other property that can be correlated to compressive strength. Thus, to evaluate structural capacity of an existing building or structural capacity under construction loading, it is necessary to have not only an estimate of the equivalent cylinder or cube strength but also an estimate of the characteristic strength of the concrete as it exists in the structure. If in-place tests are used then: (a) a valid relationship between the results of in-place tests and the compressive strength of cylinders or cubes must be established, and (b) there must be an agreed statistical procedure to convert the estimated in-place cylinder or cube strength to characteristic strength.

For example:

- a) Historically, most strength relationships have been assumed to be straight lines but ACI Committee 228 (ACI, 1995) recommends a more rigorous analysis based on a power function. While the latter may yield more accurate strength predictions, it requires a lot more data points to be determined. This may not be practical on site and therefore if such a relationship is to be used then the data must be from previous projects, i.e. a “general” correlation, like the one

recommended by the pull-out manufacturer (Petersen and Poulsen, 1993) (see Chapter 2, §13 – pull-out technique), where the aggregates and mix proportions may differ from the specific mix to be used for the project at hand.

- b) While specific mix correlations are likely to have between six and nine data points, the manufacturer's correlation will have a lot more data points over a wider range of strengths. Both are important factors in determining the best-fit line for a strength correlation which will be close to the true one.

Attempts to estimate the accuracy of the above methods for obtaining the strength relationship have been indirect. The direct method would require comparison of the estimated strength by the in-place test with the compressive strength obtained from cores. Cores, because of the large number required, are not an option especially for new construction. Thus the indirect method relies on the use of a combination of test methods, e.g., maturity method together with pull-out tests (Soutsos et al, 2000), in order to obtain the strength estimates. Traditionally, some measure of the strength of the concrete in the structure has been obtained by using field-cured cylinders or cubes prepared and cured in accordance with ASTM C31/C31M (ASTM, 2003). These cylinders or cubes are cured on or in the structure under, as nearly as possible, the same conditions as the concrete in the structure. Cylinders or cubes are usually obtained from one batch of concrete while the in-place tests are usually carried out over the whole structural element, e.g., a concrete slab, which may have required several deliveries of concrete. It is therefore impossible, because of the variability of delivered concrete, to have a direct comparison between in-place tests and concrete cubes. It is not therefore surprising that ACI Committee 228 has called for: *“Additional fundamental research to improve the understanding of how in-place tests are related to concrete strength and how the tests results are affected by factors other than strength”* (ACI, 2003).

### 1.3 For What Purpose?

Sound and proven statistical procedures should be used to interpret in-place tests. It is not sufficient to simply average the values of the in-place test results and then compute the equivalent compressive strength by means of the previously established relationship. It is necessary to account for the uncertainties that exist. In designing a structure to safely resist the expected loads, the engineer uses the specified compressive strength,  $f_{cy}$  and  $f_{cu}$  for cylinders and cubes respectively. The strength of the concrete in a structure is variable and the specified or characteristic compressive strength is taken to be approximately the strength that is expected to be exceeded with about 90% and 95% probability, i.e. 10% (ACI 214R-02 (ACI, 2004) in the USA) and 5% (Design of Normal Concrete Mixes (Teychenne et al, 1988) in the UK) of tests are expected to fall below the specified strength). The statistical procedures for interpretation of non-destructive test results appear to differ in the way that they take into account the variability of the in-place strength. It has been shown that the within-test variability of in-place test results is generally greater than for compressive test results. (Stone et al, 1986) showed that the differences in the

“rigorous”, “Danish” and “tolerance factor” methods could be as high as 40% when the in-place tests had high variability. It is not therefore surprising that ACI Committee 228 (ACI, 2003) called for: “*Experimental studies to compare the in-place specified or characteristic strength estimated by different statistical methods with the values obtained from many core tests. Only then can the reliability of the statistical methods be evaluated.*”

The above described deficiencies have been impediments to widespread adoption of in-place tests. There is now a revived interest internationally in these methods and in investigating whether improvements in concrete strength predictions can be achieved by a combination of non-destructive test methods.

## 2 Description of the Techniques

Key features of non-destructive test methods will be briefly described. Reviews of the history and technical basis of these testing methods have been reported by other authors [(Carino, 1994), (ACI, 1995), (Bungey and Millard, 1996), (Malhotra and Carino, 2004)]. Details of available equipment are given in CIRIA Technical Note 143 (Bungey, 1992).

Several in situ tests can be used for compressive strength assessment. Among them, Rebound Hammer, Ultrasonic Pulse Velocity and Resistivity Methods have been presented in the preceding chapter. The reader is invited to refer to this chapter where their basic principles, reliability and limitations have yet been discussed. The pull-out test has also been briefly presented in Chapter 2. Additional information is given here. Lastly, two other techniques, namely Penetration Resistance and Pull-off test will be presented in the following.

### 2.1 Penetration Resistance

The underlying principle of this test is that, for standard test conditions, the depth of penetration of a probe, see Fig. 3.1, is inversely proportional to the compressive strength but in fact, no theoretical basis for this has been established. However, like the rebound hammer, this is a hardness tester and the probe penetration does relate to some property of the concrete below the surface. It has thus been possible to develop empirical correlations between strength properties and the penetration of the probe.

The driver, which is also shown in Fig. 3.1, utilizes a carefully standardized powder cartridge. This imparts a constant amount of energy to the probe irrespective of firing orientation, and produces a velocity of 183 m/s which does not vary by more than  $\pm 1\%$ . The power level can be reduced when dealing with low strength concretes simply by locating the probe at a fixed position within the driver barrel. For lightweight concrete special power cartridge and probe are also available. The





**Fig. 3.1** Penetration resistance probes and associated equipment

driver is pressed firmly against a steel locating plate held on the surface of the concrete which releases a safety catch and permits firing when the trigger is pulled. After firing, the driver head and locating plate are removed and any surface debris around the probe is scraped or brushed away to give a level surface. A flat steel plate is placed on this surface, and a steel cap screwed onto the probe to enable the exposed length to be measured to the nearest 0.5 mm with a spring-loaded calibrated depth gauge.

Manufacturers of penetration resistance probes and associated equipment supply curves and tables relating the exposed length of the probe to the strength for concretes containing coarse aggregates with various values of hardness. However, the manufacturers' tables do not always give satisfactory results. Therefore, it is recommended that the relationship between strength and depth of penetration is established by experiments for the particular concrete which is to be investigated.

The result is likely to represent the concrete at a depth of 25-75 mm from the surface rather than just the property of the surface layer as in the surface hardness test. The test however leaves an 8 mm hole in the concrete and may even fracture the area around the point of penetration. The test has been reported to be efficient for determining the formwork removal time and as a substitute for core testing. (Swamy and Al-Hamed, 1984) reported that penetration resistance can be used to estimate the early age compressive strength better than small diameter cores. The test procedure is described in ASTM C 803 (ASTM, 2003) and in BS 1881: Part 207 (BS, 1992).

## **2.2 Pull-out Test**

The pull-out test is based on the concept that the compressive strength of concrete is related to the maximum pull-out force which can be applied to an embedded insert before the concrete fails. There are two basic categories of pull-out test: one

which involves an insert having to be cast into the concrete and the other where the insert is introduced into a drilled hole in the hardened concrete.

The first published reports of these types of tests were in the USA and USSR in the late 1930's. These early tests were however not popular because they were quite cumbersome and unrefined. It was not until some thirty years later that practical feasible versions of these tests were developed. The two main parties involved in these developments were in Canada and Denmark. The principal difference was in the shape of the inserts and the loading technique used. In both cases however a cone of concrete was 'pulled out' and the force required to achieve this was translated to compressive strength by the use of an empirical calibration curve.

### **2.2.1 Pull-out with inserts cast into the concrete**

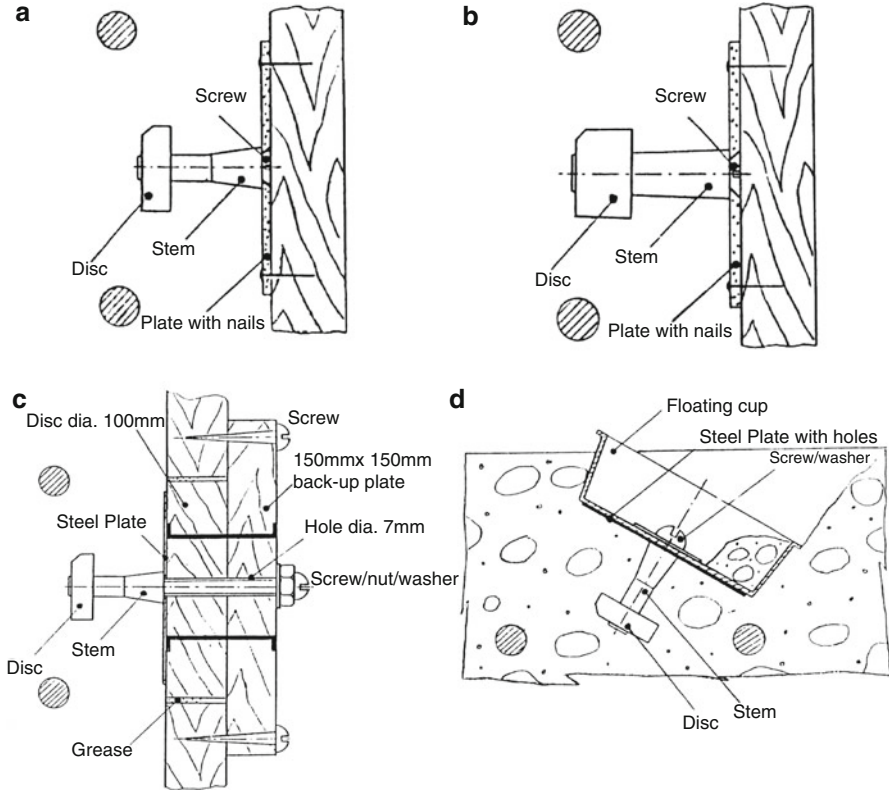
The fundamental principle behind this test is to measure the tensile force required to 'pull-out' a metal insert which has been cast into the concrete. Load is applied through a manually operated jack which bears against the concrete surface through a reaction ring of 55 mm internal diameter. There are two main types of insert, one which is attached directly to the formwork and another which is fixed to a plastic buoyancy cup which 'floats' on the top surface of the concrete for use on slabs. Both types of insert can be seen in Fig. 3.2.

The basic geometry of both inserts is the same, i.e. each has a 25 mm diameter disc attached to a removable stem which locates the disc 25 mm below the concrete surface, see Fig. 3.2. There are two different strength classes of insert available, 0-50 kN and 0 - 110 kN. The main difference between these two is the thickness of the disc (approximately 8 mm for the 0 - 50 kN inserts and 16 mm for the 0 - 110 kN inserts). To prevent the disc rotating when the stem is being removed a 15 mm chamfer is formed on one side of the disc, see Fig. 3.2.

The testing procedure is described at the relevant section in Chapter 2, as the use of a calibration curve to estimate the concrete compression strength from the peak force recorded during the test.

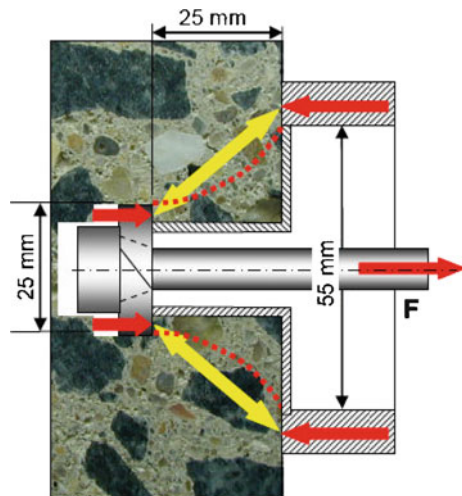
### **2.2.2 Pull-out with an expanding ring inserted into an undercut groove**

The pull-out with an expanding ring, see Fig. 3.3, inserted into an undercut groove was developed for situations where testing cannot be pre-planned. The basic geometry of the pull-out test described in Section 2.3.1 has been maintained. The procedure consists of drilling a 45 mm deep, 18 mm diameter core hole, after which a 25 mm diameter groove is cut at a depth of 25 mm using a portable reaming machine. The expanding ring insert is then placed and expanded into the groove using a pull-bolt assembly, see Fig. 3.4. The conventional pull-out test jack is then used as previously described but testing must continue until the cone of concrete has been removed to allow retrieval of the pull-bolt assembly. The expandable ring can be recovered and re-compressed for re-use if required although this procedure may not



**Fig. 3.2** Pull-out inserts: (a) L-40 (0-50kN) (b) L-41 (0-110kN) (c) L-42 attached through a wooden shutter port hole and (d) L-49 floating type

**Fig. 3.3** Basic geometry of the pull-out test with an expanding ring inserted into an undercut groove (after [http://www.germann.org/Articles/download\\_files](http://www.germann.org/Articles/download_files))



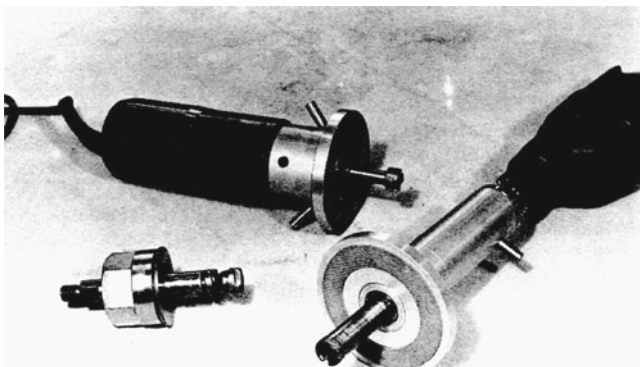


Fig. 3.4 Equipment needed for undercut groove (after Teychenne et al, 1988)

always be successful. The cube compressive strength is estimated using an empirical correlation chart similar to that used with the other type of insert.

### 2.3 Pull-off Test

The collapse of roofs made of prestressed High Alumina Cement (HAC) in 1973-1974 in the UK resulted in a ban on the use of HAC in structural applications (Midgley, 1990). All buildings in which HAC had been used came under suspicion as it was gradually accepted that the conversion of  $CAH_{10}$  and  $C_2AH_8$  to  $C_3AH_6$  at temperatures above  $20^\circ C$  could cause loss of strength (Neville, 1963). As a result, there was an immediate need for evaluating the conditions of the existing structures made from HAC, leading to an increasing awareness of the need for an in-situ test that would not seriously weaken members under investigation but would give a reliable estimate of the concrete's compressive strength. A new generation of tests was thus developed and amongst them was pull-off test (Long, 1979). Loading was initially applied via a universal testing machine in the laboratory, but in order to permit in-situ testing, portable hydraulic equipment was developed. Further developments included a digital read-out. This mechanical system was purposely designed for ease of use on site (Long and Murray, 1981). Figure 3.5 shows a currently available pull-off test equipment.

The pull-off method involves bonding a circular steel probe to the surface of the concrete by means of an epoxy resin adhesive. Slowly increasing tensile force is then applied to the probe and, as the tensile strength of the bond is greater than that of concrete, the latter will eventually fail in tension. The amount of overbreak is usually small so the area of failure can be taken as being equal to that of the probe. To avoid overbreak, partial coring may be performed (see § 3.1.4). A nominal tensile strength for the concrete can be obtained by dividing the force applied by the area of the probe. The test is covered by EN 1542, developed for measuring the bond strength of repair products.



Fig. 3.5 Portable Pull-off Tester (left), circular steel probe (right)

### 3 Calibration Aspects and Assessment of Characteristic In-situ compressive strength

#### 3.1 Calibration Aspects

The objective of an in-place test is to obtain an estimate of the properties of concrete in the structure. Very often the desired property is the compressive strength. To make a strength estimation it is thus necessary to have a known relationship between the result of the in-place test and the strength of the concrete for the particular concrete mix concerned. The usual practice in determining the strength relationship is to treat the average values of the replicate air-cured cube compressive strength and in-place test results at each strength level as one data pair. The data pairs are plotted using the in-place test value as the independent value (or X variable) and the compressive strength as the dependent value (or Y variable). Regression analysis is performed on the data pairs to obtain the best-fit estimate of the strength relationship.

Most part of the information discussed in this section originates in a large experimental program, namely the Cardington project, developed in the 1980s in the UK. However calibration issue shares many points in common independently of the non destructive technique used. These points will be addressed in the following. They are:

- the factors that can affect the correlation. These factors can originate from the material, e.g. concrete components, from the environment, e.g. temperature or humidity or from the testing procedure;
- the statistical relevance of the correlation and the possibility to use it in order to estimate the strength of a similar or a different concrete;
- the use of these correlations for estimating “low properties” (e.g. characteristic strength).

Calibration aspects of the following non-destructive tests will be briefly described here for: (1) Rebound Hammer, (2) Penetration Resistance, (3) Pull-out test, (4) Pull-off test, (5) Ultrasonic Pulse Velocity (UPV) measurements, and (6) Resistivity Methods.

### 3.1.1 Rebound Hammer

The correlation between the  $Q$  value provided by the test and the compressive strength of a concrete element is represented by a conversion curve (see Chapter 2, § 12). Conversion curves are available for a wide range of compressive concrete strengths, including low and high strength concrete  $f_c < 10$  MPa and up to 110 MPa. Depending on the range of compressive strength under test, it is advantageous to use various combinations of hammer type and plunger.

Conversion curves for different types of modern concrete may also be preset in modern digital rebound hammer equipment. The new equipment has a differential optical absolute velocity encoder guaranteeing high accuracy in measurements. Measurements are not affected by impact direction and therefore there is no need for any correction to be applied.

A large variety of conversion curves have been proposed by researchers and manufacturers, e.g.

$$f_c = 1.398 Q - 20.17$$

where  $Q$  is the rebound number and  $f_c$  the strength of a concrete between 14 and 56 days old [Proceq, 2007].

In the lower range of compressive strengths up to approximately 40 MPa, the mushroom plungers exhibit a conversion curve with a lower gradient when compared to those of the standard plungers. This yields a better prediction for the compressive strength based on the measured  $Q$  value. Further to this, the variation of the measured values is lower when compared to the standard plunger. The standard plunger can cause some damage to the test surface when used on low strength concrete up to approximately 10 MPa. This in turn led to greater variation of the measured values on a particular concrete and also on measurements between different concretes. The mushroom plunger should not however be used for concrete strengths above 40 MPa as it is not possible to ensure sufficient accuracy in strength estimates. The standard plunger should be used above 40 MPa.

Accuracy of compressive strength estimates can be improved by establishing a specific conversion curve for the concrete under investigation. The shape of the relationship between  $Q$  and strength depends on the authors. It can be linear or bilinear, exponential, polynomial or power law.

Moisture condition type of aggregate and carbonation depth of the material can affect the strength estimate [Kim et al, 2006] and some standards (e.g. Chinese standards JGJ/T 23-2001) offer recommendations for compensating these effects.

### 3.1.2 Penetration Resistance

Empirical relationships between penetration and strength are required. Calibration is hampered by the minimum edge distance requirement which prevents splitting. Although it may be possible to use standard 150 mm cubes or cylinders for tests at low power, the specimens must be securely held during the test. A holding jig for cylinders is available and cubes are most conveniently clamped in a compression-testing machine, although no data concerning the influence of applied compressive strength are available. It is recommended that groups of at least six specimens from the same batch are used, with three tested in compression and three each with one probe test, and the results averaged to produce one point on the calibration graph.

Where the cube strength of the concrete is greater than 26 MPa it is necessary to use a combination of cubes or cylinders for compressive testing and larger slab or beam specimens from the same batch for probing. Relationships between penetration and strength for the two different power levels are not easily related, and it is therefore necessary to produce calibration charts for each experimentally.

Calibration tables in which aggregate hardness is taken as the only variable influencing the penetration/strength relationship are available from manufacturers. However, these appear to ignore that the aggregate type and its amount can also have a large influence. Use of calibration tables that are based on crushed rock may give an overestimate of the compressive strength of concretes with rounded gravel as the aggregate.

The test is not greatly affected by operator technique, although verticality of the bolt relative to the surface is obviously important and a safety device in the driver prevents firing if alignment is poor. It is claimed that an average coefficient of variation for a series of groups of three readings on similar concrete of the order of 5% may be expected, and that a correlation coefficient of greater than 0.98 can be achieved for a linear calibration relationship for a single mix. 95% limits of about  $\pm 20\%$  on predicted strengths may be possible for a single set of three probes, given adequate calibration charts.

### 3.1.3 Pull-out test

Historically, most strength relationships have been assumed to be straight lines, and ordinary least-squares analysis has been used to estimate the corresponding slopes and intercepts. Figure 3.6 shows that the Y intercepts and the slopes of the strength correlations vary considerably. The data used in Fig. 3.6 are from work undertaken as part of the European in-situ concrete frame building project which was located in a large airship hangar at Cardington in the UK (Bungey et al, 2000). This facility was operated as a laboratory by Building Research Establishment Ltd (BRE). The full scale seven-storey in-situ advanced reinforced concrete building frame, designed to Eurocode 2 by Buro Happold, encompassed a range of different mixes (w/c between 0.25 and 0.52), including high strength concretes (28-day compressive strength between 47.2 and 102.8 MPa) and advanced construction techniques.



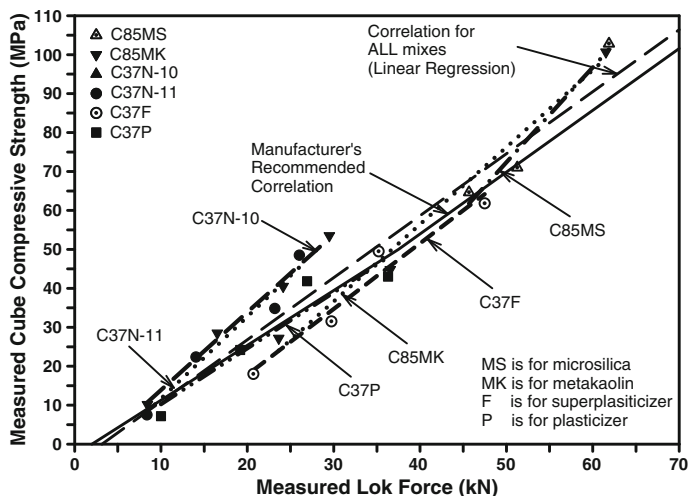


Fig. 3.6 Lok test strength correlations (after Bungey et al, 2000)

It must be noted that the manufacturer of one pull-out type of equipment recommends (Petersen, 1997) two different relationships for Lok force readings according to the ultimate load value:

$$f_c = -2.82 + 1.41 F_u \quad \text{if } F_u \leq 37 \text{ kN} \quad \text{and}$$

$$f_c = -9.52 + 1.59 F_u \quad \text{if } 37 \text{ kN} \leq F_u \leq 70 \text{ kN}$$

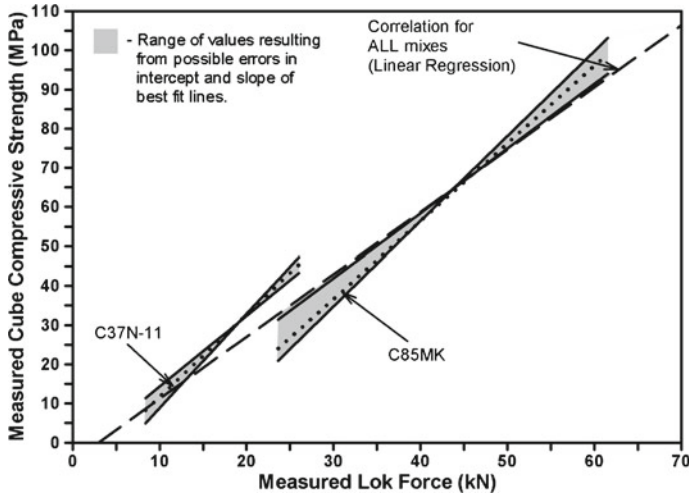
where  $F_u$  is the Lok force (kN) and  $f_c$  is the air-cured concrete cube compressive strength (MPa).

The difference in the slopes of strength correlations of normal and high strength concrete mixes have been the subject of further investigation. Figure 3.7 shows the possible errors in intercept and slope of the best fit lines determined using the least squares method for a normal and a high strength concrete. It is seen, especially in the case of the high strength concrete, that the envelope of possible best-fit lines almost encompasses the general correlation for all mixes. The manufacturer of the Lok test jack has indicated that, in addition to the number of data points, a wide range of values, i.e. from as low as possible to as high as possible, is also an important factor in determining the best-fit line for a strength correlation which will be very close to the true line. In this case, the possible errors in intercept and slope will be very small. Therefore the accuracy of the strength predictions at either side of the average of all Lok force values will improve.

In order to get a wide range of values, all the data points from the different mixes were grouped together. These were only sufficient for a single equation to be determined for the whole range of Lok force values. The equation of the combined strength correlation, based on air-cured cube compressive strengths, was found to be:

$$f_c = -4.71 + 1.59 F_u$$





**Fig. 3.7** The possible errors in intercept and slope of the best fit lines determined using the least squares method for a normal and a high strength concrete

The linear regression equation obtained when all mixes were grouped together is very close to the Manufacturer’s Correlation (Petersen, 1997), see Fig. 3.6, which has been derived from a wide range of concrete mixes made with gravel, limestone and granite aggregates. This line crosses the Manufacturer’s recommended correlation at a Lok force of 10.5 kN but because of its different slope it results in an estimated in-situ strength which is higher by 4.8 MPa at a Lok force of 37 kN. Beyond this Lok force, the Manufacturer’s recommended correlation has the same slope.

ACI Committee 228 [ACI, 2003] recommends a more rigorous analysis based on the regression analysis of the average of the natural logarithms of the test results at each strength level. For a linear relationship, the equation is as follows:

$$\ln C = \alpha + \beta \ln I$$

where  $\ln C$  is the average of natural logarithms of compressive strengths and  $\ln I$  is the average of natural logarithms of in-place test results. The above equation can be transformed into a power function:

$$C = e^\alpha I^\beta$$

This not only allows for a non-linear strength relationship, if such a relationship is needed, but it also satisfies one of the underlying assumptions of the ordinary least squares method of analysis (constant error in the Y value). It is generally accepted that the within-test variability of standard cylinder or cube compression tests is described by a constant coefficient of variation. Therefore, the standard deviation increases with increasing compressive strength. It follows that by taking the natural logarithms of groups of test results, which have the same coefficient of

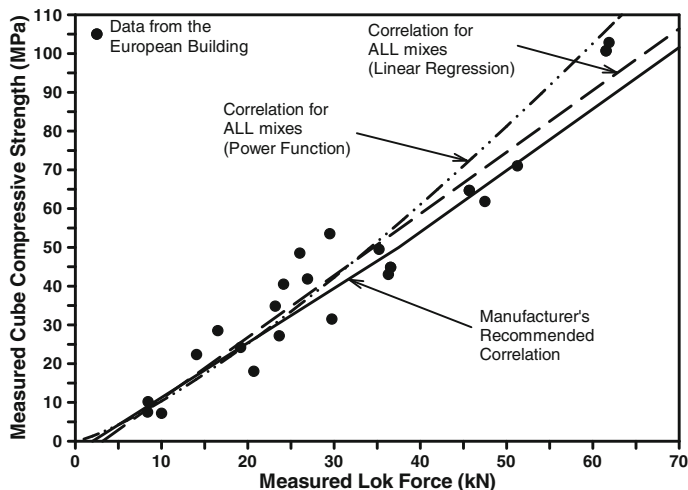
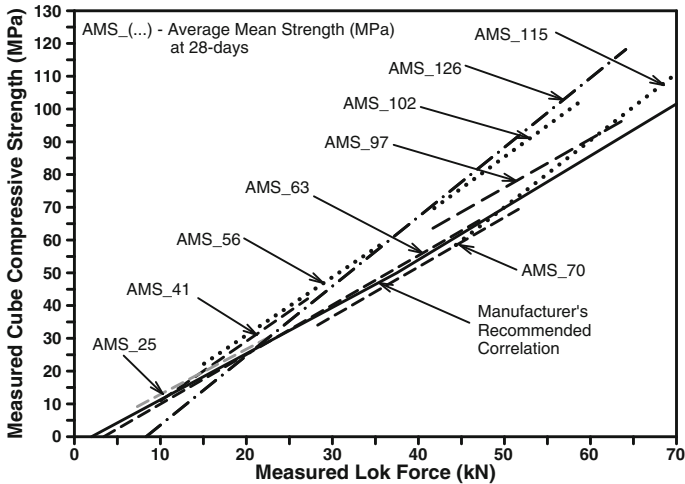


Fig. 3.8 Lok test strength correlation based on a power function

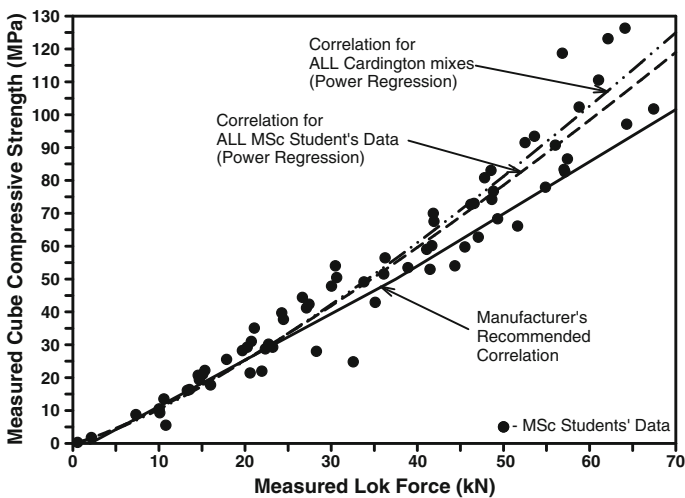
variation, the standard deviations of the logarithm values in each group will have the same value. The calculations for this more rigorous procedure are outlined in the ACI Committee 228 report (ACI, 2003).

The relationship obtained with the above procedure is shown in Fig. 3.8. There is a surprising similarity between the power function and the linear regression equations obtained for strengths in the range 5 to 40 MPa. It is only above the compressive strength of 40 MPa that the two correlations appear to deviate from each other resulting in a difference of 12 MPa at the Lok force of 60kN. The linear correlation gives the lower value of 90 MPa compared to 102 MPa estimated by the power function. (Price and Hynes, 1996) have suggested that (a) pull-out tests become less sensitive to changes in compressive strength at high strength levels, and (b) strength correlations obtained for high strength concretes show increasing divergence from the manufacturer's recommended correlation at higher strength levels. Several series of tests were subsequently carried out by undergraduate and postgraduate student at the University of Liverpool [(Teng, 1999), (Kouris, 2001), (Papadopoulou, 2003), (Lim, 2001)] in an attempt to confirm these suggestions. Granite aggregate had to be used in order to achieve the high strengths, up to 126 MPa at 28-days, required for this work.

Figure 3.9 shows the strength correlations, based on linear regression, for the individual mixes with various average mean strengths (AMS) at 28-days. The manufacturer's recommended correlation appears to be below the correlation obtained for strengths greater than 70 MPa, i.e. it underestimates/gives safe estimates of the in-situ concrete strength. Power function regression analysis of all the data obtained by the postgraduate students, see Fig. 3.10, show clearly the divergence at higher strength levels from the manufacturer's recommended correlation. The correlation for specimens cast and tested in the laboratory also shows surprisingly good agreement with



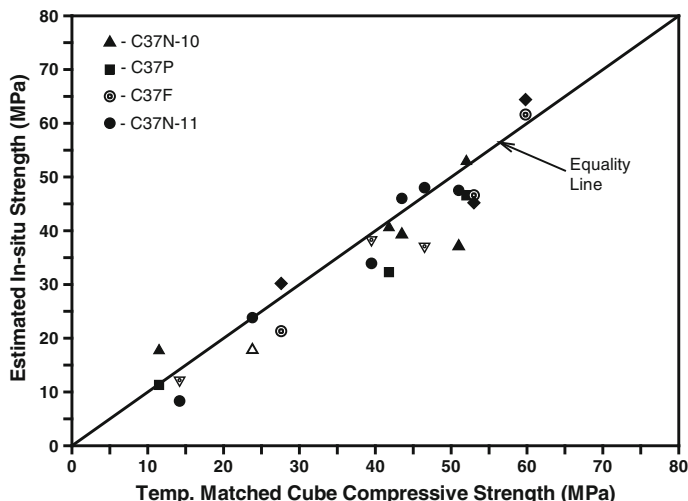
**Fig. 3.9** Pull-out test strength correlations determined for granite concretes (after [(Teng, 1999), (Kouris, 2001), (Papadopoulou, 2003), (Lim, 2001)])



**Fig. 3.10** Power function pull-out test strength correlations w (after [(Teng, 1999), (Kouris, 2001), (Papadopoulou, 2003), (Lim, 2001)])

the one obtained from the Cardington mixes. Based on these studies it was felt that the power function relationship was the more appropriate one to use for the whole range of mixes used for the European Reinforced Concrete Building project.

The wisdom of assuming that all the data obtained from the different mixes belong to one population, to give a strength relationship which is close to the true one, can only be tested in the context of the overall in-situ strength estimates.



**Fig. 3.11** In-situ strength (pull-out) versus Temperature Matched Cube results

The strength correlations determined previously have been used to estimate the in-situ strengths based on measurements on the structure. These are compared to strengths obtained from air-cured and temperature matched cured cubes, at different ages.

The in-situ strengths should ideally be related to strengths obtained from temperature matched cured cubes, see Fig. 3.11. The average coefficient of variation from this equality line was found to be 13.9%. Unfortunately, this comparison was only possible for the C37 mixes, as no temperature matched cured cubes for the C85 concretes were available for testing. Although temperature matched cured cubes, using sensors located in the middle of the pour, should have the same temperature curing regime as that of the concrete in the structural element, there may be differences in the compaction which can still lead to differences in strengths, e.g., the average difference found between the top and soffit strengths of slabs at mid-bays was 13.6 %, the highest compressive strength being at the soffit. (Murray and Long, 1987) have reported similar coefficients of variation of strengths within individual structural members for a car park. It is not therefore surprising that the in-situ strengths have an average coefficient of variation of 13.9% from the equality line.

Figure 3.12 shows the estimated strengths for columns and slabs, versus the measured compressive strengths obtained from air-cured companion cubes. The general trend is that early age strengths are higher in the structural element, while the 28-day strengths are lower than those of cubes cured alongside the structure. This is due to the difference in the temperature curing regime of the concretes in a structural element and in air-cured cube moulds. The effect of subjecting concrete to a high temperature regime during its early life is to accelerate the early strength gain of the concrete but to impair the long term strength development. The peak temperatures in the column and in the air-cured cube for the C85MS concrete were 41°C and 16°C

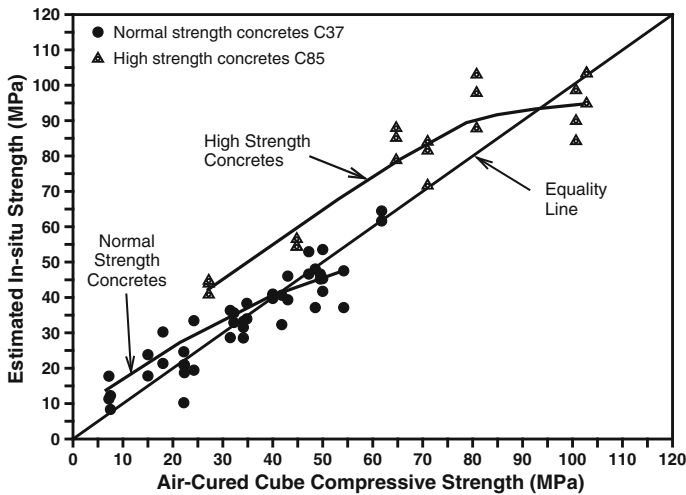
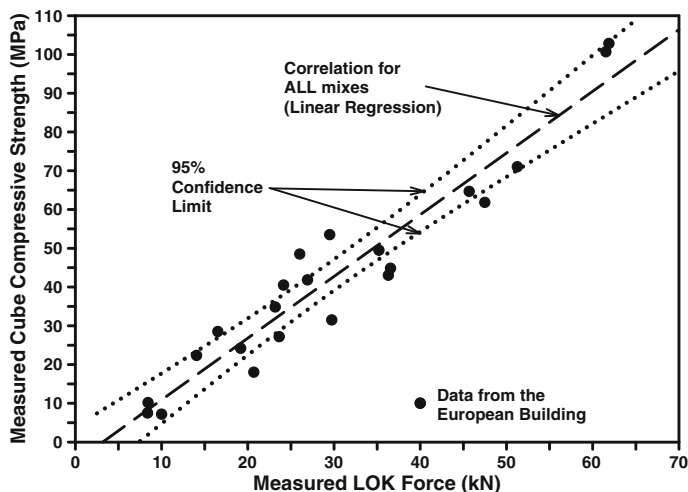


Fig. 3.12 In-situ strength (pull-out) versus Air-Cured Cube Strength

respectively. Similar trends were obtained for the other mixes but the temperature differences were smaller, e.g., for the C37N-10 the peak temperatures were 24°C and 14°C in the column and in the air-cured cube, respectively. The ambient temperature was approximately 8°C in the first few days after casting of the C85MS and C37N-10 concretes.

Grouping mixes might offer better strength predictions from the limited number of in-situ test results as the confidence interval for an estimate is affected by the number of points used to establish the strength relationship. The relative width of the confidence interval reduces exponentially as the number of test points is increased, e.g., the reduction is significant with every additional test point up to a total of six to nine points. More than nine tests would probably not be economical (ACI, 2003). The number of test points intended for use on the Cardington Project was at ages 1, 3, 7, 14 and 28-days. This was cut down to four test points because of the non-availability of companion cubes for testing at 14-days. The number was, for at least one mix (C85MK), further reduced to three because of the non-availability, at the start of the project, of the necessary Lok-test accessories to test high strength concrete inserts.

The strength correlation for all mixes combined had a 95% confidence interval of  $\pm 4$  MPa at the average concrete compressive strength of 43 MPa. It must be noted that the confidence statement applies to the line as a whole, and therefore it is expected that the confidence interval for  $y$  corresponding to all the chosen  $x$  values will simultaneously be correct 95% of the time that the calibration is repeated (i.e. take a sample of the same size and determine the respective confidence interval). A confidence interval for a point on the line, i.e. a confidence interval for  $y'$  (the true value of  $y$  and the mean value of  $Y$ ) corresponding to a single value of  $x = x'$ , will be smaller. The wider interval is the “price” paid for making joint statements about  $y$  for any number of or all of the  $x$  values, rather than the  $y$  for a single  $x$ . It must be



**Fig. 3.13** The confidence interval for the whole range of strengths considered for the strength correlation

noted that the confidence interval increases on both sides of the 43 MPa concrete compressive strength (the average of all the strengths used to obtain the strength correlation), see Fig. 3.13.

According to (Stone et al, 1986) and (Stone and Reeve, 1986), the ordinary least squares method will underestimate the uncertainty of the strength relationship since it is based on the assumption that (a) there is no error in the average value of in-situ tests ( $X$  value); yet these, with the exception of maturity indices, generally have greater within-test variability than compression tests ( $Y$  value), and (b) the error (standard deviation) in the  $Y$  value is constant; yet the standard deviation increases with increasing compressive strength.

The more rigorous method is more complex and requires an electronic spreadsheet or computer program for practical implementation. The values obtained from the correlation tests, i.e. Lok tests and cube compressive strengths, are used to compute the lower confidence limit ( $Y_{\text{low}}$ , i.e. the desired confidence level has been taken to be 95%) of any estimates to be undertaken with the use of this correlation. This has been computed using error of fit given by Mandel's procedure (Mandel, 1984), the standard deviation of the estimated value of compressive strength given by the procedure recommended by (Stone and Reeve, 1986), and the Student  $t$ -value for  $m$  (the number of replicate Lok tests) obtained from (Natrella, 1963). The lower confidence limit for the average concrete strength is then obtained from the equation (ACI, 2003):

$$Y_{\text{low}} = Y - (t_{m-1,\alpha} s_Y)$$

where  $Y_{\text{low}}$  is the lower confidence limit at 95% confidence level,  $t_{m-1,\alpha} s_Y$  is the Student  $t$ -value for  $m-1$  degrees of freedom and 95% confidence level and  $m$  is the number of replicate Lok tests.

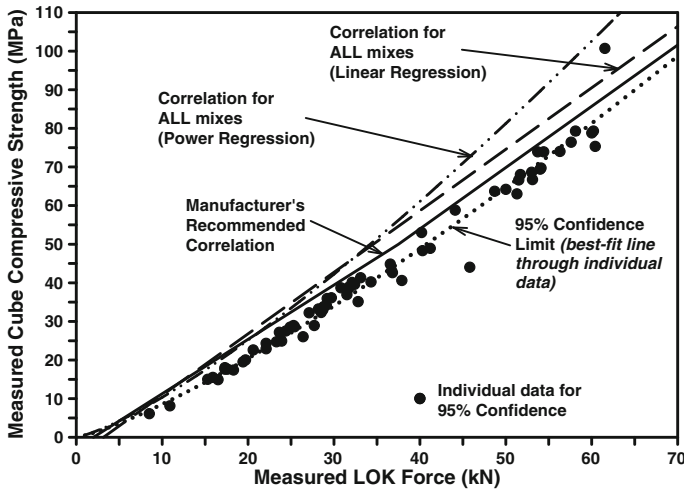


Fig. 3.14 The confidence interval determined with a power function regression analysis

Since the data for this research program have been analyzed using a power function, a comparison with the strength correlation used to obtain them is appropriate, see Fig. 3.14. Despite the finding that the 95% confidence limit is 20 MPa at 100 MPa, it is encouraging that at low strengths the strength relationship and the 95% confidence limit lines converge. Early stripping of flat slab formwork for this project required a target mean strength of 19 MPa and for this the 95% confidence limit is 3.5 MPa.

According to BS1881: Testing Concrete, Part 201: Guide to the use of non-destructive methods of test for hardened concrete [BS, 1986]: “*Estimated compressive strengths from pull-out tests are unlikely to have 95% confidence limits of better than  $\pm 20\%$  of the mean when a general calibration is used or  $\pm 10\%$  when a specially prepared calibration for the aggregate type in use is available.*”

The results from the Cardington project reconfirm that the 95% confidence limit is around  $\pm 20\%$  of the mean when a general power function correlation is used. Values for a wide range of concrete strengths, e.g., from 0 to 120 MPa are required to determine a power function correlation. Therefore specially prepared correlations for the type of concrete available for a specific project will have to be based on correlations obtained by linear regression.

### 3.1.4 Pull-off test

Several factors affecting the compressive strength/pull-off correlation and these will be described next.

**Effect of the modulus of concrete:** (Bunney and Madandoust, 1992), based on a finite element analysis, concluded that high stress concentrations may occur below

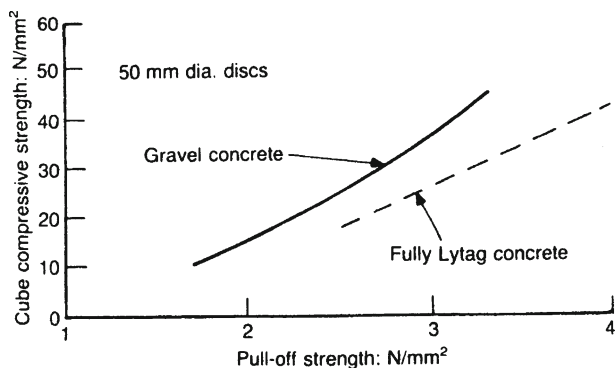


Fig. 3.15 Effect of aggregate type on the compressive strength/pull-off correlation

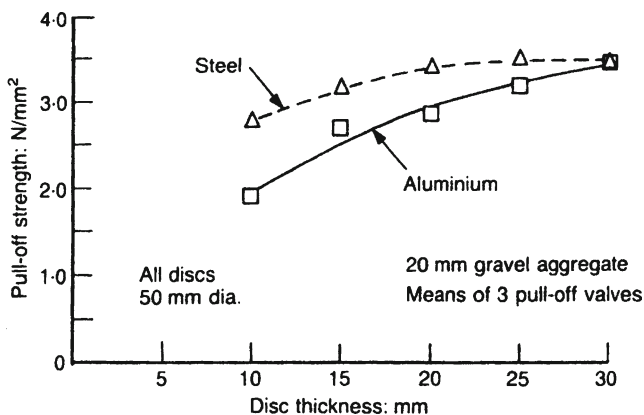
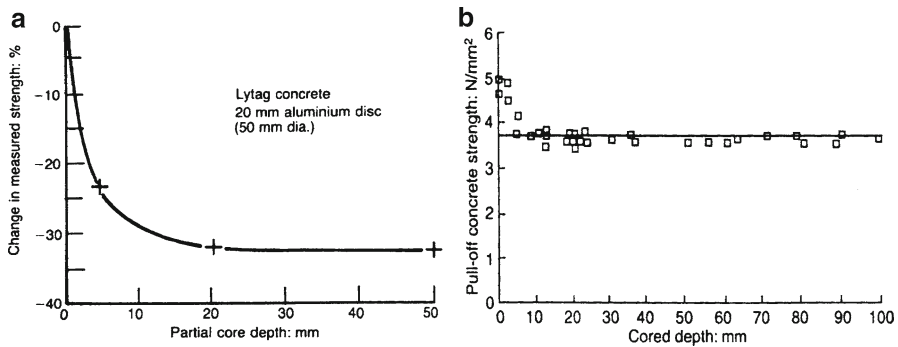


Fig. 3.16 Effect of the disc material and thickness

the central region of the disc in concretes with high elastic modulus. Figure 3.15 shows that the compressive strength/pull-off correlation is dependent on the aggregate type used and thus on the modulus of the resulting concretes. Pull-off failure is expected to be at a lower applied load as the modulus of the concrete increases.

**Effect of disc material and thickness:** (Bungey and Madandoust, 1992) indicated that increased disc thickness, e.g., to 30 mm, provided much greater uniformity of interface stresses. Figure 3.16 shows that the steel and the aluminium discs provide similar results when their thickness is 30 mm. (Bungey and Madandoust, 1992) concluded that in order to achieve a fairly uniform stress in the concrete, the disc needed to be at least 20 mm thick for steel and 30 mm for aluminium. This factor may however be less critical when testing the adhesion of repair materials since the stress will be distributed through the depth of repair material, giving a more uniform stress distribution at the interface [(Cleland and Long, 1997), (Austin et al, 1995)]. EN 1542:1999 specifies a disc “with a diameter of  $50 \pm 0.5$  mm and with a thickness of at least 20 mm if made of steel, or with a thickness of at least 30 mm if made of





**Fig. 3.17** Effect of the depth of partial coring: (a-left) 20mm-thick aluminium discs, (b-right) 25mm-thick steel discs

aluminium” (EN, 1999). BS 1881-207:1992 requires that the thickness of the disc should not be less than 40% of its diameter. This ratio should be increased to 60% when using an aluminium disc (BS, 1992).

**Effect of the depth of partial coring:** It has been well established that the failure load of a partially cored test is lower than that for a surface test in the same specimen. However, as shown in Fig. 3.17a, when 20 mm aluminium discs are used, the reduction did not vary beyond depths of 20mm<sup>(48)</sup>. Similar trend has also been observed from the HAC concrete (Mc Comb, 1983). While the 25 mm thick steel discs (as shown in Fig. 3.17b) are used (Cleland and Long, 1997), for core depth of 5 mm or more, the failure load was found to be independent of core depth.

The theoretical stress analyses investigation carried out by (Bungey and Madandoust, 1992) also suggested that when the depth of coring is beyond 20 mm, comparable results can be obtained irrespective the disc materials. Nonetheless, if 30 mm thick discs are used, comparable results can be obtained at even smaller coring depths irrespective of disc materials. In the BS 1881-207:1992 (BS, 1992) for testing the surface strength of concrete, the depth of partial coring is not specified. For testing repair overlays, (Cleland and Long, 1997) considered that the effect of the depth of partial coring is less relevant since failure is usually occurred at the interface between the repair and the base concrete, rather at the base of the core. In the current EN 1542:1999, it requires that the partial coring should “drill through the repair product or system to a depth of (15±5) mm into the concrete substrate” (EN, 1999).

**Effect of the moisture condition:** It has been found that the effect of the moisture condition of the concrete at which the test is carried out is insignificant. The only effect is on the strength development of adhesive. However, the use of a recently available adhesive has removed this effect, enabling probes to be bonded to wet concrete. As a result, the pull-off test also can be used to test in-situ strength of concrete at an early age (Long and Murray, 1981).

**Effect of the loading rate:** BS 1881-207:1992 (BS, 1992) specifies a loading rate of  $0.05 \pm 0.03 \text{ MPa}\cdot\text{s}^{-1}$ , while EN 1542:1999 (EN, 1999) requires that the loading rate

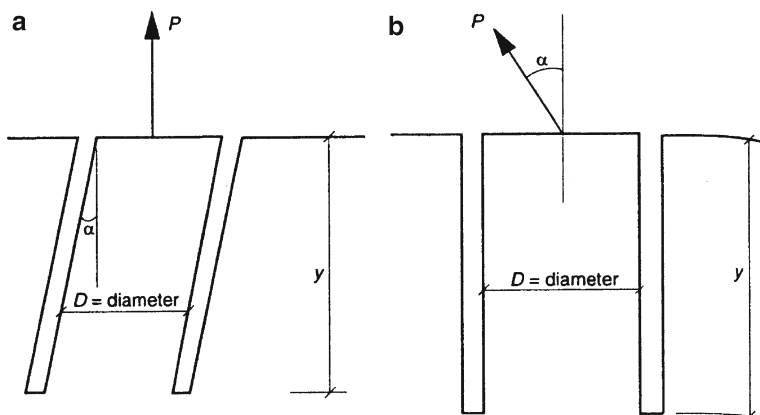


Fig. 3.18 Causes of eccentricity from coring

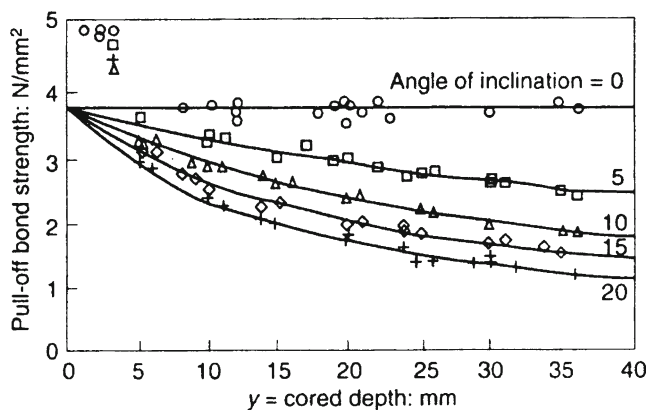


Fig. 3.19 Effect of core perpendicularity

should not be greater than  $1 \text{ MPa}\cdot\text{s}^{-1}$ . However, there is no evidence that this is a particularly critical factor. The above rate can be achieved easily using the equipment in which the rate is determined by the speed of cranking a handle.

**Effect of the core perpendicularity:** For partial coring test, the inaccuracy in coring may cause eccentricity as shown in Fig. 3.18 and consequently the measured pull-off bond strength is reduced (Fig. 3.19, from (Cleland and Long, 1997)). However, for small values of  $\alpha$ , the ratio of the failure load for any value of  $\alpha$  to the failure load at zero misalignment is given by:

$$P_{\alpha} / P_0 = 1 / [1 + (8 \tan \alpha / D)y]$$

where  $\alpha$ ,  $D$  and  $y$  are as shown in Fig. 3.18.

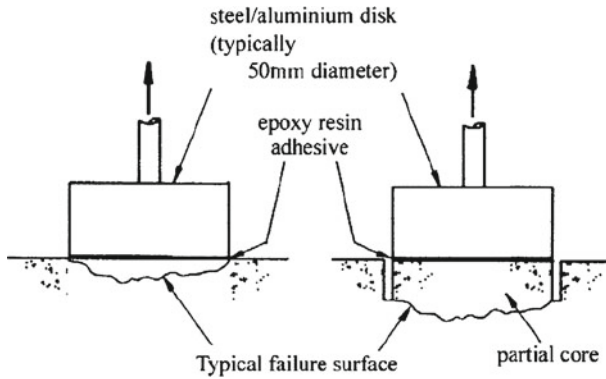
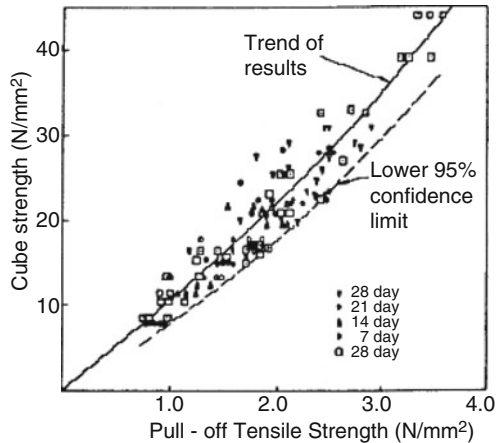


Fig. 3.20 Strength testing procedure

Fig. 3.21 Correlation curve



It is worth mentioning that an important requirement for pull-off testing equipment is that it can apply an almost pure axial load with no bending. During the development of pull-off test equipment, this problem was initially solved by using a ball and socket joint, but it was later found sufficient to use a much smaller diameter high-tensile steel connecting rod to reduce any moment transfer effects and simultaneously achieve a self-aligning system (Long and Murray, 1981).

The driving force for the development of pull-off test is to measure in-situ the strength of concrete structures. Fig. 3.20 shows two ways of testing concrete strength on site, viz. on the surface and on the partial cores (Long and Murray, 1981).

It was found that for tests on HAC concrete partial coring was necessary to eliminate errors caused by the hard shell effect, whereas on OPC concrete uncured specimens gave significantly more consistent results, as the aggregate was not disturbed or weakened by the drilling. However, the tensile strength calculated from the pull-off load is of little use to structural engineers. But, with a calibration curve such as that shown in Fig. 3.21, the equivalent cube compressive strength of the concrete

under test can be estimated. This practice has been accepted as a standard approach in the UK (BS, 1992) and recommended by (ACI, 2003) for assessing the in situ concrete strength.

It is worth mentioning that as discussed in section 3 the correlation between tensile strength and compressive strength can be influenced by aggregate as well as the disc material and thickness. Therefore, (BS, 1992) requires that a correlation should be established for the particular concrete under investigation and the apparatus being used. Nonetheless, (Johnston, 1967) indicated a single curve could be sufficient for most of the available aggregates. This is also reflected in (BS, 1992) in specifying that “in some circumstances, use of a general correlation may be adequate”. In-situ case studies on a multi-story car park, multispan flyover, precast prestressed HAC concretes and a high performance concrete bridge deck overlay (FHWA, 2000) also revealed that pull-off test is a simple, reliable and easy-to-use partially destructive test method for testing concrete strength in-situ.

### 3.1.5 Ultrasonic pulse velocity (ASTM C 597)

The basic problem is that the material under test consists of two separate constituents, matrix and aggregate, which have different elastic and strength properties. The relationship between pulse velocity and dynamic elastic modulus of the composite material measured by resonance tests on prisms is fairly reliable. Although this relationship is influenced by the value of dynamic Poisson's ratio, for most practical concretes made with natural aggregates the estimate of modulus of elasticity should be accurate within 10%.

The relationship between elastic modulus (or pulse velocity) and strength of the composite material cannot be defined simply by consideration of the properties and proportions of individual constituents, see Fig. 3.22. This is because of the influence of aggregate particle shape, efficiency of the aggregate/matrix interface and variability of particle distribution, coupled with changes of matrix properties with age. Although some attempts have been made to represent this theoretically, the complexity of the interrelationships is such that experimental calibration for elastic modulus and pulse velocity/strength relationships is normally necessary. Aggregate type may vary in type, shape, size, and quantity, and the cement type, sand type, water/cement ratio and maturity are all important factors which influence the matrix properties and hence strength correlations.

Strength calibration for a particular mix should normally be undertaken in the laboratory with due attention to the factors listed above. Pulse velocity readings are taken between both pairs of opposite cast faces of cubes of known moisture condition, which are then crushed in the usual way. Ideally, at least ten sets of three specimens should be used, covering as wide a range of strengths as possible, with the results of each group averaged. A minimum of three pulse velocity measurements should be taken for each cube, and each individual reading should be within 5% of the mean for that cube. Where this is not possible, cores cut from the hardened concrete may sometimes be used for calibration, although there is a danger that drilling damage may affect pulse

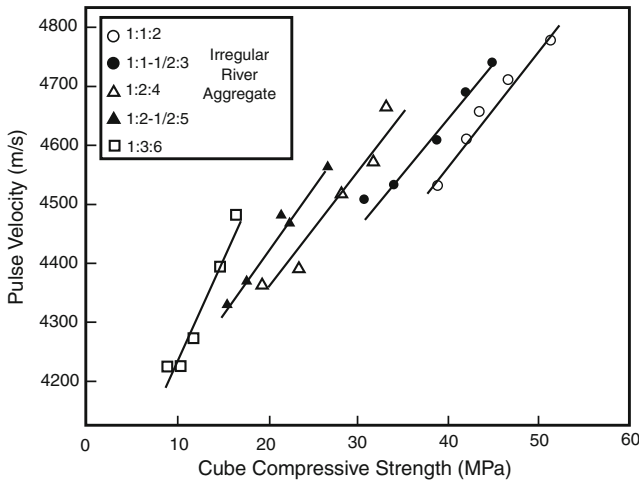


Fig. 3.22 Effect of cement to aggregate ratio on the relationship between pulse velocity and compressive strength (Naik and Malhotra, 1991)

velocity readings. Wherever possible, readings should be taken at core locations prior to cutting. Provided that cores are greater than 100 mm in diameter, and that the ends are suitably prepared prior to test, it should be possible to obtain a good calibration, although this will usually cover only a restricted strength range.

Although the precise relationship is affected by many variables, the curve may be expected to be of the general form:

$$f_c = A e^{bV}$$

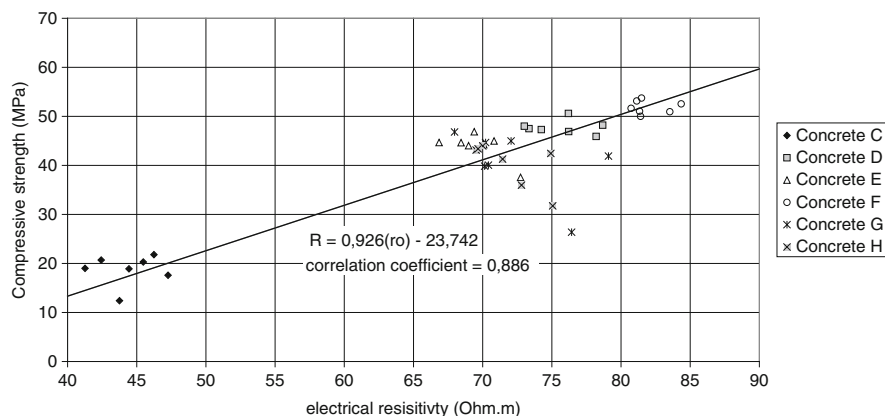
where  $f_c$  is the equivalent cube strength,  $V$  is the pulse velocity and  $A$  and  $B$  are constants. Hence a plot of log cube strength against pulse velocity is linear for a particular concrete. It is therefore possible to use a curve derived from reference specimens to extrapolate from a limited range of results from cores.

(Bungey, 1980) has suggested that if a reliable correlation chart is available, together with good testing conditions, it may be possible to achieve 95% confidence limits on a strength prediction of  $\pm 20\%$  relating to a localized area of interest. Expected within-member variations are likely to reduce the corresponding accuracy of overall strength prediction of a member to the order of  $\pm 10$  MPa at the 30 MPa mean level. Accuracy decreases at higher strength levels, and estimates above 40 MPa should be treated with great caution.

Although not perfect, there may be situations in which UPV measurements may provide the only feasible method of in-situ strength estimation, and if this is necessary it is particularly important that especial attention is given to the relative moisture conditions of the calibration samples and the in-situ concrete. Failure to take account of this is most likely to cause an underestimate of in-place strength, and this underestimate may be substantial.

**Table 3.1** Volumetric composition of the 6 concrete mixes

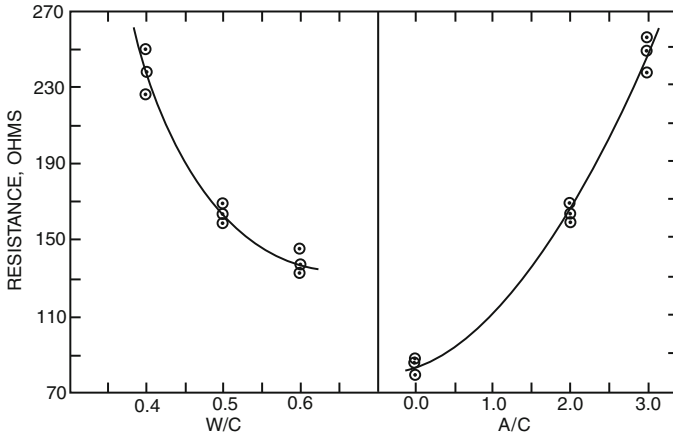
Concrete	c		w/c	w (kg or l)	Aggregates (in l)			
	(kg)	(l)			0/3	3/8	8/15	12.5/20
C	400	129	0.58	232	223.99	415.34	-	-
D	400	129	0.50	200	234.78	436.11	-	-
E	400	129	0.50	200	234.78	221.33	214.67	-
F	400	129	0.50	200	234.78	221.33	107.33	107.33
G	400	129	0.50	200	234.78	-	436.11	-
H	400	129	0.50	200	234.78	-	-	436.11

**Fig. 3.23** Compressive strength / resistivity relationship

### 3.1.6 Resistivity Methods

Relationships between the electrical and mechanical properties (resistivity and strength) have been determined for several concretes (Lataste, 2002). In order to have concretes of different porosity, and distribution of pore size, the aggregate grading was varied, see Table 3.1. Concrete cylinders 320 mm (height) x 160 mm (diameter) were cured in water for 28 days before carrying out electrical resistivity measurements and subsequently crushing them to obtain the compressive strength. The compressive strength/resistivity relationship shown in Fig. 3.23 is based on seven samples for each mix. Series C had a very high water-cement ratio while series G and H used gap graded aggregates. A good strength/resistivity correlation is obtained if series G and H are ignored.

It has also been advocated that the mechanical properties of the concrete can be related to its porosity. Measuring the latter with electrical resistivity may give an indication of the compressive strength of the concrete, see Fig. 3.24 (Woelfl and Lauer, 1980).



**Fig. 3.24** Influence of water to cement ratio and aggregate to cement ratio on the electrical resistance of concrete

**Table 3.2** Relative merits of non-destructive tests

Test method	Cost	Speed of test	Damage	Representativeness	Reliability of absolute strength correlations
<i>General Applications</i>					
Core	High	Slow	Moderate	Moderate	Good
Pull-out	Moderate	Fast	Moderate/Minor	Near surface only	Moderate/Good
Penetration resistance	Moderate	Fast	Minor	Near surface only	Moderate
Pull-off	Moderate	Moderate/Fast	Minor	Near surface only	Moderate/Good
<i>Comparative Assessment</i>					
Ultrasonic Pulse Velocity	Low	Fast	None	Good	Poor
Rebound	Very Low	Fast	Very minor	Surface only	Poor

### 3.1.7 Comparison of the techniques

Relative features of various concrete strength test methods are summarized in Table 3.2. In the common situation where an assessment of material strength is required, it is unfortunate that the complexity of correlation tends to be greatest for the test methods which cause the least damage. Although surface hardness and pulse velocity tests cause little damage, are cheap and quick, and are ideal for comparative and uniformity assessments, their correlation for absolute strength prediction poses many problems. Core tests provide the most reliable in-situ strength assessment but also cause the most damage and are slow and expensive. They will often be regarded as essential

when investigating existing structures, and their value may be enhanced if they are used to form a basis for calibration of non-destructive or partially-destructive methods which may then be adopted more widely. Partially-destructive methods generally require less-detailed calibration for strength but cause some surface damage, test only the surface zone, and may suffer from high variability. The availability of strength correlations and the accuracy required from the strength predictions may be important factors in selecting the most appropriate methods to use. This must be coupled with the acceptability of making good any damaged areas for appearance and structural integrity. For monitoring strength in new construction, it will be necessary to develop or obtain appropriate strength correlations before construction commences.

Previous studies by (Bungey and Millard, 1996) have established that surface hardness testing is unreliable at early ages, and that whilst ultrasonic pulse velocity measurements can yield good early age strength estimates usage is usually precluded by the need for access to two opposite faces. Where testing is required on one face, penetration resistance testing is quick and suitable for large members such as slabs, but this again has been shown to be unreliable at low strength values. The previous studies concluded that pull-out testing was the most reliable and practicable technique at low strength levels.

### ***3.2 Assessment of characteristic in-situ compressive strength by indirect methods***

Concerning USA and European standards, despite the correction factors associated with curing, compaction, age, etc., the in-situ strength of concrete needs to be converted into a 10<sup>th</sup> or 5<sup>th</sup> percentile, in order to be used in structural analysis. Different statistical procedures including distinct assumptions about strength population are considered by each, in order to estimate the correspondent percentiles. This also happens when the in-situ strength is estimated through indirect methods such as the rebound hammer, ultrasonic pulse velocity and pull-out tests, requiring always a calibration with cores from the same concrete (and under the same conditions) as the one that is about to be assessed.

In the USA, this calibration can be carried out in moulded cubes and in cores drilled from existing structures while in Europe only the last one is allowed. In this section will be briefly describes the different standard procedures to asses in-situ strength of concrete in structures based on indirect methods. For an appropriate use of the procedures, the respective standard should be consulted.

#### **3.2.1 USA standards**

ACI Committee 228 has reviewed four statistical methods for evaluating in-place test results. Two of the suggested methods are briefly described below.



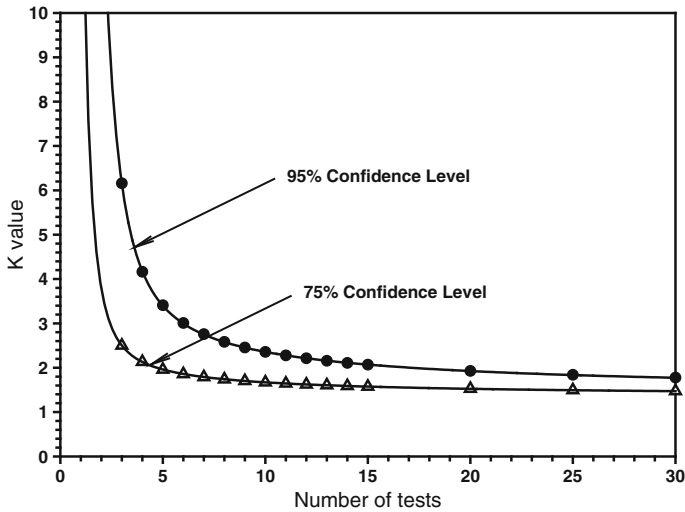


Fig. 3.25 One-sided tolerance factor for 10% defective level

*The “Tolerance Factor Approach”*

The estimate of the tenth percentile strength  $Y_{0.10}$  can be determined, for a normal distribution function, as follows (Bickley, 1982)

$$Y_{0.10} = Y - K s_y$$

where  $Y_{0.10}$  corresponds to a 10% probability of being defective  $Y$  is the sample average strength,  $K$  in the one-sided tolerance factor and  $s_y$  is the sample standard deviation.

“Sample” in this case refers to tests performed at several locations on the structure. As such, multiple tests performed at a single location only contribute one single value to the sample. The tolerance factor is determined from statistical characteristics of the normal probability distribution and depends on the number of group of tests  $n$  at different locations on the structure, the confidence level, and the defect percentage. Values of  $K$  can be found in standard statistical references (Natrella, 1963). Figure 3.25 shows how the  $K$  value varies with the number of group of tests performed on site but also with the required confidence level. Hindo and Bergstrom (ACI, 2003) suggested that only 75% is used for ordinary structures, 90% for very important buildings, and 95% for crucial parts of nuclear power plants. It is obvious that as the variability of the test results increases or as fewer tests are performed, the tenth-percentile strength will be a smaller fraction of the sample average strength.

Two criticisms for this method are (ACI, 2003):

- the strength relationship is presumed to have no error; and,
- the variability of the compressive strength in the structure is assumed to be equal to the variability of the in-place test results.

While the second factor will make the estimates overly conservative, the first factor will have the opposite effect. This method is simple to use, requiring only tabulated statistical factors and a calculator, but because its underlying assumptions have been questioned, a rigorous method has been proposed.

### *The “Carino’s alternative method”*

The rigorous method is more complex and requires an electronic spreadsheet or computer program for practical implementation (Carino, 1993). The values obtained from the correlation tests, e.g., for pullout tests and cube compressive strengths, are used to compute the lower confidence limit ( $Y_{\text{low}}$  with the desired confidence level, e.g., 75%) of any estimates to be undertaken with the use of this correlation (following the procedure discussed at §3.1.3). This requires use of the error of fit given by Mandel’s procedure (Mandel, 1984), the standard deviation of the estimated value of compressive strength according to (Stone and Reeve, 1986), and the Student t-value for  $m$  (the number of replicate in-situ tests) obtained from (Natrella, 1963). The lower confidence limit for the average concrete strength is then obtained from the equation (ACI, 2003):

$$Y_{\text{low}} = Y - (t_{m-1,\alpha} s_Y)$$

where  $Y_{\text{low}}$  is the lower confidence limit at 95% confidence level,  $t_{m-1,\alpha}$  is the Student t-value for  $m-1$  degrees of freedom and 95% confidence level and  $m$  is the number of replicate Lok tests.

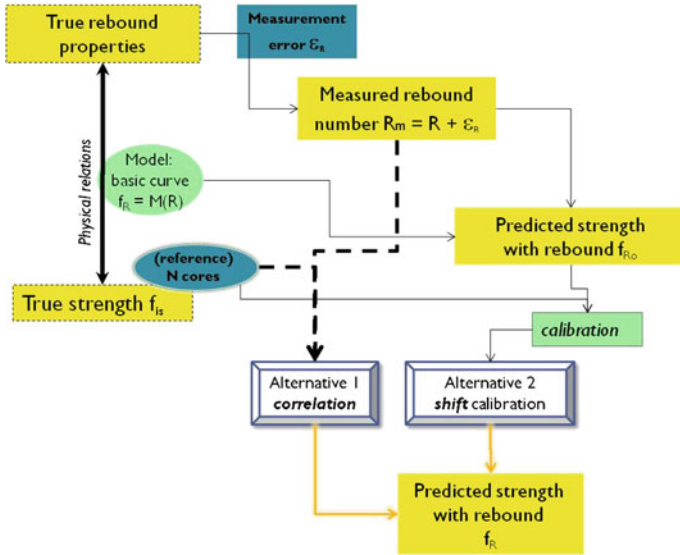
The tenth percentile strength  $Y_{0.10}$  is then computed from (ACI, 2003):

$$Y_{0.10} = Y_{\text{low}} - 1.282 s_{cf}$$

where  $s_{cf}$  is the standard deviation of the logarithm of concrete strength in the structure and is obtained from the assumption that the ratio of the standard deviation of compressive strength to the standard deviation of indirect tests in the field is the same as that obtained during the laboratory correlation testing. This equation accounts for the variability of the in-situ compressive strength, i.e. it converts the average in-situ strength from several locations to a characteristic strength for the structure.

### **3.2.2 European standards**

Two alternative methods for assessment of in-situ compressive strength are provided (EN 13791, 2007) as it can be seen on Fig. 3.26. Alternative 1 (use of correlation) requires at least 18 core test results to establish the relationship between the in-situ compressive strength and the test result by the indirect method. Alternative 2 (calibration of a prior model) requires a basic curve, provided by the standards and a relationship determined from a limited number of cores.



**Fig. 3.26** The two alternatives from EN 13791, here the non destructive technique is rebound (after Breyse et al, 2010)



**Fig. 3.27** Prestressed concrete storage tanks in Stargard (Poland)

*Basic curve approach*

Results from an in-situ investigation of several prestressed concrete storage tanks in Stargard (Poland), see Fig. 3.27, carried out in 2007 when the structures were approximately ten years old, are used to demonstrate the procedure for estimating

**Table 3.3** Determination of the relationship between Rebound number and in-situ compressive strength (Stargard prestressed concrete tanks, strength in MPa)

Location	#01	#02	#03	#04	#05	#06	#07	#08	#09
Rebound readings	44	46	51	51	45	41	50	42	50
	41	48	49	51	43	44	51	43	49
	43	45	51	51	48	42	48	41	51
	45	46	48	51	44	43	48	44	50
	44	43	44	53	46	47	51	48	51
	46	43	51	51	47	46	49	46	48
	46	42	46	47	49	44	50	43	49
	43	45	51	48	43	43	50	45	49
	46	41	52	49	45	44	51	44	52
Standard deviation	1.7	2.1	2.7	1.8	2.1	1.9	1.2	2.1	1.3
Rebound number (median)	44	44.5	51	51	45	44	50	44	50
Core strength $f_{is}$	25.3	27.5	31.6	36.6	28.9	26	32.9	26.7	35
Predicted strength (basic curve) $f_R$	41.6	42.5	53.7	53.7	43.4	41.6	52.0	41.6	52.0
$df = f_{is} - f_R$	-16.3	-15.0	-22.1	-17.1	-14.5	-15.6	-19.1	-14.9	-17.0
New predicted strength	20.7	21.6	32.8	32.8	22.4	20.7	31.1	20.7	31.1

the in-situ compressive strength and how this is then used to calculate the characteristic in-situ compressive.

A test region containing nine test locations was selected. A test result for rebound hammer was obtained at each test location in accordance with EN 12504-2 and a core was taken and tested in accordance with EN 12504-1. The results are shown in Table 3.3 for the region used for calibration and in Table 3.4 for the concrete in regions that are about to be assessed.

The basic curve given by EN 13791 writes  $f_R = 1.73R - 34.5$ . The average  $df_{m(n)}$  of the differences between the measured value on the core  $f_{is}$  and the value given by the basic curve  $f_R$  was found to be 16.9 MPa. The sample standard deviation of shifts,  $s$ , was found to be 2.4 MPa. The amount by which the basic curve needed to be shifted,  $\Delta f$ , used to estimate the in-situ compressive strength, was obtained from

$$\Delta f = df_{m(n)} - k_1 s$$

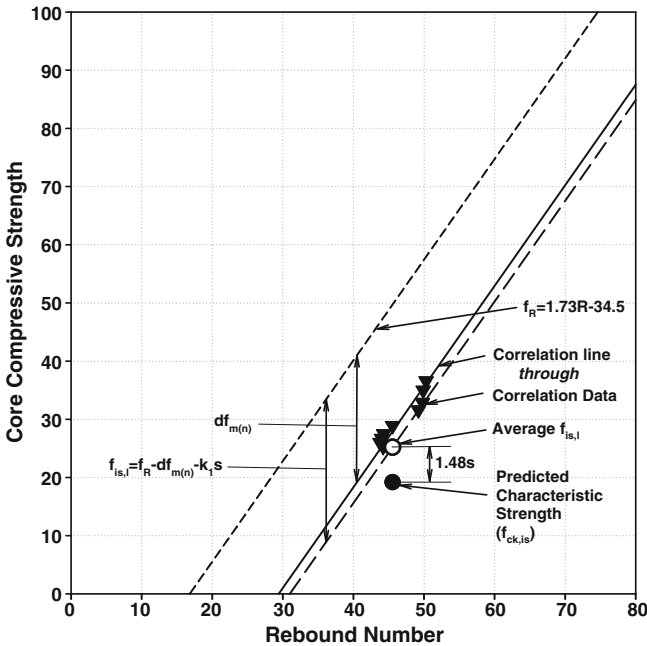
which is added to  $f_R$ . The value of  $k_1$  for nine paired test results is given as 1.67.

This last step ensures that the curve is not only shifted by adding the average value but it includes a downward shift of  $k_1 s$ , so that the predicted core strength is on the safe side. In the example given, the shift will be of  $-16.9 - 1.67 \times 2.4 = -20.9$ . This has been done in Table 3.4. The strength correlations obtained are shown in Fig. 3.28.

In Table 3.3, the estimated strength is  $f_R = 1.73R - 34.5 - df_{m(n)}$  with  $df_{m(n)} = 16.4$  MPa. The final estimation  $f_{is,1} = 1.73R - 34.5 - df_{m(n)} - k_1 s$ .

**Table 3.4** Determination of the in-situ compressive strength for the concrete used in the Stargard Prestressed Concrete Tanks (s is standard deviation of rebound numbers,  $f_R$  is estimated strength and  $f_{is,1}$  is the final value of the estimated in situ compressive strength)

Testing area	Rebound readings									$R_{median}$ [ - ]	$f_{is,1}$ [MPa]
	1	2	3	4	5	6	7	8	9		
<b>P-1</b>	50	47	45	47	46	49	51	49	45	47	<b>25.9</b>
<b>P-2</b>	44	45	42	43	46	44	40	41	41	43	<b>19.0</b>
<b>P-3</b>	42	42	43	43	39	43	41	45	48	43	<b>19.0</b>
<b>P-4</b>	49	47	49	45	45	46	47	49	51	47	<b>25.9</b>
<b>P-5</b>	45	45	41	46	47	46	45	48	45	45	<b>22.4</b>
<b>P-6</b>	41	41	45	41	43	47	45	44	45	44	<b>20.7</b>
<b>P-7</b>	49	51	46	47	47	43	49	47	50	47	<b>25.9</b>
<b>P-8</b>	47	50	49	45	46	52	51	45	47	47	<b>25.9</b>
<b>P-9</b>	51	50	51	47	53	49	51	49	52	51	<b>32.8</b>
<b>P-10</b>	52	53	45	51	52	48	51	52	51	51	<b>32.8</b>
<b>P-11</b>	42	42	43	44	46	47	45	43	43	43	<b>19.0</b>
<b>P-12</b>	42	43	46	43	41	41	43	40	44	43	<b>19.0</b>
<b>P-13</b>	43	45	46	48	43	42	43	43	42	43	<b>19.0</b>
<b>P-14</b>	49	51	45	49	50	45	46	47	49	49	<b>29.3</b>
<b>P-15</b>	38	38	39	39	38	38	38	39	38	38	<b>10.3</b>
	average										<b>23.1</b>



**Fig. 3.28** Strength correlation for rebound hammer tests for the prestressed concrete storage tanks in Stargard (Poland)

The last step is the estimation of the characteristic strength. Clause 7.3.3 of EN 13791 applies and the characteristic strength of the concrete is the lower of:

$$\text{Average} - 6 = 23.1 - 6 = 17.1 \text{MPa}$$

$$\text{Minimum} + 4 = 10.3 + 4 = 14.3 \text{MPa}$$

If the low result is due to a local defect, for example honeycombing, and it was agreed to remove this area, this result could be excluded from the calculation of the characteristic in-situ strength.

For design purposes one may want to divide the 17.1 MPa by 0.85 to get the characteristic strength of test specimens, i.e. 20.1 MPa.

The procedure appears to work well when the correlation specimens have a low standard deviation. This may not always be the case and there are worries that this procedure leads to very low estimates of the characteristic in-situ strength.

#### *Alternative 1 – Direct correlation with cores*

The Alternative 1 presented in EN 13791 consists in choosing at least 18 test locations from the structure and obtaining one pair of results – one indirect test result and the compressive strength of one core. The relationship between the in-situ compressive strength and the indirect test is established by the tolerance lower limit for a coverage of 90%. This alternative has been criticized (Monteiro and Gonçalves, 2009) due to three reasons:

- high number of cores needed for calibration (minimum of 18 cores);
- incomplete information about the procedure;
- use of a tolerance interval for establishing the relationship between in-situ strength and indirect test results.

The first reason makes this approach prohibited in most cases where characteristic in-situ strength is about to be assessed, since, according to the same standard, 15 cores are enough to do it without the need of indirect tests. However, in particular cases, such as the assessment of characteristic in-situ strength for applying the compressive prestress in a large number of concrete elements, the number of cores required for calibration may not be so relevant.

Concerning the second reason, the EN 13791 indicates that the relationship between in-situ strength and indirect test results shall be obtained from the tolerance limit for individual observations which gives a safety level where 90% of the strength levels are expected to be higher than the estimated value. This tolerance limit shall be calculated through regression analysis using the best-fit regression model. However, the standard does not give any indication about the confidence level and the statistical distribution of both variables (e.g., if the measurement error of the indirect test is neglected or not) that should be adopted. These last two aspects may affect significantly the estimated characteristic strength.

The third reason concerns the use of a tolerance limit to establish the relationship which can be excessively conservative. Tolerance limits are used to predict a

percentile of the compressive strength which, in this case, corresponds to calculating a characteristic value of concrete strength within each test location. The reasons behind this choice remains unpublished but, statistically, it is not consistent with the procedure used for assessing in-situ strength with cores only, where, in the case of taking more than one core in each test location (replicates), the mean value is used as a test result. To be consistent, a confidence limit should be used instead.

### *Determining the characteristic in-situ strength*

EN 13791 uses a completely distinct approach to determine the 5<sup>th</sup> percentile (or the characteristic) in-situ strength of concrete from attest region,  $f_{ck, is}$ . After the calculation of the relationship line (obtained by any of the two above approaches), each indirect test result (obtained from each test location from the test region of concrete that is about to be assessed) is converted into in-situ strength results,  $f_{i, is}$ . The characteristic in-situ strength is then taken as:

$$f_{ck, is} = \min[f_{m(n), is} - 1.48s; f_{is, lowest} + 4]$$

where  $f_{m(n), is}$ ,  $f_{is, lowest}$  and  $s$  are the average, minimum and standard deviation if the converted  $f_{i, is}$  respectively. The value of  $s$  shall not be, however, less than 3 MPa.

### 3.2.3 Comparison between approaches

In Table 3.5 are summarized the main differences between the Carino's and EN 13791 Alternative 1 methods.

**Table 3.5** Recommendations and minimum requirements for calibration. Comparison between ACI Carino's alternative method versus EN 13791 – Alternative 1 (Direct correlation with cores)

	ACI 228 (2003)	EN 13791
Min. number of test locations	6 to 9	18
Min. number of cores by each test location	2	1
Min. total number of cores	12 to 18	18
Replicates in each test location	Rebound hammer UPV Pull-out	9 5 3
Influence of measurement error on indirect test results during calibration	Mandel's procedure	10 Not defined Not defined
Assumed statistical distribution for in-situ strength	Lognormal	No indications
Assumed statistical distribution for indirect test results	Lognormal	No indications

(continued)

**Table 3.5** (continued)

	ACI 228 (2003)	EN 13791
Regression model	Power	Best fit line
Relationship line	Approximated non simultaneous confidence limit	Tolerance limit for individual observations
Confidence level	– 75% for ordinary structures – 90% for very important buildings – 95% for crucial parts of nuclear power plants	No indications
Influence of measurement error on indirect test results during the assessment of in-situ strength	Included	No indications
Influence of external factors (e.g., moisture content of concrete)	Not included or neglected	Not included or neglected
Correction of the estimated standard deviation of the predicted in-situ strength	Assumes that the standard deviation ration between compressive strength and the indirect test result during calibration remains the same in the field	No corrections
Combination of indirect methods	Not covered by the standard	

## 4 Multivariate analysis and modeling for strength assessment of concrete

In this section, the issue of combining several non destructive techniques, to take profit of their various advantages (see Table 3.2) will be discussed. After having recalled the seminal work, we will discuss the question of conversion curves (here surfaces). Thus the role played by the driving parameters, namely the quality of the model and the measurement error, will be highlighted, both on synthetic data (that will make the understanding easier) and on field data.

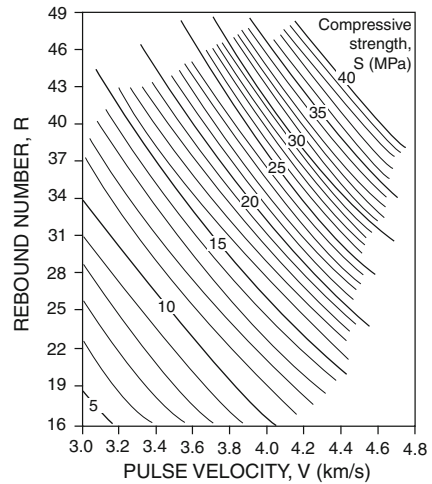
### 4.1 Back into history: the *SonReb* method

The term “combined methods” refers to the use of two or more in-place test methods to estimate concrete strength. By combining results from more than one in-place test, a multivariable correlation can be established to estimate strength. Combined methods are reported to increase the reliability of the estimated strength.

A combined Ultrasonic Pulse Velocity and Rebound Number method, known as the SONREB method, was developed largely due to the efforts of RILEM Technical Committees 7 NDT and 43 CND. A general relationship between compressive strength of concrete, rebound hammer number, and ultrasonic pulse velocity, in



**Fig. 3.29** Diagram enabling the determination of concrete strength from rebound and UPV measurements



accordance with the tentative recommendations for “in situ concrete strength estimation by combined non-destructive methods” RILEM Committee TC 43 CND, 1983, forms the basis of SONREB technique. Figure 3.29 shows this relationship in the form of a “nomogram”. By knowing the rebound hammer and pulse velocity, the compressive strength is estimated.

A series of correction coefficients, can be applied in order to improve the accuracy of prediction obtained from the “nomogram”. These coefficients account for the type of cement, the cement content, the aggregate type, the aggregate fine fraction (less than 0.1 mm) and the maximum size of aggregates.

The accuracy of the estimated strength (the range comprising 90% of all the results) is considered to be (1) 10 to 14% when the correlation relationship is developed with known strength values of cast specimens or cores and when the composition is known, and (2) 15 to 20% when only the composition is known.

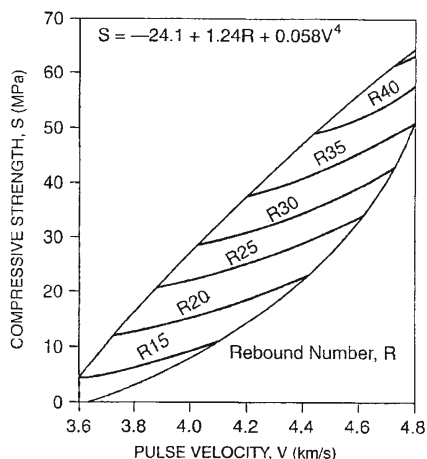
In fact, the “nomogram” is no more than a conversion curve in the case where the strength is estimated from the value of two non destructive parameters instead of a single one. It results a series of curves like on Fig. 3.29, instead of a single one. Two main issues have been pointed after these seminal works:

- the use of correcting coefficients is not practicable in the field, since it is difficult to identify the constituents of concrete,
- the value of these coefficients as well as the basic correlations were fitted on a series of concrete and cannot be extrapolated to the general case.

This is the reason why different “nomograms” can be found in a variety of sources, like that of Fig. 3.30 (IAEA, 2002). In this case, the relation between strength  $f_c$  and non-destructive parameters shows a 4<sup>th</sup>-power variation for the pulse velocity, which has also been identified by (Meynink and Samarín, 1979).

Many studies over the last fifty years, both on laboratory specimens and on structures using cores, have tried to improve the quality of the correlation between

**Fig. 3.30** The “Australian method” for estimating concrete strength (after IAEA, 2002)



measured parameters and concrete strength. Combination of ultrasonic pulse velocity and rebound hammer measurements has been extensively studied for improving strength estimates. The combination of other techniques, like penetration resistance (Machado et al, 2009), pull-out tests (Ferreira et al, 1999) or drilling (Radonjanin, 2010) was also extensively studied. (Naus, 2009) provided several other examples.

The principle behind the combination of methods is that a certain factor, e.g., moisture content, may affect the measurements of different non destructive techniques and the correlations with strength in a distinct way. If this is the case, then combining the two measurements should enable the elimination of the adverse effect of moisture condition of the specimen and improve the confidence in the concrete strength estimates. The cost of several investigations may however prove to be prohibitive and one can expect that, at most, only two techniques will be used.

## 4.2 Developing multivariate relationships as conversion curves

### 4.2.1 Specify a shape of equations

Facaoaru (Facaoaru, 1961, Facaoaru, 1970) was the pioneer in this field. He applied the combination by taking the mean of three UPV measurements and the mean of six readings for rebound numbers R, and then determined the compressive strength by using three-dimensional surfaces (called “nomograms”) where the concrete strength is expressed as a function of two variables, *i.e.*:

$$f_c = f(\text{UPV}, R)$$

Many studies have been carried out to improve these correlations, either for univariate curves  $f_c = f(\text{UPV})$  or  $f_c = f(R)$  or for bivariate correlations. It appears that:

- several functions/relationships, i.e. linear, power function, exponential, etc., have been used for the equations but they appear to be globally equivalent in terms of efficiency. Arioglu (Arioglu et al, 1996) compared seven functions with one set of data. The determination coefficient  $r^2$  for all of these was between 0.94 and 0.98, indicating that all could be used within the range of data;
- even if the type of function is fixed, the parameters identified by the authors exhibit a high variation:
- for strength-rebound number relationship,  $f_c = f(R) = a R^b$ , the  $b$  exponent was found to vary from 1.12 to 3.44 with an average value of 2.38 (Almeida, 1993, Pascale et al, 2000, Brozovsky, 2009a, Lima et al, 2000, Fabbrocino, 2005),
- for strength-UPV relationship,  $f_c = f(\text{UPV}) = a \text{UPV}^b$ , the  $b$  exponent was found to vary from 5.54 to 8.13 with an average value of 6.25 (Almeida, 1993, Drochytka, 2008, Fabbrocino, 2005, Pascale et al, 2000),
- for the combined relation  $f_c = f(\text{UPV}, R) = a \text{UPV}^b R^c$ , the variability is the same, with average values being 2.39 for  $b$  and 1.44 for  $c$  (Arioglu et al, 1996, Di Leo et al, 1994, Gasparik, 1992, Giacchetti et al, 1980, Pucinotti, 2010, Tanigawa, 1984).

The high variability of these coefficients has many causes:

- relationships identified on laboratory specimens or on cores,
- existence of many uncontrolled factors, like the concrete properties, the water content, the way of coring, the core size and shape, etc., which have all been listed by the authors,
- measurement error of NDT technique is not usually accounted to establish correlations.

A “universal law”, which could be used for any concrete has been searched by many. Others have tried combining several sets of data (Turgut, 2004, Qaswari, 2010, Evangelista et al, 2003, Nash't et al, 2005) to find such a law. These efforts have been in vain. The question as to which function is to be used still remains unresolved. Only a power law is therefore considered in the following discussion.

#### 4.2.2 Determination of multivariate relationships

NDT measurements (rebound hammer, UPV and pull-out force) have been obtained from seven Italian bridges that were tested at many locations on several piers and beams (Gennari-Santori, 2005). Cores were taken at thirteen locations after NDT measurements were carried out and the compressive strength was determined. Determining a multivariate relationship from these data would provide a practical tool for estimating strength: (a) at other locations on these bridges, where there were only NDT measurements and (b) on similar bridges. Table 3.6 summarizes the results obtained at the thirteen locations.

**Table 3.6** Measurement results for three NDT and core strength at 13 locations (from Gennari-Santori, 2005)

V (m/s)	R	F (kN)	$f_c$ MPa
4459.2	41.6	27.8	29.3
4519	45.0	42.3	35.1
4476	48.1	43.9	46.6
4243	43.1	33.7	43.3
4745	43.6	25.6	35.7
4355	44.7	27.3	27.8
4603	44.2	34.8	41.4
4477	40.5	23.5	25.1
4214	42.7	34.8	24.9
5086	50.3	49.8	63.8
4329	49.3	27.3	32.4
4373	47.1	30.5	33.0

**Table 3.7** Coefficients of determination for mono- and multivariate relationships

	Power exponents			
	R	UPV	F	$r^2$
$f_c = a R^b$	2.62			0.41
$f_c = a UPV^b$		3.41		0.43
$f_c = a UPV^b R^c$	1.91	2.52		0.62
$f_c = a UPV^b R^c F^d$	1.02	2.07	0.53	0.75

**Table 3.8** Improvement of correlation by combining two NDT measurements

	$r^2$ (R)	$r^2$ (V)	$r^2$ (R and V)
Gonçalves, 1995	0.86	0.72	0.94
Gennari-Santori, 2005	0.41	0.50	0.62
Proverbio, 2005	0.82	0.46	0.86
Nash't, 2005	0.77	0.59	0.80

Several mono- and multivariate relationships have been identified (see Table 3.7). All relationships have low values for the coefficient of determination  $r^2$ . However, when the relationship is multivariate, i.e. combining several tests for a single relationship, the coefficient of determination is greatly improved. Similar improvements have been reported by others as shown in Table 3.8.

The combination is expected to improve the coefficient of determination, but this improvement can be small if one technique is much more reliable than the other. Strength correlations for UPV measurements may not be very reliable (Kheder, 1998, Yun et al, 1988) because of the uncertainties and variability in the moisture content of the structure at the time of testing. We will try to explain how the influence of these uncontrolled factors can be used, by combination of UPV and another technique (here rebound).

### 4.3 *Understanding the possibilities and limits of multivariate correlations*

#### 4.3.1 **Using simulations to better understand what happens during NDT measurements**

Since it is impossible to fully control all parameters in practice (either in the lab or in the field), a synthetic approach, based on virtual data, will be advantageous in order to better understand on what factors the efficiency of combination depends.

The general principles of this synthetic approach works in four steps:

- *Step 1 - generation.* A data set of material properties is generated, the focus being given on material strength  $f_c$  and on moisture content, through saturation rate  $X$ . These two parameters are randomly simulated according to a prior statistical distribution representing the material variability.
- *Step 2. – measurement.* Non destructive measurements are simulated and two values  $V$  (for UPV velocity) and  $R$  (for rebound) are generated. These values are calculated in two steps: (a) a theoretical value is generated, according to the relationships  $V(f_c, X)$  and  $R(f_c, V)$  and then, (b) a random error is added, corresponding for each technique, to the measurement error.
- *Step 3 – calibration.* The calibration stage consists in comparing the non destructive measurement values and the concrete strength (which can be determined after coring), and to identify the mono- or multivariate regression laws  $f_{c\text{ est}} = f(R, V)$ .
- *Step 4 – validation.* Because of the measurement errors, model error and statistical uncertainty (limited size of the sample taken for calibration), the estimated strength differs from the true strength (which, in this synthetic approach, is available and was generated at Step 1). The comparison between estimated and true values provides information about the quality of the NDT evaluation.

How representative the synthetic approach is depends on the care with which simulations are performed. Specific attention must be paid so that the statistical distributions, the correlations between parameters and the various sensitivities (e.g. influence of saturation rate on UPV velocity or on strength) required to build the synthetic data at Step 1 are similar to those in the “real world”.

The simulations have been performed with the following average properties:  $f_c = 30$  MPa,  $X = 85$  %. Such a concrete has a rebound number  $R = 35$  and an ultrasonic pulse velocity  $V = 4365$  m.s<sup>-1</sup>. When the strength and/or saturation rate differ from their average value,  $R$  and  $V$  vary accordingly. Power relationships have been chosen to describe this dependency, being the exponents selected after a careful analysis of the literature.

$$R = 35(f_c / 30)^{1/mf} (X / 85)^{1/mx} \quad (3.1)$$

$$V = 4365(f_c / 30)^{1/nf} (X / 85)^{1/nx} \quad (3.2)$$

The signs and values of the exponents depend on the sensitivity of NDT measurements ( $R$ ,  $V$ ) to the strength  $f_c$  or to the unknown variable  $X$ .

When the saturation rate  $X$  is taken as the random variable,  $m_x$  is negative (rebound decreases if water content increases) while  $n_x$  is positive (the UPV increases with the water content). If another unknown variable were to be considered, like carbonation level, both  $m_x$  and  $n_x$  could be positive. All exponent values have been calibrated after having considered the literature and experimental data:

- $m_f$  and  $n_f$  were taken to be 2.38 and 6.25 for  $R$  and UPV respectively, which correspond to average values from the literature, as seen above,
- $m_x$ , which describes the sensitivity of rebound to water content has been taken to be  $-1/3$ . This value is in agreement with Czechian Standard CSN 731373 which introduces a correcting factor  $\alpha_w$  for the rebound value, which varies from 0.85 (dry concrete) to 1.05 (water saturated concrete) (Brozovsky, 2009b),
- $n_x$ , which describes the sensitivity of UPV to water content, has been taken to be 0.20, in agreement with SENSO experimental data, where the velocity increased from 4365  $\text{m}\cdot\text{s}^{-1}$  for  $X = 85\%$  to 4630  $\text{m}\cdot\text{s}^{-1}$  for the same concrete saturated (LMDC-SENSO, 2009).

### 4.3.2 What an uncontrolled factor can change

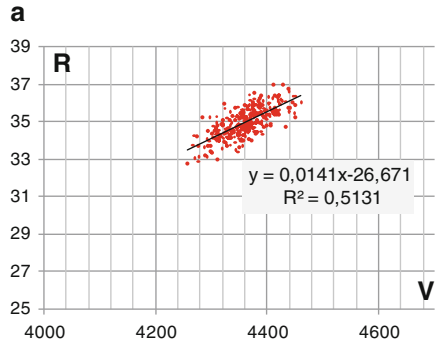
In a first series of simulations, we consider perfect measurements (no error is introduced at Step 2 on  $R$  and  $V$ ), but with some material variability. The standard deviation on strength is equal to 1.5 MPa (which corresponds to a coefficient of variation (c.o.v. = standard deviation/mean value)  $\text{c.o.v.}(f_c) = 5\%$ ). Three levels of variability are considered for the uncontrolled factor  $X$ :  $\text{c.o.v.}(X) = 2\%, 5\%, 10\%$ . The three following Figs. (Fig. 3.31a-c) plot the existing correlation between  $R$  and UPV simulated measurements.\*

These figures highlight the role of the uncontrolled parameter. If  $X$  was constant, because of the positive influence of strength on both  $R$  and  $V$  ( $m_f$  and  $n_f$  exponents have the same sign), it would result in a positive correlation between  $R$  and  $V$ . This correlation would even be perfect in case of no measurement error. However, because  $m_x$  and  $n_x$  have a different sign in Eq. 3.1–3.2,  $X$  variations have an adverse effect on  $R$  and  $V$ : a large  $X$  value increases  $V$  but decreases  $R$ . Then a negative correlation between  $R$  and  $V$  results.

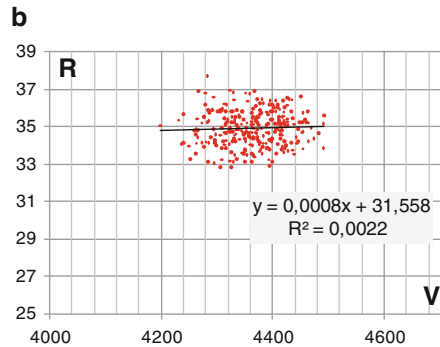
This negative correlation (due to  $X$  variations) superimposes to the (former) positive correlation (due to  $f_c$  variation). Depending on the range of variation of the uncontrolled parameter  $X$ , the result can be: (a) a positive correlation for a small range of  $X$ , (b) no correlation, for an intermediate range of  $X$ , (c) a negative correlation for a large range of  $X$ .

The final correlation depends on the respective weights of the two possible causes, which comes from the respective scatters (c.o.v.) of  $f_c$  and  $X$ . The positive correlation dominates when the water content  $X$  varies in a limited range, and the negative correlation dominates when it varies in a large range, by comparison to that of concrete strength (here constant). This confirms the interest of combining these two NDT measurements, because of their different sensitivity to the uncontrolled parameter.

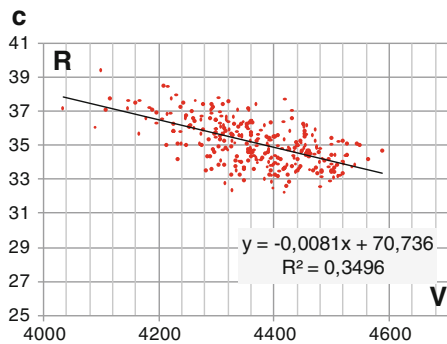
**Fig. 3.31a** Correlation between UPV and Rebound number R (c.o.v.(X) = 2%)



**Fig. 3.31b** Correlation between UPV and Rebound number R (c.o.v.(X) = 5%)



**Fig. 3.1c** Correlation between UPV and Rebound number R (c.o.v.(X) = 10%)



### 4.3.3 The influence of the measurement error

The NDT measurements are simulated by adding a random error to the true (theoretical) NDT value. The magnitude of “reasonable” measurement errors is chosen in agreement with the SENSO experimental data, where a large number of measurements were performed specifically to determine this variability. The standard errors for the rebound number and for UPV were respectively measured to be 2 and 90 m.s<sup>-1</sup>. These values give us the magnitude of standard error that can be used in simulations (Balayssac, 2008, LMDC-SENSO, 2009).

The simulation process consists of:

- (a) *Step 1 - generation.* Generating first a pair of “true” strength  $f_c$  and “true” saturation rate  $X$ . These variables follow a Gaussian distribution with respective means of 30 MPa and 85 % and respective coefficients of variation  $c.o.v.(f_c) = 15\%$  and  $c.o.v.(X) = 10\%$ , which is a relatively high level of uncontrolled variation. The range of material variability has been chosen in agreement with experimental data. Brozovski found a c.o.v. ranging from 10 to 12% (Brozovsky, 2009a), and Moczko found between 8 and 13 % (Breysse et al, 2010). Of course, this range can be much larger if very different concretes are included in the experimental data, with the risk of introducing additional uncontrolled factors (composition of concrete, age, etc.).
- (b) *Step 2. – measurement.* NDT measurements are simulated by calculating the theoretical values for  $R$  and  $V$  according to Equations 3.1–3.2, and by adding the measurement noise. The ranges for the measurement error are in agreement with those found during the SENSO program (SENSO-LMDC, 2009) and on Polish bridges by Moczko (Breysse et al, 2010), but also with data provided by Brozovski, who found  $(c.o.v.(R) = 7\%$  if the measurement is done with Czechian standard and 12% with the European standard) (Brozovsky, 2009a).
- (c) *Step 3 – calibration.* Considering that strength can be identified on cores or control specimens (without error measurement) and, from that, identifying three regression models linking the strength to one or two NDT measurements:

$$- \text{ Monovariate regression with } R : f_c = 30 (R / 35)^m \quad (3.3)$$

$$- \text{ Monovariate regression with } V : f_c = 30 (V / 4365)^n \quad (3.4)$$

$$- \text{ Bivariate regression with } R \text{ and } V : f_c = 30 (R / 35)^m (V / 4365)^n \quad (3.5)$$

The ranges of strength and saturation ratio being given, the quality of the regression models depends on the “noise”, which increases with the measurement errors on  $R$  and  $V$ .

To be representative of real situations for calibration, it is considered that the models are identified from 13 pairs (or triplets) of strength-NDT parameter value. This number is identical to that in Table 3.6 from measurements (Gennari-Santori, 2005). It corresponds to an investigation program which remains limited regarding the quantity of cores.

- (d) *Step 4 – validation.* In the last step, the identified models are used as three alternatives so as to estimate strength at points where  $R$  and/or  $V$  are measured, by using Equations (3.3) to (3.5). The simulation is performed on a data set of 300 strength values.

Table 3.9 gives the  $r^2$  coefficients between estimated and real strengths when varying the measurement error. All coefficients correspond to an average value on 3 simulations: the identification on 13 cores and the estimation stage on 300 points is repeated three times and the  $r^2$  values are averaged.

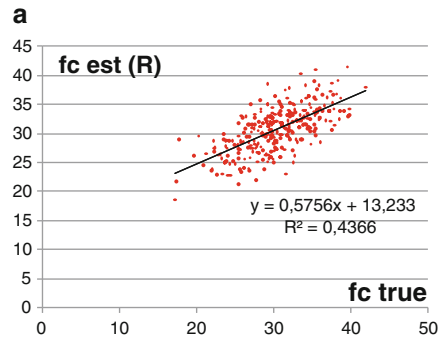
Figures. 3.32a-c show the quality of fit (for a single simulation) between real and estimated strength in the case where the measurement error is  $2 / 60 \text{ m.s}^{-1}$ .



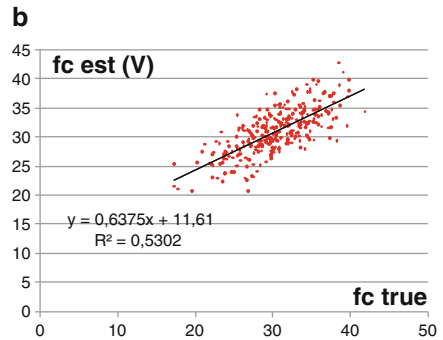
**Table 3.9** Determination coefficient between true and estimated strength for several measurement errors (sd for standard deviation) and regression models used

Measurement error	sd (R)	0	1	2	2	3
	sd(V) (m/s)	0	30	60	90	90
model Eq. (3)	r <sup>2</sup> (R)	0.80	0.66	0.44	0.47	0.28
model Eq. (4)	r <sup>2</sup> (UPV)	0.64	0.59	0.53	0.41	0.41
model Eq. (5)	r <sup>2</sup> (R, UPV)	1	0.92	0.76	0.66	0.59

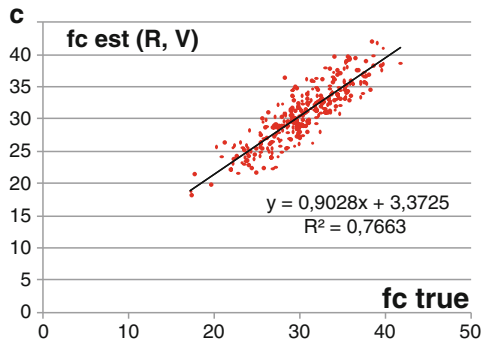
**Fig. 3.32 a** Correlation between true strength and strength estimated with rebound



**Fig. 3.32b** Correlation between true strength and strength estimated with UPV.



**Fig. 3.32c** Correlation between true strength and strength estimated by combining rebound and UPV



It is interesting to first check the consistency between these synthetic results and those found in the literature, obtained from field measurements. The determination coefficients from Table 3.9 can be positively compared with those from Table 3.8. The main reason for differences is the magnitude of the measurement error, which is considered in these simulations as a parameter.

The results also show that:

- The quality of estimation is highly sensitive to the quality of measurements, which justifies the great care with which the NDT measurements have to be performed,
- The combination significantly increases the fit and reduces the error on estimation. This is also visible on Fig. 3.32c where the scattering of the cloud of points is reduced when the measurements are combined. Here, most of the points lay in the [-5, + 5] MPa range around the real value. As a consequence, if one considers that the aim is not the “local estimation” of strength but that of the average value of strength or that of fixed percentiles (characteristic values), their estimation will also be improved.

This simulation has been limited to a case where the relative influence of the uncontrolled variable (here X) on the two NDT measurements was adverse. When it is not the case (e.g. if the uncontrolled parameter is the carbonation depth, which increases both for UPV and R), combination of techniques is also applicable, but less efficient.

In any case, the simulation of synthetic data is helpful for quantifying the practical added-value of combining the techniques, once the computer has been fed with realistic “virtual physics”. This means that, to be representative, the prior models used in the simulations to link material properties and NDT measurement values must mimic the real world at best.

#### 4.4 Calibration process and combination of NDT on real data

The European Standard EN 13791 explains how NDT measurements can be used to estimate in situ concrete strength. The process requires: (a) using a “prior” curve, which links the strength and the NDT value, (b) calibrating, through a “shifting process”, so as to fit the results in agreement with a number of reference values obtained by coring.

We will depart here from this standardized approach, and show how, while using the same principles, the strength estimation can be efficiently improved by combining NDT data. The field data are those of Table 3.6 (Gennari-Santori, 2005). Three alternatives will be compared, all using power law models, and having the generic shape:

$$(f_c / f_{c_{ref}}) = (R / R_{ref})^{mf} (UPV / UPV_{ref})^{nf} \quad (3.6)$$

In this equation, the “reference values” enable to work without units. They do not influence the results. Their values are:  $f_{c_{ref}} = 30$  MPa,  $R_{ref} = 35$ ,  $UPV_{ref} = 4365$  m.s<sup>-1</sup>.

**Table 3.10** Quality of the strength estimate for the different approaches ( $\Delta$  is the mean value of absolute error)

	Approach 1	Approach 2a	Approach 2b	Approach 3
	Specific model	prior curve (R) + shift	prior curve (UPV) + shift	prior curve (R, UPV) + shift
Exponent on R	1.91	2.38	-	1.44
Exponent on V	2.52	-	6.25	2.39
$r^2$	0.625	0.390	0.492	0.619
$\Delta$ (MPa)	5.1	7.7	7.7	5.2

The alternatives are:

- (a) *Approach 1*. Building specific regression models, directly on the data set (i.e. 13 triplets R, UPV,  $f_c$  cores). The statistical fitting leads to  $m_f = 1.91$  and  $n_f = 2.52$ .
- (b) *Approach 2*. Estimating strength from one NDT measurement (either R - *Approach 1a*. or UPV - *Approach 1b*) and the corresponding calibration curve. The estimations are shifted so as to obtain the same average value for estimated strengths as for true strengths measured on cores.

The prior model used are:

$$(f_c / f_{c,ref}) = (R / R_{ref})^{2.38} \quad (3.7)$$

and

$$(f_c / f_{c,ref}) = (UPV / UPV_{ref})^{6.25} \quad (3.8)$$

where the values of the exponents used are in agreement with those in the literature (see § 4.2.1).

- (c) *Approach 3*. Estimating strength from two NDT measurements (R and UPV) and the corresponding calibration curve. The estimations are shifted so as to obtain the same average value for estimated strengths as for true strengths measured on cores.

The prior model used is:

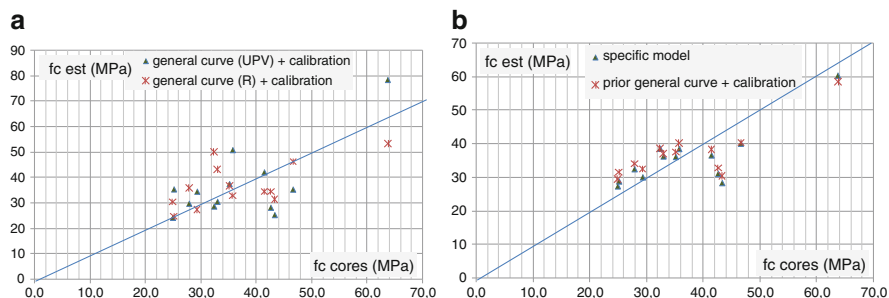
$$(f_c / f_{c,ref}) = (R / R_{ref})^{1.44} (UPV / UPV_{ref})^{2.39} \quad (3.9)$$

where the values of the exponents have been taken in agreement with the literature (see § 4.2.1).

Thanks to the shifting process, the values taken for the exponents in Equations (3.7) to (3.9) have only a small influence on the quality of the final estimate. Figures 3.33a-b and Table 3.10 compare what can be obtained from site data with the different approaches:

The two main conclusions are:

- That the multivariate analysis (Approach 3) is much better than the univariate analysis (Approach 2). It increases the determination coefficient and reduces the error;



**Fig. 3.33a-b** Quality of strength estimate., (a-left) using one NDT measurement and calibration, (b-right) combining two NDT measurements

- The quality of fit is comparable between Approach 3 and the specific correlation of Approach 1: the determination coefficient is roughly the same, and the average error on strength is about  $\pm 5$  MPa. Despite the fact that the exponents are very different, the estimated values are very close (Fig. 3.33b).

The use of the prior model (R, V) and calibration (Approach 3) is very practical, since it can be used as soon as one gets an idea of the real core strength values. This of course requires a “minimal number” of cores, but one can think that six cores can provide a good idea of this parameter. Once this average “true core strength” can be estimated, the combination of the multivariate regression law with the shifting process provides the estimated value of strength at any location where R and UPV are measured.

This efficiency justifies the idea of a global calibration curve. The model of Eq. (3.9) can be used as a starting point.

## 4.5 The scope of investigation and its efficient planning

### 4.5.1 Is it useful to get more NDT parameters?

The regression laws built with two NDT measurements instead of a single one improve the quality of the strength estimation. The same reasoning would lead us to consider a third (or even a fourth) NDT measurement. Since this parameter is sensitive to some uncontrolled factor, it would also probably induce some further improvements in strength estimates.

The question is then to know what a realistic limit is. The criteria that contribute to answering this are:

- the more different the sensitivities are, the more efficient the combination is. In practice, one must try to find techniques for which the variations (like those corresponding to exponents in equations (3.1) and (3.2)) have opposite signs;

- the best is to choose techniques for which the signal to noise ratio is maximum. This means that a highly repeatable measurement is of high interest. Conversely, a technique in which the measurement error is too high may be not useful;
- the cost/effectiveness ratio must be evaluated, accounting for the cost of an additional series of measurements, compared with the improvement in the value obtained thanks to an additional NDT measurement. If the first two parameters have been well chosen, the possible added-value of a third one may often be limited.

If we come back to the field data given in Table 3.7, the determination factor increases from 0.62 for a bivariate regression to 0.75 if a third parameter, the pull-out force, is also considered. The gain is not negligible, but it requires an additional series of semi-destructive tests. Using such tests, instead of a third NDT, is probably interesting, since the information provided by pull-out is more directly linked to the mechanical material response.

Other recent examples on field data confirmed that pull-out test can provide useful information, whose combination with NDT parameters (rebound or UPV) has advantages (Breyse et al, 2010). However, even if some authors have tried to fit correlations with a higher number of parameters (Proverbio et al, 2005, Pucinotti, 2007), it seems reasonable to limit the investigation to two well chosen NDT techniques, one of them being possibly a semi-destructive one, like pull-out test.

#### 4.5.2 How many points of measurement? Where?

Another question is the general planning of the investigation. As long as the objective is to estimate average and local strength values, the first issue is how spatial variations are accounted for.

We can recommend a strategy adapted from (Pfister et al, 2010). They suggested that one covers first the whole on site structure with a quick and accurate NDT, like UPV or R (or, even better, both). After this first stage, the NDT data are available and their statistical distribution is known. This must drive the choice of the locations at which cores must be taken, with respect to two criteria:

- a statistical representative sample: a minimal number  $N$  of cores has to be taken,
- a choice of the  $N$  points such as the statistical distribution of the NDT parameter on the  $N$ -sample is similar to that on the whole data set.

This second criterion ensures that: (a) the range of material properties in the structure is covered at best, which is good for the quality of the regression model, and (b) the strengths measured on cores (average and distribution) are close to those on the whole structure.

There is no definite rule regarding the minimum number  $N$  of test locations, since it depends on many factors (variability of the strength distribution in the structure, total area covered, etc.). The simulations of § 4.3. were performed while keeping this number constant ( $N = 13$ ). Its effect on the accuracy of the estimation has

been recently studied (Breyse et al, 2009, Pfister et al, 2009). It is well known from statistics that the uncertainty decreases with the square root of the number of tests, and this may lead to a very large number of tests if a high accuracy is sought.

From the existing experience, it seems that about 10 to 12 tests is probably a reasonable minimum value, knowing that it is also possible to combine more or less direct information from other sources, like:

- additional tests on reduced size cores (Brignola et al, 2008), which is relatively well correlated to the strength on standard cores (in this case, the use of correcting factors for size and shape effects is necessary),
- semi-destructive tests, like pull-out tests, which offer an interesting alternative, even for providing a good estimate of the mean strength (Moczko, 2009).

#### ***4.6 Conclusions about combination of techniques***

This section has shown, based both on field data analysis, an in-depth review of the existing literature and synthetic simulations, how and why combination of NDT can be very interesting. This combination reduces the uncertainty of the concrete strength estimation.

NDTs like rebound or UPV measurements are often regarded as giving unreliable and unsatisfactory strength estimates. Because of the wide variety of concretes and the influence of many uncontrolled parameters (curing conditions, carbonation, moisture, etc.) there is no possibility to use a “universal law” that would directly estimate the concrete strength from the NDT measurement.

It is however possible, after calibration, to correctly estimate the concrete strength, with an uncertainty of approximately +/- 5 MPa on local values. This level of accuracy is convenient for many practical purposes, like a general evaluation of residual strength of the structure, or the identification of the weakest areas.

It is suggested to begin the investigation with the NDT and to define in a second step the location of cores after an in-depth analysis of the statistical distribution of the NDT parameters. The last step is that of strength assessment, with two main options:

- that of building a specific correlation relationship for the studied structure (this is named “direct method” in the EN 13791);
- that of using a calibration curve and shifting the results according to the average strength estimated on a limited number of cores.

This method works when using a single NDT, but is improved considerably when combining the information provided by two NDT measurements. The most efficient choice is that of combining two NDT measurements which show, as much as possible, adverse sensitivity to the same uncontrolled parameter. For instance, if the main uncontrolled parameter is water content in the concrete, UPV and rebound are good candidates for being the two best techniques to use. In other cases (influence of chlorides, of carbonation, etc.) other techniques like radar measurements or electrical resistivity, can be possible candidates.

If a calibration curve is required, that of Equation (3.9), working for rebound and UPV measurements offers a good starting point:

$$(f_c / 30) = (R / 35)^{1.44} (UPV / 4365)^{2.39}$$

If other techniques are used, there is no reference curve for the moment, and the only way is that of identifying a specific correlation based on the available data.

In both cases (specific correlation relationship or calibration curve), the larger the number of cores, the more reliable is the estimate. Some possibilities exist for limiting the number of cores without reducing the quality of the estimate (using non standard cores, using other tests like penetration test or pull-out test), but the practicality of this remains to be confirmed by further studies in this field.

## 5 Data fusion to better estimate strength

### 5.1 Why to use data fusion?

The previous section has shown that it is possible to use a multivariate correlation for any NDT (velocity UPV, rebound hammer R, pull out force F, etc.) to get a better strength estimate of the concrete strength. Another approach is to develop a data fusion process. This makes use of the different techniques' sensitivities with the concrete strength to improve diagnosis reliability. Instead of working on only one relationship, the strengths resulting from each non destructive or destructive evaluation can be combined.

Two measurements would theoretically be sufficient to determine two unknown indicators by solving a set of two equations (inversion process). But imperfection and partial reproducibility of measurements on concrete lead to the need of improving diagnosis quality. Indeed, on the one hand measurements are sensitive to material heterogeneity, variability and experimental noise, and on the other hand, correlations are approximations of reality, also including modeling error. Thus relative disagreement or conflict between information sources can happen and the system of equations can rapidly become ill-conditioned. A solution is then to combine several (at least three) NDT techniques providing complementary information. In fact, the data fusion process enables us to manage such situations of relative disagreement between information sources.

Data fusion is more and more employed in the NDT field. The most commonly used methods are based on classification (like Dempster-Shafer theory) in particular for image fusion: X-ray and ultrasounds in welds [(Dromigny-Badin et al, 1997), (Kaftandjian et al, 2005)], infrared thermography and eddy current in carbon reinforced composite (Gros et al, 1999), radar wave and ultrasounds on reinforced concrete for image reconstruction (Kohl and Streicher, 2006), medical imagery in brain (Bloch, 1996), and infrared thermography images in nuclear applications

(Moysan et al, 2007). Moreover data fusion has already been used for assessing civil engineering components [(Gros et al, 1999), (Kohl and Streicher, 2006), (Horn, 2006), (Maierhofer et al, 2008)] but, as previously mentioned, its classical use is in the domain of image analysis: two or more images are compared and processed together, which enables to highlight contrast, decrease noise and make defects clearer.

## 5.2 *Data fusion in 1D*

Working in one dimension means determining only one information, indicator in our case, like porosity, saturation rate, elasticity modulus or strength. Data fusion using possibility theory has been chosen in the French project SENS0 (Balayssac, 2008) because it allows combining heterogeneous information more or less precise and reliable, to provide global quantitative information with increased quality [(Zadeh, 1999), (Bouchon-Meunier and Marsala, 2003), (Bloch, 2003)]. This theory is more appropriate for this quantitative estimation problem than methods of classification. The data fusion differs from statistical methods because it is not based on probability. It transfers the human logic to the analysis, with notions of possibility, impossibility and uncertainty called fuzzy sets.

It is possible to work in one dimension (1D), two dimensions (2D) or more. In each case, the same 3-step process must be followed:

- (a) data representation via possibility distributions and fuzzy sets
- (b) fusion process with appropriate operator of combination
- (c) decision criterion.

These steps are first explained and the results obtained in two applications, i.e. in 1D and in 2D are then presented and discussed.

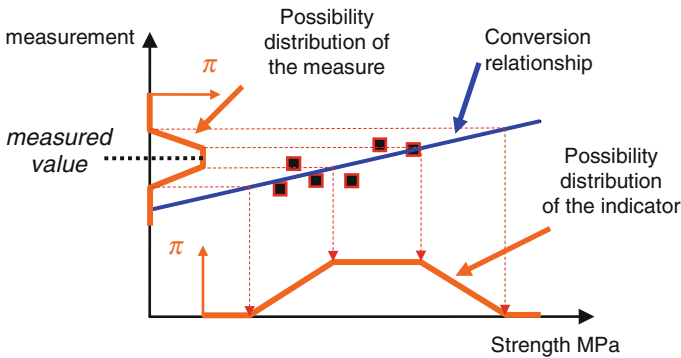
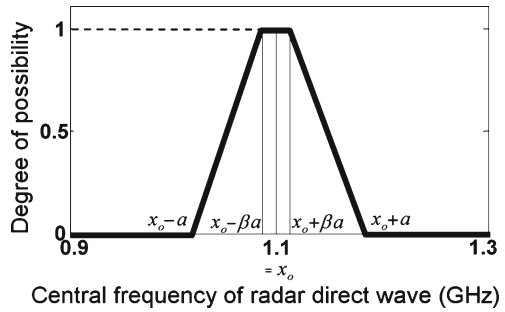
### 5.2.1 **Data representation**

The measurement and its uncertainty are represented by the existence possibility of the value measured. The possibility varies between 0 and 1. Its distribution depends on the standard deviation and it can be Gaussian, trapezoidal or triangular. One example is given in Fig. 3.34 with a trapezoidal distribution that will be taken in the following examples and applications.

Secondly, this distribution must be projected through the conversion law that links measurement results and the researched property (indicator), as seen in Fig. 3.35. As it was seen in the previous sections, many shapes of conversion curves are possible. Here the work is done with a linear relationship, identified by a linear regression analysis of the data set.



**Fig. 3.34** Possibility distribution of the central frequency of the radar direct wave



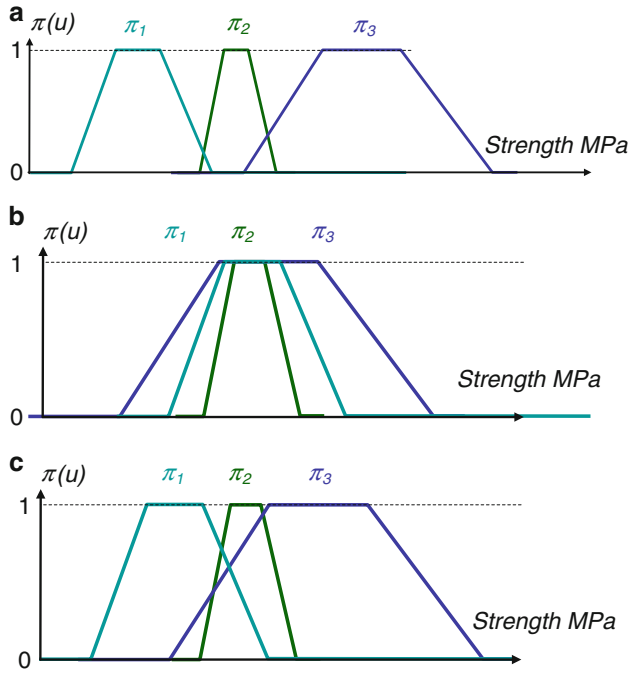
**Fig. 3.35** Propagation of the measure distribution of possibilities on the indicator (strength)

If three NDT are used independently, leading to three measurements, the projection process is repeated three times, and leads to we three possibility distributions ( $\pi_1, \pi_2, \pi_3$ ) of the indicator. Different configurations can result (Fig. 3.36).

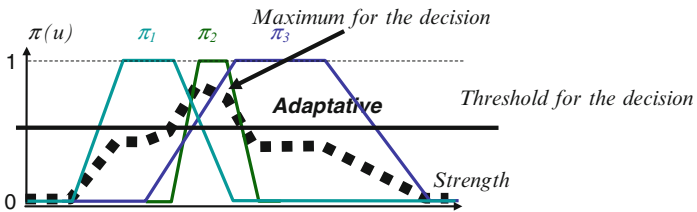
In the above figure, the concordance between the different results is low. The distributions of possibilities for the indicator deduced from the three measures are very different. In the figure at the middle, the concordance is good and the three solutions for the indicator are similar. The third figure illustrates a typical case with real on site measurements, when the concordance is neither zero nor perfect. The data fusion process must be able to account for these various cases.

### 5.2.2 Fusion process

The fusion process requires a mathematical operator. In this work, an operator proposed by Delmotte (Delmotte, 2000) has been chosen. It is a self-adapting operator, depending of the concordance. The result is a “fused” possibility distribution, like that visible as a dotted line in Fig. 3.37.

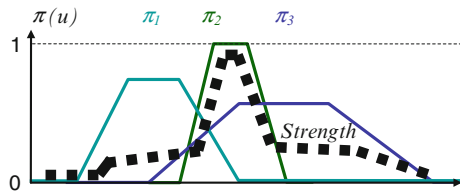


**Fig. 3.36a-c** Three possible configurations for possibility distributions obtained via three independent NT measurements



**Fig. 3.37** Typical solution of the third case obtained by Delmotte operator

**Fig. 3.38** Fused distributions including the reliability



### 5.2.3 Decision

The distribution of the possibilities for the three measurements merged generally highlights a solution, e.g. the maximum value or a range of values over a threshold as seen in Fig. 3.37. This threshold can be decided by the expert regarding the industrial context and the morphology of the fusion results. The height and the width of the distribution are quality criteria of the result after the fusion: the higher the maximum and the narrower the peak, the better the quality of the solution is.

In the SENSO project, the reliability of each technique was also accounted for. The effect of reliability is to reduce the maximum amplitude of the distribution's possibilities and to modulate each individual possibility distribution. It was introduced thanks to a quality index obtained from statistical information on the laboratory measurements and varying from 0 to 1 (LMDC-SENSO, 2009). It can also be defined by the expert, regarding the confidence that he has in the technique and in the measurement. These maximums are 0.8 and 0.6 for the  $\pi_1$  and  $\pi_3$  distributions on the example in Fig. 3.38.

The purpose of the data fusion being to find a solution with in situ measurements that are often in conflict, it would be useful to calculate a confidence index for the result of fusion. Such an index would probably help construction works manager to take a decision.

### 5.2.4 Example of strength estimate (1D problem)

In this example, we work with the same data that were used in the previous section (§ 4.2.6., Table 3.2) and issued from Italian bridges in which rebound hammer, UPV and pull-out force measurements have been obtained, at many locations on several piers and beams. Thirteen cores for different locations gave the compressive strength by destructive testing.

Empirical regression relationships can be identified from the 3 series of 13 pairs (NDT parameter, core strength). These relationships will be used as conversion curves as explained at §5.2.1. The identified relationships are:

$$\begin{aligned} V &= 15.635 f_c + 3909 & r^2 &= 0.51 \\ R &= 0.1794 f_c + 38.5 & r^2 &= 0.41 \\ F &= 0.577 f_c + 12.5 & r^2 &= 0.61 \end{aligned}$$

For the three techniques V (ultrasonic velocity), R (rebound number) and F (pull out peak load). The  $r^2$  is used as the modulating quality index introduced at § 5.2.3.

These relationships and coefficients were implemented in a program developed in the LCND laboratory. The different measurement sets are tested and combined to extract the possibility distribution maximum of the strength estimated by the fusion software and the measured one. Table 3.11 presents the strengths obtained by fusion from the three measurements, and the shift between the estimated and measured strengths. RE is the relative error:  $RE = \Delta \text{ strength} / \text{measured strength}$ .

**Table 3.11** Merged, measured and shift strength for the 13 data sets

Point	Strength S (MPa)		$\Delta S$ (MPa)	RE = $\Delta S/S$
	Merged	Measured		
<b>1</b>	28.7	29.3	0.6	0.02
2	49.4	35.1	14.3	0.41
<b>3</b>	51.2	46.6	5.6	0.10
4	34.5	43.3	8.8	0.20
5	20.4	35.7	15.3	0.43
<b>6</b>	27.9	27.8	0.1	0.00
7	39.9	41.4	1.5	0.04
8	16.8	25.1	8.3	0.33
9	36.4	24.9	11.5	0.46
<b>10</b>	66.9	63.8	3.1	0.05
11	23.4	32.4	9.0	0.28
<b>12</b>	33.4	33.0	0.4	0.01
<b>13</b>	34.5	32.8	1.7	0.05
mean	34.1	36.3	2.2	0.06

Conclusions from the results in Table 3.11 are:

- The shifts between the fused and measured results are very low for values showed in bold characters (Points 1, 3, 6, 7, 10, 12, 13) with a relative error smaller than 10 %.
- The prediction calculated for the mean value of all the results is very good.
- There are points that have a big difference between measured and merged results, i.e. poorly predicted. In these cases the possibilities distribution is generally like the one shown in Fig. 3.39 for point 5 (VC=0.43).

Figure 3.39 (point 5) and 41 (point 6) are a screen savings of the program. The window above provides the possibility distributions for the three measurements while the window below gives the fusion result. For point 5 (worst result of the whole series of data), the concordances between the three distributions are very poor. The fusion result is not good and two local solutions (maximums) are possible. The absolute maximum of the possibilities distribution after fusion ( $f_c = 20.4$  MPa) is considered to be the solution. However the “real” solution (i.e. that the strength measured on the core) is 35.7 MPa, which does not coincide with any NDT measurement!

In such a case, the strength assessment, whatever the estimated value, is not reliable enough. Because of the poor concordance, the NDT results for this point must be disregarded for strength assessment. One another possibility would be to repeat NDT measurements at the same location, in order to get a other data set.

Figure 3.40 (Point 6) shows the other extreme situation, where the concordance is high, the reliability high and the relative error very small. It can be noted that, with the same individual reliabilities, the maximum possibility of the merged solution is larger in the second situation than in the first one. Of course, intermediate situations (i.e. average quality of concordance) are not uncommon.

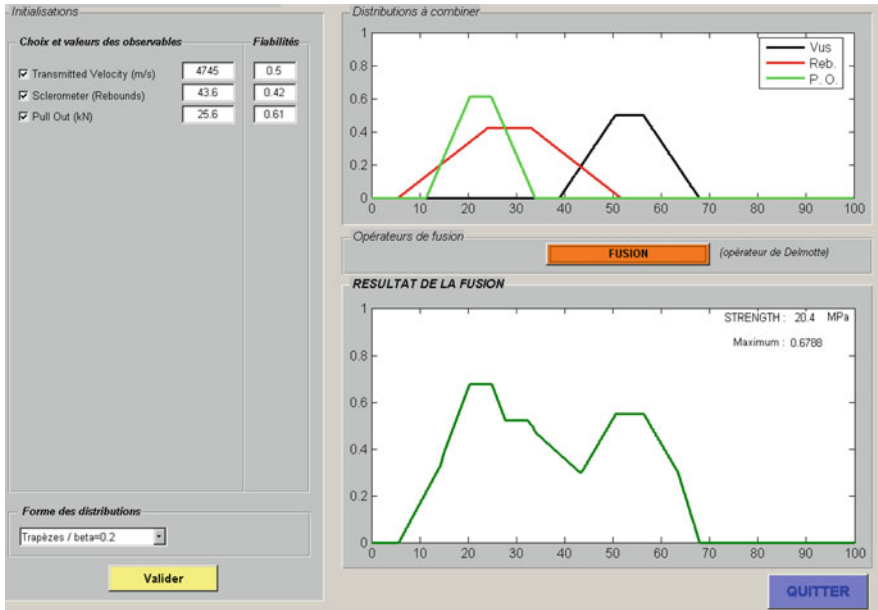


Fig. 3.39 Possibility distributions for the point 5 before and after fusion (RE=0.43)

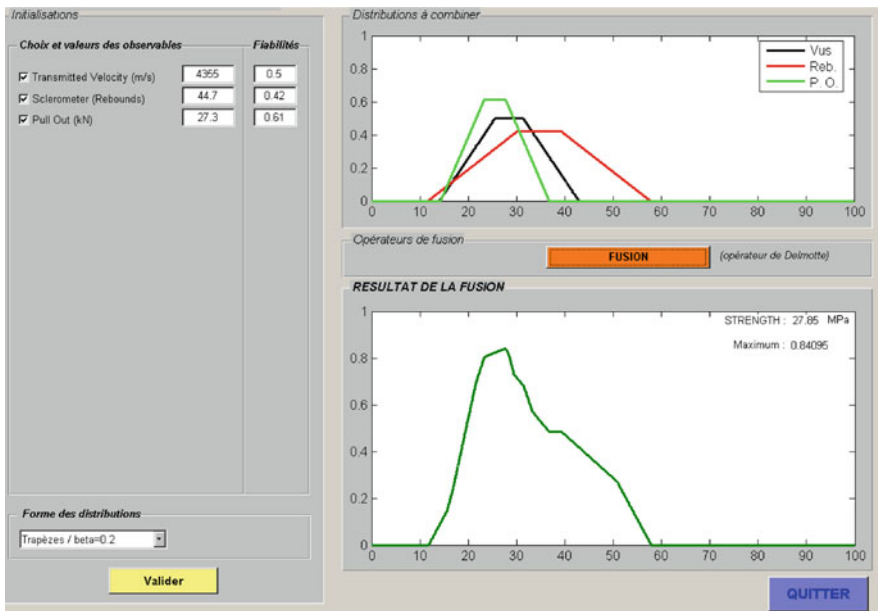


Fig. 3.40 Possibility distributions for the point 6 before and after fusion (RE=0.00)

This example of data fusion in 1D has shown that it is possible to improve the estimation of the concrete strength by combining several (here three) measurements. The fusion result is deterministic but it is more than a single strength value. Depending on good or bad concordance between the measurements results obtained by different techniques we can conclude that:

- in the case of good concordance, the level of possibility increases and reinforces the confidence that we can get in the predicted value of strength,
- in the case of average concordance, we may have different predicted value of strength and the choice is very difficult. Data fusion gives a solution which is a “best compromise” with its confidence level,
- if the concordance is really too bad, the fusion result clearly indicated that the solution proposed cannot be trusted and that the measurements have to be carried on again.

### ***5.3 Data fusion in 2D***

Working in two dimensions (2D) means working on two indicators that are interdependent, i.e. when the determination of the one depends on the second. For example the measurements of the UPV vary with the porosity and the water saturation rate. So if we work with bilinear regressions built for two well chosen measurements, we can extract the two pieces of information simultaneously.

This same basic property justified the use of multivariate analysis at §4, when it was assumed that two measurements having a different sensitivity to uncontrolled factors may carry more information if analyzed together. The main difference here is that there is no a privileged parameter (e.g. strength) and a secondary one, considered as an uncontrolled source of noise (e.g. moisture) but two parameters taken at the same level.

In the SENSO project, the goal was to provide quantitative evaluation of the following indicators: porosity rate, water saturation, modulus of elasticity, mechanical strength, chloride content and carbonation degree, by using and combining different NDT methods. Because there are dependencies between different indicators, the work was developed for the following pairs of indicators (Ploix et al, 2009): porosity rate and water saturation – water saturation and elasticity modulus – water saturation and strength.

A large number of measurements were carried on in the laboratory on a representative range of concretes. 90 specimens were cast with controlled compositions and w/c ratios and they were conditioned at different levels of water saturation (Balayssac, 2008). The different NDT (radar, electrical resistivity and capacity, infrared thermography, impact echo and ultrasounds) had been used to characterize and quantify the dependence of the measurement results to the changes of the indicators. Around 80 measurable quantities were identified.

This large database allowed assessing empirical relationships (bilinear regressions) for each technique between the measured parameter and the two varying indicators. These relationships and the level of variability associated with each measurement were indispensable input for the data fusion process based on possibility theory.

### 5.3.1 Data representation

Following the same procedure as in the 1D case (Figs. 3.34 and 3.35) the possibility distribution was propagated from the measurement to the properties. This is illustrated in Fig. 3.41.

The horizontal plan (Fig. 3.41a) corresponds to the value of the NDT measurement (here central frequency of radar = 1.1 GHz) and the inclined one to the bilinear regression. The distribution of the possibilities for radar frequency in the case of porosity and water saturation determination is given in Fig. 3.41b. It corresponds to pairs of porosity rate and water saturation values compatible with the radar measurement. It is described by a “trapezoidal tunnel of possibilities” whose magnitude varies from 0 to 1. The most important possibility value is 1 on the top of the tunnel.

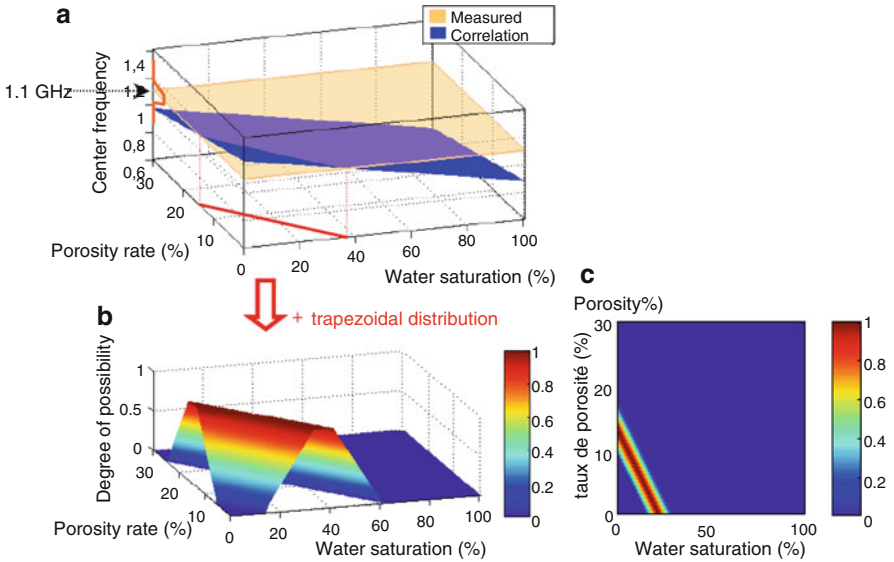
### 5.3.2 Data fusion process in 2D

The example shown below is obtained with four NDT measurements: UPV = 3961 m/s, impact-echo  $f = 5368$  Hz, resistivity  $R = 502 \Omega \cdot m$  ( $\log(R) = 2.7$ ), Radar wave arrival time = 1.19 ps. So we get four traces that cross as shown in Fig. 3.42a.

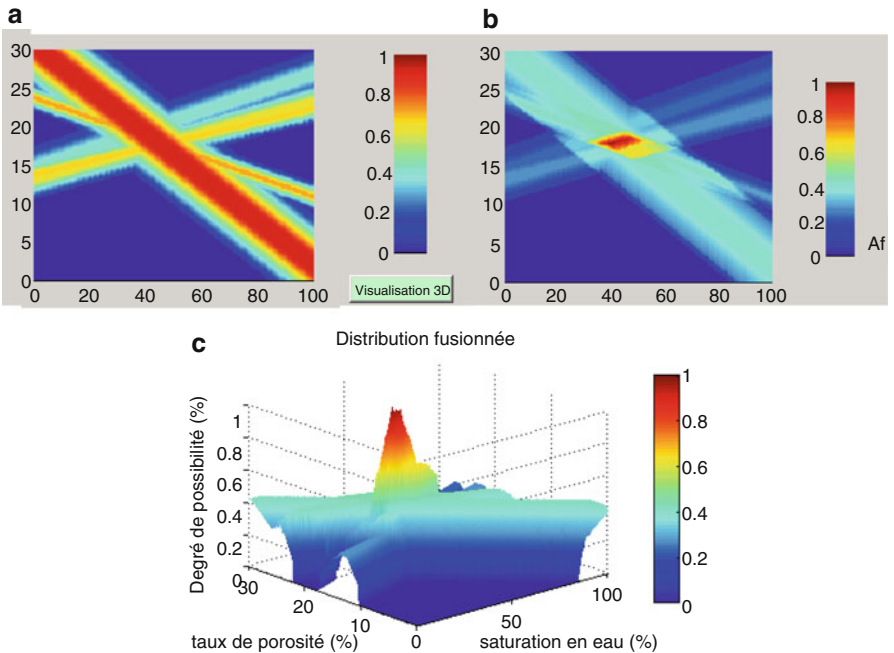
The fusing operator is the same as in 1D (Delmotte') and the fusion results are given by the Fig. 3.42b. The zone of crossing is highlighted and the solution corresponds to the maximum value of possibility. Like in 1D, it is possible to extract from the possibility distribution surface a confidence index, i.e. the confidence that we have in the results. The morphology, as a peak (Fig. 3.42c) indicates a solution that emerges from the possibility surface. In this situation, a single solution emerges for which the confidence is high: we can trust the calculated solution.

### 5.3.3 Example of strength estimation (2D problem)

The experimental data were obtained by using many different NDT on a series of specimens from eight concrete mixes and five water saturation rates (dry, about 40%, 65%, 80% and saturated). The destructive tests of strength determination were carried out according to ISO 1920-4. The data at extreme levels (dry and saturated) were used for building the conversion curves (multivariate relationships) between each NDT measurement and the pair of properties (strength, water saturation). Only results regarding strength estimate are discussed here.



**Fig. 3.41** Principle of the propagation: **a**) bilinear correlation (conversion surface) between radar centre frequency and {porosity rate; water saturation}, **b**) Possibility distribution for one measurement **c**) The same seen from above



**Fig. 3.42** Possibility distributions for four NDT measurements and fused by possibility theory



**Table 3.12** Merged, measured and error in strength estimate for 8 mixes in the laboratory

Mix	Strength S (MPa)		$\Delta S$	$RE = \Delta S/S$
	Merged	Measured	(MPa)	Point
G1	72.9	89	16.1	0.22
G2	43.3	50	6.7	0.15
G3	43.5	42	1.5	0.03
G3a	40.5	38	2.5	0.06
G4	36.6	37	0.4	0.01
G5	45	42	3.0	0.07
G7	38.3	39	0.7	0.02
G8	20.2	25	4.8	0.24

Table 3.12 shows the results of the evaluation from NDT and experimental measurements and their comparisons on 8 mixes. When the strength and the NDT measurements were determined from the same curing conditions (water saturation rate = 100 %), the results can be good as shown in Table 3.12. In the majority of cases the relative error was under 10%.

Work is still in progress to find the best combination of NDT in order to improve the quality of assessment, depending on the property that is looked for.

## 6 Conclusions

In strength determination by NDT, the objective is to reinforce confidence in the estimation. When the various measurements to be combined lead to compatible assessment, the data fusion process finds the best compromise and also evaluates the level of confidence of this assessment. When the measurements show some discrepancy, this discrepancy is highlighted by the data fusion process that provides an assessment but tells that it is not so reliable. In that situation, it remains possible to carry on new NDT measurements at the same point.

Of course, in data fusion, as it is the case when one uses a single technique, or when one combines two techniques and uses a multivariate regression model, always requires a calibration step. This calibration step comes to identify the “conversion curve” (or conversion surface) that links the measured value to the parameter(s) that are influencing this value.

It has been explained in this chapter:

- How a variety of non destructive techniques can be used in order to assess the concrete strength, and how their use can be limited because of the variety of concretes, the variability in environmental conditions or the existence of many uncontrolled factors.
- How conversion curves (or surfaces) can be calibrated and used in order to provide a quantitative estimate of local and/or characteristic strength. A specific focus has been given on the quality of the estimate and on how it depends on the number of points used in the assessment process.

- Recent research results on multivariate analysis (giving a new youth to classical procedures like the SonReb method) and on data fusion process have been discussed.

In all cases, the need to have a good knowledge of experimental measurement conditions has been pointed. It is always important to get information about the measurement variability (which influences the final quality of the assessment) and about the possible uncontrolled influent factor. This knowledge can make it possible to correct their influence, in order to improve the final assessment.

The development of tools like data fusion offers opportunity for obtaining in the next future not only the strength assessed value but also the quality of this assessment.

## References

- ACI Committee 214 (2004) Recommended Practice for Evaluation of Strength Test Results of Concrete, ACI 214R-02, ACI Manual of Concrete Practice p. 20.
- ACI Committee 228 (2003) In-place Methods for Determination of Strength of Concrete, Technical Committee Document 228.1R-03, PO Box 19150, Detroit, MI 48219, p. 44.
- ACI Committee 318 (2005) Building Code Requirements for Structural Concrete and Commentary, ACI 318-05/318R-05, American Concrete Institute, Jan. 2005, p. 430.
- Almeida, I. R. (1993) Emprego do esclerômetro e do ultra-som para efeito da avaliação qualitativa dos concretos de alto desempenho, Professorship thesis, Univ. Federal Fluminense, Niterãi, Brasil, 124pp.
- Arioglu E., Köyliüoglu (1996) Discussion of prediction of concrete strength by means of non destructive test methods by Ramyar and Kol, *Cem. Concr. World*, 3, 33–34.
- ASTM C 803M-03 (2003) Standard test method for penetration resistance of hardened concrete, Annual Book of ASTM Standards, Vol. 04.02: Concrete and aggregates.
- ASTM C31/C31M-03a (2003) Standard Practice for Making and Curing Concrete Test Specimens in the Field, p. 5.
- Austin S., Robins P., Pan, Y. (1995) Tensile bond testing of concrete repairs, *Materials and Structures*, 28, pp. 249–259.
- Balayssac J.P. (2008) SENSO: a French project for the evaluation of concrete structures by combining non destructive methods, Sacomatis, RILEM conf., 1-2/9/2008, Varenna, It.
- Bickley J. A. (1982) Variability of Pullout Tests and In-Place Concrete Strength, *Concrete International*, Vol. 4, No. 4, April 1982, pp. 44–51.
- Bickley J. A. (1984) Evaluation and acceptance of concrete quality by in-place testing, *Proc. Int. Conf. on In Situ/Nondestructive Testing of Concrete*, Ottawa, Canada, Oct. 1984, Editor: V. M. Malhotra, SP-82, ACI, Detroit, pp. 95–109.
- Bloch I. (1996) Some aspects of Dempster-Shafer evidence theory for classification of multimodality medical images taking partial volume effect into account, *Pattern Recognition Letters* 17, 905–919.
- Bloch I. (2003) Fusion d'informations en traitement du signal et des images, *Hermes – Lavoisier*.
- Bouchon-Meunier B., Marsala C. (2003) *Logique Floue, Principes, Aide à la Décision*, Hermes – Lavoisier
- Breyse D., Soutsos M., Moczko A., Laurens S. (2010), Quantitative non destructive assessment of in-situ concrete properties : the key question of calibration, *Structural Fault and Repairs conf.*, Edimburgh, 15–17 June 2010.
- Brignola A., Curti E., Parodi S., Riotta G. (2008) Compressive strength of concrete cores with samples of different diameter, *Int. RILEM Conf., SACoMaTIS*, 1-2 sept. 2008, Varenna, Italy.

- Brozovsky J. (2009a) Determination of high performance concrete strength by means of impact hammer, 10th Int. Conf. of the Slovenian Soc. for NDT, 1-3 sept. 2009, Ljubljana, 233–241.
- Brozovsky J. (2009b) Evaluation of calculation correlation efficiency as mentioned in EN13791 in order to determination concrete compression strength by non destructive testing, 10th Int. Conf. of the Slovenian Soc. For NDT, 1-3 sept. 2009, Ljubljana, 221–231.
- BS 1881: Part 201 (1986) Testing Concrete: Guide to the use of non-destructive methods of test for hardened concrete,” BSI, London, UK, p. 22.
- BS 1881: Part 207 (1992) Testing Concrete - Recommendations for the assessment of concrete strength by near-to-surface tests, BSI, London, 16p.
- Bungey J. H. (1980) The Validity of Ultrasonic Pulse Velocity Testing of In-place Concrete for Strength, NDT International, IPC Press, Dec. 1980, pp. 296–300.
- Bungey J. H., Madandoust R. (1992) Factors influencing pull-off tests on concrete, Magazine of Concrete Research, 44, No. 158, Mar. pp. 21–30.
- Bungey J. H., Millard S. G. (1996) Testing of concrete in structures,” Third Edition, Blackie Academic & Professional, 286 p.
- Bungey J. H., Soutsos M. N., Long A. E., Henderson, G. D. (2000) A Radical Re-Design Of The In-Situ Concrete Frame Process – Task 6: Early Age Acceptance Of Concrete (Improved Quality Management), BRE Ltd., Report BR 387, p. 94.
- Bungey J.H. (1992) Testing Concrete in structures - A guide to equipment for testing concrete in structures, CIRIA TN 143, 87 p.
- Carino N. J. (1993) Statistical Methods to Evaluate In-Place Test Results, ACI SP-141: New Concrete Technology – Robert E. Philleo Symp., Ed. Liu, T.C. and Hoff, G.C., ACI, Farmington Hills, Michigan, pp. 39–64.
- Carino N. J. (1994) Nondestructive testing of concrete: History and challenges, Proc. of V. Mohan Malhotra Symp. “Concrete Technology: Past, Present, and Future,” Edited by P. K. Mehta, SP-144, ACI, Detroit, 1994, pp. 623–678.
- Carino N. J., Woodward K. A., Leyendecker E. V., Fattal S. G., (1983) Review of the Skyline Plaza Collapse, *Concr. Int.: Design and Construction*, Vol. 5, No. 7, July 1983, pp. 35–42.
- Cleland D. J., Long A. E. (1997) The pull-off test for concrete patch repairs, Proc. ICE, Structure and Buildings, 1997, 122, Nov. pp. 451–460.
- Delmotte F. (2000) Un nouvel opérateur de fusion adaptatif, *Traitement du Signal* 17, 299–311.
- Di Leo A., Pascale G. (1994) Prove non distruttive sulle costruzioni in cemento armato, Convegno prove non distruttive par l’affidabilità e la sicurezza delle strutture civile, Saie’94, Giornale AICAP.
- Drochytka R. et al (2008) Progressive building materials with utilization of secondary raw materials and their impact on structures durability, Final Report Project VVZ CEZ MSM:0021630511, Brno.
- Dromigny-Badin A., Rossato S., Zhu Y.M. (1997) Fusion de données radioscopiques et ultrasonores via la théorie de l’évidence, *Traitement du Signal* 14, 499–510.
- EN 12504-2, Testing concrete in structures – Part 2 :non destructive testing – determination of rebound number
- EN 13791 (2007) Assessment of in-situ compressive strength in structures and precast concrete, CEN, Brussels, 28p.
- EN 1542:1999 (1999) Products and systems for the protection and repair of concrete structures – Test methods – Measurement of bond strength by pull-off’, BSI, London.
- Evangelista A.C., Shehata I., Shehata L. (2003) Parameters that influence the results of non-destructive test methods for concrete strength, Int. Symp. NDT-CE 2003, Berlin.
- Fabbrocino G., Di Fusco A.A., Manfredi G. (2005) In situ evaluation of concrete strength for existing constructions: critical issues and perspectives of NDT methods, fib symposium, Keep attractive concrete, Budapest.
- Facaoaru I. (1961) Contribution à l’étude de la relation entre la résistance du béton à la compression et de la vitesse de propagation longitudinale, *RILEM* 22, 125–164.
- Facaoaru L. (1970) Non destructive testing of concrete in Romania, Symp. On NDT of concrete and timber, London, ICE, 39–49.

- Ferreira A.P., Castro P.F. (1999) Application of NDT to concrete strength estimation, Int. Symp. on NDT Contribution to the Infrastructure Safety Systems, 22–26 nov. 1999, Torres, Brasil.
- FHWA (2000) Tensile bond strength of a high performance concrete bridge deck overlay, Field test report, FHWA MCL Project#9904, Federal Highway Administration, Office of Pavement Technology, Department of Transportation, 10p.
- Fib TG8.10 (2011) Performance based specifications for concrete, <http://www.fib-international.org>
- Gasparik J. (1992) Prove non distruttive nell'Edilizia, Quaderno Didattico, AIPND, Brescia.
- Gennari-Santori A. (2005) NDT measurements on the concrete elements of the bridges – Techn. Rep. 74.05, CND Controlli Non Distruttivi s.r.l., ANAS – SS761 Val Seriana.
- Giacchetti R., Lacquaniti L. (1980) Controlli non distruttivi su impalcati da ponte in calcestruzzo armato, Nota Tecnica 04, Univ. degli Studi di Ancona, Facoltà di ingegneria.
- Gros X.E., Bousigue J., Takahashi K. (1999) NDT data fusion at pixel level, NDT&E International 32, 283–292.
- Harrison T. A. (1996) The Specification of durability by performance – When?, Radical Concrete Technology, Ed.R. K. Dhir and P. C. Hewlett, E & FN SPON, pp 413–425.
- Harrison T.A. (1987) Formwork striking times - methods of assessment, CIRIA Report 73, 2nd Edn, 40 p.
- Horn D. (2006) Reliability analysis combining multiple inspection techniques, Proc. ECNDT, Berlin.
- IAEA (2002) Guidebook on non-destructive testing of concrete, Training course series n°17, Vienna.
- ISO 1920-4, Testing of concrete — Part 4: Strength of hardened concrete
- JGJ/T 23-2001, J 155-2001, Technical specification for inspection of concrete compressive strength by rebound method (in Chinese).
- Johnston C.D. (1967) Concrete and its constituent materials in uniaxial tension and compression, PhD Thesis, QUB, 310 p.
- Jones, R. (1962) Non-destructive testing of concrete. Cambridge: Cambridge University Press.
- Kaftandjian V., Zhu Y.M., Dupuis O., Babot D. (2005) The combined use of the evidence theory and fuzzy logic for improving multimodal nondestructive testing systems, IEEE Trans. on Instrumentation and Measurement 54, 1968–1977
- Kheder G. (1998) Assessment of in situ concrete strength using combined non destructive testing, Proc. 1<sup>st</sup> Int. Arab Conf. on Maintenance and Rehabilitation of Concrete Structures, Cairo, 59–75.
- Kim J.K., Kim C.Y., Yi S.T., Lee Y. (2006) Effect of carbonation on the rebound number and compressive strength of concrete, Cem. Concr. Composites, 31, 139–144.
- Kohl C., Streicher D. (2006) Results of reconstructed and fused NDT-data measured in the laboratory and on-site at bridges, Cement & Concrete Composites 28, 402–413
- Kouris, G. (2001) In-place assessment of C&DW derived aggregate concrete,”MSc (Eng) Dissertation, The University of Liverpool, p. 198.
- Kropp J, Hilsdorf H. K. (Editors) (1995) Performance criteria for Concrete Durability, RILEM Report 12, E & FN SPON, 327 p.
- Lataste J. F. (2002) Evaluation non destructive de l'état d'endommagement des ouvrages en béton armé par mesures de résistivité électrique, PhD. Univ. Bordeaux 1., 294 p.
- Lew H. S. (1980) West Virginia Cooling Tower collapse caused by inadequate concrete strength, Civil Engineering - ASCE, Vol. 50, No. 2, pp. 62–67.
- Lim Y. L. (2001) In-place strength assessment of high-strength concrete,” MSc (Eng) Dissertation, The University of Liverpool, 2001, p. 78.
- Lima F.B., Silva M.F.B. (2000) Correlação entre a resistência à compressão do concreto e a sua dureza superficial, Proc. IV Congresso de Engenharia Civil, Ed. Interciência, Juiz de Fora , pp. 429–440.
- LMDC-SENSO, Stratégie d'évaluation non destructive pour la surveillance des ouvrages en béton, final report, 274 p., 2009
- Long A. E. (1979) Improvements in or relating to strength testing brittle materials', British Standard Patent No. 1549842, Aug. 1979.

- Long A. E., Murray, A. M. (1981) Pull-off' test for in situ concrete strength, *Concrete*, December, pp. 23–24.
- Machado M.D., Shehata L.C.D., Shehata I.A.E.M. (2009) Correlation curves to characterize concretes used in Rio de Janeiro by means of non destructive tests, *Ibracon structures and materials journal*, 2, 2, 100–123, june 2009.
- Maierhofer C., Zacher G., Kohl G. C., Wöstmann J. (2008) Evaluation of radar and complementary echo methods for NDT of concrete elements, *J. of Nondestructive Evaluation* 27, 47–57
- Malhotra V. M., Carino N. J. (Editors) (2004) *Handbook on nondestructive testing of concrete*, CRC Press, Boca Raton.
- Mandel, J. (1984) Fitting Straight Lines When Both Variables are Subject to Error," *Journal of Quality Technology*, 16, 1, p. 1–14.
- McComb, A. (1983) An investigation of the hard-shell effect in HAC concrete, BSc Project, QUB.
- Meynink P., Samarin A. (1979) Assessment of compressive strength of concrete by cylinders, cores and non destructive tests, *RILEM Symp. Proc. On Quality control of concrete structures*, Swedish Concr. Res. Inst., Stockholm, 127–134.
- Midgley H. G. (1990) High alumina cement in construction – a future based on experience, *Proc. Int. Symp. held at Queen Mary and Westfield College, University of London*, 9-11 July 1990, Edited by R.J. Mangabhai, E. & F.N. SPON, pp. 1–13.
- Moczko A. (2009) Determination of actual in-situ compressive strength in concrete bridges, 10<sup>th</sup> ACI Int. Conf. on recent advances in concrete technology, 14-16 oct. 2009, Sévillá, Spain.
- Monteiro A., Gonçalves A. (2009) Assessment of characteristic strength in structures by the rebound hammer test according to EN 13791:2007, *NDTCE'09 Conf.*, Nantes, France, 30 june-3<sup>rd</sup> july 2009.
- Moysan J., Durocher A., Gueudre C., Corneloup G. (2007) Improvement of the Non-Destructive Evaluation of Plasma Facing Components by Data Combination of Infrared Thermal Images, *NDT&E International* 40, 478–485.
- Murray A. M., Long A. E. (1987) A study of the in situ variability of concrete using the pull-off method, *Proc. ICE*, Vol. 83, Part 2, Dec 1987, pp. 731–745.
- Naik T.R., Malhotra V.M. (1991) The ultrasonic pulse velocity method, *CRC handbook on nondestructive testing of concrete*, 1<sup>st</sup> edition, CRC Press, p. 169–188.
- Nash't I.H., A'bour S.H., Sadoon A.A. (2005) Finding an unified relationship between crushing strength of concrete and non-destructive tests, 3rd MENDT, Middle East NDT Conf & Exhibition, 27-30 nov. 2005, Bahrain, Manama Natrella, M. G. (1963) *Experimental Statistics*, Handbook No. 9, National Bureau of Standards, U.S. Government Printing Office, Washington, D.C., USA, p. 451.
- Naus D.J. (2009) *Inspection of nuclear power plant structures – Overview of methods and related applications*, ORNL/TM-2007/191, Oak Ridge National Laboratory, USA.
- Neville, A. M. (1963) A study of deterioration of structural concrete made with high-alumina cement, *Proc. ICE*, 25, pp. 287–324, London.
- Papadopoulou, H. (2003) *In-place strength assessment of high-strength concrete*, MSc (Eng) Dissertation, The University of Liverpool, p. 84.
- Pascale, G. Di Leo A., Carli R. (2000) Evaluation of actual compressive strength concrete by NDT", 15th World Conference on Non-Destructive Testing, Roma, 10pp.
- Petersen C.G. (1997) Lok-test and Capo-test Pullout Testing - Twenty Years Experience, *Proc. Int. Conf. on NDT in Civil Engineering*, Brit. Inst. NDT, Vol. 1, pp 77–96.
- Petersen, C. G., Poulsen E. (1993) Pull-out testing by LOK-test and CAPO-test with particular reference to the in-place concrete of the Great Belt Link, *Dansk Betoninstitut A/S*, Datavej 36, DK-3460 Birkerød, Denmark, Nov. 1993, 140 p.
- Petersons, N. (1964) *Strength of concrete in finished structures*. Gothenburg: Elanders Boktryckeri Aktiebolag.
- Pfister V., Luprano V.A.M., Tundo A. (2009) Misura di velocita ultrasonora e resistenza a compressione su calcestruzzo: analisi statistiche sulla costruzione delle curve di correlazione, *AIPnD 2009*, consulted on [ndt.net](http://ndt.net) (may 2010).
- Ploix M.A., Garnier V., Breyse D., Moysan J. (2009) Possibilistic data fusion for evaluating concrete structures, *NDTCE'09*, Nantes, 30/6–3/7 2009.

- Price W. F., Hynes J. P. (1996) Nondestructive Testing of High Strength Concrete” Proc. 4th Int. Symp. on Utilisation of High Strength/High Performance Concrete, ENPC, Paris, pp 636–643.
- Price W.F., Hynes J.P. (1996) Insitu strength testing of high strength concrete, Mag. of Conc. Res. Vol. 48, No. 176, pp. 189–197.
- Proceq S.A. (2007) Product brochures, Original Schmidt hammer and SilverSchmidt hammer.
- Proverbio E., Venturi V. (2005) Reliability of nondestructive tests for on site concrete strength, 10 DBMC, Lyon, 17–20 avril 2005.
- Pucinotti R. (2007) The use of multiple combined non destructive testing in the concrete strength assessment: applications on laboratory specimens, HSNDT int 2007, consulted on ndt.net (may 2010).
- Qaswari H.Y. (2000) Concrete strength by combined non destructive methods simply and reliably predicted, Cem. Concr. Res., 30, 739–746.
- Radonjanin V., Malesev M., Drakulic Z. (2010) New semi-destructive method for evaluation of concrete compressive strength, Structural Fault and repair conf., Edimburg, june 2010.
- RILEM (1993) Draft recommendation for in situ concrete strength determination by combined non-destructive methods, Mat. Str., 26, 43–49.
- RILEM TC-230 PSC (2008) Performance-based specifications and control of concrete durability, <http://www.rilem.net/tcDetails.php?tc=230-PSC>
- Sanja A., Verikari E. (Editors) (1996) Durability Design of Concrete Structures, RILEM Report 14, E & FN SPON, 165 p.
- Skrantaev, B. G. & M. Y. Leshchinsky (1966) Complex methods of nondestructive testing of concrete in construction and structural works. RILEM Bull., 30, 99.
- Soutsos M.N., Bungey J.H., Long, A.E., Henderson G.D. (2000) In-Situ Strength Assessment Of Concrete – The European Concrete Frame Building Project, Proc. Int. Symp. NDT-CE2000, Univ. of Tokyo, Japan, 25-27 April, 2000, Editor Taketo Uomoto, pp. 583–592.
- Stone W. C., Carino N. J., Reeve C. P. (1986) Statistical Methods for In-Place Strength Prediction by the Pullout Test, ACI J., Vol. 83, No. 5, Sept.-Oct. 1986, pp. 745–755.
- Stone W. C., Reeve C. P. (1986) New Statistical Method for Prediction of Concrete Strength from In-Place Tests, Cement, Concrete, and Aggregates, Vol. 8, 1, pp. 3–12.
- Swamy R.N., Al-Hamed A.H. (1984) The use of pulse velocity measurements to estimate strength of air-dried cubes and hence in situ strength of concrete, ACI special publ., SP 82–13, p. 247–276.
- Tanigawa Y., Baba K., Mori H. (1984) Estimation of concrete strength by combined nondestructive testing method, ACI SP-82, 1, 57–65.
- Teng M. L. (1999) Lok-test strength correlations for different aggregates, Third year (BEng) Project, The University of Liverpool, April 1999, p. 80.
- Teychenne D. C., Nicholls J. C., Franklin R. E., Hobbs, D. W. (1988) Design of Normal Concrete Mixes, BRE, Department of the Environment (DoE), London, 1988.
- The Concrete Society (1965) A framework for durability design and performance based specification of concrete, 4th working draft, April 1995, 64 p.
- Turgut P. (2004) Research into the correlation between concrete strength and UPV value, NDT.net, dec. 2004, Vol 12, n.12
- Voellmy, A. (1954) Examination of Concrete by Measurements of Superficial Hardness. In: International Symposium on Nondestructive Testing of Materials and Structures. RILEM, Paris.
- Woelfl G.A., Lauer K. (1980) The electrical resistivity of concrete with emphasis on the use of electrical resistance for measuring moisture content, Cement Concrete and Aggregates, Vol. 1, No 2, pp. 64–67.
- Yun C.H., Choi K.R., Kim S.Y., Song Y.C. (1988) Comparative evaluation of nondestructive methods for in-place strength determination, Nondestructive Testing, Special Publication SP-112, ACI, Detroit, pp.111–136.
- Zadeh L.A. (1999) Fuzzy sets as a basis for a theory of possibility, Fuzzy Sets and Systems 100 Suppl., 9–34.

# Chapter 4

## Control of thickness/dimensions of pavements, foundations, elements and piles

Johannes Hugenschmidt, Martin Krause, Denys Breysse,  
Ernst Niederleithinger, and Alexander Taffe<sup>1</sup>

This chapter is devoted to the assessment of the geometry of concrete components. This is of interest for many structures, for which the testing solutions may differ, according to the environment and to constraints like accessibility. We have chosen to discuss possible solutions for pavements, thin elements (mainly concrete slabs and tunnel shells) and foundations (shallow foundations and piles).

### 1 Problem description, testing tasks

#### 1.1 Pavement

##### Testing problem

The thickness of pavements on bridge decks is relevant if the pavement or parts thereof have to be removed without destroying the sealing which is in most cases present between the pavement and the concrete surface. In combination with a

---

<sup>1</sup>Other contributors to this chapter are G. Ballivy, X. Dérobert, A. Kodjo, F. Pires and L. Olson.

J. Hugenschmidt (✉)  
EMPA, Zurich, Switzerland  
e-mail: Johannes.Hugenschmidt@empa.ch

M. Krause • E. Niederleithinger • A. Taffe  
BAM, Bundesanstalt für Materialforschung und –prüfung, Berlin, Germany

D. Breysse  
Université Bordeaux 1, I2M, GCE (Civil and  
Environmental Engineering Department), France



geodetic survey the pavement thickness also allows for the calculation of the height of the concrete surface beneath the pavement which is in many cases relevant for the planning of rehabilitation. The thickness of single pavement layers is of little interest on bridges. The condition of pavements is an issue. However the definition of damage and its relation to the results of non-destructive testing is not straightforward.

**Methods:** Ground Penetrating Radar (GPR)

### **Level of interpretation**

NDT inspections are carried out covering the whole surface of bridge decks, along single lines and on limited areas. As modern GPR equipment is capable of acquiring hundreds of measurements per second, data are in many cases acquired along single or parallel lines. In the case of parallel lines, the spacing between those lines is a cost relevant factor.

### **Accuracy/Uncertainty**

An accuracy of better than 10 mm is often required and can be obtained with the help of a limited number of cores for calibration.

### **Special difficulties**

The inspection of pavement thickness is a routine application of the GPR method. Adapted equipment is required (high temporal sampling rate of GPR unit and high frequency (> 1GHz) antennas).

## **1.2 Thin elements**

### **1.2.1 Thickness of inner shells of tunnels**

#### **Testing problem**

The aim is to control the thickness of inner shells of tunnels, especially for indicating reduced thickness. The main purpose is the quality assurance (in Germany, this is recommended by Ministry of Transport, BASt - Federal Highway Research Institute). An important aspect is the protection of the sealing which is located between the rock and the internal shotcrete layer. The layer thickness is typically 15 cm to 60 cm.

**Methods:** Ultrasonics, Impact Echo, Ground Penetrating Radar (GPR)

#### **Level of interpretation**

The whole length of tunnels has to be inspected. When using Ultrasonics or Impact-Echo, the acquisition grid is usually 80 cm x 80 cm, and 40 cm x 40 cm around joints. In areas of estimated anomalies it has to be reduced to 10 cm x 10 cm.



When GPR is used, the distance between single measurements can be reduced to values of less than 1 cm in the direction of the antenna movement. Results of large areas have to be presented in single plots to enable an overall view of the situation.

### **Accuracy/Uncertainty**

A typical value if the desired uncertainty of the measurement is 2 cm.

### **Special difficulties**

Quality assurance demands the measurement of large areas. For the interpretation of the results, point measurements are evaluated and then combined. They are visualised as line scans (for details see Chapter 2). In the case of difficult site conditions (e.g. dense reinforcement, rough surfaces or anomalies) advanced data processing may be useful. When using Ultrasonics or Impact-Echo, the location and density of the rebar should be known or measured with adequate methods (e.g. commercial imaging systems or GPR).

A thickness measurement requires a sufficient physical contrast between the layers. For example, if there is no sealing, the difference in the acoustic impedance between concrete and the next layer (e.g. lime stone) may not be large enough.

Areas, where reduced thickness is indicated, have to be repaired. This is usually carried out with special injection mortars (or synthetic resin). The success of the repair can only be verified by mechanical methods, if there is a good bonding between the concrete and the injection mortar.

## **1.2.2 Concrete slabs**

### **Testing problem**

Bottom slabs of factory floors or car parks are typically 10 cm to 20 cm thick. As far as structural safety is concerned, the exact fulfilment of predefined thicknesses is not a crucial point. But since the production costs of large surfaces are very high, there is often a dispute between customer and contractor about the correct use of materials (cement, concrete, cast plaster; often special plaster). In this case, an accurate thickness control may be useful.

**Methods:** Ultrasonics, Impact-Echo, GroundPenetrating Radar (GPR)

### **Level of interpretation**

As bottom slabs can be very large, the inspection can range from single locations of special interest to acquisition grids of 1m x 1m (Ultrasonics and Impact-Echo).

### **Accuracy/Uncertainty**

The desired accuracy is 1 cm or better because of the high material cost.

### **Special difficulties**

When high accuracy is demanded (uncertainty lower than 10 mm), the signal velocity has to be known very accurately. Since there is a variation between 1 % and 5 %, the velocity has to be calibrated following the demand of uncertainty.

## **1.3 Shallow foundations**

### **Testing problem**

Many foundations of demolished structures have the potential of reuse. In order to evaluate their integrity, several questions have to be answered. Important results have been obtained within the research project RUFUS (Reuse of Foundations for Urban Sites; EU 5<sup>th</sup> framework) (Taffe and Niederleithinger, 2006).

Relevant parameters are:

- Geometry of slabs
- Location of piles and strip foundations between slabs
- Structures and materials beneath the foundation (soil, lean concrete layers,)
- Reinforcement size and location, often several layers
- Integrity: honeycombing, badly compacted areas, cracks

**Methods:** Ultrasonics, Impact-Echo, Ground Penetrating Radar (GPR)

### **Level of interpretation**

Since foundation slabs are usually heavily reinforced, a dense acquisition grid is often necessary to obtain the required information. The interpretation of single point measurements is rarely sufficient.

**Uncertainty (accuracy):** 2 to 5 cm, 5 %

### **Special difficulties**

In order to decide, which NDT-method is applicable, the reinforcement ratio and/or the density and diameter of rebar should be known. Commercially available equipment such as cover-meters can be used to obtain that information.

Measurements with GPR are much faster than methods applying mechanical waves, but GPR is more sensitive to dense reinforcement and depth of penetration may be limited because of moisture in young concrete.

For ultrasonic echo methods, a smooth surface is required.

The depth of inspection for acoustic methods (ultrasonic-echo, impact-echo) is limited by the first reflecting layer. This is also valid for very thin air-filled layers or sealings (e.g. bituminous sealings).

The accuracy (uncertainty) of the measurement depends on the exact knowledge and the homogeneity of the signal velocity. It can be measured with cores or estimated from the signal velocity at the surface.

A reflection from the bottom of the foundation slab is required for the investigation of the slab thickness. This reflection will only take place if there is a sufficient contrast

in physical properties between concrete and the subjacent material (density and/or elastic modulus for acoustic methods, capacitive measurements and/or conductivity for GPR). In addition, because of the limited resolution of all reflection methods, the bottom reflection may not be separable from a low lying layer of rebar which would reduce the accuracy of the thickness measurement.

## ***1.4 Deep foundations, piles and shafts***

### **Testing problem**

Deep foundations are mostly below the ground and therefore not accessible to visual inspection. The quality of foundations should be verified to ensure structural integrity to carry the required loads without bearing capacity failures and to limit displacements of the structure to acceptable levels. This quality control can help to avoid or limit an overdesign of the foundation. In particular, the following parameters are relevant:

- the pile length, which has to be in conformity with the design,
- the cross-section, which must correspond to what had been planned, to obtain a correct service load of the pile,
- the overall quality of concrete, including the possibility of localized anomalies (voids, areas where concrete and soil are mixed...).

Cast-in drilled holes (CIDH) piles are also inaccessible to visual inspection and very prone to contain zones of compromised cross-section due to the casting process, like the collapse of the excavation prior to concrete placement. Quality control must be employed to identify such problems. Non-destructive evaluation (NDE) after construction can be used to check the acceptability of the construction work in meeting the performance specifications.

**Methods:** Ultrasonics, Seismics and Radioactive Testing

### **Level of interpretation**

The estimation of the length is the first objective. A numerical value is expected to verify that the pile reaches a layer of good properties or has enough friction.

Regarding the cross-section, irregularities (necks or bulges) which could induce a lower pile strength and their vertical position are important.

Heterogeneities and voids should be detected and their locations both in the vertical and horizontal directions have to be defined together with their magnitude (what percentage of the cross-section is affected).

Defects and heterogeneities affect the carrying capacity (to vertical or lateral loadings) of foundations. However, once defects are detected/localized/quantified, their influence on the mechanical properties is still unknown. It is suggested to define criteria for the characterization of heterogeneities (size or volume or the percentage of variation of material physical properties like wave velocity) before final decisions regarding the pile integrity are taken.

**Accuracy/Uncertainty:** 4 % (with known signal velocity)

### **Special difficulties**

The main difficulty is that these structures are not directly accessible. During the construction works, their upper surface, waiting to be connected to the superstructure, remains free, but it is not the case when existing structures are inspected. Some techniques require equipped tubes and can only be used if this has been planned before the construction. Another difficulty, common to many NDE techniques, is that the assessment requires assumptions (like the wave speed), which can induce some uncertainty on the results.

## **2 Common techniques**

### **2.1 Pavement**

The inspection of pavement thicknesses on bridges is a common application of the GPR method. Pavement thicknesses are investigated on whole bridge decks or parts thereof. Data are usually acquired along lines, the combination of several lines can lead to pseudo-3D results. There are many reasons for pavement inspections on bridge decks. The knowledge of the pavement thickness can avoid the destruction of the sealing when the asphalt is removed during rehabilitation work. The combination of a GPR inspection with surveying of the asphalt surface provides a detailed knowledge of the height of the concrete surface beneath the pavement. There are systems from several manufacturers, producing antennas in a wide range of frequencies. For the investigation of pavements, horn antennas are useful because they can be operated in non-contact mode. This facilitates the use of mobile acquisition units for large surveys (Fig. 4.1).

#### **2.1.1 Example of the use of GPR for thickness survey**

A ramp leading to a bridge (Sihl flyover) is shown in Fig. 4.2. A GPR survey was carried out on this ramp using EMPA's mobile acquisition system presented in Fig. 4.1.

The acquisition parameters and the equipment used can be summarized as follows:

GPR unit: GSSI SIR-20      Antennas: GSSI Model 4205 horn; 1.2GHz  
Acquisition speed: 10 km/h      Traces/m: 40      Samples/Scan: 512

As there are no standards for acquisition parameters available, they have to be selected carefully based on the knowledge of the GPR method, the problem under inspection and the actual situation (e.g. traffic situation, availability of additional information, budget, etc.).

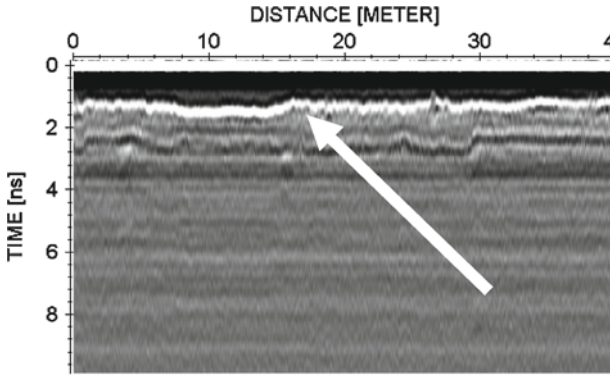
A 40 m long radargram from this ramp is presented in Fig. 4.3. The reflection at the asphalt – concrete interface is marked with a white arrow. The corresponding

**Fig. 4.1** Mobile GPR acquisition unit

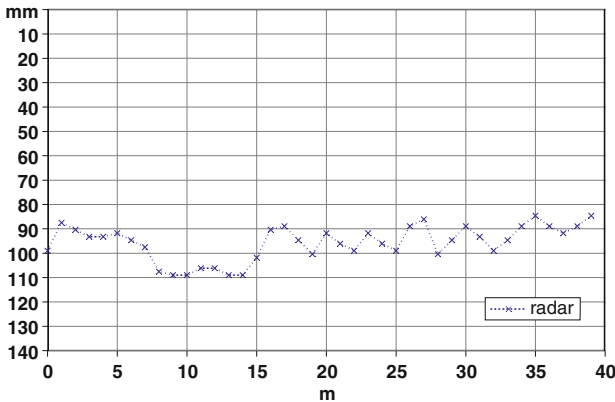


**Fig. 4.2** Ramp of Sihl Flyover

GPR result for the pavement thickness is shown in Fig. 4.4. The signal velocity used for the conversion from time to depth/thickness was 0.143 m/ns. This velocity was obtained with the help of a borehole. In order to examine the quality of the GPR results, the pavement was removed along the line with an excavator (Fig. 4.5) and the pavement thickness was measured manually with a ruler. Thus, the GPR results could be compared with the real pavement thickness.



**Fig. 4.3** Data set from Sihl flyover, vertical axis – time in nanoseconds, horizontal axis – length in meters



**Fig. 4.4** GPR result for thickness of asphalt pavement, vertical axis-pavement thickness in mm, horizontal axis-length in meters

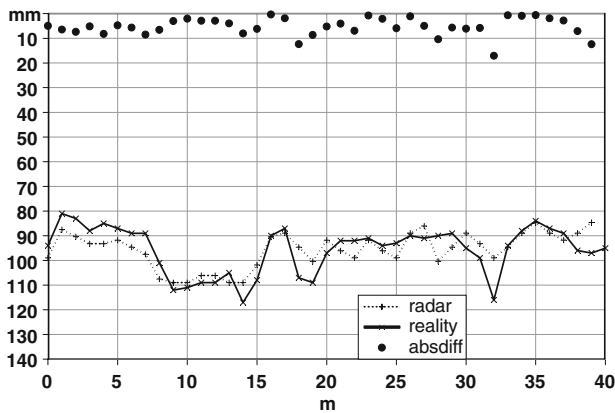
In Figure 4.6 the GPR result (dotted line) is presented together with the real pavement thickness (solid line) and the absolute differences (dots) between reality and GPR result. Obviously, there is a good agreement between GPR result and reality. The mean difference between GPR results is 5 mm, the maximum difference is 17 mm.

### 2.1.2 Accuracy and reliability of results

EMPA has carried out a research project sponsored by the Swiss Federal Roads Authority. GPR inspections were carried out on five bridges designated for demolition. Results were laid open before the bridges were taken down. During demolition GPR



**Fig. 4.5** Pavement opening with excavator



**Fig. 4.6** Comparison between GPR result and reality for thickness (in mm) of asphalt pavement: dashed line-GPR result, solid line-reality as measured with ruler along opened pavement, dots-absolute difference between GPR result and reality

results were verified by measuring pavement thicknesses with a ruler along the edges of lines where the pavement had been removed with a milling machine or along lines where the pavement had been opened with an excavator (see example above). Details of this approach are described in ASTM standards (see reference below). The mean difference between GPR results and results obtained with the ruler was 9mm. GPR results for the pavement thickness were obtained on 95% of the sections inspected. No result was obtained on 5% of the sections inspected because of various reasons such as that that was no pavement (on joints, gully holes,...) or because of the limited vertical resolution of the GPR method in zones where the concrete-cover of rebar was too small. Other studies resulted in similar accuracies as listed in Table 4.1.

**Table 4.1** Accuracy of GPR results for pavement thickness measurements, Results from various studies

References	
[Maser et al., 1994]	Expected accuracy: $\pm 7.5\%$ (typically 12.7mm)
[Maser, 1996]	Accuracy (vs. Cores): 3-10%
[FDoT, 2000]	Difference GPR prediction-measurements (field data): 1.5-20mm for Marshall sections, $\gg 20$ mm for Superpave sections
[Willet and Rister, 2002]	GPR calculated thicknesses vs. core thicknesses: $\pm 0-6$ mm
[Al-Qadi et al., 2003]	Average thickness uncertainty: 3.7-6.7%
[Hugenschmidt and Mastrangelo, 2006]	Mean absolute uncertainty (field data): 9mm

### 2.1.3 Guidelines

- Standard Guide for Using the Surface Ground Penetrating Radar Method for Subsurface Investigation, Annual Book of ASTM Standards 2005, Section four, Construction, Volume 04.09 Soil and Rock (II), D5714, Designation: D 6432 – 99
- ASTM D6087-03 (2003), “Standard Test Method for Evaluation asphalt-covered concrete bridge decks using ground-penetrating radar”, ASTM Int., PA, US, 4 p.
- Merkblattüber das Radarverfahren zur Zerstörungsfreien Prüfung im Bauwesen (Instruction leaflet about the radar method for non-destructive-testing in civil engineering), German Society for Non-Destructive-Testing, February 2008, revised edition.

## 2.2 Thin elements

### 2.2.1 Thickness of inner shells of tunnels

The inner shells of tunnels are usually concrete slabs in the range of 10 cm to 40 cm as described in §1.2.1. For thickness measurement, three methods are principally suited: Ultrasonic echo, Impact echo and GPR.

The quality assurance of thickness of inner shells of tunnels using NDT-Methods is described in a guideline of the German Ministry of Transport (BMVBS). It is recommended for all tunnels funded with public money, the costs have to be considered in the tender [BASt, 2001, Guideline RI-ZFP-TU]. For the measurement only engineering offices and companies are permitted, which have passed a qualification test at a concrete slab. This is organised and controlled by the Federal Highway Research Institute (Bundesanstalt für Straßenwesen, BASt).

#### Ultrasonic echo

Since the control of the thickness is demanded at many points all over the surface, all equipment with ultrasonic A-scan indication can be used. The data are stored



following the measuring grid and visualised afterwards. The criterion of clear echo indication has to be taken into account, which is normally a signal to noise ratio of 6 dB (factor 2).

If a measurement point is situated above a reinforcing bar, the determination of the thickness may be hindered. In this case the point has to be moved some centimeters to obtain a good back wall reflection. In case of dense reinforcement or large diameter, the location of rebar may be determined with electromagnetic methods during a preparatory study.

As a fast measurement procedure is desirable, ultrasonic equipment with dry contact transducers (point contact) is preferred, since they don't need coupling agent. The equipment that is currently commercially available uses shear waves.

### Impact echo

Commercially available impact-echo equipment working with steel ball excitation or solenoid driven impactors is suitable for point measurements. Near the edges of the casting segment the user has to be careful because of possible edge effects. The thickness is determined via the Fourier Transform of the time signal. As there is currently no general criterion available for the quality assessment of this signal, experienced and trained operators are required.

For the determination of the thickness, the signal velocity has to be calibrated. Since thickness measurements are mainly used for quality assurance on new structures, this is effectuated normally on test specimens, which are produced simultaneously with the tunnel wall. In many cases the knowledge of the absolute thickness is less relevant than the localization of areas with reduced thicknesses (see §1.2.1). Thus, an exact frequency reading is often more relevant than an accurate knowledge of the signal velocity because this velocity can be assumed near to constant on structures of constant design and age.

#### Example combining Ultrasonic echo and Impact echo

In a new tunnel on Germany's motorway A1 (Fig. 4.7) the thickness of the inner concrete shell was inspected using Impact Echo and Ultrasonic Echo. Signal velocities were calibrated using test specimens that were produced in parallel to the construction of the inner shell, a first reference point with known depth to an added metal reflector and a second reference point with known concrete thickness. It turned out, that only the second reference point enabled a precise comparison between known concrete thickness and the corresponding reflection in the recorded dataset. This applied to both Ultrasonic Echo and Impact Echo and is probably due to the unfavourable geometry of the specimens and the lack of a unique correspondence between reflections and the position of the metal plate for the first reference point.

In Figs. 4.8 and 4.9 the results of the two methods are compared. The thicknesses obtained with both methods are almost identical.



Fig. 4.7 Inner shell of a new tunnel on Germany’s motorway A1

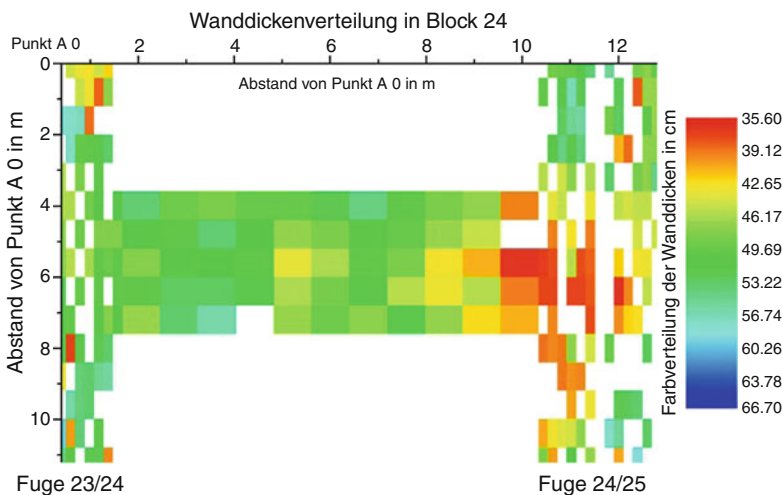


Fig. 4.8 Thickness of inner shell obtained with Ultrasonic Echo

### Ground Penetrating Radar (GPR)

As modern GPR equipment works with high pulse repetition frequencies, GPR is used normally as a line scanning method. The distance between two measuring points along a scanning line is very small. Thus the method simultaneously localises rebar, which is useful additional information.

A disadvantage of the GPR method is that it is rather sensitive to moisture. This means that the electromagnetic waves are attenuated by the moisture content of young concrete. Additionally the method is more sensitive to the shielding effect of rebar than the acoustic methods.

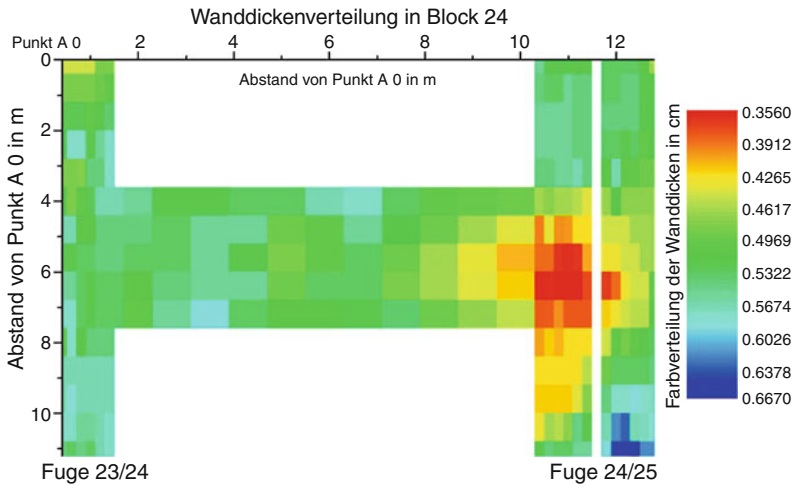


Fig. 4.9 Thickness of inner shell obtained with Impact Echo

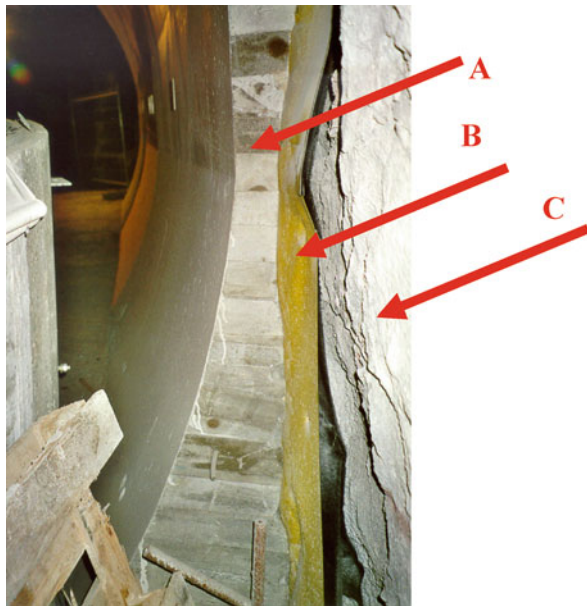


Fig. 4.10 Tunnel wall with waterproofing-membrane

Example of use of GPR

A field experiment [Hugenschmidt, 2003] was carried out on a 12 m long test site, where different wall types were available and where the details of their construction were well known. Figure. 4.10 shows a view of the section inspected. The concrete is marked with arrow “A”, the sealing with arrow “B” and rock

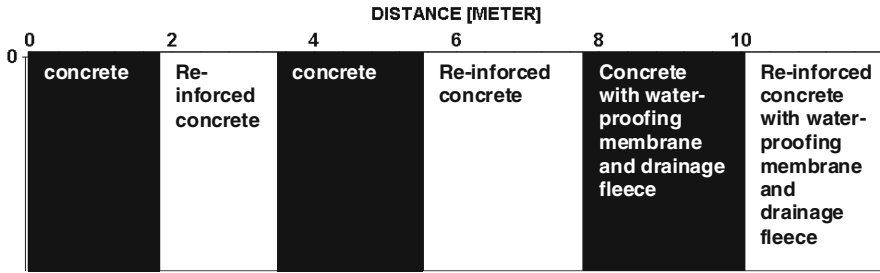


Fig. 4.11 Wall types on inspected section

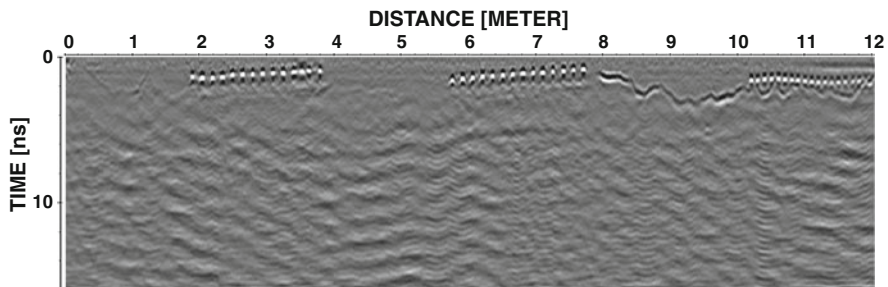


Fig. 4.12 GPRdata from tunnel wall, length = 12 m

covered with shotcrete with arrow “C”. An overview over the different wall types is presented in Fig. 4.11.

The dataset presented in Fig. 4.12 was acquired in longitudinal direction with the GSSI model 5100 antenna. The distance between the concrete surface of the tunnel wall and the rock surface (not equal to the concrete thickness in sections with waterproofing membrane because of a drainage fleece between membrane and rock) is varying between 0.15m and 0.4m. It is known as it had been recorded as transverse sections in distances of 0.5m before the wall was built. The maximum distance of 0.4m should not cause problems with the depth of penetration of the antenna used [Hugenschmidt, 2003].

In sections where the membrane is present, there is a clear reflection from the concrete-membrane interface. No reflection is caused by the concrete-rock (siliceous limestone) interface. This is likely due to the similarity in material properties of concrete and rock.

### 2.2.2 Guidelines

- Merkblattüber das RadarverfahrenzurZerstörungsfreienPrüfungimBauwesen (Instruction leaflet about the radar method for non-destructive-testing in civil engineering), German Society for Non-Destructive-Testing, February 2008, revised edition

- RI-ZFP-TU: Richtlinie für die Anwendung der zerstörungsfreien Prüfung von Tunnelinnenschalen; Ausgabe 2007-12. In: ZTV-ING, Teil 5: Tunnelbau: Geschlossene Bauweise, Anhang A. Verkehrsblatt-Sammlung Nr. S1056 (2007), pp 29-35
- Guidance on Radar Testing of Concrete Structures, Concrete Society Technical Report 48, The Concrete Society, Slough, UK.

## 2.3 *Shallow foundations*

The choice of technique depends mainly on the thickness of the foundation and the amount of reinforcement. In some cases (e.g. recently completed structures) the moisture content within concrete may also be relevant. Although the success of NDT-techniques depends on many additional aspects, mechanical methods such as Ultrasonic echo or Impact echo will have in many cases a larger depth of penetration than GPR.

### 2.3.1 **Examples of NDT investigations**

Ultrasonic inspections were carried out on the Large Concrete Slab (LCS) (Fig. 4.13) with varying amounts of rebar described in more detail in §4.2.2. Broadband low-frequency transducers were used. Dry point contact sensors that do not need a coupling agent have been used [Shevaldykin et al. 2003].

For a reliable imaging of the complex geometry an automated transducer positioning system (scanner) has been used (Fig. 4.14). Data (8000 measuring points) have been recorded and processed with the help of reconstruction calculation. The so-called SAFT (Synthetic Aperture Focusing Technique) focuses signals received at many aperture points by coherent superposition, yielding a high-resolution image of the region of interest. The following images are results of SAFT-reconstruction. Various sections through the reconstructed data volume can be processed and layers with significant reflections become obvious and visualise internal objects and geometry.

Figures 4.15 and 4.16 show the section parallel to the surface at depth of 125cm and 75cm. The expected reflection of the back wall of the different slabs and the strip foundation at corresponding depth are clearly visible. In upper left and upper right corner (dashed circles) two small areas show no back wall reflection. This is where the pile heads are located because the signals propagate from the slab further into the piles and are not reflected at the depth of the back wall.

For the reinforcement ratio along a-a, the vertical cross section is presented in Fig. 4.17. The back wall for both depths is clearly visible. The interrupted back wall reflection between  $y = 700\text{mm}$  to  $y = 1000\text{mm}$  results from the pile head in that area.

For the high reinforcement ratio along b-b (Fig. 4.18) only in the non-reinforced sections a clear back wall signal appears. In the sections with upper and lower reinforcement a strong reflection in the surface near depth is visible but no significant reflection of the back wall occurs. Only a weak signal at the 75cm section allows depth estimation.

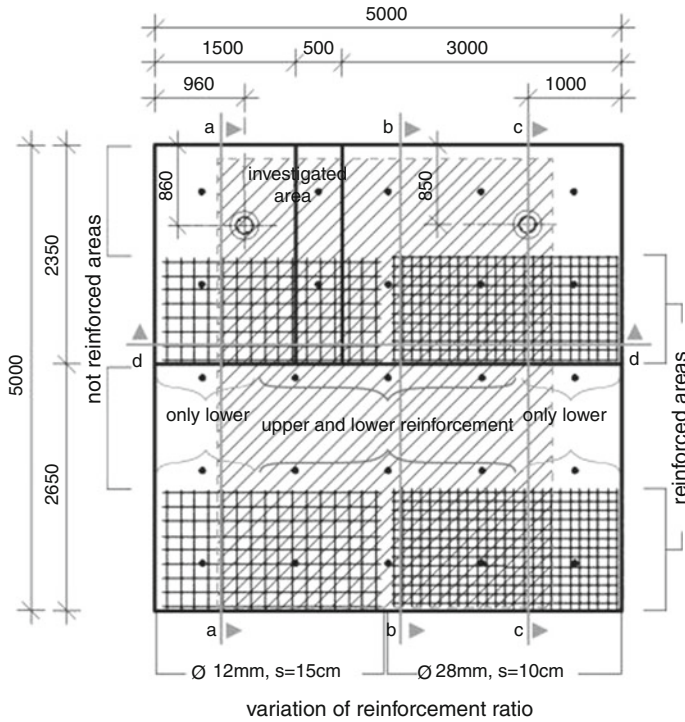


Fig. 4.13 Investigated section of the foundation slab including pile heads and strip foundation

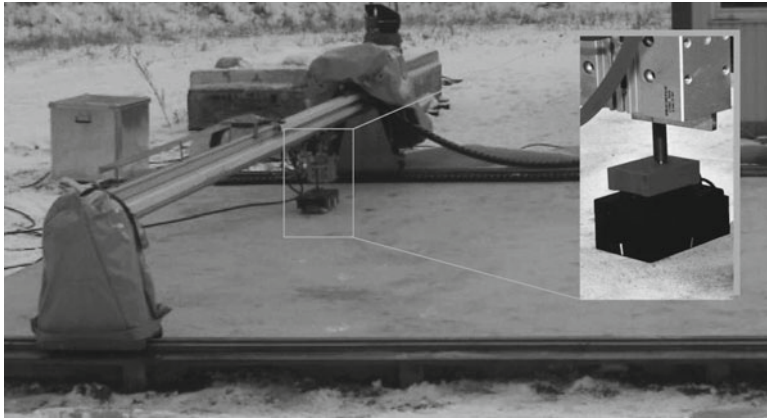
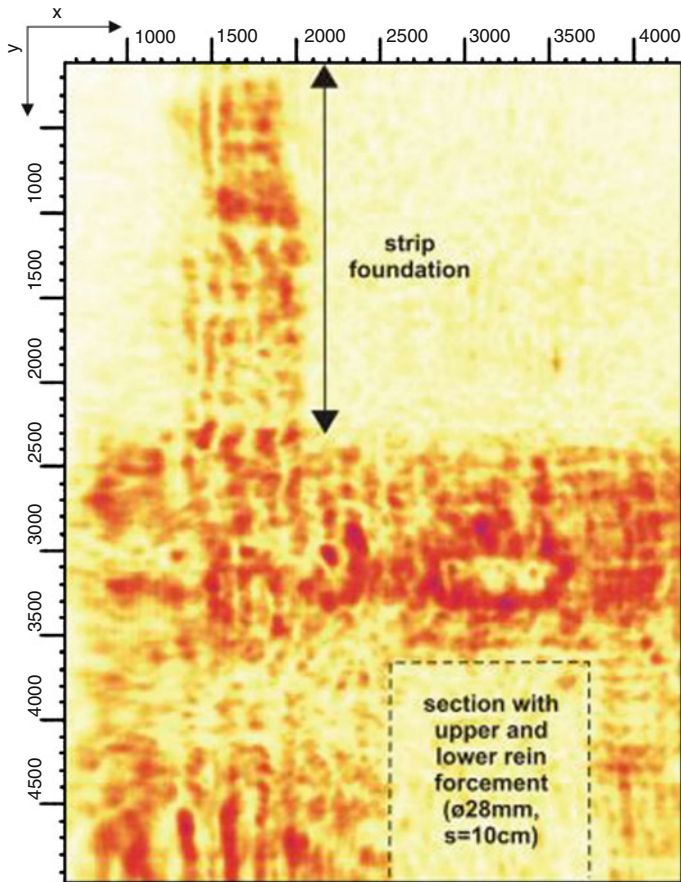


Fig. 4.14 Automated ultrasonic measurement at test site

If the 28mm diameter reinforcement is present only in the lower level, as shown along section c-c, the reinforcement bars produce a reflection in addition to the back wall reflection a few centimetres above (Fig. 4.19). Only in the 7cm section the reflections from the reinforcement and the back wall can be distinguished.





**Fig. 4.15** Section parallel to the surface at depth of 125 cm indicating the strip foundation

The three sections of Figs. 4.17 to 4.19 show that the back wall (dashed line) does not match in every section with the recorded reflection. The reason is that only one approximated ultrasonic velocity has been considered. The difference between measured reflection and expected reflection indicates that for every section its ultrasonic velocity depending on the reinforcement ratio has to be considered. This will be part of further investigations in the validation process of thickness measurement with ultrasonic echo.

Cross-section d-d shown in Fig. 4.20 also reveals the geometry of the slab and the location of the piles. The back wall reflections at 75cm and the bottom of the strip foundation at 125cm are clearly visible. Also the detected width of the strip foundation of 50cm and its location agree well with reality. The interrupted back wall echoes at the depth of 75 cm between  $x=800$  mm and 1100 mm and  $x=3850$  mm and 4150 mm mark the location of the pile heads.

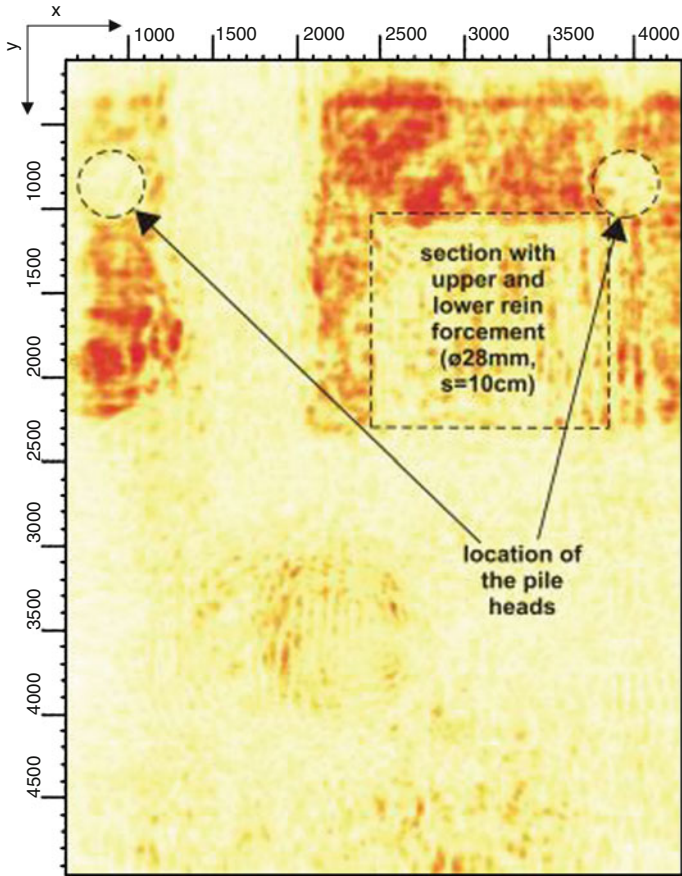


Fig. 4.16 Section at depth of 75 cm indicating the pile heads

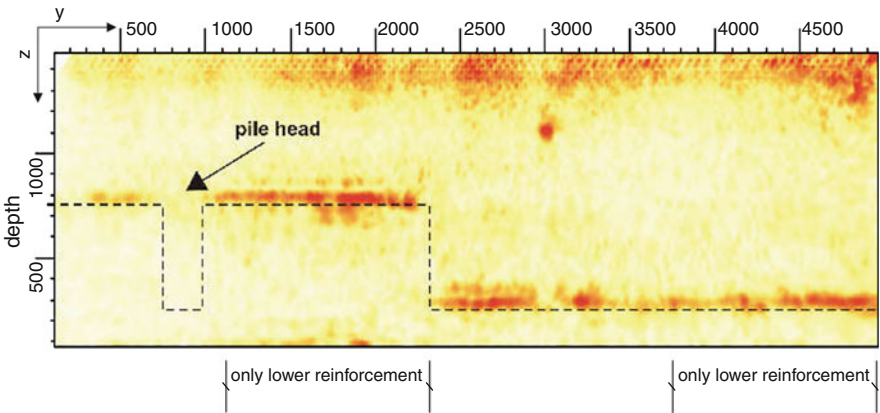


Fig. 4.17 Cross section a-a with  $\text{Ø}12$ ,  $s=15$  cm (only lower reinforcement)



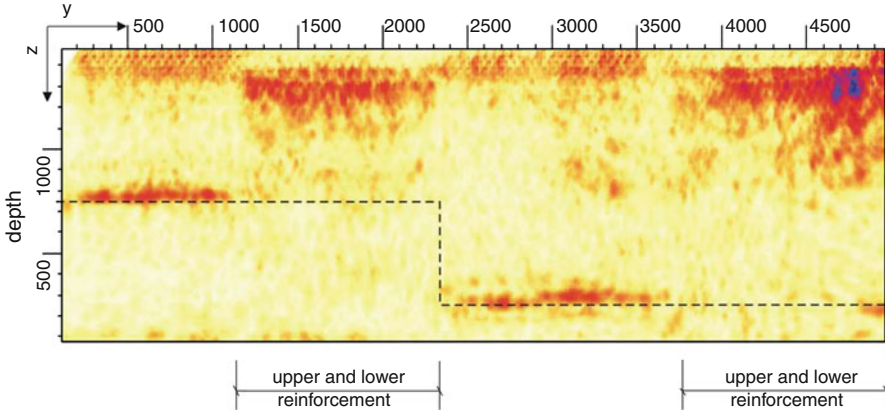


Fig. 4.18 Cross section b-b Ø28, s=10 cm (upper and lower reinforcement)

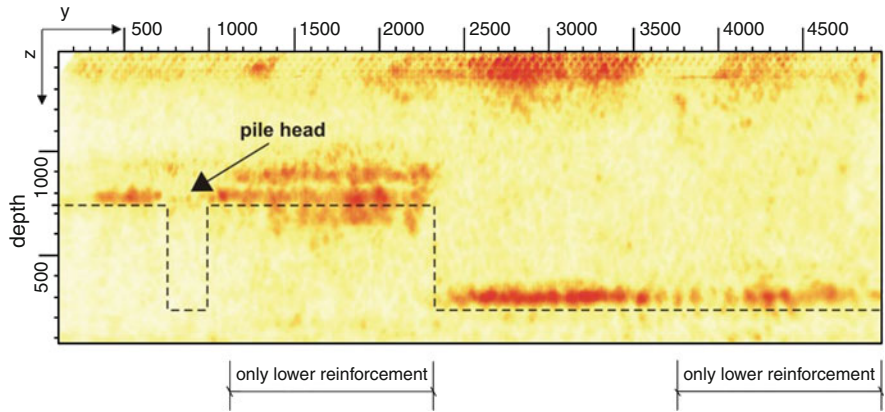


Fig. 4.19 Cross section: c-c Ø28, s=10 cm (only lower reinforcement)

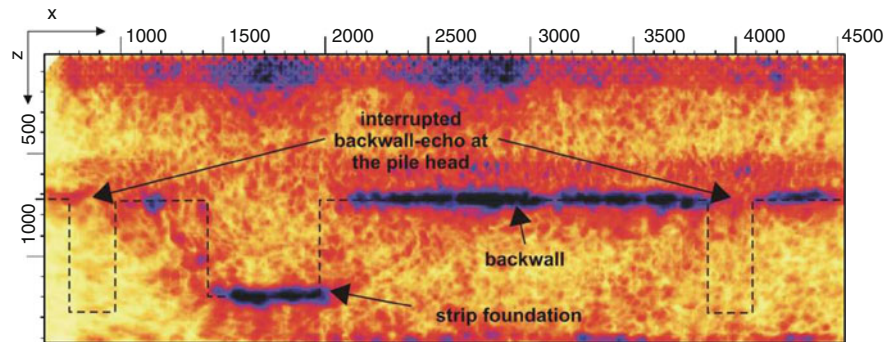


Fig. 4.20 Cross section d-d revealing the slab geometry and location of the pile heads

**Table 4.2** Ability of the different (common and special) techniques for the investigation of piles

		Sonic			Logging			Seismic	
		PET	IR	IL	CSL	CSLT	SSL	PST	Radio
Requires access tubes in/near the pile					in	in	in	near	in
Pile length		+	+	+				+	
Cross-section variations			+	+	+	+		+	
Voids, zones of bad concrete...	Detection	+	+	+	+ <sup>1</sup>	+ <sup>1</sup>	+	+	+
	Location on z	+	+	+	+	+	+	+	+
	Extension on z			+	+	+	+		+
	Location in the section				+	+			

Legend: PET = pile echo testing, IR = impulse response, IL = impedance logging, CSL = crosshole logging, CSLT = crosshole logging tomography, SSL = single hole sonic logging, PST = parallel seismic test

<sup>1</sup>: with limits on the perimeter of the pile

### 2.3.2 Guidelines

- Standard Guide for Using the Surface Ground Penetrating Radar Method for Subsurface Investigation, Annual Book of ASTM Standards 2005, Section four, Construction, Volume 04.09 Soil and Rock (II), D5714, Designation: D 6432–99
- Merkblattüber das RadarverfahrenzurZerstörungsfreienPrüfungimBauwesen (Instruction leaflet about the radar method for non-destructive-testing in civil engineering), German Society for Non-Destructive-Testing, February 2008, revised edition
- Reuse of Foundations for Urban Sites, A Best Practise Handbook, result of a research project in the frame of the 5<sup>th</sup> frame work, IHS BRE press, 2006.
- Guidance on Radar Testing of Concrete Structures, Concrete Society Technical Report 48, The Concrete Society, Slough, UK.

## 2.4 Deep foundations, shafts and piles

Two families of techniques, both based on propagation of mechanical waves, are used in common practice for cast in place piles quality assessment (“PET” for pile echo testing or PIT for pile integrity testing), the first being based on the analysis of the echo of sonic waves, the second relying on the ultrasonic transparency analysis between a transmitter and a receiver. Two of these methods have been standardized in several countries and they have several variants which are briefly described in the following. Table. 4.2 synthesizes the ability of various common and special techniques.

In the following, Sonic (PET) and Crosshole Logging (CSL) are discussed as common techniques, thus the other techniques will be presented at §3.

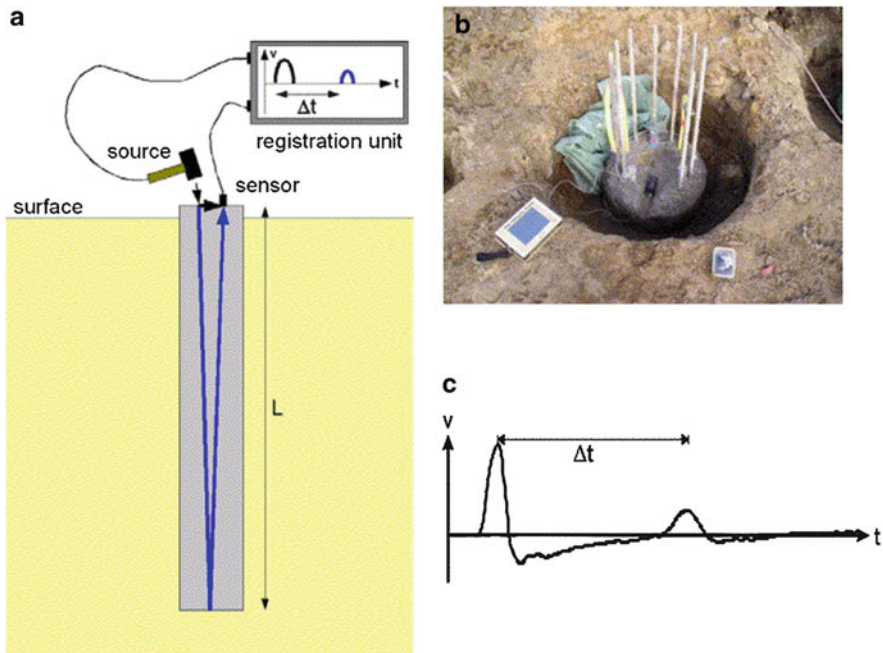


Fig. 4.21 Principle of sonic echo measurement, after [Niederleithinger and Taffe, 2006]

### 2.4.1 Sonic echo – Pile echo testing

Pile echo testing (PET), also known as low strain dynamic test, sonic echo test and low strain integrity test) is a method for condition assessment and length control. The name “low strain dynamic test” stems from the fact that when a light impact is applied to a pile it produces a low strain. The impact produces a compression wave that travels down the pile. The lower end of the pile or changes in the cross sectional area, such as a reduction in diameter or material changes, such as defects, produce wave reflections.

PET, which originated from the Netherlands [van Koten and Middendorp 1980], is the most common method for testing the integrity and length of piles of all kinds. In its original form, the test involved a vibration imposed through an electro-dynamic device, such as to impose a sinusoidal force of constant amplitude. Thanks to advances in signal processing, it is now performed with a single hand held hammer. It has been normalized in widely accepted standards (ASTM 5882, NF P 94 160-2, DGGT EAP). The test also requires an accelerometer or geophone placed on top of the pile to measure the response to the hammer impact, and a data acquisition and interpretation electronic instrument.

Pile length  $L$  is estimated from the  $\Delta t$  time of arrival of the wave, the velocity  $c$  being given (Fig. 4.21):

$$L = c \Delta t / 2$$



**Fig. 4.22** Performing the Impulse response method

The quality of the length assessment depends on the quality of the wave velocity estimation. The assessment will not identify small but perhaps structurally significant variations in  $c$  through weak concrete zones.

The Impulse response method (IR) or Transient Dynamic Response (TDR) test is an extension of the sonic echo test. The method is based on measuring the frequency and amplitude response of a pile induced by an impulse [Davis, 2003]. It requires an instrumented hammer to measure the impulse force on the pile top force in addition to motion (Fig. 4.22). The time domain signal is converted to frequency using the Fast Fourier Transform.

This response, known as Mechanical Admittance (or mobility), contains all the information necessary to check pile integrity and to analyse soil influences (ACI, see guidelines). At low frequency the response is generally linear allowing measurement of pile-head stiffness, while, at higher frequency, the resonating harmonics of the pile are detected.

Length is estimated from the distance between resonating peaks in the frequency domain (Fig. 4.23):

$$L = c / (2\Delta f)$$

where  $c$  is the velocity of longitudinal waves in concrete and  $\Delta f$  is the distance between two resonating peaks.

The quality of the length assessment depends on the quality of the wave velocity estimation.

The mean amplitude ( $P_m - Q_m$  in Fig. 4.23) of the resonating portion of the curve is a function of the impedance  $I$  of the pile, which depends on the pile cross-section  $A$ , the concrete density  $\rho_c$  and the wave velocity:

$$I = \rho_c A c = 1 / \sqrt{(P_m Q_m)}$$

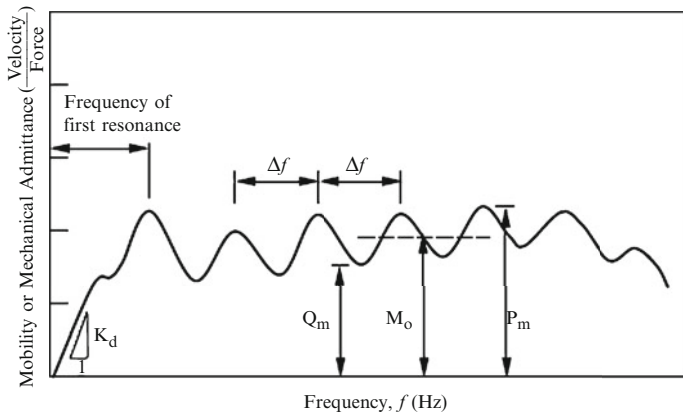


Fig. 4.23 Mobility curve

The mobility is the inverse value of the impedance. It is also possible to derive the mass  $M$  of the pile from the  $M_o$  value:

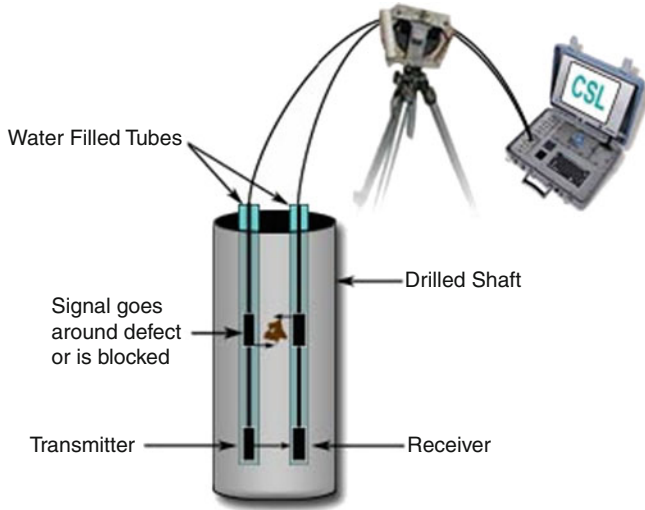
$$M = \rho_c A L = 1 / (2\Delta f M_o)$$

The main advantage of the sonic echo technique is that it is a quick and simple technique, once access is given to a clear and flat surface on top of the concrete pile (minimum age: 7 days). This crucial point for the accuracy of results requires that any weak or loose concrete has to be removed. Vibrating reinforcement or other items connected to the pile may also affect data quality. The equipment used is lightweight and portable and is very rapid in operation: a single measurement only takes about 30 seconds, so random spot checking is possible. The technique enables to identify the severity and vertical location of major defects.

The sonic techniques can be adapted for the investigation of existing structures if near head areas of the shaft are accessible. The success in assessing in-service deep foundation elements depends on several factors. Simplicity and low cost of these methods are compelling reasons for their trial before more complex and expensive means are employed.

#### Limitations:

- data interpretation requires experience and expertise.
- the accuracy of the length estimate or of the defect depth depends on an assumed stress-wave velocity,
- there are some geometrical limitations, with a length limitation of approximately 25 to 50 diameters (depending on various factors, like the soil conditions),
- multiple defects or those below a major impedance change cannot be discerned,
- small defects are often not detected, neither gradual changes in the pile section,
- the technique is not sensitive to the horizontal location of a defect in the cross-section.



**Fig. 4.24** Principle of CSL measurements (<http://www.ats-intl.com/expertise/geophysics.html>)

#### 2.4.2 Cross-hole sonic logging (CSL)

Cross-hole Sonic Logging (CSL, also named sonic coring in France) was developed in the late 1970's in France. This method requires PVC or steel tubes to be placed before casting. This is a major limitation but the technique can be very effective in assessing concrete quality and evaluating the location and extent of defects. It is a very common procedure and has been standardized (NFP, see guidelines).

It is based on the fact that the ultrasonic wave velocity is about 4000 m/s in plain concrete but changes with compaction or when voids or defects are present. The ultrasonic (typically 30 to 50 kHz) wave velocity is measured continuously between a transmitter and a receiver located at the same depth in two tubes and which are progressively moved from the pile top to its bottom end (Fig. 4.24).

The tubes are filled with water to achieve a good coupling and the test is performed when the concrete has hardened sufficiently (7 days is a common delay). The wavelength (80 mm in good concrete) provides a good resolution. As long as the first arrival time (FAT) and the energy are approximately constant, one may conclude that the concrete between the tubes is uniform and flaw-free. A marked delay in the FAT and/or a marked drop in energy indicate an inferior concrete or some anomaly (a FAT delay like 10 % is sometimes referred to as an “anomaly” when a 20 % delay is a suggested limit for a “defect” NFP 94-160-1, 2000). Of course any lack of parallelism between tubes can induce false interpretation. Figure 4.25 provides an example of how FAT and energy signals can be processed.

The process can be repeated by utilizing various combinations of access tubes to check around the shaft circumference and through its center (Fig. 4.26). It is also



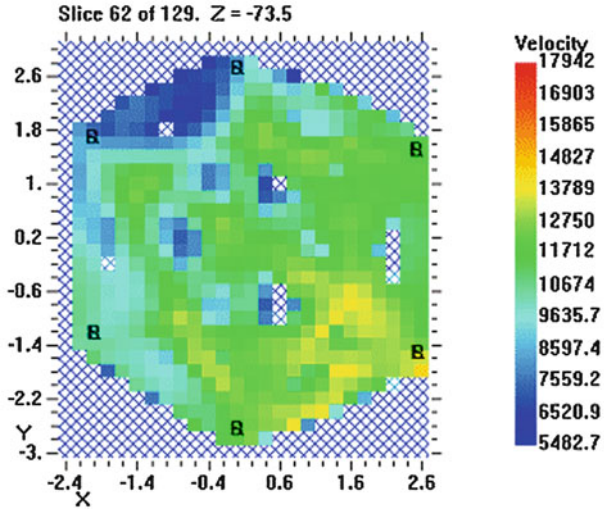


Fig. 4.25 Map of velocity at a given depth (in feet/sec) (<http://www.nci.cc/AFT/index.html>)

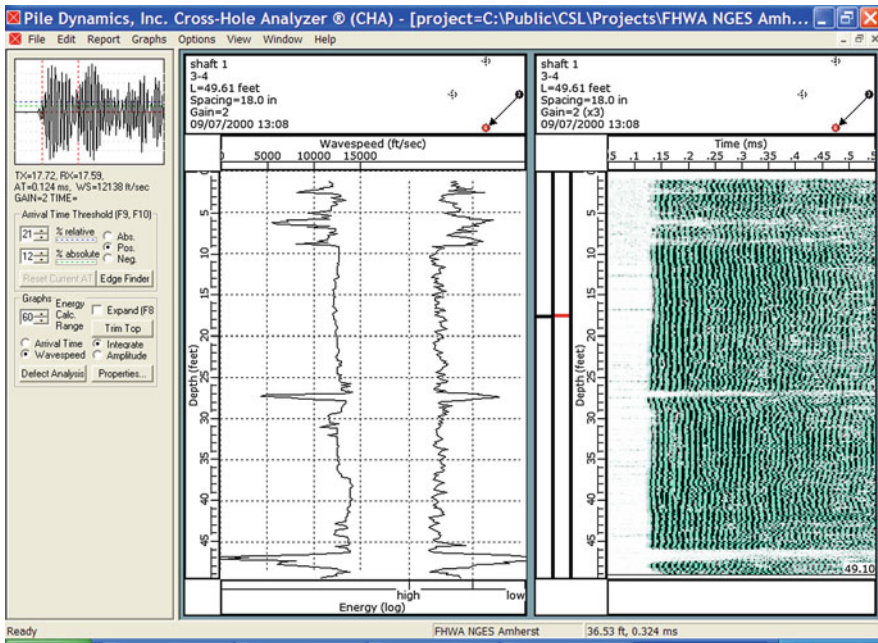


Fig. 4.26 Example of signal processing with CSL technique (after [Gray et al. 2008])

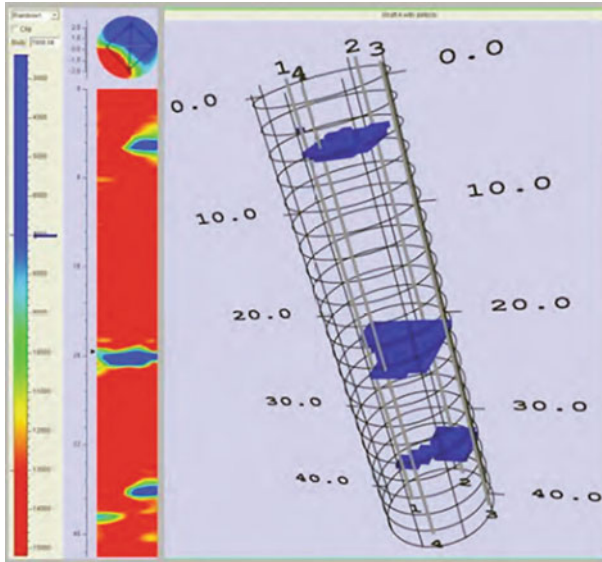


Fig. 4.27 3D-imagining: cross-hole sonic logging tomographic result (after [Hussein et al, 2005])

possible to perform tomography (the technique is then named CSLT) by varying the depth between the two probes and multiplying the ray-paths (Fig. 4.27). Its principles are identical to those of ultrasonic tomography. It is most commonly used when a defect has been identified by initial testing such as CSL. Tomography requires at least six scans per pile, which allows for a comprehensive assessment of the shaft quality.

Benefits and limits

Advantages of CSL testing include:

- no limitation on shaft length for test applicability
- provides location of defects along shaft length and in cross-section
- can detect multiple defects
- is not sensitive to soil type
- in most cases data interpretation is relatively simple

The main disadvantage of the technique is that it requires placing access tubes prior to concreting. The tested volume is that of concrete between the tubes and it does not cover the concrete outside the steel cage.

Finally, the interpretation, using tomography, requires both experience and expertise, since, e.g. artefacts can be generated in areas with a low density of information. 3D tomography provides nice pictures but the data processing is slow (cannot be done on site) and the added value can be small when compared to the time and cost required.



### 2.4.3 Guidelines and standards for piles

ACI, Non destructive methods for the Evaluation of Concrete in Structures, ACI 228.2R-98, 1998

ASTM D5882-96, Standard test method for low strain integrity testing of piles, designation, 1996

ASTM D-6760 Standard Test Method for Integrity Testing of Concrete Deep Foundations by Ultrasonic Crosshole Testing, 1/2008.

Ciria Report 144, Integrity testing in piling practice (UK).

DGGT, German Geotechnical Society, WG 2.1., Empfehlungen des Arbeitskreises Pfähle, 2007.

NFP 94-160-1, Auscultation d'un élément de fondation, Partie I - Méthode par transparence, 10/2000.

NFP 94-160-2, Auscultation d'un élément de fondation, Partie II - Méthode par réflexion, 11/1993.

NFP 94-160-4, Auscultation d'un élément de fondation, Partie IV - Méthode par impédance, 3/1994.

## 3 Special techniques and enhanced methods

### 3.1 Possible enhancements

Special techniques and enhanced methods are non-standard approaches to either standard or non-standard problems. There are several reasons for methods being non-standard such as cost, being still under development or lack of qualified specialists. Enhanced methods are expansions and/or combinations of common methods whereas special techniques include methods newly developed or existing methods applied to new applications. Enhancements often concern data processing and imaging, thanks to increasing possibilities for computations. Among these enhancements, several can be quoted:

- For GPR, Ultrasonics and Impact-Echo: Dense 3-D data acquisition, with automatic scanning systems
- For GPR and Ultrasonics: full 3-D data processing, techniques using varying transmitter-receiver offsets
- For GPR: Use of different polarizations

For all techniques, data fusion and automated combination of data from different methods into one dataset (see Chapter 8 for a detailed example on data fusion) offer new possibilities. For instance, for pile investigations, sonic echo and mobility techniques (§ 2.4.1) can be combined, mixing the information provided by the time-domain response of the sonic echo and the characteristic impedance measured with the mobility test. Thus the variation of impedance along depth, after corrections due to attenuation, is drawn in a diagram called “Impedance Log” (IL in Table. 4.2).

The question remains however of its interpretation since both the concrete quality and the pile geometry can explain variations in impedance. In addition, if a strong defect exists near the pile top, it can prevent any correct analysis of the wave propagation below.

## 3.2 *Special techniques*

### 3.2.1 **For pavements and thin elements**

The Spectral Analysis of Surface Waves (SASW) method can be potentially used to evaluate the thickness as well as the modulus profile of pavement sections. The outcome of the SASW test is the ‘dispersion curve’ which reveals the changes in phase velocity versus wavelength (or frequency). The inversion of pavement layer properties from the dispersion curve is a challenging task. For the traditional SASW test where only two receivers (at the time) are employed, the inversion concerns only the single fundamental dispersion mode. The inversion (or backcalculation) process involves minimizing the difference between the measured and theoretical dispersion curves (calculated for a set of assumed pavement sections) to find the matching pavement profile [Nazarian and Desai, 1993]. However, it was soon found that the fundamental mode dispersion curve obtained from the SASW test on pavements is dependent on the receiver locations and is actually formed by superposition of several modes of surface wave propagation [Rosset et al. 1990]. This finding led to the later inversion algorithms where the exact test set up is simulated to obtain the theoretical dispersion curve. Therefore the same distortions are reproduced in the theoretical dispersion curves as present in the measured dispersion curves. A variety of optimization algorithms have been applied to SASW backcalculation problem ranging from manual trial and error to neural network and simulated annealing [Williams and Gucunski, 1995], [Al-Hunaidi, 1998]. The backcalculation of pavement profile from the SASW test is computationally expensive and finding a unique solution of desired certainty remains a challenge.

A multi-channel variation of SASW test, the Multi-channel Spectral Analysis of Surface Waves or MASW, has been recently used in pavement evaluation applications [Ryden, 2004]. Unlike SASW, MASW takes into account higher modes of surface wave propagation [Park et al., 1999]. A corresponding two dimensional multi-modal inversion yields more accurate inverted pavement profiles, compared to SASW [Ryden and Park, 2006]. However, a multi-channel data collection adds to the complexity of field applications and data analysis.

A combination of SASW and GPR can provide complementary information regarding both the thicknesses and the material properties of pavement layers. The layer thickness information from GPR can significantly reduce the computational efforts necessary for SASW inversion. On the other hand, SASW provides invaluable information about the mechanical properties of pavement layers which cannot be obtained from GPR.

### 3.2.2 For deep foundations, shafts and piles

#### Single-hole sonic logging (SSL)

Also named “single hole ultrasonic test” (SHUT), SSL is a derivative of cross-hole testing. It has not been standardized. It was originally developed for cases where the pile was checked by core drilling, in order to increase the range of the inspection. The idea is simply to use the space left by coring for introducing two probes in the same hole. The technique has been adapted, with plastic or steel tube, and it has been shown that defects covering between 25 % and 65 % of the cross-section could be detected. It can be used in minipiles of small diameter in which it is difficult to install several tubes. It is however limited to defects adjacent to the tube and it is usually used only when a drilled shaft requires integrity assessment after construction.

#### Radioactive methods

Radioactive testing consists of lowering a gamma-gamma probe into an access tube. The gamma-gamma probe, which consists of a radioactive source and gamma photon detector separated by a length of shielded material, is lowered and raised within the tubes. During the test, gamma particles are emitted into the concrete. Some of the gamma particles are scattered back to the detector in the instrument. The test is performed continuously along the pile length with gamma count rates collected at set intervals. The counter connected to the probe gives a measure of the concrete density. Substantial drops in average bulk density readings from Gamma-Gamma tests are indicative of the presence of anomalies in the material surrounding the inspection tube. The range of inspection is limited to 75mm around the tube. It is the only method which gives high resolution information about concrete cover outside the reinforcement cage.

#### Parallel seismic testing

The principle of parallel seismic testing (PST) is comparable to that of sonic testing. It requires a small borehole in the ground parallel and close to the structure for housing a hydrophone or geophone (receiver). The length of this borehole must be larger than the assumed depth of the foundation. The main advantage of PST is that it does not need any hole within the concrete, making it well suited for existing structures. The sonic source is a shock on the head of the foundation to be investigated and the wave propagates through the pile, then through the soil between the pile and the adjacent borehole. The measurement is repeated while the receiver is progressively lowered in the borehole and a change of slope on the curve measuring the time of arrival of the wave against depth indicates the depth of the foundation. This technique provides the depth with a very good accuracy, if the borehole is near the pile. It also requires that the borehole is tubed and a good coupling (with injection) between the tube and the ground). PST results are influenced by voids and defects

in the pile but the method is not suitable for their detection, as travel time variations may also be caused by soil heterogeneities.

This technique has been standardized:

- ACI, Non destructive methods for the Evaluation of Concrete in Structures, ACI 228.2R-98, 1998
- NFP 94-160-3, Auscultation d'un élément de fondation, Partie III - Méthode sismique parallèle (MSP), 5/1993.

#### Mise à la Masse (MM), Magnetic (MT) and Induction (IT) techniques

Several other techniques are available for the measurement of the length of reinforcement in concrete piles (which does not match the total pile length in all cases), sheet piles or steel piles. *Mise à la masse* (MM) and induction techniques (IT) are active techniques applying direct (MM) or alternating (IT) electrical current to the steel at the pile top (which must be accessible therefore). The resulting electrical or electromagnetic fields are measured by a sensor moving in a PVC cased borehole (max 1 m distance recommended). The field strength drops at the level of the lower end of the reinforcement/steel pile. The magnetic technique (MT) measures the natural magnetic field strength which is influenced by the reinforcement/steel pipe. MT is less accurate and sometimes difficult to interpret, but does not require access to the pile.

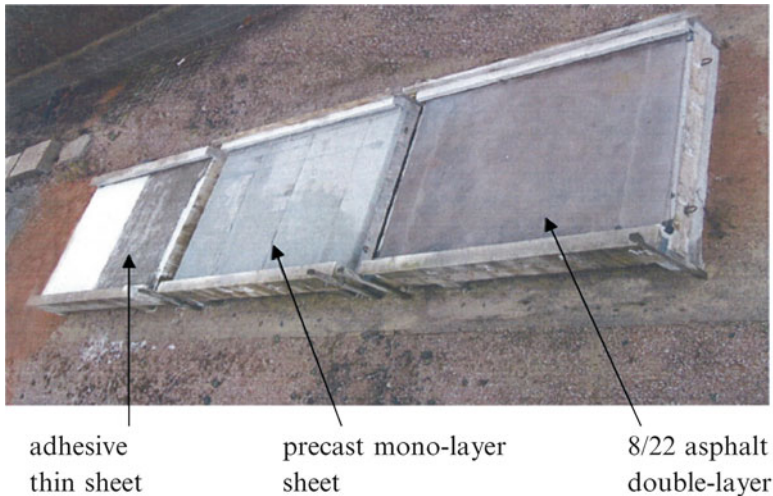
#### Combination of techniques

The combination of techniques can be used on the basis of the limitations of each single technique (for instance due to the need of access tubes) and on their ability. It is generally used to improve the quality of the assessment. For instance, the depth assessment in sonic techniques requires assumptions on the wave velocity. [Niederleithinger and Taffe, 2006] suggest, from measurements on a pilot test, to perform an additional parallel seismic test for one pile among the series to be tested. On this pile, the length being measured with a good accuracy, the velocity can be calibrated and this value can be used for the assessment in all piles in which only a sonic measurement will be performed.

## 4 Benchmarks and test sites

Test sites are purpose-built structures with known geometries and material properties. Test sites can be used in several ways such as:

- Test if a method can solve a certain problem
- Optimization of test methods
- Comparison between different methods
- Demonstration and training



**Fig. 4.28** LRPC test site, concrete slabs covered with different sealings having different defects

It is not always easy to obtain accurate information on such test-sites, which are often designed within the framework of a specific research program, and do not offer open access to the public. The following section describes some permanent test sites that are available for professionals on request.

## **4.1 Pavements and sealings**

### **4.1.1 Test deck for sealings (LRPC Autun)**

Location: LRPC, Boulevard de l'Industrie, 71405 Autun, France

Contact: Christophe Aubagnac, LRPC

This test site has been designed to test non-destructive techniques for the detection of defects related to sealings. It is composed of four concrete slabs covered with waterproofing layers (Fig. 4.28).

Three slabs are covered with different types of sealings having defined defects. The dimension of the concrete structures is 300\*260\*25 cm. They are covered with a precast mono-layer sheet, an 8/22 asphalt double-layer and an adhesive thin sheet.

### **4.1.2 Road test site (LCPC)**

Location: LCPC, Route de Bouaye, Nantes, France

Contact: Xavier Derobert, LCPC, Route de Bouaye, 44340 Bouguenais, France,  
xavier.derobert@lcpc.fr

This test site (Fig. 4.29) has been designed in order to qualify the GPR performances used for pavement layer thickness measurements. Four different structures are implemented, with local metallic plates in order to confirm some particular interfaces.

## 4.2 Thin elements

### 4.2.1 Tunnels

Reference specimen at MFPA Leipzig, Germany

Contact: Prof. Dr. Frank Dehn, phone ++49341 6582145, dehn@mfpa-leipzig.de

The shell has a total thickness of 40 cm and is made of external shotcrete, a fiber mat (2mm), a sealing (2mm) and an inner shell (Fig. 4.30).

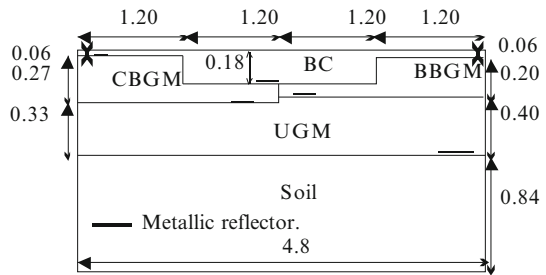
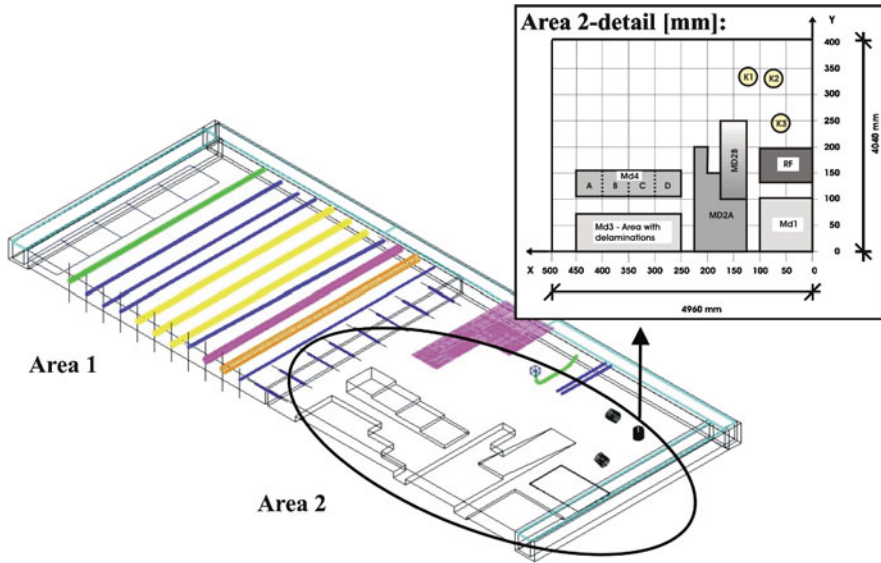


Fig. 4.29 Schematic structure of the road test site



Fig. 4.30 Test tunnel at MFPA Leipzig (after [Taffe and Gehlen, 2007])



**Fig. 4.31** Large Concrete Slab, BAM

## 4.2.2 Concrete slabs and walls

### Large concrete slab (LCS)

Location: Federal Institute for Materials Research and Testing (BAM), Unter den Eichen 87, 12205 Berlin, Germany

Contact: Martin Krause, phone: ++49 30 8104 1442, martin.krause@bam.de

The large concrete slab (LCS) is a one sided slab built by the Federal Institute for Materials Research and Testing (Fig. 4.31). It is located in Berlin, Germany. The dimensions are 4m x 10m with a thickness of 0.3m. The LCS is divided in two sections. The first section contains tendon ducts of different diameters at different depths. Some of the ducts are intentionally ungrouted. The second section has areas with smaller thickness, precast honeycombs and a reference area with a steel plate for calibration purposes. Examples of measurements performed on this specimen have been given at §2.3.1. Others will be discussed in Chapter 5 (§5.5).

### Concrete wall specimen at LRPC Lyon

Location: LRPC Lyon

Contact: Pierre Roenelle, LRPC, Lyon

A concrete wall in four parts has been built in 2003. The thickness varies from 18 to 51 cm. Many ducts have been inserted in the wall, with or without tendons (Figs. 4.32 to 4.34), and with several grouting defects [Roenelle, 2006].





Fig. 4.32 The building of the test wall at LRPC, Lyon

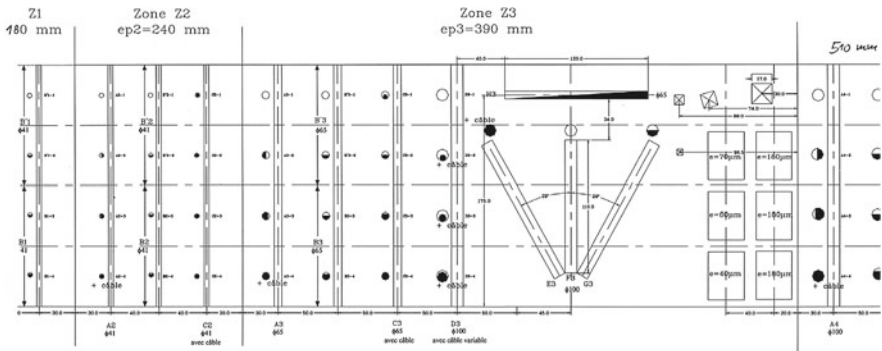


Fig. 4.33 Concrete specimen “Wall”, LCPC Lyon

### 4.2.3 Slab foundations

#### BAM Slab Foundation Test Site

Location: Horstwalde, Germany

Contact: A. Taffe, Federal Institute for Materials Research and Testing (BAM),  
Tel + 49 30 8104-4244, Alexander.taffe@bam.de

For systematic thickness measuring subject to reinforcement ratio and slab thickness a specially designed foundation slab has been constructed [Taffe et al., 2005] with the following features:

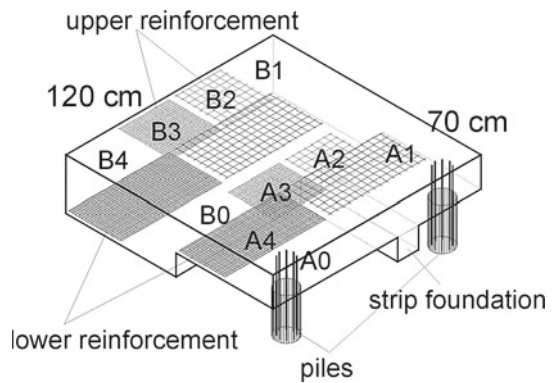
- Area: 5 x 5 m
- 2 sections, one of 75cm and one of 125cm thickness





**Fig. 4.34** Scanner for automated measurement at LCPC, Lyon

**Fig. 4.35** Drawing of the foundation with ten sections (A0-A4, B0-B4) of different reinforcement ratio as well as strip foundation and pile heads beneath the slab



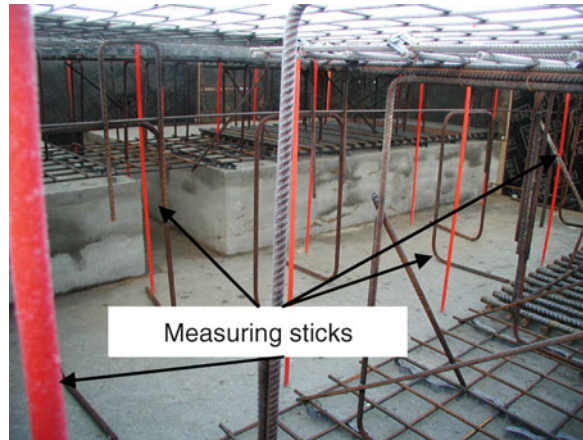
- Strip foundation (width 50 cm), height 50 cm below 70 cm slab
- Sections with 10 different reinforcement ratios
- Pile heads with diameter of 30cm below 70cm slab

The structure of the slab is shown in Fig. 4.35. Details of the specimen before concreting are depicted in Fig. 4.36. Measuring sticks are used to verify the real thickness after filling with concrete.

#### 4.2.4 Pile foundation

Test piles have been regularly used to help NDE practitioners to develop and calibrate their techniques and material. For instance, in July 1988, FHWA (Federal Highway Administration) initiated a contract research study to examine drilled shafts for the effect of defects on performance, and to develop acceptance criteria for use by

**Fig. 4.36** Photo of the foundation's inside before pouring the concrete. Measuring sticks as reference to measure true thickness



construction engineers to accept, reject, or modify a newly constructed drilled shaft. The study included the construction of 20 drilled shafts with and without defects for different soil sites located in California and Texas. All shafts were tested non-destructively using both surface reflection and direct transmission techniques to determine their effectiveness in identifying defects (<http://www.fhwa.dot.gov/engineering/geotech/pubs/century/02.cfm>).

In other cases, blind tests can be performed on real piles, and the efficiency of the technique can be checked at the end of the process by extracting the shaft. This can allow a company to demonstrate its ability to a contractor [Gray et al, 2008]. Test sites can also be used to quantify the ability of a given technique (or of an improved technique) to detect/localize/quantify model defects. These sites are often designed in relation with a company which wants to test its own material. Two such examples are:

- A test site has been used at Auburn University, Alabama (USA), in relation with a material designer (Piletest) such as to show how model soil inclusions (sand bags fixed to rebars) can be detected on four test piles by CSL or SSL [Paikowsky et al, 2000].
- A test site has also been designed in Israël [Amir, 2002], with ten short piles (diameter of 350 mm and a typical length of 3.50 m). Eight of the piles contained pre-fabricated voids, made out of thick plywood and sheet metal boxes, at a depth of between 1.50 and 2.00 from the top of the pile. CSL and SSL techniques were used, immediately after concreting, at 24 hours, 3 days and 6 days.

Other test sites can be designed with a more ambitious objective: that of improving the scientific knowledge, the expertise of practitioners or the ND techniques. Two such examples are given below.

- NDE test section of five shafts has been constructed at the National Geotechnical Experimentation Site (NGES) at Northwestern University, Michigan, to provide a controlled site where various nondestructive evaluation testing techniques could be performed (Fig. 4.37).

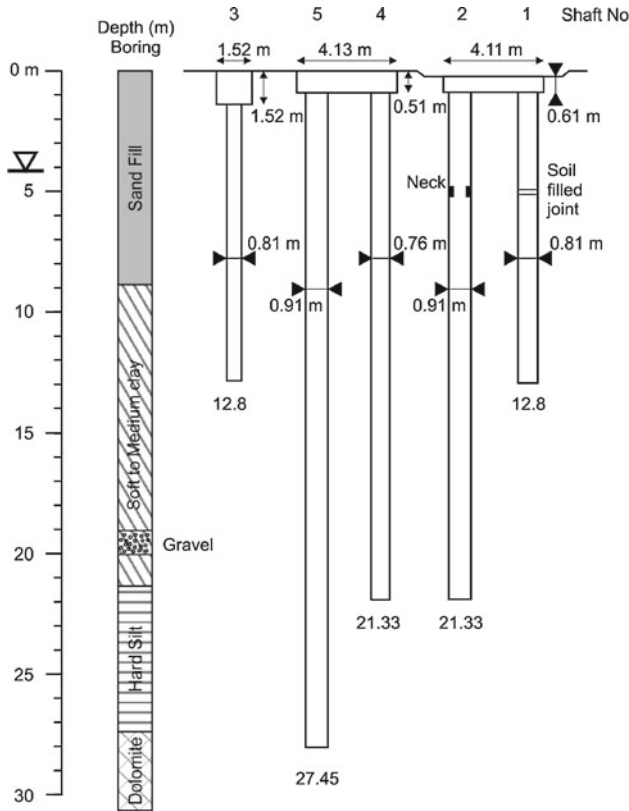


Fig. 4.37 Cross-section of NGES deep foundation test site (after [Gassman and Finno, 2000])

This site is located in Evanston, Illinois, and it was selected by the National Science Foundation (NSF) and the FHWA as a NGES in 1992. The drilled shaft section was constructed in fall of 1994 to provide a full-scale site where different non-destructive evaluation methods could be conducted to evaluate their ability to determine the integrity of inaccessible deep foundations ([http://www.iti.northwestern.edu/projects/NDE/chs\\_ch3.html#1](http://www.iti.northwestern.edu/projects/NDE/chs_ch3.html#1)). Two of these shafts were constructed with known defects (one with a horizontal crack, the second with a necking obtained with sandbags). Field test were PET, IE, CSL and PST, with the purpose of evaluating the ability of the cross-hole sonic logging test to identify the defects present in the shafts, and to determine the effects of the concrete age on the test results (four ages from 7 days to 1000 days were tested).

The “Deep Foundation Test Site” has been designed on the grounds of the University of Central Florida (USA) for the on-going and recurring testing for research and certification programs. The site is intended to be utilized to demonstrate various pile and drilled shafts, compare various load test methods, and test NDE methods like SE. It will also be possible to compare various analysis methods.

**Fig. 4.38** Pile test site under construction



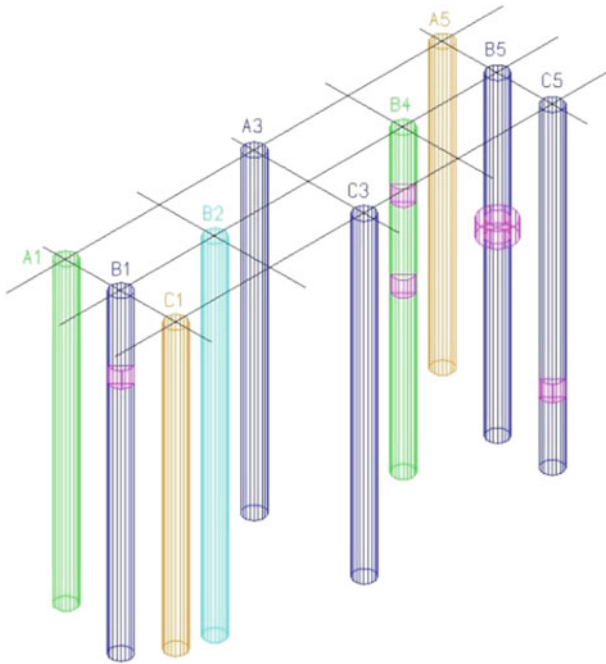
In addition, the site will be utilized for the training of Florida Department of Transportation personnel in deep foundation installation and testing methods. To our knowledge, no experimental result has been yet published from this test-site (<http://www.cce.ucf.edu/research/deep%20foundation/index.htm>).

#### **4.2.5 NDT test and validations site at Horstwalde**

Location: Horstwalde, Germany

Contact: Ernst Niederleithinger, Federal Institute for Materials Research and Testing (BAM), Unter den Eichen 87, 12205 Berlin, Germany, phone: ++49 30 8104 1443, [ernst.niederleithinger@bam.de](mailto:ernst.niederleithinger@bam.de)

In the frame of the RuFUS project [Butcher et al., 2006] a foundation test site for various NDT techniques was set up (Fig. 4.38). So far a foundations slab (described above), 10 bored piles and a set of other concrete test objects exist. The test site was designed with help from other research institutions and the industry. A major upgrade is intended, including concrete elements from foundations, utilities and road and railroad infrastructure. The test site will be available on a long-term basis for research and education.



**Fig. 4.39** Drawing of the pile test site with 10 piles with well defined pile length and location of defects

Ten bored piles with 62 cm diameter and lengths between 8.5 and 12 m (three of them with flaws) are available at the moment (Fig. 4.39). So far they have been used to validate pile length measurements by the low strain method and the parallel seismic method.

## References

- Al-Hunaidi M.O. (1998) Evolution-based generic algorithms for analysis of nondestructive surface wave tests on pavements, *NDT&E International*, Vol. 31, No. 4, pp. 273–280.
- Al-Qadi I., Lahouar S., Loulizi A. (2003) GPR: From State-Of-the-Art to the State-Of-the-Practice, Proc. NDT-CE 2003, September 16-19 2003, Berlin, Germany.
- Amir J.M. (2002) Single-Tube Ultrasonic Testing of Pile Integrity, [www.piletest.com/papers/shut/Orlando%20%2020200](http://www.piletest.com/papers/shut/Orlando%20%2020200)
- Butcher A. P., Powell J. J. M., Skinner, H.D. (2006) Reuse of foundations for urban sites, IHS BRE Press, UK; 144 p.
- Davis A.G. (2003) The non-destructive impulse response test in North America: 1985 – 2001, *NDT&E International* 36, pp. 185-193.
- FDOT, 2000, Florida Department of Transportation, ResearchCenter, Tallahassee, FL, RESEARCH TODAY, Fall 2000.
- Gassman S.L., Finno R.J. (2000) Cutoff frequencies for impulse response test of existing foundation, *J. Perf.Constructed Facilities*, 14, 1, 11-21.

- Gray K., Hussein M., Lewis C. (2008) Drilled shaft extraction, Const.Conf08, Florida DoT.
- Hugenschmidt J. (2003) Non-destructive-testing of traffic-infrastructure using GPR, Proc. NDT-CE 2003, September 16-19, Berlin, Germany.
- Hugenschmidt J., Mastrangelo R. (2006) GPR inspection of concrete bridges, *Cement & Concrete Composites*, 28, pp. 384-392.
- Hussein M.H., Likins G. (2005) Deep foundations quality control and quality assurance testing method, Florida Eng. Society, 3/2005, p. 10-13.
- Maser K. (1996) Evaluation of Pavements and Bridge Decks at Highway Speed Using Ground Penetrating Radar, Proceedings, ASCE Structures Congress XIV. Chigaco, IL, 15-18 April 1996.
- Maser K., Scullion T., Roddis W. M., Fernando E. (1994) Radar for pavement thickness evaluation, Non-destructive Testing of Pavements and Backcalculation of Moduli, ASTM STP 1198, Philadelphia.
- Nazarian S., Desai M.R. (1993) Automated surface wave method: field testing, *Journal of Geotechnical Engineering*, ASCE, Vol. 119, No. 7, pp. 1094-1111.
- Niederleithinger E., Taffe A. (2006) Early stage elastic wave velocity of concrete piles, *Cem. Concr. Composites*, 28, 317-320.
- Paikowsky S.G., Chernauskas L.R., Hart L.J., Ealy C.D., DiMillio A.F. (2000) Examination of a new cross-hole sonic logging system for integrity testing of drilled shafts, Application of stress-wave theory to piles, Nylam&Belm (eds), Balkema, Rotterdam.
- Park C.B., Miller R.D., Xia J. (1999) Multi-channel analysis of surface waves, *Geophysisc*, Vol. 64, No. 3, May-June 1999, pp. 800-808.
- Roenelle P. (2006) Contrôles, essais, mesures, Hors Série – l'Europe des END, sept. 2006.
- Rosset J.M., Chang D.W., Stoke II K.H., Aouad, M. (1990) Modulus and thickness of the pavement surface layer from SASW tests, *TRR*, No. 1260, pp. 53-63.
- Ryden N. (2004) Surface wave testing of pavements, Ph.D. thesis, LundUniversity, Lund, Sweden.
- Ryden N., Park C.B. (2006) Fast simulated annealing inversion of surface waves on pavement using phase-velocity spectra“, *Geophysics*, Vol. 71, No. 4.
- Shevaldykin V.G., Samokrutov A.A., Kozlov V.N. (2003) Ultrasonic Low-Frequency Short-Pulse Transducers with Dry Point Contact. Development and Application, Proc. Int. Symp. NDT-CE 2003, Berlin, Germany.
- Taffe A., Gehlen Ch. (2007) Anwendung der Zuverlässigkeitsanalyse auf Messungen mit zerstörungsfreien Prüfverfahren am Beispiel der Tunnelinnenschalenprüfung, Beton- und Stahlbetonbau, Volume 102, Issue 12: 812-824.
- Taffe A., Niederleithinger E. (2006) NDT investigation methods, Butcher, A.P., Powell, J.J.M. and H.D. Skinner (eds.); Reuse of Foundation For Urban Sites - A Best Practice Handbook, Berkshire, BRE Press, Kap. 6.3.3, pp. 47-55.
- Taffe A., Krause, M., Milmann, B., Niederleithinger, E. (2005) Assessment of foundation slabs with US-echo in the re-use process, in Alexander, M., Beushausen H.-D., Dehn F., MoyoP. (eds), Proc. Int. Conf. on Concrete Repair, Rehabilitation and Retrofitting (ICCRRR), 21.-23.11.05, Cape Town, South Africa, pp. 525-530.
- Van Koten H., Middendorp P. (1980) Equipment for integrity testing and bearing capacity of piles, Proc. Intl. Seminar on the Application of Stress-Wave Theory on Piles, Stockholm, Sweden, pp 69-76.
- Willet D. A., Rister B. (2002) Ground Penetrating Radar “Pavement Layer Thickness Evaluation”, Research Report KTC-02-29/FR101-00-1F, Kentucky Transportation Center, University of Kentucky, Lexington.
- Williams T.P., Gucunski N. (1995) Neural networks for backcalculation of moduli from SASW test, *Journal of Computing in Civil Engineering*, ASCE, Vol. 9. No. 1, pp. 1-8.

# Chapter 5

## Assessment of bonding, delamination and interfaces

Jean-François Lataste and Patrice Rivard<sup>1</sup>

### 1 Introduction to debonding and delamination

Concrete can be viewed as a continuous, homogeneous and isotropic material when the investigation does not consider the microstructure scale (this level will not be considered in this report). “Interface”, as generally defined, is a physical limit between two materials. Such a limit can be viewed as an alteration of the mechanical continuity of concrete, and then, as a possible alteration of its mechanical and physical properties.

Engineers are interested in the knowledge of this flaw due to its signification: either an indicator of damage (for instance, as a consequence of rebar corrosion), or a parameter conditioning the damages (due to its influence on the concrete transfer properties for example), or an internal geometrical characteristic. Generally such flaw must be considered at the local scale, at the material level, but its influence, when evolving, can finally disturb the whole structure.

The knowledge of the initial cause of the interface is important for an appropriate characterization. However, in most cases, additional information is required. The aims of an investigation can be: the detection, the identification, the location, the extension, the depth, the intensity, and the activity (possible evolution) of an interface.

So practically, the consideration of “interface” in the frame of the TC is motivated by the fact that their detection and in situ characterization is a way to assess the condition of the structure at a moment of the structure life (which is the characteristic at the date of investigation). It also allows assessing the possible

---

<sup>1</sup> Other contributors to this chapter are: O. Abraham, J.P. Balayssac, R. Felicetti, M. Fischli, V. Garnier, P. Gilles, Ch. Maierhofer, A. Moczko, L.D. Olson, J. Popovics.

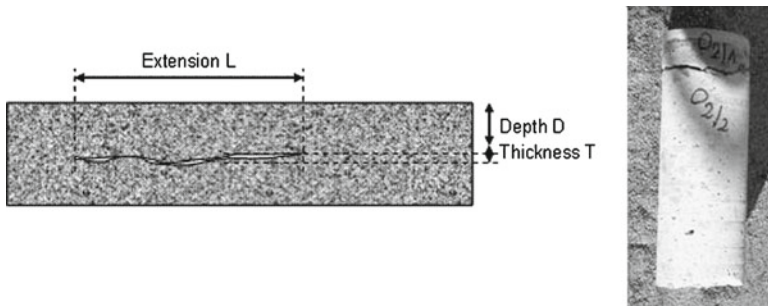
J.-F. Lataste (✉)

Université Bordeaux 1, I2M, GCE (Civil and Environmental Engineering Department), France  
e-mail: jean-francois.lataste@u-bordeaux1.fr

P. Rivard

Université de Sherbrooke, Québec, Canada





**Fig. 5.1** Example of Delamination. Core (at the right) shows a typical delamination

duration for the structure (what is the impact of the damage on the structure, and how could evolve the interface with time?).

## 2 Description /definition of the problem treated

### 2.1 *What is being looked for? At what scale? For what purpose?*

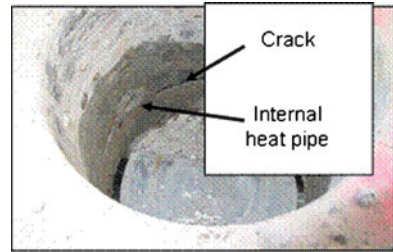
Concrete debonding can be defined as an open interface where there had been a close interface yet, such as a construction joint. We speak about debonding when this interface causes a mechanical discontinuity, a weakness. In extreme cases, the debonding can be observed as a layer filled with air or water. The presence of concrete debonding can be due to a defect during construction. A common debonding is the contact defect between a precast slab and the concrete cast over it. Another classical case of debonding in concrete bridge decks is at the separation level of the asphalt concrete overlay material from the concrete deck. In a debonded area, one would expect to find a hole, a tear, or other form of deterioration in the petromat membrane, which would allow water to accumulate between the membrane and the bridge deck.

Delamination is defined as cracks parallel to the surface. It is generally consecutive to a damage of concrete or to the structure: Fire, freeze/thaw, or rebar corrosion are classical causes of this kind of damage (Fig. 5.1). Unlike debonding, delamination is not located where there had been an interface yet. An example of common observed delamination is a splitting of the concrete at the rebar level. It stems from the expansion stress generated on the concrete by the corrosion products when the reinforcing steel is corroding. A hollow plane is then created in the concrete slab (Fig. 5.1).

Whole structures or a part of them can be investigated with regards to debonding or delamination. Multilayered debonding or delamination usually disturbs surfaces about some square decimeters to square meters. Interfaces can sit very close to the surface when they are associated with physico-chemical alterations coming from the surface (i.e. frost, fire ...). Other phenomena can generate interfaces deeper in concrete: limits between precast concrete and concrete cast on site, debonding around rebar or around internal heat pipe – Fig. 5.2 & Fig. 5.3).



**Fig. 5.2** Interface at heat pipe level in a concrete slab (P. Toussaint in Breysse et al. 2005)



**Fig. 5.3** Interface at the reinforcement level due to rebar corrosion (Naar, 2006)



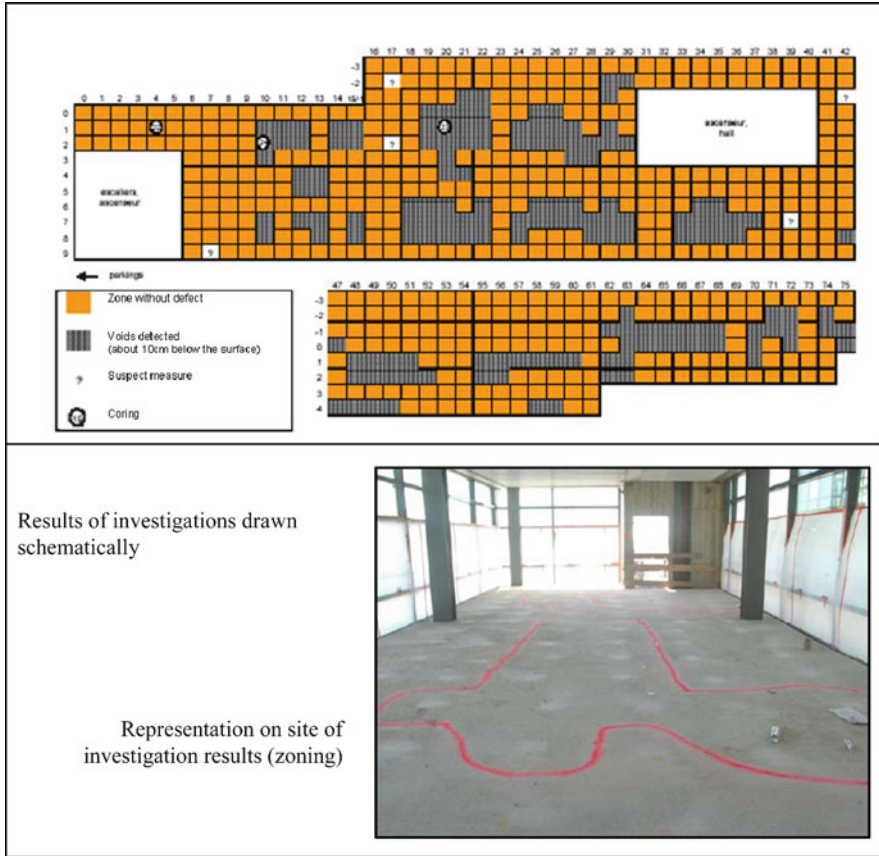
Interface investigation can be motivated by checking whether some elements of buildings complying with standards (to search for possible explanations when a problem occurs,); or, in case of damage appearance, by detecting any alteration of concrete (due to ageing, for instance). Investigations can be planned at the end of the construction (to check the conformity), during the life of structure (to diagnose an alteration), or to control the efficiency of repair works (injection for example).

The type of interface disturbs the homogeneousness of the structure and can condition its structural behavior. This interface can correspond to a preferential path for fluids to flow. Geometries and properties of these defects can vary (considering the filling, the cause, the evolution...). Interfaces can also evolve to spalling concrete. Owners can see them as source of hazard (considering the possible fall of concrete pieces from wall facing), or as an aesthetic issue (with regards to facing degradation or moss deposits).

## 2.2 What level of interpretation? Required accuracy?

### 2.2.1 Detection / localization

The first aim of an investigation involving to debonding or delamination issues is the detection of the flaw and its location. The question of detection is generally asked in term of speed of investigation with regards to the probability of detection (or non detection). The skill of the specialist consists to select the technique that

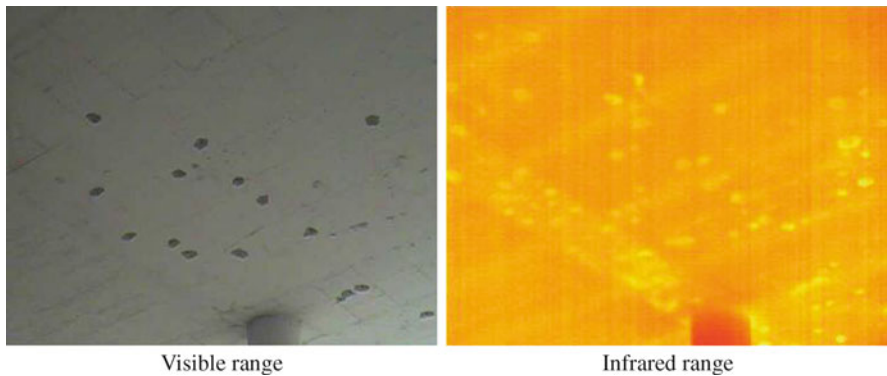


**Fig. 5.4** Region of delamination in a concrete slab determined by impact echo investigation (P. Toussaint in Breyse et al. 2005)

would allow the right adjustment of two above parameters. Techniques allowing the optimal measurement cadences are usually those that are less performing in terms of information accuracy. For instance, infrared thermography is a fast technique commonly used for investigating large surfaces but quantitative interpretation of data cannot be done. On the other hand, impact echo, a slow technique, allows characterizing interfaces sharply.

The determination of lateral extension of an interface below the surface gives information that is very useful for a better work planning. An example of a case study involving impact echo method is presented below (Fig. 5.4). The objective was to assess and localize the damaged surface. Impact echo has lead to a mapping of the damaged area in proportion relatively to the investigated surface.

Techniques based on a punctual measurement, such as impact echo or electrical resistivity, allow determining interfaces with an accuracy that depends on the measurement grid spacing. In some cases, this procedure is suitable for the problem: when the need is focused on the description of spread damages, only a global approach



**Fig. 5.5** Image of underface of an aqueduct (Gilles et al., 2007). Spalls pits are indicated by light shaded spots on the infrared image

is possible. Figure. 5.5 shows the detection and localization of spallings (few square centimeters) associated with the bad quality of spacers. These disorders are spread out spatially and the issue was only to locate altered zones within a 59m x 290m surface.

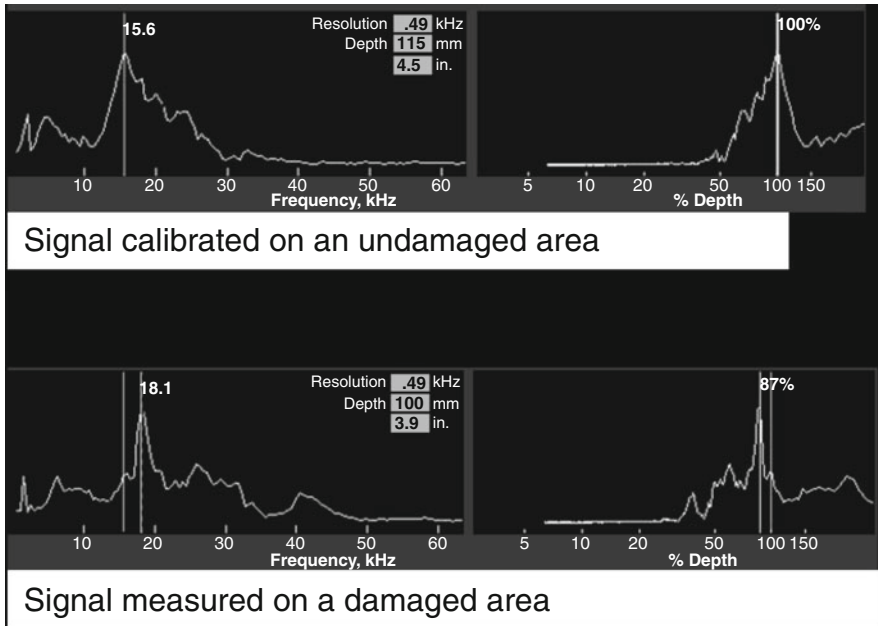
### 2.2.2 Characterization with depth

The sharp characterization of discrete interfaces in concrete is related to the determination of (1) the depth of interface, (2) the thickness of interface.

#### Depth of interface

After having detected the lateral location of alteration, the next step is characterization of its position with depth. This description is based on the material properties and must be considered as an inverse problem to be solved. A first approach consists in comparing the results with regards to their location. With impact echo, for instance, the calibration is usually made on a reference zone (known to be sound), then, further results obtained elsewhere are compared with the reference signal (Fig. 5.6).

The estimation of the interface depth from the measures values can also be performed by an inverse analysis. This approach has not been very successful up to now. One main reason is that field concrete presents variable properties that cannot be considered in models used to inverse measurements. Therefore, results analysis does not yield accurate evaluation of some characteristics of alterations. That is one of the main concerns regarding the assessment of the interface depth from the surface. The concrete is generally variable with depth (from the surface to its heart), due to the skin effect, but also to carbonation and other climatic/environmental processes or water content. These variations enhance the complexity of assessing parameters with depth due to the creation of bias. The technique effectiveness with regards to variation of concrete properties is a first consideration in the limitation of the accuracy/reliability of the diagnosis.



**Fig. 5.6** Amplitude vs. frequency of signal for the impact echo technique. (This result allows detection of delamination within a concrete slab)

Another limit of inverse analysis can be the need, to know the exact measurement “input”. With infrared thermography, for example, the natural heating or cooling of the environment (exciting thermal behavior of the concrete structure) is not mastered by operators during assessment. The work conducted with impulse infrared thermography aims at improving the interpretation: In this approach, operator controls the energy impulse. Then, the measurement of the response can be interpreted in terms of damage characteristics, such as the depth.

#### Thickness of interface

A flaw is detected because its physical properties differ from the surrounded concrete. The contrast is influenced by the physical properties of the flaw, relatively to surrounding material; but also by the volume of the flaw. For instance, considering two delaminations with the same physical properties, the thicker flaw is more easily detected than the thinner.

In favorable cases, the thickness even if it is not directly detected, can be approached: the parameter influences the final response by increasing the contrast.

For example, crack detection with electrical resistivity is possible due to the sharp electrical contrast between the crack and the concrete. The width of flaw can be “viewed” (from electrical criteria) as a variation of the material filling the crack; however both elements cannot be distinguished. Also, combination of filling material

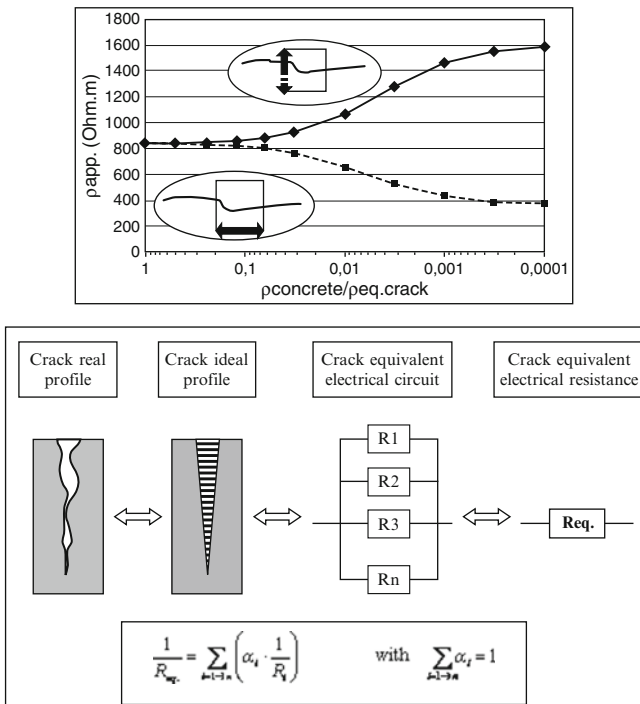


Fig. 5.7 Apparent resistivity depending on resistivity of the crack. Numerical results on resistive crack, and analogical model corresponding (Lataste et al. 2003(2))

an crack geometry can be expressed in term of electrical resistivity, stated as the “equivalent resistivity of the crack” (Fig. 5.7).

### 2.3 Why it is difficult?

The first reason may appear obvious: internal interfaces in concrete structure are not visible from the surface. For engineer and managers, the first problem to be deal with ( ) is the detection of the damage, then its location and characterization. Techniques that have been currently proposed allow either a quick detection of alterations, or a sharp description of the damage (the second being slower than the first). It does not seem possible actually to obtain both results with a single technique.

Of course, the issue of debonding detection is based on the contrast of the physical property measured by the ND technique: In other words, a delamination can only be detected if the contrast of the physical property that are measured is above the technique or equipment resolution.

The effectiveness to detect and characterize flaws with NDT, depends on the capacity to identify the “signature” of the defect on measurement. This can be done

if 1) the signal is stronger than the measurement noise (this consideration is explained above, and will not be more developed here) or 2) the data processing allows highlighting it. The direct model (analytical or numerical) is reliable enough to reach to the measurement response, for given hypothesis. Inverse analysis consists of the calculation of direct problem with hypothesis on input values. Then, by iterative steps, and improvement of the inputs, one tries to converge to a solution where the lowest gap between the measured and calculated values. This is done according to inversion methods, and in the range of uncertainties. The final result is a combination, derived from the hypothesis used for calculations, of probable characteristics of the material (physical, geometrical...) that can explain what was measured. One of the main difficulties is the knowledge, or at least, the calibration of the direct models: How to be sure (or even to control) of the reliability of the hypothesis used for direct model? How to identify the bias effect from the data that are looked for? How can the model take into account the interaction between the influencing parameters? Another issue is the mathematical technique used to find the better mathematical solution, or more practically: how to converge quickly towards the optimal solution?

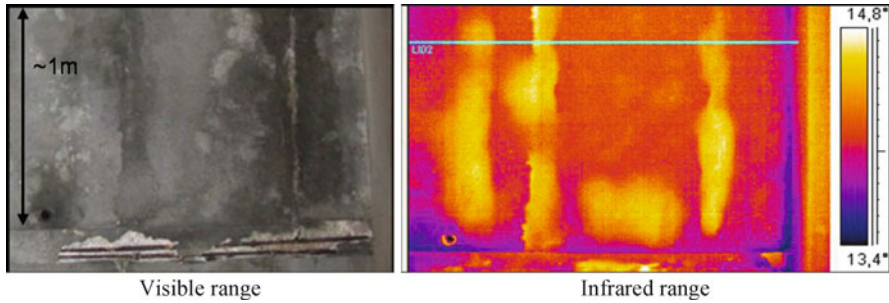
The technique resolution and the ability for engineer to represent the final results can also be improved. Some developments for sharp data imaging may improve the capacity for engineer to identify flaws. The visualization of structures or geometries associated with classical damage patterns can influence the interpretation of measurements. It is common with radar investigation to represent the layer thicknesses in pavement in 2D, with commercial softwares used for data processing.. Another example is tomography, which yields a 2D colored picture where one seems to ‘view through material’, helping engineers to understand the results. Representation of the results in term of complex parameters only understood by specialists limits the interest of the techniques: for owners who want to understand the conclusion of evaluation, and also for engineers who want to use the results even if they are not NDT specialists. Some developments are in progress in this field of results representation for easy understanding, as proposed by Mayer *et al.* (2003) who have been working on SAFT for radar signals, or Gucunski *et al.* (2009<sup>1</sup>) with regards to impact echo.

Visualization and imaging of results are in great demand for practitioners and engineers in charge of inspection. Recently the civil engineering community has identified this need in a general manner. This supports the new TC RILEM “On-site measurement of concrete and masonry structures by visualized NDT” (led by Prof. Masayasu OHTSU; see <http://www.rilem.net>).

### 3 Description of Techniques

#### 3.1 Common techniques

Most techniques presented in this document can be used to detect delaminations. Many have been tested on real cases (on site) and have proven their sensitivity to delamination. According to experts, the principal development that is needed



**Fig. 5.8** Investigation of under face of a concrete slab of bridge using passive infrared thermography (Naar, 2005). Lighter shaded zones in the infrared image (right) (up to 14,4°C), correspond to spalled regions

remains progress toward the inverse problem, either for assessing the depth of delamination (ground penetrating radar, or infrared thermography), or thickness. The issue of the exact geometrical limit of delamination can be raised for the infrared thermography, which appears to be the fastest method for the detection and location of damage in concrete.

### 3.1.1 Thermography

Thermal techniques (infrared thermography involving active or passive way) are common techniques used to detect delamination and debonding in concrete. A standard describes the use of passive infrared thermography to detect delamination in concrete bridge decks

*ASTM D4788-03: Test method for detecting delaminations in bridge decks using infrared thermography.*

The main limitation of this technique is the depth of flaws: when delaminations are too deep inside, thermography is not effective at detecting delaminations. For instance, the domain considered in the standard is concrete deck with concrete overlay as thick as 10cm:

One concern regarding this technique is that the thermal image shows only a surface view. The location of the subsurface flaw can only be localized in two dimensions, Fig. 5.8. The resolution of the measurements is related to the number of pixel per image, and depends on the distance between the camera and the investigated surface. The depth of the defect (i.e. the third dimension) requires locating the true position, which is unknown.

A second concern is the temperature contrasts: measurement conditions have to be convenient to flaw to be detected. It depends on the resolution and accuracy of scanner used and also on temperature contrasts. The structure must be warm enough to radiate heat in an enough wide band for the scanner to detect. (Alt 1996). The aim of any thermographic investigations is to detect hidden flaw (Fig. 5.8), and there is



no result obtained from inversion (depth of bond...). Generally, the required information is only relative, and no calibration is needed.

Generally the camera accuracy is about  $0.08 - 0.1^{\circ}\text{C}$ . Authors consider that the critical temperature difference between sound and damaged areas should be approximately  $0.2 - 0.3\text{ C}$  to allow detection (Clark *et al.*, 2003). This difference between sensors and true measurements is due to the external influences. Attempting to limit these, numerous considerations have to be taken into account prior to investigations (ASTM D4788-03): range in external temperature, range for wind, specific process to avoid shade on the investigated surface (i.e. drying the zone 24h prior to test), etc.

Operators have also a significant effect: the standard also reports that tests performed with several operators on the same structures, materials, and conditions lead to a variability range of 5% (ASTM D4788-03).

Work conducted on active thermography allowed determining a threshold for flaw detection. The results can be extended to passive thermography. It is given that to be detected, a defect must be closer to the surface than twice its diameter (Maldague, 1990). This is related to the equation:

$$t \approx (z^2 / a) \text{ and } PC \approx (l / z^3)$$

where  $t$  is the observation time,  $z$  the depth of delamination, and  $PC$  the contrast loss; and with  $a$  the thermal diffusivity ( $\text{m}^2 \cdot \text{s}^{-1}$ )  $= k/cp$ , and  $k$  the thermal conductivity ( $\text{W} \cdot \text{m}^{-1} \cdot \text{K}^{-1}$ ),  $c$  the specific heat ( $\text{J} \cdot \text{kg}^{-1} \cdot \text{K}^{-1}$ ),  $p$  the density.

In conclusion, the technique is easy to use, easy to read (result is an image depicting surface temperature), allows large surface to be investigated in small periods of time, and is contactless. The main limitations are the cost of the camera, and the fact that, with passive measurements, data inversion cannot be performed to provide results with depth. Furthermore, environmental conditions have great effects on heating process and on measurements. For example, a long-term investigation may be carried out during sunny days followed by raining days. It has also been shown that wind can influence the temperatures that are recorded.

### 3.1.2 Mechanical wave techniques

Measurements of concrete properties by mechanical wave techniques encompass a broad range of methods. Some of them are already well-known and broadly applied for the characterization of interface and debonding: pulse echo, impact echo, impact hammer, SASW and chain drag.

#### Ultrasonic pulse (US)

The method called pulse velocity (UPV) method consists in measuring the time of flight of an ultrasonic wave pulse between two transducers. Most commonly, this method is set up with a direct transducer arrangement, where both sides of structural



element are accessible. The increase of time can be a reliable indication of an internal defect (e.g. debonding) along the wave path in the concrete. Several standards (listed below) exist for the assessment of concrete with pulse velocity, but the detection of internal defect detection has not been standardized yet:

*EN 12504-4, Determination of ultrasonic pulse velocity, testing concrete- Part4, 14p.*

*ASTM C597: Test method of pulse velocity through concrete*

*BS1881, part 203-1986: Recommendation for the measurement of velocity of ultrasonic pulse in concrete.*

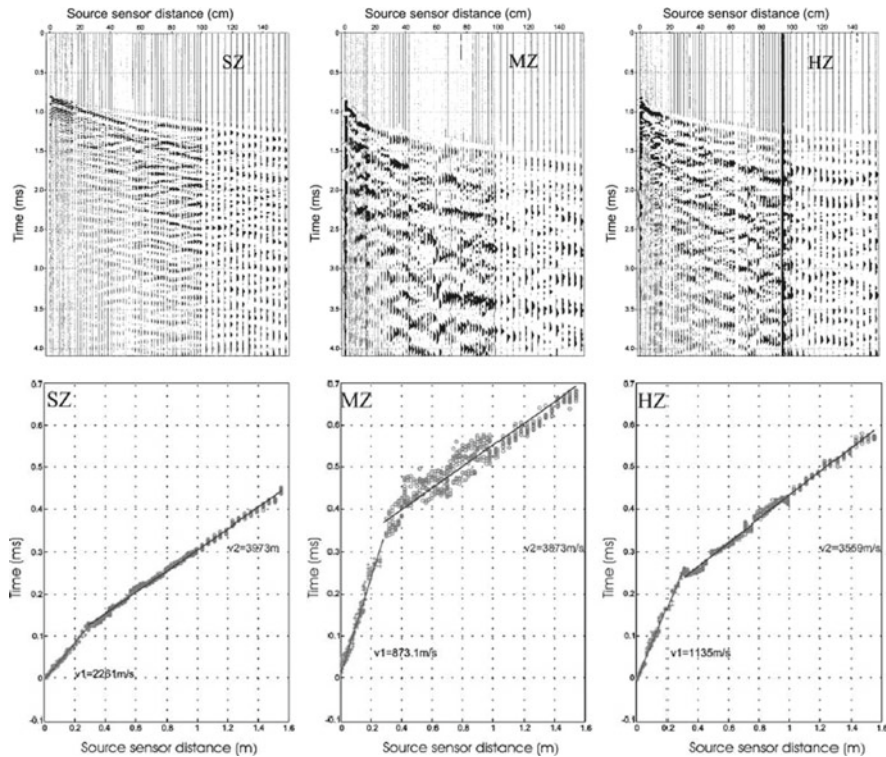
When an ultrasonic signal is sent, reflected and collected from a single surface, the technique is called Ultra Pulse Echo (UPE). If one measures the reflected signal energy, then it is also possible to estimate the depth of the interface or the flaw. Another approach, coming from geophysical fields, monitors multiple wave pulses reflected from the interface: the time of flight values for different offsets are measured. The waves refracted on interfaces can be used to assess the depths of bounded interfaces when the wave velocity increases with depth. This approach has been used on fire damaged structures, for instance (Abraham and Dérobert, 2003). Soundings that were performed on several parts of a tunnel allowed distinguishing three alteration levels and assessing the thickness of concrete layers. The sound zone (SZ) was studied as the reference for further comparison. A moderately damaged zone (MZ) and a heavily deteriorated zone (HV) are presented in Fig. 5.9. Results shows that MZ is surprisingly more damaged than HZ in term of thickness of the delaminated layer (13 cm in MZ instead of 9cm in the HZ), as well as in terms of residual properties of surface concrete (wave velocity is 2260 in the sound zone, 870 in the MZ, and 1130 in the HZ).

Both resolution and investigation depth depend on the generated frequencies: in concrete, classical frequencies are 50-200 kHz in pulse echo mode, so the investigation depths are about 10-50 cm and the resolution is about few centimeters. Higher frequencies lead to higher resolution, but reduce the investigated depth due to wave diffusion on the aggregates and energy attenuation. It must be pointed out that the surface of the flaw is detected, not the whole body.

### Impact echo (IE)

The method essentially is a spectral analysis of local vibration response of a structure. Fig. 5.10 presents recorded data (time domain plot) and processed results (frequency domain plot) allowing the interpretation: The technique is used either to detect delamination or debonding by comparison of measurements made on solid concrete, or to calculate the interface depth from the main frequency peak. In the second case, the accuracy of the technique is partly associated with the calibration of the compression wave velocity (the P-wave),

*ASTM-C1383: Test method for measuring P-wave speed and thickness of concrete plates using the impact-echo method.*



**Fig. 5.9** Recorded seismograms and time versus offset plots on fired concrete tunnel wall (Abraham and Dérobert, 2003)

The depth of a defect is approximated from the impact-echo resonance frequency according to the relation  $d \approx v/2f$  with  $d$  the defect depth,  $v$  the compression wave velocity (P-wave), and  $f$  the main peak of frequency spectrum. Note that this formula is appropriate only if the impact-echo thickness stretch mode of vibration is excited by the testing set-up. This formula is not appropriate if flexural modes of vibration are set up, which are normally associated with debonds close to the surface or with large areal extent.

Based on an analytical and experimental study, the size of the smallest detectable flaw can be defined by its lateral dimensions (for a planar crack or void) exceeding 1/3 of its depth (Sansalone and Street, 1997). The influence of the bond quality has also been studied, numerically and experimentally. Results are that IE can be used only to detect areas where interfaces are partially debonded or are about to debond (tensile strength to be negligible). The quality of debonding (delamination, interface with loose of particles, micro cracks...) does not significantly affect the results (Lin *et al.*, 1996). The unbonded fraction at the interface affects IE response as follows (Lin and Sansalone, 1996): the depth of interface with zero unbonded fractions cannot be determined; unbonded fraction up to 20% enables measuring a significant

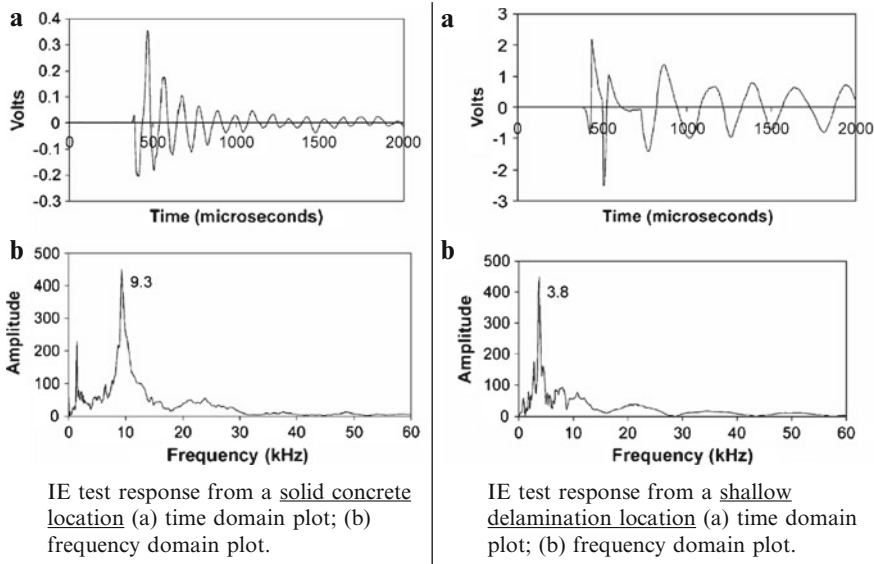


Fig. 5.10 Impact Echo response (Scott et al., 2003)

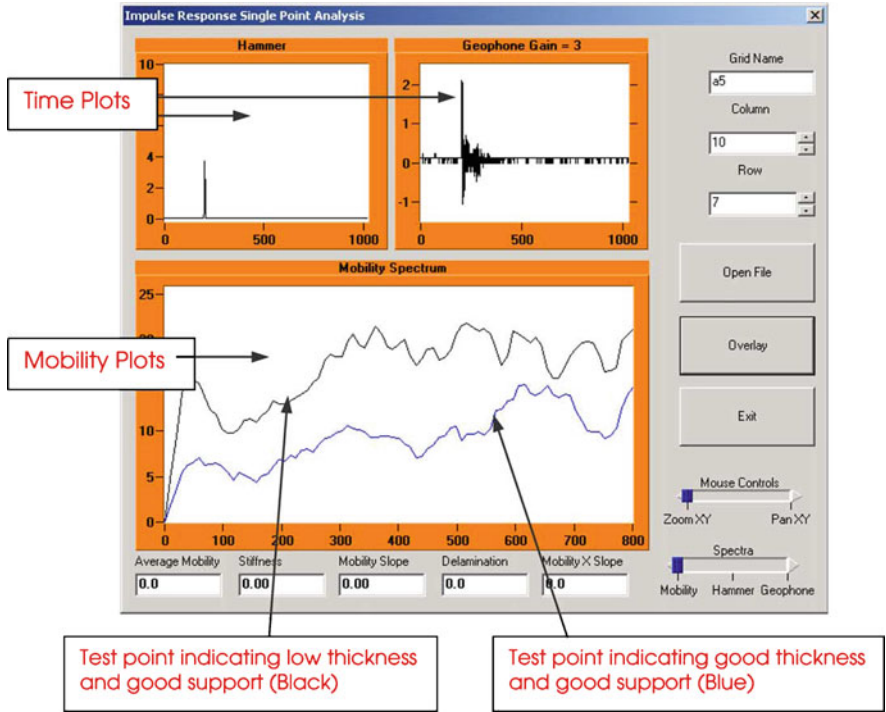
echo peak (which amplitude increases with unbonded fraction); unbonded fraction up to 80% responds similar to a crack.

Error in thickness is mainly linked to the error made on the wave velocity determination. Considering various measurement conditions (frequency, surface roughness...) errors are less than 4% if measurement process is adapted (Sansalone et al., 1997).

Tinkey et al (2007, 2008) and Olson (2010) reported on developments in impact echo scanning for more rapid testing and imaging of internal flaws such as voids, cracking, delamination, etc.. Studies were conducted on bridge concrete walls with a hand held impact echo scanner for post-tensioned ducts and on bridge decks with a bridge deck impact echo scanner, respectively.

Impulse response test method

The impulse-response uses a low-strain impact produced by an instrumented rubber-tipped hammer in order to generate local vibration resonances through the investigated element. The impact causes the element to move (vibration in the bending mode for delamination and interface parallel to the surface). A transducer placed next to the impact point measures the amplitude of the dynamic response. Normally, the transducer is a geophone type, which provides surface velocity as an output parameter. The hammer load cell and the velocity transducer data are used together in the frequency domain. Velocity divided by the force leads to the “mobility” as a function of frequency.



**Fig. 5.11** Typical output of impulse response test. The mobility plot (in m/s/N) in function of the frequency (in Hz) allow to differentiate sound zone from altered zones (Davis et al., 2005)

The technique, which has been adapted from pile integrity testing, can be used on structures to detect voids under lining, debonding of claddings, and delaminations. The mobility versus frequency curve is drawn, yielding the dynamic stiffness and the mobility range, for the tested element (Fig. 5.11). Parameters extracted are:

- the dynamic stiffness (the curve slope for low frequency),
- the frequency interval between the peaks, mainly function of the thickness of the tested element;
- the first peak mobility (for low frequency) / average mobility ratio, also called void ratio, which is the parameter used to detect delaminations.

Davis et al. (2005) (Fig. 5.11), presented two case studies where impact response has been used to detect and localise void behind a concrete lining. Mobility study allows characterising the loss of support beneath the lining: the ratio of the amplitude of the low frequency peak (below 100Hz) to the average mobility of the slab (assessed for frequency in the range 100 to 800Hz), increase in case of void. The examination of the stiffness is also used to detect delamination: increase of dynamic stiffness traducing delamination.

A similar approach, based on the analysis of acceleration of the tested surface excited by a soft tipped hammer, was reported by Sangiorgi et al. (2003). The

authors studied the response of impact hammer tests on full-scale field trials. The tests were performed for various qualities of bonds between concrete layers. The objective was to evaluate the bond between asphalt layers in a road pavement with a fractal analysis of the signal. It can be seen from the response of the bonded system that the acceleration is heavily damped. Conversely, the response of the debonded system shows high frequency vibrations in the measured acceleration response and the damping is lower than on bounded system. This is due to vibrations induced in the surfacing layer because it is not bonded to the layer below.

### Surface waves

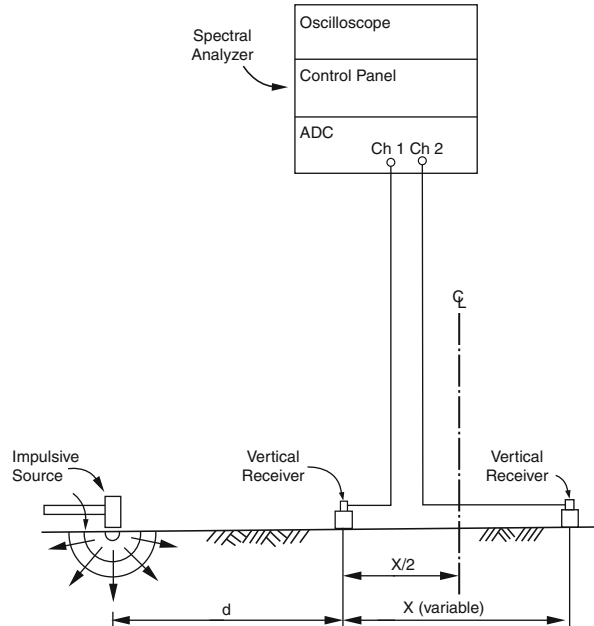
Nazarian (1984) has adapted the surface wave technique from the field of geology to the field of concrete structures. The technique called Spectral Analysis of Surface Waves (SASW), allows studying the surface waves velocity as function of wavelength. The principle is to create an impact on the surface with a hammer and monitor, in time domain, the surface wave velocities with two receivers (Fig. 5.12). Surface wave velocity varies with frequency in a layered system if the velocity in each layer is different. This frequency dependence of velocity is termed *dispersion*. The plot of surface wave velocity versus wavelength is called a dispersion curve. The material property variations with depth can be estimated from an inverse analysis of the dispersion curves. In fact, SASW is not a suitable tool for studying delaminated concrete. In case of delamination wave amplitudes are higher than those measured on sound concrete, and the spectral analysis is not needed for results interpretation. SASW is adequate for studying speed variations across successive layers in terms of depths. SASW then could be used for debonding case with partial contact. This approach has been used to assess bond quality where concrete layers can be found (Sack and Olson, 1995).

This technique is suitable for shallow investigation. The obtained results depend on the spacing of the sensors, the size and the mass of the hammer used to create the impact (which governs the energy content and the impact duration; so it partially monitors the depth of investigation).

SASW method can predict layering (by stiffness variation) within 10 % but the boundary between different layers with similar stiffness cannot be distinguished by SASW (Nazarian, 1984). Studies can be found on the use of SASW for delamination detection in concrete structures. One of them reports the case of a dam exposed to freeze-thaw, and presenting shallow delaminations (Sack and Olson, 1995). The results show the distinction between two layers. The first is the thin layer of shotcrete, characterised by a high waves speed. This surface layer on the outside is over the second layer, deeper, constituted by damaged concrete. This deeper material is characterised by slower waves speed. The condition predicted by the SASW method agreed with the repair history and coring data.

The calculated dispersion curves may show significant fluctuations due to different surface waves modes participating in the signal (Aki *et al.*, 1980)(Tokimatsu *et al.*, 1992)(Karray and Lefebvre, 2000). It breaks the basic assumption of single

**Fig. 5.12** Spectral Analysis of Surface Waves testing configuration (Nazarian, 1984)



mode propagation often implemented in the SASW method, which causes additional complication with this method. The additional modes may cause misleading conclusions. In that case wave-field transforms, as proposed by more advanced methods, such as the FK method (F: frequency, K: wave-number) (Al-Wardany *et al.*, 2009) and MASW (Ryden *et al.* 2004), have been applied to improve these problems associated with SASW. It allows a proper recovering of the dispersion curve required to assess the concrete condition.

### Chain Drag and hammer sounding

This basic technique may be considered as an acoustic sounding. However, it should be considered as a practice rather than a technology. A standard drives the investigation:

*ASTM D4580, Standard practice for measuring delaminations in concrete bridge decks by sounding.*

This procedure basically consists in dragging a chain or tapping a metal rod or hammer over the bridge deck surface. The detection of delaminations is accomplished by the operator noting dull or hollow sounds. This technique is widely used in North America, mainly for corrosion induced delamination on concrete bridge decks. This is a very low cost technique, allowing extensive application. The depth of the defect cannot be determined unless a core sample is removed. Chain drag is

a tool highly adapted to detect progressed delamination but its ability seems rather limited in detection of initial delaminations (Gucunski *et al.*, 2009<sup>2</sup>).

Inversion of the results cannot be done with this technique. Delaminated areas are marked off investigated surface. An approximate percentage of the total area delamination is then determined (Alt and Megger, 1996).

A study by Scott *et al.* (2003) highlighted the high variability associated with this technique: the delamination percentage estimate in surface varied between 2 to 69% (The variability is strongly related to operator experience and skills. The authors recommend improving the training of inspectors and suggest to inspectors to accurately document their results.

Some developments have been tested with approach similar to Chain Drag. Several investigators report hammer tapping investigations performed with a hammering trolley (Felicetti, 2008, Popovics *et al.*, 2009). A wheeled system pilots the impacts, blows are recorded by microphone connected to a lap top via an audio-card. The data processing, which is very similar to the impact echo approach, allows detecting the frequency peaks (i.e. the sounds) corresponding to altered and non altered slabs. Interpretation of data is linked to thresholds in the frequency domain. Recording and automatic data treatment decrease the importance of operators, evoked for classical chain drag.

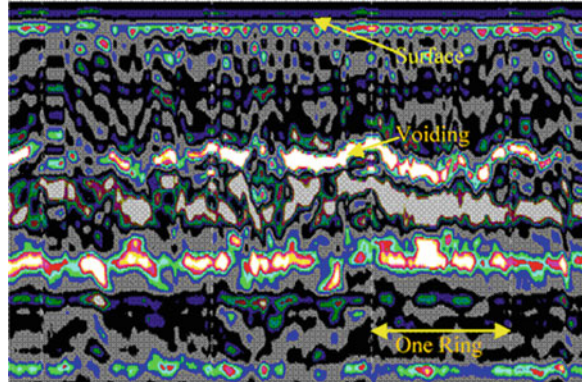
### 3.1.3 Ground Penetrating Radar (GPR)

The sensitiveness of radar for detecting delamination or debond strongly depends on the antenna frequency. When a beam of microwave energy is directed at a reinforced concrete slab, a portion of the energy is reflected at the surface of the concrete, and the remaining energy is refracted across the interface. The polarity of the reflected signal differs whether the delamination is empty or filled with water (due the permittivity contrast relatively to concrete value). When the concrete slab is delaminated, usually at the level of the top mat of reinforcement, there is an additional reflection from the deteriorated section. This additional reflection is as an indicator of the presence of a delamination in the concrete slab interface.

Radar is more adapted to detect large voids than delaminations (Fig. 5.13). Scott *et al.* (2003) tested radar on site (antenna of 1.5 and 2.4 GHz) and did not obtain consistent response to delamination. According to them, this technology may mature to allow delaminations to be detected. With a 1.5 GHz antenna adapted to concrete, the wavelength is about 6 cm, so the resolution is 3cm (about half the wavelength). Therefore, with this frequency, radar could detect delamination of few millimeters thick for strong electromagnetic properties contrast between concrete and the flaw. Radar could also detect delaminations and interfaces by their indirect effects on local properties when it is associated with a local moisture increase for instance. The concrete properties can be different close to the flaw, than further, modifying the electromagnetic wave propagation (in terms of attenuation or speed). The flaw can then be indirectly detected. An example has been given by Barnes *et al* (2008) where authors used reflected amplitude provided by radar to map moistened part of a bridge, in relation with corrosion induced delamination.



**Fig. 5.13** Results of GPR investigation to characterize voids behind precast elements after grout injection (Davis *et al.*, 2005)



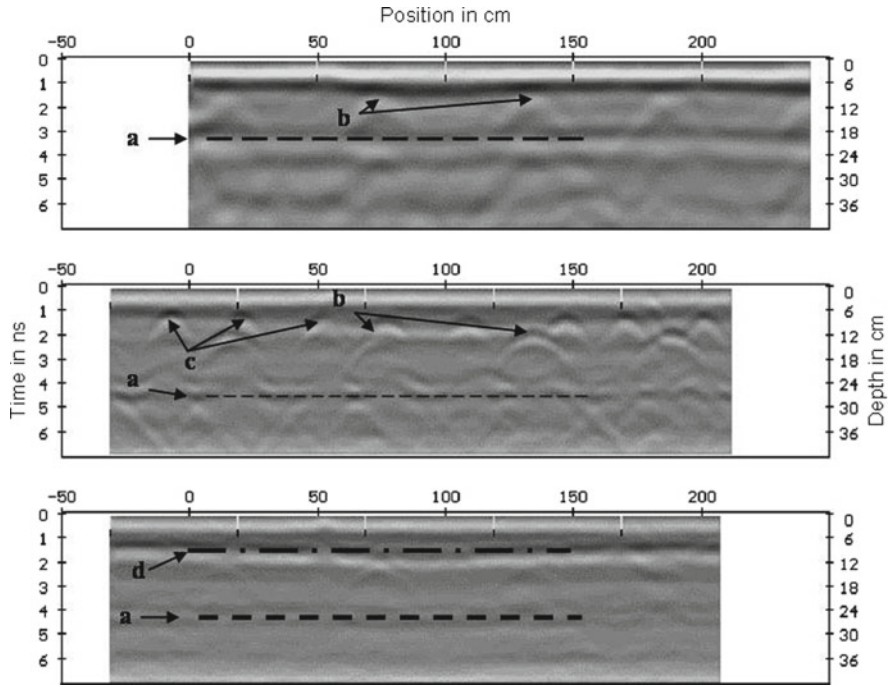
As many techniques based on wave propagations the main limit of GPR is the relation between the size of flaw and its depth; in other words, the measured resolution vs the depth of investigation. It has been shown that, in case of delaminated repaired areas at a prestressed concrete bridge, a clear reflection could be detected. Figure 5.14 displays three radargrams recorded along the same trace with a length of about 2.5 m on top of a prestressed concrete bridge. These radargrams were recorded with the 900 MHz antenna (top) and in two polarisations of the 1.5 GHz antenna (middle and bottom). The backside reflection, the position of the reinforcing bars as well as four tendon ducts can be easily detected. In the bottom radargram, where the polarisation of the electric field of the antenna was oriented perpendicular to the rebars, instead of the rebars only a continuous reflection band is visible. This reflection band could be related to a delamination, which was confirmed after opening of the area in a destructive way.

Like acoustical techniques, GPR is based on wave propagation and its power can be limited on strong interfaces: In general, it can only detect one defect at any given location. As the electromagnetic pulse travels through the concrete element and strikes an anomaly, most of the pulse energy is reflected back to the receiver. Only a small amount of electromagnetic energy is transmitted through the defect. For instance, if a pulse struck a de-bonded area, the amount of energy passing through the de-bonded area would be so small that a delamination directly under the de-bonded area would not be likely to be found. The energy reflected from the second defect, the delamination, would probably be too small to be detected or positively identified as coming from a delamination, as presented by Alt and Megger (1996). Finally, it is possible to detect the interface, but the technique does not allow sharp characterization (Colla *et al.*, 2002).

The response of radar in relation to several kinds of interface on a masonry wall is shown in the table of Fig. 5.15 – (Maierhofer *et al.*, 2001).

Clemena (2004) reported two studies conducted on radar accuracy to detect delamination in bridge decks ((Cantor *et al.*, 1982) and (Clemena, 1983)). In the first study, 90% of the area that was predicted by radar to be distressed was confirmed as such by coring. 91% of the area that was predicted to be sound concrete was also confirmed. The second study involved a comparison of radar surveys performed on several bridge





**Fig. 5.14** Radargrams of a trace recorded with different antennas: **Top: 900 MHz antenna**, polarisation perpendicular to the rebars. The backside reflection (a) as well as the tendon ducts (b) are displayed; **Middle: 1.5 GHz antenna**, polarisation parallel to the rebars. The backside reflection (a), the tendon ducts (b) and rebars (c) are visible. **Bottom: 1.5 GHz antenna**, polarisation perpendicular to the rebars. Only the reflection from the delamination is visible (d)

Results of the investigations of the different physical models

Problem	Use of radar	Accuracy and limits
Determination of moisture content	Measurement of travel time of the backside reflection and determination of permittivity, comparison to calibration curves	Between 1 and 5 vol% depending on the absolute value
Determination of moisture distribution	Measurement of travel time	No absolute values
Detection of joints in masonry made of full bricks	Possible with the 1.5 GHz antenna, unfilled joints can be detected as small hyperbolas	Low moisture and salt content is required
Detection of joints in masonry made of hollow bricks	Polarisation of the electric field of the antenna must be parallel to the joints	Low moisture and salt content is required
Control of grouting of unfilled joints	Grouting can be investigated by comparing the radargrams of empty and grouted joints	It is not possible to obtain quantitative data
Detection of layers of different materials	From the travel time, intensity and phase of reflected signals information can be gained about the permittivity of the different layers	It is not possible to distinguish between air, dry and wet mineral wool (permittivity of dry and wet mineral wool is too low)
Detection of large air voids	Large air voids in masonry can be detected easily from time slices	The minimum air voids, which was detected, had a size of 800 cm <sup>3</sup> . No smaller voids were investigated

**Fig. 5.15** Evaluation of radar capabilities relative to several interfaces (Maierhofer *et al.* 2001)

decks prior to the removal of overlays. It was found that, on an average, radar detected only 80% of the existing concrete delamination, while falsely identifying 8% of the area tested as delaminated. In these studies, radar failed to locate some of the delaminated areas, especially those that were only 1 ft (0.3 m) wide or less; partly because the strong reflections from the rebars tended to mask reflections from delaminations, which would be relatively weak in dry concrete. Barnes et al (2008) report further improvements in the identification of delamination and corrosion with GPR on decks by considering the depth of reinforcement and signal attenuation thresholds.

## 3.2 *Special techniques*

### 3.2.1 **Electrical resistivity (ER)**

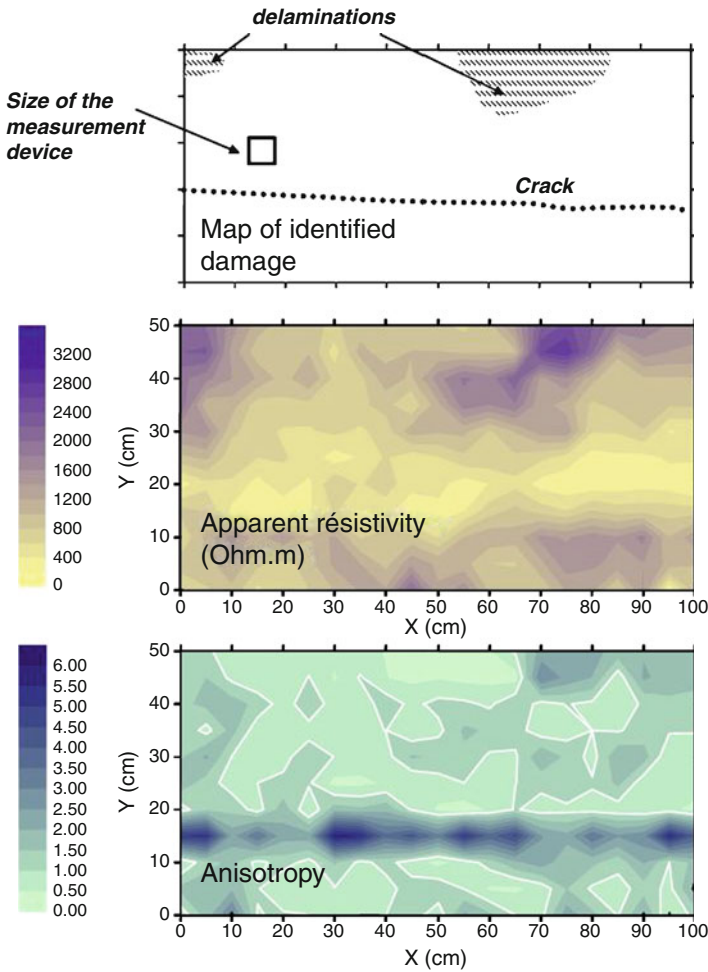
The sensitivity of ER to interface is linked to the disturbance of the investigated volume. In the case of interface (between two materials with different resistivities) or void, the electrical current circulates differently than for a homogeneous material. Figure 5.16 shows an example of the electrical response on a damaged slab on site: one can see that in this case, cracks and delamination can be detected since the resistivity increases over the delamination.). The final interpretation and the identification of delamination and cracks are based on the analysis of electrical anisotropy (Lataste *et al.*, 2003(2)).

Alt (1996) reported another case involving the detection of delamination below asphalt layer on a bridge. The measurement was performed according to ASTM D3633, allowing the characterization of the imperviousness of the membrane to water. It was not possible with this method to diagnose concrete, but the conclusion on the data interpretation was interesting: the evaluation is quite subjective, some criteria (based on resistivity values) are proposed but the suggested solution seemed to be oriented on a monitoring of resistivity according to the variations of environmental conditions.

The interpretation of resistivity variations combined with the study of electrical anisotropy variation allows detecting and locating the delamination. According to the size of the measurement device, it is possible to modify the investigated volume, then to investigate concrete to a depth of about 5-6 cm. This increase is associated with a decrease of the resolution.

The electrical resistivity increases due to an interface can be estimated according to the methodology developed in Lataste *et al.* (2003(1)) on edges influence on resistivity measurements. Indeed, if one considers delamination as a particular edge, this approach gives an optimistic range of the resistivity ability. An ideal delamination (perfect, without contact between wall filled with air, and infinitely laterally extended); and considering a noise level about 10% on resistivity measurements (classical mean values on site), can be detected and identified if:

$$z/a < 1;$$



**Fig. 5.16** Electrical resistivity used to detect and identify a delaminated zone in a concrete slab (Lataste *et al.* 2003(2))

with  $z$  the delamination depth from the surface, and  $a$  the size of device (i.e. the distance between electrodes for a four probes square device).

This threshold is not a function of the resistivity, but depends on the resistivity contrast between concrete and interface. It considers only a resistive interface. For conductive interfaces, the depth of investigation increases, but the effect on the measured apparent resistivity is less important. The threshold of  $z/a < 1$  is a reliable order of magnitude of the lateral extension, for an interface with at least  $a$ .

### 3.2.2 Impulse thermography (IT)

This technique presents the same advantages and limitations than passive infrared thermography. The difference lies mainly on the thermal solicitation rather than data processing. The need to heat the investigated surface leads to practical problems regarding the homogeneity of heating and the heating apparatus (energy supply, investigations speed...). This pulse of energy can be deployed with lamps, flashes, laser beam, and air or water jets. A “warm” or a “cold” stimulation is possible since the important point is the temperature differential that is generated (Maldagues and Marinetti, 1996). The duration of the pulse is variable from  $\mu\text{s}$ ,  $\text{ms}$ , to  $\text{s}$  depending on the thickness of material to be probed and its thermal properties. Impulse thermography allows results inversion, to go farer in flaw characterization than with passive thermography.

The investigation depth increases significantly with impulse thermography, and the inversion of results is possible. Maierhofer et al. (2002) combined experimental and numerical approaches considering voids up to 10 cm in depth. The heating time of 10 minutes allow recording temperature contrasts, which were variable during the cooling time (over 60 minutes). The value of heating time and the numerical approach enabled the determination of the depth (concrete cover) of the single defect.

## 4 Global strategy of approach towards diagnosis

The large range of ND techniques allows engineers coping with the issue of structural diagnosis. Whatever the flaw that is looked for, several techniques are more or less sensitive to its “signature”. Engineers have to choose the best technique with regards the context and the alteration. Then, they have to use several methods in combinative manners in order to optimize the investigation, either in terms of efficiency, or in terms of accuracy.

### 4.1 Complementary techniques

Taking account of the broad range of acoustic methods used for de-bonding evaluation, the complimentary aspects of the various techniques (in term of size of the object looked for) will be discussed below.

Section 3.1.2 addresses the mechanical wave techniques, covering the methods based on the analysis of the vibration induced by a mechanical impulse, whatever the source (hammer, steel ball, piezo actuator, solenoid impactor, chain, toothed wheel, etc). Five mechanical wave techniques have been cited in the present chapter, namely ultrasonic pulse echo, impact echo, impulse response, surface waves and the chain drag.

In general, three aspects can be recognized for classifying the techniques.

- the type of excitation;
- the physical principle;
- the data processing technique.

The present classification is based on the way that the data are processed for interpretation (frequency domain analysis for the impact echo, time domain analysis for the pulse echo) and also by the manner that the wave motion is excited in the structure.

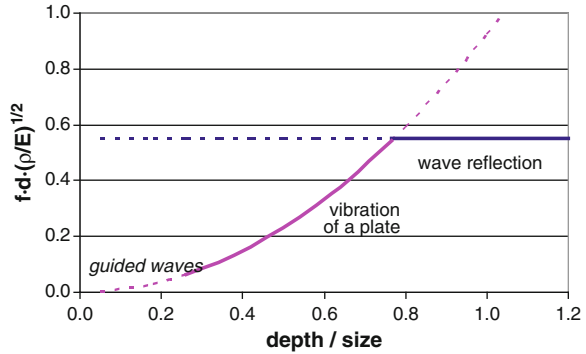
Regarding the type of excitation, these may be categorized on the basis of the frequency range and the nature of the pulses that are generated.

The classification based on the physical principle appears to be more robust: the way to implement a technique may change but the principle remains. The problem is to distinguish the principles that are being handled. Three possible schemes are proposed, depicting what happens in a structure after a mechanical pulse has been exerted.

- a) Propagation of mechanical waves through the structure: The wave (pressure or shear) is partly reflected and refracted by the interface and can be detected at the excitation point after a time delay (pulse velocity and pulse echo). Besides the interaction with the defect, the propagation of the waves is not influenced by the defect and the velocity can be assumed as a property of the investigated material.
- b) Propagation of mechanical waves within the delaminated plate: if the plate is delaminated (i.e. the surface and the top of the delamination are stress free) the dispersion curves corresponding to surface waves of the bounded media will switch to Lamb wave dispersion curves of the corresponding delaminated plate (guided wave from plates). Impact-echo and impulse response methods fall under this category, although it is possible to interpret the impact-echo vibrational response using a guided wave model (Gibson and Popovics 2005): impact echo resonance frequency corresponds to a peculiar resonance of the first symmetric Lamb wave mode where energy does not travel (zero group velocity). Specifically for the case of impact-echo, the modes of vibration that are mainly set up depend on the geometry of the debond. When the extension size of the debond is smaller than the depth, the impact-echo stretch mode is strongly excited, and the formula described in section 3.1.2 may be applied.
- c) Structural vibration of a plate: if the size of the defect is comparable or larger to its depth, the mechanical impulse activates the dynamic response of the concrete plate outlined by the delamination itself. The frequencies of the vibration modes of this plate are governed by the root of the ratio of the bending stiffness ( $\sim \text{depth}^3$ ) on the mass per unit area ( $\sim \text{depth}$ ). Hence, the frequencies are proportional to the delamination depth, and these frequency values will be significantly lower than the impact-echo stretch mode values (the impact echo rule where  $f \sim 1/\text{depth}$ ). Furthermore, there are no closed-form equations to relate frequency to depth for the flexural case. In this latter case, the chain drag method does work, and ultrasonic pulse echo may be applied to estimate depth.

Providing a criterion for determining what physical principle governs the response of the investigated member would be of considerable help in determining the most promising technique to be used for a specific problem.

**Fig. 5.17** Response of acoustical techniques in function of geometrical parameters of the fault



As a first tentative to separate the ranges pertaining to different principles the expected vibration frequencies of the impact echo (principle b) and of the vibrating plate (principle c) are plotted on the same graph (Fig. 5.17). To be more general, the frequency  $f$  is expressed in the dimensionless form:  $f \cdot d / (E / \rho)^{1/2}$ . This form is proportional to the depth of the delamination divided by a wavelength ( $d / \lambda$ ), delaminated concrete cannot be considered as infinitely extended (relatively to wavelength). Indeed, in this case  $V = (E / \rho)^{1/2}$ ; then  $\lambda = (E/\rho)^{1/2} / f$ . Where  $d$  is the depth of the interface,  $E$  is the Young modulus,  $\rho$  is the material density,  $f$  is the signal frequency,  $\lambda$  is the wave length, and  $V$  is the wave velocity.

In this form the dimensionless frequency of the impact echo is a constant for any depths.

The shape of the defect is expressed by the ratio of the depth on the size (intended as the diameter of a delaminated disc) and the vibration frequency of the plate is a parabolic function of this ratio.

Figure 5.17 shows that, for shallow delaminations (depth < 0.75 size), the mechanism based on the plate vibration yields the lowest frequency and, probably, the strongest signal. Nonetheless, a smooth transition between both ranges is expected. This graph should also be adapted for guided waves, but no work has been done yet on this topic.

## 4.2 Use for better efficiency

Infrared thermography, impulse thermography and ground penetrating radar (GPR) appear to be techniques that are sensitive to both void and bond in concrete, and allow a quick investigation of large surfaces. Other methods (acoustic: ultrasonic pulse, impact echo) are efficient for a sharp characterization of geometrical parameters (depth, limits...). A combination of these two different types of technique can be used to optimize the investigation time.

A classical methodology consists in combining a first technique to locate potential damages in a short period of time, and to use a second more time consuming) to validate or to define more accurately its parameters. Some references in literature present case studies with such approach:

1. Abraham *et al.* (2003) considered a fire damaged tunnel, and characterized layers and delamination of the tunnel. GPR and ultrasonic refraction measurements were performed. Damages were a multilayer structure of material. Conclusions were oriented on the first detection of damage with radar combined with sharp characterization with ultrasonic pulse (more time consuming method).
2. Scott *et al.* (2003) tested GPR and impact echo on corrosion induced delamination on a bridge. Main results were: impact echo is a time consuming method which (in this case) was not always conclusive; GPR is faster and easier, but not accurate enough for detection.
3. Meola *et al.* (2005) compared the results of infrared thermography, ultrasonic pulse and electrical resistivity on a masonry element in laboratory. Cork diskettes and plastic bags were incorporated in the masonry. They were manufactured of three different diameters,  $d = 40, 60$  and  $100$  mm; the thickness was approximately 1 mm for cork diskettes and 2 mm for plastic bags. A plaster layer of thickness varying from 10 to 55 mm recovered the wall. The conclusion was that infrared thermography was the faster and allowed efficient detection and location of delamination, ultrasonic pulse was more time consuming but allowed the detection of deeper delaminations, and electrical resistivity was not really efficient for delamination (sensitivity to micro-cracking, porosity...). Limitations and advantages were then considered with regards to measurement cadence and investigation depth.

### 4.3 Use for more information

Methods sensitivity to flaws is influenced by material conditions (moisture, chloride ingress...). The quality of the interpretation can be then limited by external parameters, who can biases measurement.. So the interest of investigation may appear restricted if the information obtained from measurement is not sufficiently accurate or sharp (in terms of depth of interface for instance, or geometry, or saturation degree). Repeated investigations on a same body with various non destructive techniques can be a way to obtain various informations due to sensitivity of the different techniques. The interest would be to have shaper diagnosis. Generally, such approach (i.e. investigation with several methods on a same structure) allows to rank techniques regarding their reliability, in function of damages, and for given conditions.

For investigations the use of several techniques aims at assessment of complementary information (when the different information contributes to complete results to improve interpretation). Redundant information obtained with different techniques is generally less interesting.

Some examples showing comparison of techniques on structures or test samples regarding the interfaces or delamination question are reported in literature:

1. Gucunski *et al.* (2010) assessed bridge decks subjected to induced corrosion delamination. The use of resistivity is associated with half-cell potential for corrosion assessment. Concerning delamination, they compared results from radar and impact echo: GPR provided information about deterioration of concrete and



likelihood of delamination; impact echo enabled detection and characterization of delamination deck.

2. Drdacky *et al.* investigated plaster delamination in laboratory with ultrasound, impact echo, impulse thermography. They compare results obtained with each technique, and their sensitivity on the test element.
3. Naar *et al.* (2005<sup>1</sup>) use on site electrical resistivity and infrared thermography to locate delaminations and cracks on a bridge. The use of both techniques allows distinguishing both damages, but no quantification could have been done.
4. Uomoto (2003) tested the sensitivity of NDT techniques (infrared thermography, ultrasonic pulse, impact echo) to detect voids in an experimental slab. The accuracy of each techniques was assessed and compared with regards to their advantages and limitations.
5. Maierhofer *et al.* (1998) worked on brickwork on site and appraised the sensitivity of GPR and ultrasonic pulse. Results were compared. No evident combination could have been outlined in this case.
6. Karastathis *et al.* (2002) used different NDT to assess the bond in a dam. Techniques were Acoustic method (ultrasonic pulse refraction), electrical resistivity and GPR and measurements were performed on a tunnel in the dam. They allowed detecting defects (as honey combing due to water flows).. GPR allowed rapid detection of questionable zones, ultrasonic pulse allowed sharp description of them, and electrical resistivity was chosen to describe moistening condition of materials. The complementarities of three techniques lead to a diagnosis of the whole structure.

The above cases indicated that measurements on test samples are generally a procedure to properly assess performance of techniques. The complete knowledge of the material and flaw characteristics (its depth, geometry, location ...) allows building evaluation criteria to compare ND methods. It is also another way to identify promising combination from less interesting ones.

#### **4.4 Use for better reliability**

Techniques response to an alteration is function of the characteristics of the flaw (e.g. detection is impossible under the investigation depth of the technique). These ability ranges for a technique, can vary with the material condition. Considering that the material conditions can change along a structure, the technique performance can change along this profile. So the risk of non-detection of an alteration or, inversely, the risk of a false alert with only one technique is high. The use of several techniques successively is a way to limit such risks. This approach aims at improving the detection by non-destructive measurement session. The use of several techniques leads to more reliable results because each technique detects something. It also allows rejecting all zones without any detected flaw and suggests further investigation, or sharper analysis, in zones where results were not concordant. To optimize this strategy, the selected technique must be sensitive to uncoupled parameters, and should avoid any redundancy in the results. In other words, from the engineer's



point a view, this approach is interesting only if it limits the risk of misinterpretation. The following studies reports on combination for better reliability:

1. Alt *et al.* (1996), tested GPR (no information concerning frequency) and infrared thermography on a bridge to find delamination and debonding on concrete bridge decks with asphalt concrete overlay and membrane. The authors concluded that both techniques were not certain in finding and identifying subsurface anomalies. Authors wrote about the problem of detection threshold, and of errors in detection. They underlined the important state of deterioration of the bridge to explain the lack of very clear results with GPR and infrared thermography.
2. Colla *et al.* (2002) studied interface between a concrete slab and a sleeper embedded in the concrete slab during construction. The aim was to characterize the bonding condition between sleeper and slab, and to detect and locate voids. They use impact echo, ultrasonic pulse and GPR and concluded that: impact echo was very efficient, ultrasonic pulse was adapted to delimit the extension of defects, GPR was sensitive to defects (GPR distinguished good bonding from weak or no bonding, but cannot made difference between weak and no bonding). Both acoustic techniques lead to similar results in localizing areas of good and bad bonding and delamination.
3. Weil (1998) published a study on a field structure (a stadium dome). The investigation combined infrared thermography for location of delamination and impact echo for validation of first detection. The use of a second technique (impact echo) improved significantly the information obtained with the faster technique (infrared thermography).
4. Barnes *et al.* (2008) combined radar and chain drag to map and estimate accurately the delaminated surface ratio on bridge decks. The study was based on the analysis of the reflection amplitude of the radar signal, compared with chain drag and half-cell potential. It lead to improved efficiency regarding the estimation of the damage on field structures.
5. Gucunski *et al.* (2009<sup>2</sup> and 2010), carried out investigations on bridge deck with radar (2.6Ghz and 1.5Ghz antennas), impact echo, chain drag, ultrasound, completed with half-cell potential, resistivity, as well as coring. They compared all techniques and underlined, that there were some similarities with impact echo and radar (wave attenuation). They concluded on the recognition of the potential benefits of evaluating decks using a complementary radar-impact echo approach.

#### 4.5 Case study

The case study below presents an example of technique combination. This case is not representative of the common approach, due to larger number of analysis done on a bridge, but it presents several techniques adapted to interface characterization by NDT methods (Gilles 2007).

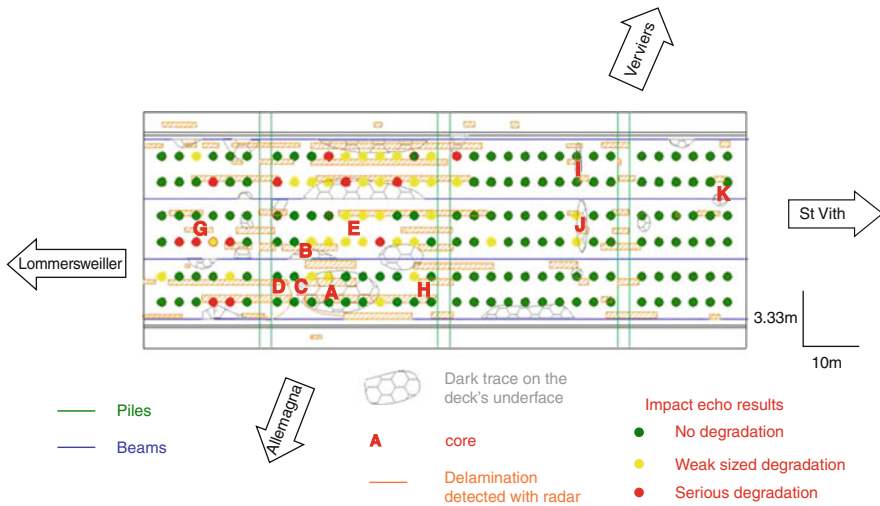
The structure is a reinforced concrete bridge exhibiting delamination related to a highly altered concrete (Fig. 5.18). The characterization of damage was first performed by coring within a selected area. Ultrasonic pulse velocity carried out on



Dark trace under bridge deck

Delamination observed on cores

**Fig. 5.18** Visual detection and destructive study of interfaces on Lommersweiler bridge, Belgium (Gilles, 2004)



**Fig. 5.19** Results of ND investigation on Lommersweiler bridge (Gilles 2004)

cores highlighted horizontal interfaces in the deck. The next step consisted in identifying the damaged zone on the whole structure.

Engineers carried out a visual inspection of external symptoms related to probable degradation, such as dark spots on the surface. They also used radar (1.5 GHz coupled antenna) to record profiles along 1400m in total length. Impact echo measurements were performed along a regular mesh of 1.3m x 3m to obtain 192 measurement points. All these results are represented on the same document as comparison (Fig. 5.19).

The final conclusion of this study indicated a very good correlation between radar and impact echo results, as confirmed by the petrographic examination conducted on cores.

## 5 Benchmark and test site

Tests body and test site are a simple mean to test technique effectiveness and accuracy with regards to controlled parameters.. Numbers of test site are then elaborated relatively to the development of a technique.. So it can be found on several sites, the same kind of “objects” (in term of geometry for instance). This is due to the similar NDT improvements needs, studied by various research teams. This is, finally, very consistent with actual engineers concerns.

Existing test site designed for the detection of interface can be broken in three large groups:

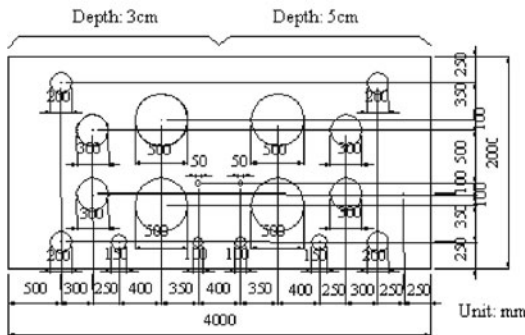
The first group considers the study of interface and delamination. Generally, the flaw is ideal, made by a plastic sheet embedded in concrete in an attempt to simulate a delamination. The irregularity of limits and the variation in its thickness are not taken into account. In this group we can list:

The University of Sherbrooke (Canada) built a concrete slab in 2008 with hidden objects, simulated flaws at various depths (Fig. 5.20). Interfaces (polystyrene sheets of 5mm thick and blocks with 50mm thick) are present, then honey combings (polystyrene bloc with holes simulating heterogeneous void), plastic pipes, and complex shapes. For all, several sizes can be found, and they are at various locations relatively to the reinforcement level.

The BAM (Berlin, Germany) proposed an experimental body, to compare techniques in relation to several disorders. The Large Concrete Slab (LCS), built to study problems in tendon ducts, thickness and geometry variations, and internal



**Fig. 5.20** Test site in Sherbrooke (Canada, Quebec)



Location of defects inside the concrete specimen (Ex. defect depth: 3cm and 5cm)



Concrete slab specimen



Arrangement of defects

**Fig. 5.21** Test slab done for impact acoustic method evaluation (Asano et al., 2003)

elements (gravel pockets), and the concrete elements for investigating voids at various depths and thicknesses Taffe *et al.* 2003. An area with different contact bonding conditions between two concrete layers (15 cm each) is also found. This area consists of five sections (approx. 70 x 70 cm<sup>2</sup>) with two concrete layers.

In the frame of the TC RILEM ON SITE FOR MASONRY, Drdacky *et al.* presented a trials wall to study subsurface defects (as plaster detachment for instance).

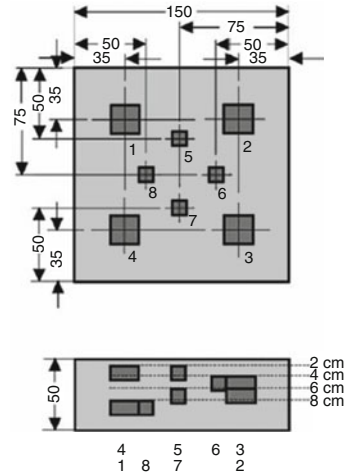
Asano et al. (2003) presented the results of impact acoustic methods, obtained on a test slab specifically made to evaluate reliability of these methods (Fig. 5.21). Thin voids (0.5cm thickness) are disposed with several depths and with various diameters, (leading to various depth/size ratios).

The second group is constituted of test sites where interfaces are not directly simulated but where flaws are quite similar to interfaces. Generally, the simulated flaws present a surface that can be compared to a very strong interface:

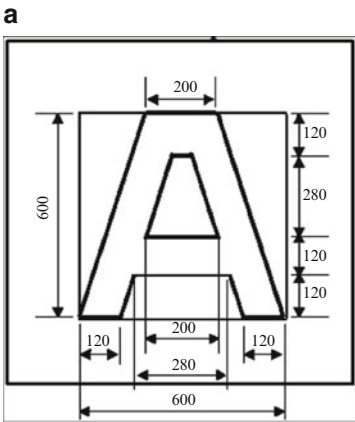
The BAM proposed an experimental concrete body. Voids are simulated with polystyrene blocks of few centimeters in thickness (Fig. 5.22).

Uomoto (2003) worked on a test body presenting voids in the concrete (Fig. 5.23). Several techniques, such as infrared thermography (active and passive way, for a combined interpretation), sonic method, and impact echo were tested in an attempt to compare results of each approach.

In this group we could also list the University of Sherbrooke slab that has been presented above.



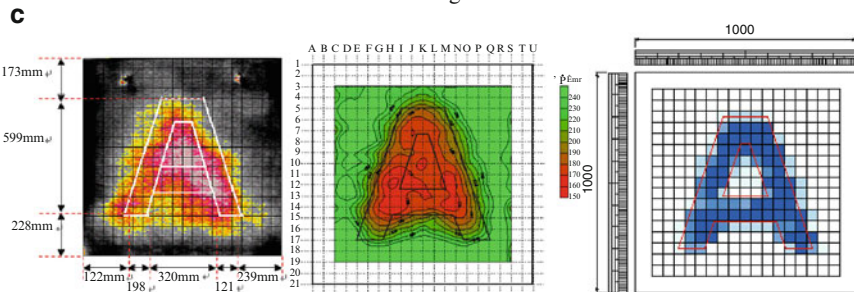
**Fig. 5.22** Concrete test specimen with voids, general view (with apparatus for investigation with impulse thermography) and scheme (Maierhofer et al., 2002)



Detail of a specimen



Apperance of specimen before concrete casting



example of results respectively with thermography (combination of active and passive), ultrasonic, and impact echo

**Fig. 5.23** Experimental element for NDT sensitivity study (Uomoto 2003)



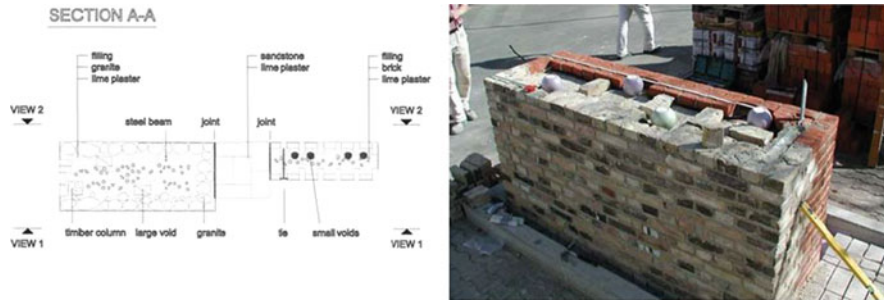


Fig. 5.24 Masonry wall at BAM for NDT sensitivity study (Maierhofer *et al.* 2003)

The third and last group is composed of test site designed for assessment of ND Techniques relatively to interfaces, but elaborated for building materials other than concrete:

LCPC Colibri test site (in Nantes, France) has been designed for development of debonding detection in road pavements. The site allowed testing techniques (impact echo) in a combined way. Results were obtained on the techniques ability in term of accuracy (Simonin *et al.*, 2006).

BAM Masonry wall (Fig. 5.24), hiding several kinds of objects and heterogeneities as voids (in the test specimen simulated by ceramic vases). The structure developed for the European research program “on site for masonry” has been used to test ultrasonic impulse-echo, and impact echo.

Beyond the possibilities of testing new developments, the main interest of tests sites that are specifically devoted to interface is relies on the opportunity of comparing and gauging different techniques. Indeed, as explain above, these sites have been built with regards to a particular issue, or to test any techniques. there are no more general test sites allowing today large and objective comparison between methods. A test site would be the mean to objectively assess the limits of techniques, and to evaluate the new development regarding a common state of the art for all methods. Such site would allow the standardization of techniques but also definition of the technique better methodology for measurements. Finally it would contribute to the training of NDT operators.

Finally, the parameters that should be taken into account on a test site specifically dedicated to interface are:

- Depth and extension of interface, from very close to the surface (few millimeters) to very depth interfaces (more than few decimeters),
- Local delamination and larger debonding (as defined in the first part of this chapter),
- Various thicknesses and partially debonded interface, with different unbonded fractions at the interface,
- Various concrete and various conditions: the aim is here to assess the influences of bias factor, such as concrete moisture, aggregate size (especially for mechanical waves techniques), interface position relatively to reinforcement layer, ...

## 6 Conclusion

Interfaces are particular flaws, consisting in planar discontinuity. Their detection and characterization with NDT are mainly related to the variation of physical/mechanical properties of the material filling the discontinuity or on both part of it. It must be point out that the effectiveness of any techniques also decrease with depth.

Engineers can count on several techniques, from very basic ones (chain drag for instance) to very sophisticated procedure (e.g. impulse thermography). Every ND technique can provide specific information regarding the interface. The selection of one (or more) techniques will depend on:

- the cost
- the timeframe
- the type of information to be collected
- the precision and accuracy needed

In a general manner, it can be inferred that mechanical wave methods are particularly sensitive to delamination and debonding. They can differ in their sensitivity according to the geometrical parameters of the flaw (extension, depth ...). With the appropriate technique, engineers can perform a sharp characterization of the flaw. Generally, mechanical wave methods have been advantageously completed with infrared thermography or ground penetrating radar. These techniques provide a large surface covering. They also allow a rapid detection and location of the flaws before a more detailed characterization with slower methods.

In an attempt to improve the effectiveness and reliability of the diagnosis, the TC RILEM group recommends to combine two (or more) techniques. Combination can be only the use of successively several techniques whom each technique improve the results of the previous investigation (for instance infrared thermography + impact echo). Combination could also mean the use of several techniques that would be interpreted together. This procedure allows taking into account various factors that affect techniques to reach to a sharp assessment of flaw properties. In fact, this approach is in progress (see chapter 8) and represents new development expected by engineers. This next step, associated with the development of visual representation of results, will allow automated measuring.

The TC Rilem Group considers that the standardization of NDT can also contribute to the improvement of diagnosis. The Operator experience and skills, its knowledge of the technique that is used and numbers of influencing factors strongly condition the quality of results. Therefore, the operator formation and training, as well as equipment calibration, would improve the performance of NDT. The definition and construction of benchmark test site could be a way to appraise the ability of a team to diagnose a structure with NDT. This consideration, which has been developed on interfaces in this chapter, could be generalised to the whole field of NDT. It appears to be a way to promote NDT in civil engineering.

## References

- Aki T. and Richards P.G. (1980) *Quantitative Seismology : Theory and Methods*, 2 Volumes, Freeman.
- Abraham O., Dérobert X. (2003) Non-Destructive Testing of fired tunnel walls: the Mont Blanc tunnel case study, *NDT&E international*, 36, pp. 411–418.
- Alt D., Meggers D. (1996) Determination of bridge deck subsurface anomalies by infrared thermography and ground penetrating radar: Polk-Quincy viaduct I-70, Topeka, Kansas, Kansas Department of Transportation, Report No. FHWA-KS-96-2, 18p.
- Al Wardany R., Ballivy G., Rivard P. (2009) Condition assessment of concrete in hydraulic structure by surface wave non-destructive testing, *Materials and Structures*, 42(3): 251–261.
- Asano M., Toshiro K., Minoru K., Keitetsu R. (2003) Impact acoustic methods for defects evaluation in concrete, *NDT-CE2003*, Berlin, 16-19 Sept., 8p
- ASTM D4788-03: Test method for detecting delaminations in bridge decks using infrared thermography.
- ASTM, Standard test method for electrical resistivity of pavement membrane system, *ASTM D3633-88* (1991).
- Barnes C.L., Trottier J-F., Forgeron D. (2008) Improved concrete bridge deck evaluation using GPR by accounting for signal depth-amplitude effects, *NDT&E Int.*, 41:427–433
- Breyse D., Abraham O. (2005) *Méthodologie d'évaluation non destructive de l'état d'altération des ouvrages en béton*, Presses de l'ENPC, ISBN 2-85978-405-5, 555p.
- Cantor, T. and Kneeter, C. (1982) Radar as applied to evaluation of bridge decks, *Transp. Res. Rec.*, 852,37 (in *Clemena*, 2004)
- Clark M.R., McCann D.M., Forde M.C. (2003) Application of infrared thermography to the non destructive testing of concrete and masonry bridges, *NDT&E Int.*, 36, pp. 265–275.
- Clemena, G.G. (1983) Nondestructive inspection of overlaid bridge decks with ground-penetrating radar, *Transp. Res. Rec.*, 899, 21.
- Clemena G.G. (2004) Short-Pulse Radar Methods, in *Handbook on non destructive testing of concrete*, Chapter 13, edited by CRC Press, 21p.
- Colla C., Krause M., Maierhofer C., Höhberger H.J., Sommer H. (2002) Combination of NDT techniques for site investigation of non-ballasted railway tracks, *NDT&E Int.*, 35, pp. 95–105.
- Davis A.G., Lim M.K., Germann Petersen C. (2005) Rapid and economical evaluation of concrete tunnel linings with impulse response and impulse radar non-destructive methods, *NDT&E Int.*, 38, pp.181–186.
- Drdacky M., Lesak J., Potential of NDT methods (US, IE, Thermovision, acoustic tracing, laser Doppler interferometry) for plaster delaminations, EC Project “on site for masonry” (coord. Ch. Maierhofer).
- EN 12504-4, Determination of ultrasonic pulse velocity, *Testing concrete- Part4*, 14p.
- Felicetti R. (2008) Assessment of industrial pavement via the impact acoustics method, *Sacomatis, Varenna (Italy)*, 1-2 September 2008, pp. 127–136.
- Gibson, A., Popovics, J.S. (2005) A Lamb wave basis for impact-echo method analysis, *ASCE Journal of Engineering Mechanics*. 141 (4), pp. 438–443.
- Gilles P. (2004) *Investigation et réparation des ouvrages atteints de pourrissement de dalles de tablier de ponts*, *Infra et Diagno'béton*, Quebec, 18p.
- Gilles P., Toussaint P. (2007) *Les besoins en CND d'un gestionnaire d'ouvrages d'art*, *Diagno'béton*, Aix en Provence, 4p.
- Gucunski N., Wang Z., Fang T., Maher A. (2009<sup>1</sup>) Rapid deck condition assessment using 3D visualisation of impact echo data, *NDT CE*, Nantes, June 30th-July 3rd, 6p.
- Gucunski N., Feldmann R., Romero F., Kruschwitz S., Abu-Hawash A., Dunn A. (2009<sup>2</sup>) *Multimodal Condition Assessment of Bridge Decks by NDE and Its Validation*, *Proc. 2009 Mid-Continent Transportation Research Symp.*, Ames, Iowa, 18p.



- Gucunski N., Kruschwitz S., Feldmann R. (2010) Comparative study of bridge deck deterioration detection and characterization by multiple NDE methods, Structural Faults and Repairs, Edinburgh UK, 12p.
- Karastathis V.K., Karmis P.N., Drakatos G., Stavrakakis G. (2002) Geophysical methods contributing to the testing of concrete dams: Application at the Marathon Dam, Journal of Applied Geophysics, 50, pp. 247-260.
- Karray M, Lefebvre G. (2000) Identification and isolation of multiple modes in Rayleigh waves testing methods. In: Proceedings of the use of geophysical methods in construction, sessions of Geo-Denver, ASCE, Denver, pp 80–94.
- Lataste JF., Sirieix C., Breyse D., Frappa M. (2003<sup>1</sup>) Improvement of electrical resistivity measurement for non destructive evaluation of concrete structures, 2nd Int. RILEM workshop on life and aging management on concrete structures, Paris (F), May 5-6 2003, pp. 93-102 (ISBN 2-912143-36-5).
- Lataste JF., Sirieix C., Breyse M., Frappa M. (2003<sup>2</sup>) Electrical resistivity measurement applied to cracking assessment of reinforced concrete structures in civil engineering, NDT&E Int., 36(6), ISSN 0963-8695, pp. 383-394.
- Lin J.M., Sansalone M. (1996) Impact Echo studies of interfacial bond quality in concrete: Part I – Effects of unbonded fraction of area, ACI Materials J., pp. 223-232.
- Lin J.M., Sansalone M., Poston R. (1996) Impact Echo studies of interfacial bond quality in concrete: Part II – Effects of Bond tensile strength, ACI Materials J., pp. 318-326.
- Maierhofer C., Krause M., Wiggenhauser H. (1998) Non-destructive investigation of sluices using radar and ultrasonic impulse echo, NDT&E Int., 31, pp. 421-427.
- Maierhofer C., Leipold S. (2001) Radar investigation of masonry structures, NDT&E Int., 34, pp. 139-147.
- Maierhofer C., Brink A., Röllig M., Wiggenhauser H. (2002) Transient thermography for structural investigation of concrete and composites in the near surface region, Infrared Physics & Technologie, 43, pp. 271-278.
- Maierhofer C., Krause M., Niederleithinger E., Wiggenhauser E. (2003) Non-destructive testing methods at BAM for damage assessment and quality assurance in civil engineering, NDT-CE, Berlin, 16-19 Sept, 14p.
- Maldague X. (1990) Evaluation non destructive par thermographie infrarouge, IEEE Canadian review, pp.11-15.
- Maldague X., Marinetti S. (1996) Pulse phase infrared thermography, J. Appl. Phys., Vol. 79, n. 5, 1: 2694-2698.
- Mayer K., Zimmer A., Langenberg K.J., Kohl C., Maierhofer C. (2003) Nondestructive Evaluation of Embedded Structures in Concrete: Modeling and Imaging, NDT-CE, Berlin, 16-19 Sept, 8p.
- Meola C., Di Maio R., Roberti N., Carlomagno G.M. (2005) Application of infrared thermography and geophysical methods for defect detection in architectural structures, Engineering failure Analysis, 12, pp. 875-892.
- Naar S. (2005) Aide au diagnostic des ouvrages en béton : couplage de méthodes non destructives, XXIIIe AUGC, 10p.
- Naar S. (2006) Evaluation non destructive des ouvrages en béton par mesures de résistivité électrique et thermographie infrarouge passive, Thèse de l'Université Bordeaux 1, 268p.
- Nazarian S. (1984) In situ determination of elastic moduli of soil deposits and pavement systems by spectral analysis of surface waves method, Doct. Diss., The University of Texas at Austin, 486p.
- Olson, L.D. (2010) Recent Advances in NDE and SHM of Bridge Superstructure with Sonic and Radar Methods, FHWA Bridge 2010 Conference Proceedings, Orlando, Florida 12p.
- Popovics, J.S., Gibson, A., Hall, K.S., Shin, S.W. (2009) Developments in air-coupled contactless sensing for concrete, in NDTCE09: 7<sup>th</sup> Int. Symp. on Nondestructive Testing in Civil Engineering, edited by O. Abraham and X. Derobert, LCPC Press, Paris.
- Ryden, N., Park, C.B., Ulriksen, P., Miller R.D. (2004) Multi-modal approach to seismic pavement testing, Journal of Geotechnical Engineering, 130, (6), pp. 636-635.

- Sack D.A., Olson L.D. (1995) Advanced NDT methods for evaluating concretes bridges and other structures, *NDT&E Int.*, 28 (6), pp. 349-357.
- Sangiorgi C., Collop A.C., Thom N.H. (2003) A non destructive impulse hammer for evaluating the bond between asphalt layers in a road pavement, *NDT-CE*, Berlin, 16-19 Sept., 8p.
- Sansalone M., Streett W.B., *Impact Echo: Non destructive testing of concrete and masonry*, Bullbrier Press, Jersey Shore, PA.
- Sansalone M., Lin J.M., Streett W.B. (1997) A procedure for determining P-Wave speed in concrete use impact echo testing using a P-Wave speed measurement technique, *ACI Materials Journal*, pp. 531-539.
- Scott M., Rezaizadeh A., De La Haza A., Santos C.G., Moore M., Graybeal B., Washer G. (2003) A comparison of nondestructive evaluation methods for bridge deck assessment, *NDT&E Int.*, 26, pp. 245-255.
- Simonin JM et Abraham O. (2006) Two complementary seismic method for the detection and the characterisation of delamination in road structures, *NDE CE*, St louis.
- Taffe A., Borchardt K., Wiggengerhauser H. (2006) Specimen for the improvement of NDT-methods Design and Construction of a large concrete slab for NDT methods at BAM, P011, *NDT-CE*, Berlin, 16-19 Sept., 7p
- Tinkey, Y. and Olson, L.D. (2007) Sensitivity Studies of Grout Defects in Post-tensioned Bridge Ducts Using Impact Echo Scanning Method, *Transportation Research Record: Journal of the Transportation Research Board*, Volume 2028, pp. 154-162.
- Tinkey, Y. and Olson, L.D. (2008) Applications and Limitations of Impact Echo Scanning for Void Detection in Post-tensioned Bridge Ducts, *Journal Transportation Research Record: Journal of the Transportation Research Board*, Volume 2070, pp. 8-12.
- Tokimatsu K, Tamura S, Kojima H (1992) Effects of multiple modes on Rayleigh wave dispersion, *J Geotech Eng ASCE*, 118:1529–1543.
- Uomoto T. (2003) Utilization of NDI to Inspect Internal Defects in Reinforced Concrete Structures, *NDT-CE*, Berlin, 16-19 Sept., 7p.
- Weil G.J. (1993) Non destructive of a bridge highway and airport pavement, *NDT of concrete in the infrastructure*, Deardon, Michigan, pp. 93-105.
- Weil G.J. (1998) Non destructive Testing of the Concrete Roof Shell at the Seattle Kingdome, *SPIE Vol. 3361*, pp. 177-187.

# Chapter 6

## Localization of grouting faults in post tensioned concrete structures

Martin Krause<sup>1</sup>

### 1 Introduction

#### 1.1 *State of the art and existing guidelines and recommendations*

The investigation of post-tensioned tendon ducts is one of the very important and fascinating testing problems for concrete structures. Much progress was achieved in the past two decades including multidisciplinary research. This includes large area measuring. The progress of research and development bases on four columns:

- Measurement and evaluation at large scale test specimens applying automated equipment
- Application at large scale post tensioned test specimens
- Reconstruction calculation for visualisation of results
- Modelling of elastic wave propagation for better understanding of effects.

The application of the methods is in an intermediate state between: practical application, validation, writing of recommendations and guidelines, even standards for certain methods, research for more reliable methods, development of automated methods for fast application.

This text is intended for a brief description of the state of the art of existing methods including some historical aspects of development of methods. There are other interesting publications of committees working on providing information and

---

<sup>1</sup>Other contributors to this chapter are: O. Abraham, L. Alver, D. Breyse, J.P. Balayssac, M. Forde, A. Kodjo, A. Moczko, C. G. Petersen, J. Popovics, F. Rivard.

M. Krause (✉)

BAM, Bundesanstalt für Materialforschung und –prüfung, Berlin, Germany  
e-mail: martin.krause@bam.de

explaining NDT methods for concrete in order bringing forward their application [Forde, 2006]. Additionally in the United Kingdom recommendations for design and tailing, duct and grouting systems as well as certification of post-tensioned operations and training are published. Details about overall design strategy and protection systems are outlined [Concrete Society, 2002].

Several groups of experts are also working on this topic: ACI 228, COFREND, DGZfP (German Soc. NDT, through its Technical Committee NDT-CE with its subcommittees and recommendations for ultrasonics, impact-echo, RADAR, radiography, quality assurance, education [DGZfP, 2010], COST Materials Action 534, dealing with Impact-Echo. The material published by these groups is considered for the present text as far as possible.

## 1.2 Fields of application

In principle there are three fields of application: regular inspection of prestressed structures, quality assurance of repair, quality assurance of new structures.

Grouting faults are appearing in all areas of tendon ducts, and there are many structures with large areas of ungrouted ducts [FDoT, 2003, Eichinger et al, 2000]. The regular damage assessment of bridges, which are planned to be demolished is a very important activity in this field [Vogel, 2002]. Following a technical report of the Concrete Society of the United Kingdom about 30 % of the post-tensioned concrete structures suffer from voids and ungrouted tendons [Concrete Society, 2002].

Many developed countries are active in this field. For instance, in Germany application of advanced NDT is part of Maintenance of Engineering Structures (BMS, Bauwerk-Management System) of Bundesanstalt für Straßenwesen (BASt, Federal Highway Research Institute). All state owned bridges are regularly inspected following the standard DIN 1078 (inspection interval 3 years and 6 years (general inspection)). If there are some abnormalities, which cannot easily be classified, a so called OSA (*Objektbezogene Schadensanalyse*, Structure related Damage Analysis) takes place [BASt, 2010]. Then NDT-CE-methods are applied by engineering offices or research institutes.

## 2 Overview of Methods

Principally the methods for assessing the grouting of metallic tendon ducts are divided in three groups:

- Radiography with X-rays and  $\gamma$ -Radiation (see § 3)
- Methods with mechanical waves, including impact-echo and ultrasonic methods (see § 4 to 6). There is a wide variety of techniques and variants, that will be detailed in the following. Mechanical wave methods are divided in Impact-Echo and Ultrasonic methods. Impact-Echo was the first mechanical wave method which was widely applied at prestressed concrete structures for testing post tensioned tendon ducts. Thus section 4 is dedicated to this subject.

- Development of broadband low frequency ultrasonic transducers and imaging techniques since the 1990 decade enable application of ultrasonic echo technique for concrete structures. These techniques (including ultrasonic through transmission) are described in sections 5 and 6. They are related to modelling and reconstruction techniques, which can only briefly mentioned in this state of the art [Langenberg et al, 2002], [Langenberg et al, 2009]
- Impulse radar, which can be used for plastic ducts (see § 7.1).

Transient thermography is widely applied in NDT. So it is obvious to apply it for concrete structures. There are encouraging results, but it seems that its application is restricted to the near surface region because of the relatively small penetration depth of the heating pulses in concrete. It will be briefly treated (see §7.2).

### 3 Radiography with X- and $\gamma$ -Radiation

High energy electromagnetic waves were already applied in civil engineering in the nineteen-thirties for investigating welded joints. It is obvious that the best state-of-the-art technical solutions are always applied to prestressed concrete structures in order to achieve a contrast between grouted and voided regions. Current  $\gamma$ -radiography is sometimes used as reference method in addition to mechanical waves.

#### 3.1 X-rays

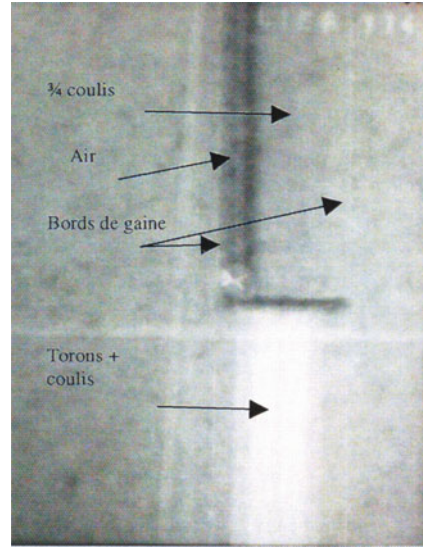
Radiography with X-rays was already carried out in the thirties of last century for testing steel structures. However to investigate tendon ducts in concrete structures the penetration depth has to be large enough. This means energy of 320 keV and more for 20 cm thick concrete elements. For higher energy linear and circular accelerators are used with X-ray energy between 2 and 6 MeV.

With linear accelerators, even thicker concrete elements can be tested with  $\gamma$ -radiography. Since the source can easily be switched on and off the application is somewhere easier than the handling of the radiation sources. Applications at concrete bridges, which are around 1 m thick, are described in France [Duffay and Piccardi, 1985], [Lanneau, 1993].

#### 3.2 Gamma-Radiation

The application of  $\gamma$ -radiography is performed in several modifications. There are two typical types of sources: Iridium 192 (up to 38 cm concrete) and Cobalt 60 (typically up to 60 cm concrete). The sensors are films or phosphor imaging plates. Guidelines are published e.g. in Germany [DGZfP, 1990] and France [AFNOR, 2011] or by international bodies [IAEA, 2002].

**Fig. 6.1** Localisation of grouting faults with Gammagraphy in a specimen at CETE de Lyon (after [Roennelle and Abraham, 2006])



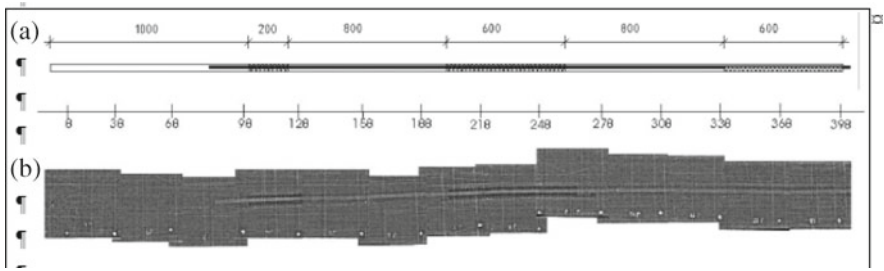
**Fig. 6.2** Plastic tubes for Cobalt 60 source at Large Concrete Slab at BAM (after [Taffe et al, 2003])



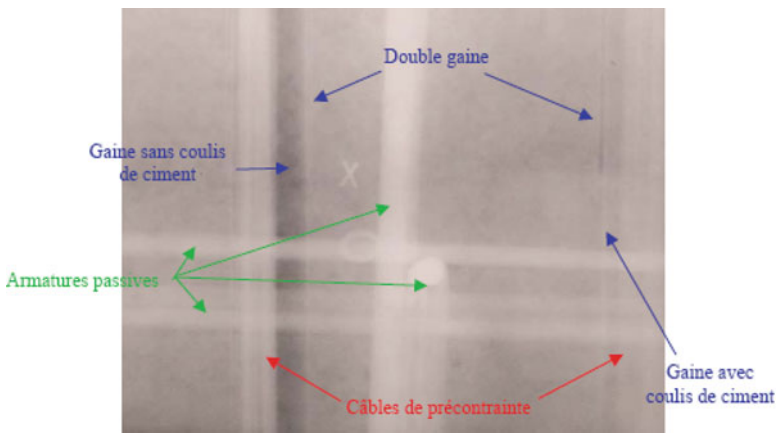
The capability of Cobalt 60 sources is demonstrated at specimens constructed at BAM and LCPC Lyon (Figs. 6.1 to 6.3) ([Roennelle and Abraham, 2006], [Taffe and al, 2003], [Krause et al, 2008]).

In Figs. 6.4 and 6.5 two examples are shown which demonstrate the capability of gammagraphy to localize ungrouted areas of tendon ducts, non-prestressed rebars and non tightened strands 0.

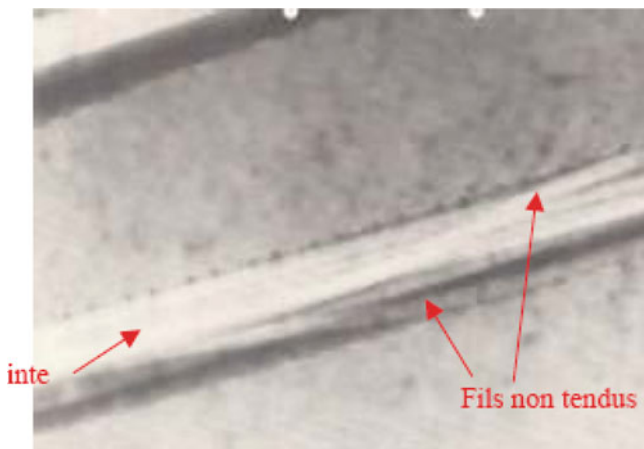
The sensitivity of phosphor imaging plates depends on the thickness of the phosphor layer. With a typical layer thickness of about 0.3 mm ( ) they can be used for digital radiography of concrete. The required exposure time is comparable with the fluorescent screen-film systems. For better image quality higher exposure time is recommended.



**Fig. 6.3** Plan of tendon duct (diameter 40 mm) with artificial grouting faults (a) and verification with Gammagraphy with Cobalt 60 source (b); measured at Large Concrete Slab of BAM

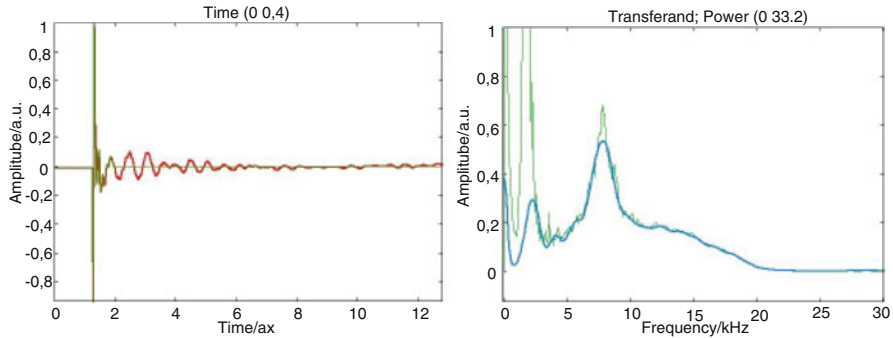


**Fig. 6.4** Gammagraphy of bridge element with Cobalt 60 source



**Fig. 6.5** Non prestressed strands imaged with Cobalt 60 source





**Fig. 6.6** Result of Impact-Echo point measurement for a specimen (thickness 0.25 m) containing tendon ducts (diameter 41 mm) [Algernon, 2007]

Of course it has to be stated out that radiographic techniques demand strict application of safety and radiation protection. This is regulated in the radiation protection ordinances in the different countries.

## 4 Echo Methods with mechanical waves: Impact Echo

The acoustic echo methods are divided in impact-echo and ultrasonic echo (see §5). Both can principally be used for point measurement. Equipment and evaluation software is available for this purpose furnished by different manufacturers. These methods are briefly described. Imaging methods are in the intermediate state between development and application. Several examples at specimens and post-tensioned concrete structures are described.

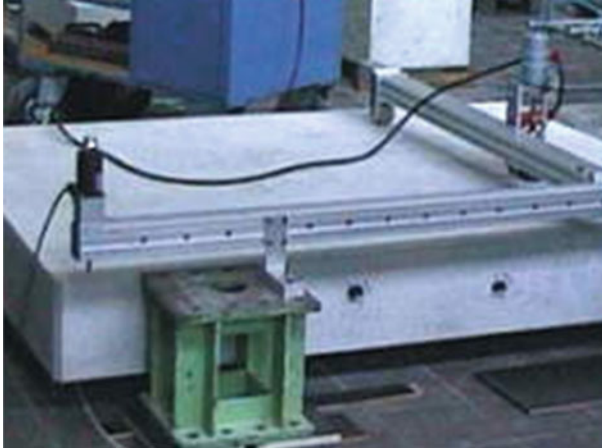
### 4.1 Application of the impact-echo method for tendon ducts

As described in Chapter 2 (§ 3), impact-echo is a mechanical wave method based on analysis of the multiple reflections after a mechanical impact and their evaluation in the frequency mode (Fast Fourier Transform, FFT).

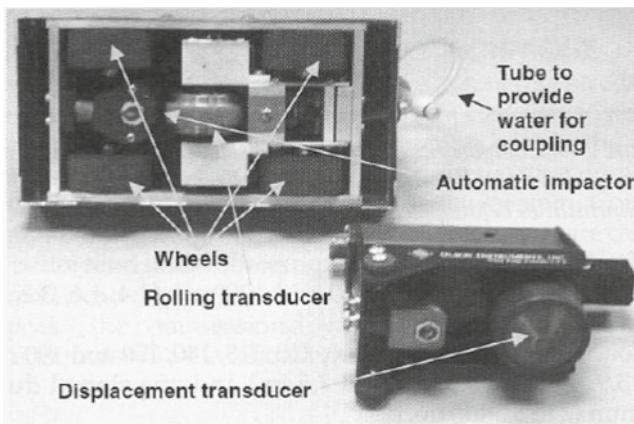
An example measured at a concrete specimen containing grouted and ungrouted tendon ducts (diameter 41 mm) is depicted in Fig. 6.6.

Concerning the assessment of this method for tendon ducts opinions slightly differ. The method was standardised in USA in 1986 and there are manufacturers and publications who certify a good reliability for localizing grouting faults in tendon ducts by point evaluation [Sansalone and Streett, 1997], [Lin and Lin, 1997]. Other authors deduced after thorough studies that this is only possible applying imaging evaluation [Lausch et al, 2002], [Große et al, 2007]. One of the reasons is appearance of disturbing effects caused by geometry. In recent years applications working with point evaluation for tendon ducts presented at international conferences became





**Fig. 6.7** Automated pneumatic scanning device with IE applied on a test specimen (after [Lausch et al, 2002])



**Fig. 6.8** Impact Echo scanning device with rolling transducer (after [Tinkey et al, 2005])

irrelevant, whereas imaging results were presented numerously [Wiggenhauser and Schickert, 2003], [Al Qadi and Washer, 2006].

There are impressive results for measurement and evaluation of large building elements with imaging impact echo ([Tinkey et al, 2005], [Abraham and Cote, 2002], [Colla et al, 1999], [Maierhofer et al, 2004]). Two examples of scanning devices are depicted in Figs. 6.7 and 6.8. The first is an application of impact-echo system mounted on an automated pneumatic scanning system, the second is an impact echo scanning device with a rolling transducer assembly incorporating multiple sensors.

Also microphones are applied for non-contact measurement [Zhu and Popovics, 2007]. Some examples are cited in the next sections. Laser interferometers are also under study for they have the advantage of being very large frequency band sensors

([Abraham et al, 2009], [Abraham and Popovics, 2010]). Their main disadvantage is that they often require surface preparation.

Another approach of evaluating Impact Echo data is in discussion since several years. It is based on the assumption of higher frequency modes after impact excitation. It is named Stack Imaging of Spectral Amplitudes Based on Impact-Echo (SIBIE [Ata et al, 2007]). Research results are briefly described in § 4.4.

There are different approaches to explain the origin of multiple reflections after mechanical impact in concrete. The easiest explanation is the appearances of resonant multiple reflections at a plane reflector, which are analysed by Fourier transform techniques. But this method needs correction factors for different geometrical shape of concrete elements [Sansalone and Streett, 1997].

[Gibson and Popovics, 2005] have analyzed the multiple reflections after impact excitation as guided waves (Lamb waves). In slab like components the resonant wave is explained as a resonance of the mode  $S_1$  of a symmetric Lamb wave. Thus the calibration factor ( $\beta=0.96$ ) as introduced by [Sansalone and Streett, 1997] for the resonance frequency of slabs is not necessary.

In the simplest way the wave velocity can be measured from at a point of known thickness of the slab. When it is not possible, the velocity must be measured at cores, for example. Since they have a differing geometry, other wave modes can occur (e.g. dilatational waves) and conversion factors must be applied. These factors depend on Poisson ratio. For surface waves other effects have to be considered. This has less importance for localizing grouting faults, thus these aspects are not discussed in detail in this overview.

The criteria for distinguishing between grouted and ungrouted tendon ducts are described differently in the literature. There are two main criteria:

1. Change in the multiple reflection frequency between concrete/air and concrete/steel interfaces (quotient 4 instead of quotient 2 in Eq. 1)
2. Shift of the back wall echo frequency to lower frequency when the duct is ungrouted.

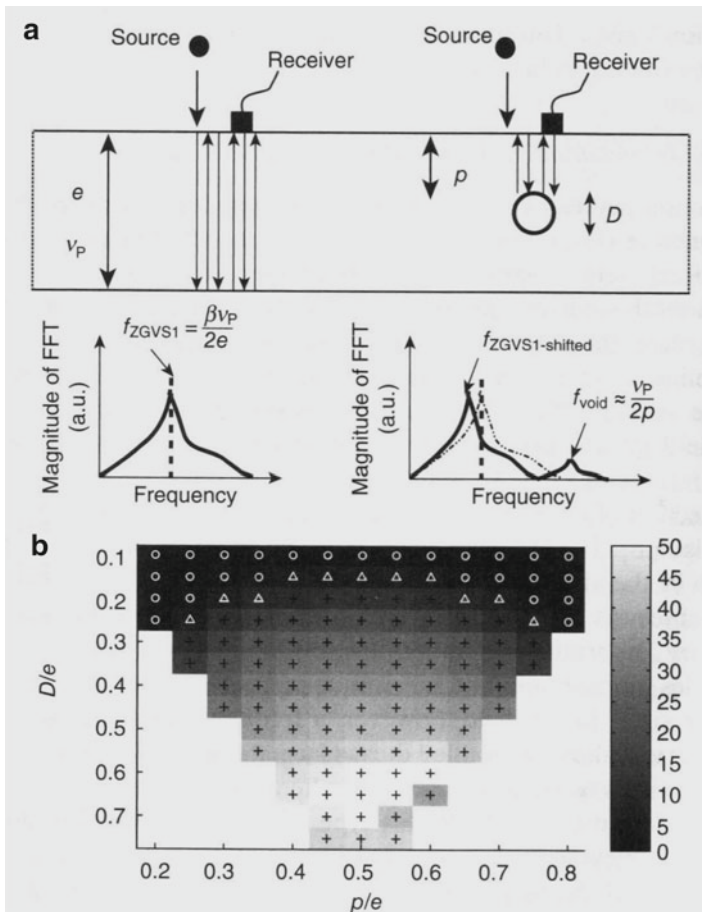
*Short comment on criterion 1:*

This is the most frequent criterion applied for impact echo point measurement. In [Sansalone and Streett, 1997] it is described as switch between pressure waves and tension waves depending on the type of reflecting interface (concrete/air or concrete/steel, respectively). It theoretically reduces the impact-echo frequency to one half. Another approach of explanation is the sign of the reflection coefficient, which switches from positive (concrete/steel) to negative (concrete/air) (phase jump). Recent experimental and theoretical considerations show that the frequency shift is much smaller as suggested for typical tendon duct diameters [Schubert and Köhler, 2008].

Imaging impact echo works mainly with criterion 2.

*Short comment on criterion 2:*

For the effect that the back wall frequency is shifted to lower frequencies (indicating larger thickness) the influence is twofold. The basic explanation considers the ray



**Fig. 6.9** (a) Schematic diagram of the impact-echo method for the detection of a small-sized void (b) Finite element evaluation of the thickness resonance frequency shift, in percent, above a void [Abraham and Popovics, 2010]

path of the longitudinal waves: in case of a void, the ray path becomes larger, which means a higher frequency of the multiple reflections.

Voids in concrete, especially in tendon ducts are reflectors for elastic waves, but they also reduce the concrete strength in their vicinity. This has the consequence that the elastic constant and the vibration frequency are changed in relation to the position of the void relative to the centre of the concrete slab. Following this argumentation the shift of the back wall echo caused by a void depends on the concrete cover of the tendon ducts [Lausch et al, 2002]. Experimental results of that shift are presented in § 4.3 (impact echo imaging).

There are thorough theoretical considerations, which consider both effects [Roellenle and Abraham, 2006]. In Fig. 6.9, the principle of the frequency shifted by the presence of a voided tendon duct is demonstrated. Here ZGVS1 indicates the

Zero Group Velocity of the Symmetric mode of a lamb wave. The thickness resonance frequency is shifted towards lower frequency caused by the void (diameter  $D$ ). The lower part of the Fig. 6.9(b) shows the result of a finite element evaluation of the frequency shift in dependence of the diameter  $D$  and concrete cover  $p$  of the void [Abraham and Popovics, 2010].

## 4.2 Point and Linear Measurement and evaluation

In reality the impact echo signal often is superimposed by disturbing signals caused by geometry. Additionally impact echo theory only works properly for plane reflectors. Cylindrical targets as tendon ducts and even unstructured targets as honeycombing can lead to different behaviour of multiple reflections. The clearness of the signals mainly depends on the ratio between depth and diameter of the target. Following [Sansalone and Streett, 1997], ducts can be measured until a ratio of 3, other authors describe the difficulties, but they don't consider it as realistic to deduce an exact limit ([Lausch et al, 2002], [Große et al, 2007]).

In the Advice Notes from UK [Forde, 2006] a special carefulness is proposed, when the reflection objects are cylindrical like metal ducts. After this the advice is a need to pay attention to the input frequencies and the consequential wavelength in relation to the duct diameter. The proposed impact echo frequency runs from a minimum frequency of 19 kHz excited with an impactor diameter of 15 mm to a maximum frequency of 69 kHz excited with impactor diameter of 4 mm. In the first case the minimum target diameter is 105 mm ( $\lambda$ ) and the depth range runs from 105 mm to 840 mm. In the latter case the minimum target diameter is 58 mm ( $\lambda$ ) and the depth range runs from 29 mm to 232 mm.

Figure 6.10a) shows the frequency response from a voided duct whilst Fig. 6.10b) shows the frequency response from a fully grouted duct. These results were taken at the middle of a concrete beam to reduce any border effects. It can be seen that from Fig. 6.8 the initial peak (fT) has moved forward from 4.9 (plain concrete), and there is a peak with a higher frequency, these being typical of a voided duct. In Fig. 6.8 the initial fT has not moved forward and there is a frequency peak at 6 kHz [Forde, 2006].

The difficulties to read proper impact echo results in point measurement was one of the reasons to develop the impact-echo imaging possibilities described in the following § 4.3.

## 4.3 Impact-Echo imaging

In applying point-measuring methods in a way that several data points are collected along a line, imaging techniques can be used. This method is improved into a scanning test method to visualize test results as an Impact-Echogram, similar to a B-scan in ultrasonic pulse echo or a GPR radargram. The amplitude of the

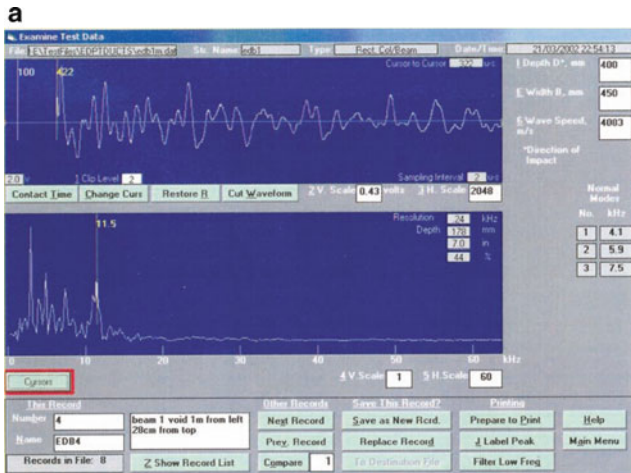


Fig. 6.10a) Result of an impact-echo test over an ungrouted (voided) tendon duct



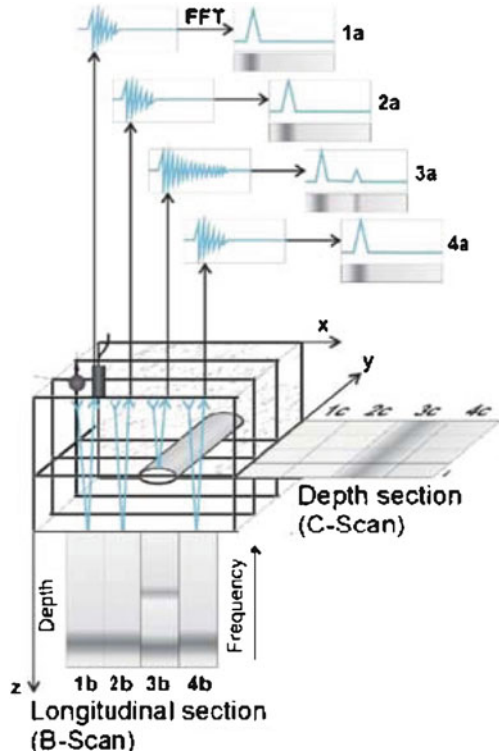
Fig. 6.10b) Result of impact-echo test over a grouted tendon duct [Forde, 2006]

frequency power spectrum is displayed colour coded or in greyscale over the position of the measurements and frequency like shown in Fig. 6.11 ([Colla et al, 1999], [Große et al, 2007]).

With automated testing in dense measurement grids Impact-Echo measurements can image very detailed the thickness of a concrete slab. When scanning is extended to a 2-dimensional grid, IE-results can be shown as 3-D images as shown in Fig. 6.12.

Usually impact-echo imaging of ducts works indirectly. This is demonstrated in Fig. 6.13a)-b), where the shift of the resonance frequency of the back wall signal is clearly visible. As mentioned above, several effects influence the shift of the back

**Fig. 6.11** Principle of Impact-echo imaging (Layout: D. Schaurich)



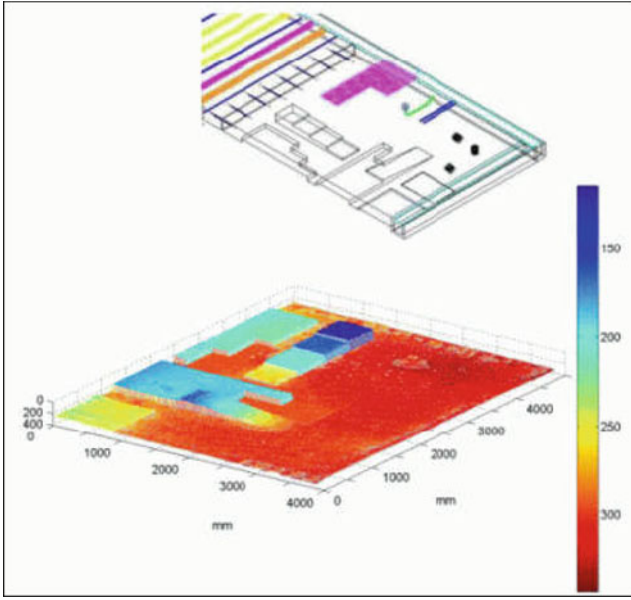
wall echo: diameter, grouting condition, stiffness, concrete cover, position in the concrete slab ([Lausch et al, 2002], [Wiggenhauser, 2003], [Große et al, 2007]).

In a systematic study at a test specimen under laboratory condition it was shown that ungrouted and grouted areas can be indicated by impact echo imaging. This is demonstrated in Fig. 6.14. The built in grouting faults are depicted in part a) of the Fig. Part b) shows the impact-echo B-scan. The different shift of the back wall resonance below the duct is clearly visible. Apparently regions having a stronger shift correspond to voids in the tendon duct. Regarding the impact-echo c-scan in part c) of Fig. 6.14, the ungrouted areas are imaged in the correspondent depth section ([Maierhofer et al, 2004], [Wiggenhauser et al, 2007]).

Another approach to measure and image the shift of the back wall echo is to use a laser interferometer as receiver. It was realized at a test slab, which is 0.25 m thick and includes various tendon ducts - filled and empty - together with an empty thick steel pipe. The source is maintained at a fixed distance from the wall with a wheel so that the impact is reproducible. The presence of empty tendon duct are clearly seen on the C-SCAN at a frequency nearby the impact-echo thickness resonance frequency ([Abraham et al, 2010], [Abraham et al, 2010]).

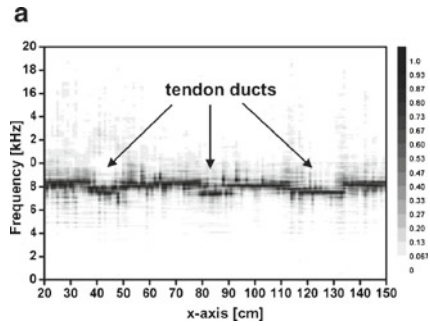
Experimental studies about indicating voids by the shift of back wall echo also were also performed applying the impact echo scanner described above (see Fig. 6.8). An example is shown in Fig. 6.15. It demonstrates that the back wall echo show a smaller increase of apparent thickness over a well-grouted steel duct and a more significant



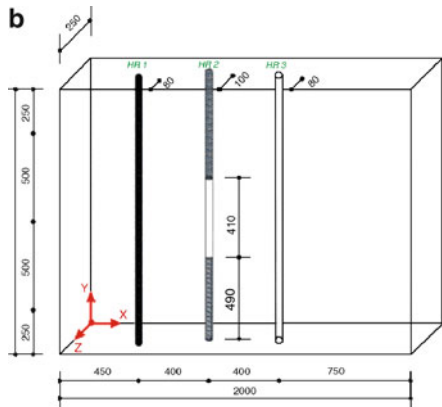


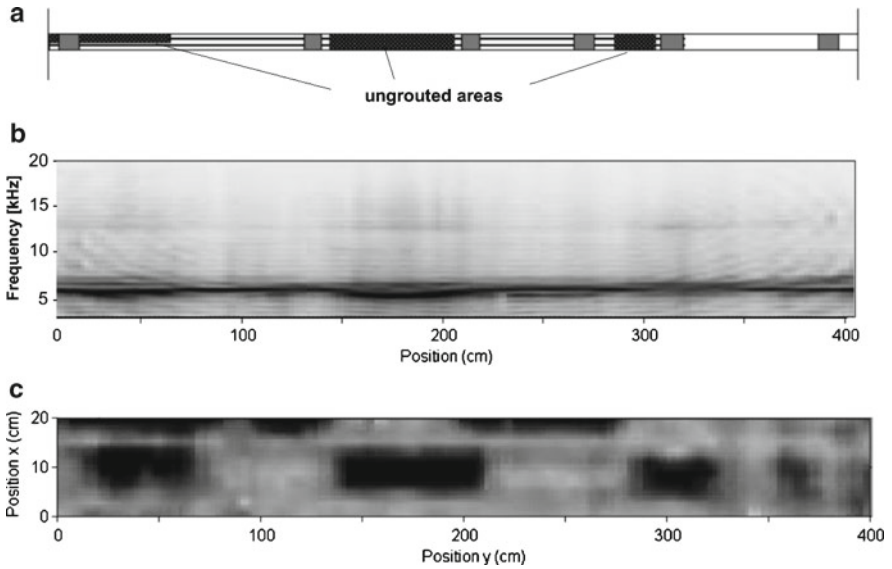
**Fig. 6.12** Imaging of IE results of the Large Concrete Slab at BAM, Berlin

**Fig. 6.13a)** Impact echogram of concrete specimen with tendon ducts (grouted and ungrouted without strands)

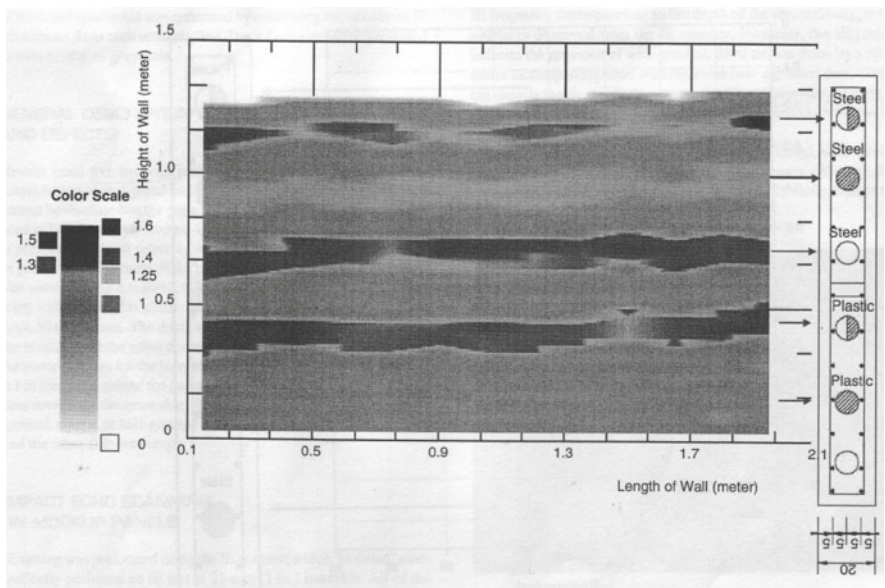


**Fig. 6.13b)** Specimen with three tendon ducts, different concrete cover and grouting condition (after [Lausch et al, 2002])



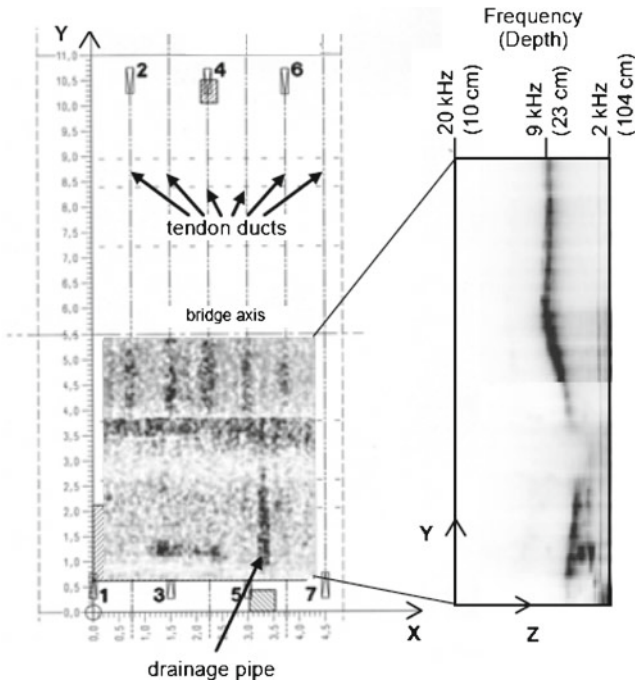


**Fig. 6.14** Impact echo imaging of tendon duct with artificial voids: **a)** plan, **b)** Impact echogramm (longitudinal section above duct, B-scan; backwall echo 6.16 kHz, shifted backwall echo around ducts., **c)** Depth section for shifted backwall echo (5.63 kHz) (after [Große et al, 2007])



**Fig. 6.15** Result of impact echo scanning experiment of a specimen with a thickness of 0.2 m. Visualisation of actual thickness indicated corresponding to the colour scale [Tinkey and Olson, 2008]





**Fig. 6.16** Results of impact-echo-measurements on a bridge deck; left: C-scan parallel to the measurement surface at 8.6 kHz, right: projection of all B-scans parallel to the y-axis

increase of apparent thickness over empty and partially grouted ducts [Tinkey and Olson, 2008]. These experiments were carried out on tendons without strands.

#### *Examples from application at bridges*

On-site investigations with impact-echo at concrete structures up to a thickness of 83 cm show, that the back wall of these concrete structures could be reliably detected. The localization of tendon ducts and the assessment of the grouting conditions at the tendon ducts of the bridges are often difficult. As shown at the example of results in Fig. 6.16 the lateral position of tendon ducts could be determined by a displacement of the reflection from the backside of structure during on-site performances.

In Fig. 6.16, two images of an impact echo data set are shown as results of measurements on a deck of a box girder bridge. On the right side a B-scan projection is presented. The backside, which is partially not parallel to the surface, is clearly visible at a frequency of approximately 9 kHz. This frequency is equivalent to the thickness in the middle of the deck (approx. 24 cm). On the left side of this figure a C-scan (slice parallel to the surface) in the depth of the backside is shown. The lateral positions of the tendon ducts are clearly visible from  $y = 3.7$  m to  $y = 5.4$  m as displacements of the backside reflection. A drainage pipe causes high intensity between the tendon ducts nos. 5 and 6. At these measurements the distance between the top of the deck that means the measurement surface and the tendons was not determinable. Otherwise the concrete cover of the tendons could be determined carrying

out measurements on the bottom side of the deck. Here, wave reflections from the tendons were directly detected as well [Wiggenhauser et al, 2007].

#### 4.4 Interpretation and research: the SIBIE procedure

For a better evaluation of impact-echo data and in order to improve the method, an imaging technique has been applied to the data in the frequency domain. This procedure is named SIBIE (*Stack Imaging of Spectral Amplitudes Based on Impact-Echo*) [Ohtsu and Watanabe, 2002]. SIBIE procedure is an improved alternative method to interpret impact echo data. It is an imaging technique applied to the impact-echo data in frequency domain.

In the procedure, first, a cross-section of concrete is divided into square elements. Then, resonance frequencies due to reflections at each element are computed. The travel distance from the input location to the output through the element is calculated for each square element.

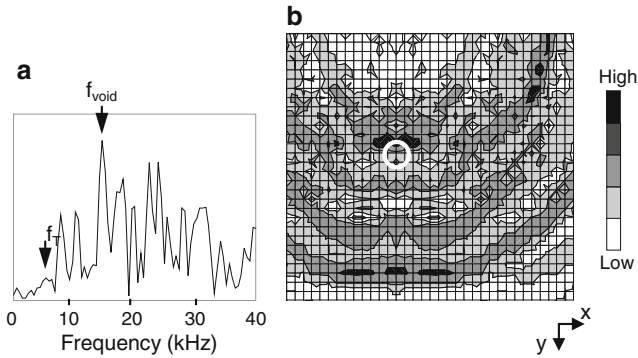
Following the developers of the method, there are two resonance frequencies due to reflections at each element are calculated:

$$f'_2 = C_p / r_2 \text{ and } f_R = C_p / R$$

where  $C_p$  is the velocity of P-wave,  $r_2$  is the distance between an element and the output location,  $R$  is the total travel distance. Spectral amplitudes corresponding to these two resonance frequencies in the frequency spectrum are summed up at each mesh. Thus, reflection intensity is estimated as a stack image at each element. The minimum size of the square mesh  $\Delta$  for the SIBIE analysis should be approximately equal to  $C_p \Delta t/2$ , where  $\Delta t$  is the sampling time of a recorded wave.

Following the authors, SIBIE has been successfully applied to void detection within tendon ducts as well as surface-crack depth identification ([Ata et al., 2007], [Alver and Ohtsu, 2007], [Alver et al, 2004]). In these papers results on locations of voids and depths of surface-cracks identified by SIBIE are described. One example of the method is described below, following citation [Alver and Ohtsu, 2006]. It is the result of application of impact-echo method and SIBIE procedure to a concrete specimen with a metal-duct, presented in Fig. 6.17. The frequency spectrum obtained by an impact-test of the specimen is shown in Fig. 6.17a). The resonance frequency of the void  $f_{\text{void}}$  is indicated with an arrow and is assigned as close to the calculated value [ $f_{\text{void}} = C_p / 2d$ ], as possible. SIBIE analysis was carried out by using a frequency spectrum shown in Fig. 6.17a) and a result is shown in Fig. 6.17b). Black colour of the high reflection zones is clearly observed in front of the void. Following the authors in this way it is demonstrated that SIBIE is able to identify such voids within tendon-ducts.

During several discussions on conferences, the presenters of SIBIE-results were asked to prove the existence of two resonance frequencies additionally for large concrete specimens in order not to avoid confusion resonances with geometrically caused multiple reflections and oscillations of the specimen. This should be especially important in case of cracks, because following the usual Impact Echo theory there are no multiple reflections between measuring surface and crack tip.



**Fig. 6.17** a) Frequency response and b) SIBIE result by impact test of a concrete specimen with metal duct

## 5 Echo Methods with mechanical waves: Ultrasonic Echo

The mechanical wave methods are divided in impact-echo (see §4) and ultrasonic echo and ultrasonic through transmission, that will be presented in §5 and §6. Both can be used for point measurement. Equipment and evaluation software is available for this purpose furnished by different manufacturers. These methods are briefly described.

Since about 1995 imaging and reconstruction methods are developed for measuring data, which are taken in a line or a measuring mesh (2D data acquisition). For both Impact-Echo and ultrasonic echo methods, large progress was achieved; examples are summarized in this text.

### 5.1 Introduction, principle

The frequency range for ultrasonic echo measurement in concrete elements leads from 20 kHz to 200 kHz. Pressure-waves (longitudinal waves) as well as shear waves (transverse waves) are applied. For basics about ultrasonic low frequency echo methods for reinforced concrete see e.g. [Schickert and Krause, 2010].

From the research work of the last 15 years it can be followed that there are two criteria for localizing grouting faults in tendon ducts:

1. In the magnitude representation air inclusions show significant higher reflection intensity (total reflection) than for grouted steel rebar or strands. This criterion follows from the different reflection coefficients of the interface concrete/air and concrete/steel as is applied since 1995 ([Krause et al, 1997], [Jansohn et al, 2002], [Krause et al, 2003], [Schickert, 2005].).
2. In imaging the phase value or signal shape of the reflected signal the distinction between air filled areas and grouted steel bars or strands is realized by the phase difference of  $180^\circ$ . This criterion considers the phase difference between the reflections at the interface concrete/air (material with smaller acoustic impedance)

relative to the reflection concrete/steel (larger acoustic impedance). It recently was redeveloped applied as a part of acoustical imaging [Mayer et al, 2008 and 2008b]. Up to now this criterion is only developed for few types of tendon ducts. The systematic automated application and research on site conditions are subjects of actual research and development project [Krause et al, 2011].

A third effect is known from several measuring results at tendon ducts: in several cases reflecting signals are appearing in the SAFT-B-scans (*Synthetic Aperture Focusing Technique*) corresponding to the depth of the bottom side of the tendon duct. In completely voided areas the reflection happens always at the top side of the duct (smallest concrete cover relative to the measuring surface) [Krause et al, 2011]).

Especially in older post-tensioned structures it may happen that the duct is correctly grouted but the mortar was shrinking during hardening and will cause minor delaminations between duct and grouting mortar. This means that such a duct would show the same ultrasonic reflection properties than a completely voided duct. Experiences with opened ducts show that the shrinking process is not always uniform. For example light rust films may partially cause bonding between duct and grouting mortar. However it should be noted that high ultrasonic back scatter intensity of ducts does not inevitably indicate poor grouting conditions. Up to now the main aim of the method is to indicate suspicious areas. For the final assessment minor destructive opening of the tendon ducts seems useful.

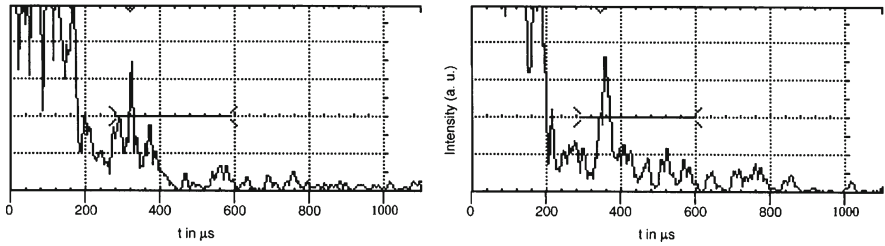
## 5.2 *Ultrasonic Point Measurement and evaluation*

Tendon ducts can clearly be recognised as reflectors in single reflection curves. This follows from the fact that reflection coefficients at steel tendons as well as at air inclusions have large values ( $R_{\text{steel}} = 60\%$  and  $R_{\text{air}} = 100\%$ ; idealized for plan and thick reflectors). Since modern ultrasonic echo equipment is capable to measure back wall reflections in concrete for up to 0.5 m or 1.50 m depending on the site conditions, tendon ducts having a diameter of 40 mm or more result in a clear echo, when they have typical concrete covers between 50 mm and 150 mm. Of course the position of the probes has to be directly above the duct and the wave propagation must not be shielded by reinforcing bars.

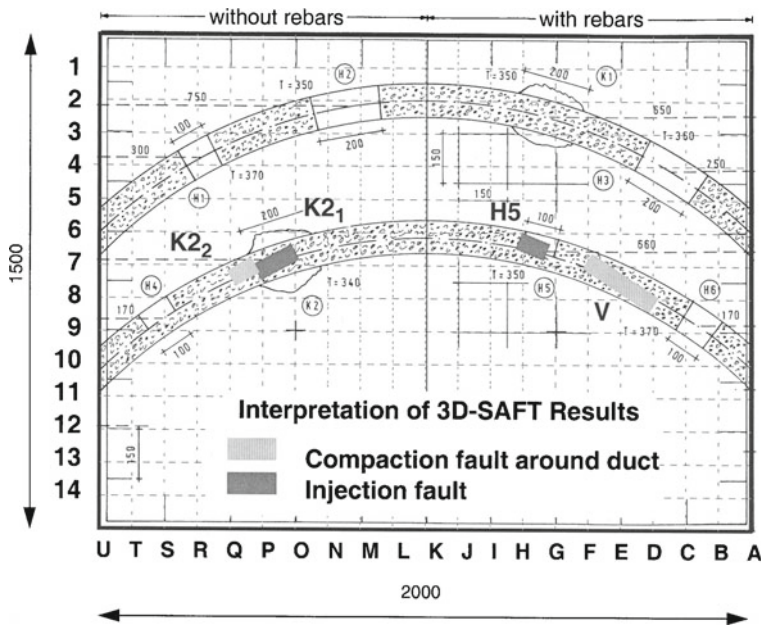
One example of indicating an artificial compaction fault around a duct is presented in Fig. 6.18. P-wave transducers were applied in T/R mode (transmitter and receiver separated but close together [Taffe et al, 2008]).

## 5.3 *Linear Measurement and 2D representation of the data*

When several measuring points are combined to a measuring line, the results are normally represented in a cross section or longitudinal section (also called ultrasonic B-scan), respectively. In this B-scans the magnitude of the reflection is represented



**Fig. 6.18** Ultrasonic pulse echo with interpretation of ultrasonic echo time curve (A-scan) measured above a compaction fault, hence the concrete cover is reduced (left); right: reflection at steel

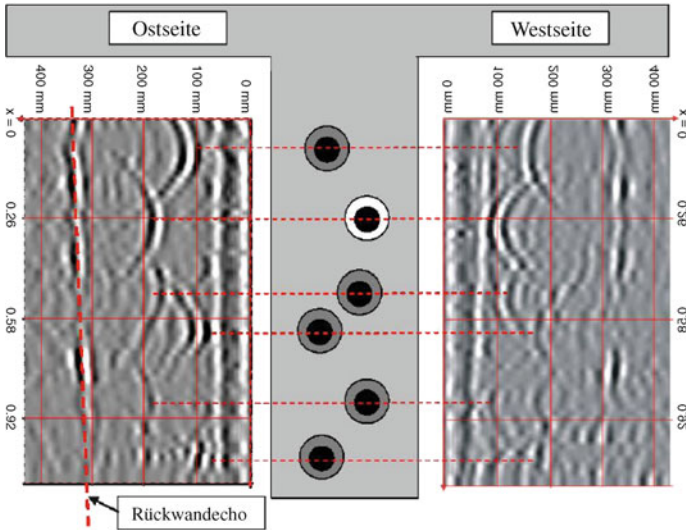


**Fig. 6.19** Interpretation of results obtained with ultrasonic imaging (experiments for lower duct)

in grey values or false colours. From this low and high reflecting areas can be indicated [Krause et al, 1997].

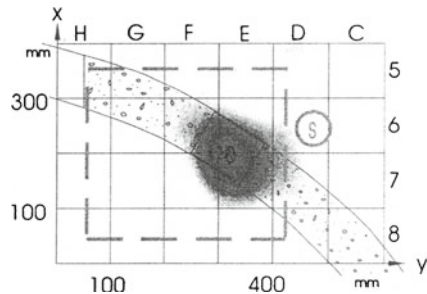
Application of shear wave dry contact equipment enables measuring above tendon ducts and representing their reflecting magnitude. There are results successfully assigned to ungrouted areas in tendon ducts [Kroggel et al, 2002]. The reflection magnitude gives hints for compaction faults around and grouting faults in tendon ducts (specimen sketch see Fig. 6.19, upper duct).

These results were obtained in a round robin test at BAST (Federal Highway Institute) at two specimens with artificial voids and different amount of non prestressed reinforcing bars [Krause et al, 2002]. In this double blind tests also ultrasonic imaging methods were applied, which partly indicated voids in tendon ducts.



**Fig. 6.20** Reflection signals from a grouted and ungrouted area of a tendon duct in a prefabricated road bridge (diameter 80 mm concrete cover: 100 mm to 200 mm [Sodeikat and Dauberschmidt, 2008])

**Fig. 6.21** Imaging of void in tendon duct with Laser interferometer and reconstruction calculation

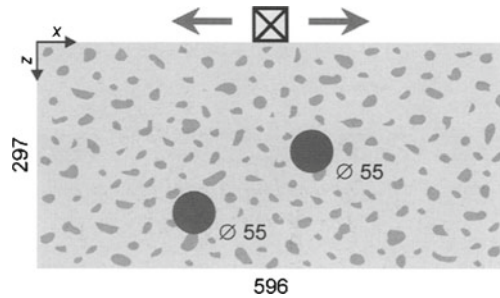


These experiments were carried applying a laser interferometer as ultrasonic receiver (see §5.4.1., Fig. 6.21).

Analysing the pulse shape and estimating and the value of the reflected pulse in ultrasonic B-scans is rarely possible in practical application. The signal from of the reflecting pulse is overlaid by backscatter effects of concrete (structural noise) so that the phase jump between two different locations of the probe normally is not visible clearly enough for a reliable assessment of grouting condition. One example is depicted in Fig. 6.22.

It is an example measured at a prefabricated road bridge in Germany applying the equipment mentioned above with actual evaluation software being able to switch between raw data (HF signal) and rectified data [Sodeikat and Dauberschmidt, 2008] (see Fig. 6.20).

**Fig. 6.22** Sectional view of the two-hole test specimen (dimensions in mm) [Schickert 2005]



## 5.4 Linear and 2D Measurement followed by Imaging with Reconstruction calculation (magnitude evaluation)

### 5.4.1 Examples in the laboratory

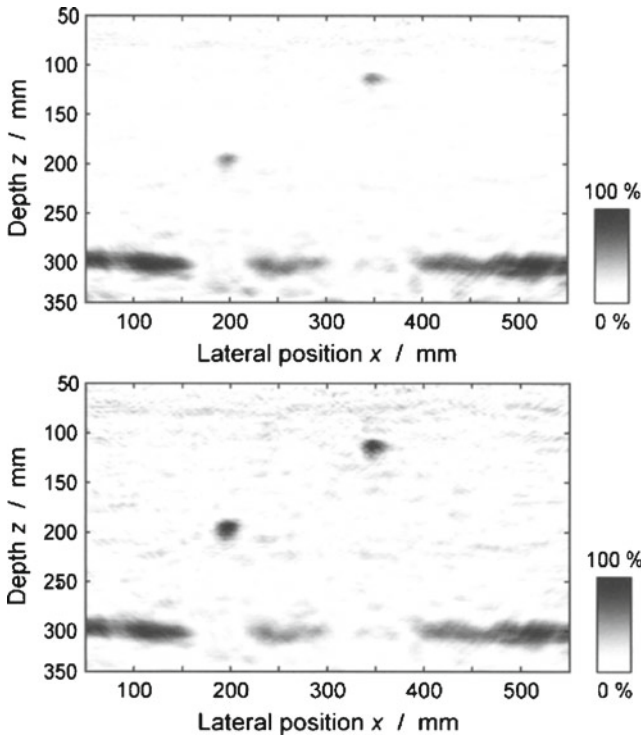
The examples described in the two previous sections are limited to few applications. The most impressive success in the last years was achieved applying linear and 2D measurements with successive imaging. This imaging is performed using reconstruction calculation with SAFT-Synthetic Aperture Focusing Technique. Here 2D and 3D applications in the heuristic time shifting approach [Schickert et al, 2003] as well as with Fast Fourier transform [Mayer et al, 2008] are applied.

The first example of 3D imaging of a void in a tendon duct was presented in 1996 in the frame of a round robin test carried out at a test specimen with artificial grouting faults in a tendon duct without strands [Krause et al, 1997]. The example depicted Fig. 6.21 was measured applying a broadband pressure wave pulse ( $f = 85$  kHz) and a 2D scanning laser interferometer as receiver. For good signal/noise ratio retro reflecting colour was used.

The capability for imaging holes with linear measuring and 2D-reconstruction is demonstrated in Figs. 6.22 and 6.23. Applying broadband transducers excitation with rectangular pulses are guided along the known position of a tendon duct, and the data are registered with high repetition frequency. Applying a commercial equipment development together with statistical analyzing methods the localization of air inclusions is possible [Schickert 2005]. Figures 6.22 and 6.23 presents a result obtained at a borehole, which is partially filled with cement. Applying statistical evaluation a noise threshold is defined. Then the reflection magnitude indicates the filling degree of the duct.

The intensity criterion (No.1 in §5.1) is applied with shear waves and pressure waves. For both automated scanning systems are available. For shear waves dry contact transducers described above are applied. They are mounted in large scanners, which can measure surfaces up to  $40 \text{ m}^2$  non-stop, because they don't need any





**Fig. 6.23** SAFT reconstructions, depth corrected using reference reflectors (top) and noise statistics (down) [Schickert 2005]

coupling agent (Fig. 6.24). For automated measuring the p-wave transducers were coupled by water (Fig. 6.25). Another possibility for fast ultrasonic echo measurement is described in § 5.6.

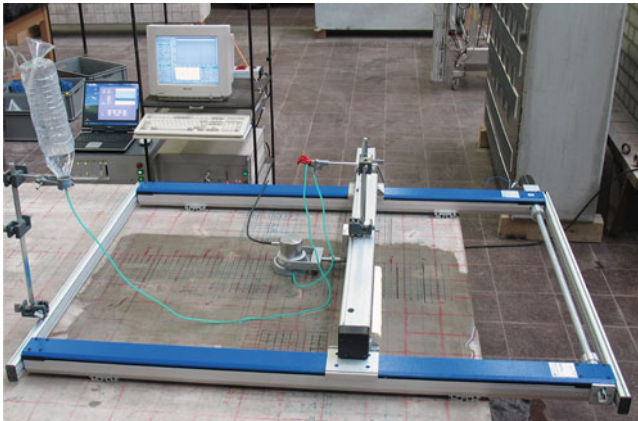
Comparative tests were performed in the frame of the research group FOR 384. Figure 6.26 presents a test specimen with 80 mm tendon ducts containing 12 reinforcing wires (diameter 12 mm; side view Fig. 6.27a).

Figures 6.27a) and 6.28 show the experimental results for ultrasonic measurement and SAFT-reconstruction. In Fig. 6.27a) the shear wave measurements (ultrasonic frequency 55 kHz) are presented with 3D-SAFT reconstruction imaging ([Krause et al, 2003], [Krause et al, 2006]). In this case a longitudinal section parallel to the duct is presented (ultrasonic SAFT B-scan parallel  $x$ ). In Fig. 6.28 the results of linear SAFT reconstruction of p-wave measurement are depicted (centre frequency 200 kHz of transmitting pulse). The jump in ultrasonic reflection magnitude appears at  $x = 800$  mm in both measuring curves and corresponds to the change of grouting conditions.

A second feature in Fig. 6.27a) corresponds to the depth of reflecting signals from the interior of tendon ducts (criterion #2 described in §5.1). As can be seen in



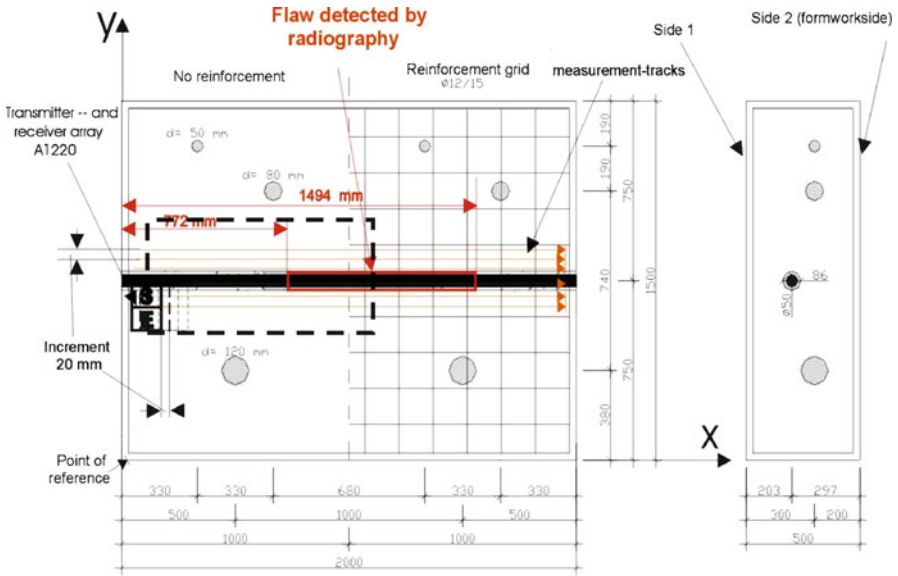
**Fig. 6.24** 2D scanner working with linear drives and a pneumatic system to press the point contact transducers without coupling agent (at BAM Berlin)



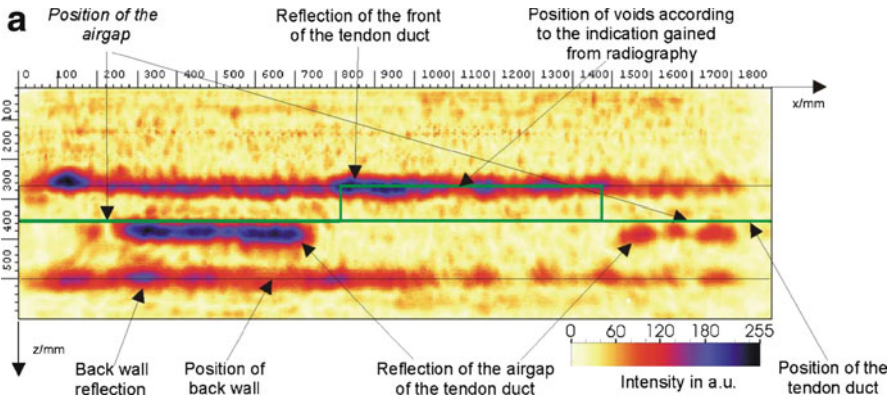
**Fig. 6.25** Ultrasonic measuring head for pressure waves mounted in a 2D scanner working in pulse echo mode with water coupling (at MFPA Weimar)

Fig. 6.27b), the tendon duct has an air inclusion at the bottom side, which arrived unintentionally during the grouting process, being bedded on the opposite side (see photograph in Fig. 6.27b). The reflection line at  $z = 380$  mm is obviously related to the existence of the air inclusion, but the measured depth doesn't exactly correspond to a direct reflection at the air inclusion.

The effect of a second signal for well grouted ducts measured with shear waves was also observed in practical applications at post tensioned concrete bridges [Krause et al, 2011]. The effect is not yet completely understood. It depends on the way, how the ultrasonic waves pass the grouting mortar and steel wires and/or propagate along the interface around the tendon duct (concrete/steel sheet/grouting mortar). An explanation

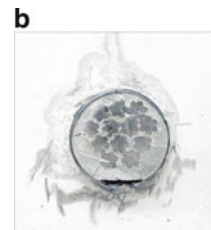


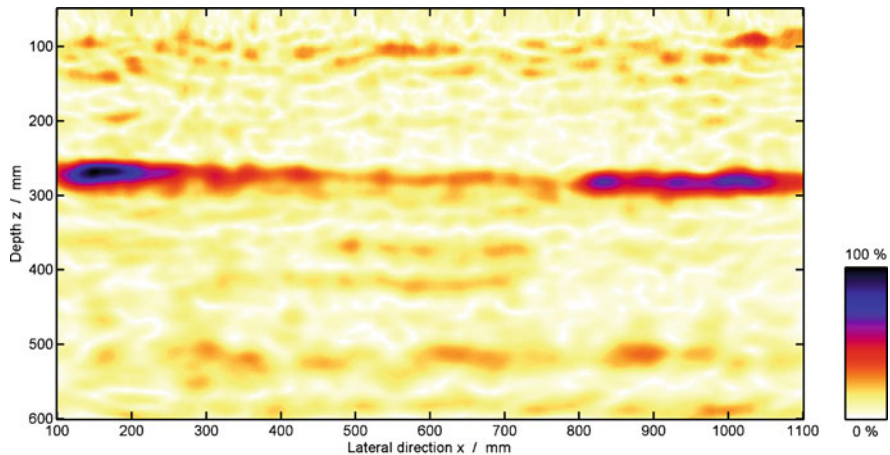
**Fig. 6.26** Construction plan of test specimen BAM.NB.FBS.1, containing artificial voids in a tendon duct and styrodur balls. The location of the void in the duct was localized using  $\gamma$ -radiography. Rectangle: Area of pressure wave measurement MFPA Weimar (Fig. 28); Arrows: area of presented shear wave measurement BAM (Fig. 27)



**Fig. 6.27a)** Result of imaging tendon duct in specimen FBS1 with shear waves: B-scan above the tendon duct from 3D-SAFT reconstruction. Polarization axis parallel x

**Fig. 6.27b)** Side view of tendon duct on FBS1 (photograph)





**Fig. 6.28** Result of imaging tendon duct in specimen FBS1 with pressure waves: B-scan above the tendon duct from 2D-SAFT reconstruction

with help of 3D modelling calculation including EFIT (*Elastodynamic Finite Integration Technique*) is still in the works [Krause et al, 2009].

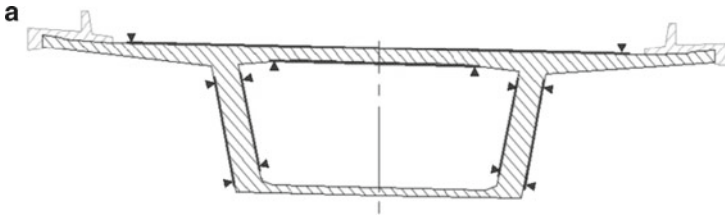
#### 5.4.2 Applications at post-tensioned concrete bridges

In order to assess and to improve the NDT methods for practical application, BAM together with partners regularly performs automated radar and ultrasonic-echo measurements on post-tensioned bridges. Investigations are carried out on areas on the inner and/or outer-side of webs and on the bottom and/or topside of decks with transverse pre-stressing (e.g. [Streicher et al, 2006], [Helmerich et al, 2008]). Those areas are marked with dark lines in a typical cross section (Fig. 6.29a). With exception of topside measurement, traffic on bridges is not affected by those activities.

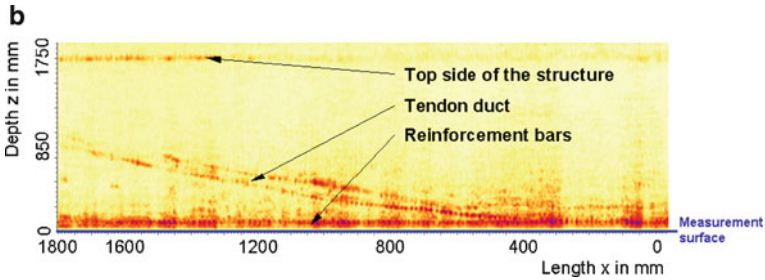
Figure 6.29b) depicts an example of a large scale measurement of a tendon duct measured by means of scanning ultrasonic echo (shear waves 55 kHz) from the bottom side of the bridge. The duct is imaged in the depth range from  $z = 100$  mm to 870 mm. Signals from the bottom side of the duct (close to ultrasonic probe) and partly from the area of the far side are recognisable. Further investigation of those effects is ongoing [Krause et al, 2011]. With ultrasonic 3D reconstruction (3D-SAFT) also tendons arranged behind others can be imaged. As an example Fig. 6.29c) presents from an investigated web.

#### 5.5 Reconstruction calculation using phase evaluation

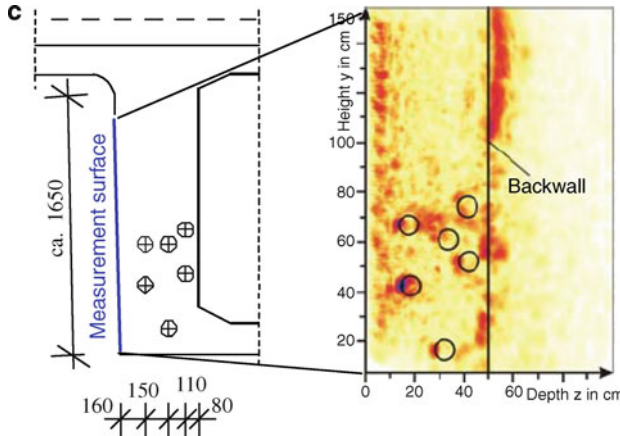
A qualitative distinction between steel and air reflections in concrete becomes possible, when the phase values of the ultrasonic signals are considered in the SAFT reconstruction calculation. This result was achieved within in the frame of the



**Fig. 6.29a)** Investigated areas on box girder bridges using automated NDT-methods



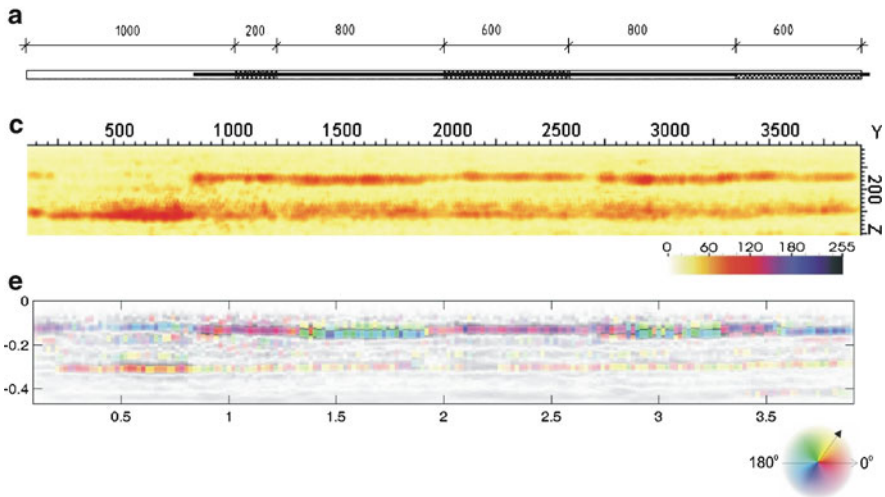
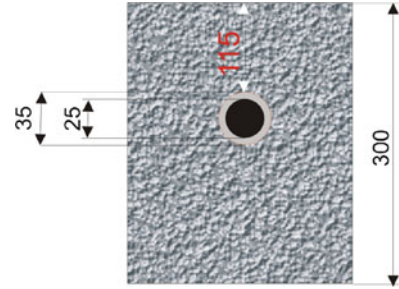
**Fig. 6.29b)** SAFT-B-projection of ultrasonic echo data, imaging the curvature of a tendon duct in the longitudinal section of a T-beam bridge [Streicher et al, 2006]



**Fig. 6.29c)** Arrangement of tendon ducts in the cross section of a box girder web, left: according to construction plan, right: located at a SAFT-B projection by ultrasonic echo [Wiggenhauser et al, 2007]

research group FOR 384 ([Mayer et al, 2006], [Patent, 2006]). A first study describes the method capability [Mayer et al, 2008]. In the following, two exam-ples are presented. The first was carried out at the Large Concrete Slab (LCS, see also Chapter 6, § 4.2.2), which was designed and constructed at BAM in order to realize typical

**Fig. 6.30** Geometry and concrete cover for tendon D3 in LCS



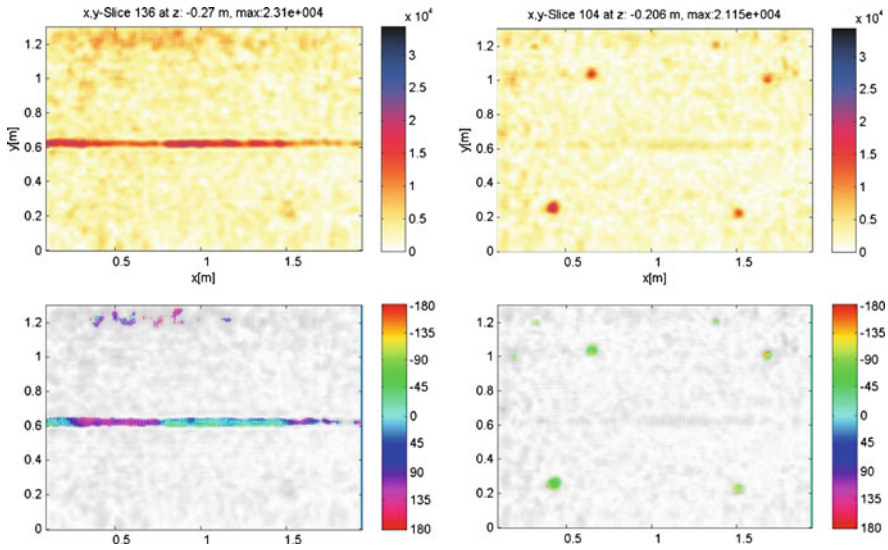
**Fig. 6.31** Results for tendon duct D3 in LCL: **a)** Sketch of the specimen with desired grouting faults; **c)** Result of scanning with 55 kHz shear waves, polarization parallel to the ducts: magnitude representation in a B-scan of 3D-SAFT reconstruction; **e)** Phase values of reflecting pulses around the maximum of each reflector calculated from FT-SAFT reconstruction

testing tasks for the comparison of different NDT methods and their validation [Taffe et al, 2003].

One part of this concrete slab contains 11 tendon ducts in the diameter range from 40 mm to 120 mm having concrete cover between 80 mm and 200 mm with artificial grouting faults. The grouting was performed similar to industrial application (pressure grouting). The geometry of tendon D3 is depicted in Fig. 6.30. It has a concrete cover of 115 mm. It is a steel bar in a duct having a diameter of 35 mm. The experiments were carried out using a 55 kHz point contact transducer working with an automated scanner.

Figure 6.31 depicts the results of ultrasonic imaging experiments of the tendon D3 in comparison with the plan of artificial grouting faults (shaded in Fig. 6.31a)). Their location was verified applying  $\gamma$ -radiography. Figure 6.31c) depicts the magnitude





**Fig. 6.32** Ultrasonic imaging of artificial grouting faults and styrodur balls by means of 3D-SAFT phase evaluation (depth sections (C-scans)) specimen FBS1, SAFT-B-scans of magnitude already shown in Fig. 6.27., see also plan Fig. 6.26. The upper parts of the figures show the magnitude and the lower part the phase value of the reflected pulse, respectively. Left: depth section of the top side of the tendon duct ( $z = 270$  mm); Right: Depth section in the depth of styrodur balls ( $z = 206$  mm). Significant phase value difference between reflection at air inclusions / styrodur and steel.

of ultrasonic reflection intensity as longitudinal section along the tendon duct (ultrasonic B-scan). There is no significant change in reflection intensity at ungrouted areas.

Otherwise the phase evaluation shown in Fig. 6.31e) shows a very clear difference between air filled and well grouted areas. The colour coded image indicates a shift of the phase value of  $180^\circ$  between grouted and ungrouted areas.

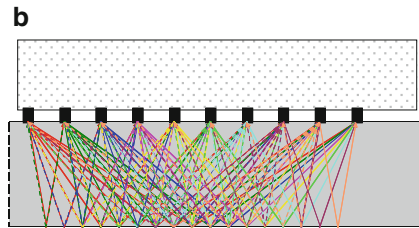
This means that the phase evaluation clearly indicated the difference between air filled and grouted areas, and allows distinguishing between reflection at air and reflection at steel. This is not possible from the intensity representation in this case.

The second example concerns the specimen containing artificial grouting faults and styrodur balls already presented and discussed in section 4.5.1 (Figs. 6.26 to 6.28). The phase evaluation demonstrates the capability to characterise even small air inclusions. Figure 6.32 shows the C-scan (depth section) in the depth corresponding to of the top side of the tendon duct ( $z = 270$  mm), whereas Fig. 6.26 shows the plane of the styrodur balls ( $z = 206$  mm). All balls in the diameter range from 120 mm to 30 mm are imaged. The phase difference between air inclusions ( $\phi = 0$  to  $45^\circ$ ) and steel ( $\phi = -130^\circ$ ) is significant.

**Fig. 6.33a)** Linear array with dry contact transducers



**Fig. 6.33b)** Principle of data acquisition



## 5.6 Ultrasonic Echo with Linear Array

In order to accelerate the ultrasonic data acquisition, a linear array was developed in co-operation between BAM and ACSYS ([Kozlov et al, 2006], [Krause et al, 2008]). It consists of 10 lines à 4 dry contact shear wave transducers working with 50 kHz. The distance of the lines is 35 mm in the present modification. The transducers and the electronics are mounted in a handheld box easily to be applied at concrete surfaces (Fig. 6.33a). The ten lines are switched as a multistatic array, that means one line acts as transmitter and all others as receiver, then the second as transmitter, and so forth as shown in Fig. 6.33b). The data transfer is organized in the way that the whole data set is measured and stored in less than 1 second per location.

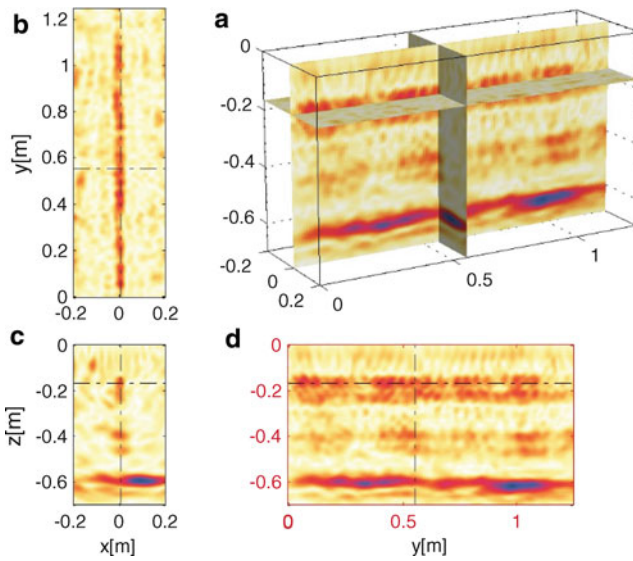
The data measured along a line can be combined to one data set and are evaluated with fast FT-SAFT reconstruction calculation. Together with 3D imaging technique the scatterers and reflectors in the volume of interest can quickly be analyzed on site with cross and longitudinal sections as well as depth sections and phase evaluation (corresponding to ultrasonic B- and C-scans).

In Fig. 6.34 one practical application is presented as example. The aim was to verify if and where are tendon ducts inside of a cross girder, which is 60 cm thick. The data were measured along a line (length 1.16 m) with a step width of 2 cm (orientation of the array perpendicular to the measuring line). The result of the 3D-FT-SAFT reconstruction is shown in Fig. 6.34: the cuboid at the right (a) represents the reconstructed volume (surface: 0.40 m x 1.26 m, depth: 0,70 m). The other parts of the graph represent the different sections, which can be interactively adjusted by three planes. The measuring system with linear SAFT reconstruction also is distributed and applied as commercial equipment [Kozlov et al, 2006].

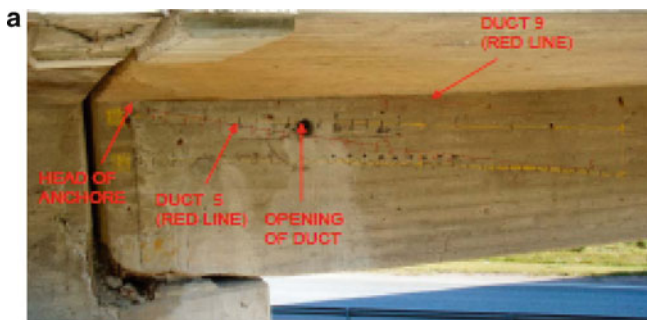
There are numerous reports on practical application of the Linear Scanner system with evaluation software for magnitude representation [De la Haza et al, 2008]. Here several 2D-SAFT evaluations of the array positioning perpendicular to the tendons are combined to one representation showing the reflection magnitude of the tendon duct.

In Figs 6.34a) to 6.34d) an application on a prestressed box girder bridge is presented [Rapaport, 2010]. There are four layers of tendon ducts in the girder, the upper layer has a concrete cover of 125 mm was measured step by step as described above (Fig. 6.34b).

In a section measured on the right border two tendons are imaged in the reconstructed SAFT-C-scan (Fig. 6.35d)): for tendon 5 (bottom) a high reflection



**Fig. 6.34** Result of measurement at a cross girder measured with linear array and 3D imaging with FTSAFT: **a)** Cuboid of the reconstructed volume, three plains are selectable for the different sections: **b)** Depth section (C-scan), **c)** Cross section (B-scan parallel x), **d)** Longitudinal section (B-scan parallel y)



**Fig. 6.35a)** Investigation area at prestressed concrete bridge. Concrete cover of first layer of tendons: 125 mm



Fig. 6.35b) Positioning of linear array



Fig. 6.35c) Verified grouting fault at duct 5

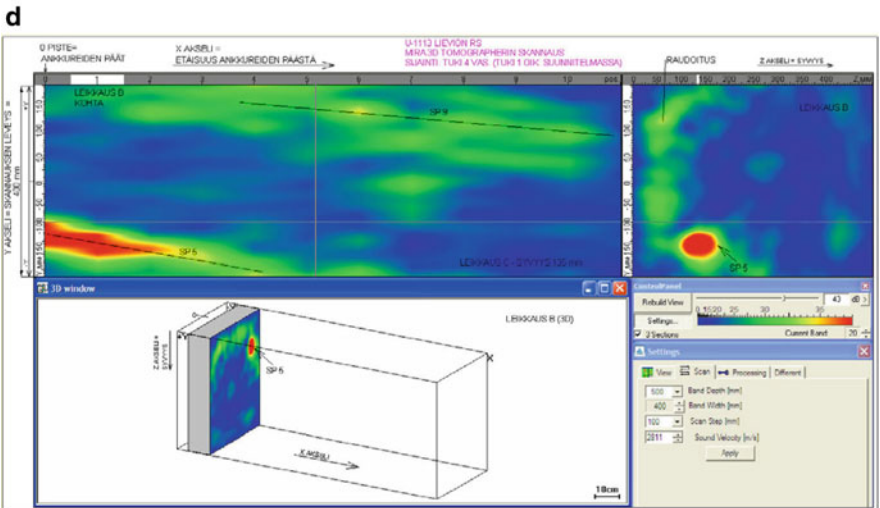


Fig. 6.35d) Magnitude representation of duct 9 (top) and 5 (bottom) of right (right border of measuring area shown in Fig. 6.35a)

magnitude relative to duct 9 (top) is measured indicating bad grouting conditions. This was verified by opening duct 5 (photograph Fig. 6.35c)) and endoscopy. At other locations of the same bridge it was verified that a duct showing similar reflectivity as duct 9 was well grouted.

## 6 Ultrasonic Through Transmission

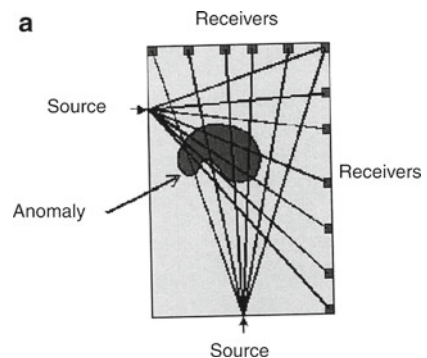
Ultrasonic through transmission is frequently applied in order to measure (determine) the elastic parameters of building materials. From ultrasonic velocity of pressure waves and shear waves the elasticity modules and Poisson's ratio can be calculated.

The distribution of ultrasonic velocity in a building element may give basic information about its integral homogeneity and integrity. The velocity is influenced by the composition of the material as well as by heterogeneities, voids, deteriorated areas, and moisture. By measuring the distribution of the velocity such areas can be localized and classified.

There are several possibilities of ultrasonic through transmission tests. The simplest one is measuring the direct transit time with ultrasonic transmitters positioned directly opposite to the receiver. Other methods are adapted from the crosshole sonic logging method, where two transducers are positioned step by step along lines at both sides of the building element ([Olson and Hollema, 2003], [Binda et al, 2001]). Thus e.g. the velocity distribution in the wall can be roughly deduced. These methods are restricted for the application of coplanar surfaces.

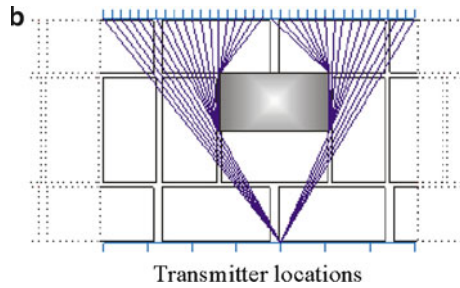
A more sophisticated method is the calculation of the velocity distribution by means of tomographic calculation, based on an inversion applying the so called Radon-transformations. From this, generally an accurate image of the velocity distribution in the inner of the investigated object can be deduced and is imaged in corresponding slices. This method is widely used in metal and plastic investigation as well as medical application [Wüstenberg et al, 2008]. In building engineering this technique was recently developed for masonry (bricks and natural stones) [Wendrich et al, 2006].

Typical ray path examples are depicted in Figs. 6.36a) and 6.36b) for 4-sided and 2-sided access. In the latter also diffraction is taken into account. A principally difficulty for tomographic reconstruction in through transmission arrangement is that voids are regions of quasi zero transmission ( $c$  is nearly equal to zero). The convergence criterion of the algorithm is less distinct in this case.



**Fig. 6.36a)** Ray path scheme for 4-sided access of transducers

**Fig. 6.36b)** Ray path scheme for 2-sided access with void (application for masonry)



For concrete ultrasonic tomography is not used rather often. One example is detecting voids and honeycombing in concrete columns in the frequency range 100 kHz to 200 kHz [Schickert, 2004].

For prestressed concrete structures, tomographic surveys of different concrete beams are described in the British Advice Notes [Forde, 2006]. Examples are shown, where voiding in ducts is clearly detected by ultrasonic tomography and verified by impact-echo.

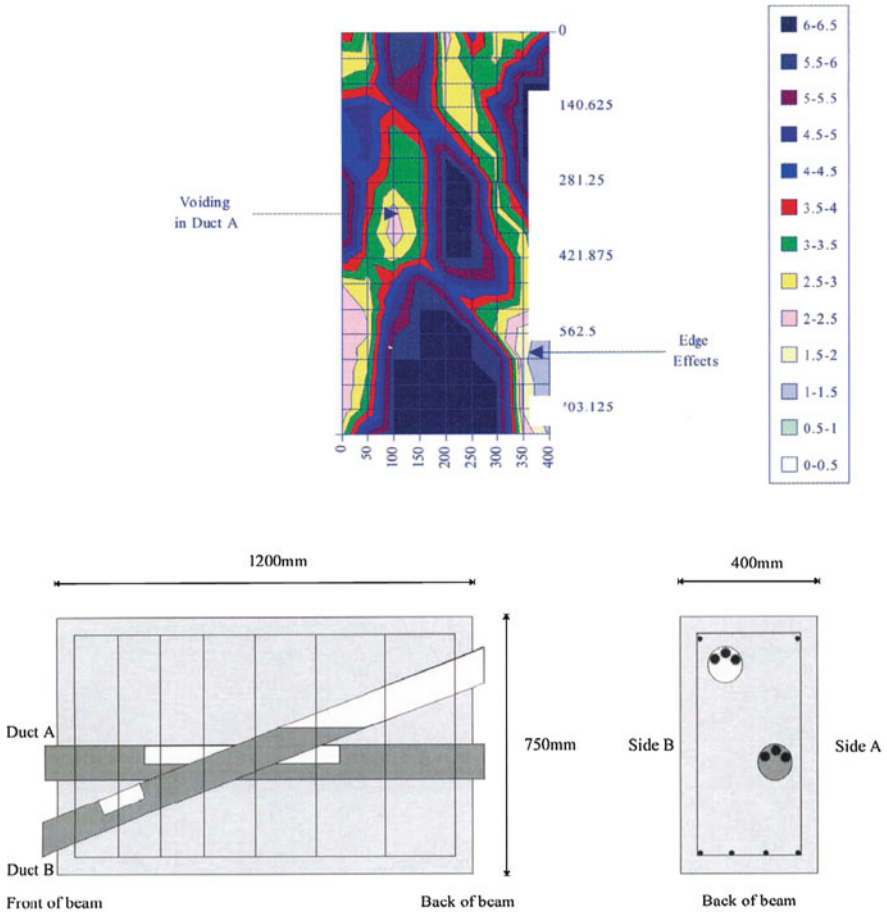
An application at a concrete bridge girder is described in [Martin et al, 2001]. Two test beams were examined: a 10 m long beam at the Transport Research Laboratory (TRL), Crowthorne, UK and a short test beam constructed at Stanger Science and Environment, Elstree, UK. The ducts were 40 mm in diameter in the first test and 100-mm diameter in the second one.

As example the result of a beam from the second test is shown in Fig. 6.37. The beam is 750 mm deep (the plan of the beam is given at the lower part of Fig. 6.37). The measuring field is 400 mm wide with grid locations at 100 mm spacing - using all four faces. A voiding is indicated by a low velocity. Apparent areas of low velocity in the corners are due to the reduced number of transit paths producing unreliable results. It has to be noted that edge effects or errors occur when there is a corner or low density of transmission/reception rays in a model. Edge effects or errors are highlighted in the cross-sections. The method is somewhat time consuming and so should be used in conjunction with a simpler testing method, e.g. sonic impact-echo, which identifies areas of interest. The smaller the ducts to be investigated, the smaller the required distances between testing stations. This therefore significantly increases the testing time.

## 7 Other methods

### 7.1 Radar for plastic ducts

For analysing steel tendon ducts radar is not suitable because shielding of electromagnetic waves. In contrast it is possible to apply Radar in case of post tensioned structures using tendon ducts made of plastic.

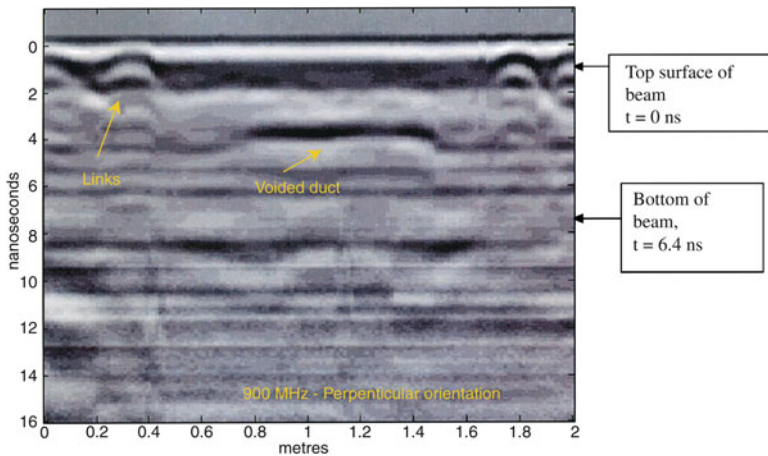


Note: The voids are formed by an air gap or a polystyrene box-out

Fig. 6.37 Tomographic Survey of a cross-section of a concrete beam (after [Martin et al, 2001])

Radar Antennas in the frequency range of 500 MHz, 900 MHz and 1.5 GHz were tested at test specimens containing plastic tendon ducts of 90 mm and 63 mm diameter in beams made from concrete with maximum aggregate size of 20 mm [Forde, 2006]. As depicted in Fig. 6.38 the voided part of the duct (concrete cover 230 mm) is imaged showing a time of flight of  $t = 4$  ns. Otherwise the reinforcing bars put in the specimen (spacing 20 mm) cause quite intense reflection of Radar pulses, which might hinder the image of the voided duct. Theoretical calculations lead to the conclusion that the perpendicular polarisation is more sensitive to the imaging of the voided plastic duct than the parallel orientation.

Ground-penetrating radar (GPR) inspection was conducted on fourteen concrete specimens by [Pollock et al, 2008]. Based on the GPR surveys conducted in this



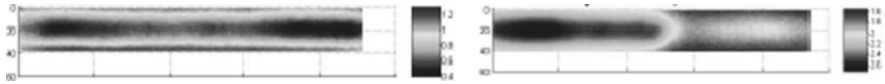
**Fig. 6.38** Indication of voided plastic duct by means of 900 GHz antenna (test specimen)

study, it is apparent that the detection of simulated voids within grouted ducts embedded in concrete is possible with a 1.5 GHz GPR system. Although none of the post-tensioning strands and simulated air voids within the grouted steel ducts was detectable, simulated voids within plastic ducts were generally detectable in GPR images. In another study [Conner et al, 2006], GPR was successfully used as a local inspection technique to precisely locate simulated voids as small as 1.5 in. (thick) adjacent to post-tensioning strands in grouted HDPE (High Density Polyethylene) ducts embedded in concrete slabs at depths of 5 to 20 centimeters.

## 7.2 Active Thermography

Thermal imaging can be used to detect simulated air voids within grouted post-tensioning ducts, thus locating areas where the post-tensioning steel strands are vulnerable to corrosion. [Pollock et al, 2008] prepared specimens with voids. For the thermal imaging inspections, six concrete specimens were constructed to simulate the walls of post-tensioned box girder bridges. The most important deduction taken from these inspections was that ducts and simulated voids were more detectable in the 20 cm thick specimens than in the 30 cm thick specimens. Inspections revealed the majority of the simulated voids in the former case, while, only one thicker specimen inspection indicated the presence of simulated voids (out of four voids in two ducts). Also, ducts were much clearer and visible in the thermal images of the thinner specimens.

[Rieck and Hillemeier, 2003] used transient thermography to monitor the grouting of steel ducts. All voids in the ducts could be detected using the heat of hydration of the cement lime inside the ducts. Even voids in tendons with a concrete



**Fig. 6.39** Phase image of the beam without (left) and with (right) defect, at 0.78 mHz (after [Brachelet and al, 2009])

cover of 12 cm could be detected at an early stage. Applying thermal impulse heating and IR imaging for the same specimen, the voids in the tendon ducts could be localized up to a concrete cover of 7 cm.

Another heating source was used by [Brachelet and al, 2009], which consisted in induction heating, with a magnetic field. The analysis of both magnitude and phase on thermal images has shown that it is possible to identify the ungrouted areas (Fig. 6.39). The major drawback remains the relative slowness of the procedure. Further studies should focus on the design of the inductor and the heating time optimization.

Up to now, transient IR thermography for localizing grouting faults was mainly developed in laboratory, but very little on site application is reported. The contact-free aspect of this method is very attractive, when rapid measurements are desired. Although this method is very powerful for testing materials such as steel and carbon fibre laminates, the maximum penetration depth in concrete seems to be limited to only about 100 mm.

## 8 Conclusions

Most applications concerning non-destructive testing of tendon ducts deal with metal ducts. Because of the shielding of electromagnetic waves off metal surfaces, radar is principally not applicable in this task. It can however be used in a first step, to locate the ducts on which other methods are applied.

**Radiography** applying X- and Gamma Radiation is the oldest method to investigate the interior of steel and concrete structures. They still play an important role for NDT of post tensioned concrete bridges because of the capability of penetrating thick concrete elements up to 1 m. Using digital imaging plates instead of films these methods have become much more sensitive during the last decade.

Principally the method requires that the building element is accessible from both sides. Using radioactive radiation sources the thickness is limited to about 0.7 m, applying linear accelerators (or betatrons) even a thickness up to 1 m is feasible with an acceptable expenditure of time.

The first applicable **mechanical wave** method applied for this purpose was Impact Echo. The first version of Impact-Echo, developed at the end of 1980s, involves equipment which is not too complex and rather easy to use. Impact-Echo was widely applied in the 1990s and had the advantage of dry coupling on concrete surfaces. Even though evaluation in the frequency domain works best for planar slabs, the method was also applied for post tensioned structures with more complicated

geometry. Since mid-1990s, several commercial equipments came into the market and numerous applications were reported with partially verified results.

Basic research on this method at the beginning in the 1990s showed that the geometry of building elements affects the signals recorded. Based on principles of multiple reflections at tendon ducts, other concepts such as back wall frequency shift and influence of stiffness were thoroughly investigated. The originally affirmed reduction of Impact-Echo frequency to its half in case of metallic reflection could never be confirmed for grouted tendon ducts.

The principle of impact echo imaging deduced from 2-D measurements was developed and produced representations in analogy to ultrasonic evaluation (B-scan or Impact-Echogram according to longitudinal or cross section, respectively; C-scan according to depth section). However technical disputes on how to characterize the condition of tendon ducts remain.

Due to the advances in 2-dimensional Impact-Echo measurement, partly as a result of automated scanning systems used since 2003, the point measurement evaluation for tendon duct characterisation has become less common. At the same time modelling of wave propagation gained importance for interpreting the data and clarifying the results. For the theoretical background of Impact-Echo the aspect of Lamb waves published in 2005 was very important.

SIBIE (Stack Imaging of Spectral Amplitudes) is a new analysis scheme for impact echo based on spatial summation of the first and second harmonics. However real-world applications of SIBIE to characterize tendon ducts have not yet been reported.

The **ultrasonic echo** technique for evaluation of concrete elements has been developed in 3 phases:

In the 1990s broadband transducers in the appropriate frequency range (around 100 kHz) were developed. Simultaneously Synthetic Aperture techniques for imaging and modelling via Elastodynamic Finite Integration Techniques (EFIT) were developed and first applications on structures took place. Contactless measurement with laser interferometer was also used.

With the development of dry contact shear wave transducers in 2000, large areas could be measured much faster than before. This development also facilitated the construction of automated scanners for large structure evaluation (up to 40 m<sup>2</sup>). Also new reconstruction programs and modelling of wave propagation helped further advancement and application of ultrasonic imaging. Several types of multistatic measuring equipment were developed and commercial NDT-testing of post tensioned concrete members began.

Since 2005, when the phase evaluation of the reflected signal was integrated in reconstruction calculation, the evaluation of testing results became more reliable. Validation and development of commercially available scanning systems in recent years has drawn a lot of attention.

More precise measuring capacities give rise to new questions. For example it is not yet completely understood how elastic waves penetrate or circulate around tendon ducts depending on their inner condition. Another point is the possibility to investigate the condition of tendon ducts in the second or third layer. The research work in such areas has only begun.



Nevertheless the potential of the method is rather promising leading to further research and development of equipment. The capability seems to be limited only by poor surface conditions or dense reinforcing layers.

Impact-Echo and ultrasonic echo field measurements have revealed very impressive results. Since dry contact transducers are also available for ultrasonic measurement in the appropriate frequency range, ultrasonic echo is sometimes advantageous because it can provide a better spatial resolution.

The use of ultrasonic through transmission method for inspection of tendon ducts has not been documented in the past years since 2002. One difficulty could be that air filled areas correspond to very low velocity whereas algorithms for through transmission are more precise for regions with greater wave speed.

Radar measurements (for plastic ducts only) and transient IR thermography (mainly used on laboratory) are alternative solution. The contact-free aspect of IR thermography is very attractive, when rapid measurements are desired. However, the penetration depth (in the case of dense reinforcements) and the slow time response for thermography put practical limits for on site measurements.

In order to advance reliable application of all testing methods three points seem to be useful:

- Precise description of the methods and quantitative assessment of their potentials and limitations. Controlled test sites and setting benchmarks have been developed for this purpose but there are still shared experiments.
- Educating and developing training courses for NDT engineers.
- Persuading owners and stakeholders that NDT can reduce the lifetime costs through quality assurance.

The activities of RILEM TC INR-207 were part of these actions. Next step may be to update existing and work out new standards. All this may encourage more producers, developers and engineering offices to come into the market with new equipment, software and offers.

## References

- Abraham O., Cote P. (2002) Thickness Frequency Profile for the detection of voids in tendon duct. *ACI Structural Journal* 99, 3, pp. 239-247.
- Abraham O., Cottineau L.M., Valade M., Bedaoui S., Argoul P. (2009) Laser interferometer robot for the detection of voids in tendon ducts with the impact echo method, *Int. Conf. NDT-CE 2009*, Nantes, France.
- Abraham O., Popovics J., Cottineau L.M., Durand O. (2010) Laser ultrasonics for civil engineering: some applications in development for concrete non destructive testing, *Int. Conf. Laser Ultrasonics*, 2010, Bordeaux, France.
- Abraham O., Popovics J. (2010) Non destructive evaluation of reinforced concrete. Chapter 21: impact echo, pp. 466-489, ed. Maierhofer C., Reinhardt H.W., Dobman G., Woodhead Publ. Ltd.
- AFNOR (2001) NF A09-202 Non-destructive testing - General principles for radiographic examination of reinforced concrete and prestressing materials by X- and gamma.
- Algeron D. (2007) Measurements at specimen in Lyon (CETE-LCPC), private comm..

- Al-Qadi I., Washer G. (2006) NDE Conference on Civil Engineering, A Joint Conference of the 7<sup>th</sup> Structural Materials Technology: NDE/NDT for Highways and Bridges and the 6<sup>th</sup> Int. Symp. NDT-CE, 14.-18. August 2006, St. Louis, MO, USA, CD-ROM.
- Alver N., Ohtsu M. (2006) Visual identification of defects in concrete by SIBIE procedure. In: Al-Quadi, I. and G. Washer (eds.); Proc. NDE Conference on Civil Engineering, 14-18. August 2006, St. Louis, MO, USA.
- Alver N., Ohtsu M. (2007) BEM analysis of dynamic behavior of concrete in impact-echo test. Construction and Building Materials, Elsevier, Vol. 21, 3, pp. 519-526.
- Alver N., Takaki K., Ohtsu M. (2007) Visual identification of surface-crack depth in concrete by SIBIE. JCA Proc. of Cement & Concrete (Japan Cement Association), Vol. 60, pp. 199-204.
- Ata N., Mihara S., Ohtsu M. (2007) Imaging of ungrouted tendon ducts in prestressed concrete by improved SIBIE. NDT&E International 40, p. 258-264.
- BASt (2010) [http://www.bast.de/nn\\_82260/EN/e-Aufgaben/e-abteilung-b/e-referat-b4/e-schadensanalyse/e-schadensanalyse.html](http://www.bast.de/nn_82260/EN/e-Aufgaben/e-abteilung-b/e-referat-b4/e-schadensanalyse/e-schadensanalyse.html)
- Binda L., Saisi A. Tiraboschi C. (2001) Application of sonic tests to the diagnosis of damaged and repaired structures, NDT&E International 34, pp.123- 138.
- Brachelet F., Du T., Defer D., Antczak E. (2009) Detection of poor filling in prestressed beams specimen by inductive thermography and transfer function analysis, NDTCE'09, Non-Destructive Testing in Civil Engineering, Nantes, France, June 30th – July 3rd, 2009
- CETE (2006) Centre d'Etudes techniques de l'Equipement de Lyon, La Gammagraphie sur les ouvrages d'art.
- Colla C., Schneider G., Wiggenhauser, H. (1999) Automated Impact-Echo: Method improvements via 2-D and 3-D imaging of concrete elements, In: Proceedings of Structural Faults and Repair, London, pp. 1-11.
- Concrete Society, the (2002) Durable post-tensioned concrete bridges, Concrete Soc. Technical Report No. 47, Second Edition, Century House, Crowthorne, Berkshire RG45 6YS, UK.
- Conner J.M., Pollock D.G., Khaleghi, B. (2006) Detection of Simulated Voids in Grouted Ducts using Ground-Penetrating Radar, Proc. 2006 Concrete Bridge Conference, Portland Cement Association
- De la Haza A., Petersen C. G., Samokrutov A. (2008) Three dimensional imaging of concrete structures using ultrasonic shear waves, In: Forde, M. C. (ed.); Proc.12th Int. Conf. Structural Faults and Repair, Edinburgh, Scotland, 10.-12. Juni 2008.
- DGZfP (2010) <http://www.dgzfp.de/Fachaussch%C3%BCsse/ZfPimBauwesen.aspx>
- DGZfP (1990) 90DGZ1 Merkblatt für die Durchstrahlungsprüfung von Stahlbeton und Spannbeton (B1), Deutsche Gesellschaft für Zerstörungsfreie Prüfung e.V., Berlin.
- Dufay J.C., Piccardi J. (1985) SCORPION, premier système de radioscopie télévisée haute énergie pour le contrôle non destructif des ouvrages d'art en béton précontraint », Bulletin de liaison des Laboratoires des Ponts et Chaussées, N°139, pp 77-84, Sep-Oct 1985.
- Eichinger E. M., Diem J., Kolleger J. (2000) Bewertung des Zustandes von Spanngliedern auf der Grundlage von Untersuchungen an Massivbrücken der Stadt Wien. Institut für Stahlbeton und Massivbau, Heft 1.
- FDoT (2003) Florida Department of Transportation Central Structures Office: Test and Assessment of NDT Methods for Post-Tensioning Systems in Segmental Balanced Cantilever Concrete Bridges. DMJM & HARRIS.
- Forde M. (2006) Advice Notes NDT Highway Structures, GB, [http://www.trl.co.uk/online\\_store/reports\\_publications/papers\\_articles/cat\\_paper\\_highway\\_engineering/](http://www.trl.co.uk/online_store/reports_publications/papers_articles/cat_paper_highway_engineering/).
- Gibson A., Popovics J. (2005) Lamb Wave Basis for Impact-Echo Method Analysis. Journal of Engineering Mechanics, ASCE 5, pp. 438-443.
- Große Ch., Beutel R., Wiggenhauser H., Algernon D., Schubert F. (2007) Impact-Echo. Bergmeister, K., Wörner, J.-D. (Hrsg.); BetonKalender 2007, Verkehrsbauten-Flächentragwerke. Berlin: Verlag Ernst & Sohn, Bd. 1, Kapitel V Echoverfahren in der zerstörungsfreien Zustandsuntersuchung von Betonbauteilen, Absch. 3, S. 496-505.
- Helmerich R., Niederleithinger E., Algernon D., Streicher D., Wiggenhauser H. (2008) Bridge inspection and condition assessment in Europe, Transport. Res. Record, TRB, Vol 2044, pp. 31-38.

- IAEA (2002) Guidebook on non destructive testing of concrete structures, Int. Atomic Energy Agency, Vienna.
- Jansohn, R. and J. Scherzer (2002) Improper filled ducts detected by ultrasound reflection, In: Proceedings of the 8th ECNDT, 17.-21. June 2002, Barcelona, Spain, CD-ROM.
- Kozlov V.N., Samokrutov A.A., Shevaldykin V.G. (2006) Ultrasonic Equipment for Evaluation of Concrete Structures Based on Transducers with Dry Point Contact. In: Al-Qadi, I. and Washer G. (eds.); Proc. NDE Conference on Civil Engineering, 14.-18. August 2006, St. Louis, MO, USA, pp. 496-498.
- Krause M., Bärmann R., Frielinghaus R., Kretzschmar F., Kroggel O., Langenberg K., Maierhofer Ch., Müller W., Neisecke J., Schickert M., Schmitz V., Wiggenhauser H., Wollbold F. (1997) Comparison of pulse-echo methods for testing concrete. In: NDT&E International Sonderheft, Vol. 30, 4, pp. 195-204.
- Krause M., Wiggenhauser H., Krieger J. (2002) NDE of a Post Tensioned Concrete Bridge Girder Using Ultrasonic Pulse Echo and Impact Echo, Proc. Structural Materials Technology (SMT), NDE/NDT for Highways and Bridges Topical Conference, 10.-13. September 2002, The Westin Cincinnati, Cincinnati, OH, USA
- Krause M., Mielentz F., Milmann B., Streicher D., Müller W. (2003) Ultrasonic imaging of concrete elements: State of the art using 2D synthetic aperture. In: DGZfP (ed.); Int. Symp. NDT-CE Berlin, Germany, September 16-19, 2003.
- Krause M., Milmann B., Schickert M., Mayer K. (2006) Investigation of Tendon Ducts by Means of Ultrasonic Echo Methods: A Comparative Study. Proceedings of the 9th Eur. Conf. on NDT, September 25-29, 2006, Berlin: DGZfP, BB 103-CD, Tu.3.2.1.
- Krause M., Gräfe B., Mielentz F., Milmann B., Friese M., Wiggenhauser H., Mayer K. (2008) Ultrasonic Imaging of Post-tensioned Concrete Elements: New Techniques for Reliable Localization of Grouting Defects. In: Alexander M. G., Beushausen H.-D., Dehn, F. and Moyo P. (eds.); Proc. Concrete Repair, Rehabilitation and Retrofitting II, ICCRRR 2008, 24.-26.11.2008, Kapstadt, CD-ROM, pp. 521-527.
- Krause M., Milmann B., Mielentz F., Streicher D., Redmer B., Mayer K., Langenberg K.-J., Schickert M. (2008) Ultrasonic Imaging Methods for Investigation of Post-Tensioned Concrete Structures: A Study of Interfaces at Artificial Grouting Faults and its Verification. Journal of Nondestructive Evaluation, 27, pp. 67-82.
- Krause M., Mayer K., Friese M., Milmann B., Mielentz F., Ballier G. (2011) Progress in ultrasonic tendon ducts imaging, In: Derobert, X. and O. Abraham (eds.);EJECE No 77, in print.
- Kroggel O., Scherzer J., Jansohn R. (2002) The Detectability of Improper Filled Ducts with Ultrasound Reflection Techniques. <http://www.ndt.net/article/v07n03/kroggel/kroggel.htm>, NDT.net 7, 3, No. 03,
- Krüger M., Große C.U. (2006) Crack depth determination using advanced impact-echo techniques, ECNDT.
- Langenberg K.J., Marklein R., Mayer K. (2002) Applications to Nondestructive Testing with Ultrasound, in E. R. Pike, P. C. Sabatier (eds.), Scattering: Scattering and Inverse Scattering in Pure and Applied Science, pp. 594-617, Academic Press, London, UK.
- Langenberg K.J., Marklein R., Mayer K. (2009) Theoretische Grundlagen der zerstörungsfreien Materialprüfung mit Ultraschall, Oldenbourg Wissenschaftsverlag GmbH München.
- Lanneau P. (1993) Mise en oeuvre de l'accélérateur linéaire portable MINAC pour des contrôles radiographiques de chantier, Revue pratique de contrôle industriel., vol. 32, no182, pp. 40-43,
- Lausch R., Wiggenhauser H., Schubert F. (2002) Geometrieeffekte und Hüllrohrortung bei der Impaktechopprüfung von Betonbauteilen - Experimentelle und modelltheoretische Ergebnisse. In: DGZfP-Jahrestagung 06.-08. Mai 2002 in Weimar, DGZfP-Berichtsband BB 80-CD, Plakat 34, Berlin (2002).
- Lin Y., Lin K. (1997) Transient impact response of bridge I-girders with and without flaws. ASCE Journal of Bridge Engineering, 2(4), 131-138.
- Maierhofer Ch., Krause M., Mielentz F., Streicher D., Milmann B., Gardei, A., Kohl Ch. Wiggenhauser H. (2004) Complementary application of radar, impact-echo and ultrasonics for

- testing concrete structures and metallic tendon ducts. in: Proc. 83rd Annual Meeting Transportation Research Board of the National Academies, 11.-15. January 2004, Washington, D.C.
- Martin, J., Broughton, K., Giannopolous, A., Hardy, M. and M. Forde: Ultrasonic tomography of grouted duct post-tensioned reinforced concrete bridge beams. *NDT&E International* 34 (2001), p. 107-113.
- Mayer K., Langenberg K.-J., Krause M., Maierhofer Ch., Milmann B., Kohl Ch. (2006) Characterization of Ultrasonic and Radar Reflector Types in Concrete by Phase Evaluation of the Signal and the Reconstructed Image. In: Proc. 9th European Conference on NDT, September 25-29, 2006, Berlin: DGZfP, BB 103-CD, We.1.3.4.
- Mayer K., Langenberg K.-J., Krause M., Milmann B., Mielentz F. (2008) Characterization of Reflector Types by Phase-Sensitive Ultrasonic Data Processing and Imaging, *J. of Nondestructive Evaluation* 1-3, 27, pp. 35-45.
- Mayer, K., Milmann, B., Krause, M. and F. Mielentz (2008b) Methode zum Nachweis von Verpressfehlern in Spannbeton durch Phasenauswertung bei Ultraschallecho-Verfahren, *ZfP-Zeitung* 112 (2008) 12, S. 37-40
- Ohtsu M., Watanabe T. (2002) Stack imaging of spectral amplitudes based on impact-echo for flaw detection. *NDT&E International*, Vol. 35, No. 3, pp. 189-196.
- Olson L.D., Hollema D.A. (2003) Crosshole Sonic Logging and Velocity Tomography Imaging of Drilled Shaft Foundation, Int. Symp. NDT- CE 2003, Berlin.
- Patent (2006) Patentanmeldung DE 10 2006 027 132.7: Verfahren zum Detektieren von Fehlstellen in Betonbauteilen, BAM, Bundesanstalt für Materialforschung und -prüfung, Universität Kassel. Anmeldetag: 02.06.2006.
- Pollock D.G., Dupuis K.J., Lacour B., Olsen K.R. (2008) Detecting voids in prestressed concrete bridge using thermal imaging and ground penetrating radar, WA-RD 717.1, WSDot Res. Rep., dec. 2008.
- Rapaport, G., inc. Ramboll, Finland: Scanning By MIRA 3D Tomographer, case study, 2010, unpublished.
- Rieck C., Hillemeier B. (2003) Detecting Voids Inside Ducts of Bonded Steel Tendons Using Impulse Thermography. in: DGZfP (ed.); International Symposium Non-Destructive Testing in Civil Engineering (NDT-CE) in Berlin, Germany, September 16-19, 2003, Proceedings on BB 85-CD, P21, Berlin.
- Roënelle P., Abraham O. (2006) Détections de vides dans les gaines de précontraintes par la méthode écho, In: Abraham, O. (ed.), *Champs physiques et propagation dans les sols et les structures du génie civil*, ISSN 1167-4865, LCPC, pp. 81-93.
- Sansalone M., Streett W. (1997) *Impact-Echo*. Jersey Shore, PA: Bullbrier Press.
- Schickert M., Krause M., Müller W. (2003) Ultrasonic Imaging of Concrete Elements Using Reconstruction by Synthetic Aperture Focusing Technique. *Journal of Materials in Civil Engineering (JMCE)*, ASCE Vol. 15, 3, pp. 235-246.
- Schickert M. (2004) Ultraschall-Tomographie an Betonbauteilen, in: DACH-Jahrestagung, 17-19 may 2004, Salzburg.
- Schickert M. (2005) Progress in ultrasonic imaging of concrete. *Materials and Structures* 38; 11, pp. 807-815
- Schickert, M. and M. Krause (2010) Ultrasonic evaluation of reinforced concrete structures, in: Maierhofer, Ch., Reinhardt, H.-W. and G. Dobmann (eds.): *Non-destructive evaluation of reinforced concrete structures*, Woodhead Publishing Limited, Cambridge, Part II.22, pp. 490-530
- Schubert F., Köhler B. (2008) Ten lectures on Impact-Echo. *Journal of Nondestructive Evaluation* 27, 1-3, pp. 5-21.
- Sodeikat Ch., Dauberschmidt Ch. (2008) Anwendung von Georadar und Ultraschall – Fallbeispiele aus der Praxis eines Ingenieurbüros. In: Tagungsband zur Fachtagung Bauwerksdiagnose 2008, Praktische Anwendungen Zerstörungsfreier Prüfungen und Zukunftsaufgaben, 21.-22.02.2008, Berlin, Berichtsband BB 112-CD, Vortrag 13.
- Streicher D., Algernon D., Wöstmann J., Behrens M., Wiggenhauser H. (2006) Automated NDE of post tensioned bridge using imaging echo methods, ECNDT, Berlin, 25-29 Sept. 2006.

- Taffe A., Borchardt K., Wiggenhauser H. (2003) Specimen for the improvement of NDT-methods - Design and construction of a Large Concrete Slab for NDT methods at BAM. In: DGZfP (ed.); Int. Symp. NDT-CE.
- Taffe A., Kind T., Stoppel M., Wiggenhauser H. (2008) OSSCAR - Development of an On-Site SCanner for automated non-destructive bridge testing. In: Alexander M. G., Beushausen H.-D., Dehn, F. and Moyo P. (eds.); Proc. Concrete Repair, Rehabilitation and Retrofitting II, ICCR 2008, 24.-26.11.2008, Kapstadt, CD-ROM, pp. 541-545.
- Tinkey Y., Olson, L., Wiggenhauser H. (2005) Impact Echo Scanning for Discontinuity Detection and Imaging in Post tensioned Concrete Bridges and Other Structures. *Materials Evaluation* 63, 1, pp. 64-69.
- Tinkey Y., Olson L.D. (2008) Application and Limitations of Impact Echo Scanning for Void Detection in Post tensioned Bridge Ducts, *Transport Research Record: Journal of the Transportation Research board* No. 2070, Washington, D.C., pp. 8-12.
- Vogel T. (2002) Zustandserfassung von Brücken bei deren Abbruch - Erkenntnisse für Neubau und Erhaltung. *Bauingenieur* 77, 12, 559-567.
- Wendrich A., Trela C., Krause M., Maierhofer C., Effner U., Wöstmann J. (2006) Location of voids in masonry structures by using radar and ultrasonic traveltime, ECNDT, Berlin.
- Wiggenhauser H., Schickert M. (2003) Non-destructive Testing in Civil Engineering, Proceedings Berlin 2003
- Wiggenhauser, H. (2003) Duct inspection using scanning impact-echo, In: DGZfP (Ed.); International Symposium Non-Destructive Testing in Civil Engineering (NDT-CE) in Berlin, Germany, September 16-19, 2003, Proceedings on BB 85-CD, V101, Berlin (2003).
- Wiggenhauser H., Streicher D., Algernon D., Wöstmann J., Behrens M. (2007) Automated Application and Combination of Non-Destructive Echo Methods for the Investigation of Post-Tensioned Concrete Bridges. In: Long, A. and J. Bungey (eds.); Proceedings of Concrete Platform, Belfast, 19.-20.04.2007, Proc. and CD-ROM, pp. 261-270.
- Wüstenberg H., Erhard A., Austel W., Klanke H.P. (1988) Ultrasonic echo tomography. A new procedure for defect presentation. *Ultraschall- Echo- Tomographie, ein neues Verfahren für die Darstellung von Fehlern. Konferenz- Einzelbericht: Pressure Vessel Technology. 6<sup>th</sup> Int. Conf.*, pp1481 – 1492, Oxford: Pergamon Press.
- Zhu J., Popovics J. (2007) Imaging Concrete Structures Using Air-Coupled Impact-Echo. *Journal of Engineering Mechanics, ASCE*, 6, p. 628-640.

# Chapter 7

## Ruptures of prestressing cables

Jean-Paul Balayssac, Carmen Andrade, Javier Sanchez Monteiro, and Horst Scheel<sup>1</sup>

### 1 Definition of the problem

#### 1.1 What is looked for?

The structures involved are **prestressed concrete structures**. The aim is to detect either **failures of prestressing cables (or strands)** or as a **preventive measure to detect corrosion or damages** before failure.

The corrosion of prestressed cables has been the cause of few structural failures with a high impact, since they occurred without any warning. The most famous case is that of the 32-year old small Ynys-y-Gwas bridge in the UK, of segmented concrete post-tensioned construction, which suddenly collapsed in 1985. Due to the lack of safety (or impossibility to assess it), Britain had a moratorium on post-tensioned bridge construction in 1998.

The forensic investigation of the Ynys-y-Gwas bridge collapse [Woodward et al, 1989] confirmed that the collapse was caused by the intrusion of water and

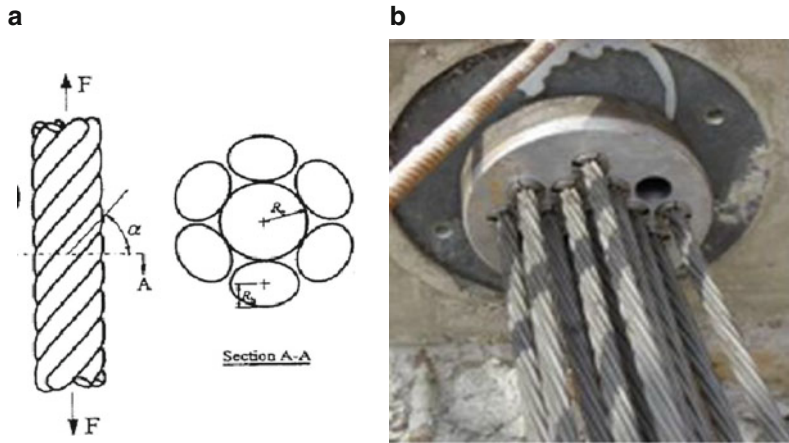
---

<sup>1</sup>Johannes Hugenschmidt and Denys Breysse have also contributed to this section.

J.-P. Balayssac  
Université de Toulouse, UPS, INSA, LMDC  
(Laboratoire Matériaux et Durabilité des Constructions), France  
e-mail: jean-paul.balayssac@insa-toulouse.fr

C. Andrade • J. S. Monteiro  
Eduardo Torroja Institute for Construction Science, Madrid, Spain

H. Scheel  
Technische Universität Berlin, Institut für Bauingenieurwesen,  
Fachgebiet Baustoffe und Baustoffprüfung, Germany



**Fig. 7.1** Example of a strand (a) and of a cable (b) with many strands in the same duct at the anchorage

chlorides at the joints which corroded the internal cables insufficiently protected with cardboard. The bridge gave no visible warning signs of cracking, and as one had no way to inspect the internal cables it was impossible to forecast the accident. Intrusion of contaminants can also occur due to faulty grout, as with Lowes Speedway which suddenly collapsed in Charlotte ( North Carolina, USA), on 2000, 20th may, injuring 114 people.

A strand is made up of several wires (usually seven), and the cable is generally made up several strands (Fig. 7.1). Usually the tendon is the whole system composed by both the cable and the duct filled by the grout.

The assessment of the prestressing cables is important to confirm if the design strength of the structure is always available. Field experiments show that most of the prestressed structures that will need maintenance in the future rely on proven techniques with cable systems. These cables are using different design and technology. Prestressed concrete consists in two predominant fabrication or construction categories: pre-tensioned and post-tensioned.

Pre-tensioned systems are generally used within prefabricated concrete beams and in this case the cables are anchored by bond with surrounding concrete. Post-tensioned structures can use only internal tendons (i.e. inside concrete) or both internal and external tendons (i.e. outside concrete) (box girder bridges). Internal tendons consist of many strands surrounded by a metallic or plastic duct. The duct is filled with a grout or with grease. In this case, the cables are difficult to investigate because the depth of concrete cover can reach many decimeter and also due to the presence of the metallic duct. External tendons consist of many strands fully encapsulated within a continuous high density polyethylene duct filled with grout or grease. The advantage of external prestressed tendons is an easier access for inspection and monitoring than internal tendons.

In post-tensioned concrete structures, it has been found many times that the ducts had big voided sections (due for example to bad injection) and were filled



**Fig. 7.2** An example of corrosion of strands with broken wires [Chauvin, 2005]



only partially. These voids can be present in some critical areas of the ducts for example in the anchorage areas, where corrosion can be initiated. Indeed, chloride-bearing water can find its way through anchorage inside the ducts and eventually initiate a corrosion mechanism at the anchorage and subsequently of the prestressing steel inside the ducts. In pre-tensioned concrete structures the surface of the concrete can be in contact with corrosive media (de-icing salts or marine environment for bridges for example) and in the case of bad waterproofing, the chlorides can reach and depassivate the prestressing steel.

Many kinds of corrosion can occur, either a general corrosion or a pitting corrosion which leads to a stress corrosion cracking because the steel is under tension. Moreover, sometimes, corrosion reactions lead to the evolution of atomic hydrogen, which can be subsequently absorbed into the steel leading to hydrogen embrittlement of the steel and subsequently to failure. These damages can also be increased by creep and also by fatigue and fretting fatigue. See Fig. 7.2 for an example of corroded and broken wires.

## 1.2 At what scale?

Three levels of investigation can be distinguished:

**Level 1-** at the scale of the whole of the structure: for a complete assessment of the structure. This consists of a monitoring of the structure by acoustic emission for example or by vibration analysis. Usually, acoustic emission is able to detect and to localize ruptures of wires. Private companies are able to provide such delivery for long time monitoring of structures. Sometimes if the structure is sensitive, the monitoring can be used as a surveying mean. Regarding the resolution of the localization it depends on the number of sensors and usually it is not very high.

**Level 2-** at the scale of a part of the structure (a girder, a part of the deck): after a visual discriminative inspection or a monitoring which has permit to define some critical zones. The aim is to localize the failures with a good accuracy. This can be

usually achieved by magnetic technique (remanent magnetic method or magnetic flux leakage). Several special techniques are also described in the literature (electromagnetic resonance measurement, eddy current ...).

**Level 3-** at the scale of a cable: this can be used to define what kind of damage is involved in the rupture. For example, to check if the duct is correctly filled by the grout or if there is an active corrosion. For an assessment of the grouting quality, radiography or radioscopy can be used which provides an image of the entire tendon. But the size of sounded area remains limited. Moreover for safety reasons (the technique uses radioactive rays) it is more and more difficult to implement it, particularly in the vicinity of habitations. Some studies are now in progress to study the efficiency of Impact Echo for the detection of voids inside the grout.

Any level can't give a complete answer for the diagnosis of a structure. It would be important to provide a global approach which allows a global diagnosis of the structure, first a discrimination of critical zones and then a more accurate sounding of these zones.

### ***1.3 For what purpose?***

The assessment of the ability of an existing concrete bridge to function must take into account the condition of the prestressing cables. Many failures of tendons have been observed around the world which demonstrates the importance of this problem. A lack of appropriate data can induce a very expensive and destructive assessment of the cables integrity. But, up to now, no methodology for assessing the integrity of the tendons is available. Generally this consists of fixed-interval inspections made by visual observation of the structural elements. But in most cases the rupture of wire or strands is not visible at the concrete surface. A re-bonding of the broken wires by friction on the grout is usual and so the behavior of the structure may remain almost the same. For example, about the Ynys-y-Gwas in the U.K. [Wood, 2008], it was impossible to see any warnings before the collapse. Indeed, the first visible phenomenon is a bending or shearing cracking which results in important prestressing losses. At this stage a lot of stresses are transmitted to the passive reinforcement and a sudden failure of the structure is possible.

So, without any information from a visual inspection, the choice of areas to implement a reliable assessment of the cable by means of destructive or partially destructive techniques is very difficult. Only non destructive testing methods can be implemented to allow a representative diagnosis of a complete structure. Further, no effective means exist for quantitatively measuring condition of the strand. No methodology for integrating results of such measurements into the strength and serviceability rating computations are available. Ideally, a technique able to investigate prestressed reinforcement in concrete and to generate data regarding residual strength of the reinforcement would permit to reach these objectives.

There is a need for investigating the cable condition e.g. how many wires are broken, or is there an active corrosion? Quantitative information, which must be accurate and reliable are required to be used in a process of re-calculation, in order to place the structure in its life cycle; this point is very important because it's conditioning the reliability of the assessment.

Two different approaches can be considered:

- the cable investigation in order to detect a failure and then to go far in the diagnosis: what is the cable condition particularly how many wires are broken, is there an active corrosion which can rapidly induce an other failure?
- the investigation of the cable condition (even if no failure is suspected) in order to quantify the probability of development of corrosion or to detect the presence of un-grouted areas where corrosion can be initiated. This approach could be rather considered as preventive.

## 2 Description of the techniques

For on site non destructive evaluation of rupture of cables, three common techniques can be considered. These are:

- Radiography,
- Magnetic methods: Remanent magnetism method “RMM” or magnetic flux leakage “MFL”,
- Acoustic emission.

For these techniques a presentation is made for detailing their principle, their limits and example(s) of application, including usual combinations not applied for improving the detection of failures, but for a better implementation. For example, ground penetrating radar for the localization of the cables and impact echo for a detection of voids in the duct can be efficiently used. Sometimes, an endoscope is introduced just behind the anchorages to assess the integrity of the cables (corrosion can be detected for example) [Poston and West, 2004]. But these observations are limited to the vicinity of anchorages.

Other techniques are in a development phase [Laguerre, 2003], [Wichmann et al., 2003] but, up to now, they are only used on laboratory applications, considered as special techniques. However, two types of special techniques will be briefly described at §2.4:

- the Electromagnetic Resonance Measurement (ERM) developed by Holst and Wichmann [Wichmann et al, 2003], [Holst et al, 2007], since it has been already tested on full scale models,
- the electrochemical techniques, that could be useful for the characterization of cable corrosion.

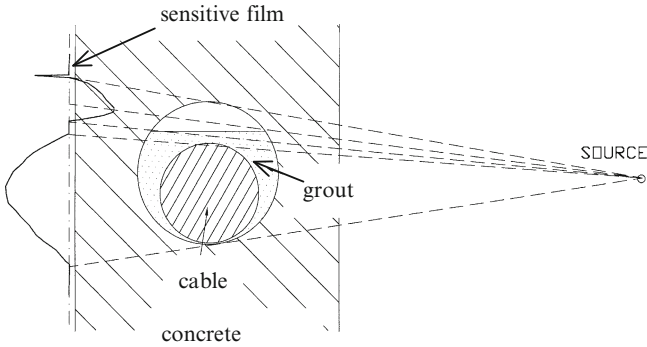


Fig. 7.3 Principle of radiography

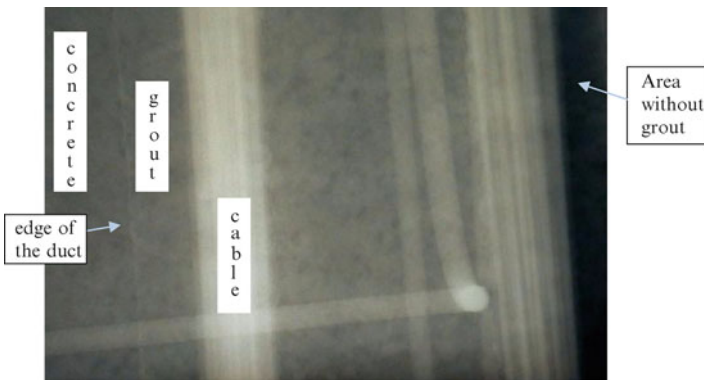


Fig. 7.4 Example of radiogram – sounding of an internal tendon [AFGC-B7, 2005]

## 2.1 Radiography

### 2.1.1 Principle

In radiography, the radiation source is either X-rays or gamma rays. Gamma rays or X-rays are emitted by an artificial source (Cobalt 60 or Iridium 192). In the case of X-rays, accelerators are used to obtain higher energy. It's a technique by transmission and the radiation attenuation through the material is measured with a sensitive film located on the opposite face to the one where the source is located (Fig. 7.3).

The optical density related to the grey levels of the sensitive film is analyzed. The quality of the images is generally good because the attenuating characteristics of steel, concrete, and air differ greatly (Fig. 7.4).

Field applications of radiography include the detection of reinforcement, voids, and cracks, the quality of grouted post-tensioned tendons and the failure of cables. Radioscopy is a different form of radiography in which the transmitted radiation is converted into visible light and recorded by a video camera. Radioscopy has been used in France for the detection of grouting defects.

The radiographic techniques can provide very useful information because of their ability to observe cross-sectional images of the object. They are applicable for every kind of prestressed concrete structures. However, these methods currently pose the problem of safety and other limitations. With further advancements in portable radiography equipment for field applications, such techniques could be more widely used. In particular, safety increasing, and imaging speed advances to permit practical scanning rates should greatly improve the technique.

Classically, industrial radiography is able to observe:

- the presence of cavities inside the concrete
- the presence of grout inside the prestressing ducts and also its defects
- the position of tendons
- the position of the reinforcement and the diameter of the rebars
- the discontinuities of the ducts
- the broken wires or cables in some cases
- etc.

### 2.1.2 Limitations of the technique

- Global limitations:

- Like it's a technique by transmission, two faces of the structure must be accessible
- Depth limitation: 60 cm for gamma rays but 120 cm can be reached with X-rays
- Only small surfaces can be sounded due to the limitation of the surface of sensitive film
- Steel bars (cables or reinforcement bars) can mask the target
- Important weight of the common radiation sources which doesn't enable the investigation of all the parts of a structure.
- Like the technique is hazardous, security area is required around the structure. Sometimes it's impossible
- The implementation of the technique is expensive if very large areas need to be sounded. For this reason radiography is sometimes relegated to use only in specific conditions [Poston and West, 2004].

- Limitations for the detection of broken wires:

Besides the above limitations, its low resolution for the detection of damages on the cables is the main disadvantage of the technique: the width of the fracture must be important enough to be detected. Moreover it is linked to the depth limitation.



**Fig. 7.5** Implementation of the technique at the intrados of a bridge deck (on the left) and a source of Iridium (on the right) – LPC France

### 2.1.3 Application

Field applications are currently made for grouting defects investigation, but also, in some cases, for the detection of broken wires [AFGC-B7, 2005], [Dérobert et al, 2002], [Ciolko and Tabatabai, 1999]. For example, in France, radiography (and also radioscopy) is usually implemented (Fig. 7.5) by means of gamma and also X-rays (Scorpion II, Laboratoire des Ponts et Chaussées, in France) [Dufay et al, 1985]. The methodology for the implementation of the technique on reinforced and pre-stressed structures is defined in a standard [NF A 09-202].

### 2.1.4 Combinations with other NDT methods

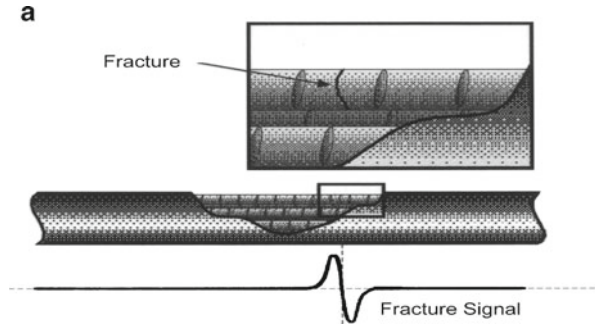
- Usual: radar for a fast localisation of the ducts. It's important if the plans of the structure are not available.
- Unusual: impact echo for a fast detection of voids in the ducts [Poston and West, 2004].

## 2.2 Magnetic methods

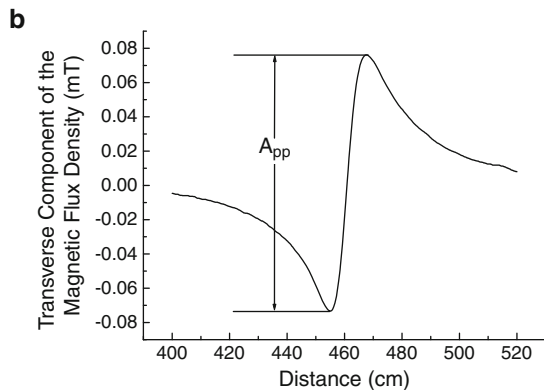
### 2.2.1 Principle [Scheel and Hillemeier, 2003]

The magnetic field resulting from a magnetized tendon or a magnetized steel wire is comparable to the magnetic field of a bar magnet. In the vicinity of a fracture a magnetic dipole-distribution is formed and, accordingly, a magnetic leakage field in

**Fig. 7.6a** Transverse component of the magnetic flux leakage measured above a cable fracture



**Fig. 7.6b** The peak-peak-amplitude ( $A_{pp}$ ) of the transverse component as a measure of the strength of the leakage field



the surrounding region. The transverse component of the magnetic flux density, measured at the concrete surface is shown in Fig. 7.6a. The characteristic leakage field allows detecting fractures of prestressing steel wires (Fig. 7.6b).

Two methods are presented in the literature, the Magnetic Flux leakage (MFL) and the Remanent Magnetism Method (RMM), but their physical principle is the same. In practice, these methods consist of applying a steady-state magnetic field to the cable and so the use of a scanning magnetic flux sensor allows detecting the changes in the applied field caused by the ruptures or the cracks.

In order to draw unequivocal conclusions from the magnetic flux density measured at the concrete surface to potential fractures, the external magnetization of the prestressing steel has to generate a magnetic state where all irreversible magnetization processes in the prestressing steel are completed. This is necessary in order to erase the unknown magnetic history of the steel. Without this magnetization the measured magnetic signals could be caused by various former unknown magnetization processes (e.g. transport by lifting magnets). By this way, a homogeneous magnetization of the cables is achieved.

The magnetization of the cables is performed from the concrete surface with an electromagnet. A remanent magnetization of the cables is achieved up to a concrete cover of 30 cm. It is ineffective to magnetize the cables before they are installed, in



order to avoid pre-magnetization because the magnetization will be destroyed partially and locally by the mechanical impacts during the construction process. This might produce signals similar to fracture signals. Demagnetization in the region of a fracture will disturb a fracture signal. The magnetized cable has a magnetic field similar to that of a bar magnet. Fractures of a single prestressing wire within a bundle of wires inside the metal sheathing are detectable by characteristic leakage fields. Figure 7.6b shows the transverse component (relative to the direction of the steel wires) of the remanent magnetic flux density measured at the concrete surface. At the location of a fracture the measurement curve of the transverse component shows a reversing polarity. The peak-peak-amplitude ( $A_{pp}$ ) of the transverse component of the leakage field is used to measure the strength of a fracture signal (Fig. 7.6b).

### 2.2.2 Influences on the measurement

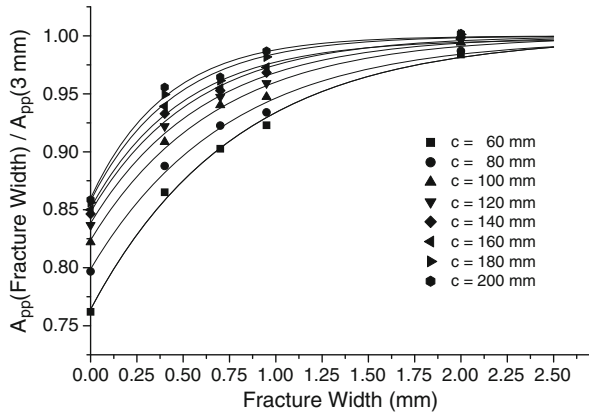
Various influences have to be considered in order to locate the position of steel fractures in remanent magnetized tendons and to evaluate the extent of damage:

- concrete cover: the total magnetization of cable is possible up to 30 cm depth,
- cross-sectional area of the prestressing steel wires,
- number of prestressing steel wires in the tendon,
- number of single wires that are broken in the cross-sectional area where the signal occurs,
- bonding between the prestressing steel wires and the grouting mortar (fracture width),
- interfering signals caused by other ferromagnetic components, especially mild reinforcement,
- magnetic and magneto-elastic material properties of the type of prestressing steel.

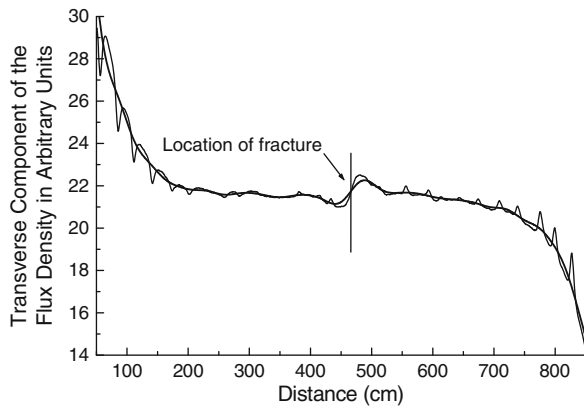
The peak-peak-amplitude of the transverse component of the leakage field for a certain cable depends on:

- the number of single wires that are broken in the cross-sectional area where the signal occurs,
- the concrete cover: the peak-peak-amplitude decreases when the concrete cover increases and increases when the number of single broken wires increases,
- the fracture width (distance between the fracture surfaces): the peak-peak-amplitude increases when the fracture width increases (Fig. 7.7),
- the degree of prestressing: the peak-peak-amplitude increases or decreases depending on the type of steel with the increase of tensile stress,
- the presence of the reinforcement in case of a high reinforcement ratio. If the reinforcement ratio is usual, while the magnetization of prestressing steel can be maximized by the chosen magnetization procedure up to remanence (the maximum residual magnetization), the magnetization of the mild reinforcement decreases to small values [Scheel and Hillemeier, 1997]. Specific procedures for data processing can also be used for removing the part of the signal induced by the reinforcement [Sawade, 2007].

**Fig. 7.7** Relative peak-peak-amplitude of the transverse component of the leakage field as a function of the fracture width for different concrete covers

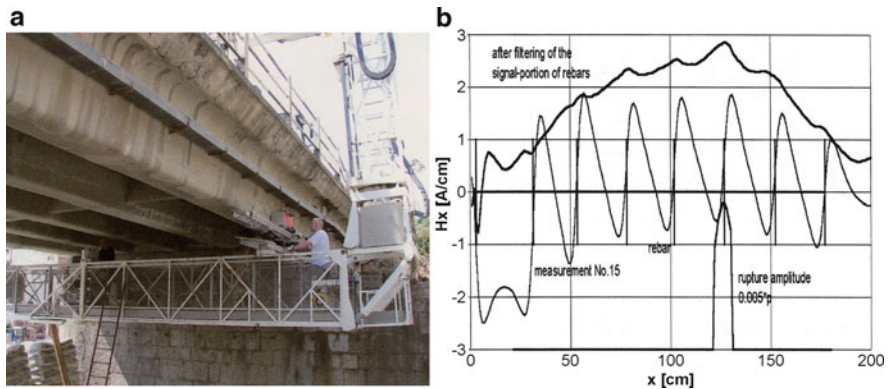


**Fig. 7.8** Effect of FFT filter smoothing



The interfering signals caused by the mild reinforcement and other ferromagnetic components are greatly reduced by the applied magnetization procedure; but they are not completely eliminated. In order to reduce these signals and to distinguish them from fracture signals, the following data processing can be applied:

- Simple addition of two measurement data arrays:  
Two arrays with the magnetic flux density data of the system in different magnetic states, in which the residual magnetizations of the mild reinforcement have different signs, but not the residual magnetizations of the prestressing steel wires, are added. The signals caused by all types of mild reinforcement decrease, whereas the signals caused by the prestressing steel increase.
- Fourier Transformation filter smoothing (Fig. 7.8):  
The signals with a small width compared to the width of a fracture signal are filtered out. FT filter smoothing suppresses signals caused by transverse reinforcement (e.g. by stirrups), if their distances do not vary too much. It also filters the signals of ferromagnetic components with a small width compared to



**Fig. 7.9** Application of Magnetic Flux Leakage technique for a girder inspection

the width of the fracture signal, e.g. nails, binding wires etc. Noise with a frequency greater than 5 Hz (depending on the measurement speed) is also filtered out. Fig. 7.8 shows a measurement curve and the resulting FFT filter smoothed curve: the measurement curve shows small peaks caused by the residual magnetization of stirrups. The smoothed curve shows the significant fracture signal while the stirrup peaks are filtered out.

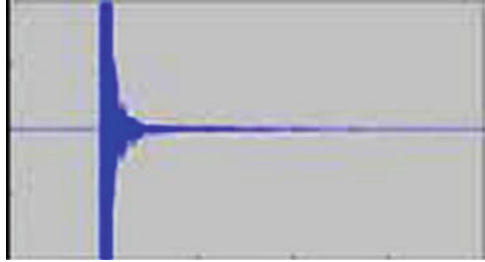
- Deconvolution of the (smoothed) curve with fracture signals.
- Calculation of the cross correlation function of the (smoothed) curve and fracture signals.

### 2.2.3 Application

Several publications upon laboratory validations [Scheel and Hillemeier, 2003], [Makars and Desnoyers, 2001], [Altschuler and Pignotti, 1995] are available. Concerning field applications, Scheel and Hillemeier have implemented the technique on the vertical surfaces of prestressed beams, on the upper surface of a bridge deck [Hillemeier and Scheel, 2004] and on parking structures [Scheel and Hillemeier, 2003]. Krause and colleagues have successfully implemented the technique for the detection of broken wires inside a bridge deck [Krause et al, 2000].

Fig. 7.9a presents an example of application on a girder of a highway bridge with one broken single-rod tendon (which was in a metallic duct) [Sawade, 2007]. Fig. 7.9b presents the different signals obtained along a 2 m long profile. First it is possible to see rough signal which was obtained by the measurement (called measurement N°15 on the picture). The rapid changes of the field amplitude are linked to influence of the reinforcing bars. After filtering the signal portion induced by the reinforcing bars (see 2.2.2.), the upper signal is obtained. The position of the rupture clearly appears on the diagram which plots the variation of the rupture signal at about 125 cm (bottom curve).

**Fig. 7.10** Wire break: typical response of a sensor (time domain)



#### 2.2.4 Combinations with other NDT methods

- Usual: radar can be used for the localisation of the cables and a more efficient magnetisation of the steel.
- Unusual: impact echo for a fast and non expensive detection of voids in the ducts. Indeed, in these areas corrosion can process and so the probability of broken wires is higher.

### 2.3 Acoustic Emission

#### 2.3.1 Principle

When an acoustic emission occurs at a source within a material due to inelastic deformation or to cracking it generates a stress wave which can be detected by an adapted receiver. The signal recorded by the receiver can be affected by the nature of the source, the geometry of the tested specimen and the characteristics of the receiver. The sensors used are broad-band or resonant piezo-electric accelerometers which convert the surface displacement into an electric signal. Acoustic emission testing is a “passive” monitoring method in which the detection system waits for the occurrence and capture of stress wave emissions associated with cracking, corrosion, or wire breaks. By contrast, classical flaw detection methods, such as ultrasonics, are considered “active” because a stress wave is sent into the test object to identify the presence of defects.

In the case of a prestressed cable the failure provides a sudden release of energy. This energy can be dissipated by means of acoustic waves through the surrounding media. The signals generated by wire failures must be detected above general noise levels and distinguished from events which are not of interest. By using several characteristics of the acoustic events including frequency spectrum it is possible to classify wire breaks and to reject environmental noise. Furthermore to assess the implication of each event on the structure it is important to locate the source of each emission. By analyzing the time taken by the energy wave caused by the failure as it travels through the concrete up to the different sensors, it is possible to calculate the location of the broken wire. Fig. 7.10 shows a typical acoustic response of wire

break (in a strand of an internal tendon in this case) monitored by a sensor 10 m away [De Wit, 2004].

The quality of the structure assessment is linked to the importance of the monitoring. More important is the number of inspection points better is the assessment. In many applications the acoustic data are transmitted via the Internet for processing and analysis.

Moreover some studies are currently implemented for testing the sensitivity of acoustic emission to the detection of corrosion development. It seems that the energy released by corrosion development is not very important versus all the environmental noises.

### 2.3.2 Limitations

- The breaking phenomenon is very short in time so it's necessary to monitor continuously during a long time (sometimes several years). Moreover the data acquisition must be done with a sufficiently high sampling rate.
- The technique does not provide any information on failures that occurred before its implementation
- Accuracy of the localisation: it depends on the number of sensors. By mean of multiplexing, usually it is possible to acquire on 32 channels, but it is not a general limitation [De Wit, 2004].

#### *First example*

It concerns the monitoring of a bridge in Switzerland. The monitoring is done by the company ADVITAM (SOUNDPRINT System) in collaboration with the Institute of Structural Engineering (ETH) in Zurich [Flicker and Vogel, 2007], [Hovhanessian, 2005]. The bridge is prestressed by internal tendons (63 cables with 12 wires of 7 mm diameter - system Freyssinet P50). 11 natural failures of the wires are monitored and localized with accuracy between 10 and 60 cm. In order to test the reliability of the technique, artificial failures are generated with an accelerated corrosion process. These artificial ruptures are also detected and localized (Fig. 7.11) with accuracy between 20 and 50 cm. The results confirm that the detection quality of the ruptures can be disabled by a bad grouting of the duct. Indeed, in this case, the high attenuation of the signal may disturb the data processing [Hovhanessian and Laurent, 2005].

#### *Second example*

It concerns a study realized both on laboratory beams and bridges in Japan [Yuyama et al, 2007]. AE is tested for the detection of wire failures due to corrosion. On a laboratory beam (Fig. 7.12) the failure is introduced by artificial corrosion (by applying anodic current) and the influence of grouting conditions is tested. The results show that the amplitude of the waves exceeds 100 dB and the source location is possible for the failures of unbonded and partially grouted cables. When the cable is fully grouted even if the detection is possible the location is not easily performed. Nevertheless, about 82% of the wire breaks are detected. Different resonant sensors

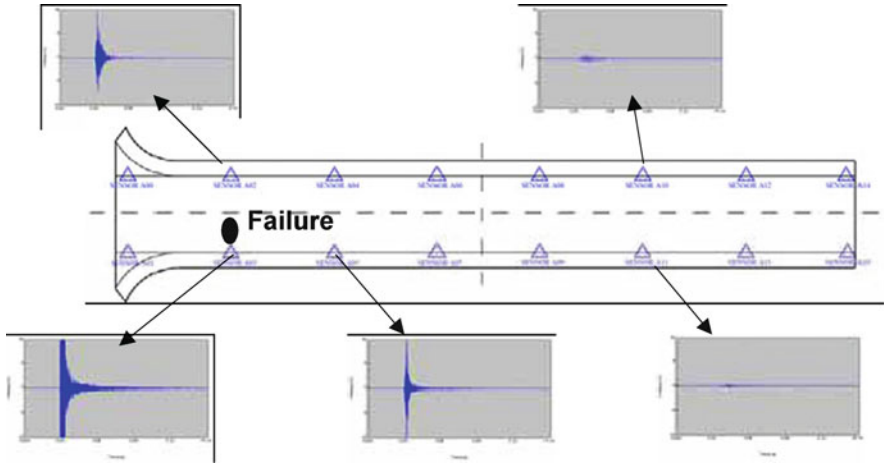


Fig. 7.11 Artificial failure of a wire: response of different sensors (after [Hovhannessian, 2005])

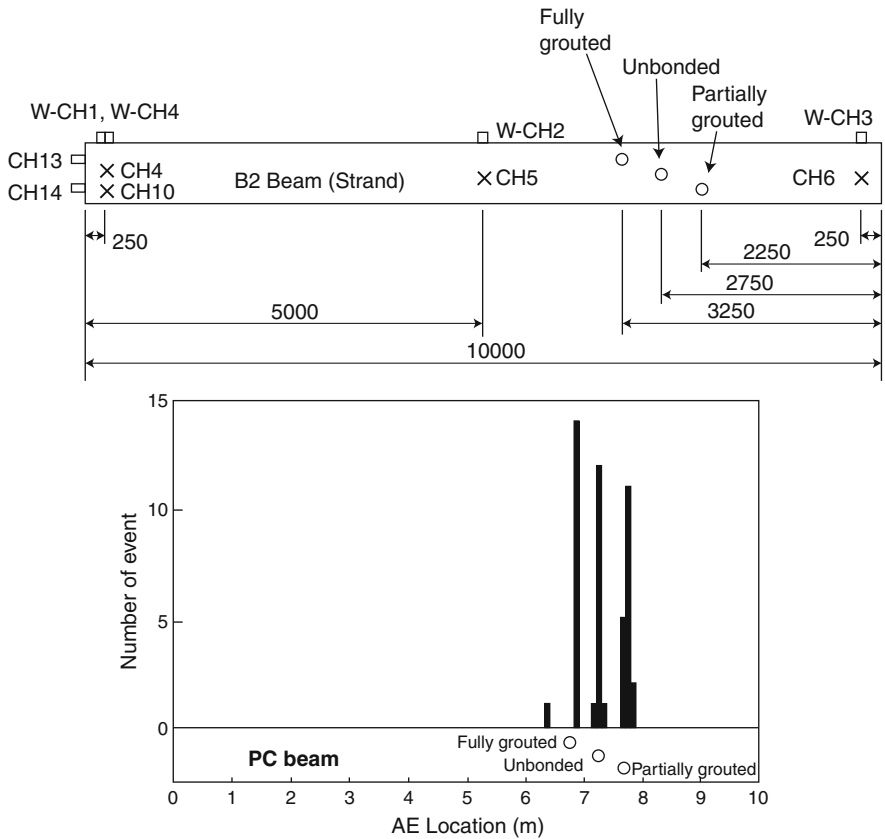


Fig. 7.12 Laboratory beam and location of wire failures (after [Yuyama et al, 2007])

are tested (30 kHz, 60 kHz and 150 kHz) and it is clearly demonstrated that the sensitivity increases as the resonant frequency of the sensor decreases. The amplitudes detected by 30 kHz sensors are very high (over 100 dB), those by 60 kHz are high (60-100 dB) and those by 150 kHz are low (50-80 dB).

For the field tests two bridges (a box girder beam and a T-shaped beam) are tested. The activity due to wire breaks is compared to those resulting from traffic noises. Even if traffic noise is a major AE source, the results show that the amplitudes are higher than 90 dB, continuing for 1-2 s. The ratio of wire failures detected under traffic conditions are about 80% for one bridge and 90% for the other one. The location of the source is also possible on the bridges with an error less than 8%. Other tests show that the attenuation of the waves during propagation is about 30 dB while it travels about 7 m (using a 60 kHz resonant sensor).

A literature review provides other examples of detection of cable ruptures on bridges [De Wit, 2004], on pipes [Travers, 1997] and on nuclear containments [Graves and Tabatabai, 1998].

### 2.3.3 Combinations with other NDT methods

Radar can be used for a best localisation of tendons but it is not necessary for the implementation of the technique. Nevertheless, it could be used if a destructive assessment is done after a localisation of rupture.

## 2.4 *Special techniques*

### 2.4.1 Electrochemical techniques

#### Description

Electrochemical techniques are largely used for the characterization of reinforced concrete corrosion [Andrade et al., 1978&2002]. Both description and implementation of these techniques are detailed into RILEM and ASTM recommendations [ASTM C876-91], [RILEM, 2000&2003&2004]. The main electrochemical techniques for measuring corrosion are:

- The **Corrosion Potential**,  $E_{\text{corr}}$ , which informs on the state of the metallic surface with respect to the surrounding electrolyte. If the steel is corroding with the production of oxides, the  $E_{\text{corr}}$  is very negative and if the steel surface is covered by a passive oxide film the  $E_{\text{corr}}$  is less cathodic or even in the positive range with respect to the saturated calomel electrode (SCE).
- The **concrete Resistivity** ( $R_e$ ) which indicates the porosity of concrete and the degree of water saturation of concrete pores. Values below 50  $\Omega\text{m}$  indicates pore saturated concrete and values above 500  $\Omega\text{m}$  indicate very dense or dry concrete. The  $R_e$  needs to be referred to a particular volume or regular geometry.



**Fig. 7.13** “Barrios de Luna”  
Bridge



- The  $R_p$  (polarization resistance) technique which enables the calculation of the **corrosion rate**,  $I_{\text{corr}}$  in  $\mu\text{A}/\text{cm}^2$  or the  $V_{\text{corr}}$  in  $\text{mm}/\text{year}$ .

In a reinforced concrete structure the measurement informs on the state of the reinforcement closer to the placement of the electrodes, so only the first layer of bars can be measured. However, in the case of post-tensioned elements in which a layer of non prestressed reinforcement is placed between the concrete surface and the ducts, the measurement of the prestressing cable is shielded by this intermediate layer, which in addition is usually electrically connected to the ducts. The only way to monitor the cables is to open a window in the concrete and to put the counter electrode directly on the grout surrounding the cables. In the following sections two examples are presented, a first one on cables of a suspended bridge and a second one on cables in a prestressed concrete bridge.

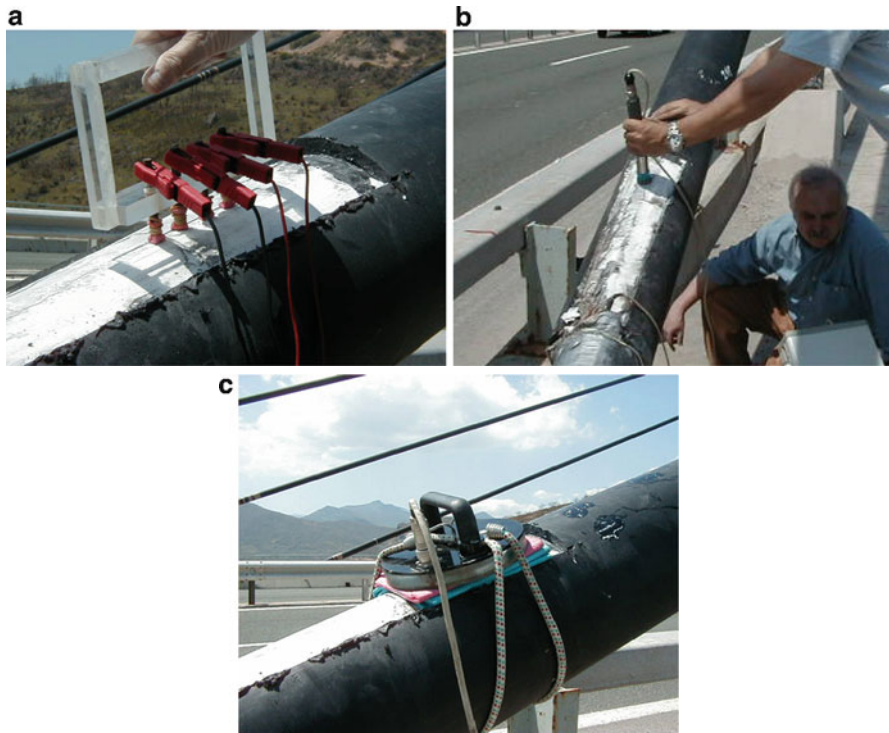
#### Examples of application

##### a) Example 1: measurement in tendons of a suspended bridge (Barrios de Luna Bridge)

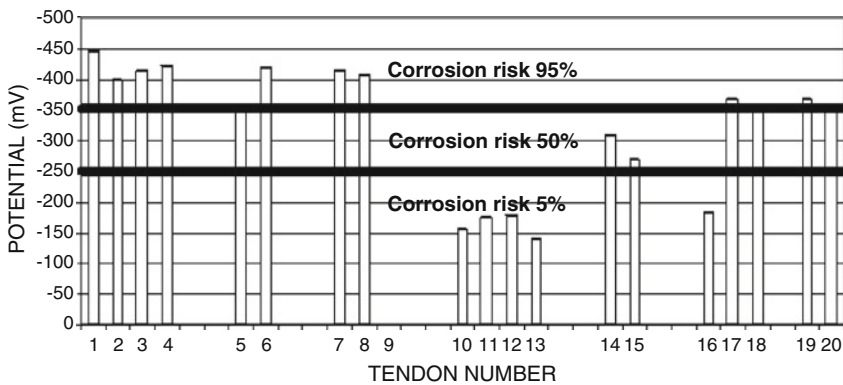
The bridge was built in 1983; it is a cable-stayed bridge with three spans. The main span is 440 meter long (Fig. 7.13). The bridge is suspended by means of 228 tendons. Each cable has some high strength steel cable of 1.5 cm diameter. The measurement was made by removing the plastic duct and placing the corrosion rate meter directly on the grout (see Fig. 7.14c).

Once it is achieved an electrical connectivity, it is possible to measure different electrical and electrochemical parameters: resistivity (Fig. 7.14a), potential (Fig. 7.14b) and corrosion rate (Fig. 7.14c). All these parameters let us to evaluate the service life of the bridge.

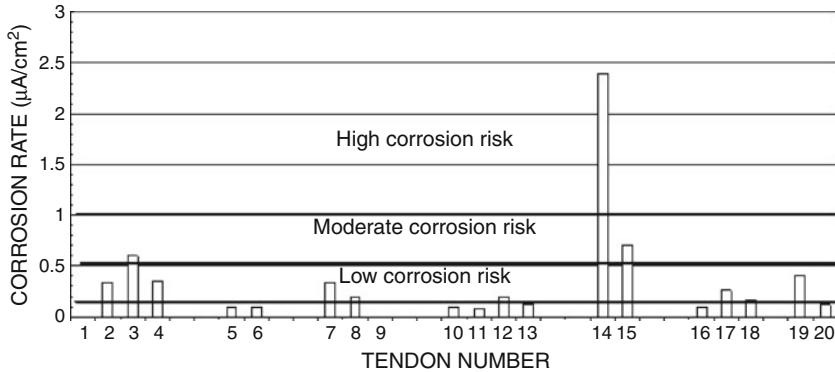
Fig. 7.15 and Fig. 7.16 show the potential and corrosion rate values of different tendons. Assuming that the process is that of generalized corrosion and that the standards used for the assessment of reinforced concrete corrosion are relevant in



**Fig. 7.14** Electrical and electrochemical measurements. (a) Resistivity measurement, (b) Electrochemical potential (c) Corrosion rate



**Fig. 7.15** Electrochemical potential of tendons



**Fig. 7.16** Corrosion rate of tendons

this case, it is possible to distinguish three levels of corrosion according to electrochemical potential. And according to corrosion rate measurements it is possible to quantify this risk of deterioration. All these data are necessary to evaluate the residual life of these components.

A lot of values of the potential registered were in the range “moderate to high corrosion risk” (i.e. more than 50%) following ASTM standard. The potential readings are only qualitative and they serve to indicate that the tendons are in a situation where the corrosion is likely to grow.

The quantification is made through the corrosion rate (Fig. 7.16). It has been detected that several points show values of the corrosion rate higher than  $0.1 \mu\text{A}/\text{cm}^2$ .

*b) Example 2: Measurement in post-tensioned elements*

This example concerns a bridge built in 1992 and formed by five spans of 48, 60, 100, 60 and 48 meters. It has a composite section (steel – concrete) which is variable in height and width through the five spans. Over supports, negative bending moment is supported, both by a strong lower plate and seven stiffeners, and a passive and active reinforcement and several prestressing tendons.

When concreting, a change in the water table level of the well, used for concreting, allowed the sea water to penetrate into the water well, and finally the amount of chlorides in the concrete was around 7 times higher than the maximum allowed by standards ( $\sim 0.4\%$  in weight of cement). Thus, the corrosion in the concrete deck was detected since construction.

During eight years the bridge was continuously monitored in order to know the corrosion rate with the aid of a portable corrosion rate meter with modulated confinement of the current (Fig. 7.17). The results obtained in two sections of the deck are represented in the form of a distribution (Fig. 7.18).

The connection was done on the passive reinforcement as it was verified that it was electrically connected to the tendons. Therefore it was not necessary to make direct connection to the ducts. In addition, as the chlorides were added in the mix,



Fig. 7.17 Corrosion rate measured in-situ

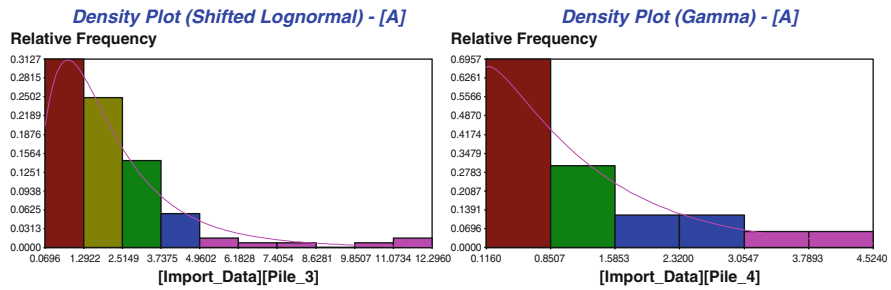


Fig. 7.18 Distributions of measured corrosion rate in sections 2 and 3

the corrosion of the passive reinforcement was the same than that of the tendons. This was verified in one case, where direct measurement on the grout was made after performing a window in the duct (Fig. 7.17).

The cover of the duct was removed in several places in order to verify the loss in cross section and directly observe the type of corrosion.

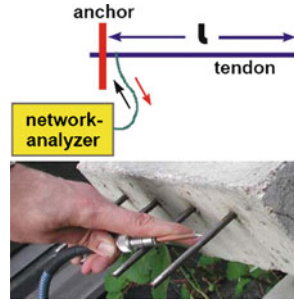
The results obtained showed that the corrosion was in general not too high (current density about  $0.2 \mu\text{A}/\text{cm}^2$ ) except in one of the sections where the values were higher, reaching sometimes values of  $0.5 \mu\text{A}/\text{cm}^2$ . The conclusions obtained were that the corrosion was not low in three sections of the bridge and moderate in one. The expected life of the tendons was calculated from around 15 to 40 years.

However the failure risk would depend on whether stress corrosion cracking (SCC) develops or not. It is not known at present how to predict the occurrence or not of SCC. SCC would be one of the worst scenarios for the prediction. When it occurs, the failure is much quicker than when produced by normal corrosion.

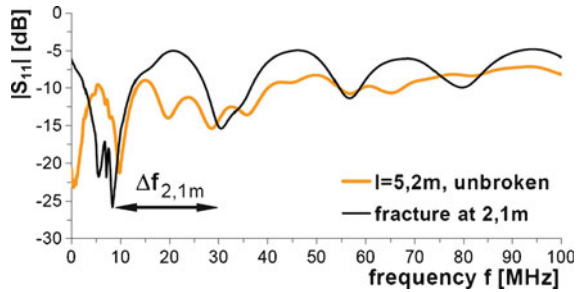
### 2.4.2 Electromagnetic Resonance RF-Measurement (ERM)

The technique uses the electromagnetic resonance of the prestressing steel to detect and localize steel fractures and flaws in prestressing cables. The principle of the method is to consider the prestressing cable itself as a resonator located in a material

**Fig. 7.19** Principle of ERM measurement



**Fig. 7.20** Reflection parameter S11 versus frequency f for a 5.2 m long strand in air with and without fracture



with electromagnetic losses (concrete). An electromagnetic wave of variable frequency is coupled to the end of the cable (Fig. 7.19) and the reflection coefficient is S11 is scanned over a large spectrum (from low to high frequencies) by mean of a vector network analyser. The resonance frequencies are recorded and the spacing between two adjacent resonance frequencies  $\Delta f$  (Fig. 7.20) is inverse in proportion to the length  $l$  of the tendon, from the source and up to the fracture, and also depends on the dielectric permittivity of the surrounding material  $\epsilon_r$  as it is shown in the following equation [Holst et al., 2008].

$$l = \frac{c_0}{2 \cdot \Delta f \cdot \sqrt{\epsilon_r}}$$

with  $c_0$  : vacuum speed of light

One of the difficulties of the technique is to evaluate the permittivity of the surrounding medium. If it is unknown, the distance to the fracture can be determined by comparing the ratio of the measured spacings on the broken wire with the ones of an unbroken wire. The possible limits of the methods are:

- the presence of voids (filled with air or with a salt solution) in the grout which can induce a important change of the dielectric permittivity,
- the contact between the cable and the metallic duct, and in this case the duct is investigated and not the cable.

## 2.5 *Calibration aspects*

A calibration is not necessary in all the cases. If the aim of the sounding is only limited to the detection of failures on the cables and not to the evaluation of the number of broken wires, some of the techniques are able to provide such information with rather good reliability. For instance, magnetic technique has proved efficiency for detecting broken wires and moreover, for this technique, sensitivity studies realized in laboratory conditions [Scheel and Hillemeier, 2003] can be used for a calibration procedure on site.

On the other hand, sometimes, a full diagnosis of the whole tendon can be required in order to provide reliable information for a re-calculation of the structure. In this case, information like the number of broken wires, the condition of the wires (for instance is there a corrosion activity) are necessary to be provided to the engineers.

Moreover, for a prognosis of the evolution of the cable condition, another kind of information can be required like, the quality of the grout, the activity degree of the corrosion process, the presence of chlorides and so on. In this case a relative calibration could be helpful, because up to now it remains very difficult to provide data regarding these different points by non intrusive means. Thus, the only available mean to achieve this calibration consists on making a window through the structure, up to the cable. As the depth of the cable is usually at least 20 or 30 cm (more in some cases) the window is very disabling for the integrity of the structure.

## 2.6 *Evaluation and comparison of the techniques*

Only radiography, magnetic and acoustic emission are compared. The evaluation is presented in the following Table 7.1 regarding several characteristics [Ciolko and Tabatabai, 1999]. For a given characteristic each of the three techniques is ranked (with  $A > B > C$ ). A mark "A" doesn't systematically mean that the technique is very good and on the other hand "C" is not a depreciation of the technique. These marks have to be rather considered like a relative classification of the three techniques.

## 3 **What can be done for a better assessment?**

### **Combination possibilities**

For a recalculation process what is important is to detect and to localize the ruptures or the damages and if possible to quantify the number of broken wires. Up to now, to be accurate and reliable, the answer to this question requires a windowing in the structure so as to observe the cable. But this process is heavy and can alter the integrity of the structure. The combination of techniques could be used so as to optimize the interventions and to decrease the windowing operations. Radiography which is an imaging technique, usually provides relevant information about the whole tendon

**Table 7.1** Comparison of the techniques (R = radiography, M = magnetic techniques, AE = acoustic emission, IE = impact echo)

Characteristics	Details	R	M	AE
Applications	Pre-tensioned structures	A	A	B <sup>2</sup>
	Post-tensioned structures with metallic ducts	A	A <sup>3</sup>	A
	Post-tensioned structures with plastic ducts	A	A	A
Ability	Detection of cable or wire failures	B	A	A
	Number of broken wires	C	B	C
	Localisation of failures	C	B	A
	Detection of wire damage	C	B	C
	Detection of corrosion	C	C	C
Operational characteristics	Contact/Surface Coupling	A	A	C
	Need of continuous monitoring <sup>4</sup>	A	A	C
Device details	Equipment Weight	C	B	A
	Sensor Weight	C	B	A
Efficiency	Number of readings (tests) required for a given surface	C	B	C
	Time expended for data gathering for a given surface	C	A	C
	Interfering effects of multiple steel layers (shadowing)	C	C	A
	Resolution versus detection of failures	C	A	C
Level of interpretation	Immediate readings	A	C	C
	Time expended for data interpretation for a given surface	B	B	C
	Calibration aspects <sup>5</sup>	C	C	C
Standards and guidelines	Standards	A	C	C
	Guidelines	A	A	A
Combination considerations	For a better implementation of the technique	Radar, IE, Magnetic	Radar, IE	Nothing
	For a better assessment	Magnetic	Radio	Magnetic, Radio
Safety parameters	Protection required for users and passers-by	C	B	A
Required staff and training time	Total crew size	C	A	A
	Required training time	B	B	B
Cost considerations <sup>6</sup>	Cost of implementation	C	B	B

<sup>2</sup>: some experts underline the difficulty to assess pre-tensioned prestressed structures with AE

<sup>3</sup>: the shadowing effect of the duct can reduce the signal but it is possible to keep 60 to 80% which can be sufficient in many cases [Scheel, 2003] Nevertheless the junction of the metallic ducts can disturb the measurement.

<sup>4</sup>: continuous monitoring can disable the diagnosis since the assessment is not immediate

<sup>5</sup>: calibration is destructive and consists in doing a window through the structure up to the cable

<sup>6</sup>: for information



(cable integrity and also, in the same time, quality of the grout), but its implementation is expensive and hazardous. A limitation or a rationalization of radiography investigations by a first sounding with other methods (magnetic, acoustic emission, impact echo) could be proposed. The magnetic methods are able to identify and to localize the ruptures on a cable.

Nevertheless, for a global assessment of the structure, neither the magnetic methods, nor the radiography can be helpful. A monitoring technique such as acoustic emission is able to localize areas where failures occur, at the global scale of the structure. But this localization is not accurate. Once this localization is done, magnetic technique could be very useful to localize the rupture with higher accuracy. In chosen areas, radiography could be performed to go further in the diagnosis and to define the condition of the whole tendon (presence of grout, defect in the duct...). Nevertheless, to go further and to establish a prognosis of the structure evolution, another important point is the definition of the origin of the rupture of the cable. Particularly, if there is a bad grouting what is the nature of the medium surrounding the cable or is there a favorable condition for the development of corrosion? If corrosion is involved what is its activity level? But for such level of investigation a windowing remains necessary.

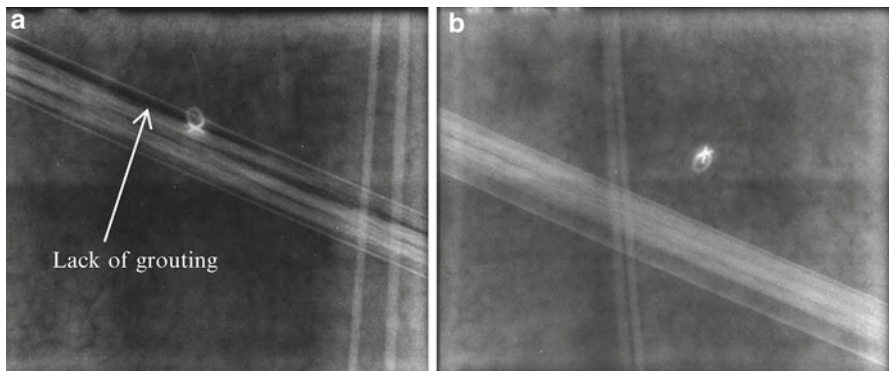
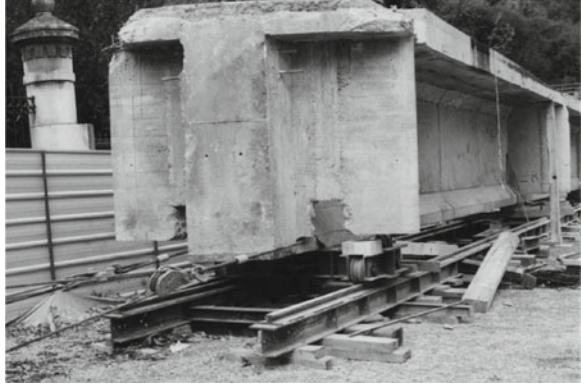
The following describes an example where the techniques were combined. It concerns a prestressed concrete bridge located in Foix in the South of France. This bridge was placed under survey since 1995, because some recalculations have shown that a single rupture of cable could involve a sudden failure of the bridge. So a monitoring of the bridge by AE has been performed during a period of three years [Robert et al, 2000] in order to survey the behaviour of the bridge and to identify the ruptures.

The dimensions of the post-tensioned test beam are 2.10 m high and approximately 9.50 m long. The height of the web is 1.10 m and its thickness is 0.20 m. Its reinforcement is composed of vertical bars and 11 post-tensioned tendons, including five anchorages at the end stringer and six in the top.

During this period the five prestressed beams of the bridge were monitored and 13 events which have been linked to failures of wires or cables have been identified. One of the beams has cumulated 7 events which were all localized at its extremity. The intensity of the last event monitored was so high that the bridge owner decided to close the bridge and shortly after the bridge has been demolished.

During the bridge demolition, it was decided to perform an autopsy on the beam that presented the highest level of presumed defects in order to validate the acoustic monitoring. In addition, prior to the destruction of the beam (see Fig. 7.21), an experimental program to evaluate numerous non-destructive testing (NDT) methods was initiated. So, Impact Echo, radar and radiography were implemented on the areas where failures had been detected [Dérobert et al, 2002]. Radar was only used for the localization of tendons. For the radiographic investigation, a radiographic numerical system, called the digital phosphor system (DPS) which scans into a numerical film, has been used. Its major advantages, in comparison with the classical radiographic technique, consist of an accurate positioning of the prestressed ducts and tendons as well as of reinforcement bars. In the vicinity of the detected failures by

**Fig. 7.21** Post-tensioned beam



**Fig. 7.22** Radiographic films

AE, two zones were investigated. The radiographic films obtained are presented on Fig. 7.22. The first zone revealed a complete lack of grouting (dark area above the cable) around the tendons (dark areas) in the central duct (Fig. 7.22a), while the second one indicates a correct injection in the central duct (Fig. 7.22b).

Even if the quality of the radiographic films was rather good, the technique was not able to reveal the presence of failures on the cable in these zones.

Another interesting approach of this study is the implementation of the IE technique for the detection of voids in the ducts. The results clearly emphasize the ability of the technique to detect the empty duct which was revealed by the radiography.

So, after performing NDT, the beam was completely destroyed by hydro-demolition. After completely removing the tendons, the autopsy permitted to confirm the fractures detected by AE. The observation of the cables showed that they were manually greased in order to provide adequate protection against corrosion given the age of the bridge. But in some specific locations, the lack of grease reflects stress corrosion with wire fracture and, in two cases, a cable fracture.

## 4 Benchmarking sites: examples

Even if the problem is more and more important, too few non destructive techniques are available for detecting the failures of prestressing cables. Moreover there is a lack of guidelines or recommendations regarding the implementation of these techniques for the diagnosis of ruptures of prestressing cables. Existing methods use very different approaches and are not efficient at the same scale.

Acoustic emission which is a monitoring technique can detect occurring ruptures and localize them. But it does not allow quantifying the number of broken wires which is nevertheless one of the more important information regarding a recalculation process of the structure. Magnetic techniques are able to localize existing ruptures but without possibility of quantifying the number of ruptures. Radiography is interesting by providing an image of the whole tendon but, up to now, it remains difficult to reveal the presence of wire failures due to insufficient resolution. Moreover radiography is hazardous and its implementation requires a protection area around the structure. Nevertheless, despite of this disadvantage which makes it rather heavy to implement, radiography can also provide information on the grouting quality which can be one of the origins of the failure of the cables, in case of corrosion for instance.

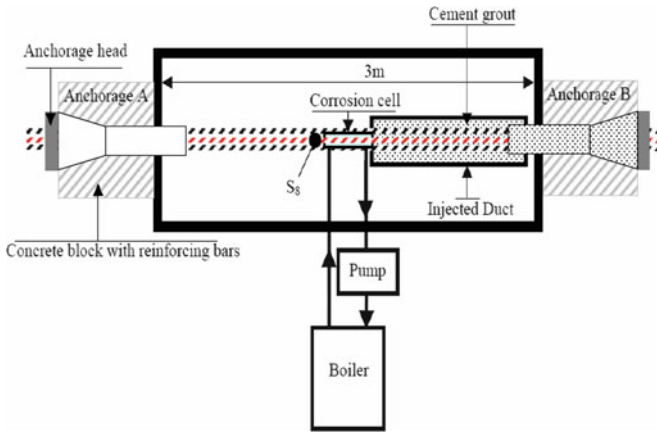
Our aim is to show that a combination of these three techniques should efficiently improve the assessment of prestressing cables. The main interest of the combination could be the gradual assessment of the cable integrity: firstly at the level of the whole structure by an acoustic monitoring, secondly on a part of the structure by magnetic techniques implemented on the supposed damaged cable if it is accessible, and finally at the scale of the cable, by radiography done on the damaged area.

Some benchmarking sites could be designed for this purpose. The rupture of the wires could be induced by means of an accelerated corrosion of the cables like it was proposed by Flicker and Vogel (see 2.3.3.) or by Sawade [Sawade, 2007]. In this last example, in a prestressed beam, a cable was treated with a solution of  $\text{NH}_4\text{SCN}$  and HCL and polarized with  $-1200$  mV (Fig. 7.23). The cable has been monitored by magnetic flux leakage measurements at different time intervals.

Another study performed by Perrin et al [Perrin et al, 2009] also permitted to detect failures on a strand by acoustic emission on a simulated prestressed concrete structure (Fig. 7.24). A full anchorage was used and the strand was placed inside an injected duct. The full anchorages were composed by a concrete block with reinforcing bars and an anchorage head. A duct was placed on a half part of the strand. The anchorage B and the duct were injected with a cement grout. A corrosion cell was placed in the middle of the strand and a corrosive solution composed with 250 g/l of ammonium thiocyanate ( $\text{NH}_4\text{SCN}$ ) was placed in the cell and kept at a constant temperature of  $50^\circ\text{C}$  due to liquid circulating from a boiler. This structure was instrumented with an acoustic emission monitoring system with 12 different sensors.

Such examples of simulated or simplified structures could be used for a reliable control of the cable ruptures by means of a corrosion accelerated process and for implementing the three techniques in combination. This should allow a better

**Fig. 7.23** Laboratory prestressed beam for detecting a wire failure by magnetic flux leakage method [Sawade, 2007]



**Fig. 7.24** Simulated structure for monitoring wire failure by acoustic emission [Perrin et al, 2009]

knowledge of the sensitivity of the different techniques and also their limits. So, some guidelines or recommendations regarding both implementation of the techniques and use in combination could be written.

## 5 Conclusions

The detection of broken wires or broken cables in prestressed concrete structures remains one of the most important challenges for Non Destructive Testing in Civil Engineering. This is a difficult topic due to the complexity of prestressing technol-

ogy. Indeed, in post-tensioned structures, the cables are placed in a duct (generally metallic) filled by a cement grout. The thickness of concrete above the duct can attain many decimeter, which makes difficult the assessment from the surface. Moreover a passive reinforcement mesh placed between the surface and the tendons can disturb the signal propagation of the NDT methods.

This chapter discussed three techniques which can be considered as relevant for this concern, since they have been successfully used on real structures:

- radiography, imaging technique allowing the assessment of both the grout and the duct. Identification of broken wires can be possible in some cases;
- magnetic techniques, able to detect broken wires up to 30 cm depth;
- acoustic emission, a monitoring technique able to detect and to localize ruptures when they occur.

These techniques were detailed, illustrated by case studies and their performances were compared. Standards or guidelines are available for radiography but not for magnetic techniques or acoustic emission. For this last technique, which is commonly implemented on bridges by several companies, some guidelines should be written.

Some possibilities of combination of these techniques and an example on a bridge beam were presented, but this example is probably unique. However, given the usual difficulties for investigating the cable integrity which requires a windowing to achieve a reliable diagnosis, the combination of the three techniques detailed above could be considered. Testing sites to define the sensitivity of the techniques and the added value of the combination should be also developed.

Finally there is also an important need of development of new methods, not only for the detection of broken wires but also for identifying the origins of the ruptures of cables (corrosion assessment, contamination of the cable environment by chlorides ...). In a predictive approach, so as to predict new ruptures, reliable methods for measuring the speed of corrosion should be also developed.

## References

- AFGC-B7 (2005) *Méthodologie d'évaluation non destructive de l'état d'altération des ouvrages en béton armé*, Ed. D. Breyse et O. Abraham, Chap. B7 « Méthodes END gamma-radio », Presses de l'Ecole Nationale des Ponts et Chaussées.
- Altschuler E., Pignotti A. (1995) Nonlinear model of flaw detection in steel pipes by magnetic flux leakage", *NDT&E International*, Vol.28, N°1, pp 35–40.
- Andrade C., Alonso C. Sarría. J. (2002) Corrosion rate evolution in concrete structures exposed to the atmosphere, *Cement and concrete composites*, Vol.24, pp 55–64.
- Andrade C., Martínez I., Castellote M., Zuloaga P. (2006) Some principles of service life calculation of reinforcements and in situ corrosion monitoring by sensors in the radioactive waste containers of El Cabril disposal (Spain), *J. Nuclear Materials*, Vol. 358, pp 82–95.
- Andrade C., Sarria J., Alonso C. (1999) Relative humidity in the interior of concrete exposed to natural and artificial weathering, *Cem. Concr. Res.*, Vol. 29, pp. 1249–1259.
- Andrade C., Gonzalez, J.A. (1978) Quantitative measurements of corrosion rate of reinforcing steels embedded in concrete using polarization resistance measurements, *Werkst. Korros.*, Vol. 29, N° 515.

- ASTM C876-91, Standard Test Method for Half Cell Potentials of Uncoated Reinforcing Steel in Concrete.
- Chauvin G. (2005) La réparation de la route de la Corniche à Marseille : les désordres, les investigations, le projet de réparation, les contraintes du maître d'ouvrage, les réparations, les difficultés rencontrées, le coût de l'opération », X<sup>ème</sup> colloque sur les Ouvrages d'Art, Toulouse, 19 et 20 octobre 2005, <http://www.le-pont.com/Histo/programme/interventions/chauvin-corniche-marseille.pdf>
- Ciolko A.T., Tabatabai H. (1999) Nondestructive Methods for Condition Evaluation of Prestressing Steel Stands in Concrete Bridges”, Final Report, Phase I: Technology Review, March 1999.
- De Wit M. (2004) Acoustic monitoring for wire break detection – Case study, First Workshop of COST 534 “NDT assessment and new systems in prestressed concrete structures”, ETH Zurich, Ed. Bernhard Elsener and Rob Polder, 13 October 2004
- Dérobot X., Aubagnac C., Abraham O. (2002) Comparison of NDT techniques on a post-tensioned beam before its autopsy”, NDT&E International, Vol.35, p.541–548.
- Dufay J.C., Piccardi J. (1985) SCORPION, premier système de radioscopie télévisée haute énergie pour le contrôle non destructif des ouvrages d'art en béton précontraint », Bulletin de liaison des Laboratoires des Ponts et Chaussées, N°139, pp 77–84, Sep-Oct 1985.
- Elsener B., Bóhni H. (1990) Corrosion Rates of Steel in Concrete, N.S. Berke, V.Chaker and D. Whiting (Eds.), ASTM STP 1065, pp. 143–156.
- Feliú S., Gonzalez J.A., Andrade C. (1996) Multiple-electrode method for estimating the polarization resistance in large structures, J. Appl. Electrochemistry, 26, pp 305–309.
- Fricker S., Vogel T. (2007) Site installation and testing of a continuous acoustic monitoring, Constr. Build. Mat., Volume 21, Issue 3, March 2007, 501–510.
- Graves H.L., Tabatabai H. (1998) Acoustic Monitoring of Containment Tendons” Nuclear Engineering and design, Vol.181, pp.225–233.
- Hillemeier B., Scheel H. (2004) Location of prestressing wire breaks with the remanent magnetism method – recent developments: application to highly reinforced concrete members and fast location of prestressing wire breaks in bridge decks and parking lots, Second FIB Workshop on Durability of post-tensioning tendons, , ETH Zurich, Ed. Bernhard Elsener, 11-12 October 2004.
- Host H., Wichmann H.J., Hariri K., Budelmann H. (2008) Detection and Localization of Fractures and Flaws in Pressured Tendons by means of Electromagnetic Resonance RF-Measurements, COST 534 “NDT assessment and new systems in prestressed concrete structures”, Final Report, 2008.
- Hovhanessian G., Laurent E. (2005) Ecoute acoustique et durabilité des ouvrages en béton précontraint », Journées GC'2005, Paris, 5 et 6 octobre 2005.
- Hovhanessian G. (2005) Bilan de 10 années d'écoute acoustique, Colloque le Pont, Toulouse France, 19 et 20 octobre 2005.
- Krause H.J., Wolf W., Glaas W., Zimmermann E., Faley M.I., Sawade G., Neudert G., Gampe U., Krieger J. (2000) SQUID system for magnetic inspection of prestressed tendons on concrete bridges, Proc. 15<sup>th</sup> WCNDT, Roma.
- Laguerre L. (2003) Non destructive evaluation of slender steel members using elastic guided waves, Int. Symp. NDT-CE 2003, Berlin, Germany.
- Makars J., Desnoyers R. (2001) Magnetic field techniques for the inspection of steel under concrete cover, NDT&E International, Vol.34, pp.445–456.
- Mindess S. (2004) Acoustic Emission Methods, in CRC Handbook on Non-destructive Testing of Concrete, 2<sup>nd</sup> Edition, CRC Press, Boca Raton, Fl.
- NF A 09-202 (1999) principes généraux de l'examen radiographique, à l'aide de rayons X et gamma, des matériaux béton, béton armé et béton précontraint.
- Perrin M., Gaillet L., Tessier T., Idrissi H. (2009) Acoustic emission for prestressing strands corrosion assessment”, NDTCE'09, Nantes, France, June 30<sup>th</sup>-July 3<sup>rd</sup>, 2009.
- Poston R.W., West J.S. (2004) North American Strategies for Monitoring, Maintenance and Repair of post-tensioning Tendons, Second FIB Workshop on Durability of post-tensioning ten-

- dons, Swiss Federal Institute of Technology, ETH Zurich, Ed. Bernhard Elsener, 11-12 October 2004.
- RILEM TC-154 EMC (2000) Electrochemical techniques for measuring corrosion in concrete”, Recommendations, Mat. Str., Vol.33, 36 and 37, 2000 to 2004.
- Robert J.L., Brevet P, Bruhat D., Gervais J.P. (2000) La surveillance acoustique-auscultation des OA: application au pont de Foix, Bull.AFGC, 2, pp 113–8.
- Sawade G. (2007) Magnetic flux leakage measurement method, Final Workshop of COST 534, “NDT assessment and new systems in prestressed concrete structures”, Univ. Paul Sabatier, Toulouse, France, 26-27 November 2007.
- Sawade G. (2004) Magnetic leakage measurements on prestressed concrete, First Workshop of COST 534, “NDT assessment and new systems in prestressed concrete structures”, ETH Zurich, Ed. B. Elsener and R. Polder, 13 October 2004.
- Scheel H., Hillemeier B. (1997) Capacity of the remanent magnetism method to detect fractures of steel in tendons embedded in prestressed concrete, NDT&E Int., Vol.30, N°4, pp.211–216.
- Scheel H., Hillemeier B. (2003) Location of Prestressing Steel Fractures, Concrete J. of Materials in Civil Engineering, Volume 15, Issue 3, pp. 228–234, May/June 2003.
- Travers F.A. (1997) Acoustic Monitoring of Prestressed Concrete Pipe, Constr. Build. Mat., Vol.11, 3, pp. 175–187.
- Wichmann H.J., Holst A., Hariri K., Budelmann H. (2003) Detection and localization of fractures in tendons by means of electromagnetic resonance measurement, Int.Symp. NDT-CE 2003, Berlin, Germany
- Wood J.G.M., L'ingénierie forensique. Approche anglaise, Colloque Le Pont, Toulouse, 21-22 oct. 2008.
- Woodward R.J., Williams F.W., Collapse of Ynys-y-Gwas bridge, West Glamorgan, Proc. ICE, Part 1, Vol. 86, pp. 1177–1191, 1989.
- Yuyama S., Yokoyama K., Niitani K., Ohtsu M., Uomoto T. (2007) Detection and evaluation of failures in high-strength tendon of prestressed concrete bridges by acoustic emission, Constr. Build. Mat., Vol. 21, pp.491–500.



# Chapter 8

## Non destructive assessment of concrete structures: combination of different techniques for addressing new challenges

Denys Breysse and Vincent Garnier

### 1 Introduction: a new challenge for combination

The combination of techniques is central to this book. In the six previous chapters it has been discussed, how geometrical parameters or material properties can be assessed. However, it has not been analyzed in detail, from an analytical point of view, how and why these combinations work. What are the possible limits and their most interesting fields of interest? In this last chapter, our objective is to highlight some general principles so as to better understand what (and why) can be efficient strategies of combination. New challenges will be addressed and priorities for future developments will be identified.

The first part of this chapter tries to make some general, theoretical statements. Then examples will follow and conclusions will be drawn. However, these conclusions will not be case-specific or application specific: they will remain valid for all problems that have been addressed in the different chapters of this book.

Chapter 1 described what experts are expecting when they combine several NDT methods. These expectations were classified in Type [A], [B] and [C] cases. In all the cases cited, the combination of techniques remained more or less a comparison between independent sets of results, whatever the techniques used and whatever the type of structure or the kind of problem analyzed (mechanical or alkali-aggregate damage, delamination detection, strength assessment...). A more ambitious way of combining NDT methods will be presented here and named: Type [D] combination.

The idea of Type [D] combination is to combine two techniques, such as the result given by the first measurement can be corrected according to the second

---

D. Breysse (✉)

Université Bordeaux 1, I2M, GCE (Civil and Environmental Engineering Department), France  
e-mail: denis.breysse@u-bordeaux1.fr

V. Garnier

Université de la Méditerranée, IUT Aix-en-Provence, France

measurement value. The “SonReb” method, which has been developed many years ago to estimate on site concrete strength [Malhotra, 1981], is an example of such a combination. The Rebound number gives a first assessment of the concrete strength, which is corrected with Ultrasonic Pulse Velocity (UPV). In practice, the user can read the concrete strength in a chart where iso-strength curves are a combined function of Rebound and UPV (see Chapter 3 for more details).

A Type [D] combination can have two main fields of application:

- when the first measurement is sensitive to two influential parameters, a second technique, sensitive to one or two of these parameters, enables the inversion of the system and the quantification of each parameter,
- if the first technique is sensitive to one influential parameter, but also to a bias factor (e.g., temperature) the bias effect can be reduced by measuring a second parameter which is also sensitive to this bias.

In both cases, the generic problem results from using a single NDT method that is sensitive to two or more parameters. In this situation, it is not possible to derive the value of a first parameter from a unique measurement. A contrario, a second technique, also sensitive to these two parameters (or only to the second one) can enable an elimination of the effect of the second parameter. The second parameter can be material property (internal) or environmental (e.g. air temperature and humidity).

The problem can be expressed in terms of sensitivity of measurements to influential variables. This explains why NDT has so many drawbacks. When NDT methods are considered as not being reliable, this means that one cannot simply derive the value of the influential variable which is looked for from that of the measured value. Calibration curves or additional measurements on cores are required (see Chapter 3 for the case of concrete strength assessment).

The ideal case would be when one has a unique influential variable  $Y$  and a unique relationship giving the NDT parameter value  $T$ :

$$T = f(Y)$$

In that ideal case, the inversion  $Y = f^{-1}(T)$  would provide the  $Y$  value. It will be shown why real situations are not so simple and this issue will be addressed in more detail in the following.

Sensitivity is a key point for better understanding what happens. Table 8.1 illustrates the sensitivity of four different non destructive techniques to several properties of concrete. It is drawn from a national review of the state-of-the-art recently published in France [Breyse and Abraham, 2005] and from results obtained from a benchmark research program [Balayssac, 2005, Sbartai et al. 2006]. The + or - signs correspond to a positive (effect varying with cause) or negative (consequence varying against cause) sensitivity. In the Table, “-” means a moderate negative effect and “--” a strong negative effect, “0” denotes no significant influence, “?” means that the effect is unsure at our present state of knowledge).

Let us consider as an example the Young modulus  $E$  or concrete strength  $R_c$  evaluation, using ultrasonic wave propagation. The P-wave velocity  $V$  is known to be related to these parameters (this issue has been addressed in detail in Chapter 3). Thus,

**Table 8.1** Sensitivity of NDT methods to several important concrete properties

	Radar	Capacimetry	Electrical resistivity	Ultrasonic waves
Water content	Velocity: -- Amplitude: --	--	--	Velocity: + Attenuation: –
Porosity	-	-	-	Velocity: YES (+ if saturated, – if dried)
Chloride content	Velocity: -- Amplitude: 0	0 ?	- ?	0
Rebars	Bias		Bias	bias

if one knows the  $V = f(E)$  model (or the  $V = g(R_c)$  model), a velocity measurement  $V$  would provide the value of  $E$  (resp.  $R_c$ ) by inversion of this  $f$  (resp.  $g$ ) model.

However, in practice, three additional difficulties may be faced:

- the exact models  $f$  or  $g$  are not known and they can only be approximated (by empirical relations, based on statistical analysis, or by using theoretical models). For instance,  $f$  can be based on the elasticity theory whereas  $g$  is taken from an empirical model. The use of calibration is therefore common, since it enables reducing the model error by comparing the estimations with the measurements, and by adapting the value of some model parameters. In any case a model error remains;
- each measurement, including that of velocity  $V$  itself, has some error or uncertainty: two successive measurements at the same point under identical conditions will not give the same results. If measurements are used for calibration, this measurement error has also an influence on model error,
- other parameters (temperature or humidity for instance) can influence the relation between  $Y$  and  $T$ . The consequence is an additional model error if these parameters are not considered.

For all these reasons, it is crucial to understand why and how the combination of techniques can result in added value:

- if two parameters, which a given technique is sensitive to, vary simultaneously, the reason for the measured variation cannot be identified without additional information. This is, for example, the case when a variation in water content (due to varying environmental conditions) is superimposed to a variation in the concrete microstructure (porosity of the cement paste). In this case, it is not possible to establish a direct link between the observed variation of the measured property (wave velocity, electrical resistivity...) and the physical cause. This is, of course, a crucial point for diagnosis since a variation of the microstructure can reveal some defect or damage when the water content may also vary simply because of the environment at the time of measurement (temperature, sun exposure, rain or wind...),
- the combination of two non-destructive techniques can provide additional information only if the sensitivity to the two parameters is different for the two techniques.

## 2 The identification / inversion problem

### 2.1 *Understanding the complexity of the problem*

We will develop here a very general formulation that can be applied to all assessment problems addressed in this book: strength assessment, damage detection, geometry assessment... The basic idea is that one always has at least one property  $Y$  that is looked for, and at least one NDT measurement  $T$ . The physical property measured with the NDT usually differs from the parameter one wants to evaluate.

Several levels of uncertainty arise from physical considerations and modelling, from the measurement process itself and from the material variability. A more detailed insight into the physics of the involved phenomena is necessary for a better understanding. Let us call:

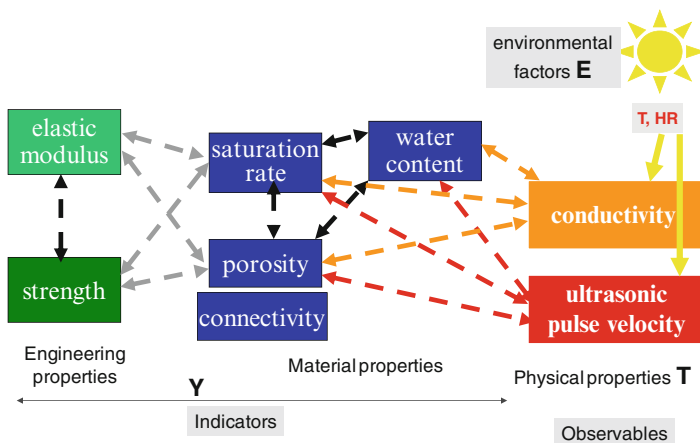
- **Y the property that is looked for** (dimension, strength, modulus, activity of corrosion...)
- and **T the measured value** (electrical resistivity, magnitude or time of arrival of a signal, electrical potential...).

NDT is based on the assumption that some correlation exists between  $Y$  and  $T$ , for instance between a length  $Y$  and the time of arrival  $T$  of a signal. Figure 8.1 illustrates what kind of relationships can exist between various material properties and why NDT interpretation is such a complex task. The black and grey arrows denote some correlation between properties and the orange and red arrows denote some sensitivity of a technique to parameters. At the center, one finds **material properties** (in blue boxes), which are representative of the material: porosity and connectivity on one hand, water content and saturation rate on the other hand. The former can be considered as constant with time (at least at short term, since they can slowly vary due to chemical processes), while the latter can vary due to environmental changes and concrete hygroscopicity. On the left part of the diagram, one finds the **engineering properties** which are related to material properties (grey double arrows). Finally, on the right part, one has **physical properties T** measured through NDT (here electrical conductivity and UPV), which depend on material properties (red double arrows) but also on some disturbing factors, for instance temperature (orange arrows). **Environmental factors E** must also be taken into consideration, since they influence the  $T$  values.

This graph in Fig. 8.1 shows that:

- the assessment of  $Y$  parameters does not reduce to the inversion of a simple  $T = f(Y)$  relation,
- any existing correlation between two techniques (here conductivity and US pulse velocity) also follows a very complex scheme, which must be understood before being used.

NDT measurements can be sensitive to both the engineering parameters (strength or Young modulus), which are rather stable with time, and to the water content, which can vary at short term according to environmental conditions. One can consider for example the case of corrosion assessment, since electrochemical



**Fig. 8.1** Generic diagram of relations between engineering and material properties Y, NDT measurements T and environmental factors E

measurements are known to be highly influenced by environmental conditions (temperature, humidity) [Andrade et al, 2002]. In this case:

- one cannot say if the measured variations result from a variation of the engineering parameter or water content,
- one has to take into account this sensitivity for quantifying the engineering parameter.

This is a main cause that hinders the practical use of NDT. Considering that a measurement T is sensitive to a first parameter Y, whose value is expected, and to one or several “influence factors” E, the effect of these influence factors has to be eliminated or at least reduced during the data processing.

## 2.2 Formalizing the problem

Before going further with practical examples, it is important to consider the main factors that can influence the quality of the identification / inversion problem. This will help to understand why the combination of techniques can be more or less efficient.

### 2.2.1 The weight of sensitivities

Let us look at this issue, using a very general formalism. What has been told in previous section remains valid if one considers two (or more) T parameters and two (or more) Y parameters. If one considers, for instance, two measured variables  $T_1$  and  $T_2$  and two material parameters  $Y_1$  and  $Y_2$  to be evaluated, one can write

$$T_1 = f_1(Y_1, Y_2) \quad \text{and} \quad T_2 = f_2(Y_1, Y_2) \quad [1]$$

where  $f_{i,i=1,2}$  are the “models” linking  $Y_i$  and  $T_i$ . The efficiency of the combination of techniques will increase with increasing values of the “crossed sensitivity”  $G$ :

$$G = [(\partial T_1 / \partial Y_1)(\partial T_2 / \partial Y_2) - (\partial T_1 / \partial Y_2)(\partial T_2 / \partial Y_1)] / [(\partial T_1 / \partial Y_1)(\partial T_2 / \partial Y_2)] \quad [2]$$

A value of  $G$  equal to zero means that the two techniques have exactly the same sensitivities to the two  $Y_i$  parameters, being thus totally redundant. In that situation, there is no interest to combine them, except if one just looks for mutual confirmation (Type [A] combination). When looking for interesting combinations, one has to consider the sign and values of the four partial derivatives  $\partial T_i / \partial Y_i$ ,  $i = \{1, 2\}$ . The priority is therefore the identification of techniques whose “crossed sensitivity” is different.

For instance, if one assumes that  $\partial T_1 / \partial Y_1$  and  $\partial T_2 / \partial Y_2$  have the same sign, techniques such as:

$$\text{SGN}(\partial T_1 / \partial Y_2) \neq \text{SGN}(\partial T_2 / \partial Y_1) \quad [3]$$

have a high interest, since they increase the  $G$  value. In practice, this means that both techniques are positively sensitive to the first parameter  $Y_1$ , but that the second parameter  $Y_2$  has an adverse effect on the two techniques: it decreases the first measurement when it increases the second one.

This case has been addressed into details in Chapter 3, when we described the Sonreb technique, as a useful combination for concrete strength assessment: the Sonreb consists in combining two techniques (US velocity and rebound) which are positively sensitive to strength, while having a different sensitivity to concrete water content.

The priority is to find techniques maximizing the upper term in the expression for  $G$  (Eq. [2]). Two things are relevant:

- (a) the sensitivity of each individual technique to the  $Y$  parameters,
- (b) the relations between these sensitivities, the best being when the sensitivities of the two techniques are very different, thus maximizing  $G$ .

This can be illustrated in practice by using empirical relationships which have been identified during the SENS0 program [Balayssac, 2008]. These relationships are similar to the conversion curves discussed in Chapter 3. Here linear models are considered:

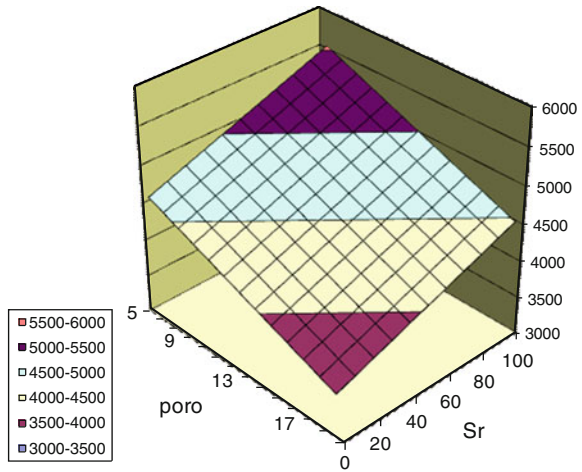
$$T_1 = A_1 Y_1 + B_1 Y_2 + C_1 \quad \text{and} \quad T_2 = A_2 Y_1 + B_2 Y_2 + C_2 \quad [4]$$

In this case,  $G$  writes:

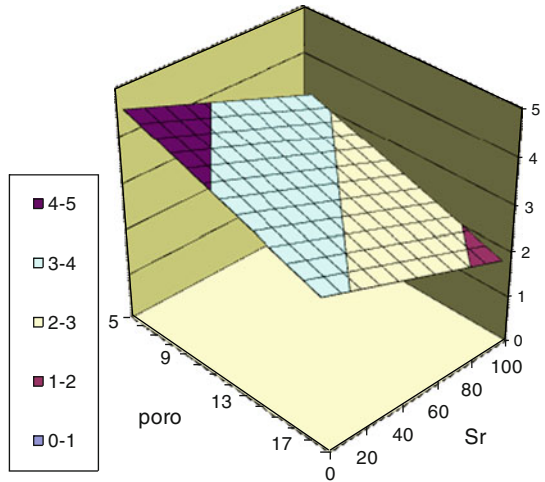
$$G = (A_1 B_2 - B_1 A_2) / A_1 B_1 \quad [5]$$

The absolute value of  $G$  is minimal when  $A_1 B_2 = B_2 A_1$ , i.e. when the two expressions are exactly proportional. Each model can be represented by a plane in three dimensions, like in Figs. 8.2 and 8.3 for two different techniques (ultrasonic

**Fig. 8.2** Model for US velocity (technique T2 in Table 8.2, see below) as a function of saturation rate (in %) and porosity (in %)



**Fig. 8.3** Model for the logarithm of electrical resistivity (technique T3 in Table 8.2, see below) as a function of saturation rate (in %) and porosity (in %)



velocity and electrical resistivity). The two measurements have a good complementarity if the orientation of the two planes is clearly different.

Figures 8.2 and 8.3 show how the US velocity and the electrical resistivity both decrease when the porosity increases, while the influence of an increase of saturation is different: the US velocity increases but the electrical resistivity decreases. This different sensitivity is the key point when combining the techniques.

The level of complementarity can be expressed:

- through the angle  $\alpha$  between the vectors perpendicular to the two planes:

$$\alpha = \arccos\left[\frac{1 + A_1 A_2 + B_1 B_2}{\sqrt{(1 + A_1^2 + B_1^2)(1 + A_2^2 + B_2^2)}}\right] \quad [6]$$



- and (more exactly) through the angle  $\alpha'$  between two horizontal lines belonging to the two respective planes:

$$\alpha' = \arccos[(A_1 A_2 + B_1 B_2) / \sqrt{\{(A_1^2 + B_1^2)(A_2^2 + B_2^2)\}}] \quad [7]$$

The G function of Eq. [2] writes here:

$$G = (A_1 B_2 - A_2 B_1) / A_1 B_2$$

and  $G = 0$  corresponds to  $A_1 B_2 - A_2 B_1$ , which means that the two models are proportional. This condition also corresponds to  $\alpha' = 0$  in Eq. [7]. The larger the  $\alpha'$  value, the better the complementarity of the two techniques. The  $\alpha'$  coefficient can be named “complementarity index”.

One can note that it is also possible to consider normalized parameters, replacing the equations:

$$T_1 = A_1 Y_1 + B_1 Y_2 + C_1$$

with

$$T_1 / C_1 = a_1 Y'_1 + b_1 Y'_2 + 1 \quad [8]$$

where  $Y'_i = Y_i / Y_{i\text{ref}}$ ,  $a_1 = A_1 Y_{1\text{ref}} / C_1$  and  $b_1 = B_1 Y_{2\text{ref}} / C_1$ . In these expressions,  $Y_{i\text{ref}}$  are arbitrary reference values, with the same units as  $Y_i$ . Please note that the  $a_i$  parameters in Eq. [8] have no unit.

### 2.2.2 The weight of measurement noise

The quality of the measurement is an important factor. Since the measured values  $T_{1M}$  and  $T_{2M}$  will differ from the “true” properties  $T_{1T}$  and  $T_{2T}$ , the better the reproducibility, the better the efficiency of combination. One can write

$$T_{1M} = T_{1T} + \varepsilon_1 \quad \text{and} \quad T_{2M} = T_{2T} + \varepsilon_2 \quad [9]$$

with measurement errors  $\varepsilon_1$  and  $\varepsilon_2$ . These errors include:

- random errors and systematic errors, e.g. due to the processing device,
- additional noise factors, among which low scale material variability and the influence of environmental factors (like temperature and humidity) not considered explicitly in the models.

Because of measurement errors, one often chooses to repeat the measurements in a limited area around the reference point of measurement (see Chapter 3 for rebound). The repetition leads to averaging regarding local variability. This issue has been recently addressed into details by [Breyse et al, 2008a], since the number of reasonable repetitions for each technique can be quantified as a function of the level of accuracy that is looked for and of the level of repeatability of the technique itself. Thus, the inversion of the system of equations:

$$T_{iM} = f_i(Y_1, Y_2) \quad \text{and} \quad T_{2M} = f_2(Y_1, Y_2) \quad [10]$$

with  $T_{iM}$  instead of  $T_{iT}$  cannot yield the exact values of  $Y_1$  and  $Y_2$ .

### 2.2.3 The importance of the quality of the model

A last important element has to be considered: the inversion process requires solving the direct problem. Since the physical reality can only be approached by models, one must be aware that  $f_i$  and  $f_i$  are only models of the reality. Thus, model errors (or uncertainties) will result in uncertainties and errors in  $Y$  estimates.

This is the reason why inversion problems in NDT often require a good (prior) calibration stage where a relationship between  $Y$  and  $T$  is established before proceeding to inversion.

Analytical models, empirical relations drawn from data sets, additional laboratory tests or complimentary semi-destructive tests can be used to improve the quality of calibration.

### 2.2.4 The global problem

To summarize the above considerations, the general problem finally is to identify the material properties  $Y_j$  ( $j=1,2$ ) from the  $T_{iM}$  measurement with:

$$T_{iM} = f_i(Y_j, E_k) + \varepsilon_i(E_k) \quad [11]$$

$$T_{iT} = F_i(Y_j, E_k) \quad [12]$$

where  $T_{iT}$  and  $T_{iM}$  are the true (expected) and measured values respectively,  $F_i$  and  $f_i$  are the true (unknown) and identified relationships, and  $\varepsilon_i$  is the measurement error. Two important differences exist between Eq. [11] and Eq. [12]:

- the identified (assumed)  $f_i$  is not identical to the true  $F_i$ ,
- the measurement uncertainties  $\varepsilon_i(E_k)$  the “true” NDT value is not known.

In addition, the inversion problem can be ill-conditioned when the “cross-sensitivity”  $G$  (see Eq. [2]) or the “complementarity index”  $\alpha'$  (see Eq. [8]) is small.

Three general rules can now be drawn for an efficient combination of NDT:

Alternative ways are offered by a variety of meta-heuristic methods which avoid formalizing the direct problem. For instance, neural networks have recently proved to be very efficient for identifying material parameters in concrete [Sbartai et al, 2009]. These non explicit methods require a learning stage (equivalent to the calibration process) and the range of validity of the model remains limited to datasets which are similar to that used during learning. The parameters of the neural network must be identified for each new concrete. This is a limit for a wider use of such models.

### General rules for an efficient combination of Non Destructive Techniques

The optimization of the combination of NDT techniques requires:

- (a) the **selection of NDT techniques offering the best as possible “cross-sensitivity”** G to the influencing parameters,
- (b) the **reduction of the measurement uncertainties**, including the consequences of uncontrolled environmental conditions,
- (c) to use a model which is the **best possible description** of the physical reality.

**Table 8.2** Best selected NDT observables

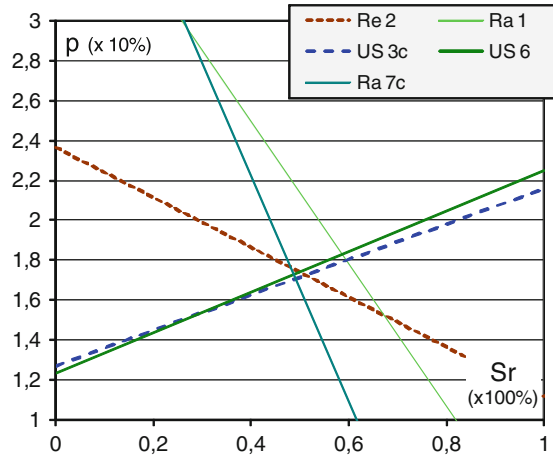
	Family of NDT	Measured quantity	code	unit
T <sub>1</sub>	mechanical waves	group velocity of surface waves	US3c	m.s <sup>-1</sup>
T <sub>2</sub>	mechanical waves	UPV of compression waves	US6	m.s <sup>-1</sup>
T <sub>3</sub>	electrical	logarithm of electrical resistivity	Re2	Ω.m
T <sub>4</sub>	radar (electromagnetic)	amplitude of a radar signal	Ra1	without unit
T <sub>5</sub>	radar (electromagnetic)	time of arrival of a radar signal	Ra7c	ns

### 3 Practical case of Type [D] combination for concrete properties assessment

The two examples discussed in this section have been developed during the SENSO project. SENSO is a specific research program that has been designed under the auspices of French National Agency of Research (ANR) such as to quantify the relations between indicators (influential parameters) and observables (measurements). A large series of NDT observables and concrete material properties (indicators) have been considered, namely: strength, elastic modulus, porosity, water content, carbonation depth, chloride content, amount of micro cracking. Various sources of uncertainties (measurement uncertainties, material variability, model errors...) have been systematically quantified. The full programme will not be described here in detail since the reader can refer to the literature [Balaysac, 2008, Breyse et al, 2008c].

Analysis of the variability of NDT measurements at various scales had lead experts to select five NDT observables that show a very good repeatability or/and are sensitive to the indicators. These are given at Table 8.2. The two examples discussed in the following are drawn from results obtained with these observables.

**Fig. 8.4** Regression lines enabling estimation of porosity and saturation rate from measurements of the various observables (see Table 8.2 for legend)



### 3.1 Porosity and water content assessment by combining two NDT methods

For each of the five observables, multiregression linear models were identified from statistical analysis of datasets for a series of indicators. The first example focuses on the combined influence of porosity and saturation rate on Young modulus. This combined influence is well known, for instance, on acoustic parameters, since the US velocity depends on porosity (thus Young modulus) but also varies with water content [Soltani et al, 2009].

Two observables show significant complementarity if they have a different sensitivity to indicators as it was expressed in Eq. [2] and Eq. [8]. Figure 8.2 and 8.3 show multi-regression models in 3-dimensions for observables  $T_2$  and  $T_3$  (quantities to be measured) and the two indicators porosity and water content. The different orientations in space of the two regression surfaces corresponds to different partial derivative values  $dTi/dYi$  and confirms the good complementarity between surface wave velocity and electrical resistivity. This is equivalent to a “good value” of the coefficient  $G$  defined in Eq. [2]).

Since the orientation of the planes in the 3D-space is very different, any couple of values ( $T_2, T_3$ ) will provide a well-conditioned pair of equations, enabling a good inversion of the system. This can be seen in Fig. 8.4, which represents the projection onto the horizontal plane (porosity, saturation rate  $Sr$ ) for a given series of measurements. The angles  $\alpha'$  between the different lines are directly visible in this figure.

Figure 8.4 shows that the information provided by four out of the five observables is very consistent. The fifth one (radar measurement  $T_4$ , RAI) gives a contradictory information. This is the result of the model used for radar. It has been assumed a priori that a multiregression linear model was appropriate for this technique and the relevant regression coefficients were identified and kept in the model. In fact, the  $T_4$  dependency on porosity is statistically non significant and it should have been

removed from the model, keeping only the  $S_r$  dependency, thus resulting in vertical line in Fig. 8.4. Figure 8.4 shows how the Type [D] combination works, since, as soon as two techniques show a good level of complementarity, the system inversion and the determination of the couple of indicators is possible. It also shows that the two US techniques (US8, US3c) provide consistent but redundant information. If the assessment would be relying on these two methods only, the system of equation would be ill-conditioned and a large uncertainty would result.

### 3.2 *Young modulus assessment by combining two or more NDT measurements*

#### 3.2.1 Strategy of combination

The second example describes the application of the same logic to Young modulus assessment. The estimation of concrete Young modulus is a common challenge for structural assessment. Sonic and ultrasonic measurements are widely used for the condition assessment of building materials. For elastic materials, there is a theoretical relationship between the velocity of P-waves and the elasticity modulus  $E$ :

$$E = c V_L^2 \rho \quad \text{or} \quad V_L^2 = E / c \rho \quad [13]$$

where  $V_L$  is the velocity of P-waves (in  $\text{m}\cdot\text{s}^{-1}$ ),  $\rho$  is the volumetric mass (in  $\text{kg}\cdot\text{m}^{-3}$ ) and  $c$  is a constant which depends on the Poisson's ratio  $\nu$ . Thus, if linear elasticity is assumed and values are assigned to  $\nu$  and  $\rho$ , the measurement of  $V_L$  directly leads to a value of the Young modulus.

Changes in environmental conditions such as temperature or relative air humidity, modify the water content in concrete, thus both Young modulus  $E$  and  $V_L$ . Another difficulty is that the material mass density  $\rho$  may change (as it is probably the case for the Poisson's ratio  $\nu$ ), and it cannot be longer assumed as constant in Eq. [12].

To summarize, the fact that environmental conditions cannot be fully controlled will influence:

- (a) the real parameter to identify  $E$ ,
- (b) the non destructive measurement of  $V_L$ ,
- (c) the relation between  $E$  and  $V_L$ . If a model has been identified for this relation, changing the environment will induce model errors.

Since UPV measurements are very easy to handle, they have been often combined to a secondary technique for material assessment. One approach is to combine them with another technique that is also sensitive to water content. Capacitive measurements [Sirieix et al, 2007], GPR measurements [Saisi et al, 2001, Laurens et al, 2003], IR thermography [Sirieix et al, 2007, Kandemir-Yucel et al, 2007] or electrical resistivity [Sirieix et al, 2007, Breyse et al, 2008b] have been used for this purpose. However a more formal approach appears to be necessary.

In the SENSO program, a statistical analysis of measurement results recorded while varying the concrete composition and the saturation rate enabled the selection of the relevant observables. Multiple regression relationships between material properties (here saturation rate  $S_r$  and Young modulus  $E$ ) and NDT measurements  $T$  were identified [LMDC-SENSO, 2009]:

$$T_1 = 1128 + 4.87 S_r + 26.4 E \quad [14]$$

$$T_2 = 2644 + 8.77 S_r + 39.1 E \quad [15]$$

$$T_3 = 1.94 - 0.015 S_r + 0.053 E \quad [16]$$

$$T_4 = 0.541 - 0.0016 S_r + 0.0014 E \quad [17]$$

$$T_5 = 0.956 + 0.00379 S_r - 0.0032 E \quad [18]$$

where  $S_r$  and  $E$  are the saturation rate (in %) and the saturated Young's modulus (in GPa).  $T_1$  to  $T_5$  are the same five NDT observables as in Table 8.2, with the same units (the units of the numerical coefficients are such as the relationships are consistent; e.g. in Eq. [14],  $T_1$  is in  $m \cdot s^{-1}$ , and the unit of the coefficient 26.4 is  $m \cdot s^{-1} \cdot GPa^{-1}$ ).

These equations can be replaced with normalized equations ([14'] to [18']), in which  $S_{r,ref} = 100$  and  $E_{ref} = 10$  GPa:

$$T_1 = 1128(1 + 0.432 S_r / S_{r,ref} + 0.234 E / E_{ref}) \quad [14']$$

$$T_2 = 2644(1 + 0.332 S_r / S_{r,ref} + 0.148 E / E_{ref}) \quad [15']$$

$$T_3 = 1.94(1 - 0.786 S_r / S_{r,ref} + 0.274 E / E_{ref}) \quad [16']$$

$$T_4 = 0.541(1 - 0.289 S_r / S_{r,ref} + 0.025 E / E_{ref}) \quad [17']$$

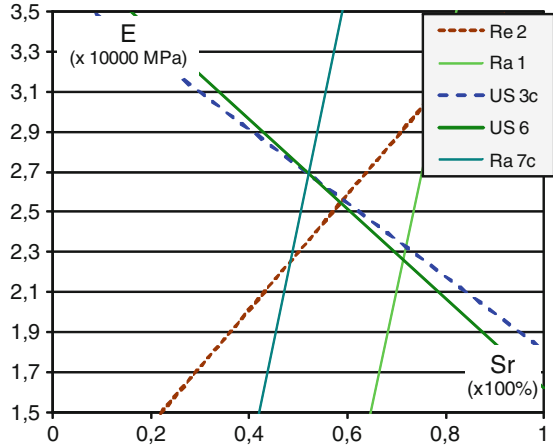
$$T_5 = 0.956(1 + 0.397 S_r / S_{r,ref} - 0.034 E / E_{ref}) \quad [18']$$

In this case, the numerical coefficients are without unit. Their sign and magnitude is directly related with the sensitivity as it was discussed at Section 2.2.1. The different signs of these partial derivatives  $dT_i/dY_j$  ( $Y_1 = S_r$ ,  $Y_2 = E$ ) in Eq [14]-[18] or [14']-[18'] show that the degree of complementarity can be more or less important between any two of these five techniques.

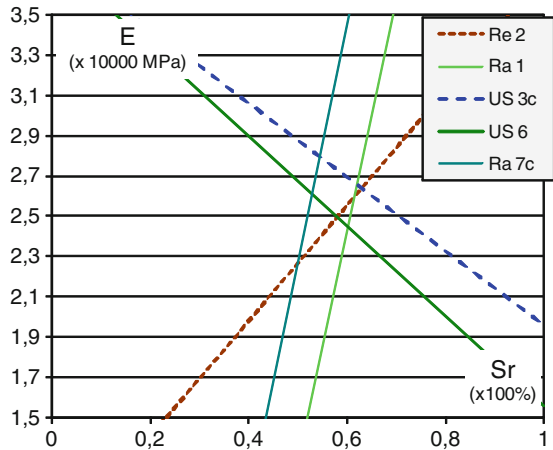
### 3.2.2 Assessment results

Figures 8.5 and 8.6 show the regression lines corresponding to the measured values  $T_i$  in the  $S_r$ - $E$  plane with the five observables  $T_1$ - $T_5$  for two specimens (two slabs) made of the same concrete ( $w/c = 0.55$ ) and kept under the same conditions.

**Fig. 8.5** Use of linear regression model to identify the  $\{S_r, E\}$  values for one concrete specimen (code for techniques in Table 8.2)



**Fig. 8.6** Use of linear regression model to identify the  $\{S_r, E\}$  values for a second concrete specimen, identical to that of Fig. 8.5 (code for techniques in Table 8.2)



If both the measurements and the (statistical regression) models were perfect, all lines should cross in a unique point. If the material was homogeneous, the two graphs would be identical. Any difference between theory and practice is due to one of three reasons: measurements are not perfect, the linear regression model is an approximation, and the material is not homogeneous.

The complementarity of the techniques involved here (crossed-sensitivity, quantified by  $G$  in Eq. [2]) can be clearly seen since the lines have different slopes. If the two techniques with mechanical waves ( $T_1/US3c$  and  $T_2/US6$ ) give parallel lines, the two radar measurements ( $T_4/Ra1$  and  $T_5/Ra7c$ ) give two different parallel lines and the last technique, electric resistivity ( $T_3/Re2$ ) has a different slope. The larger the difference between slopes, the better the complementarity, with an optimum when the  $\alpha'$  angle is between  $60$  and  $120^\circ$  (this angle is calculated accordingly to Eq. [9] and cannot be directly read on figures, because of different scales on the two axes).



We can also note that the two radar measurements do not provide consistent results (neither between them, nor with the three other techniques). The reason of this fact will be explained in the following section. This poor consistency may induce conflicts between the possible values estimated for  $S_r$  and  $E$ .

### 3.2.3 Quality of the assessment and influential parameters

Figures 8.5 and 8.6 show the results corresponding to five observables (which have been selected from a larger set, since a lot of information has been obtained during the SENSO experimental program), but the method works as soon as two observables are available. Nevertheless, the assessment is not perfect, since the lines do not meet in a unique point. To give some basis for comparison, the measured value of  $S_r$ , estimated by weighing the slabs is between 47 and 54 % and the measured Young's modulus, obtained on cylinders, is about 27 GPa. The  $S_r$  value seems to be slightly overestimated, but the Young modulus is accurately estimated. The differences between reality and estimation have two main explanations:

- the model error: the lines correspond [Eq. 13 to 17]. These relationships are empirical regressions identified between a data set and a measurement set. Linear relationships between  $Y_i$  and  $T_i$  have been systematically assumed. It will be shown below that this assumption may be inappropriate.
- the measurement uncertainty: changing the measured value moves each line parallel to itself. Thus the location of each line on the ( $S_r$ ,  $E$ ) plane is only approximate, the magnitude of the uncertainty depending on the measurement uncertainty and on the regression coefficients of the linear relationships [14] to [18].

It can be seen from Figs. 8.5 and 8.6 (drawn from measurements on a pair of twin slabs) that the position of the lines is very similar, showing a high consistency. However, one can note slight differences between the two slabs, indicating that the measurement values are different. This is a consequence of the measurement variability (see Eq. [8]) that could be caused by noise, material variability and environmental conditions.

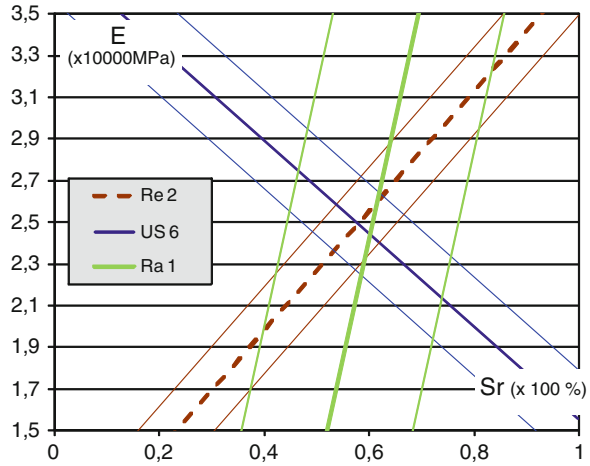
Since this point appears to be of specific importance for quantifying the influence on the quality of the assessment, the experimental strategy in the SENSO program has consisted in systematically quantifying the variability, either due to the repeatability of the technique/measurement, or due to the material variability. This was done by recording multiple measurements, for each technique: (a) at a given point on a specimen, (b) at various points on a given specimen, (c) between specimens.

This variability can be expressed in terms of  $T_i$  variance or standard deviation. For instance, for the five observables, the standard deviations  $sd$  are:

$$sd(T_1) = 41.2; \quad sd(T_2) = 11.5; \quad sd(T_3) = 0.11; \quad sd(T_4) = 0.025; \quad sd(T_5) = 0.020.$$

The smaller is the standard deviation, the more accurate the estimation of  $\{S_r, E\}$  when using the Eq. [14] to [18] for inversion. In addition, the knowledge of the

**Fig. 8.7** Use of linear regression model to identify the  $\{S_r, E\}$  values with range of uncertainties (code for techniques in Table 8.2)



standard deviation for each measurement provides information about the level of accuracy of the estimate (a slightly different value of the measurement would correspond to a slight displacement of the line in the  $E-S_r$  diagram). For instance, if one considers the resistivity measurement  $T_3$ , with  $sd(T_3) = 0.11$ , this leads to an uncertainty of about  $\pm 0.11/0.015 = \pm 6\%$  on  $S_r$  and of about  $\pm 0.11/0.053 = \pm 2$  GPa on  $E$ . Fig. 8.7 provides the corresponding information. It is similar to Fig. 8.6 but only three techniques have been kept for the sake of clarity. For each of these techniques, the bandwidth corresponding to  $\pm$  one standard deviation is drawn. It can be seen that US (US6 -  $T_2$ ) and resistivity (Re2 -  $T_3$ ) are more efficient because of their smaller  $sd$  ranges than radar (Ra1 -  $T_4$ ).

Looking at the bandwidths also provides a range of values for  $\{S_r, E\}$  pairs directly visible in the Figure. It can be said here that Young modulus ranges between 23 and 27 MPa and that saturation rate ranges between 50 and 65 %.

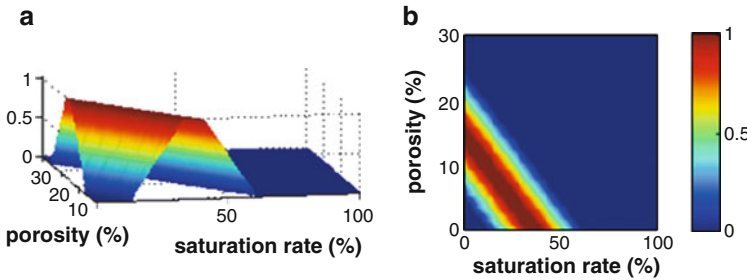
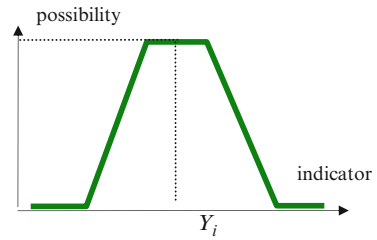
## 4 Data fusion

The deterministic process of combination presented in the previous section has two main limitations:

- there is no information on the quality of the results and no confidence interval for estimated values,
- there is no solution to the possible conflict between the solutions given by different observables.

It has been shown at Chapter 3 that data fusion can offer interesting possibilities for solving these problems. Data fusion has been used for the assessment of civil engineering components [Gros et al, 1999, Kohl et al, 2006, Streicher et al. 2006,

**Fig. 8.8** Possibility distribution  $\Pi(Y_i)$  for an observable as a trapezoidal function of the indicator



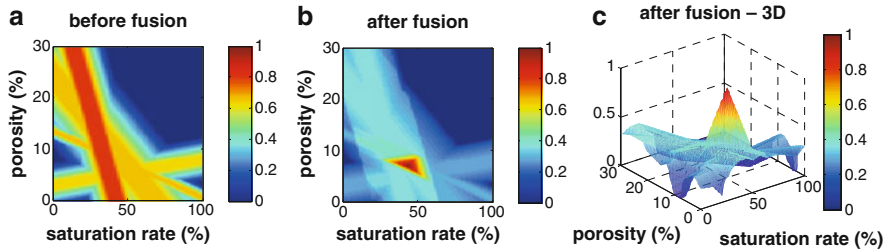
**Fig. 8.9** Possibility distribution for one observable and two indicators:  $Y_1$  (porosity (%)) and  $Y_2$  (water saturation rate (%)). (a) 3D image, (b) top view in the  $\{Y_1, Y_2\}$  plan

Horn 2006, Maierhofer 2008, Huginschmidt and Kalogeropoulos 2009], but it is mainly used for image analysis where two or more images are compared and processed together. This can highlight contrast or defects and reduce noise. One technique proposed by Dempster-Shafer [Shafer, 1976] allows to segment the image which is a way to detect cracks or inclusions.

When dealing with material properties, values of indicators that vary continuously have to be estimated. This is the reason why frameworks like the theory of probabilities or the theory of possibilities can be helpful. The theory of possibilities is able to take into account the conflict between assessments originating from different observables. It thus can be used to combine the information provided by several ND techniques.

If one considers first one technique and one observable  $T_i$  for one indicator  $Y_i$ , the value of the possibility  $\Pi(Y_i)$  ranges between 0 (= impossible) to 1 (= sure). The shape of the distribution  $\Pi(Y_i)$  (Fig. 8.8) depends on the quality of the inversion  $Y_i = f^i(T_i)$ . The width of the plateau where  $\Pi(Y_i) = 1$  is reduced if the observable is highly discriminant regarding  $Y_i$ .

If one now considers one observable and two indicators  $Y_1$  and  $Y_2$ , the inversion of the  $f_i$  model (Eq. [1]) leads to an infinite number of  $\{Y_1, Y_2\}$  pairs corresponding to the regression model. With a deterministic approach, this corresponds to a line, like on Figs. 8.5-8.6. However, data fusion assumes that the result is a distribution of possibility, for any  $\{Y_1, Y_2\}$  pair, as illustrated in Fig. 8.9 for determining the porosity (%) and the water saturation rate (%) from a single measurement.



**Fig. 8.10a-c** Distribution of possibilities for porosity and saturation, originating from several ND methods (after [Ploix et al, 2009]). (a, b) before and after fusion, (c) 3D view

Different NDT methods lead to different results. A further step is required to fuse the different distributions which have been created in the first step. This methodology has been used [Ploix et al, 2009; LMDC-SENSO, 2009] in the SENSO Programme, working with many techniques on a common data set and a common library of models (empirical bilinear regression models) as discussed in the previous section. Fig. 8.10 shows what kind of results can be obtained.

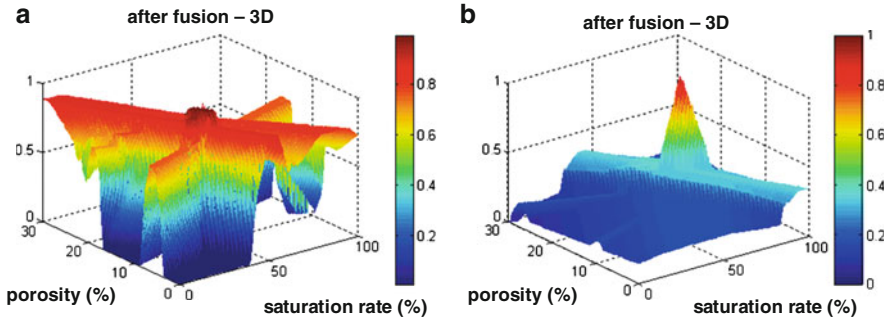
The image on the left shows the distribution for four observables ( $T_1$  to  $T_4$ ) for the assessment of water saturation rate (%)  $Y_1$  and porosity (%)  $Y_2$ . The central image shows what is obtained after the application of a mathematical operator for data fusion. The last picture (Fig. 8.10c) presents the same information in a 3D view.

Data fusion has three main advantages:

- visual representation that highlights the results and makes assessment easier;
- an adaptive mathematical operator, for the assessment of the concordance between partial results provided by each observable. The concordance is maximum when there are no conflicts between the possibility distributions originating from the different observables;
- the possibility to quantify a confidence index. It is determined by analysing the “solution peak” morphology.

In Figs. 8.11 a-b, two situations are compared. They correspond to cases where the expert’s confidence in the techniques/measurements is low (left) or high (right). In the first case, even if the value of an observable has been obtained, other results cannot be fully excluded. In the second case, once a value has been measured, it excludes many possibilities that would be incompatible with it. This difference is accounted for through the mathematical operator used for fusing the different distributions of possibility. It leads to a final solution that is more or less contrasted regarding the final assessment (Figs. 8.11a-b). In the picture on the left, the “solution peak” is weak and the extraction of a solution is uncertain. On the contrary, the image on the right shows a peak that emerges from the solution set and that is discriminant [LMDC-SENSO, 2009].

Data fusion is a complementary tool that makes the combination process more systematic and that adds the interest of visual representation. It can be also helpful



**Fig. 8.11a-b** Probability distributions after fusion with bad confidence (left) and good confidence (right)

to select the best observable(s) and to allow for the development of automatic quantitative protocols. However, one should keep in mind that the eye and expertise of NDT practitioners remains essential. The mathematical process, even if automatic, is based on choices derived from expert knowledge regarding the confidence they give to their techniques. This defines the shape of each individual distribution of probabilities (Fig. 8.8) through the shape of the mathematical operator for fusion.

## 5 Quality of techniques and quality of assessment

This chapter was devoted to analyze how non destructive techniques can be combined in a formal way, to improve the conclusions provided by single techniques. The methodology was developed on examples in relation with the material or engineering properties of concrete (porosity, Young's modulus, saturation rate). This methodology can also be used for other material parameters (e.g. concrete strength) and for geometrical assessment (e.g. depth assessment, delamination assessment...).

It has to be kept in mind that the "Type [D]" combination is based on the inversion of the  $f_i$  models which link what is measured ( $T_i$ ) to what has to be assessed ( $Y_i$ ).

Thus, modelling remains a necessary step. It has been shown that the final quality of the assessment depends on three sets of parameters:

- (a) the **noise**
- (b) the **quality of the models** used for inversion/identification
- (c) the **choice of the relevant techniques** for each specific purpose, based on their (individual) **sensitivities** and (when combined) **complementarity**.

## 5.1 *Effect of the noise*

The two main challenges are its reduction and quantification. The measurement noise is partly due to the material heterogeneity at micro-scale and partly due to lack of repeatability. The reduction is only possible for repeatability. The best way would be the definition of standard procedures, which are currently still uncommon for non destructive assessment of concrete. RILEM can take its part, by mobilizing experts for a series of known techniques. The standard procedures must not only concern the equipment but, more globally, the way measurements are done. Of course, technical improvements on devices and equipment can also contribute to increased measurement quality.

The definition and use of national/international reference sites would also be positive, since they would offer the possibility of comparing techniques and procedures, in order to select the best ones (regarding the repeatability of measurements). Such test sites have been designed, more often at a national scale and for a given purpose (e.g. check the limits of a given device for defect detection). The idea would be to write common specifications, and perhaps to prepare an international benchmark on a series of reference test sites.

It is also of primary importance to quantify the repeatability for each technique. The repeatability depends on the specimen (laboratory specimens, on site structures...), on the device used, on the conditions during measurement (e.g. control of external conditions, way of preparing the surface, of positioning the measurements). The repeatability must also be quantified at a very local scale (in a delimited area of few cm<sup>2</sup>) and at more global scale, thus including the effects of material variability in a “normal homogeneous concrete”. Developing a database that would combine data about repeatability would be of great value, since knowing the variance of measurements is required before: (a) selecting the “best” techniques, (b) identifying the scatter/uncertainty in assessment.

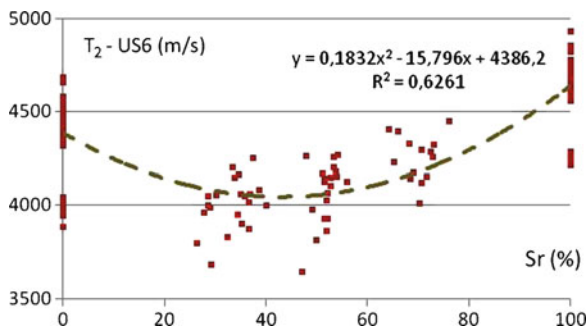
## 5.2 *Quality of the models used for inversion/identification*

The models discussed here were mainly based on statistical data analysis. Such empirical modeling can be developed for larger series of indicators (including carbonation, chloride content...) and observables. But the models must also be improved. If one considers statistical regression, the linear models are not well suited to describe the complexity of the physics involved.

For instance, the measurements in the SENSO program have shown [LMDC-SENSO, 2009] that the ultrasonic velocity does not vary monotonously with water content as shown on Fig. 8.9. Measured values from 8 different concretes (with varying w/c, different aggregate type and size), and five levels of saturation from  $S_r = 0\%$  to  $S_r = 100\%$  [Balayssac, 2008] are shown.

Eq. [15] which expresses a bilinear dependency for pulse velocity of compression waves on saturation rate and porosity is only valid when  $S_r$  is larger than 40%,

**Fig. 8.12** Non linear dependency of compression waves velocity to saturation rate



while it leads to significant errors for drier specimens. If one focuses on sensitivity to saturation rate (Fig. 8.12) an alternative model writes (porosity here remaining an uncontrolled parameter):

$$T_2 = 0.1832 S_r^2 - 15.796 S_r + 4386.2$$

The velocity of waves exhibits a non monotonous variation and the model inversion would lead to values different from those provided by Eq. [15]. This non linearity had yet been observed on other porous materials, like stones, and justified by theoretical considerations at the pore scale. It can be however noted that in the range  $S_r = [30 \%, 100 \%]$  which corresponds to the practical range on real structures, the linear dependency remains a good approximation.

More care can be devoted to the development of models laying on some physical basis, and not only on empirical/statistical considerations. Such models can provide a better understanding of the measurement process itself, which could lead to an improvement of techniques.

An alternative is the use of heuristic models, which do not explicitly formalize the relationships existing between inputs (indicators) and output (observables – NDT measurements) but identify and quantify possible links. Neural networks have been used for building materials. However, since such models do not provide an explicit relation, inversion is not possible. Thus it is the inverse relation ( $Y_i = g(T_i)$ ) which has to be identified by the heuristic model.

In any case, empirical models, more or less based on physical reasoning and modeling, or heuristic models, the development of reference sites and measurements databases would provide the basis for modeling. The model error has also to be systematically quantified, since it contributes to the uncertainty of the final assessment. Of course, this model error has a lowest limit, due to the measurement uncertainty.

### 5.3 Complementarity and efficiency of combination

Now, the efficiency of combinations can be assessed itself. It can be counterproductive to repeat redundant measurements or to perform additional measurements that



do not provide any additional information. We have therefore suggested an approach for analyzing this efficiency.

Using the example of multivariate models, Figs. 8.2 and 8.3 and Equations [6] and [7] have shown how the complementarity can be illustrated and quantified. To be more general, the problem can be reduced to that of the different sensitivity of two (or several) techniques to two (or several) indicators. If the  $T_i = f_i(Y_j)$  relationships are known, the quality of complementarity is easily quantified from the partial derivatives on the corresponding surfaces. Thus, developing a general analysis of possible efficient combinations would require first the development of the knowledge database of models.

In the short term it is possible to justify the choice of efficient combinations of techniques for a given assessment purpose using existing information. Some challenges that should be addressed in the future:

- Improving the on site strength assessment of concrete: the SonReb process could be reanalyzed and possibly improved by quantifying the level of complementarity between rebound and velocity of surface waves, but also with possible alternative techniques, like resistivity measurements or pull-out semi-destructive tests.
- The issue of carbonation depth assessment is a key question, since the carbonated layer has a strong influence on the material behavior and therefore on many ND measurements. It can be considered as a disturbing factor for measurements carried out for other reasons, preventing their accurate analysis. Alternatively carbonation can be considered as a testing problem of its own and addressed through the combination of well chosen techniques.
- The chloride content assessment requires some destructive tests and analysis. It appears however that several techniques (mainly electromagnetic or electrical, (Hugenschmidt and Loser, 2008)) are sensitive to chloride content, thus opening new possibilities of development.

This list is not limitative and the future development of practical use of NDT will depend mainly on their ability to provide quantitative results, ideally directly usable by the engineer. Throughout this book it has been tried to show how recent progress has been achieved and what could be future improvements.

NDT assessment often remains a field for specialists because of the complexity of measurements and post-processing. But, the limiting factor is much more scientific knowledge and the capacity of experts to formalize the problems than the data processing itself.

Of course it would be a good point to develop tools and softwares supporting the final assessment, This is not an easy task when several sources of information lead to different (and possibly contradictory) results. The development of methods like data fusion, which can provide more explicit outputs will be helpful and will contribute to a wider use of NDT for concrete assessment.

## References

- Andrade C., Alonso C., Sarria J. (2002) Corrosion rate evolution in concrete structures exposed to the atmosphere, *Cement and concrete composites*, Vol. 24, pp. 55–64.
- Balayssac, J.P. (2005) Evaluation de la dégradation du béton d'enrobage et aide au diagnostic et à la réparation des ouvrages, Projet RGC&U, Contract 01V0550, Final report, 2/2005.
- Balayssac J.P. (2008) SENSO: a French project for the evaluation of concrete structures by combining non destructive methods", *Sacomatis, RILEM conf.*, 1-2/9/2008, Varenna, It.
- Balayssac J.P., Laurens S., Arliguie G., Ploix M.A., Breyse D., Dérobert X., Piwakowski B. (2009) Evaluation of concrete structures by combining non-destructive testing methods (SENSO project), NDT-CE, Non-destructive testing in Civil Engineering, Nantes, 30 june-3 july 2009.
- Breyse D., Abraham O. (2005) Guide méthodologique de l'évaluation non destructive des ouvrages en béton armé, Presses ENPC, Paris, 550 pages.
- Breyse D., Lataste J.F., Balayssac J.P., Garnier V. (2008a) Quality and accuracy of concrete assessment provided by NDT measurement, 6<sup>th</sup> Int. Workshop on probabilities and materials, Darmstadt, 26-28 oct. 2008.
- Breyse D., Soutsos M., Lataste J.F. (2008b) Assessing stiffness and strength in reinforced concrete structures: added-value of combination of nondestructive techniques, 1st Medachs conf., Lisbon, 28-30 jan 2008.
- Breyse D., Elachachi S.M., Balayssac J.P., Laurens S. (2008c) Méthodologie de qualification des observables issus du contrôle non destructif pour diagnostiquer l'état du béton, *Eur. J. of Environmental and Civil Engineering*, 12, 459–472.
- Gros X.E., Bousigue J., Takahashi K. (1999) NDT data fusion at pixel level, *NDT&E Int.*, 32, 283-29.
- Horn D. (2006) Reliability Analysis Combining Multiple Inspection Techniques, *Proc. NDT-CE Conf.*, Berlin.
- Hugenschmidt J., Kalogeropoulos A. (2009) The inspection of retaining walls using GPR, *J. Appl. Geophys.*, 67, 4, 335–344
- Hugenschmidt J., Loser R. (2008) Detection of chlorides and moisture in concrete structures with ground penetrating radar, *Mater Struct*, 41, 4, 785–792
- Kohl C., Streicher D. (2006) Results of reconstructed and fused NDT-data measured in the laboratory and on-site at bridges, *Cem. Concr. Composites*, 28, 402–413.
- Laurens S., Balayssac J.P., Rhazi J., Klysz G., Arliguie G. (2003) Non destructive evaluation of concrete moisture by GPR technique: experimental study and direct modeling, *NDT-CE'03*, 16-19 sept. 2003.
- LMDC-SENSO (2009) Stratégie d'évaluation non destructive pour la surveillance des ouvrages en béton, final report, 274 p..
- Maierhofer C., Zacher G., Kohl C., Wöstmann J. (2008) Evaluation of Radar and Complementary Echo Methods for NDT of concrete elements, *J. Nondestructive Evaluation*, Vol. 27, p. 47–57.
- Malhotra, V.M. (1981) Rebound, penetration resistance and pulse velocity tests for testing in place, The Aberdeen Group.
- Ploix M.A., Garnier V., Breyse D., Moysan J. (2009) Possibilistic data fusion for evaluating concrete structures, *NDTCE'09*, Nantes, 30/6-3/7 2009.
- Saisi A., Valle S., Zanzi L., Binda L. (2001) Radar and sonic as complementary and/or alternative tests in the survey of structures, *Arch 2000*, UNESCO Icomos conf. 10-12 sept. 2001.
- Sbartai Z.M., Laurens S., Balayssac J.P., Ballivy G., Arliguie G. (2006) Effect of concrete moisture on radar signal amplitude, *ACI Mat. J.*, 419-426, nov-dec. 2006.
- Sbartai Z.M., Laurens S., Viriyametanont K., Balayssac J.P., Arliguie G. (2009) Non-destructive evaluation of concrete physical conditions using radar and artificial neural networks, *Constr. Building materials*, 23, 837–845
- Shafer G. (1976) *A mathematical theory of evidence*, Chichester, Princeton Univ. Press, 297 p.

- Sirieix C., Lataste J.F., Breysse D., Naar S., Dérobert X. (2007) Comparison of nondestructive testing: Infrared thermography, electrical resistivity and capacity methods for assessing a reinforced concrete structure, *J. Building Appraisal* 3, 1, 77–88.
- Soltani F., Lafhaj Z., Goueygou M. (2009) Experimental determination of the relationship between porosity and surface wave parameters of fully and partially saturated cement paste, NDT-CE, Non-destructive testing in Civil Engineering, Nantes, 30 june-3 july 2009.
- Streicher D., Algernon D., Wöstmann J., Behrens M., Wiggenhauser H. (2006) Automated NDE of post-tensioned concrete bridges using imaging echo methods, NDT-CE Berlin.

# RILEM Publications

The following list is presenting our global offer, sorted by series.

## RILEM PROCEEDINGS

**PRO 1:** Durability of High Performance Concrete (1994) 266 pp., ISBN: 2-91214-303-9; e-ISBN: 2-35158-012-5; *Ed. H. Sommer*

**PRO 2:** Chloride Penetration into Concrete (1995) 496 pp., ISBN: 2-912143-00-4; e-ISBN: 2-912143-45-4; *Eds. L.-O. Nilsson and J.-P. Ollivier*

**PRO 3:** Evaluation and Strengthening of Existing Masonry Structures (1995) 234 pp., ISBN: 2-912143-02-0; e-ISBN: 2-351580-14-1; *Eds. L. Binda and C. Modena*

**PRO 4:** Concrete: From Material to Structure (1996) 360 pp., ISBN: 2-912143-04-7; e-ISBN: 2-35158-020-6; *Eds. J.-P. Bournazel and Y. Malier*

**PRO 5:** The Role of Admixtures in High Performance Concrete (1999) 520 pp., ISBN: 2-912143-05-5; e-ISBN: 2-35158-021-4; *Eds. J. G. Cabrera and R. Rivera-Villarreal*

**PRO 6:** High Performance Fiber Reinforced Cement Composites (HPFRCC 3) (1999) 686 pp., ISBN: 2-912143-06-3; e-ISBN: 2-35158-022-2; *Eds. H. W. Reinhardt and A. E. Naaman*

**PRO 7:** 1st International RILEM Symposium on Self-Compacting Concrete (1999) 804 pp., ISBN: 2-912143-09-8; e-ISBN: 2-912143-72-1; *Eds. Å. Skarendahl and Ö. Petersson*

**PRO 8:** International RILEM Symposium on Timber Engineering (1999) 860 pp., ISBN: 2-912143-10-1; e-ISBN: 2-35158-023-0; *Ed. L. Boström*

**PRO 9:** 2nd International RILEM Symposium on Adhesion between Polymers and Concrete ISAP '99 (1999) 600 pp., ISBN: 2-912143-11-X; e-ISBN: 2-35158-024-9; Eds. *Y. Ohama and M. Puterman*

**PRO 10:** 3rd International RILEM Symposium on Durability of Building and Construction Sealants (2000) 360 pp., ISBN: 2-912143-13-6; e-ISBN: 2-351580-25-7; Eds. *A. T. Wolf*

**PRO 11:** 4th International RILEM Conference on Reflective Cracking in Pavements (2000) 549 pp., ISBN: 2-912143-14-4; e-ISBN: 2-35158-026-5; Eds. *A. O. Abd El Halim, D. A. Taylor and El H. H. Mohamed*

**PRO 12:** International RILEM Workshop on Historic Mortars: Characteristics and Tests (1999) 460 pp., ISBN: 2-912143-15-2; e-ISBN: 2-351580-27-3; Eds. *P. Bartos, C. Groot and J. J. Hughes*

**PRO 13:** 2nd International RILEM Symposium on Hydration and Setting (1997) 438 pp., ISBN: 2-912143-16-0; e-ISBN: 2-35158-028-1; Ed. *A. Nonat*

**PRO 14:** Integrated Life-Cycle Design of Materials and Structures (ILCDES 2000) (2000) 550 pp., ISBN: 951-758-408-3; e-ISBN: 2-351580-29-X, ISSN: 0356-9403; Ed. *S. Sarja*

**PRO 15:** Fifth RILEM Symposium on Fibre-Reinforced Concretes (FRC) – BEFIB'2000 (2000) 810 pp., ISBN: 2-912143-18-7; e-ISBN: 2-912143-73-X; Eds. *P. Rossi and G. Chanvillard*

**PRO 16:** Life Prediction and Management of Concrete Structures (2000) 242 pp., ISBN: 2-912143-19-5; e-ISBN: 2-351580-30-3; Ed. *D. Naus*

**PRO 17:** Shrinkage of Concrete – Shrinkage 2000 (2000) 586 pp., ISBN: 2-912143-20-9; e-ISBN: 2-351580-31-1; Eds. *V. Baroghel-Bouny and P.-C. Aïtcin*

**PRO 18:** Measurement and Interpretation of the On-Site Corrosion Rate (1999) 238 pp., ISBN: 2-912143-21-7; e-ISBN: 2-351580-32-X; Eds. *C. Andrade, C. Alonso, J. Fullea, J. Polimon and J. Rodriguez*

**PRO 19:** Testing and Modelling the Chloride Ingress into Concrete (2000) 516 pp., ISBN: 2-912143-22-5; e-ISBN: 2-351580-33-8; Soft cover, Eds. *C. Andrade and J. Kropp*

**PRO 20:** 1st International RILEM Workshop on Microbial Impacts on Building Materials (2000) 74 pp., e-ISBN: 2-35158-013-3; Ed. *M. Ribas Silva (CD 02)*

**PRO 21:** International RILEM Symposium on Connections between Steel and Concrete (2001) 1448 pp., ISBN: 2-912143-25-X; e-ISBN: 2-351580-34-6; Ed. *R. Eligehausen*

**PRO 22:** International RILEM Symposium on Joints in Timber Structures (2001) 672 pp., ISBN: 2-912143-28-4; e-ISBN: 2-351580-35-4; Eds. *S. Aicher and H.-W. Reinhardt*

**PRO 23:** International RILEM Conference on Early Age Cracking in Cementitious Systems (2003) 398 pp., ISBN: 2-912143-29-2; e-ISBN: 2-351580-36-2; Eds. *K. Kovler and A. Bentur*

**PRO 24:** 2nd International RILEM Workshop on Frost Resistance of Concrete (2002) 400 pp., ISBN: 2-912143-30-6; e-ISBN: 2-351580-37-0, Hard back; Eds. *M. J. Setzer, R. Auberg and H.-J. Keck*

**PRO 25:** International RILEM Workshop on Frost Damage in Concrete (1999) 312 pp., ISBN: 2-912143-31-4; e-ISBN: 2-351580-38-9, Soft cover; Eds. *D. J. Janssen, M. J. Setzer and M. B. Snyder*

**PRO 26:** International RILEM Workshop on On-Site Control and Evaluation of Masonry Structures (2003) 386 pp., ISBN: 2-912143-34-9; e-ISBN: 2-351580-14-1, Soft cover; Eds. *L. Binda and R. C. de Vekey*

**PRO 27:** International RILEM Symposium on Building Joint Sealants (1988) 240 pp., e-ISBN: 2-351580-15-X; Ed. *A. T. Wolf*, (CD03)

**PRO 28:** 6th International RILEM Symposium on Performance Testing and Evaluation of Bituminous Materials, PTEBM'03, Zurich, Switzerland (2003) 652 pp., ISBN: 2-912143-35-7; e-ISBN: 2-912143-77-2, Soft cover; Ed. *M. N. Partl* (CD06)

**PRO 29:** 2nd International RILEM Workshop on Life Prediction and Ageing Management of Concrete Structures, Paris, France (2003) 402 pp., ISBN: 2-912143-36-5; e-ISBN: 2-912143-78-0, Soft cover; Ed. *D. J. Naus*

**PRO 30:** 4th International RILEM Workshop on High Performance Fiber Reinforced Cement Composites – HPRFCC 4, University of Michigan, Ann Arbor, USA (2003) 562 pp., ISBN: 2-912143-37-3; e-ISBN: 2-912143-79-9, Hard back; Eds. *A. E. Naaman and H. W. Reinhardt*

**PRO 31:** International RILEM Workshop on Test and Design Methods for Steel Fibre Reinforced Concrete: Background and Experiences (2003) 230 pp., ISBN: 2-912143-38-1; e-ISBN: 2-351580-16-8, Soft cover; Eds. *B. Schnütgen and L. Vandewalle*

**PRO 32:** International Conference on Advances in Concrete and Structures, 2 volumes (2003) 1592 pp., ISBN (set): 2-912143-41-1; e-ISBN: 2-351580-17-6, Soft cover; Eds. *Ying-shu Yuan, Surendra P. Shah and Heng-lin Lü*

**PRO 33:** 3rd International Symposium on Self-Compacting Concrete (2003) 1048 pp., ISBN: 2-912143-42-X; e-ISBN: 2-912143-71-3, Soft cover; Eds. *Ó. Wallevik and I. Nielsson*

**PRO 34:** International RILEM Conference on Microbial Impact on Building Materials (2003) 108 pp., ISBN: 2-912143-43-8; e-ISBN: 2-351580-18-4; Ed. *M. Ribas Silva*

**PRO 35:** International RILEM TC 186-ISA on Internal Sulfate Attack and Delayed Ettringite Formation (2002) 316 pp., ISBN: 2-912143-44-6; e-ISBN: 2-912143-80-2, Soft cover; Eds. *K. Scrivener and J. Skalny*

**PRO 36:** International RILEM Symposium on Concrete Science and Engineering – A Tribute to Arnon Bentur (2004) 264 pp., ISBN: 2-912143-46-2; e-ISBN: 2-912143-58-6, Hard back; Eds. *K. Kovler, J. Marchand, S. Mindess and J. Weiss*

**PRO 37:** 5th International RILEM Conference on Cracking in Pavements – Mitigation, Risk Assessment and Prevention (2004) 740 pp., ISBN: 2-912143-47-0; e-ISBN: 2-912143-76-4, Hard back; Eds. *C. Petit, I. Al-Qadi and A. Millien*

**PRO 38:** 3rd International RILEM Workshop on Testing and Modelling the Chloride Ingress into Concrete (2002) 462 pp., ISBN: 2-912143-48-9; e-ISBN: 2-912143-57-8, Soft cover; Eds. *C. Andrade and J. Kropp*

**PRO 39:** 6th International RILEM Symposium on Fibre-Reinforced Concretes (BEFIB 2004), 2 volumes, (2004) 1536 pp., ISBN: 2-912143-51-9 (set); e-ISBN: 2-912143-74-8, Hard back; Eds. *M. Di Prisco, R. Felicetti and G. A. Plizzari*

**PRO 40:** International RILEM Conference on the Use of Recycled Materials in Buildings and Structures (2004) 1154 pp., ISBN: 2-912143-52-7 (set); e-ISBN: 2-912143-75-6, Soft cover; Eds. *E. Vázquez, Ch. F. Hendriks and G. M. T. Janssen*

**PRO 41:** RILEM International Symposium on Environment-Conscious Materials and Systems for Sustainable Development (2005) 450 pp., ISBN: 2-912143-55-1; e-ISBN: 2-912143-64-0, Soft cover; Eds. *N. Kashino and Y. Ohama*

**PRO 42:** SCC'2005 – China: 1st International Symposium on Design, Performance and Use of Self-Consolidating Concrete (2005) 726 pp., ISBN: 2-912143-61-6; e-ISBN: 2-912143-62-4, Hard back; Eds. *Zhiwu Yu, Caijun Shi, Kamal Henri Khayat and Youjun Xie*

**PRO 43:** International RILEM Workshop on Bonded Concrete Overlays (2004) 114 pp., e-ISBN: 2-912143-83-7; Eds. *J. L. Granju and J. Silfwerbrand*

**PRO 44:** 2nd International RILEM Workshop on Microbial Impacts on Building Materials (Brazil 2004) (CD11) 90 pp., e-ISBN: 2-912143-84-5; Ed. *M. Ribas Silva*

**PRO 45:** 2nd International Symposium on Nanotechnology in Construction, Bilbao, Spain (2005) 414 pp., ISBN: 2-912143-87-X; e-ISBN: 2-912143-88-8, Soft cover; Eds. *Peter J. M. Bartos, Yolanda de Miguel and Antonio Porro*

**PRO 46:** ConcreteLife'06 – International RILEM-JCI Seminar on Concrete Durability and Service Life Planning: Curing, Crack Control, Performance in Harsh Environments (2006) 526 pp., ISBN: 2-912143-89-6; e-ISBN: 2-912143-90-X, Hard back; Ed. *K. Kovler*



**PRO 47:** International RILEM Workshop on Performance Based Evaluation and Indicators for Concrete Durability (2007) 385 pp., ISBN: 978-2-912143-95-2; e-ISBN: 978-2-912143-96-9, Soft cover; Eds. *V. Baroghel-Bouny, C. Andrade, R. Torrent and K. Scrivener*

**PRO 48:** 1st International RILEM Symposium on Advances in Concrete through Science and Engineering (2004) 1616 pp., e-ISBN: 2-912143-92-6; Eds. *J. Weiss, K. Kovler, J. Marchand, and S. Mindess*

**PRO 49:** International RILEM Workshop on High Performance Fiber Reinforced Cementitious Composites in Structural Applications (2006) 598 pp., ISBN: 2-912143-93-4; e-ISBN: 2-912143-94-2, Soft cover; Eds. *G. Fischer and V.C. Li*

**PRO 50:** 1<sup>st</sup> International RILEM Symposium on Textile Reinforced Concrete (2006) 418 pp., ISBN: 2-912143-97-7; e-ISBN: 2-351580-08-7, Soft cover; Eds. *Josef Hegger, Wolfgang Brameshuber and Norbert Will*

**PRO 51:** 2<sup>nd</sup> International Symposium on Advances in Concrete through Science and Engineering (2006) 462 pp., ISBN: 2-35158-003-6; e-ISBN: 2-35158-002-8, Hard back; Eds. *J. Marchand, B. Bissonnette, R. Gagné, M. Jolin and F. Paradis*

**PRO 52:** Volume Changes of Hardening Concrete: Testing and Mitigation (2006) 428 pp., ISBN: 2-35158-004-4; e-ISBN: 2-35158-005-2, Soft cover; Eds. *O. M. Jensen, P. Lura and K. Kovler*

**PRO 53:** High Performance Fiber Reinforced Cement Composites HPRCC5 (2007) 542 pp., ISBN: 978-2-35158-046-2; e-ISBN: 978-2-35158-089-9, Hard back; Eds. *H. W. Reinhardt and A. E. Naaman*

**PRO 54:** 5<sup>th</sup> International RILEM Symposium on Self-Compacting Concrete, 3 Volumes (2007) 1198 pp., ISBN: 978-2-35158-047-9; e-ISBN: 978-2-35158-088-2, Soft cover; Eds. *G. De Schutter and V. Boel*

**PRO 55:** International RILEM Symposium Photocatalysis, Environment and Construction Materials (2007) 350 pp., ISBN: 978-2-35158-056-1; e-ISBN: 978-2-35158-057-8, Soft cover; Eds. *P. Baglioni and L. Cassar*

**PRO56:** International RILEM Workshop on Integral Service Life Modelling of Concrete Structures (2007) 458 pp., ISBN 978-2-35158-058-5; e-ISBN: 978-2-35158-090-5, Hard back; Eds. *R. M. Ferreira, J. Gulikers and C. Andrade*

**PRO57:** RILEM Workshop on Performance of cement-based materials in aggressive aqueous environments (2008) 132 pp., e-ISBN: 978-2-35158-059-2; Ed. *N. De Belie*

**PRO58:** International RILEM Symposium on Concrete Modelling CONMOD'08 (2008) 847 pp., ISBN: 978-2-35158-060-8; e-ISBN: 978-2-35158-076-9, Soft cover; Eds. *E. Schlangen and G. De Schutter*

**PRO 59:** International RILEM Conference on On Site Assessment of Concrete, Masonry and Timber Structures SACoMaTiS 2008, 2 volumes (2008) 1232 pp., ISBN: 978-2-35158-061-5 (set); e-ISBN: 978-2-35158-075-2, Hard back; Eds. *L. Binda, M. di Prisco and R. Felicetti*

**PRO 60:** Seventh RILEM International Symposium (BEFIB 2008) on Fibre Reinforced Concrete: Design and Applications (2008) 1181 pp, ISBN: 978-2-35158-064-6; e-ISBN: 978-2-35158-086-8, Hard back; Ed. *R. Gettu*

**PRO 61:** 1<sup>st</sup> International Conference on Microstructure Related Durability of Cementitious Composites (Nanjing), 2 volumes, (2008) 1524 pp., ISBN: 978-2-35158-065-3; e-ISBN: 978-2-35158-084-4; Eds. *W. Sun, K. van Breugel, C. Miao, G. Ye and H. Chen*

**PRO 62:** NSF/RILEM Workshop: In-situ Evaluation of Historic Wood and Masonry Structures (2008) 130 pp., e-ISBN: 978-2-35158-068-4; Eds. *B. Kasal, R. Anthony and M. Drdácký*

**PRO 63:** Concrete in Aggressive Aqueous Environments: Performance, Testing and Modelling, 2 volumes, (2009) 631 pp., ISBN: 978-2-35158-071-4; e-ISBN: 978-2-35158-082-0, Soft cover; Eds. *M. G. Alexander and A. Bertron*

**PRO 64:** Long Term Performance of Cementitious Barriers and Reinforced Concrete in Nuclear Power Plants and Waste Management – NUCPERF 2009 (2009) 359 pp., ISBN: 978-2-35158-072-1; e-ISBN: 978-2-35158-087-5; Eds. *V. L'Hostis, R. Gens, C. Gallé*

**PRO 65:** Design Performance and Use of Self-consolidating Concrete, SCC'2009, (2009) 913 pp., ISBN: 978-2-35158-073-8; e-ISBN: 978-2-35158-093-6; Eds. *C. Shi, Z. Yu, K. H. Khayat and P. Yan*

**PRO 66:** Concrete Durability and Service Life Planning, 2<sup>nd</sup> International RILEM Workshop, ConcreteLife'09, (2009) 626 pp., ISBN: 978-2-35158-074-5; e-ISBN: 978-2-35158-085-1; Ed. *K. Kovler*

**PRO 67:** Repairs Mortars for Historic Masonry (2009) 397 pp., e-ISBN: 978-2-35158-083-7; Ed. *C. Groot*

**PRO 68:** Proceedings of the 3<sup>rd</sup> International RILEM Symposium on 'Rheology of Cement Suspensions such as Fresh Concrete' (2009) 372 pp., ISBN: 978-2-35158-091-2; e-ISBN: 978-2-35158-092-9; Eds. *O. H. Wallevik, S. Kubens and S. Oesterheld*

**PRO 69:** 3<sup>rd</sup> International PhD Student Workshop on 'Modelling the Durability of Reinforced Concrete' (2009) 122 pp., ISBN: 978-2-35158-095-0; e-ISBN: 978-2-35158-094-3; Eds. *R. M. Ferreira, J. Gulikers and C. Andrade*

**PRO 71:** Advances in Civil Engineering Materials, Proceedings of the 'The 50-year Teaching Anniversary of Prof. Sun Wei', (2010) 307 pp., ISBN: 978-2-35158-098-1; e-ISBN: 978-2-35158-099-8; Eds. *C. Miao, G. Ye, and H. Chen*

**PRO74:** International RILEM Conference on ‘Use of Superabsorbent Polymers and Other New Additives in Concrete’ (2010) 374 pp., ISBN: 978-2-35158-104-9; e-ISBN: 978-2-35158-105-6; Eds. *O.M. Jensen, M.T. Hasholt, and S. Laustsen*

**PRO75:** International Conference on ‘Material Science - 2<sup>nd</sup> ICTRC - Textile Reinforced Concrete - Theme 1’ (2010) 436 pp., ISBN: 978-2-35158-106-3; e-ISBN: 978-2-35158-107-0; Ed. *W. Brameshuber*

**PRO76:** International Conference on ‘Material Science - HetMat - Modelling of Heterogeneous Materials - Theme 2’ (2010) 255 pp., ISBN: 978-2-35158-108-7; e-ISBN: 978-2-35158-109-4; Ed. *W. Brameshuber*

**PRO77:** International Conference on ‘Material Science - AdIPoC - Additions Improving Properties of Concrete - Theme 3’ (2010) 459 pp., ISBN: 978-2-35158-110-0; e-ISBN: 978-2-35158-111-7; Ed. *W. Brameshuber*

**PRO78:** 2<sup>nd</sup> Historic Mortars Conference and RILEM TC 203-RHM Final Workshop – HMC2010 (2010) 1416 pp., e-ISBN: 978-2-35158-112-4; Eds. *J. Válek, C. Groot, and J. J. Hughes*

**PRO79:** International RILEM Conference on Advances in Construction Materials Through Science and Engineering (2011) 213 pp., e-ISBN: 978-2-35158-117-9; Eds. *Christopher Leung and K.T. Wan*

**PRO80:** 2<sup>nd</sup> International RILEM Conference on Concrete Spalling due to Fire Exposure (2011) 453 pp., ISBN: 978-2-35158-118-6, e-ISBN: 978-2-35158-119-3; Eds. *E.A.B. Koenders and F. Dehn*

## RILEM REPORTS

**Report 19:** Considerations for Use in Managing the Aging of Nuclear Power Plant Concrete Structures (1999) 224 pp., ISBN: 2-912143-07-1; e-ISBN: 2-35158-039-7; Ed. *D. J. Naus*

**Report 20:** Engineering and Transport Properties of the Interfacial Transition Zone in Cementitious Composites (1999) 396 pp., ISBN: 2-912143-08-X; e-ISBN: 2-35158-040-0; Eds. *M. G. Alexander, G. Arliguie, G. Ballivy, A. Bentur and J. Marchand*

Report 21: Durability of Building Sealants (1999) 450 pp., ISBN: 2-912143-12-8; e-ISBN: 2-35158-041-9; Ed. *A. T. Wolf*

**Report 22:** Sustainable Raw Materials – Construction and Demolition Waste (2000) 202 pp., ISBN: 2-912143-17-9; e-ISBN: 2-35158-042-7; Eds. *C. F. Hendriks and H. S. Pietersen*

**Report 23:** Self-Compacting Concrete state-of-the-art report (2001) 166 pp., ISBN: 2-912143-23-3; e-ISBN: 2-912143-59-4, Soft cover; Eds. *Å. Skarendahl and Ö. Petersson*

**Report 24:** Workability and Rheology of Fresh Concrete: Compendium of Tests (2002) 154 pp., ISBN: 2-912143-32-2; e-ISBN: 2-35158-043-5, Soft cover; *Eds. P. J. M. Bartos, M. Sonebi and A. K. Tamimi*

**Report 25:** Early Age Cracking in Cementitious Systems (2003) 350 pp., ISBN: 2-912143-33-0; e-ISBN: 2-912143-63-2, Soft cover; *Ed. A. Bentur*

**Report 26:** Towards Sustainable Roofing (Joint Committee CIB/RILEM) (CD 07), (2001) 28 pp., e-ISBN: 2-912143-65-9; *Eds. Thomas W. Hutchinson and Keith Roberts*

**Report 27:** Condition Assessment of Roofs (Joint Committee CIB/RILEM) (CD 08), (2003) 12 pp., e-ISBN: 2-912143-66-7

Report 28: Final report of RILEM TC 167-COM 'Characterisation of Old Mortars with Respect to Their Repair' (2007) 192 pp., ISBN: 978-2-912143-56-3; e-ISBN: 978-2-912143-67-9, Soft cover; *Eds. C. Groot, G. Ashall and J. Hughes*

**Report 29:** Pavement Performance Prediction and Evaluation (PPPE): Interlaboratory Tests (2005) 194 pp., e-ISBN: 2-912143-68-3; *Eds. M. Partl and H. Piber*

**Report 30:** Final Report of RILEM TC 198-URM 'Use of Recycled Materials' (2005) 74 pp., ISBN: 2-912143-82-9; e-ISBN: 2-912143-69-1 – Soft cover; *Eds. Ch. F. Hendriks, G. M. T. Janssen and E. Vázquez*

**Report 31:** Final Report of RILEM TC 185-ATC 'Advanced testing of cement-based materials during setting and hardening' (2005) 362 pp., ISBN: 2-912143-81-0; e-ISBN: 2-912143-70-5 – Soft cover; *Eds. H. W. Reinhardt and C. U. Grosse*

**Report 32:** Probabilistic Assessment of Existing Structures. A JCSS publication (2001) 176 pp., ISBN 2-912143-24-1; e-ISBN: 2-912143-60-8 – Hard back; *Ed. D. Diamantidis*

**Report 33:** State-of-the-Art Report of RILEM Technical Committee TC 184-IFE 'Industrial Floors' (2006) 158 pp., ISBN 2-35158-006-0; e-ISBN: 2-35158-007-9, Soft cover; *Ed. P. Seidler*

**Report 34:** Report of RILEM Technical Committee TC 147-FMB 'Fracture mechanics applications to anchorage and bond' Tension of Reinforced Concrete Prisms – Round Robin Analysis and Tests on Bond (2001) 248 pp., e-ISBN 2-912143-91-8; *Eds. L. Elfgren and K. Noghabai*

**Report 35:** Final Report of RILEM Technical Committee TC 188-CSC 'Casting of Self Compacting Concrete' (2006) 40 pp., ISBN 2-35158-001-X; e-ISBN: 2-912143-98-5 – Soft cover; *Eds. Å. Skarendahl and P. Billberg*

**Report 36:** State-of-the-Art Report of RILEM Technical Committee TC 201-TRC 'Textile Reinforced Concrete' (2006) 292 pp., ISBN 2-912143-99-3; e-ISBN: 2-35158-000-1, Soft cover; *Ed. W. Brameshuber*

**Report 37:** State-of-the-Art Report of RILEM Technical Committee TC 192-ECM 'Environment-conscious construction materials and systems' (2007) 88 pp., ISBN: 978-2-35158-053-0; e-ISBN: 2-35158-079-0, Soft cover; Eds. N. Kashino, D. Van Gemert and K. Imamoto

**Report 38:** State-of-the-Art Report of RILEM Technical Committee TC 205-DSC 'Durability of Self-Compacting Concrete' (2007) 204 pp., ISBN: 978-2-35158-048-6; e-ISBN: 2-35158-077-6, Soft cover; Eds. G. De Schutter and K. Audenaert

**Report 39:** Final Report of RILEM Technical Committee TC 187-SOC 'Experimental determination of the stress-crack opening curve for concrete in tension' (2007) 54 pp., ISBN 978-2-35158-049-3; e-ISBN: 978-2-35158-078-3, Soft cover; *Ed. J. Planas*

**Report 40:** State-of-the-Art Report of RILEM Technical Committee TC 189-NEC 'Non-Destructive Evaluation of the Penetrability and Thickness of the Concrete Cover' (2007) 246 pp., ISBN 978-2-35158-054-7; e-ISBN: 978-2-35158-080-6, Soft cover; *Eds. R. Torrent and L. Fernández Luco*

**Report 41:** State-of-the-Art Report of RILEM Technical Committee TC 196-ICC 'Internal Curing of Concrete' (2007) 164 pp., ISBN: 978-2-35158-009-7; e-ISBN: 978-2-35158-082-0, Soft cover; *Eds. K. Kovler and O. M. Jensen*

**Report 42:** 'Acoustic Emission and Related Non-destructive Evaluation Techniques for Crack Detection and Damage Evaluation in Concrete' – Final Report of RILEM Technical Committee 212-ACD (2010) 12 pp., e-ISBN: 978-2-35158-100-1; *Ed. M. Ohtsu*

# RILEM Publications published by Springer

## RILEM BOOKSERIES (Proceedings)

**VOL. 1:** Design, Production and Placement of Self-Consolidating Concrete (2010) 466 pp., ISBN: 978-90-481-9663-0; e-ISBN: 978-90-481-9664-7, Hardcover; Ed. *K. Khayat and D. Feyes*

**VOL. 2:** High Performance Fiber Reinforced Cement Composites 6 – HPRCC6 (2011) 584 pp., ISBN: 978-94-007-2435-8; e-ISBN: 978-94-007-2436-5, Hardcover; Ed. *G.J. Parra-Montesinos, H.W. Reinhardt and A.E. Naaman*

**VOL. 5:** Joint fib-RILEM Workshop on Modelling of Corroding Concrete Structures (2011) 290 pp., ISBN: 978-94-007-0676-7; e-ISBN: 978-94-007-0677-4, Hardcover; Ed. *C. Andrade and G. Mancini*

**For the latest publications in the RILEM Bookseries, please visit**  
<http://www.springer.com/series/8781>

## RILEM STATE-OF-THE-ART REPORTS

**VOL. 3:** State-of-the-Art Report of RILEM Technical Committee TC 193-RLS ‘Bonded Cement-Based Material Overlays for the Repair, the Lining or the Strengthening of Slabs or Pavements’ (2011) 198 pp., ISBN: 978-94-007-1238-6; e-ISBN: 978-94-007-1239-3, Hardcover; Ed. *B. Bissonnette, L. Courard, D.W. Fowler and J-L. Granju*

**VOL. 4:** State-of-the-Art Report prepared by Subcommittee 2 of RILEM Technical Committee TC 208-HFC ‘Durability of Strain-Hardening Fibre-Reinforced Cement-Based Composites’ (SHCC) (2011) 151 pp., ISBN: 978-94-007-0337-7; e-ISBN: 978-94-007-0338-4, Hardcover; Ed. *G.P.A.G. van Zijl and F.H. Wittmann*

**VOL. 5:** State-of-the-Art Report of RILEM Technical Committee TC 194-TDP 'Application of Titanium Dioxide Photocatalysis to Construction Materials' (2011) 60 pp., ISBN: 978-94-007-1296-6; e-ISBN: 978-94-007-1297-3, Hardcover; Ed. *Yoshihiko Ohama and Dionys Van Gemert*

**VOL. 7:** State-of-the-Art Report of RILEM Technical Committee TC 215-AST 'In Situ Assessment of Structural Timber' (2010) 152 pp., ISBN: 978-94-007-0559-3; e-ISBN: 978-94-007-0560-9, Hardcover; Ed. *B. Kasal and T. Tannert*

**For the latest publications in the RILEM State-of-the-Art Reports, please visit**  
<http://www.springer.com/series/8780>

# Index

## A

- Acoustic
  - emission, 58–63, 307, 309, 317–320, 326–328, 330–332
  - event, 62, 317
  - impedance, 27, 28, 45, 189, 279, 280
  - tomography, 210–212
- Active thermography, 92–97, 236, 297–298
- Antenna (radar), 5, 6, 9–13, 32, 33, 47, 63–70, 170–173, 178–180, 188–190, 192, 196, 198–201, 206, 234, 235, 243–246, 250, 251, 253–255, 259, 264, 265, 272, 287, 295–298, 300, 309, 312, 317, 320, 327, 328, 337, 344, 345, 348, 350
- Archie's law, 77–78
- Artificial defects (failure), 318, 319
- A-scan, 22, 29, 31, 32, 196, 281
- Asphalt concrete, 228, 253
- Attenuation of elastic waves, 18

## B

- Basic curve, 107, 150–154
- Bridge deck, 5, 6, 48, 52, 56, 67, 70, 97, 144, 187, 188, 192, 196, 228, 235, 239, 242–244, 251, 253, 277, 312, 316
- Bridge girder, 50, 295
- B-scan, 22, 32–34, 37, 47, 272, 274, 276, 277, 280, 282, 284, 286, 287, 289, 290, 292, 299
- Burst, 61, 62

## C

- Calibration
  - on cores, 35, 148, 154, 164
  - curve, 75, 95, 106, 107, 109, 113, 115, 116, 126, 143, 150, 167, 168, 170, 171, 245, 336
- Carbonation, 105–107, 109, 130, 162, 166, 170, 178, 231, 344, 354
- Chain drag, 236, 242, 243, 248, 249, 253, 259
- Characteristic strength assessment, 148–156
- Combination, 1–14, 34, 71, 84, 110, 123, 124, 130, 131, 156, 158, 160, 161, 166–172, 181, 187, 192, 210, 213, 214, 216, 232, 234, 250, 252, 253, 257, 259, 309, 312, 317, 320, 326–332, 335–356
- Concrete strength, 2, 9, 12, 18, 22, 104, 107, 110, 112, 114, 117, 119–182, 271, 336, 340, 353
- Conversion curve, 105–107, 130, 156–172, 175, 179, 181, 340
- Correlation, 11, 18–20, 22, 106, 107, 109, 115–117, 122–124, 128–140, 143–148, 150, 152–166, 168–171, 180, 255, 316, 338
- curve, 109, 116, 143
- Corrosion
  - activity, 2, 80, 326, 328, 338
  - potential, 320
  - rate, 80, 321–324
- Coupling (of transducers), 18, 21, 30, 38, 285
- Cover (determination), 69, 248, 277
- Crack detection, 25, 62, 232
- Cross-hole sonic logging (CSL), 206, 210–212, 222, 223
- C-scan, 21, 32–34, 37, 274, 277, 290–292, 299



**D**

- Damage detection, 3, 25, 83, 338
- Data fusion, 120, 171–182, 213, 350–353, 356
- Debonding, 48, 52, 55, 227–229, 233, 235–238, 240, 241, 253, 258, 259
- Deep foundations, 22, 191–192, 206–213, 215–216, 223
- Defect detection, 2, 5, 237, 354
- Delamination, 2, 3, 5, 6, 13, 14, 22, 26, 40, 45, 52, 54–56, 89, 91, 92, 97, 227–259, 280, 335, 353
- Dielectric permittivity, 64, 325
- Direct transmission, 22–24, 222
- Dispersion curve, 42, 214, 241, 242, 249
- Dynamic
  - modulus, 21
  - stiffness, 54, 57, 240

**E**

- Elastic waves, 17, 18, 34, 58, 60, 263, 271, 299
- Electrical impedance, 81
- Electrical impedance spectroscopy (EIS), 81, 84
- Electrical resistivity, 5–10, 12, 77–84, 146, 170, 178, 230, 232, 233, 246–247, 251, 252, 337, 338, 341, 344–346
- Electrochemical measurements, 80, 322
- Electrodes, 71–76, 79, 81, 247, 320, 321
- Electromagnetic resonance, 308, 309, 324–325
- Electromagnetic waves, 64, 65, 198, 243, 265, 295, 298, 325
- Emissivity, 85–88, 95
- Environment (influence of the), 83, 338, 339, 342, 346

**F**

- Fast Fourier Transform (FFT), 44, 51, 93, 95, 208, 268, 283, 315, 316
- Fire damage, 228
- Freeze-thaw, 228, 241
- Frequency
  - of waves, acoustics, 39
  - of waves, radar, 11, 171, 179, 243

**G**

- Gammagraphy, 266, 267
- Gamma-ray, 98, 101

- Ground penetrating radar (GPR), 47, 63–70, 188–192, 196–201, 206, 213, 214, 218, 235, 243–246, 250, 251, 253, 259, 272, 296–297, 309, 346
- Group velocity, 41, 249, 272, 344
- Grouting faults, 263–300

**H**

- Hammer sounding, 242–243
- Hardness, 101, 102, 104, 108, 109, 120, 124, 125, 131, 147, 148
- Honeycombing, 2, 5, 40, 48, 52, 55, 154, 190, 272, 295
- Humidity (evaluation), 3, 69, 83, 87, 129, 336, 337, 339, 342, 346

**I**

- Impact
  - echo imaging, 271–278, 299
  - echo scanning, 239, 269, 276
  - hammer, 236, 241
- Impulse
  - response, 5, 51–57, 206, 208, 239–241, 249
  - thermography, 92–95, 248, 250, 252, 257, 259
- Indirect transmission, 23, 24
- Infrared camera, 86, 88, 92–94
- Infrared thermography, 5, 6, 12–14, 85–97, 171, 178, 230, 232, 235, 248, 250–253, 256, 259
- Interface, 27–29, 40, 44, 45, 48, 49, 60, 65, 78, 81, 90, 100, 105, 140, 141, 144, 192, 200, 218, 227–259, 270, 279, 285
- Interpretation (of measurements), 2, 57, 77, 83, 189, 234

**L**

- Lok test, 132, 134, 137, 138, 150
- Longitudinal waves, 18, 27, 208, 271, 279

**M**

- Magnetic
  - methods, 197, 309, 312–326, 328
  - susceptibility, 64
- Magnetic flux leakage (MFL), 313, 316
- Maxwell's equations, 64

## Measurement

error, 154–156, 159, 161–166, 169, 337, 342, 343

noise, 164, 234, 342–343, 354

Mechanical admittance, 208, 209

Mobility curve, 52, 54, 55, 209

Moisture content, 3, 5, 8–10, 71, 72, 75, 156, 158, 160, 161, 198, 201, 245

Multi-channel analysis of surface waves (MASW), 42, 214, 242

Multivariate analysis, 120, 156–171, 178, 182

## N

Nielsen source, 59

Nomogram, 157, 158

## P

Parallel seismic testing, 215–216

Passive thermography, 89–92, 236, 248

Pavement thickness, 188, 192–196

Penetration depth, 72, 74, 75, 90, 98, 265, 298, 300

Penetration resistance, 120, 124–125, 130, 131, 147, 148, 158

Phase velocity, 27, 28, 41, 42, 214

Pile echo testing (PET), 206–210, 223

Pile integrity technique (PIT), 206

Pile length estimation, 207

Piles, 22, 51, 187–225, 240, 254, 324

PIT. *See* Pile integrity technique

Planck's law, 85

Polarization resistance, 77, 321

Porosity, 3, 8, 9, 19, 22, 26, 78, 82–84, 146, 172, 178–180, 251, 320, 337–339, 341, 344–346, 351–355

assessment, 345–346

Possibility distribution, 172–177, 179, 180, 351, 352

Post-tension, 48, 73, 98, 121, 239, 263, 264, 268, 280, 287, 297, 305, 306, 311, 321, 323–324, 327–329, 332

Post-tensioned bridge, 287, 305

Pressure waves, 18, 27, 39, 270, 279, 283, 285, 287, 294

Prestressing cables, 305–332

Pull-off test, 120, 124, 128–130, 139–144

Pull-out test, 110–117, 120, 123–128, 130–140, 148, 158, 169–171

Pulse echo, 5, 17, 27, 34, 47, 236, 237, 248, 249, 258, 272, 281, 285

Pulse phase thermography, 92, 93, 95–96

P-waves, 18, 22, 27, 29, 39, 40, 44, 346

## Q

Quality of assessment, 2, 181, 353–356

## R

Radiation, 85–87, 92, 93, 98, 101, 264–268, 298, 310, 311

Radiography, 98–101, 264–268, 286, 298, 308–312, 326–330, 332

Radiometric equation, 86, 87

Rayleigh wave, 18, 26, 35, 39, 41–44, 60

Ray path, 35, 212, 271, 294, 295

Rebar corrosion, 77, 80, 82, 84, 227–229

Rebound hammer, 5, 101–110, 120, 124, 130, 148, 152, 153, 155–159, 171, 175

Reflection of waves (acoustics), 250

Reflection of waves (radar), 65, 245

Remanent magnetism, 309, 313

## S

SAFT. *See* Synthetic aperture focusing technique

SASW. *See* Spectral analysis of surface wave

Saturation degree, 78, 251

Schmidt hammer, 106

Sensitivity (of a NDT), 1, 10, 11, 14, 162, 170, 252, 257, 258, 336, 337, 339, 344, 347

Shallow foundations, 187, 190–191, 201–207

Shear waves, 18, 21, 27, 29, 31, 33, 35, 39, 52, 197, 279, 283, 285, 286, 289, 294

Shotcrete, 188, 200, 218, 241

SIBIE. *See* Stack imaging of spectral amplitudes based on impact-echo (SIBIE)

Sonic echo, 207–210, 213

SonReb method, 12, 156–158, 182, 336

Specific heat, 236

Spectral analysis of surface wave, 26, 41, 214, 241, 242

Stack imaging of spectral amplitudes based on impact-echo (SIBIE), 49, 50, 270, 278–279, 299

Surface waves, 6, 18–20, 26, 31, 35, 39–44, 58, 60, 214, 241–243, 248, 249, 270, 344, 345, 356

S-waves, 14, 18, 21, 27, 39, 40, 44, 60, 209

Synthetic aperture focusing technique, 33, 34, 36–38, 201, 234, 280, 283, 284, 286–292

**T**

- Tendon, 3, 14, 31, 32, 37, 38, 50, 60, 98, 100, 219, 244, 245, 255, 263–292, 295–300, 306, 308, 310–312, 314, 316, 318, 320–326, 328–330, 332
- Tendon duct, 3, 14, 31, 32, 37, 38, 50, 69, 219, 244, 245, 255, 263–292, 295, 296, 298–300

## Test site

- concrete wall, 219–220
- large concrete slab (LCS ), 219
- pavement, 187–188
- pile foundation, 191, 221–224
- sealing, 217–225
- slab foundation, 220–221
- tunnel, 218–219

Thermal conductivity, 92, 93, 236

Thermal diffusivity, 90, 236

Thermogram, 92, 94–96

Thickness evaluation, 43, 48, 63–65, 69–70, 187–189

Time of flight (of elastic waves), 18, 24, 27, 29, 35, 236, 237, 296

Transducers, 18–24, 26, 28–36, 38, 44–49, 51, 53, 197, 201, 236, 239, 265, 269, 280, 283–285, 289, 291, 294

Transverse waves, 18, 27, 31, 60, 279

Traveltime, 65

Tunnel shell thickness, 188–189

**U**

Ultrasonic echo, 6, 17, 27–38, 47, 190, 196–198, 201, 203, 265, 268, 279–293, 299, 300

Ultrasonic imaging, 281, 289, 290, 299

Ultrasonic pulse, 3, 22, 28, 34, 35, 47, 120, 124, 130, 144–148, 156, 158, 161, 236–237, 248–253, 272, 281, 336

Ultrasonic pulse echo, 47, 248, 249, 272, 281

Ultrasonic pulse velocity (UPV), 3, 22, 34, 120, 124, 130, 144–148, 156, 158, 161, 237, 253, 336

Ultrasonics in transmission, 17–27

UPV. *See* Ultrasonic pulse velocity**V**

Void detection, 278

**W**

Water content, 3, 12, 73, 76, 77, 159, 162, 170, 231, 337–340, 344–346, 354

Water content assessment, 345–346

Wave length, 21, 24, 50, 250

Wavelength (radar), 63

Wavelength (thermography), 85–86

Wave velocity (radar), 63, 344

Wire failure, 317–320, 327, 330, 331

**X**

X-ray, 98, 99, 101, 171, 264, 265, 310–312

**Y**

Young modulus, 250, 336, 338, 345–350

Young modulus assessment, 346–350

**Z**

Zoning, 4–6